THE DEADLY SECRETS OF C. DIFFICILE - INSIGHTS INTO HOST-PATHOGEN INTERACTION, VOLUME II

EDITED BY: Meina Neumann-Schaal, Uwe Groß, Dieter Jahn and Ingo Just

PUBLISHED IN: Frontiers in Microbiology

frontiers Research Topics

frontiers

Frontiers eBook Copyright Statement

The copyright in the text of individual articles in this eBook is the property of their respective authors or their respective institutions or funders. The copyright in graphics and images within each article may be subject to copyright of other parties. In both cases this is subject to a license granted to Frontiers.

The compilation of articles constituting this eBook is the property of Frontiers.

Each article within this eBook, and the eBook itself, are published under the most recent version of the Creative Commons CC-BY licence. The version current at the date of publication of this eBook is CC-BY 4.0. If the CC-BY licence is updated, the licence granted by Frontiers is automatically updated to the new version.

When exercising any right under the CC-BY licence, Frontiers must be attributed as the original publisher of the article or eBook, as applicable.

Authors have the responsibility of ensuring that any graphics or other materials which are the property of others may be included in the CC-BY licence, but this should be checked before relying on the CC-BY licence to reproduce those materials. Any copyright notices relating to those materials must be complied with.

Copyright and source acknowledgement notices may not be removed and must be displayed in any copy, derivative work or partial copy which includes the elements in question.

All copyright, and all rights therein, are protected by national and international copyright laws. The above represents a summary only. For further information please read Frontiers' Conditions for Website Use and Copyright Statement, and the applicable CC-BY licence.

ISSN 1664-8714
ISBN 978-2-88976-037-4
DOI 10.3389/978-2-88976-037-4

About Frontiers

Frontiers is more than just an open-access publisher of scholarly articles: it is a pioneering approach to the world of academia, radically improving the way scholarly research is managed. The grand vision of Frontiers is a world where all people have an equal opportunity to seek, share and generate knowledge. Frontiers provides immediate and permanent online open access to all its publications, but this alone is not enough to realize our grand goals.

Frontiers Journal Series

The Frontiers Journal Series is a multi-tier and interdisciplinary set of open-access, online journals, promising a paradigm shift from the current review, selection and dissemination processes in academic publishing. All Frontiers journals are driven by researchers for researchers; therefore, they constitute a service to the scholarly community. At the same time, the Frontiers Journal Series operates on a revolutionary invention, the tiered publishing system, initially addressing specific communities of scholars, and gradually climbing up to broader public understanding, thus serving the interests of the lay society, too.

Dedication to Quality

Each Frontiers article is a landmark of the highest quality, thanks to genuinely collaborative interactions between authors and review editors, who include some of the world's best academicians. Research must be certified by peers before entering a stream of knowledge that may eventually reach the public - and shape society; therefore, Frontiers only applies the most rigorous and unbiased reviews.
Frontiers revolutionizes research publishing by freely delivering the most outstanding research, evaluated with no bias from both the academic and social point of view. By applying the most advanced information technologies, Frontiers is catapulting scholarly publishing into a new generation.

What are Frontiers Research Topics?

Frontiers Research Topics are very popular trademarks of the Frontiers Journals Series: they are collections of at least ten articles, all centered on a particular subject. With their unique mix of varied contributions from Original Research to Review Articles, Frontiers Research Topics unify the most influential researchers, the latest key findings and historical advances in a hot research area! Find out more on how to host your own Frontiers Research Topic or contribute to one as an author by contacting the Frontiers Editorial Office: frontiersin.org/about/contact

THE DEADLY SECRETS OF C. DIFFICILE - INSIGHTS INTO HOST-PATHOGEN INTERACTION, VOLUME II

Topic Editors:
Meina Neumann-Schaal, German Collection of Microorganisms and Cell Cultures GmbH (DSMZ), Germany
Uwe Groß, University Medical Center Göttingen, Germany
Dieter Jahn, Technische Universitat Braunschweig, Germany
Ingo Just, Hannover Medical School, Germany

Citation: Neumann-Schaal, M., Groß, U., Jahn, D., Just, I., eds. (2022). The Deadly Secrets of C. Difficile - Insights Into Host-Pathogen Interaction, Volume II. Lausanne: Frontiers Media SA. doi: 10.3389/978-2-88976-037-4

Table of Contents

frontiers | Frontiers in Microbiology

EDITORIAL
published: 06 April 2022
doi: 10.3389/fmicb.2022.896979

Editorial: The Deadly Secrets of *C. Difficile*—Insights Into Host-Pathogen Interaction, Volume II

Meina Neumann-Schaal[1,2]*, *Uwe Groß*[3], *Ingo Just*[4] *and Dieter Jahn*[2,5]

[1] Research Group Metabolomics, Leibniz-Institute DSMZ–German Collection of Microorganisms and Cell Cultures, Braunschweig, Germany, [2] Braunschweig Integrated Centre of Systems Biology (BRICS), Braunschweig, Germany, [3] Institute of Medical Microbiology and Virology, University Medical Center Göttingen, Göttingen, Germany, [4] Institute of Toxicology, Hannover Medical School, Hannover, Germany, [5] Institute of Microbiology, Technische Universität Braunschweig, Braunschweig, Germany

Keywords: *Clostridioides* (*Clostridium*) *difficile*, *Clostridioides* (*Clostridium*) *difficile* infection, host pathogen interaction, toxins A and B *Clostridium difficile*, binary toxin CDT

Editorial on the Research Topic

The Deadly Secrets of *C. Difficile*—Insights Into Host-Pathogen Interaction, Volume II

INTRODUCTION

Clostridioides (formerly *Clostridium*) *difficile* is an anaerobic, spore-forming bacterium, widely distributed in soil, water, animals, and the gut of healthy humans (Hall and O'Toole, 1935; al Saif and Brazier, 1996; Lawson et al., 2016). The symptoms of *C. difficile* infection (CDI) range from relatively mild diarrhea to severe life-threatening pseudomembranous colitis, toxic megacolon with bowel perforation and a concomitant sepsis (Lessa et al., 2015). In the last two decades, an emerging number of nosocomial and community-acquired infections was reported worldwide (Bartlett, 2006; Rupnik et al., 2009; Lessa et al., 2015). CDI is commonly, but not necessarily associated with previous administration of antibiotics. Further risk factors are age, cancer treatment and immunosuppression. However, CDI also affects individuals without these classical risk factors (Bignardi, 1998; Rupnik et al., 2009).

THE CLOSTRIDIAL TOXINS AND BEYOND

C. difficile harbors different secreted and surface proteins responsible for the colonization of the colon and a subsequent inflammatory reaction in *C. difficile* infection. The most important and best characterized ones are three large clostridial toxins: toxin A and toxin B and in some bacterial strains, the binary toxin CDT.

In an approach by Petersen et al., toxin-catalyzed GTPase glucosylation resulted in subsequent cell cycle arrest which on the other hand was causative for decreased repair capacity of the colonic epithelium and delayed epithelial renewal. The role of toxin A and toxin B in treatment of *C. difficile* infection is elucidated in a study by Papatheodorou et al. to understand how important cholesterol is for the translocations process of the toxins into the cytoplasm. Two further publications focus on the role of the binary toxin CDT. In a study by Marquardt et al., binary toxin-induced activation of the innate immune system (MAIT cells) was identified to be partially MR1-dependent and allow hypervirulent *C. difficile* to overcome cellular barriers. Proteomic analysis of the cellular effects of the binary toxin on human cells by Stieglitz et al., showed only moderate changes on the overall proteome level but strong changes in the phosphorylation level. CSNK2A1 might act as an effector kinase in response to CDT.

OPEN ACCESS

Edited and reviewed by:
Axel Cloeckaert,
Institut National de Recherche pour l'Agriculture, l'Alimentation et l'Environnement (INRAE), France

***Correspondence:**
Meina Neumann-Schaal
meina.neumann-schaal@dsmz.de

Specialty section:
This article was submitted to Infectious Agents and Disease, a section of the journal Frontiers in Microbiology

Received: *15 March 2022*
Accepted: *16 March 2022*
Published: *06 April 2022*

Citation:
Neumann-Schaal M, Groß U, Just I and Jahn D (2022) Editorial: The Deadly Secrets of C. Difficile—Insights Into Host-Pathogen Interaction, Volume II. Front. Microbiol. 13:896979. doi: 10.3389/fmicb.2022.896979

In a review by Nibbering et al., both, current knowledge on toxin and non-toxin based host immune response are summarized and compared. The authors highlight that future research should focus on the immune responses to non-toxin proteins and non-toxigenic strains as starting point for non-antibiotic therapeutic approaches.

PHYSIOLOGY AND HOST RESPONSE

In the host, *C. difficile* is exposed to the host immune response and multiple stress factors. With the increasing knowledge on the pathogen itself, multifactorial systems in the human host get into focus. Biofilms are discussed as a form of persistence for *C. difficile* in the human host. Brauer et al. used a proteomics approach for understanding the biofilm formation and the role of proteins on the cell surface and the underlying regulatory network. Motility as one of the key patterns in biofilm formation is addressed in two further publications.

The regulation of flagellin synthesis was studied by Zhu et al. showing that the carbon storage regulator A modulates flagellin expression along with indirect effects of the flagellin assembly factor FliW. Schwanbeck et al. studied the swimming behavior in depending on environmental parameters, specifically also addressing the viscoelastic properties of the environment. Three further articles focus on different aspects of the host microbiome and the influence on *C. difficile*. In a review on recent developments, Vasilescu et al. focus on the microbiota profiles in infants and adults colonized or infected with *C. difficile* and provide insights into the role of protective microbial species. The impact of bile acids on *C. difficile* was studied by Metzendorf et al. and showed the effects on flagella, toxins and specifically the membrane composition. A study by Aguilar-Zamora et al. with isolates from patients in Mexico showed a high share of multidrug resistant strains and the importance of whole genome sequencing.

CONCLUSION AND OUTLOOK

The research on *C. difficile* of the last years gives in fact deeper insights into the process of pathogenesis but also increases complexity. Complexity is further increased by the diversity of strains. The simple story of two villains—toxins A and B—is thing of the past. The studies of this volume contribute to the idea that secreted proteins/toxins and adhesion proteins are in addition to the toxins modulators of the host response. CDT seems to affect the immune system rather to act as cytotoxin. Persistence of *C. difficil*e is no longer more simply based on sporulation but biofilm formation contributes as well. The gut microbiome not only interacts with *C. difficile*—outgrowth and sporulation—but also with colonic mucosa and the gut immune system. All these interdependencies define the gut environment to be protective or permissive for inflammation and the clinical outcome. Thus, the understanding of the effects of atoxinogenic, that means asymptomatic *C. difficile* strains on colonic mucosa and the immune system evolves to be the foundation of the development of non-antibiotic treatment of CDI.

AUTHOR CONTRIBUTIONS

All authors listed have made a substantial, direct, and intellectual contribution to the work and approved it for publication.

REFERENCES

al Saif, N., and Brazier, J. S. (1996). The distribution of *Clostridium difficile* in the environment of South Wales. *J. Med. Microbiol.* 45, 133–137. doi: 10.1099/00222615-45-2-133

Bartlett, J. G. (2006). Narrative review: the new epidemic of *Clostridium difficile*–associated enteric disease. *Ann. Intern. Med.* 145, 758–764. doi: 10.7326/0003-4819-145-10-200611210-00008

Bignardi, G. E. (1998). Risk factors for *Clostridium difficile* infection. *J. Hosp. Infect.* 40, 1–15. doi: 10.1016/S0195-6701(98)90019-6

Hall, I. C., and O'Toole, E. (1935). Intestinal flora in new-born infants: with a description of a new pathogenic anaerobe, *Bacillus difficilis*. *Am. J. Dis. Child* 49:390. doi: 10.1001/archpedi.1935.01970020105010

Lawson, P. A., Citron, D. M., Tyrrell, K. L., and Finegold, S. M. (2016). Reclassification of *Clostridium difficile* as *Clostridioides difficile* (Hall and O'Toole 1935) Prevot 1938. *Anaerobe* 40, 95–99. doi: 10.1016/j.anaerobe.2016.06.008

Lessa, F. C., Mu, Y., Bamberg, W. M., Beldavs, Z. G., Dumyati, G. K., Dunn, J. R., et al. (2015). Burden of *Clostridium difficile* Infection in the United States. *N. Engl. J. Med.* 372, 825–834. doi: 10.1056/NEJMoa1408913

Rupnik, M., Wilcox, M. H., and Gerding, D. N. (2009). *Clostridium difficile* infection. *Nat. Rev. Microbiol.* 7, 526–536. doi: 10.1038/nrmicro2164

Conflict of Interest: The authors declare that the research was conducted in the absence of any commercial or financial relationships that could be construed as a potential conflict of interest.

Publisher's Note: All claims expressed in this article are solely those of the authors and do not necessarily represent those of their affiliated organizations, or those of the publisher, the editors and the reviewers. Any product that may be evaluated in this article, or claim that may be made by its manufacturer, is not guaranteed or endorsed by the publisher.

Copyright © 2022 Neumann-Schaal, Groß, Just and Jahn. This is an open-access article distributed under the terms of the Creative Commons Attribution License (CC BY). The use, distribution or reproduction in other forums is permitted, provided the original author(s) and the copyright owner(s) are credited and that the original publication in this journal is cited, in accordance with accepted academic practice. No use, distribution or reproduction is permitted which does not comply with these terms.

frontiers in Microbiology

ORIGINAL RESEARCH
published: 10 June 2021
doi: 10.3389/fmicb.2021.682111

What's a Biofilm?—How the Choice of the Biofilm Model Impacts the Protein Inventory of *Clostridioides difficile*

*Madita Brauer[1], Christian Lassek[1], Christian Hinze[1], Juliane Hoyer[2], Dörte Becher[2], Dieter Jahn[3], Susanne Sievers[1] and Katharina Riedel[1]**

[1] Department for Microbial Physiology and Molecular Biology, Institute of Microbiology, University of Greifswald, Greifswald, Germany, [2] Department for Microbial Proteomics, Institute of Microbiology, University of Greifswald, Greifswald, Germany, [3] Braunschweig Integrated Centre of Systems Biology (BRICS), Institute of Microbiology, Technische Universität Braunschweig, Braunschweig, Germany

The anaerobic pathogen *Clostridioides difficile* is perfectly equipped to survive and persist inside the mammalian intestine. When facing unfavorable conditions *C. difficile* is able to form highly resistant endospores. Likewise, biofilms are currently discussed as form of persistence. Here a comprehensive proteomics approach was applied to investigate the molecular processes of *C. difficile* strain 630Δ*erm* underlying biofilm formation. The comparison of the proteome from two different forms of biofilm-like growth, namely aggregate biofilms and colonies on agar plates, revealed major differences in the formation of cell surface proteins, as well as enzymes of its energy and stress metabolism. For instance, while the obtained data suggest that aggregate biofilm cells express both flagella, type IV pili and enzymes required for biosynthesis of cell-surface polysaccharides, the S-layer protein SlpA and most cell wall proteins (CWPs) encoded adjacent to SlpA were detected in significantly lower amounts in aggregate biofilm cells than in colony biofilms. Moreover, the obtained data suggested that aggregate biofilm cells are rather actively growing cells while colony biofilm cells most likely severely suffer from a lack of reductive equivalents what requires induction of the Wood-Ljungdahl pathway and *C. difficile's* V-type ATPase to maintain cell homeostasis. In agreement with this, aggregate biofilm cells, in contrast to colony biofilm cells, neither induced toxin nor spore production. Finally, the data revealed that the sigma factor SigL/RpoN and its dependent regulators are noticeably induced in aggregate biofilms suggesting an important role of SigL/RpoN in aggregate biofilm formation.

Keywords: biofilm, colony biofilm, aggregate biofilm, *Clostridioides difficile*, proteomics, cell surface antigens, RpoN signaling

OPEN ACCESS

Edited by:
George Grant, University of Aberdeen, United Kingdom

Reviewed by:
Thomas Candela, Université Paris-Saclay, France
Anthony Buckley, University of Leeds, United Kingdom

****Correspondence:***
Katharina Riedel
riedela@uni-greifswald.de

Specialty section:
This article was submitted to Infectious Diseases, a section of the journal Frontiers in Microbiology

Received: *17 March 2021*
Accepted: *12 May 2021*
Published: *10 June 2021*

Citation:
Brauer M, Lassek C, Hinze C, Hoyer J, Becher D, Jahn D, Sievers S and Riedel K (2021) What's a Biofilm?—How the Choice of the Biofilm Model Impacts the Protein Inventory of Clostridioides difficile. Front. Microbiol. 12:682111. doi: 10.3389/fmicb.2021.682111

INTRODUCTION

In recent years, the anaerobic gastrointestinal pathogen *Clostridioides difficile* has established itself as one of the major causative agents of pseudomembranous colitis and toxic megacolon (Wiegand et al., 2012; Nasiri et al., 2018; Martínez-Meléndez et al., 2020; Doll et al., 2021). *C. difficile* does not only produce enterotoxins that damage the gastrointestinal epithelium (Fletcher et al., 2021) but

also forms easily transmittable spores that significantly contribute to *C. difficile's* efficient spreading in the environment, hospitals and elderly homes (McLure et al., 2019; Hernandez et al., 2020; Werner et al., 2020; Khader et al., 2021). If conditions are favorable, e.g., after antibiotic-induced dysbiosis when the reduced microbiome fails to convert primary bile acids into secondary bile acids, *C. difficile* spores are able to germinate to successively colonize the large intestine (Theriot et al., 2014; Pike and Theriot, 2020). Even though antibiosis mostly stops the acute infection, *C. difficile* spores as well as some vegetative cells survive in the intestine and can subsequently cause a relapse as soon as antibiotic concentrations are sufficiently low (Goulding et al., 2009; Chilton et al., 2018; Castro-Córdova et al., 2020; Feuerstadt et al., 2021; Normington et al., 2021). Initially, sporulation was assumed to be one of the major prerequisites for *C. difficile's* persistence under clinical circumstances. However, recent publications failed to correlate sporulation efficiency of a certain strain with the corresponding virulence and persistence potential, i.e., highly infectious strains do not necessarily produce more spores than other strains (Sirard et al., 2011; Oka et al., 2012; Plaza-Garrido et al., 2015; Gómez et al., 2017). In conclusion, persistence does obviously not solely rely on sporulation but also on additional features of *C. difficile* (Smits, 2013). In this context, biofilm formation was proposed to be a major additional factor (Dawson et al., 2012; Đapa et al., 2013). Surface-associated biofilms, consisting of multiple microorganisms embedded in a slimy extracellular matrix, represent a form of community lifestyle for many bacteria (Hansen et al., 2007; Oliveira et al., 2015; Ren et al., 2015). Many nosocomial infections caused by *Staphylococcus aureus*, *Streptococci* and numerous other pathogens rely on biofilms (Jamal et al., 2018). In this context, biofilm formation has been frequently linked to pro-longed infection and persistence (Burmølle et al., 2010; Jamal et al., 2018). An important feature of biofilms is their extracellular matrix, which mostly consists of extracellular DNA (eDNA), lipids, proteins and polysaccharides. The extracellular matrix provides protection against chemical and mechanical stress and confers resistance to therapeutics and the host immune system (Karygianni et al., 2020). Anaerobic bacteria, including *C. difficile* have also been found to produce biofilms *in vitro*, and biofilm-like structures have been observed on the intestinal mucosal surface of *C. difficile* infected mice (Donelli et al., 2012; Lawley et al., 2012; Soavelomandroso et al., 2017).

Initial biofilm studies using *C. difficile* revealed mechanisms of formation and involved components comparable to those determined for other bacteria (Dawson et al., 2012; Vuotto et al., 2018). For instance, the involvement of adhesion-mediating cell surface structures, such as flagella, pili and various adhesion molecules, has been reported (Reynolds et al., 2011; Đapa et al., 2013; Pantaléon et al., 2015). Similarly, c-di-GMP signaling, quorum sensing, and regulators, such as Spo0A and CodY, are involved in coordination of the process of biofilm formation (Đapa et al., 2013; Purcell et al., 2016; McKee et al., 2018b; Dubois et al., 2019). Knockout mutants of some genes encoding certain proteins commonly linked to biofilm formation, such as adhesion and cell signaling proteins, were found impaired in biofilm formation *in vitro* and revealed a reduced infection and persistence behavior in rodent models (Barketi-Klai et al., 2011; Dawson et al., 2012; Đapa et al., 2013; Batah et al., 2017; McKee et al., 2018a; Slater et al., 2019). Corresponding cell-cell aggregates were observed in a CDI murine model and multispecies biofilms have been shown to be a reservoir for *C. difficile* spores in triple-stage chemostat human gut model (Lawley et al., 2012; Soavelomandroso et al., 2017; Normington et al., 2021). While these data clearly indicate that biofilm formation is indeed an important virulence factor our knowledge on the physiology of *C. difficile* biofilms is still scarce. Moreover, it remains to be determined whether *in vitro* biofilm model systems sufficiently resemble *in vivo* biofilm formation. Currently, *in vitro C. difficile* biofilms are often studied in plastic microtiter plates, where cells initially attach to the surface, followed by a maturation of the biofilm and a final detachment of cell-cell-aggregates (Dawson et al., 2012; Đapa et al., 2013; Dubois et al., 2019). Similar biofilms have been observed in continuous-flow micro-fermenters (Poquet et al., 2018). Alternatively, colony biofilms on agar plates and related biofilm models have been used (Crowther et al., 2014; Semenyuk et al., 2014; James et al., 2018). Inconsistent results from *in vitro* experiments suggest that biofilm physiology strongly depends on the chosen strain, growth conditions and phase as well as the experimental setup (Đapa et al., 2013; Maldarelli et al., 2016; Mathur et al., 2016; Pantaléon et al., 2018). For example, differences in flagella production and contribution to biofilm formation has been reported for different strains and phases of biofilm formation (Đapa et al., 2013; Maldarelli et al., 2016). Analogously, a comprehensive RNA-seq approach revealed that the expression levels of some genes which had previously been linked to biofilm formation were significantly different between *C. difficile* colony biofilms grown on agar plates and biofilms formed on glass beads (Maldarelli et al., 2016).

Considering the strong evidence that *C. difficile* colonizes the gut in a biofilm-like manner a profound molecular characterization of *C. difficile* biofilms is crucial, e.g., for the targeted development of therapeutics and vaccines. Since most vaccines are directed against cell-surface exposed structures, the comprehensive characterization of *C. difficile's* cell-surface proteins and polysaccharides in biofilms is of particular importance (Bruxelle et al., 2017; Kirk et al., 2017a; Péchiné et al., 2018; Bradshaw et al., 2019). Here, we applied a comparative proteomics approach to investigate the proteome repertoire of *C. difficile* strain 630Δ*erm* grown either as aggregate or colony biofilm to (i) identify proteins contributing to biofilm formation of one or the other growth condition and (ii) elucidate the underlying regulatory networks.

MATERIALS AND METHODS

Bacterial Strains and Media

The reference strain *C. difficile* 630Δ*erm* (DSM28645) (Hussain et al., 2005; van Eijk et al., 2015) was grown at 37°C in an anaerobic workstation (Toepffer Lab Systems, Germany) in Brain Heart Infusion (BHIS; Oxoid (Thermo Fisher Scientific), Waltham, MA) supplemented with L-cysteine (0.1%(wt/vol), Sigma-Aldrich, St. Louis, MO), and yeast extract (5 mg/ml; Carl

Roth, Germany) as described earlier (Đapa et al., 2013). Prior to cultivation, spores were allowed to germinate for 72 h in BHIS medium. Subsequently, the germinated cells were used to inoculate pre-cultures which were grown for 18 h in BHIS medium. For planktonic growth main cultures were inoculated to an optical density of 0.05 at 600 nm.

Growth of Colony and Aggregate Biofilms

The growth of colony biofilms was performed as previously described with some modifications (Semenyuk et al., 2014). Briefly, BHI medium was supplemented with yeast extract and agarose (1.5% v/v) and autoclaved for 15 min. Subsequently, sterile-filtered cysteine in BHI medium was added to the medium, mixed and transferred to petri dishes. Plates were allowed to dry for 24 h in the anaerobic chamber. Prior to cultivation, a filter membrane with a pore size of 0.45 μm (cellulose ester, Sigma-Aldrich, St. Louis, MO) was placed on top of the BHIS agar plate. Per plate 100 μl of *C. difficile*-containing BHIS medium were placed on top of the filter membrane. The BHIS medium was inoculated by an exponentially grown *C. difficile* main culture (OD_{600nm}: ∼0.5) in a 100-fold dilution. Plates were wrapped with parafilm in order to protect them from drying. The colony biofilms were grown for three and six days at 37°C in the anaerobic environment.

Aggregated biofilms were cultivated as previously reported with some modifications (Dawson et al., 2012). Briefly, sterile 6-well plates (polystyrene, Corning, NY) were filled with 2 ml *C. difficile*-containing BHIS medium. The BHIS medium was inoculated by an exponentially grown *C. difficile* main culture (OD_{600nm}: ∼0.5) in a 100-fold dilution. The 6-well plates were placed in a plastic bag to avoid evaporation of the medium. Cells were grown for three and six days at 37°C in the anaerobic environment.

Cell Harvest and Protein Extraction

Planktonically-grown cells were harvested after 6 and 12 h of cultivation at 6.000 × g for 20 min and pellets were stored at −80°C. Filter membranes with colony biofilms were placed into 15 ml reaction tubes and stored at −80°C. In order to separate aggregated cells from free-living planktonic cells the culture-medium was carefully removed from the 6-well plates and pooled (one 6-well plate = one biological sample). The pooled culture-medium was filtered through a 10 μm filter (Isopore^{TM} PC Membrane, Merck Millipore, Tullagreen, Ireland), washed with 5 ml of 0.9% NaCl (w/v) and subsequently the filter was stored at −80°C. The filtrate containing the planktonic cells was centrifuged at 6.000 × g and the cell pellet was stored at −80°C.

The samples (cell pellets of filtrate samples and membrane filters of both biofilm types) were kept in 0.6–1 ml of an urea-containing buffer (7 M urea, 2 M thiourea, 50 mM dichlorodiphenyltrichloroethane (DDT), 4% (w/v) 3-[(3-cholamidopropyl) dimethylammonio]-1-propanesulfonate (CHAPS), 50 mM Tris-HCl). Cell lysis was performed by sonication in six cycles on ice as done previously (Sonoplus, Bandelin, Berlin, Germany, Otto et al., 2016; Berges et al., 2018). Cell debris was removed by centrifugation at 6,000 × g for 20 min at 4°C. 200 μl of the resulting lysates were precipitated by ice-cold acetone (in a 1:7 ratio v/v) for 20 h at −20°C. Subsequently, samples were allowed to warm up at RT and were centrifuged at 22,000 × g for 45 min at RT. The supernatant was discarded and the pellets were dried at RT. The protein pellets were solubilized in 100 μl of an SDS-containing urea-buffer (7 M urea, 2 M thiourea, 1% SDS v/v). In order to estimate the relative protein concentration, 10 μl of each sample was mixed with SDS-loading buffer and separated by SDS-PAGE (Criterion TGX Precast Gels 12%, Biorad, Hercules, CA, Laemmli, 1970). Protein gels were fixed for 1 h at RT (40% EtOH, 10% glacial acidic acid and 50% H_2O), washed in H_2O and stained by the Flamingo fluorescent dye (Biorad, Hercules, CA) for 1 h at RT. Remaining dye was removed by a washing step in H_2O and fluorescence signals of the samples were obtained by Typhoon scanner (GE Healthcare, Little Chalfont, United Kingdom). The fluorescence signals of the gel image were quantified by ImageQuant (Biorad, Hercules, CA). These fluorescent signal intensities were used for normalization to load comparable protein amounts (30 μg of protein per sample) on the final SDS-Gel. For each sample, the entire gel lane was cut into 10 gel blocks and proteins were digested in-gel with trypsin as follows: the excised gel pieces were destained using 50% (v/v) methanol in 100 mM NH_4HCO_3. Subsequently, gel pieces were dehydrated using 100% ACN and allowed to dry. Modified trypsin (sequencing grade, Promega, Germany) was added to a final ratio of 1:10 (trypsin/sample) in 50 mM Tris/HCl, pH 7.5 and the sample incubated at 37°C overnight. Peptides were iteratively extracted from the gel by a four-step procedure, using ACN, 5% (v/v) formic acid in ddH_2O and further two steps of ACN. Peptide-containing supernatants were pooled and completely dried using a Speedvac concentrator (Eppendorf AG). Samples were subsequently resolved in buffer A (5% (v/v) ACN, 0.1% (v/v) formic acid) and desalted using ZipTips (C18, Millipore). Desalted peptides were again vacuum-dried and stored at −20°C. Finally, the samples were solubilised in 10 μL 0,1% acetic acid solution and transferred into vials for MS-analysis.

Mass Spectrometric Measurement and Data Analysis

Samples were subjected to LC-MS/MS measurements using an EASYnLC 1,000 (Thermo Fisher Scientific, Odense, Denmark) with self-packed columns [(Luna 3 μC18(2) 100A, Phenomenex, Germany)] in a one-column setup on-line coupled to an Orbitrap Elite (Thermo Fisher Scientific, Bremen, Germany) setting parameters as previously described (Berges et al., 2018).

Database search and intensity based absolute quantification (iBAQ) was achieved using the MaxQuant proteomics software package (Cox and Mann, 2008; Tyanova et al., 2016a; version: 1.6.10.43). A protein sequence database of *C. difficile* strain 630Δ*erm* containing 3781 entries was obtained from UniProt. Common laboratory contaminants and reverse sequences were added by the MaxQuant software. Parameters were set as follows: Trypsin cleavage with a maximum of two missed cleavages was assumed and oxidation of methionine was set as

variable modification. Default parameters were used for protein identification. For label-free protein quantification unique and razor peptides were considered with a minimum ratio count of 2. Match between runs was enabled with default settings within each sample group. *C difficile* proteins were considered as identified if they were identified with at least two unique peptides in at least two out of three biological replicates. riBAQ values were calculated as published previously (Shin et al., 2013). Averaged riBAQs were used to calculate log2 fold changes. Proteins significantly altered in their abundance between two conditions were identified by two-way analysis of variance (ANOVA) followed by a Tukey *post hoc* test using the Perseus software package (Tyanova et al., 2016b; version: 1.6.2.2). Cellular localization of identified proteins was predicted by PSORTb (Yu et al., 2010; version: 3.0).

Voronoi-Regulon Treemaps

Global protein expression patterns were analyzed and visualized using Voronoi treemaps (Bernhardt et al., 2013) which were adapted to illustrate regulons of several well defined global regulators of *C. difficile* as described in the literature. For this purpose, data extracted from eight transcriptomic studies was used to generate a scaffold for the Voronoi-regulon-treemaps. In these previous studies, regulons of fourteen global regulators were characterized, i.e., SigB (Kint et al., 2017), SigH (Saujet et al., 2011), SigD (El Meouche et al., 2013), SigL/RpoN (Soutourina et al., 2020), CodY (Dineen et al., 2010), CcpA (Antunes et al., 2012), Fur (Ho and Ellermeier, 2015), Hfq (Boudry et al., 2014), c-di-GMP (McKee et al., 2018b), Spo0A (Pettit et al., 2014), SigF, SigE, SigG, and SigK (Fimlaid et al., 2013). The corresponding regulons, comprising negatively as well as positively regulated genes, differ in size in the range of 30 to more than 400 genes (**Table 1**). In total, these transcriptional regulators modulate the expression of 1252 different *C. difficile* genes. For the illustration of the defined regulons each regulated gene was assigned to its corresponding regulator(s). Additionally, the regulatory effect (positive or negative) of a regulator on the expression of a specific gene is indicated by a plus or minus symbol. Finally, *C. difficile* log2 fold changes of biofilm models compared to filtrate samples were mapped onto the regulon maps.

RESULTS AND DISCUSSION

A Comparative Proteomics Approach to Investigate the Protein Repertoire of *C. difficile* Biofilms

In order to identify proteins required for and/or characteristic of *C. difficile* biofilm formation the protein inventory of biofilm- and planktonically-grown bacteria was comparatively analyzed. Two different types of biofilms were investigated: 1. colony biofilms on agar plates and 2. aggregate biofilms formed in 6-well plates. Although colonies on agar plates do not meet the traditional criteria of a biofilm, the densely packed cells likewise present a form of multicellular growth attached to a biotic surface (Gingichashvili et al., 2017; Kesel et al., 2017) and it cannot be excluded that the growth conditions that bacteria face during this form of multicellular living are relevant during infection. Colony biofilms were directly analyzed after scraping them off the plates. Aggregate biofilms from 6-well plates were harvested by filtration and cells that passed the filter were analyzed in parallel as non-biofilm fraction. Previous studies investigating *C. difficile* biofilm gene expression by RNA-seq used planktonically-grown cells as reference (Maldarelli et al., 2016; Poquet et al., 2018). Thus, planktonically-grown cells from exponential (6 h) and stationary (12 h) growth phase were also included in this study (**Figure 1**).

Principal component analyses revealed that the various proteome parameters obtained for every tested condition clustered together within the biological replicates but revealed a clear cut separated distribution in dependence of the growth condition and time (**Supplementary Figure 1**). This was also true for the data obtained for cells from the filtrate (sample C of **Supplementary Figure 1**) of the aggregate biofilms which clearly separated from the corresponding biofilm cells (sample B of **Supplementary Figure 1**), although both types of cells experienced the same cultivation time and growth medium along with nutrient limitation and accumulated waste products. We propose physiological differences between these cells to be mainly attributed to cell aggregation/biofilm formation and therefore used the filtrate samples as the reference for non-biofilm conditions rather than the planktonic cells (sample A of **Supplementary Figure 1**) which were not further considered.

Global hierarchical cluster analyses on all proteins that were found differentially expressed between the six remaining data sets using ANOVA (analysis of variance) yielded four major clusters A–D (**Figure 2** and **Supplementary Table 2**). Cluster A contained proteins with higher abundance in 6-day old filtrate cells and consisted of a high proportion of membrane

TABLE 1 | Selected regulators of *C. difficile* gene expression.

Regulator	Regulatory event	Regulon size (genes)	References
SigB	General stress response	663	Kint et al., 2017
SigH	Transition phase	490	Saujet et al., 2011
SigD	Motility, toxin production	146	El Meouche et al., 2013
SigL/RpoN	Amino acid catabolism	114	Soutourina et al., 2020
CodY	Regulation of metabolism	160	Dineen et al., 2010
CcpA	Carbohydrate catabolism	313	Antunes et al., 2012
Fur	Iron acquisition	125	Ho and Ellermeier, 2015
Hfq	Posttranscriptional (pleiotropic) regulation	203	Boudry et al., 2014
c-di-GMP	Motility	160	McKee et al., 2018b
Spo0A	Sporulation	297	Pettit et al., 2014
SigF	Sporulation (forespore)	181	Fimlaid et al., 2013
SigE	Sporulation (mother cell)	164	Fimlaid et al., 2013
SigG	Sporulation (forespore)	34	Fimlaid et al., 2013
SigK	Sporulation (mother cell)	30	Fimlaid et al., 2013

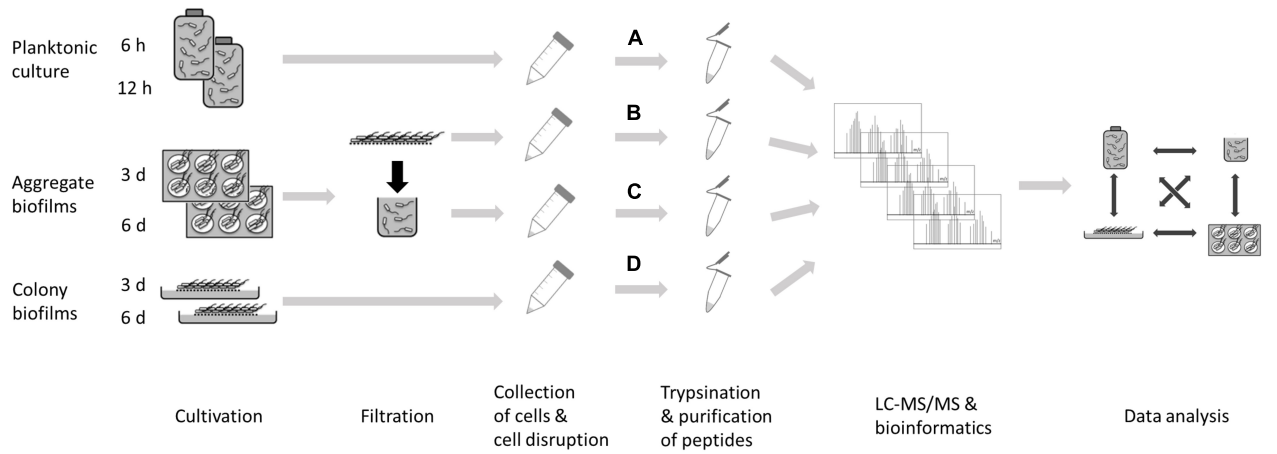

FIGURE 1 | Experimental setup for a comparative proteomics approach to investigate biofilm formation in *C. difficile*. *C. difficile* strain 630Δerm was grown as planktonic culture for 6 and 12 h **(A)**, or as aggregate biofilm in six-well plates for 3 or 6 days **(B)** or as colony biofilm on solid growth medium for 3 or 6 days **(D)**. In addition, cells from the filtrate of aggregate biofilms were analyzed **(C)**. Cells were harvested and their protein repertoire was subsequently analyzed using a LC-MS/MS approach.

proteins (54%) while all other clusters contained approximately 75% cytosolic proteins. In line with this, cluster A contained transporters for cations and amino acids. The largest cluster B contained 607 proteins of high abundance in aggregate biofilms which were assigned to the functional categories "cell wall biosynthesis", "cell surface polysaccharide biosynthesis", "flagella biosynthesis", "regulation and cell signaling", and "amino acid and carbohydrate metabolism". Cluster C was composed of 99 proteins highly abundant in colony biofilms, and the 267 proteins of cluster D were found in higher abundance in colony biofilms and filtrate cells. Both clusters share a high proportion of cell-wall proteins including the S-layer protein SlpA and 12 of the 28 cell wall proteins (CWPs) encoded in one operon with SlpA. Additionally, "fermentation and energy generation" proteins of cluster C were assigned to the Wood-Ljungdahl pathway and the corresponding glycine cleavage system, and to subunits of the V-type ATPase, but also "sporulation"-related proteins such as CotA, CotB, and SipL were observed.

In agreement with transcriptome data comparing biofilm and non-biofilm cells (Maldarelli et al., 2016; Poquet et al., 2018), we identified genes encoding cell-surface exposed proteins, but also genes from the categories "energy metabolism", "stress response", "virulence" and "regulation and cell signaling" as biofilm signature.

Production of Cell Surface-Associated Proteins in *C. difficile* Biofilms

Adhesion to epithelial cells as well as cell-cell-aggregation is mainly mediated by cell-surface exposed proteins, polysaccharides and cell appendices such as pili and flagella (Đapa et al., 2013; McKee et al., 2018a; Arato et al., 2019). Notably, proteins from the respective categories were found differently expressed between colony and aggregate biofilms (**Figure 3** and **Supplementary Table 3**). Most flagella proteins (i.e., FliE, FliF, FliG, FliH, FliM, FlgE, FlgG, FhlA, FhlF) and type IV pili proteins (i.e., PilT, PilB2, and PilM2) were detected in higher concentrations in aggregate biofilms than in colony biofilms and filtrates. Similar behavior was observed for proteins involved in cell wall biogenesis like enzymes of the *mur* operon (i.e., MurB, MurE, MurG), enzymes involved in lipoteichoic acid synthesis (GtaB, GtaB1) and modification (DltA), enzymes of the Cell Wall Glycopolymer (CWG) locus (CD2783 to CD2769), and proteins of membrane-lipid biosynthesis encoded by the *fab* operon (i.e., FabD, FabH, FabK). In contrast, the S-layer protein SlpA and most CWPs (i.e., Cwp12, Cwp16, Cwp19, Cwp22, Cwp84) were of significantly lower abundance in aggregate biofilms.

Flagella and Type IV Pili

While comparable RNA-seq based expression profiles were observed for cell wall and S-layer biogenesis genes when aggregate biofilms and planktonic cells were compared (Poquet et al., 2018), transcription of flagella genes has been found to be reduced in aggregate and colony biofilms in comparison to planktonic cells of *C. difficile* (Maldarelli et al., 2016; Poquet et al., 2018). However, both transcriptomic studies were performed with biofilms grown in different setups and to different timepoints. Hence, flagella might be required for aggregate biofilm growth in our rather static set up, but might be obsolete or even obstructive for biofilm formation in continuous flow systems (Poquet et al., 2018) or for biofilms grown on glass beads (Maldarelli et al., 2016). As discussed above, somewhat contradictory observations have been obtained regarding the role of flagella during *C. difficile* biofilm formation (Đapa et al., 2013; Jain et al., 2017) that may either reflect the complexity of the regulatory system underlying flagella expression in *C. difficile* (El Meouche et al., 2013; Soutourina et al., 2013; Anjuwon-Foster and Tamayo, 2017, 2018) and/or the different functions of flagella that depend on their posttranslational modification state (Twine et al., 2009; Faulds-Pain et al., 2014;

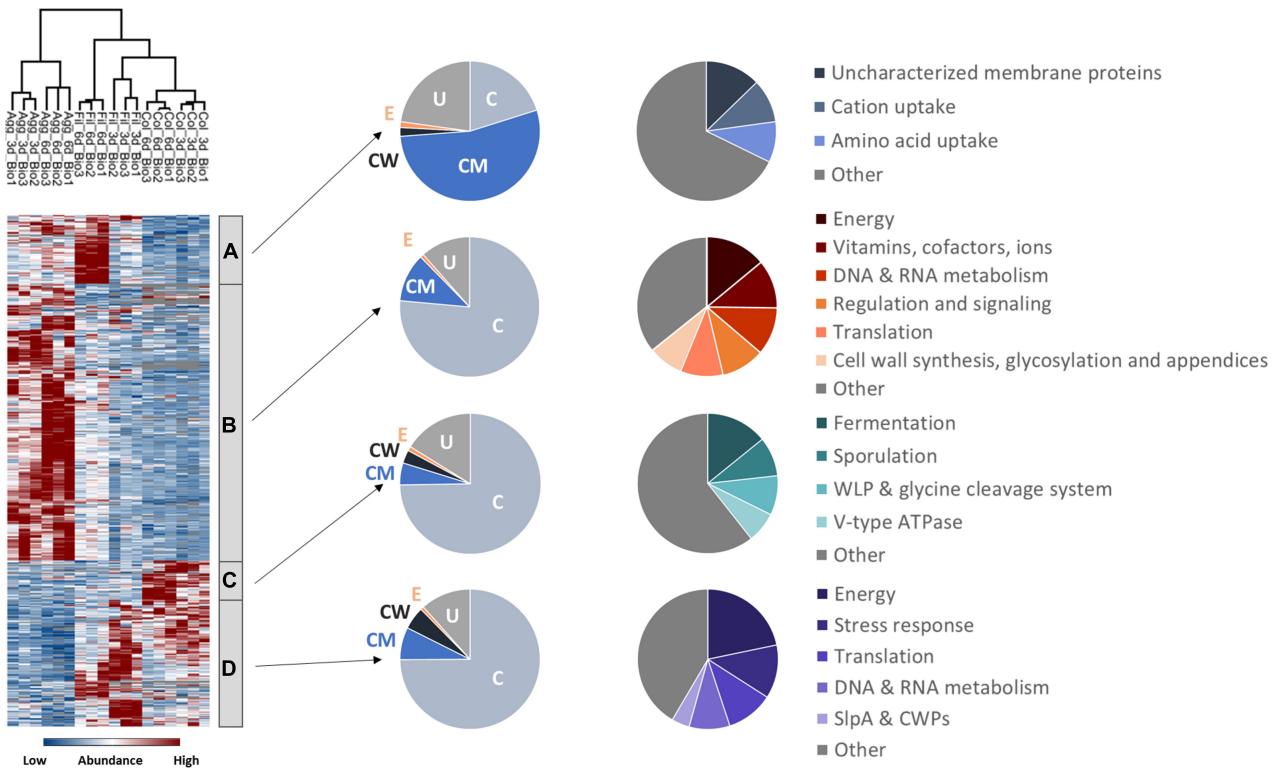

FIGURE 2 | Hierarchical cluster analyses of *C. difficile* proteome data sets. The heatmap on the left side shows differentially abundant proteins between aggregate biofilms (Agg), filtrate cells (Fil), and colony biofilms (Col) from day three (3d) and day six (6d) for three biological replicates (Bio1-3). Z-transformed abundance values are displayed as a color gradient where blue colors indicate weakest abundance levels and red colors the strongest abundance levels among the growth conditions with maximum z-scores of +/–1.5. Hierarchical clustering revealed four major cluster **(A–D)** representing 6-day old filtrate cells cluster **(A)**, aggregate biofilms **(B)**, colony biofilms **(C)** or both, colony biofilms and filtrate samples **(D)**. In the pie charts on the right the various clusters shown on left were further analyzed with regard to the subcellular location (middle: C for cytoplasmic; CM for cytoplasmic membrane; CW for cell wall; E for extracellular; U for unassigned). In addition, proteins within a cluster were grouped according to their function and the most prominent functional groups of each cluster are presented in the pie charts on the right (WLP for Wood-Ljungdahl pathway). A detailed list of all significantly differentially abundant proteins including fold changes can be found in **Supplementary Table 2** (**Supplementary Material**). Agg: Aggregate biofilms; Col: Colony biofilms; Fil: Filtrate samples; 3d: Samples from day three; 6d: Samples from day six; C, cytoplasmic; CM, cytoplasmic membrane; CW, cell wall; E, extracellular; U, unassigned; WLP, Wood-Ljungdahl pathway; CWPs, cell wall proteins.

Bouché et al., 2016; Valiente et al., 2016). Additionally, biofilms are often composed of subpopulations (Vlamakis et al., 2008; Besharova et al., 2016) and flagella in one or the other modification state might be relevant for one subpopulation and obstructive for the other. Alterations of flagella post-translational modifications were shown to impact motility and cell-cell-aggregation properties of *C. difficile* (Faulds-Pain et al., 2014; Valiente et al., 2016). Significant upregulation of *C. difficile's* conserved glycosyltransferase CDIF630erm_00362 in conjunction with the flagella proteins in aggregate biofilms in our study might suggest that flagella in aggregate biofilms were glycosylated. The CDIF630erm_00362 gene is encoded directly downstream of *fliC* which is essential for flagella formation and the bacterium's virulence *in vivo* (Valiente et al., 2016). Obviously, flagella are not always required for biofilm formation in *C. difficile* but might be beneficial depending on their state of modification in some cases.

In contrast, there is growing consensus that type IV pili are dispensable for early biofilm development, but required in mature biofilms of *C. difficile* (Maldarelli et al., 2016; Purcell et al., 2016; McKee et al., 2018a). We found type IV pili-associated proteins like PilT, PilB2 and PilM2 in aggregate biofilms and in lower amounts in filtrates but not in colony biofilms. Therefore, our data suggest that aggregate biofilms in contrast to colony biofilms obviously utilized glycosylated flagella and certain pili components during their formation.

Cell Surface Glyco-Polymers and Teichoic Acids

Proteins from the PSII locus for the synthesis of the teichoic-acid-like cell-surface polysaccharide II (e.g., CDIF630erm_03033, CDIF630erm_03035, CDIF630erm_03041), GtaB and GtaB1 providing UDP-glucose for teichoic acid synthesis and DltA involved in D-alanylation of teichoic acids were detected in aggregate biofilms and in lower amounts in the filtrates, and even lower or not in colony biofilms. Polysaccharide II is one of three of *C. difficile's* cell surface polysaccharides (Ganeshapillai et al., 2008; Reid et al., 2012; Willing et al., 2015). The ubiquitously found polysaccharide, attached to the cell surface, represents either an important antigen or is masking surface antigens with higher inflammatory potential. Its presence in *C. difficile* biofilms

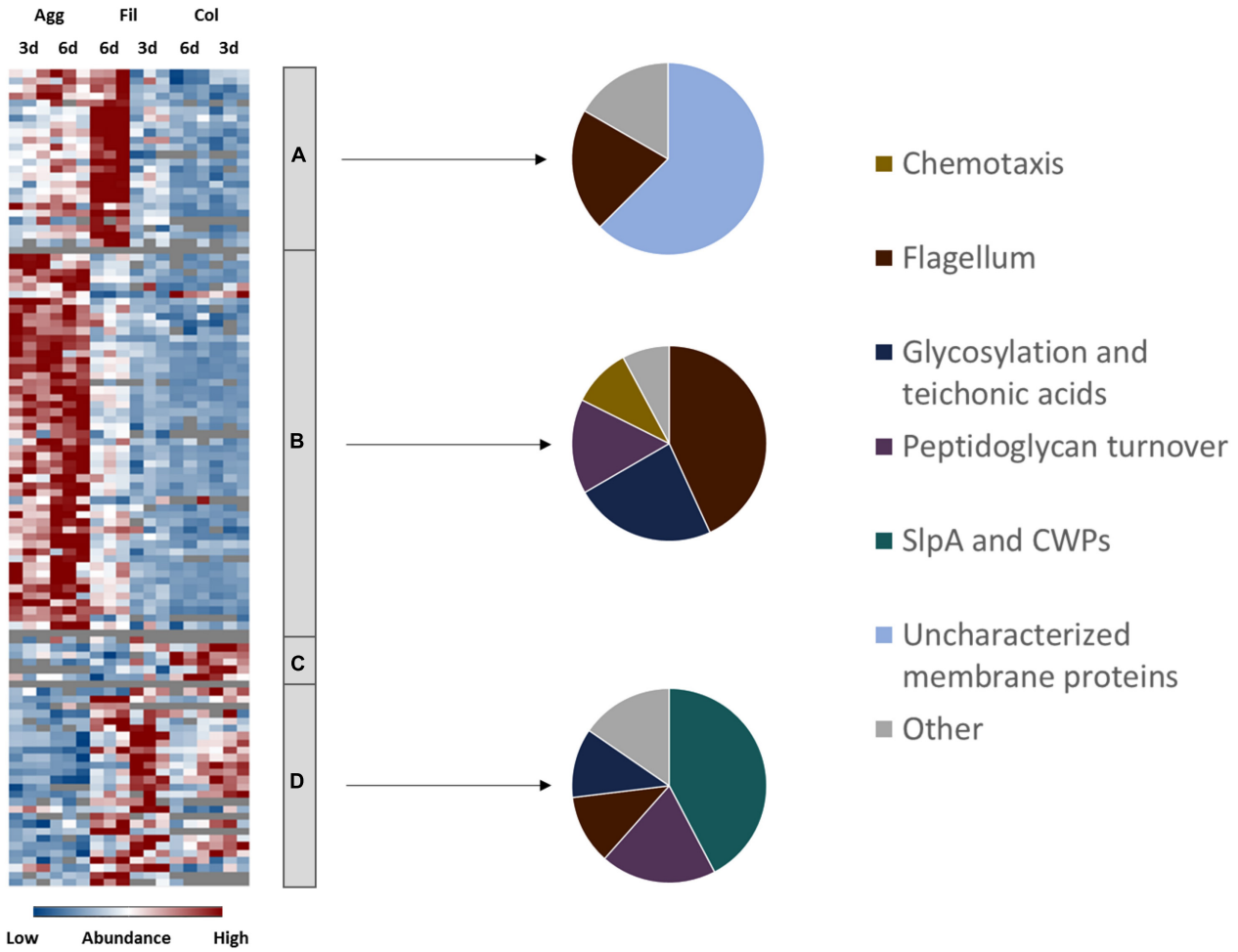

FIGURE 3 | Differential abundance of cell surface-associated proteins. 108 surface-associated proteins were found differentially abundant (blue is down, red is up) between aggregate biofilms (Agg), filtrate samples (Fil) and colony (Col) from day three (3d) and day six (6d). Z-transformed abundance values are displayed as a color gradient where blue colors indicate weakest abundance levels and red colors the strongest abundance levels among the growth conditions with maximum z-scores of +/–1.5. The heatmap on the left site shows that they were found in all 4 clusters, representing the 6-day old filtrate cells cluster **(A)**, aggregate biofilms **(B)**, colony biofilms **(C)** or both, colony biofilms and filtrate samples **(D)**. Pie charts on the right reveal that each individual cluster comprised mostly proteins from a specific functional group of cell surface-associated proteins. A list of the underlying proteins for this heatmap including their fold changes in abundance can be found in **Supplementary Table 3**. Agg, Aggregate biofilms; Col, Colony biofilms; Fil, Filtrate samples; 3d, Samples from day three; 6d, Samples from day six; CWPs, cell wall proteins.

was reported before (Đapa et al., 2013; Chu et al., 2016). Likewise, lipoteichoic acids revealed a significant immunogenic potential. They have been found to fulfill numerous functions in antibiotic resistance, cell wall homeostasis, cell division and metabolism (McBride and Sonenshein, 2011; Schade and Weidenmaier, 2016).

The S-Layer

The S-layer covers the cell surface of *C. difficile* and consists of the main S-layer protein SlpA which is encoded in one operon with 28 CWPs. *C. difficile's* S-layer protein SlpA and the 28 CWPs have been shown to be immunogenic (Péchiné et al., 2011; Bruxelle et al., 2016; Mizrahi et al., 2018). Deletion of the S-layer encoding genes renders a pathogenic *C. difficile* strain apathogenic (La Riva et al., 2011; Kirk et al., 2017b; Vaz et al., 2019). Furthermore, the S-layer, was found to play a role in cell-cell-aggregation and attachment to epithelial cells (Waligora et al., 2001; Merrigan et al., 2013; Bradshaw et al., 2017; Kirk et al., 2017b; Richards et al., 2018). Interestingly, the proteome data revealed that SlpA and 23 of its adjacent CWPs could be identified in colony biofilms and filtrate samples but were almost not detected in aggregate biofilms. This is in line with observations made by Janoir et al. (2013) who reported the downregulation of SlpA in the late stage of a mouse colonization model. The cysteine protease Cwp084, which was among the lower abundant CWPs, is responsible for the proteolytic processing of S-layer proteins (Kirby et al., 2009; Gooyit and Janda, 2016). Interestingly, a *cwp84* mutant produces more biofilm mass compared to the wildtype (Pantaléon et al., 2015). Since the mutant was unable to cleave the SlpA precursor protein, a different more hydrophobic

surface and different matrix proteome composition was observed, which might lead to an enhanced surface attachment of the cells, potentially explaining the increased biofilm production (La Riva et al., 2011; Pantaléon et al., 2015). Pantaléon et al. (2015) further detected most CWPs in the biofilm matrix (Cwp5, Cwp6, Cwp 9, Cwp14, Cwp21) and supernatant (CwpV, Cwp2, Cwp11, Cwp12, Cwp13, Cwp16, Cwp18, Cwp19, Cwp22, Cwp25, Cwp66) rather than in the surface proteome by comparative MALDI TOF analyses.

The Potential Role of PrkC Kinase During Biofilm Formation of *C. difficile*

Cwp7 was one of the few CWPs that revealed a differential expression pattern between the analyzed growth conditions and was significantly lower abundant in colony biofilms than in filtrates although not as low in aggregate biofilms as most other CWPs. Interestingly, a previous investigation showed that deletion of the membrane-associated serine/threonine kinase PrkC which is involved in cell wall homeostasis and antimicrobial resistance led to the downregulation of almost all CWPs but to an upregulation of Cwp7. Additionally, the Δ*prkC* mutant showed an increased release of polysaccharide II into the supernatant, was less motile and produced more biofilm (Cuenot et al., 2019). Although PrkC was found to be significantly higher abundant in the 3-day old aggregate biofilms and significantly lower abundant in 6-day old colony biofilms, the similar expression pattern of aggregate biofilms and the Δ*prkC* mutant suggest a possible role of PrkC in the regulation of biofilm formation in *C. difficile*.

In summary, aggregate biofilms analyzed here were characterized by higher abundance of potentially glycosylated flagella, type IV pili proteins, proteins required for cell surface polysaccharide synthesis and proteins involved in cell wall and membrane turnover compared to colony biofilms while SlpA and CWPs were lower abundant in aggregate biofilms compared to colony biofilms.

Energy Metabolism

The unique energy metabolism of *C. difficile* preferentially utilizes amino acids through a process called Stickland fermentation which firstly produces ATP via substrate level phosphorylation (Stickland, 1934; Neumann-Schaal et al., 2015). Secondly, various carbohydrates are the basis for a complex mixed acid fermentation (Riedel et al., 2017; Hofmann et al., 2021). Some of the involved processes are coupled via the membrane associated Rnf complex to the formation of an ion gradient which in turn drives ATP formation via a classical F_OF_1-ATPase (Müller et al., 2008). Alternative carbon sources like ethanolamine are used additionally (Nawrocki et al., 2018; Hofmann et al., 2021). When preferred amino acids and glucose are depleted from the medium, *C. difficile* is able to generate energy from lactate fermentation and to fix CO_2 via the Wood-Ljungdahl pathway (Köpke et al., 2013; Hofmann et al., 2021).

Although all biofilm and filtrate cells were obviously subject to nutrient limitations due to extended incubation time, proteomic profiles for proteins involved in various pathways of energy generation indicated an aggregate- and colony biofilm specific energy metabolism (**Figure 4** and **Supplementary Table 4**).

Amino Acid Utilization

Several systems of the oxidative and reductive branches of the Stickland amino acid fermentation were found differentially produced under the different biofilm conditions investigated in comparison to the filtrate samples. To start with, proteins from the *CDIF630erm_00522-. . .-etfA1* operon (AcdB, EtfA1, EtfB1) for the reductive fermentation of leucine and phenylalanine to 3-phenylproprionate/isocoproate and the activator protein of the 2-hydroxyisocaproyl-CoA dehydratase, HadI, were higher abundant in aggregate biofilms compared to other culture conditions. The reductive fermentation of leucine and phenylalanine is indirectly coupled to the Rnf complex via ferredoxin (Kim et al., 2006; Schiffels and Selmer, 2019). In agreement, proteins from the Rnf complex (RnfB, RnfC, RnfD, RnfG) were higher abundant in filtrate and aggregate biofilms than in colony biofilms. In contrast, the proline reductase (PrdA, PrdB) for reductive degradation of proline to 5-aminovalerate, which is directly coupled to the Rnf complex (Jackson et al., 2006), showed the highest abundance levels in filtrate samples. Similarly, the subunits of the glycine reductase (GrdB, GrdC, GrdD) and associated proteins TrxA2 and TrxB3 for degradation of glycine to acetate were higher abundant in filtrate cells than in biofilm cells. Enzymes of the oxidative branch for fermentation of branched chain (VorA1, VorB1, VorC1, Ptb1) and aromatic amino acids (CDIF630erm_02622, IorA, IorB, Ptb1) were higher abundant in colony biofilms. To react to the reduced availability of nutrients, both filtrate samples and aggregate biofilms were found to have transporters for the uptake of amino acids such as those encoded by the *app* operon for oligo-peptide transport and MetNQ required for methionine uptake. In contrast, colony biofilms showed an overall lower abundance of any kind of transporters which might reflect the even more impaired diffusion of nutrients inside the dense biofilm matrix. It cannot be excluded that membrane protein extraction was less efficient for colony biofilms and reinforced this observation. However, overall only a very minor bias toward cytoplasmic and against membrane proteins was observed and significant changes in protein formation between the different analyzed conditions caused by regulatory processes were clearly visible.

Carbohydrate Utilization

C. difficile degrades carbohydrates via glycolysis and the pentose-phosphate pathway yielding pyruvate (Hofmann et al., 2018). Proteome analysis showed that enzymes of both pathways, such as PfkA, Pgi, Tpi, and Eno from the glycolysis and Tal, Tal1, RpiB1, RpiB2, Rpe1, and Tkt' from the pentose-phosphate pathway, were higher abundant in filtrate samples. This is in contradiction to results of Poquet et al. (2018) who reported induction of glycolysis and pentose-phosphate pathway in aggregate biofilms compared to planktonically-grown cells. However, both data sets agree on active carbohydrate utilization within aggregate biofilms. As observed for amino acid uptake systems, both filtrate samples and aggregate biofilms revealed the presence of PTS systems for the uptake of carbohydrates. Moreover, aggregate biofilms revealed an extensive amount of enzymes for the utilization of carbohydrates which underlines

the importance of carbohydrates for *C. difficile* under infection-relevant conditions (Theriot et al., 2014; Jenior et al., 2017, 2018; Fletcher et al., 2018). Also, Dubois et al. (2019) reported that induction of biofilm formation by deoxycholate was enhanced in the presence of fermentable carbohydrates.

Ethanolamine Utilization

An abundant nutrient source in the gut is the membrane lipid phosphatidylethanolamine. The derived amino alcohol ethanolamine can serve as carbon and nitrogen source. Availability of ethanolamine has been shown to reduce virulence in *C. difficile* and to delay the onset of CDI in a hamster model (Nawrocki et al., 2018). Interestingly, proteins involved in ethanolamine utilization were more or less exclusively identified in filtrate cells. However, e.g., in *Entercoccus faecalis* ethanolamine utilization is dependent on the presence of cobalamin (Del Papa and Perego, 2008). Assuming similar regulation in *C. difficile*, induction of cobalamin biosynthesis pathways in the aggregate biofilms (**Supplementary Table 1**) suggests that these biofilms were limited in cobalamin what might explain the inhibition of ethanolamine utilization gene expression under these growth conditions.

Utilization of the Intermediate Products Pyruvate and Acetyl-CoA

The intermediate product of the glycolysis as well as alanine oxidation, pyruvate, is further metabolized to either acetyl-CoA and formate via the pyruvate formate-lyase PflDE or to lactate by the lactate dehydrogenase Ldh (Dannheim et al., 2017; Hofmann et al., 2018). Acetyl-CoA is in turn degraded to acetate by Ptb1 and AckA or to butyrate via the butyrate fermentation pathway encoded in the *bcd2-. . .-thlA* and *4hbD-. . .-CDIFerm_02583* operons (Hofmann et al., 2018). Formate can be further metabolized to hydrogen by the formate hydrogenases FdhD and FhdF and the hydrogenases HydN1, HydN2, and HydA (Berges et al., 2018). According to our proteome data, several proteins for butyrate fermentation (ThlA1, Hbd, Crt2, EtfB3, Ptb, AbfD) and the hydrogenase HydN2 were found in higher amounts in colony biofilms and in lower amounts in aggregate biofilms. In contrast, the electron bifurcating lactate dehydrogenase encoded by CDIF630erm_01319-01321 was detected in higher amounts in aggregate biofilms. Pyruvate formate-lyase PflDE was found induced in biofilms compared to filtrate cells.

Expression of F_OF_1-Type and V-Type ATPase

Rarely observed among bacteria, *C. difficile* encodes for two ATPases. In addition to its F_OF_1-ATPase, which uses the membrane potential to generate ATP, *C. difficile* encodes a Na^+– or H^+ -transporting V-type ATPase which uses ATP to maintain the ion gradient across the membrane and which has been linked to the Wood-Ljungdahl pathway and glycine cleavage system before (Saujet et al., 2011; Poquet et al., 2018). While the subunits of the F_OF_1-ATPase were overall lower abundant in both biofilm types compared to filtrate cells, the V-type ATPase subunits were significantly higher abundant in colony biofilms but less abundant in aggregate biofilms compared to filtrate cells. This suggests that the V-type ATPase is of importance for the colony biofilms.

Role of the Wood-Ljungdahl Pathway

In line with this, several proteins from the Wood-Ljungdahl pathway (WLP) were higher abundant in colony biofilms while repressed in aggregate biofilms in comparison to filtrate cells. With the exception of AcsABE that were found higher abundant in aggregate biofilms, almost all enzymes of the WLP, such as the carbon monoxide dehydrogenase (CooS, CDIFerm_00297, CDIFerm_00298), Fhs, FchA, FoldD, MetV and MetF, and the glycine cleavage system proteins (GcvTPA, GcvPB), which provide 5,10-methylene-tetrahydrofolate for the WLP, were significantly higher abundant in colony biofilms but lower abundant in aggregate biofilms compared to filtrate cells. The WLP, also known as the reductive Acetyl-CoA pathway, is able to generate acetyl-CoA from CO_2 (Stupperich et al., 1983; Köpke et al., 2013). Moreover, the WLP has recently been suggested as an electron sink to maintain cell homeostasis in the absence of Stickland acceptors (Gencic and Grahame, 2020). Taken together, the higher levels of proteins from the oxidative branch of Stickland fermentation, of butyrate fermentation and of the V-type ATPase discussed above as well of WLP proteins in colony biofilms strongly support the hypothesis that the WLP plays an important role in maintaining cell growth in environments depleted in reductive equivalents and potentially maintains the membrane potential in concert with the coupled V-type ATPase (Gencic and Grahame, 2020). Of note, Poquet et al. (2018) reported a downregulation of WLP, glycine cleavage system and V-type ATPase genes in aggregate biofilms compared to planktonic cells which is in line with results of this proteome analysis.

In conclusion, higher production of proteins for less favorable energy pathways such as the Wood-Ljungdahl pathway and the lactate dehydrogenase and lower production of proteins for more favorable energy pathways and enzymes such as the proline and glycine reductase as well as glycolysis in biofilm cells compared to filtrate cells suggest that biofilms were more affected by the nutrient limitation than filtrate cells. However, both biofilms obviously responded differently. Presence of several PTS and enzymes for carbohydrate uptake and degradation and the induction of cofactor biosynthesis proteins in aggregate biofilms suggest that aggregate biofilms are (1) rather active cells that are able to invest ATP to take up nutrients from the environments and (2) permeable enough to allow nutrients to reach cells inside the biofilm. In contrast, the observed uniform induction of WLP, V-type ATPase, butyrate fermentation and oxidative branch of the Stickland fermentation in colony biofilms compared to aggregate biofilm and filtrate cells likely points at severe limitation of reductive equivalents in colony biofilms that rather supports survival than reproduction.

Stress Response and Virulence

In general, biofilm cells are embedded inside an extracellular matrix that protects cells from antibiotics and disinfectants but at the same time also impairs diffusion of nutrients and waste products (Anwar et al., 1992; Karygianni et al., 2020).

Consequently, cells from the inner biofilm have to cope with nutrient limitation and accumulation of waste products. To survive such stressful conditions *C. difficile's* genome encodes for various stress response systems as a first line of defense (Sebaihia et al., 2006). If conditions remain unfavorable, *C. difficile* initiates toxin synthesis or, as a last resort, sporulation (Onderdonk et al., 1979; Lawley et al., 2009; Underwood et al., 2009). Analysis of *C. difficile's* stress reponse systems revealed that both biofilm types and filtrate cells revealed different expression of stress response and virulence-associated pathways similar to the results for the energy metabolism (**Figure 5** and **Supplementary Table 5**).

Stress Response

As a strictly anaerobic pathogen, *C. difficile* requires an effective oxidative stress response to be able to react to oxygen and reactive oxygen species (Neumann-Schaal et al., 2018). Interestingly, our proteome data set revealed that some of *C. difficile's* oxidative stress response proteins, such as the rubrerythrin Rbr and the reverse rubrerythrins Rbr2 and Rbr3, were drastically lower abundant in aggregate biofilms compared to filtrate samples but slightly higher abundant in colony biofilms than in filtrate samples. Since PerR, a transcriptional regulator which represses oxidative stress response proteins, is inactive in strain Δerm due to a single nucleotide polymorphism in the *perR* gene (Troitzsch et al., 2021), these effects are possibly a result of post-transcriptional regulation. On the other hand, 6-day old colony biofilms revealed an induction of some oxidative stress response proteins such as NorR and SodA. Since no molecular oxygen was present in any of the tested conditions, the oxidative stress response proteins identified here were either expressed to react to other oxidative species such as reactive nitrogen species or other yet unknown signals not present in aggregate biofilms. Similarly, other stress response-associated proteins such as DnaK, GrpE, GroL, and ClpC, which were previously shown to be induced in response to heat stress, bile acids and antibiotics (Jain et al., 2011; Ternan et al., 2012; Chong et al., 2014; Sievers et al., 2019), were significantly lower abundant in aggregate biofilms compared to filtrate samples while the transcriptional regulators CtsR and HrcA, which repress the above mentioned proteins in other firmicutes species (Schulz and Schumann, 1996; Derré et al., 1999), were higher abundant in aggregate biofilms compared to the filtrate samples. In general, aggregate biofilms seemed to face less stress than colony biofilms and filtrate samples.

Antibiotic Resistance

In contrast, antibiotic resistance-associated proteins such as ClnA and ClnR involved in cationic antimicrobial peptide resistance (Woods et al., 2018), the tetracycline resistance protein TetM (Mullany et al., 1990) and putative multidrug ATP-type transport proteins such as CDIF630erm_00291, CDIF630erm_00940, and CDIF630erm_02245 revealed highest protein levels in aggregate biofilms, but were rarely detected in colony biofilms. Indeed, most studies addressing antibiotic resistance of *C. difficile* biofilms consistently showed that biofilms are more resistant to various antibiotics such as metronidazole (Semenyuk et al., 2014), vancomycin and linezolide (Tijerina-Rodríguez et al., 2019). In addition to impaired diffusion through the dense extracellular matrix and differential regulation of antibiotic resistance markers (Høiby et al., 2010) increased mutation rates as a result of accumulating metabolic waste products as well as increased horizontal gene transfer that is often observed in biofilms where cell densities are particularly high are assumed to boost antibiotic resistance of biofilms (Molin and Tolker-Nielsen, 2003; Boles and Singh, 2008; Levin and Cornejo, 2009; Ryder et al., 2012). Accordingly, levels of proteins required for homologous recombination and DNA repair (RecN, RuvB, RadA, UvrABC, MutLS, SbcCD, LexA) were significantly higher in aggregate biofilms than in filtrate samples. In line with this, it was shown before, that the induction of the SOS response (RecA, UvrABC) in a *lexA* deletion mutant resulted in an increased biofilm mass further demonstrating the importance of gene transfer and genetic evolution for efficient biofilm formation (Walter et al., 2015). Again, colony biofilms revealed even lower protein amounts of mentioned proteins than filtrate cells.

Toxin Synthesis

Both forms of biofilms had in common a decreased production of toxin A and B compared to filtrate samples although the effect was more pronounced in aggregate biofilms. In agreement, toxin B mRNA levels were previously determined to be lower in aggregate biofilms than in colony biofilms. Toxin A mRNA levels were found to be decreased in aggregate biofilms vs. planktonic cells (Maldarelli et al., 2016; Poquet et al., 2018). Worth mentioning, toxin expression in *C. difficile* underlies a sophisticated regulatory network that is tightly coupled to the energy metabolism (Dineen et al., 2007; Antunes et al., 2011; Dubois et al., 2016; Hofmann et al., 2018). In summary, although both biofilms revealed significantly different expression profiles with regard to energy metabolism, toxins were found downregulated in both biofilm models indicating that the biofilm lifestyle rather facilitates persistence than infection.

Sporulation

Although biofilms were initially assumed to be hot spots of sporulation and a potential reservoir for spores during persistence, recent data suggest that this may not be the case and only a few spores can be found in *C. difficile* biofilms which additionally were determined to be different from other spores with regard to germination efficiency and heat resistance (Đapa et al., 2013; Semenyuk et al., 2014; Pizarro-Guajardo et al., 2016; Dubois et al., 2019). Moreover, it was reported that sporulation rates in biofilms vary between strains and do not correlate with severity of disease (Semenyuk et al., 2014). In agreement with the previous observations, we determined that sporulation and spore proteins such as spore coat proteins CotA, CotB, SipL, and SpoIVA were less abundant in aggregate biofilms than in filtrate samples which matches the concomitant higher abundance of the negative regulators of sporulation, KipI and Soj, in aggregate biofilms (Đapa et al., 2013; Poquet et al., 2018; Dubois et al., 2019). In contrast, we found spore proteins significantly higher abundant in colony biofilms. This, however, matches the observation that the carbohydrate utilization- and the amino acid uptake systems App and Opp, whose expression was found negatively correlated with sporulation

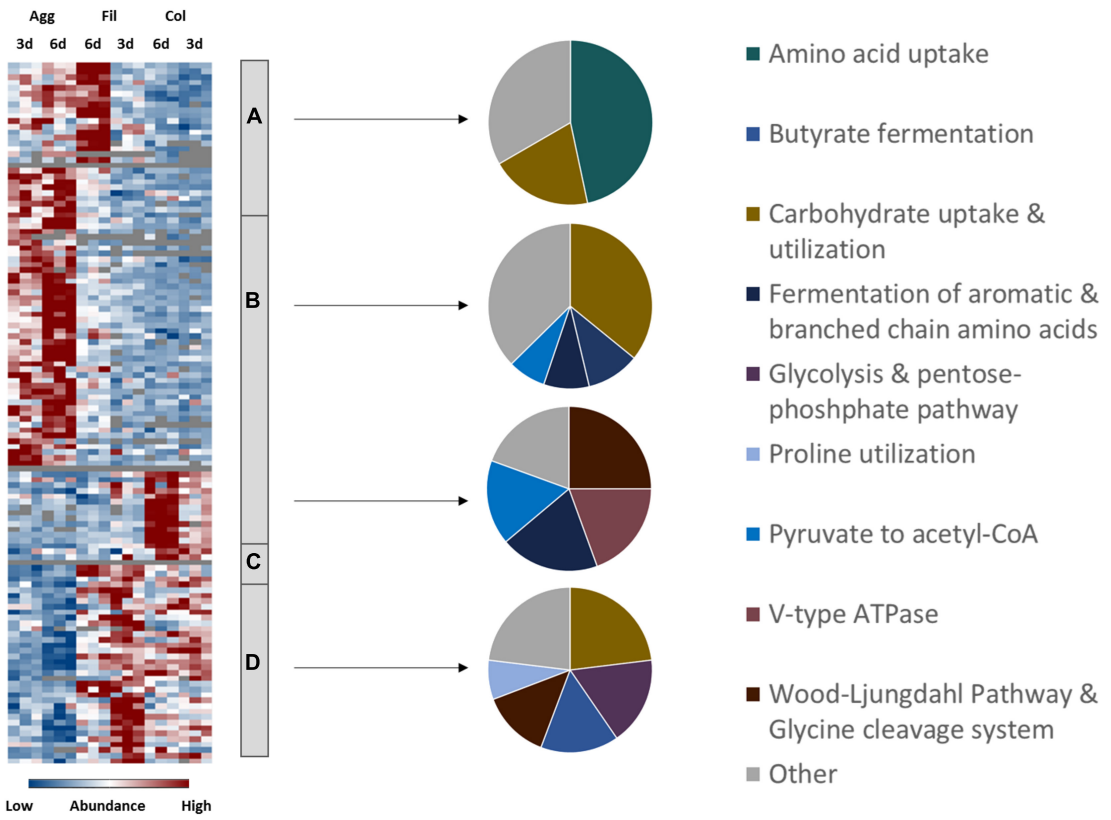

FIGURE 4 | Differential abundance of energy metabolism-associated proteins. 185 metabolism-related proteins were found differentially abundant between aggregate biofilms (Agg), filtrate samples (Fil) and colony (Col) from day three (3d) and day six (6d). Z-transformed abundance values are displayed as a color gradient where blue colors indicate weakest abundance levels and red colors the strongest abundance levels among the growth conditions with maximum z-scores of +/–1.5. The heatmap on the left site shows that they were found in all 4 clusters, representing the 6-day old filtrate cells cluster **(A)**, aggregate biofilms **(B)**, colony biofilms **(C)** or both, colony biofilms and filtrate samples **(D)**. Pie charts on the right reveal that each individual cluster comprised mostly proteins from a specific functional metabolic pathway. A list of proteins from this heatmap including their fold changes in abundance can be found in **Supplementary Table 4**. Agg, Aggregate biofilms; Col, Colony biofilms; Fil, Filtrate samples; 3d, Samples from day three; 6d, Samples from day six.

before (Antunes et al., 2012; Edwards et al., 2014), as well as proteins involved in translation, ribosome maturation and cell division such as RumA, MiaB, BipA, Obg, and InfB showed lower abundance in our colony biofilms than in aggregate biofilms and filtrate samples. Again, these data indicate a higher metabolic activity of *C. difficile* in aggregate biofilms and in filtrate samples compared to colony biofilms.

Taken together, the lower response levels of aggregate biofilms to unknown metabolic stresses and lower sporulation rates but higher production of antibiotic resistance markers suggest that the extracellular matrix of aggregate biofilms is possibly less dense than in colony biofilms what insufficiently protects cells from antibiotics but prevents accumulation of waste products and allows diffusion of nutrients. While Poquet et al. (2018) who cultivated aggregate biofilms in continuous flow systems argued that the constant renewal of medium is responsible for the observed metabolic activity and low sporulation rates, the data presented here indicate that aggregate biofilms comprise active growing cells regardless of the nutrient supply. Overall, the differential expression of sporulation proteins depending on the choice of biofilm model is an interesting observation and further underlines the urgent need to answer the question of which type of biofilm is produced in the host.

Global Regulatory Circuits and Cell Signaling

Finally, proteins involved in regulation and cell signaling were analyzed to uncover which regulatory circuits possibly underlie the observations discussed in the previous sections. In view of the extensive remodeling of the cell envelope and of metabolic pathways and the tight control of toxin synthesis and sporulation, it was not surprising that multiple central regulatory networks have been affected during biofilm formation in *C. difficile* (Đapa et al., 2013; Purcell et al., 2017; Dubois et al., 2019). For example, c-di-GMP signaling and quorum sensing were shown to be required for biofilm formation before (Đapa et al., 2013; Purcell et al., 2017; Slater et al., 2019). Moreover, several publications have reported that deletion of various regulatory proteins including Spo0A (Dawson et al., 2012; Đapa et al., 2013), Hfq (Boudry et al., 2014), CcpA (Dubois et al., 2019), CodY (Dubois et al., 2019), and as mentioned above

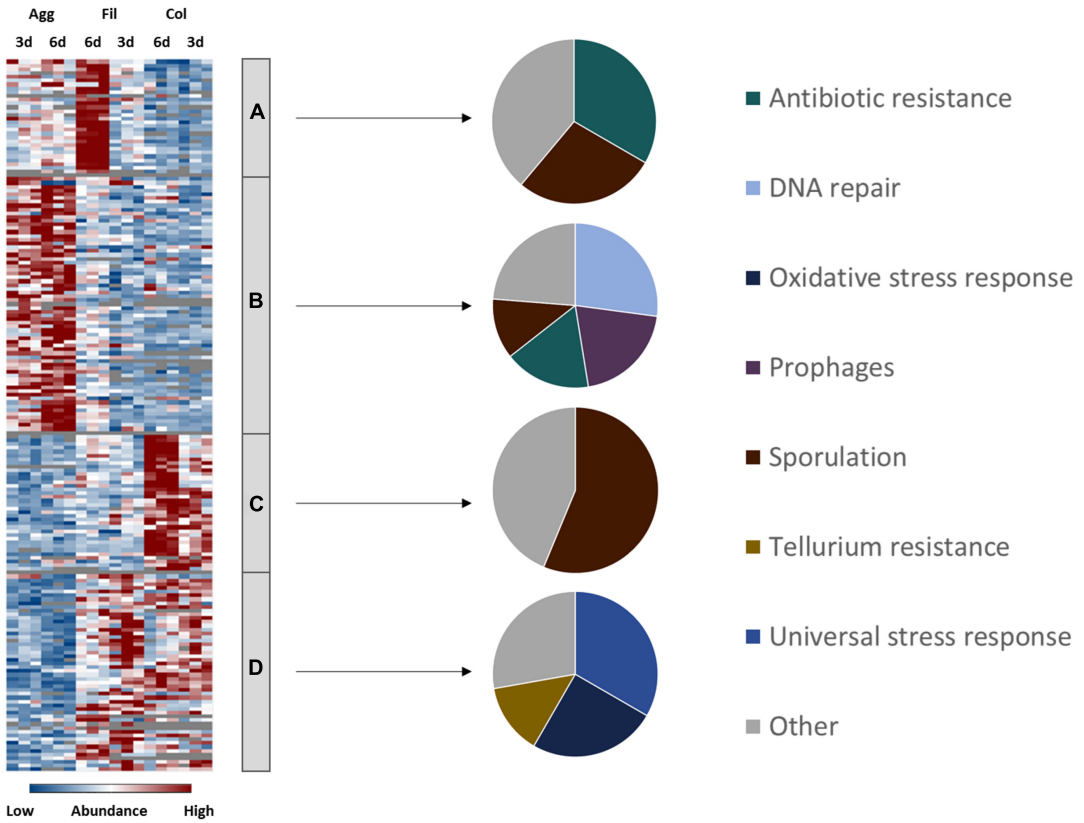

FIGURE 5 | Differential abundance of virulence, antibiotic resistance and stress response-associated proteins. 129 proteins assigned to virulence, antibiotic resistance and stress-response related pathways were found differentially abundant (blue is down, red is up) between aggregate biofilms (Agg), filtrate samples (Fil) and colony (Col) from day three (3d) and day six (6d). Z-transformed abundance values are displayed as a color gradient where blue colors indicate weakest abundance levels and red colors the strongest abundance levels among the growth conditions with maximum z-scores of +/−1.5. The heatmap on the left site shows that they were found in all 4 clusters, representing the 6-day old filtrate cells cluster **(A)**, aggregate biofilms **(B)**, colony biofilms **(C)** or both, colony biofilms and filtrate samples **(D)**. Pie charts on the right reveal that each individual cluster comprised proteins from specific stress response and resistance systems. A list of proteins from this heatmap including their fold changes in abundance can be found in **Supplementary Table 5** (**Supplementary Material**). Agg, Aggregate biofilms; Col, Colony biofilms; Fil, Filtrate samples; 3d, Samples from day three; 6d, Samples from day six.

LexA (Bordeleau et al., 20119) impaired biofilm formation in *C. difficile*. In agreement, proteome data sets presented here suggested that especially aggregate biofilm formation involved complex gene regulatory network restructuring and induction of various transcriptional regulators and two component system proteins (**Figure 6** and **Supplementary Table 6**).

In order to visualize and analyze the complex gene regulatory networks that were active in the different biofilm setups and to potentially assign some of the afore-discussed features of each biofilm type to specific regulatory systems, regulon analyses were performed. To do so, available global expression data of *C. difficile* strains deleted or overexpressed in central regulators were used to assign *C. difficile* proteins to their respective regulons. Subsequently, our proteome data were mapped onto obtained regulons and the results were visualized in Voronoi treemaps (**Figure 7**).

Key Regulators of Colony Biofilms

In accordance with the observed induction of sporulation proteins in colony biofilms discussed above, the obtained regulon maps revealed the induction of regulons for the sporulation sigma factors SigE, SigF, SigG, and SigK and the master regulator of sporulation, Spo0A, in the 6-day old colony biofilms (**Figure 7**). While SigE and SigF were previously shown to be not required for biofilm formation (Dubois et al., 2019), Spo0A was frequently reported to be essential for biofilm formation in *C. difficile* (Đapa et al., 2013; Dubois et al., 2019). Moreover, proteins from the SigH and Fur regulon were found upregulated in colony biofilms. Upregulation of Fur proteins might be the result of the impaired diffusion of ions inside the biofilm matrix. The sigma factor SigH is required during transition from exponential growth to stationary phase and was demonstrated to regulate sporulation, toxin production and surface-associated proteins (Saujet et al., 2011). Several of the proteins and operons found to be differentially abundant between colony and aggregate biofilms, such as the flagella operons, the S-layer protein SlpA, the V-type ATPase operon, the oxidative stress response and the glycine reductase complex, were shown to be under control of SigH suggesting that SigH might considerably shape the colony biofilm metabolism (Saujet et al., 2011). In contrast, proteins from the

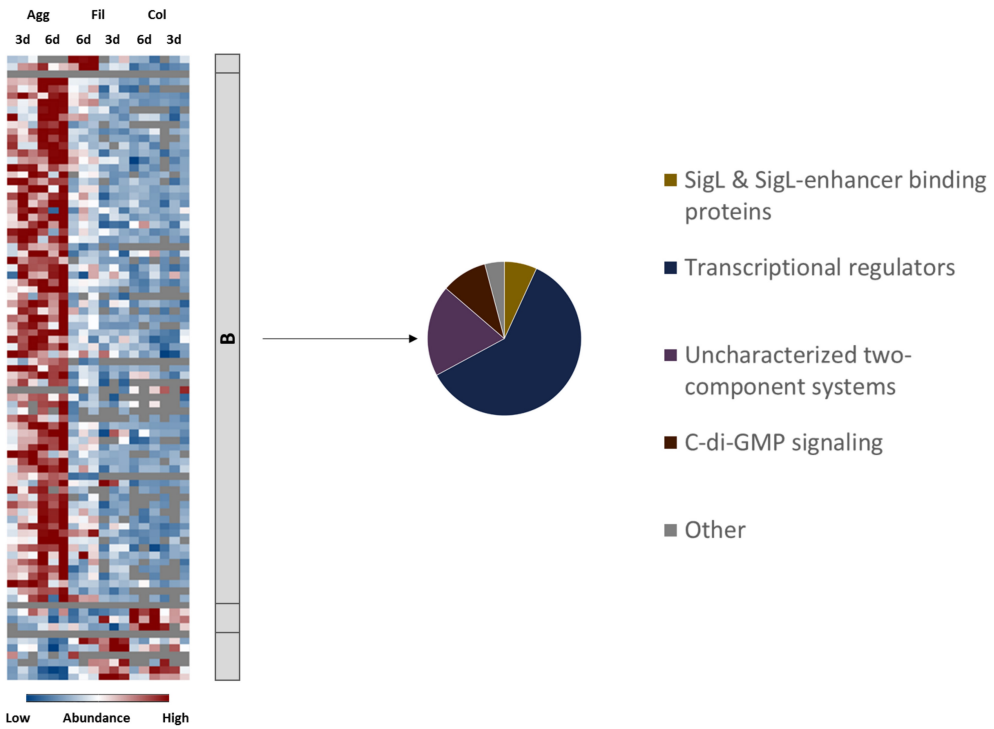

FIGURE 6 | Differential abundance of signaling and regulatory proteins. 84 proteins annotated as regulatory or signaling proteins were differentially abundant (blue is down, red is up) between aggregate biofilms (Agg), filtrate samples (Fil) and colony (Col) from day three (3d) and day six (6d). Z-transformed abundance values are displayed as a color gradient where blue colors indicate weakest abundance levels and red colors the strongest abundance levels among the growth conditions with maximum z-scores of +/−1.5. The heatmap on the left site shows that they were found in all 4 clusters, representing the 6-day old filtrate cells cluster **(A)**, aggregate biofilms **(B)**, colony biofilms **(C)** or both, colony biofilms and filtrate samples **(D)**. The pie chart on the right reveals that proteins from Cluster B comprised proteins from four major groups of regulatory and signaling proteins. A list of proteins from this heatmap including their fold changes in abundance can be found in **Supplementary Table 6** (**Supplementary Material**). Agg, Aggregate biofilms; Col, Colony biofilms; Fil, Filtrate samples; 3d, Samples from day three; 6d, Samples from day six.

regulon of the motility regulator SigD and the c-di-GMP regulon were rather low abundant in colony biofilms.

Activation of c-di-GMP Signaling in Aggregate Biofilms

c-di-GMP signaling relies on the production of the second messenger c-di-GMP. In contrast to other Gram-positive bacteria, *C. difficile's* genome encodes for a large number of functional diguanylate cyclases and phosphodiesterases suggesting special importance of c-di-GMP signaling in *C. difficile* (Bordeleau et al., 2011). Out of these c-di-GMP associated proteins, the diguanylate cyclases CDIF630erm_01581, CDIF630erm_02043, and CDIF630erm_03665, and the phosphodiesterases PdcA, CDIF630erm_00875 and CDIF630erm_01792 were found significantly upregulated in aggregate biofilms compared to filtrate samples or were even exclusively identified in aggregate biofilms. As shown previously, elevated c-di-GMP levels promote expression of type IV pili that subsequently mediate attachment of the gut bacteria to epithelial cells, cell aggregation and biofilm formation in *C. difficile* strain R20291 (Purcell et al., 2012, 2016; McKee et al., 2018a). In contrast, flagella proteins that are known to be negatively regulated by c-di-GMP were highly abundant in the aggregate biofilm samples indicating that other regulatory circuits likely interfere with c-di-GMP signaling (Purcell et al., 2012; McKee et al., 2013, 2018b).

The Role of SigL/RpoN in Aggregate Biofilms

Our data suggest that the alternative sigma factor SigL/RpoN, encoded by CD630_31760 and also known as σ^{54}, plays an important role in the gene regulation of aggregate biofilms (**Figures 6**, **7**). The SigL/RpoN regulon has frequently been observed to significantly contribute to biofilm formation in various species by positive regulation of motility (Jagannathan et al., 2001; Saldías et al., 2008; Francke et al., 2011; Iyer and Hancock, 2012), enhancement of extracellular DNA levels inside the extracellular matrix (Iyer and Hancock, 2012) and remodeling of metabolic pathways to adapt to nutrient conditions inside the biofilm (Arous et al., 2004; Francke et al., 2011; Xu et al., 2014; Hayrapetyan et al., 2015). Initially described as sigma regulator induced by nitrogen limitation (Hirschman et al., 1985; Weiss and Magasanik, 1988) SigL/RpoN was later found in most bacterial species to be activated in response to various stressful conditions, such as osmostress and low temperatures (Francke et al., 2011; Nie et al., 2019). The SigL/RpoN regulon in *C. difficile* and other *Clostridiales*

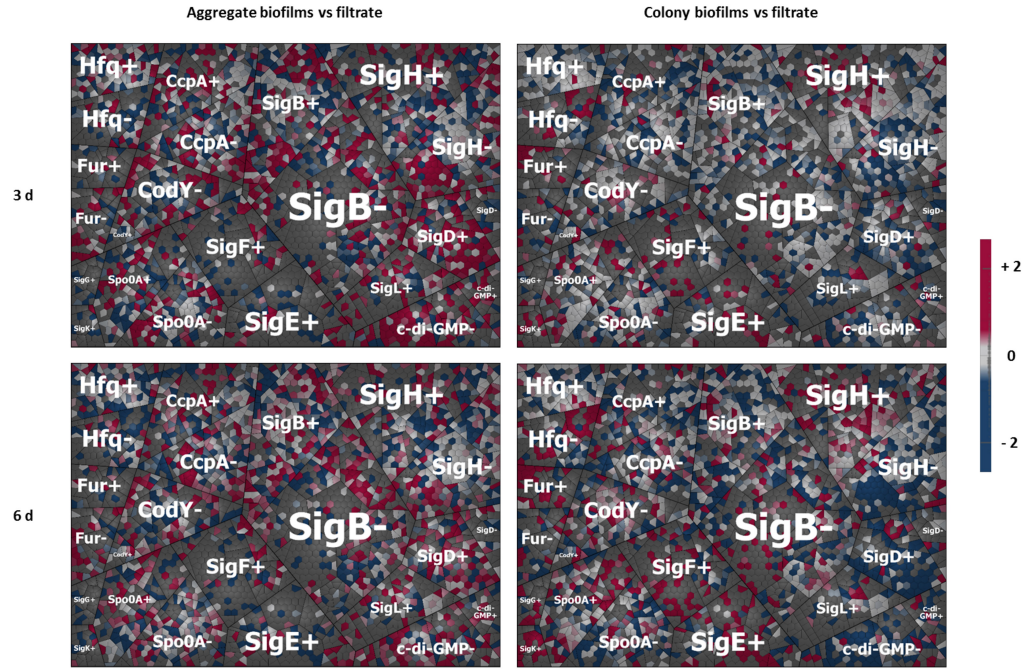

FIGURE 7 | Regulon maps for aggregate and colony biofilms both vs. filtrate samples. Shown are four Voronoi regulon treemap maps. They are summarizing the mapping of our proteome data onto *C. difficile's* hitherto characterized regulons created based on available gene expression (transcriptome) data from the literature. All proteins regulated by a respective regulator were depicted as single cells clustered together with all other protein under the control of the same regulator either positively (+) or negatively (–) controlled by the respective regulators. The log2 fold changes of each biofilm sample relative to the corresponding filtrate sample were directly mapped to visualize the impact of a respective regulator on the sample set. Red cells represent proteins induced in biofilm samples relative to filtrate samples while blue cells present proteins downregulated in biofilms relative to filtrate samples. The upper left panel shows the data for aggregate biofilm vs. the filtrate sample after 3 days (3d); lower left panel aggregate biofilms after 6 days (6d); upper right panel colony biofilm after 3 days; lower right panel colony biofilms after 6 days. "+" stands for proteins positively regulated by the respective regulator, "–" for proteins negatively regulated by the respective regulator. A detailed list of all proteins including fold changes and additional information on regulon and operon affiliation can be found in **Supplementary Table 6**.

has recently been characterized leading to the discovery of 30 SigL/RpoN-dependent promoters. Of these 30 SigL/RpoN-dependent promoters, 23 were adjacent to a gene sequence encoding for a SigL/RpoN-dependent regulator, a group of regulators also known as enhancer binding proteins (EBP). Thereby SigL/RpoN was identified as an important central regulator controlling amino acid and carbohydrate catabolism pathways in *C. difficile* (Nie et al., 2019; Soutourina et al., 2020). Interestingly, 15 of the 23 proposed EBPs for *C. difficile* were identified in this study. Thirteen EBPs were solely present or detected in higher amounts in aggregate biofilms compared to filtrate samples and colony biofilms suggesting an important role of the SigL/RpoN regulon during aggregate biofilm formation. Indeed, the activation of the SigL/RpoN regulon most likely explains some of the energy-related observations discussed above. For instance, the *CDIF630erm_00522-. . .-etfA1* operon for reductive fermentation of branched chain amino acids, which was higher abundant in aggregate biofilms compared to filtrate samples, is positively controlled by the EBP LeuR which was among the EBPs higher abundant in aggregate biofilms. Similarly, several PTS systems are under control of SigL/RpoN and its EBPs (Soutourina et al., 2020). For instance, the galactitol-specific PTS component CDIF630erm_00104, the mannose-specific PTS components CDIF630erm_00408 and CDIF630_00409 and the ribitol-specific PTS component CDIF630erm_00620 were either found in higher amounts or exclusively in aggregate biofilms. Since toxin synthesis was recently found to be negatively controlled by SigL/RpoN in *C. difficile*, also the low production of toxins in aggregate biofilms might be a result of SigL/RpoN regulation (Dubois et al., 2016). Overall, our proteome data suggest that SigL/RpoN has an important role in aggregate biofilm formation.

Other Regulatory Circuits Involved in Aggregate Biofilm Formation

Furthermore, the regulon maps revealed a slightly higher induction of proteins from the SigB, CcpA, and CodY regulons in aggregate biofilms than in colony biofilms which may have contributed to the remodeling of the energy metabolism in aggregate biofilm cells (Dineen et al., 2010; Antunes et al., 2012; Kint et al., 2017). In addition, activation of SigB may have contributed to repression of sporulation proteins (Kint et al., 2017). Minor changes in the Spo0A regulon in aggregate biofilms suggest that Spo0A is possibly required for initial or early biofilm formation or cellular adaptation in general rather than maturation and maintenance of biofilm homeostasis. In contrast, the quorum sensing protein LuxS, which was previously shown to be essential for biofilm formation in *C. difficile* (Đapa et al., 2013), was decreased in both aggregate and colony biofilms compared to filtrate cells. LuxS was shown to contribute to biofilm formation

via induction of prophage genes that in turn induce cell lysis resulting in higher levels of eDNA in the biofilm matrix of strain R20291 (Slater et al., 2019). Possibly, LuxS is more important in early biofilm formation due to its activation in late exponential phase (Carter et al., 2005) or rather required for adaptation to pre-longed survival in nutrient depleted conditions which is a pre-requisite of biofilm formation. Of note, proteome data of this study still demonstrated induction of prophage genes in aggregate biofilms despite the low abundance of LuxS (**Figure 5** and **Supplementary Table 5**).

To conclude, the prominent synthesis of SigL/RpoN, some of its EBPs and SigL/RpoN-dependent operons such as the operon for branched chain amino acid utilization in aggregate biofilms suggest that SigL is an important regulator of aggregate biofilm formation. In addition, c-di-GMP likely shaped the protein inventory of aggregate biofilms while colony biofilms were most likely shaped by the sporulation sigma factors Spo0A, SigE, SigF, SigG, and SigK as well as sigma factor SigH and the transcriptional regulator Fur. However, it should be stressed that biofilm formation is obviously a dynamic process that involves successive action of various regulatory proteins and pathways. Thus, the data of the presented two sample points only allow a temporal narrow view. Moreover, regulon data were not available for all regulators so that the impact of these regulators might be missed. Furthermore, proteins are often under control of several regulators what makes it difficult to unequivocally link adaptation processes to a certain regulator. Nevertheless, the data provide novel in-depth insight into the complex regulatory network of biofilm formation in *C. difficile* and likely permit helpful conclusions of the necessity of specific regulators which are less prone to bias than regulator knock-out studies.

TABLE 2 | Differential protein abundance between aggregate and colony biofilms of C. difficile.

Category	Pathway/function	Aggregate biofilms	Colony biofilms
Cell surface proteins	Flagella	↑	↓
	Cell surface glycosylation	↑	→
	S-layer	↓	→
Energy metabolism	V-type ATPase	↓	↑
	Wood-Ljungdahl-Pathway	↑	↑
	Stickland fermentation–ox. Branch	↓	↑
	Stickland fermentation–red. Branch	↑	↓
	Glycolysis	↓	↓
	Pentose phosphate pathway	↓	↓
Stress response	Antibiotic resistance	↑	↓
	DNA repair	↑	↓
	Ox. Stress response	↓	→
	Chaperones	↓	→
	Toxins	↓	↓
	Sporulation	↓	↑
	c-di-GMP signaling	↑	↓
Regulation and signaling	Quorum sensing	↓	↓
	Two-component systems	↑	↓
	SigL/RpoN regulon	↑	↓

The protein inventory of C. difficile aggregate and colony biofilms was analyzed revealing differences mainly in the categories "Cell surface proteins," "Energy metabolism," "Stress response" and "Regulation and cell signaling." Pathways or proteins with respective functions were either less abundant (↓), higher abundant (↑) or remained unchanged (→).

CONCLUSION

The comprehensive proteome data presented here shed light on the protein repertoire of *C. difficile* strain 630Δ*erm* grown in two different biofilm models. Based on the results, we confirmed that free-floating aggregate biofilms behave drastically different from sessile colony biofilms and could possibly be the more relevant biofilm model. Cells of this biofilm type were characterized by significant metabolic activity, flagellation and activation of various regulatory circuits while they neither produced spores or toxins (**Table 2**), which is in line with previous transcriptomic data (Maldarelli et al., 2016; Poquet et al., 2018). Three aspects might explain some discrepancies observed between previously reported transcriptome approaches, e.g., by Poquet et al. (2018), and the here presented proteome data set. First, discrepancies could be explained by the initially discussed different experimental set ups used to grow biofilms (6-well plates vs. continuous flow system). Second, the choice of the reference sample sets applied (filtrate cells of same age as biofilms vs. 24 h batch cultures) impedes direct comparison of data sets. Lastly, previous observations demonstrated that transcriptome and proteome data do not necessarily follow the same expression trend (Zapalska-Sozoniuk et al., 2019). Therefore, we would like to emphasize that, although detection of a protein should not be mistaken for the protein's activity, proteome data probably reveal a more reliable picture of what genes are active within the two biofilm models than transcriptome data could do and might subsequently be more relevant for vaccine and antimicrobial design. On that basis, type IV pili were validated as important cell-surface antigens in *C. difficile* biofilms while the role of flagella and the S-layer remains unclear (**Table 2**). Moreover, we did not only confirm the importance of c-di-GMP signaling in biofilm formation but further suggested a central role for SigL/RpoN in *C. difficile* biofilms and conclude that research on this well-conserved regulator is hitherto underrepresented (**Table 2**). Of note, Tremblay et al. (2021) recently suggested a role for SigL/RpoN in *C. difficile* biofilms. Likewise, the data presented here emphasize the importance to characterize various still uncharacterized transcriptional regulators and two-component systems of which several were induced in aggregate biofilms (**Table 2**). Generally, further research is necessary to completely decipher the process of biofilm formation in *C. difficile* and to identify the nature of infection-relevant biofilms. Thereby, comprehensive *in vivo* omics studies including proteomic based studies will be inevitable. Moreover, integration of such *in vivo* data, which to some extent already exist for animal model studies

and analyses of patients' stool samples, with *in vitro* data such as those presented in this study will be just as important. For instance, transcriptomic and metabolomic data obtained from mice experiments suggest that *C. difficile* consumes significant amounts of amino acids but also of several carbohydrates such as mannitol during colonization of the intestine (Theriot et al., 2014; Jenior et al., 2017; Pereira et al., 2020). Consequently, the discussed identification of carbohydrate uptake and utilization pathways in the aggregate biofilms might be highly relevant for infection conditions.

DATA AVAILABILITY STATEMENT

The datasets presented in this study can be found in online repositories. The names of the repository/repositories and accession number(s) can be found below: https://www.ebi.ac.uk/pride/archive/, PXD022830.

AUTHOR CONTRIBUTIONS

CL, KR, and DJ designed the research. CL and CH performed the research. DB and JH were involved in mass spectrometric analyses. MB and CL analyzed the data. MB, CL, DJ, SS, and KR conceptualized and wrote the manuscript. All authors contributed to the article and approved the submitted version.

FUNDING

This project was funded by the Federal State of Lower Saxony, Niedersächsisches Vorab (VWZN2889), the Federal State of Mecklenburg-Vorpommern (UG 14 001), and the Federal Ministry of Research and Education (BMBF 0315833B, Urogenomics BMF Cooperative project and InfectControl 2020 project "MOASES"). We acknowledge support for the Article Processing Charge from the DFG (German Research Foundation, 393148499) and the Open Access Publication Fund of the University of Greifswald.

ACKNOWLEDGMENTS

We thank Silvia Dittmann for technical assistance and Daniela Zühlke and Tjorven Hinzke for helpful support during data analysis.

SUPPLEMENTARY MATERIAL

The Supplementary Material for this article can be found online at: https://www.frontiersin.org/articles/10.3389/fmicb.2021.682111/full#supplementary-material

REFERENCES

Anjuwon-Foster, B. R., and Tamayo, R. (2017). A genetic switch controls the production of flagella and toxins in Clostridium difficile. *PLoS Genet.* 13:e1006701. doi: 10.1371/journal.pgen.1006701

Anjuwon-Foster, B. R., and Tamayo, R. (2018). Phase variation of Clostridium difficile virulence factors. *Gut. Microb.* 9, 76–83. doi: 10.1080/19490976.2017.1362526

Antunes, A., Camiade, E., Monot, M., Courtois, E., Barbut, F., Sernova, N. V., et al. (2012). Global transcriptional control by glucose and carbon regulator CcpA in Clostridium difficile. *Nucleic Acids Res.* 40, 10701–10718. doi: 10.1093/nar/gks864

Antunes, A., Martin-Verstraete, I., and Dupuy, B. (2011). CcpA-mediated repression of Clostridium difficile toxin gene expression. *Mol. Microbiol.* 79, 882–899. doi: 10.1111/j.1365-2958.2010.07495.x

Anwar, H., Strap, J. L., and Costerton, J. W. (1992). Establishment of aging biofilms: possible mechanism of bacterial resistance to antimicrobial therapy. *Antimicrobial. Agents Chemother.* 36, 1347–1351. doi: 10.1128/aac.36.7.1347

Arato, V., Gasperini, G., Giusti, F., Ferlenghi, I., Scarselli, M., and Leuzzi, R. (2019). Dual role of the colonization factor CD2831 in Clostridium difficile pathogenesis. *Sci. Rep.* 9:5554. doi: 10.1038/s41598-019-42000-8

Arous, S., Buchrieser, C., Folio, P., Glaser, P., Namane, A., Hébraud, M., et al. (2004). Global analysis of gene expression in an rpoN mutant of Listeria monocytogenes. *Microbiology* 150, 1581–1590. doi: 10.1099/mic.0.26860-0

Barketi-Klai, A., Hoys, S., Lambert-Bordes, S., Collignon, A., and Kansau, I. (2011). Role of fibronectin-binding protein A in Clostridium difficile intestinal colonization. *J. Med. Microbiol.* 60, 1155–1161. doi: 10.1099/jmm.0.029553-0

Batah, J., Kobeissy, H., Bui Pham, P. T., Denève-Larrazet, C., Kuehne, S., Collignon, A., et al. (2017). Clostridium difficile flagella induce a pro-inflammatory response in intestinal epithelium of mice in cooperation with toxins. *Sci. Rep.* 7:3256. doi: 10.1038/s41598-017-03621-z

Berges, M., Michel, A.-M., Lassek, C., Nuss, A. M., Beckstette, M., Dersch, P., et al. (2018). Iron regulation in Clostridioides difficile. *Front. Microbiol.* 9:3183. doi: 10.3389/fmicb.2018.03183

Bernhardt, J., Michalik, S., Wollscheid, B., Völker, U., and Schmidt, F. (2013). Proteomics approaches for the analysis of enriched microbial subpopulations and visualization of complex functional information. *Curr. Opin. Biotechnol.* 24, 112–119. doi: 10.1016/j.copbio.2012.10.009

Besharova, O., Suchanek, V. M., Hartmann, R., Drescher, K., and Sourjik, V. (2016). Diversification of gene expression during formation of static submerged biofilms by *Escherichia coli*. *Front. Microbiol.* 7:1568. doi: 10.3389/fmicb.2016.01568

Boles, B. R., and Singh, P. K. (2008). Endogenous oxidative stress produces diversity and adaptability in biofilm communities. *Proc. Natl. Acad. Sci. U S A.* 105, 12503–12508. doi: 10.1073/pnas.0801499105

Bordeleau, E., Fortier, L.-C., Malouin, F., and Burrus, V. (2011). c-di-GMP turn-over in Clostridium difficile is controlled by a plethora of diguanylate cyclases and phosphodiesterases. *PLoS Genet.* 7:e1002039. doi: 10.1371/journal.pgen.1002039

Bouché, L., Panico, M., Hitchen, P., Binet, D., Sastre, F., Faulds-Pain, A., et al. (2016). The type B flagellin of hypervirulent Clostridium difficile is modified with novel sulfonated peptidylamido-glycans. *J. Biol. Chem.* 291, 25439–25449. doi: 10.1074/jbc.M116.749481

Boudry, P., Gracia, C., Monot, M., Caillet, J., Saujet, L., Hajnsdorf, E., et al. (2014). Pleiotropic role of the RNA chaperone protein Hfq in the human pathogen Clostridium difficile. *J. Bacteriol.* 196, 3234–3248. doi: 10.1128/JB.01923-14

Bradshaw, W. J., Bruxelle, J.-F., Kovacs-Simon, A., Harmer, N. J., Janoir, C., Péchiné, S., et al. (2019). Molecular features of lipoprotein CD0873: A potential vaccine against the human pathogen Clostridioides difficile. *J. Biol. Chem.* 294, 15850–15861. doi: 10.1074/jbc.RA119.010120

Bradshaw, W. J., Kirby, J. M., Roberts, A. K., Shone, C. C., and Acharya, K. R. (2017). Cwp2 from Clostridium difficile exhibits an extended three domain fold and cell adhesion in vitro. *FEBS J.* 284, 2886–2898. doi: 10.1111/febs.14157

Bruxelle, J. F., Mizrahi, A., Hoys, S., Collignon, A., Janoir, C., and Péchiné, S. (2016). Immunogenic properties of the surface layer precursor of Clostridium difficile and vaccination assays in animal models. *Anaerobe* 37, 78–84. doi: 10.1016/j.anaerobe.2015.10.010

Bruxelle, J.-F., Mizrahi, A., Hoÿs, S., Collignon, A., Janoir, C., and Péchiné, S. (2017). Clostridium difficile flagellin FliC: evaluation as adjuvant and use in a mucosal vaccine against Clostridium difficile. *PLoS One* 12:e0187212. doi: 10.1371/journal.pone.0187212

Burmølle, M., Thomsen, T. R., Fazli, M., Dige, I., Christensen, L., Homøe, P., et al. (2010). Biofilms in chronic infections - a matter of opportunity - monospecies biofilms in multispecies infections. *FEMS Immunol. Med. Microbiol.* 59, 324–336. doi: 10.1111/j.1574-695X.2010.00714.x

Carter, G. P., Des Purdy, Williams, P., and Minton, N. P. (2005). Quorum sensing in Clostridium difficile: analysis of a luxS-type signalling system. *J. Med. Microbiol.* 54, 119–127. doi: 10.1099/jmm.0.45817-0

Castro-Córdova, P., Díaz-Yáñez, F., Muñoz-Miralles, J., Gil, F., and Paredes-Sabja, D. (2020). Effect of antibiotic to induce Clostridioides difficile-susceptibility and infectious strain in a mouse model of Clostridioides difficile infection and recurrence. *Anaerobe* 62:102149. doi: 10.1016/j.anaerobe.2020.102149

Chilton, C. H., Pickering, D. S., and Freeman, J. (2018). Microbiologic factors affecting Clostridium difficile recurrence. *Clin. Microbiol. Infect.* 24, 476–482. doi: 10.1016/j.cmi.2017.11.017

Chong, P. M., Lynch, T., McCorrister, S., Kibsey, P., Miller, M., Gravel, D., et al. (2014). Proteomic analysis of a NAP1 Clostridium difficile clinical isolate resistant to metronidazole. *PLoS One* 9:e82622. doi: 10.1371/journal.pone.0082622

Chu, M., Mallozzi, M. J. G., Roxas, B. P., Bertolo, L., Monteiro, M. A., Agellon, A., et al. (2016). A Clostridium difficile cell wall glycopolymer locus influences bacterial shape, polysaccharide production and virulence. *PLoS Pathog.* 12:e1005946. doi: 10.1371/journal.ppat.1005946

Cox, J., and Mann, M. (2008). MaxQuant enables high peptide identification rates, individualized p.p.b.-range mass accuracies and proteome-wide protein quantification. *Nat. Biotechnol.* 26, 1367–1372. doi: 10.1038/nbt.1511

Crowther, G. S., Chilton, C. H., Todhunter, S. L., Nicholson, S., Freeman, J., Baines, S. D., et al. (2014). Comparison of planktonic and biofilm-associated communities of Clostridium difficile and indigenous gut microbiota in a triple-stage chemostat gut model. *J. Antimicrob. Chemother.* 69, 2137–2147. doi: 10.1093/jac/dku116

Cuenot, E., Garcia-Garcia, T., Douche, T., Gorgette, O., Courtin, P., Denis-Quanquin, S., et al. (2019). The Ser/Thr kinase PrkC participates in cell wall homeostasis and antimicrobial resistance in Clostridium difficile. *Infect. Immun.* 87, e00005–e19. doi: 10.1128/IAI.00005-19

Dannheim, H., Riedel, T., Neumann-Schaal, M., Bunk, B., Schober, I., Spröer, C., et al. (2017). Manual curation and reannotation of the genomes of Clostridium difficile 630Δerm and C. difficile 630. *J. Med. Microbiol.* 66, 286–293. doi: 10.1099/jmm.0.000427

Đapa, T., Dapa, T., Leuzzi, R., Ng, Y. K., Baban, S. T., Adamo, R., et al. (2013). Multiple factors modulate biofilm formation by the anaerobic pathogen Clostridium difficile. *J. Bacteriol.* 195, 545–555. doi: 10.1128/JB.01980-12

Dawson, L. F., Valiente, E., Faulds-Pain, A., Donahue, E. H., and Wren, B. W. (2012). Characterisation of Clostridium difficile biofilm formation, a role for Spo0A. *PLoS One* 7:e50527. doi: 10.1371/journal.pone.0050527

Del Papa, M. F., and Perego, M. (2008). Ethanolamine activates a sensor histidine kinase regulating its utilization in *Enterococcus faecalis*. *J. Bacteriol.* 190, 7147–7156. doi: 10.1128/JB.00952-08

Derré, I., Rapoport, G., and Msadek, T. (1999). CtsR, a novel regulator of stress and heat shock response, controls clp and molecular chaperone gene expression in gram-positive bacteria. *Mol. Microbiol.* 31, 117–131. doi: 10.1046/j.1365-2958.1999.01152.x

Dineen, S. S., McBride, S. M., and Sonenshein, A. L. (2010). Integration of metabolism and virulence by Clostridium difficile CodY. *J. Bacteriol.* 192, 5350–5362. doi: 10.1128/JB.00341-10

Dineen, S. S., Villapakkam, A. C., Nordman, J. T., and Sonenshein, A. L. (2007). Repression of Clostridium difficile toxin gene expression by CodY. *Mol. Microbiol.* 66, 206–219. doi: 10.1111/j.1365-2958.2007.05906.x

Doll, M., Marra, A. R., Apisarnthanarak, A., Al-Maani, A. S., Abbas, S., and Rosenthal, V. D. (2021). Prevention of Clostridioides difficile in hospitals: a position paper of the international society for infectious diseases. *Int. J. Infec. Dis.* 102, 188–195. doi: 10.1016/j.ijid.2020.10.039

Donelli, G., Vuotto, C., Cardines, R., and Mastrantonio, P. (2012). Biofilm-growing intestinal anaerobic bacteria. *FEMS Immunol. Med. Microbiol.* 65, 318–325. doi: 10.1111/j.1574-695X.2012.00962.x

Dubois, T., Dancer-Thibonnier, M., Monot, M., Hamiot, A., Bouillaut, L., Soutourina, O., et al. (2016). Control of Clostridium difficile physiopathology in response to cysteine availability. *Infect. Immun.* 84, 2389–2405. doi: 10.1128/IAI.00121-16

Dubois, T., Tremblay, Y. D. N., Hamiot, A., Martin-Verstraete, I., Deschamps, J., Monot, M., et al. (2019). A microbiota-generated bile salt induces biofilm formation in Clostridium difficile. *npj Biofilms Microbio.* 5, 1–12. doi: 10.1038/s41522-019-0087-4

Edwards, A. N., Nawrocki, K. L., and McBride, S. M. (2014). Conserved oligopeptide permeases modulate sporulation initiation in Clostridium difficile. *Infect. Immun.* 82, 4276–4291. doi: 10.1128/IAI.02323-14

El Meouche, I., Peltier, J., Monot, M., Soutourina, O., Pestel-Caron, M., Dupuy, B., et al. (2013). Characterization of the SigD regulon of C. difficile and its positive control of toxin production through the regulation of tcdR. *PLoS One* 8:e83748. doi: 10.1371/journal.pone.0083748

Faulds-Pain, A., Twine, S. M., Vinogradov, E., Strong, P. C. R., Dell, A., Buckley, A. M., et al. (2014). The post-translational modification of the Clostridium difficile flagellin affects motility, cell surface properties and virulence. *Mol. Microbiol.* 94, 272–289. doi: 10.1111/mmi.12755

Feuerstadt, P., Boules, M., Stong, L., Dahdal, D. N., Sacks, N. C., Lang, K., et al. (2021). Clinical complications in patients with primary and recurrent Clostridioides difficile infection: A real-world data analysis. *SAGE Open Med.* 9:2050312120986733. doi: 10.1177/2050312120986733

Fimlaid, K. A., Bond, J. P., Schutz, K. C., Putnam, E. E., Leung, J. M., Lawley, T. D., et al. (2013). Global analysis of the sporulation pathway of Clostridium difficile. *PLoS Genet.* 9:e003660. doi: 10.1371/journal.pgen.1003660

Fletcher, J. R., Erwin, S., Lanzas, C., and Theriot, C. M. (2018). Shifts in the gut metabolome and Clostridium difficile transcriptome throughout colonization and infection in a mouse model. *mSphere* 3:e00089–e18. doi: 10.1128/mSphere.00089-18

Fletcher, J. R., Pike, C. M., Parsons, R. J., Rivera, A. J., Foley, M. H., McLaren, M. R., et al. (2021). Clostridioides difficile exploits toxin-mediated inflammation to alter the host nutritional landscape and exclude competitors from the gut microbiota. *Nat. Commun.* 12:462. doi: 10.1038/s41467-020-20746-4

Francke, C., Groot Kormelink, T., Hagemeijer, Y., Overmars, L., Sluijter, V., Moezelaar, R., et al. (2011). Comparative analyses imply that the enigmatic Sigma factor 54 is a central controller of the bacterial exterior. *BMC Genom.* 12:385. doi: 10.1186/1471-2164-12-385

Ganeshapillai, J., Vinogradov, E., Rousseau, J., Weese, J. S., and Monteiro, M. A. (2008). Clostridium difficile cell-surface polysaccharides composed of pentaglycosyl and hexaglycosyl phosphate repeating units. *Carbohydrate Res.* 343, 703–710. doi: 10.1016/j.carres.2008.01.002

Gencic, S., and Grahame, D. A. (2020). Diverse energy-conserving pathways in Clostridium difficile: Growth in the absence of amino acid stickland acceptors and the role of the Wood-Ljungdahl Pathway. *J. Bacteriol.* 202:e00233–e220. doi: 10.1128/JB.00233-20

Gingichashvili, S., Duanis-Assaf, D., Shemesh, M., Featherstone, J. D. B., Feuerstein, O., and Steinberg, D. (2017). *Bacillus subtilis* biofilm development - a computerized study of morphology and kinetics. *Front. Microbiol.* 8:2072. doi: 10.3389/fmicb.2017.02072

Gómez, S., Chaves, F., and Orellana, M. A. (2017). Clinical, epidemiological and microbiological characteristics of relapse and re-infection in Clostridium difficile infection. *Anaerobe* 48, 147–151. doi: 10.1016/j.anaerobe.2017.08.012

Gooyit, M. D., and Janda, K. D. (2016). Modulation of the surface-layer protein of Clostridium difficile through Cwp84 inhibition. *ACS Infect. Dis.* 2, 465–470. doi: 10.1021/acsinfecdis.6b00061

Goulding, D., Thompson, H., Emerson, J., Fairweather, N. F., Dougan, G., and Douce, G. R. (2009). Distinctive profiles of infection and pathology in hamsters infected with Clostridium difficile strains 630 and B1. *Infect. Immun.* 77, 5478–5485. doi: 10.1128/IAI.00551-09

Hansen, S. K., Rainey, P. B., Haagensen, J. A. J., and Molin, S. (2007). Evolution of species interactions in a biofilm community. *Nature* 445, 533–536. doi: 10.1038/nature05514

Hayrapetyan, H., Tempelaars, M., Nierop Groot, M., and Abee, T. (2015). *Bacillus cereus* ATCC 14579 RpoN (Sigma 54) is a pleiotropic regulator of growth, carbohydrate metabolism, motility, biofilm formation and toxin production. *PLoS One* 10:e0134872. doi: 10.1371/journal.pone.0134872

Hernandez, B. G., Vinithakumari, A. A., Sponseller, B., Tangudu, C., and Mooyottu, S. (2020). Prevalence, colonization, epidemiology, and public health significance of Clostridioides difficile in companion animals. *Front. Veter. Sci.* 7:512551. doi: 10.3389/fvets.2020.512551

Hirschman, J., Wong, P. K., Sei, K., Keener, J., and Kustu, S. (1985). Products of nitrogen regulatory genes ntrA and ntrC of enteric bacteria activate glnA transcription in vitro: evidence that the ntrA product is a sigma factor. *Proc. NatL. Acad. Sci. U S A.* 82, 7525–7529. doi: 10.1073/pnas.82.22.7525

Ho, T. D., and Ellermeier, C. D. (2015). Ferric uptake regulator Fur control of putative iron acquisition systems in Clostridium difficile. *J. Bacteriol.* 197, 2930–2940. doi: 10.1128/JB.00098-15

Hofmann, J. D., Biedendieck, R., Michel, A.-M., Schomburg, D., Jahn, D., and Neumann-Schaal, M. (2021). Influence of L-lactate and low glucose concentrations on the metabolism and the toxin formation of Clostridioides difficile. *PLoS One* 16:e0244988. doi: 10.1371/journal.pone.0244988

Hofmann, J. D., Otto, A., Berges, M., Biedendieck, R., Michel, A.-M., Becher, D., et al. (2018). Metabolic reprogramming of Clostridioides difficile during the stationary phase with the induction of toxin production. *Front. Microbiol.* 9:1970. doi: 10.3389/fmicb.2018.01970

Høiby, N., Bjarnsholt, T., Givskov, M., Molin, S., and Ciofu, O. (2010). Antibiotic resistance of bacterial biofilms. *Int. J. Antimicrobial. Agent* 35, 322–332. doi: 10.1016/j.ijantimicag.2009.12.011

Hussain, H. A., Roberts, A. P., and Mullany, P. (2005). Generation of an erythromycin-sensitive derivative of Clostridium difficile strain 630 (630Deltaerm) and demonstration that the conjugative transposon Tn916DeltaE enters the genome of this strain at multiple sites. *J. Med. Microbiol.* 54, 137–141. doi: 10.1099/jmm.0.45790-0

Iyer, V. S., and Hancock, L. E. (2012). Deletion of σ(54) (rpoN) alters the rate of autolysis and biofilm formation in *Enterococcus faecalis*. *J. Bacteriol.* 194, 368–375. doi: 10.1128/JB.06046-11

Jackson, S., Calos, M., Myers, A., and Self, W. T. (2006). Analysis of proline reduction in the nosocomial pathogen Clostridium difficile. *J. Bacteriol.* 188, 8487–8495. doi: 10.1128/JB.01370-06

Jagannathan, A., Constantinidou, C., and Penn, C. W. (2001). Roles of rpoN, fliA, and flgR in expression of flagella in Campylobacter jejuni. *J. Bacteriol.* 183, 2937–2942. doi: 10.1128/JB.183.9.2937-2942.2001

Jain, S., Graham, C., Graham, R. L. J., McMullan, G., and Ternan, N. G. (2011). Quantitative proteomic analysis of the heat stress response in Clostridium difficile strain 630. *J. Proteome Res.* 10, 3880–3890. doi: 10.1021/pr200327t

Jain, S., Smyth, D., O'Hagan, B. M. G., Heap, J. T., McMullan, G., Minton, N. P., et al. (2017). Inactivation of the dnaK gene in Clostridium difficile 630 Δerm yields a temperature-sensitive phenotype and increases biofilm-forming ability. *Sci. Rep.* 7:17522. doi: 10.1038/s41598-017-17583-9

Jamal, M., Ahmad, W., Andleeb, S., Jalil, F., Imran, M., Nawaz, M. A., et al. (2018). Bacterial biofilm and associated infections. *J. Chinese Med. Assoc.* 81, 7–11. doi: 10.1016/j.jcma.2017.07.012

James, G. A., Chesnel, L., Boegli, L., deLancey Pulcini, E., Fisher, S., and Stewart, P. S. (2018). Analysis of Clostridium difficile biofilms: imaging and antimicrobial treatment. *J. Antimicrobial. Agents Chemother.* 73, 102–108. doi: 10.1093/jac/dkx353

Janoir, C., Denève, C., Bouttier, S., Barbut, F., Hoys, S., Caleechum, L., et al. (2013). Adaptive strategies and pathogenesis of Clostridium difficile from in vivo transcriptomics. *Infect. Immun.* 81, 3757–3769. doi: 10.1128/IAI.00515-13

Jenior, M. L., Leslie, J. L., Young, V. B., and Schloss, P. D. (2017). Clostridium difficile colonizes alternative nutrient niches during infection across distinct murine gut microbiomes. *mSystems* 2:e00063–e17. doi: 10.1128/mSystems.00063-17

Jenior, M. L., Leslie, J. L., Young, V. B., and Schloss, P. D. (2018). Clostridium difficile alters the structure and metabolism of distinct cecal microbiomes during initial infection to promote sustained colonization. *mSphere* 3:e00261–e18. doi: 10.1128/mSphere.00261-18

Karygianni, L., Ren, Z., Koo, H., and Thurnheer, T. (2020). Biofilm matrixome: Extracellular components in structured microbial communities. *Trends Microbiol.* 28, 668–681. doi: 10.1016/j.tim.2020.03.016

Kesel, S., Bronk, B., von, Falcón García, C., Götz, A., Lieleg, O., et al. (2017). Matrix composition determines the dimensions of *Bacillus subtilis* NCIB 3610 biofilm colonies grown on LB agar. *RSC Adv.* 7, 31886–31898. doi: 10.1039/C7RA05559E

Khader, K., Munoz-Price, L. S., Hanson, R., Stevens, V., Keegan, L. T., Thomas, A., et al. (2021). Transmission dynamics of Clostridioides difficile in 2 high-acuity hospital units. *Clin. Infec. Dis.* 72, S1–S7. doi: 10.1093/cid/ciaa1580

Kim, J., Darley, D., Selmer, T., and Buckel, W. (2006). Characterization of (R)-2-hydroxyisocaproate dehydrogenase and a family III coenzyme A transferase involved in reduction of L-leucine to isocaproate by Clostridium difficile. *Appl. Environ. Microbiol.* 72, 6062–6069. doi: 10.1128/AEM.00772-06

Kint, N., Janoir, C., Monot, M., Hoys, S., Soutourina, O., Dupuy, B., et al. (2017). The alternative sigma factor σB plays a crucial role in adaptive strategies of Clostridium difficile during gut infection. *Environ. Microbiol.* 19, 1933–1958. doi: 10.1111/1462-2920.13696

Kirby, J. M., Ahern, H., Roberts, A. K., Kumar, V., Freeman, Z., Acharya, K. R., et al. (2009). Cwp84, a surface-associated cysteine protease, plays a role in the maturation of the surface layer of Clostridium difficile. *J. Biol. Chem.* 284, 34666–34673. doi: 10.1074/jbc.M109.051177

Kirk, J. A., Banerji, O., and Fagan, R. P. (2017a). Characteristics of the Clostridium difficile cell envelope and its importance in therapeutics. *Microbial. Biotechnol.* 10, 76–90. doi: 10.1111/1751-7915.12372

Kirk, J. A., Gebhart, D., Buckley, A. M., Lok, S., Scholl, D., Douce, G. R., et al. (2017b). New class of precision antimicrobials redefines role of Clostridium difficile S-layer in virulence and viability. *Sci. Transl. Med.* 9:eaah6813. doi: 10.1126/scitranslmed.aah6813

Köpke, M., Straub, M., and Dürre, P. (2013). Clostridium difficile is an autotrophic bacterial pathogen. *PLoS One* 8:e62157. doi: 10.1371/journal.pone.0062157

La Riva, L., de, Willing, S. E., Tate, E. W., and Fairweather, N. F. (2011). Roles of cysteine proteases Cwp84 and Cwp13 in biogenesis of the cell wall of Clostridium difficile. *J. Bacteriol.* 193, 3276–3285. doi: 10.1128/JB.00248-11

Laemmli, U. K. (1970). Cleavage of structural proteins during the assembly of the head of bacteriophage T4. *Nature* 227, 680–685. doi: 10.1038/227680a0

Lawley, T. D., Clare, S., Walker, A. W., Goulding, D., Stabler, R. A., Croucher, N., et al. (2009). Antibiotic treatment of clostridium difficile carrier mice triggers a supershedder state, spore-mediated transmission, and severe disease in immunocompromised hosts. *Infec. Immunol.* 77, 3661–3669. doi: 10.1128/IAI.00558-09

Lawley, T. D., Clare, S., Walker, A. W., Stares, M. D., Connor, T. R., Raisen, C., et al. (2012). Targeted restoration of the intestinal microbiota with a simple, defined bacteriotherapy resolves relapsing Clostridium difficile disease in mice. *PLoS Pathog.* 8:e1002995. doi: 10.1371/journal.ppat.1002995

Levin, B. R., and Cornejo, O. E. (2009). The population and evolutionary dynamics of homologous gene recombination in bacterial populations. *PLoS Genet.* 5:e1000601. doi: 10.1371/journal.pgen.1000601

Maldarelli, G. A., Piepenbrink, K. H., Scott, A. J., Freiberg, J. A., Song, Y., Achermann, Y., et al. (2016). Type IV pili promote early biofilm formation by Clostridium difficile. *Pathog. Dis.* 74:ftw061. doi: 10.1093/femspd/ftw061

Martínez-Meléndez, A., Morfin-Otero, R., Villarreal-Treviño, L., Baines, S. D., Camacho-Ortíz, A., and Garza-González, E. (2020). Molecular epidemiology of predominant and emerging Clostridioides difficile ribotypes. *J. Microbiol. Methods* 175:105974. doi: 10.1016/j.mimet.2020.105974

Mathur, H., Rea, M. C., Cotter, P. D., Hill, C., and Ross, R. P. (2016). The efficacy of thuricin CD, tigecycline, vancomycin, teicoplanin, rifampicin and nitazoxanide, independently and in paired combinations against Clostridium difficile biofilms and planktonic cells. *Gut Pathog.* 8:20. doi: 10.1186/s13099-016-0102-8

McBride, S. M., and Sonenshein, A. L. (2011). The dlt operon confers resistance to cationic antimicrobial peptides in Clostridium difficile. *Microbiology* 157, 1457–1465. doi: 10.1099/mic.0.045997-0

McKee, R. W., Aleksanyan, N., Garrett, E. M., and Tamayo, R. (2018a). Type IV pili promote Clostridium difficile adherence and persistence in a mouse model of infection. *Infec. Immun.* 86:e00943–e17. doi: 10.1128/IAI.00943-17

McKee, R. W., Harvest, C. K., and Tamayo, R. (2018b). Cyclic diguanylate regulates virulence factor genes via multiple riboswitches in Clostridium difficile. *mSphere* 3:e00423–e18. doi: 10.1128/mSphere.00423-18

McKee, R. W., Mangalea, M. R., Purcell, E. B., Borchardt, E. K., and Tamayo, R. (2013). The second messenger cyclic Di-GMP regulates Clostridium difficile toxin production by controlling expression of sigD. *J. Bacteriol.* 195, 5174–5185. doi: 10.1128/JB.00501-13

McLure, A., Clements, A. C. A., Kirk, M., and Glass, K. (2019). Modelling diverse sources of Clostridium difficile in the community: importance of animals, infants and asymptomatic carriers. *Epidemiol. Infec.* 147:e152. doi: 10.1017/S0950268819000384

Merrigan, M. M., Venugopal, A., Roxas, J. L., Anwar, F., Mallozzi, M. J., Roxas, B. A. P., et al. (2013). Surface-layer protein A (SlpA) is a major contributor to host-cell adherence of Clostridium difficile. *PLoS One* 8:e78404. doi: 10.1371/journal.pone.0078404

Mizrahi, A., Bruxelle, J. F., Péchiné, S., and Le, M. A. (2018). Prospective evaluation of the adaptive immune response to SlpA in Clostridium difficile infection. *Anaerobe* 54, 164–168. doi: 10.1016/j.anaerobe.2018.09.008

Molin, S., and Tolker-Nielsen, T. (2003). Gene transfer occurs with enhanced efficiency in biofilms and induces enhanced stabilisation of the biofilm structure. *Curr. Opin. Biotechnol.* 14, 255–261. doi: 10.1016/S0958-1669(03)00036-3

Mullany, P., Wilks, M., Lamb, I., Clayton, C., Wren, B., and Tabaqchali, S. (1990). Genetic analysis of a tetracycline resistance element from Clostridium difficile and its conjugal transfer to and from *Bacillus subtilis*. *J. General Microbiol.* 136, 1343–1349. doi: 10.1099/00221287-136-7-1343

Müller, V., Imkamp, F., Biegel, E., Schmidt, S., and Dilling, S. (2008). Discovery of a ferredoxin:NAD+-oxidoreductase (Rnf) in *Acetobacterium woodii*: a novel potential coupling site in acetogens. *Ann. N.Y. Acad. Sci.* 1125, 137–146. doi: 10.1196/annals.1419.011

Nasiri, M. J., Goudarzi, M., Hajikhani, B., Ghazi, M., Goudarzi, H., and Pouriran, R. (2018). Clostridioides (Clostridium) difficile infection in hospitalized patients with antibiotic-associated diarrhea: A systematic review and meta-analysis. *Anaerobe* 50, 32–37. doi: 10.1016/j.anaerobe.2018.01.011

Nawrocki, K. L., Wetzel, D., Jones, J. B., Woods, E. C., and McBride, S. M. (2018). Ethanolamine is a valuable nutrient source that impacts Clostridium difficile pathogenesis. *Environ. Microbiol.* 20, 1419–1435. doi: 10.1111/1462-2920.14048

Neumann-Schaal, M., Hofmann, J. D., Will, S. E., and Schomburg, D. (2015). Time-resolved amino acid uptake of Clostridium difficile 630Δerm and concomitant fermentation product and toxin formation. *BMC Microbiol.* 15:281. doi: 10.1186/s12866-015-0614-2

Neumann-Schaal, M., Metzendorf, N. G., Troitzsch, D., Nuss, A. M., Hofmann, J. D., Beckstette, M., et al. (2018). Tracking gene expression and oxidative damage of O2-stressed Clostridioides difficile by a multi-omics approach. *Anaerobe* 53, 94–107. doi: 10.1016/j.anaerobe.2018.05.018

Nie, X., Dong, W., and Yang, C. (2019). Genomic reconstruction of σ 54 regulons in Clostridiales. *BMC Genom.* 20, 1–14. doi: 10.1186/s12864-019-5918-4

Normington, C., Moura, I. B., Bryant, J. A., Ewin, D. J., Clark, E. V., Kettle, M. J., et al. (2021). Biofilms harbour Clostridioides difficile, serving as a reservoir for recurrent infection. *npj Biofilms Microbio.* 7:16. doi: 10.1038/s41522-021-00184-w

Oka, K., Osaki, T., Hanawa, T., Kurata, S., Okazaki, M., Manzoku, T., et al. (2012). Molecular and microbiological characterization of Clostridium difficile isolates from single, relapse, and reinfection cases. *J. Clin. Microbiol.* 50, 915–921. doi: 10.1128/JCM.05588-11

Oliveira, N. M., Oliveria, N. M., Martinez-Garcia, E., Xavier, J., Durham, W. M., Kolter, R., et al. (2015). Biofilm formation as a response to ecological competition. *PLoS Biol.* 13:e1002191. doi: 10.1371/journal.pbio.1002191

Onderdonk, A. B., Lowe, B. R., and Bartlett, J. G. (1979). Effect of environmental stress on Clostridium difficile toxin levels during continuous cultivation. *Appl. Environ. Microbiol.* 38, 637–641. doi: 10.1128/AEM.38.4.637-641.1979

Otto, A., Maaß, S., Lassek, C., Becher, D., Hecker, M., Riedel, K., et al. (2016). The protein inventory of Clostridium difficile grown in complex and minimal medium. *Proteomics Clin. Applicat.* 10, 1068–1072. doi: 10.1002/prca.201600069

Pantaléon, V., Monot, M., Eckert, C., Hoys, S., Collignon, A., Janoir, C., et al. (2018). Clostridium difficile forms variable biofilms on abiotic surface. *Anaerobe* 53, 34–37. doi: 10.1016/j.anaerobe.2018.05.006

Pantaléon, V., Soavelomandroso, A. P., Bouttier, S., Briandet, R., Roxas, B., Chu, M., et al. (2015). The Clostridium difficile protease Cwp84 modulates both biofilm formation and cell-surface properties. *PLoS One* 10:e0124971. doi: 10.1371/journal.pone.0124971

Péchiné, S., Bruxelle, J. F., Janoir, C., and Collignon, A. (2018). Targeting Clostridium difficile surface components to develop immunotherapeutic strategies against Clostridium difficile infection. *Front. Microbiol.* 9:1009. doi: 10.3389/fmicb.2018.01009

Péchiné, S., Denève, C., Le Monnier, A., Hoys, S., Janoir, C., and Collignon, A. (2011). Immunization of hamsters against Clostridium difficile infection using the Cwp84 protease as an antigen. *FEMS Immunol. Med. Microbiol.* 63, 73–81. doi: 10.1111/j.1574-695X.2011.00832.x

Pereira, F. C., Wasmund, K., Cobankovic, I., Jehmlich, N., Herbold, C. W., Lee, K. S., et al. (2020). Rational design of a microbial consortium of mucosal sugar utilizers reduces Clostridiodes difficile colonization. *Nat. Commun.* 11:5104. doi: 10.1038/s41467-020-18928-1

Pettit, L. J., Browne, H. P., Yu, L., Smits, W. K., Fagan, R. P., Barquist, et al. (2014). Functional genomics reveals that Clostridium difficile Spo0A coordinates sporulation, virulence and metabolism. *BMC Genom.* 15, 1–15. doi: 10.1186/1471-2164-15-160

Pike, C. M., and Theriot, C. M. (2020). Mechanisms of colonization resistance against Clostridioides difficile. *J. Infec. Dis.* 2020:jiaa408. doi: 10.1093/infdis/jiaa408

Pizarro-Guajardo, M., Calderón-Romero, P., and Paredes-Sabja, D. (2016). Ultrastructure variability of the exosporium layer of Clostridium difficile spores from sporulating cultures and biofilms. *Appl. Environ. Microbiol.* 82, 5892–5898. doi: 10.1128/AEM.01463-16

Plaza-Garrido, Á, Miranda-Cárdenas, C., Castro-Córdova, P., Olguín-Araneda, V., Cofré-Araneda, G., Hernández-Rocha, C., et al. (2015). Outcome of relapsing Clostridium difficile infections do not correlate with virulence-, spore- and vegetative cell-associated phenotypes. *Anaerobe* 36, 30–38. doi: 10.1016/j.anaerobe.2015.09.005

Poquet, I., Saujet, L., Canette, A., Monot, M., Mihajlovic, J., Ghigo, J.-M., et al. (2018). Clostridium difficile biofilm: Remodeling metabolism and cell surface to build a sparse and heterogeneously aggregated architecture. *Front. Microbiol.* 9:2084. doi: 10.3389/fmicb.2018.02084

Purcell, E. B., McKee, R. W., Bordeleau, E., Burrus, V., and Tamayo, R. (2016). Regulation of type IV pili contributes to surface behaviors of historical and epidemic strains of Clostridium difficile. *J. Bacteriol.* 198, 565–577. doi: 10.1128/JB.00816-15

Purcell, E. B., McKee, R. W., Courson, D. S., Garrett, E. M., McBride, S. M., Cheney, R. E., et al. (2017). A nutrient-regulated cyclic diguanylate phosphodiesterase controls Clostridium difficile biofilm and toxin production during stationary phase. *Infec. Immun.* 85:e00347–e17. doi: 10.1128/IAI.00347-17

Purcell, E. B., McKee, R. W., McBride, S. M., Waters, C. M., and Tamayo, R. (2012). Cyclic diguanylate inversely regulates motility and aggregation in Clostridium difficile. *J. Bacteriol.* 194, 3307–3316. doi: 10.1128/JB.00100-12

Reid, C. W., Vinogradov, E., Li, J., Jarrell, H. C., Logan, S. M., and Brisson, J.-R. (2012). Structural characterization of surface glycans from Clostridium difficile. *Carbohydrate Res.* 354, 65–73. doi: 10.1016/j.carres.2012.02.002

Ren, D., Madsen, J. S., Sørensen, S. J., and Burmølle, M. (2015). High prevalence of biofilm synergy among bacterial soil isolates in cocultures indicates bacterial interspecific cooperation. *ISME J.* 9, 81–89. doi: 10.1038/ismej.2014.96

Reynolds, C. B., Emerson, J. E., La Riva, L., de, Fagan, R. P., and Fairweather, N. F. (2011). The Clostridium difficile cell wall protein CwpV is antigenically variable between strains, but exhibits conserved aggregation-promoting function. *PLoS Pathog.* 7:e1002024. doi: 10.1371/journal.ppat.1002024

Richards, E., Bouché, L., Panico, M., Arbeloa, A., Vinogradov, E., Morris, H., et al. (2018). The S-layer protein of a Clostridium difficile SLCT-11 strain displays a complex glycan required for normal cell growth and morphology. *J. Biol. Chem.* 293, 18123–18137. doi: 10.1074/jbc.RA118.004530

Riedel, T., Wetzel, D., Hofmann, J. D., Plorin, Simon Paul, Erich Otto, et al. (2017). High metabolic versatility of different toxigenic and non-toxigenic Clostridioides difficile isolates. *Int. J. Med. Microbiol.* 307, 311–320. doi: 10.1016/j.ijmm.2017.05.007

Ryder, V. J., Chopra, I., and O'Neill, A. J. (2012). Increased mutability of *Staphylococci* in biofilms as a consequence of oxidative stress. *PLoS One* 7:e47695. doi: 10.1371/journal.pone.0047695

Saldías, M. S., Lamothe, J., Wu, R., and Valvano, M. A. (2008). Burkholderia cenocepacia requires the RpoN sigma factor for biofilm formation and intracellular trafficking within macrophages. *Infec. Immun.* 76, 1059–1067. doi: 10.1128/IAI.01167-07

Saujet, L., Monot, M., Dupuy, B., Soutourina, O., and Martin-Verstraete, I. (2011). The key sigma factor of transition phase, SigH, controls sporulation, metabolism, and virulence factor expression in Clostridium difficile. *J. Bacteriol.* 193, 3186–3196. doi: 10.1128/JB.00272-11

Schade, J., and Weidenmaier, C. (2016). Cell wall glycopolymers of firmicutes and their role as nonprotein adhesins. *FEBS Lett.* 590, 3758–3771. doi: 10.1002/1873-3468.12288

Schiffels, J., and Selmer, T. (2019). Combinatorial assembly of ferredoxin-linked modules in *Escherichia coli* yields a testing platform for Rnf-complexes. *Biotechnol. Bioeng.* 116, 2316–2329. doi: 10.1002/bit.27079

Schulz, A., and Schumann, W. (1996). hrcA, the first gene of the *Bacillus subtilis* dnaK operon encodes a negative regulator of class I heat shock genes. *J. Bacteriol.* 178, 1088–1093.

Sebaihia, M., Wren, B. W., Mullany, P., Fairweather, N. F., Minton, N., Stabler, R., et al. (2006). The multidrug-resistant human pathogen Clostridium difficile has a highly mobile, mosaic genome. *Nat. Genet.* 38, 779–786. doi: 10.1038/ng1830

Semenyuk, E. G., Laning, M. L., Foley, J., Johnston, P. F., Knight, K. L., Gerding, D. N., et al. (2014). Spore formation and toxin production in Clostridium difficile biofilms. *PLoS One* 9:e87757. doi: 10.1371/journal.pone.0087757

Shin, J.-B., Krey, J. F., Hassan, A., Metlagel, Z., Tauscher, A. N., Pagana, J. M., et al. (2013). Molecular architecture of the chick vestibular hair bundle. *Nat. Neurosci.* 16, 365–374. doi: 10.1038/nn.3312

Sievers, S., Metzendorf, N. G., Dittmann, S., Troitzsch, D., Gast, V., Tröger, S. M., et al. (2019). Differential view on the bile acid stress response of Clostridioides difficile. *Front. Microbiol.* 10:258. doi: 10.3389/fmicb.2019.00258

Sirard, S., Valiquette, L., and Fortier, L.-C. (2011). Lack of association between clinical outcome of Clostridium difficile infections, strain type, and virulence-associated phenotypes. *J. Clin. Microbiol.* 49, 4040–4046. doi: 10.1128/JCM.05053-11

Slater, R. T., Frost, L. R., Jossi, S. E., Millard, A. D., and Unnikrishnan, M. (2019). Clostridioides difficile LuxS mediates inter-bacterial interactions within biofilms. *Sci. Rep.* 9:9903. doi: 10.1038/s41598-019-46143-6

Smits, W. K. (2013). Hype or hypervirulence: a reflection on problematic C. difficile strains. *Virulence* 4, 592–596. doi: 10.4161/viru.26297

Soavelomandroso, A. P., Gaudin, F., Hoys, S., Nicolas, V., Vedantam, G., Janoir, C., et al. (2017). Biofilm structures in a mono-associated mouse model of Clostridium difficile infection. *Front. Microbiol.* 8:2086. doi: 10.3389/fmicb.2017.02086

Soutourina, O., Dubois, T., Monot, M., Shelyakin, P. V., Saujet, L., Boudry, P., et al. (2020). Genome-wide transcription start site mapping and promoter assignments to a sigma factor in the human enteropathogen Clostridioides difficile. *Front. Microbiol.* 11:1939. doi: 10.3389/fmicb.2020.01939

Soutourina, O. A., Monot, M., Boudry, P., Saujet, L., Pichon, C., Sismeiro, O., et al. (2013). Genome-wide identification of regulatory RNAs in the human pathogen *Clostridium difficile*. *PLoS Genet.* 9:e1003493. doi: 10.1371/journal.pgen.1003493

Stickland, L. H. (1934). Studies in the metabolism of the strict anaerobes (genus Clostridium): The chemical reactions by which Cl. sporogenes obtains its energy. *Biochem. J.* 28, 1746–1759. doi: 10.1042/bj0281746

Stupperich, E., Hammel, K. E., Fuchs, G., and Thauer, R. K. (1983). Carbon monoxide fixation into the carboxyl group of acetyl coenzyme A during autotrophic growth of *Methanobacterium*. *FEBS Lett.* 152, 21–23. doi: 10.1016/0014-5793(83)80473-6

Ternan, N. G., Jain, S., Srivastava, M., and McMullan, G. (2012). Comparative transcriptional analysis of clinically relevant heat stress response in Clostridium difficile strain 630. *PLoS One* 7:e42410. doi: 10.1371/journal.pone.0042410

Theriot, C. M., Koenigsknecht, M. J., Paul, E., Carlson, Gabrielle, E., Hatton, et al. (2014). Antibiotic-induced shifts in the mouse gut microbiome and metabolome increase susceptibility to Clostridium difficile infection. *Nat. Commun.* 5, 1–10. doi: 10.1038/ncomms4114

Tijerina-Rodríguez, L., Villarreal-Treviño, L., Morfín-Otero, R., Camacho-Ortíz, A., and Garza-González, E. (2019). Virulence factors of Clostridioides (Clostridium) difficile linked to recurrent infections. *Can. J. Infec. Dis. Med. Microbiol.* 2019:7127850. doi: 10.1155/2019/7127850

Tremblay, Y. D. N., Durand, B. A. R., Hamiot, A., Martin-Verstraete, I., Oberkampf, M., Monot, M., et al. (2021). Metabolic adaption to extracellular pyruvate triggers biofilm formation in Clostridioides difficile. *bioRxiv* doi: 10.1101/2021.01.23.427917.

Troitzsch, D., Zhang, H., Dittmann, S., Düsterhöft, D., Möller, T. A., Michel, A.-M., et al. (2021). A point mutation in the transcriptional repressor PerR results in a constitutive oxidative stress response in Clostridioides difficile 630Δerm. *mSphere* 6:e00091–21. doi: 10.1128/mSphere.00091-21

Twine, S. M., Reid, C. W., Aubry, A., McMullin, D. R., Fulton, K. M., Austin, J., et al. (2009). Motility and flagellar glycosylation in Clostridium difficile. *J. Bacteriol.* 191, 7050–7062. doi: 10.1128/JB.00861-09

Tyanova, S., Temu, T., and Cox, J. (2016a). The MaxQuant computational platform for mass spectrometry-based shotgun proteomics. *Nat. Prot.* 11, 2301–2319. doi: 10.1038/nprot.2016.136

Tyanova, S., Temu, T., Sinitcyn, P., Carlson, A., Hein, M. Y., Geiger, T., et al. (2016b). The Perseus computational platform for comprehensive analysis of (prote)omics data. *Nat. Methods* 13, 731–740. doi: 10.1038/nmeth.3901

Underwood, S., Guan, S., Vijayasubhash, V., Baines, S. D., Graham, L., Lewis, R. J., et al. (2009). Characterization of the sporulation initiation pathway of Clostridium difficile and its role in toxin production. *J. Bacteriol.* 191, 7296–7305. doi: 10.1128/JB.00882-09

Valiente, E., Bouché, L., Hitchen, P., Faulds-Pain, A., Songane, M., Dawson, L. F., et al. (2016). Role of glycosyltransferases modifying type B flagellin of emerging hypervirulent Clostridium difficile lineages and their impact on motility and biofilm formation. *J. Biol. Chem.* 291, 25450–25461. doi: 10.1074/jbc.M116.749523

van Eijk, E., Anvar, S. Y., Browne, H. P., Leung, W. Y., Frank, J., Schmitz, A. M., et al. (2015). Complete genome sequence of the Clostridium difficile laboratory strain 630Δerm reveals differences from strain 630, including translocation of the mobile element CTn5. *BMC Genom.* 16:31. doi: 10.1186/s12864-015-1252-7

Vaz, F., Wilson, G., Kirk, J., Salgado, P., Fagan, R., and Douce, G. (2019). Unraveling the role of C. difficile S-layer in infection and disease. *Access Microbiol.* 1:86. doi: 10.1099/acmi.ac2019.po0086

Vlamakis, H., Aguilar, C., Losick, R., and Kolter, R. (2008). Control of cell fate by the formation of an architecturally complex bacterial community. *Genes Dev.* 22, 945–953. doi: 10.1101/gad.1645008

Vuotto, C., Donelli, G., Buckley, A., and Chilton, C. (2018). Clostridium difficile biofilm. *Adv. Exper. Med. Biol.* 1050, 97–115. doi: 10.1007/978-3-319-72799-8_7

Waligora, A. J., Hennequin, C., Mullany, P., Bourlioux, P., Collignon, A., and Karjalainen, T. (2001). Characterization of a cell surface protein of Clostridium difficile with adhesive properties. *Infec. Immun.* 69, 2144–2153. doi: 10.1128/IAI.69.4.2144-2153.2001

Walter, B. M., Cartman, S. T., Minton, N. P., Butala, M., and Rupnik, M. (2015). The SOS response master regulator LexA is associated with sporulation, motility and biofilm formation in Clostridium difficile. *PLoS One* 10:e0144763. doi: 10.1371/journal.pone.0144763

Weiss, V., and Magasanik, B. (1988). Phosphorylation of nitrogen regulator I (NRI) of *Escherichia coli*. *Proc. Natl. Acad. Sci. U S A.* 85, 8919–8923.

Werner, A., Mölling, P., Fagerström, A., Dyrkell, F., Arnellos, D., Johansson, K., et al. (2020). Whole genome sequencing of Clostridioides difficile PCR ribotype 046 suggests transmission between pigs and humans. *PLoS One* 15:e0244227. doi: 10.1371/journal.pone.0244227

Wiegand, P. N., Nathwani, D., Wilcox, M. H., Stephens, J., Shelbaya, A., and Haider, S. (2012). Clinical and economic burden of Clostridium difficile infection in Europe: a systematic review of healthcare-facility-acquired infection. *J. Hospital Infec.* 81, 1–14. doi: 10.1016/j.jhin.2012.02.004

Willing, S. E., Candela, T., Shaw, H. A., Seager, Z., Mesnage, S., Fagan, R. P., et al. (2015). Clostridium difficile surface proteins are anchored to the cell wall using CWB2 motifs that recognise the anionic polymer PSII. *Mol. Microbiol.* 96, 596–608. doi: 10.1111/mmi.12958

Woods, E. C., Edwards, A. N., Childress, K. O., Jones, J. B., and McBride, S. M. (2018). The C. difficile clnRAB operon initiates adaptations to the host environment in response to LL-37. *PLoS Pathog.* 14:e1007153. doi: 10.1371/journal.ppat.1007153

Xu, Y.-B., Chen, M., Zhang, Y., Wang, M., Wang, Y., Huang, Q.-B., et al. (2014). The phosphotransferase system gene ptsI in the endophytic bacterium *Bacillus*

cereus is required for biofilm formation, colonization, and biocontrol against wheat sharp eyespot. *FEMS Microbiol. Lett.* 354, 142–152. doi: 10.1111/1574-6968.12438

Yu, N. Y., Wagner, J. R., Laird, M. R., Melli, G., Rey, S., Lo, R., et al. (2010). PSORTb 3.0: improved protein subcellular localization prediction with refined localization subcategories and predictive capabilities for all prokaryotes. *Bioinformatics* 26, 1608–1615. doi: 10.1093/bioinformatics/btq249

Zapalska-Sozoniuk, M., Chrobak, L., Kowalczyk, K., and Kankofer, M. (2019). Is it useful to use several "omics" for obtaining valuable results? *Mol. Biol. Rep.* 46, 3597–3606. doi: 10.1007/s11033-019-04793-9

Conflict of Interest: The authors declare that the research was conducted in the absence of any commercial or financial relationships that could be construed as a potential conflict of interest.

Copyright © 2021 Brauer, Lassek, Hinze, Hoyer, Becher, Jahn, Sievers and Riedel. This is an open-access article distributed under the terms of the Creative Commons Attribution License (CC BY). The use, distribution or reproduction in other forums is permitted, provided the original author(s) and the copyright owner(s) are credited and that the original publication in this journal is cited, in accordance with accepted academic practice. No use, distribution or reproduction is permitted which does not comply with these terms.

frontiers in Microbiology

ORIGINAL RESEARCH
published: 21 July 2021
doi: 10.3389/fmicb.2021.715220

Clostridioides difficile Single Cell Swimming Strategy: A Novel Motility Pattern Regulated by Viscoelastic Properties of the Environment

*Julian Schwanbeck, Ines Oehmig, Uwe Groß, Andreas E. Zautner and Wolfgang Bohne**

Institute for Medical Microbiology and Virology, University Medical Center Göttingen, Göttingen, Germany

Flagellar motility is important for the pathogenesis of many intestinal pathogens, allowing bacteria to move to their preferred ecological niche. *Clostridioides difficile* is currently the major cause for bacterial health care-associated intestinal infections in the western world. Most clinical strains produce peritrichous flagella and are motile in soft-agar. However, little knowledge exists on the *C. difficile* swimming behaviour and its regulation at the level of individual cells. We report here on the swimming strategy of *C. difficile* at the single cell level and its dependency on environmental parameters. A comprehensive analysis of motility parameters from several thousand bacteria was achieved with the aid of a recently developed bacterial tracking programme. *C. difficile* motility was found to be strongly dependent on the matrix elasticity of the medium. Long run phases of all four motile *C. difficile* clades were only observed in the presence of high molecular weight molecules such as polyvinylpyrrolidone (PVP) and mucin, which suggests an adaptation of the motility apparatus to the mucin-rich intestinal environment. Increasing mucin or PVP concentrations lead to longer and straighter runs with increased travelled distance per run and fewer turnarounds that result in a higher net displacement of the bacteria. The observed *C. difficile* swimming pattern under these conditions is characterised by bidirectional, alternating back and forth run phases, interrupted by a short stop without an apparent reorientation or tumbling phase. This motility type was not described before for peritrichous bacteria and is more similar to some previously described polar monotrichous bacteria.

Keywords: *Clostridioides difficile*, motility, viscoelastic medium, video microscopy, motility tracking, bacterial swimming strategy

OPEN ACCESS

Edited by:
Caterina Guzmán-Verri, National University of Costa Rica, Costa Rica

Reviewed by:
Jonathan David Partridge, University of Texas at Austin, United States
Mindy Engevik, Medical University of South Carolina, United States
David Courson, Old Dominion University, United States

***Correspondence:**
Wolfgang Bohne
wbohne@gwdg.de

Specialty section:
This article was submitted to Infectious Diseases, a section of the journal Frontiers in Microbiology

Received: *26 May 2021*
Accepted: *29 June 2021*
Published: *21 July 2021*

Citation:
Schwanbeck J, Oehmig I, Groß U, Zautner AE and Bohne W (2021) Clostridioides difficile Single Cell Swimming Strategy: A Novel Motility Pattern Regulated by Viscoelastic Properties of the Environment. Front. Microbiol. 12:715220. doi: 10.3389/fmicb.2021.715220

INTRODUCTION

Clostridioides (formerly *Clostridium*) *difficile* is a spore forming, obligate anaerobic pathogen that causes CDI (*C. difficile* infection), which predominantly manifests as hospital-associated diarrhoea and pseudomembranous colitis (Leffler and Lamont, 2015; Lessa et al., 2015). Clinical symptoms are associated with toxin expression, in particular toxin A and B, which undergo a complex regulation pattern (Just et al., 1995; Kuehne et al., 2010; Chandrasekaran and Lacy, 2017). An intact gut microbiome is believed to protect from *C. difficile* infection. Dysbiosis however, for example after

antibiotic treatment, favours *C. difficile* spore germination and subsequent colonisation (Buffie and Pamer, 2013; Theriot and Young, 2015; Gómez et al., 2017).

Flagellar motility and chemotaxis are important for successful colonisation and virulence of many gastrointestinal pathogens, for example *Campylobacter jejuni*, *Salmonella enterica* Serovar Typhimurium, *Helicobacter pylori,* and *Vibrio chlolerae* (Boin et al., 2004; Stecher et al., 2004; Lertsethtakarn et al., 2011; Korolik, 2019). Most *C. difficile* strains produce peritrichous flagella, which can mediate swimming motility in soft-agar based assays (Twine et al., 2009; Baban et al., 2013; Courson et al., 2019). The contribution of flagellar motility for the pathogenesis in mice was studied with the aid of *C. difficile* flagellar mutants, which were found to be reduced in their colonisation efficiency (Baban et al., 2013; Batah et al., 2017). It is also known that the *C. difficile* genome contains a region which encodes for a complete set of chemotaxis genes (Dannheim et al., 2017). Chemotaxis allows bacteria to swim up or down a chemical gradient and thus to find optimal growth conditions (Matilla and Krell, 2018). Regulation of motility by the chemotaxis system is well investigated for a variety of bacterial species. Chemical gradients are sensed by chemoreceptors, which transfer the signal via the adapter protein CheW and the histidine kinase CheA to the transducer CheY, which becomes phosphorylated (Porter et al., 2011). The phosphorylated CheY finally interacts with the flagellar motor and leads to a modulation of motility characteristics.

However, in contrast to other gut pathogens, little knowledge exists on the motility of *C. difficile* at the single cell level. A careful analysis of the *C. difficile* swimming pattern and its dependency on environmental parameters would contribute to a better understanding of *C. difficile* motility for pathogenesis and particularly for the attachment and dissemination phases, in which flagella have previously been found to play a role (Tasteyre et al., 2001; Batah et al., 2017).

Gut pathogens like *C. difficile*, as well as commensalists, have to deal with the mucosal layer in the lower intestine. The colon mucus, made up mostly of Muc2, consists of a stratified inner, attached layer which is expressed by the surface goblet cells and serves as a protective barrier for the intestines (Lai et al., 2009; Johansson et al., 2011; McGuckin et al., 2011). The pore sizes of this layer allow for small molecule diffusion, but acts as a barrier to structures in the micrometre range, partially due to steric hindrance (Lai et al., 2009). The mucus layer is partial degraded by commensalists and possesses then an increased pore size, allowing a better colonisation by bacteria (Lai et al., 2009; Johansson et al., 2011; McGuckin et al., 2011). As the layer is still cross-linked, it presumably still poses as a steric hindrance, influencing the rheological profile of the environment.

We report in this study on the swimming behaviour of *C. difficile* and its strong dependency on the viscoelastic properties of the medium across all motile clades. A comprehensive quantitative analysis of *C. difficile* motility parameters on the single cell level was obtained with the aid of the bacterial tracking programme YSMR (Schwanbeck et al., 2020). We hypothesise that this dependency on viscoelastic properties is an adaptation to the properties of the mucin rich lower intestines, which form the habitat of *C. difficile*. A large-scale quantitative analysis of the swimming behaviour leads to the conclusion that the single cell motility displayed by *C. difficile* forms a novel pattern for peritrichous bacteria, which we describe here in detail.

MATERIALS AND METHODS

Used *C. difficile* Strains

C. difficile 630 Δ*erm* [Ribotype (RT) 012, DSM 28645, CP016318.1 (Dannheim et al., 2017)], *C. difficile* R20291 (RT 027, DSM 27147, CP029423.1), DSM 100002 (RT 084), DSM 102978 (RT not determined, CP020380.1), DSM 28670 [RT SLO 237, CP012312.1 (Riedel et al., 2017)], and DSM 100005 (RT SLO 235).

Media and Strain Cultivation

C. difficile strains were grown at 37°C in BHIS (37 g/l brain heart infusion broth supplemented with 5 g/l yeast extract and 0.3 g/l cysteine) shaking at 180 rpm for liquid cultures, alternatively with 15 g/l agar for plates, or on Columbia agar with 5% sheep blood (COS, bioMérieux, Nürtingen, Germany). Cultivation was always performed under anaerobic conditions using a COY anaerobic gas chamber (COY Laboratory Products, Grass Lake, United States). The chamber was gas-flushed with 85% N_2, 10% H_2, and 5% CO_2.

Motility With Polyvinylpyrrolidone (PVP) or Mucin

For experiments with high molecular weight polymers K 90 polyvinylpyrrolidone (MW 360,000 g/mol, Carl Roth, Karlsruhe, Germany, order nr. CP15.1) and Type I-S mucin (Bovine Submaxillary glands, Merck, Darmstadt, Germany, order nr. M3895-100MG) was used. From a PVP or Mucin stock solution (see **Supplementary Text 2**), the desired end-concentration of the additive as stated in the experiment was prepared in Dulbecco's phosphate buffered saline (PBS, Merck, Darmstadt, Germany, order nr. D5652) to a volume of 90 μl. The solution was then incubated anaerobically at 37°C for at least 1 h. From a mid-exponential culture (OD_{600} 0.4–0.6) 1 ml was centrifuged at 1,500 × g for 15 min using slow acceleration and deceleration ramps during centrifugation. The supernatant was removed, and the pellet resuspended to an OD_{600} of 6 in anaerobised BHIS. From the bacterial suspension, 10 μl were added to the PVP/Mucin solution for a final volume of 100 μl and OD_{600} of 0.6.

Video Microscopy

Inside the anaerobic chamber, 4 μl of the culture were placed on an objective slide, covered with a cover slip and immediately sealed with nail polish. Except when stated otherwise, slides were recorded 15 min after sealing on a microscope at room temperature with a 10x phase contrast objective (Nikon Eclipse TE2000-S, Nikon PlanFluor 10x). Videos were recorded for 3 min at 30 fps using an Aptina CMOS Sensor 18MP 1/2.3" Colour.

For 64x phase contrast objective movies, a Leica DMR microscope with a PL APO 506082 64x objective was used. Movies were taken with a Nikon D7100 camera at 30 fps.

Single Cell Tracking With YSMR

For quantitative data of the *C. difficile* swimming parameters, we recorded video files and always analysed 10 s of motility parameters per detected bacteria with the aid of the recently developed bacterial tracking programme YSMR (Schwanbeck et al., 2020). We used a low magnification objective (10x) for video recording in order to monitor the swimming behaviour of a large number of bacteria (100–5,000) per video. All videos were analysed using YSMR v0.1.1 using the settings as set in the "**Supplementary 1_tracking.txt**" file.

Turnaround Calculation

Turnarounds were calculated using YSMR v0.1.1. Briefly, turnarounds were determined by calculating the difference in heading direction for two consecutive points. Heading directions were calculated by taking the arctan2 between the original point and one 0.3 s in the future. Turnarounds were calculated to be at positions with a relative angle change of at least 30° and an average minimum speed of at least 0.03 μm/s. The position with the greatest local angle difference was chosen as the turnaround.

Displacement Calculation

The maximum Euclidean distance between any two points reached during the analysed period of the track was calculated.

Calculations, Graphs and Video Editing

All performed calculations and graphs were created using Python 3.9.1, Seaborn 0.11.1 (Waskom, 2021), Matplotlib 3.4.1 (Hunter, 2007), SciPy 1.6.3 (Virtanen et al., 2020), Numpy 1.20.0 (Harris et al., 2020), and Pandas 1.2.1 (McKinney, 2010; Reback et al., 2021). Videos were edited using openCV-contrib-python 4.5.1.48 (Bradski, 2000).

RESULTS

C. difficile Swimming Motility in BHIS Medium

When *C. difficile* 630 Δ*erm* swimming behaviour was analysed in 100% BHIS medium or in a 10% BHIS 90% PBS mixture, the bacteria could be classified into two groups. A fraction of up to 75% was completely non-motile, whereas the motile fraction displayed an unusual motility phenotype, which is characterised by alternating, short, back and forth run phases of 0.5–3 bacterial lengths, corresponding to ∼3–15 μm (**Supplementary Movie 1**). The frequency of directional changes is very high with ∼18 turnarounds/10 s and we thus refer to this behaviour as "jitter motility." None of the bacteria displayed prolonged run phases and there is no substantial net displacement of the bacteria during movement. The motility of further five *C. difficile* strains from different clades was analysed under the same conditions. The clade 5 strain RT078, which is non-flagellated and non-motile in soft-agar assays and lacks a flagellar operon, was as expected completely immotile. All other tested strains, namely 630 Δ*erm* (clade 1), DSM 100002 (clade 1), R20291 (clade 2), DSM 102978 (clade 3), DSM 28670 (clade 4), and DSM 100005 (clade 4) displayed the jitter-motility phenotype in BHIS medium (**Supplementary Movie 1**). When *C. difficile* 630 Δ*erm* motility was analysed in 100% PBS instead of medium containing BHIS, the jitter-motility fraction was absent and bacteria were completely non-motile (data not shown).

The Motility Phenotype Changes in the Presence of the High Molecular Weight Polymers PVP and Mucin

It is well investigated that the motility of bacteria depends on the physical properties of the medium, particularly on the viscosity and on the matrix elasticity (Gao et al., 2014; Martinez et al., 2014). *C. difficile* 630 Δ*erm* cells were exposed to various glycerol concentrations from 0.05 to 25% in BHIS medium in order to increase the viscosity. None of these conditions induced increased displacement and the bacteria remained in their jitter-motility stage.

As *C. difficile* displays motility in agarose (Baban et al., 2013; Courson et al., 2019), we wondered if altering the matrix elasticity of the medium has an influence on the motility phenotype. High molecular weight polymers such as polyvinylpyrrolidone (PVP), which increase the matrix elasticity, were described to enhance motility in various bacteria in a concentration dependent manner (Schneider and Doetsch, 1974; Greenberg and Canale-Parola, 1977). When *C. difficile* was resuspended in a solution containing 3.6% PVP, bacteria displayed a dramatic change in their motility phenotype with long, alternating back and forth runs (**Supplementary Movies 2**, **3**). In this setup, motility could be observed for at least 2 h. When motility was analysed in 3.6% PVP dissolved in pure PBS without any BHIS, cells were completely immotile, suggesting that a nutrient source is required for the observed motility phenotype. We also tested the combination of 3.6% PVP and 10% glycerol in 10% BHIS. The addition of glycerol had no influence on the motility behaviour, indicating that glycerol did not inhibit the PVP-induced motility phenotype with long, alternating back and forth runs.

To exclude the possibility that the observed motility patterns are influenced by the relatively small distance between the microscope slide and the cover slide or the wall effect (Magariyama et al., 2005), we monitored the swimming behaviour also on cavity slides. The same motility pattern as with the original setup was observed for experiments with PVP (**Supplementary Movie 9**).

In order to investigate how common the observed motility phenotype is in *Clostridiodes*, we analyzed representative members from all four motile clades (Griffiths et al., 2010). The PVP-induced change of the motility phenotype occurred in all motile strains that were tested, including 630 Δ*erm* (clade 1, **Supplementary Movies 4–7**), DSM 100002 (clade 1), R20291 (clade 2), DSM 102978 (clade 3), DSM 28670 (clade 4), and DSM 100005 (clade 4) (**Supplementary Movie 8**).

We applied single cell tracking using the recently developed bacterial tracking programme YSMR (Schwanbeck et al., 2020) to analyse and quantify the motility characteristics of *C. difficile* (see **Supplementary Videos 5–7**). Per track we quantified the average speed, maximal displacement to body length ratio, arc-chord

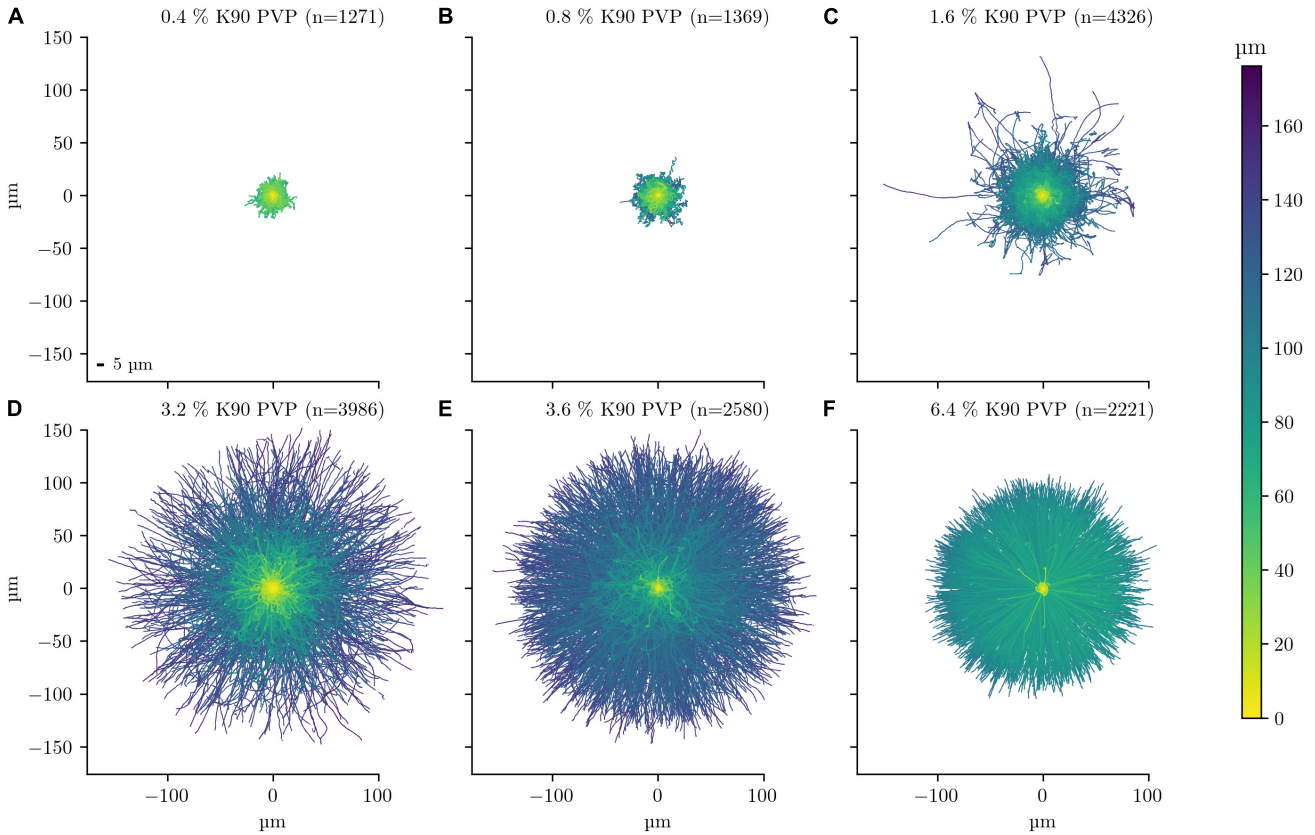

FIGURE 1 | Single cell motility dependency on PVP of *C. difficile* 630 Δ*erm*. The motility of *C. difficile* cells was tracked in the presence of six increasing K90 PVP concentrations (w/v) from 0.4 to 6.4% **(A–F)**. All observation durations were limited to 10 s for better comparability. The number of displayed tracks is stated in the title of each experiment. The starting position of each track is at the origin of the plot at position 0 µm/0 µm. The scale is identical for all six plots. Track colours denote the total travelled distance, with a colour bar on the right-hand side as a legend. A 5 µm scale bar is depicted in the lower left of subfigure **(A)**. The median cell lengths of *C. difficile* was determined to be between 4.3 and 5.7 µm (**Supplementary Table 1**).

ratio, and calculated the turnarounds. The displacement/bacterial body length ratio indicates how much ground a bacterium covered in relation to its own length. The arc-chord ratio, calculated by dividing the length between start and end point by the total distance travelled, denotes the tortuosity of the bacterial movement, with a straight travel path resulting in an arc-chord ratio of 1.

To provide a graphical overview of the PVP-induced motility change, the track of each bacterium was displayed in a rose plot for an experiment with PVP concentrations in the range between 0.4 and 6.4% (**Figure 1**). More than 1,000 tracks were analysed for each PVP concentration. Each track is displayed with its starting position set to the origin of the coordinate system (0, 0). Additionally, each tracks maximum distance is indicated by its colour. For each track three selected characteristics are displayed in a bivariate scatterplot (**Figure 2**). The arc-chord ratio and average speed of each track are each plotted against the displacement/bacterial length ratio, with individual kernel density estimates for each condition. The experiment was repeated twice on different days and for each biological replicate independent rose and scatter plots were generated (**Supplementary Figures 1–4**).

At 0.4 and 0.8% PVP the average speed of the bacteria increases (median values 3.1–4.7 µm/s and 5.84–8.88 µm/s, respectively, **Table 1**) with a corresponding, albeit small increase in displacement/body length ratio (**Figures 1A,B**, **2**). The motility phenotype at both concentrations is likely still futile, as the bacteria do not achieve notable displacement, with median displacement to length ratios below 1.5 for 0.4% and 2.5 for 0.8% PVP (**Figures 1A,B** and **Table 1**). This also is noticeable in the arc-chord ratios, which are on median between 0.08 and 0.11 (**Figure 2A** and **Table 1**). None of the bacteria revealed run phases of greater than 10 s, as can be seen in samples with higher PVP concentrations.

At 1.6% PVP the first visible shift in the motility phenotype occurs. Several individual bacteria achieve clear displacement (**Figure 1C**), indicating that the increase in PVP starts to form a medium in which *C. difficile* can be motile. Speed at 1.6% PVP is markedly increased in comparison to lower PVP concentrations (**Figure 2B**). On the population level though, bacteria still have a median displacement/bacterial length ratio between 1.3 and 3.8, and median arc-chord ratios between 0.1 and 0.13 (**Table 1**). The fraction of bacteria with continuous runs of at least 10 s was between 13 and 58%.

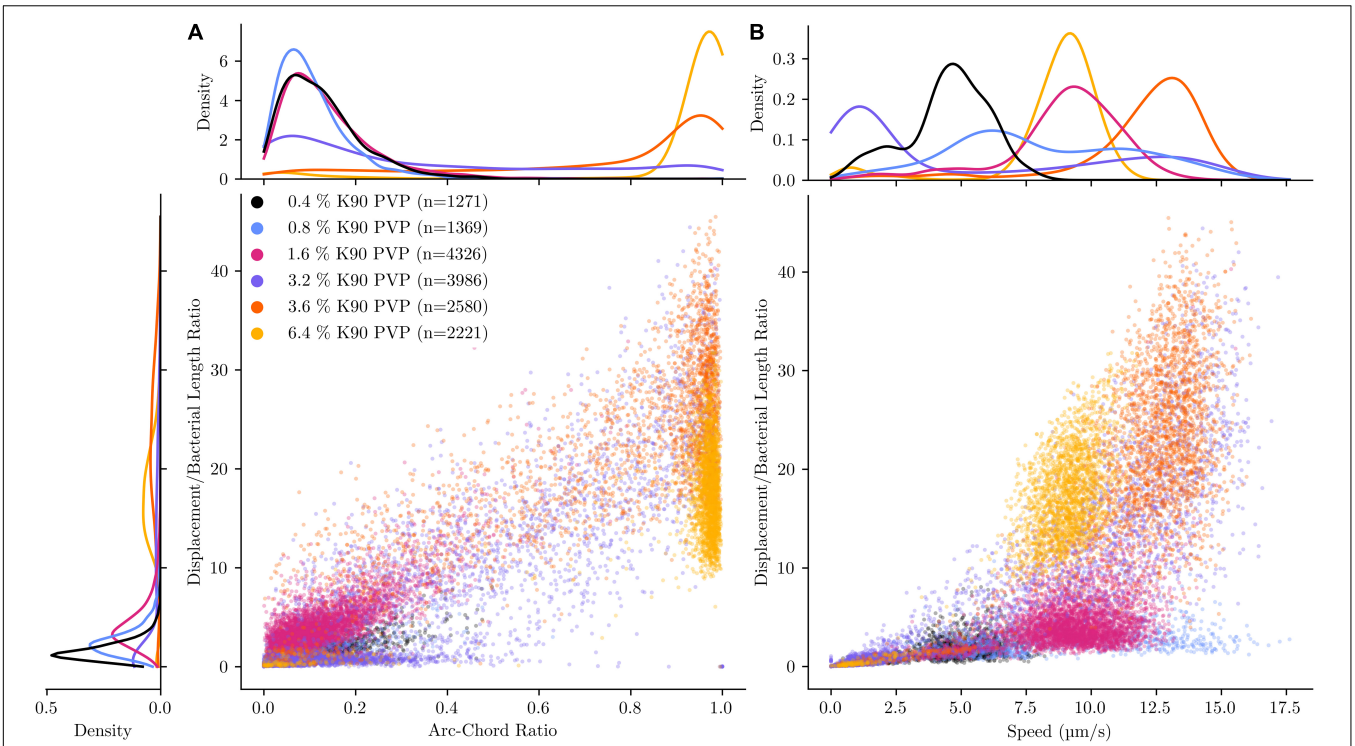

FIGURE 2 | Direct comparison of motility characteristics and statistical distribution within experiments for different PVP concentrations. The motility of *C. difficile* was tracked in the presence of six increasing K90 polyvinylpyrrolidone (PVP) concentrations. The PVP concentration starts at 0.4% and increase at a doubling rate up to 6.4%, with an additional step of 3.6% PVP. All observations were limited to 10 s for better comparability. Average speed **(A)** and arc-chord ratio (**B**, denoting tortuosity of path) are plotted against the displacement/bacterial length ratio (showing the maximal distance in body lengths each bacterium has covered) for each tracked bacterium. The kernel density estimate is plotted independently for each experiment and variable, denoting the distribution for each characteristic.

TABLE 1 | Median values for select properties for different PVP concentrations.

Condition	Median displacement/Bacterial length ratio	Median distance (µm)	Median speed (µm/s)	Median arc-chord ratio
0.4% K90 PVP (*n* = 1,271, 1,300, 1,188)	1.40, 1.38, 0.80	46.69, 46.96, 30.99	4.67, 4.70, 3.10	0.11, 0.10, 0.09
0.8% K90 PVP (*n* = 1,369, 2,486, 2,251)	2.35, 2.41, 1.48	74.84, 88.77, 58.36	7.48, 8.88, 5.84	0.09, 0.09, 0.08
1.6% K90 PVP (*n* = 4,326, 2,448, 2,034)	3.77, 1.26, 2.24	92.67, 38.20, 55.70	9.27, 3.82, 5.57	0.12, 0.10, 0.13
3.2% K90 PVP (*n* = 3,986, 2,626, 2,208)	1.15, 16.57, 12.85	21.24, 109.04, 93.01	2.12, 10.90, 9.30	0.22, 0.90, 0.92
3.6% K90 PVP (*n* = 2,580, 2,416, 2,447)	21.67, 6.29, 5.60	126.28, 58.68, 56.81	12.63, 5.87, 5.68	0.90, 0.47, 0.44
6.4% K90 PVP (*n* = 2,221, 1,454, 328)	16.80, 0.16, 0.07	90.50, 7.70, 5.15	9.05, 0.77, 0.51	0.97, 0.06, 0.03

*Values correspond to **Figure 1** and **Supplementary Figures 1**, **3** (first, second, and third given value, respectively). For a full set, including average, 25 and 75 percentiles for each property, as well as distance, displacement, and bacterial length see **Supplementary Table 1**.*

At PVP concentrations of 3.2% and higher, the majority of *C. difficile* cells display clear motility (**Figures 1C–F**, **2**). Instead of the futile short movements, long, sustained run phases with varying curvature and intermittent turnarounds are the majority. They lead to a motility phenotype that can achieve displacement from the starting position. The motility phenotype is achieving an optimum in terms of displacement/bacterial length ratio, speed, and arc-chord ratio at around 3.2–3.6% (w/v) PVP (**Figures 1D,E**, **2** and **Supplementary Figures 1–4**). The fraction of bacteria with continuous run lengths of at least 10 s was between 67 and 86%.

At a concentration of 6.4% PVP the proportion of motile bacteria decreases in the majority of experiments (**Figures 1F**, **2A** and **Supplementary Figures 1–4**). Bacteria that are still motile display very straight runs with little curvature and a median arc-chord ratio of up to 0.97 (**Table 1**). The fraction of bacteria showing continuous runs of at least 10 s was between 95 and 100%. The speed of motile bacteria is also markedly lower than with 3.6% PVP (**Figure 2** and **Supplementary Figure 2**).

C. difficile inhabits areas with high molecular weight polymers in the larger intestine such as mucins, which cover the epithelial cell layer with a gel like structure (McGuckin et al., 2011; Semenyuk et al., 2015). We used bovine submaxillary gland mucin in concentrations ranging from 2.5 to 40 mg/ml in doubling steps (**Supplementary Movie 3**). The track of each bacterium was displayed in a rose plot from

an experiment with mucin concentrations between 2.5 and 40 mg/ml (**Supplementary Figures 7–9**). At concentrations of 2.5–10 mg/ml, typical short back and forth motion was observed as in medium without PVP or at low PVP concentrations (**Supplementary Figures 7–9A–C**). However, at mucin concentrations of 20 and 40 mg/ml bacteria displays long, alternating back and forth run phases with few turning points and high net displacement (**Supplementary Figures 7–9D,E**).

C. difficile Displays a Distinct Motility Phenotype

Representative tracks from a video (**Supplementary Movie 4**) of *C. difficile* 630 Δ*erm,* as identified by the YSMR software, are shown in **Figure 3A**. The swimming motility phenotype in PVP is characterised by alternating back and forth run phases, which are indistinguishable in length and duration. There is a short stop between two run phases, but there is neither an obvious tumbling nor a sudden reorientation during the stop (**Figures 3A,B**). Nevertheless, the reverse run is not exactly mirroring the previous forward run, but their curvatures can be different. This leads to a significant net displacement of the bacterium during movement.

A manual inspection of bacterial tracks revealed no obvious difference between a forward and a backward run phase. In addition, we performed a thorough quantitative comparison of two motility parameter, speed and arc-chored ratio, before and after a stop phase. We calculated the difference in average speed and in average arc-chored ratio before and after the stop for > 300 of these events and plotted the obtained difference values (**Figure 4**). If back and forth runs possess non-identical motility parameter, a histogram of difference values would show two peaks. In contrast, the histogram shows a typical Gaussian distribution, which is indicative for identical speed values and arc-chord ratios before and after a stop. This confirms that the two run phases between a stop are indistinguishable in their motility parameters.

In summary, this characterisation of the *C. difficile* swimming phenotype reveals a novel motility type for peritrichous bacteria.

DISCUSSION

The Motility of *C. difficile* Is Dependent on Matrix Elasticity

We used single cell video microscopy in conjunction with a software-based quantification of motility parameters to characterise the motility profile of *C. difficile* under various conditions. The applied YSMR software allowed the unbiased and automated analysis of a large number of tracks per frame. It is well investigated that the motility of bacteria depends on the physical properties of the medium in which they move (Gao et al., 2014; Martinez et al., 2014; Bartlett et al., 2017; Taylor et al., 2019). When analysed in regular, water-based media without increased viscosity or matrix elasticity, *C. difficile* displayed a seemingly useless motility phenotype. Moving rapidly back and forth while achieving no notable displacement, the motility seemed to be highly energy intensive, yet ineffectual. It is unclear whether this motility phenotype has any relevance for *C. difficile* physiology and it is possible that it does not occur under natural environmental conditions.

Important physical characteristics shaping the environment include the viscosity, as well as the matrix elasticity of the medium (Gao et al., 2014; Martinez et al., 2014). Viscosity is generally accepted to be a major criterion for bacterial movement, as it plays an overwhelming role in the physics governing motility at the Reynolds number at which bacteria exist (Purcell, 1977). Increasing the medium viscosity by adding glycerol was therefore a logical first step to study motility. However, glycerol, which increases medium viscosity without affecting the matrix elasticity, did not strongly affect the swimming behaviour of *C. difficile* and effective motility could not be observed. In contrast, increase of matrix elasticity by PVP, a long-chained polymer at 360 MDa, or by mucins, both of which can form gel like structures, has a dramatic, concentration dependent effect on the swimming motility of *C. difficile*.

At PVP concentrations of 1.6%, a marked change in motility behaviour becomes visible with long, sustained run phases with varying curvature and intermittent turnarounds starting to appear that result in a net displacement of the bacterium. An optimum in terms of displacement/bacterial length ratio, speed, and arc-chord ratio is achieved at 3.2–3.6% (w/v) PVP. At 6.4% a decrease or complete cessation of movement can be observed, in which the strongly reduced number of motile cells perform very straight runs.

Our findings lead to the conclusion that the motility apparatus in *C. difficile*, across all clades, is adapted to an environment of large, high molarity molecules, which increase the matrix elasticity. Such molecules can be found in the natural environment of *C. difficile*, for example in the mucin-rich lower intestines. Association and interaction of *C. difficile* with the mucosal layer has been researched previously. Its ability to adhere to, and survive in the mucosal layer, as well as its demonstrated presence in the outer mucosal layer during infection, further indicates that the *C. difficile* motility apparatus is specialised for this environment (Tasteyre et al., 2001; Semenyuk et al., 2015; Soavelomandroso et al., 2017). It should be noted that Mucin types differ in their protein and glycosylation patterns. The bovine type I-S mucin used here is different from the human gastrointestinal mucin.

C. difficile Displays a New Swimming Strategy

Depending on the species and the number and location of flagella across the cell body, bacteria use different swimming strategies. At least four different swimming types are described in detail in the literature, but none of them matches the observed *C. difficile* swimming strategy. The swimming pattern of the peritrichous model organism *E. coli* and its regulation are particularly well investigated. *E. coli* switches between a "run" mode and a "tumble" mode (Sarkar et al., 2010). During the run mode, the counter-clockwise rotating flagella form a bundle that pushes the cell forward, leading to a straight swimming phase. In the "tumble" mode the clockwise rotation

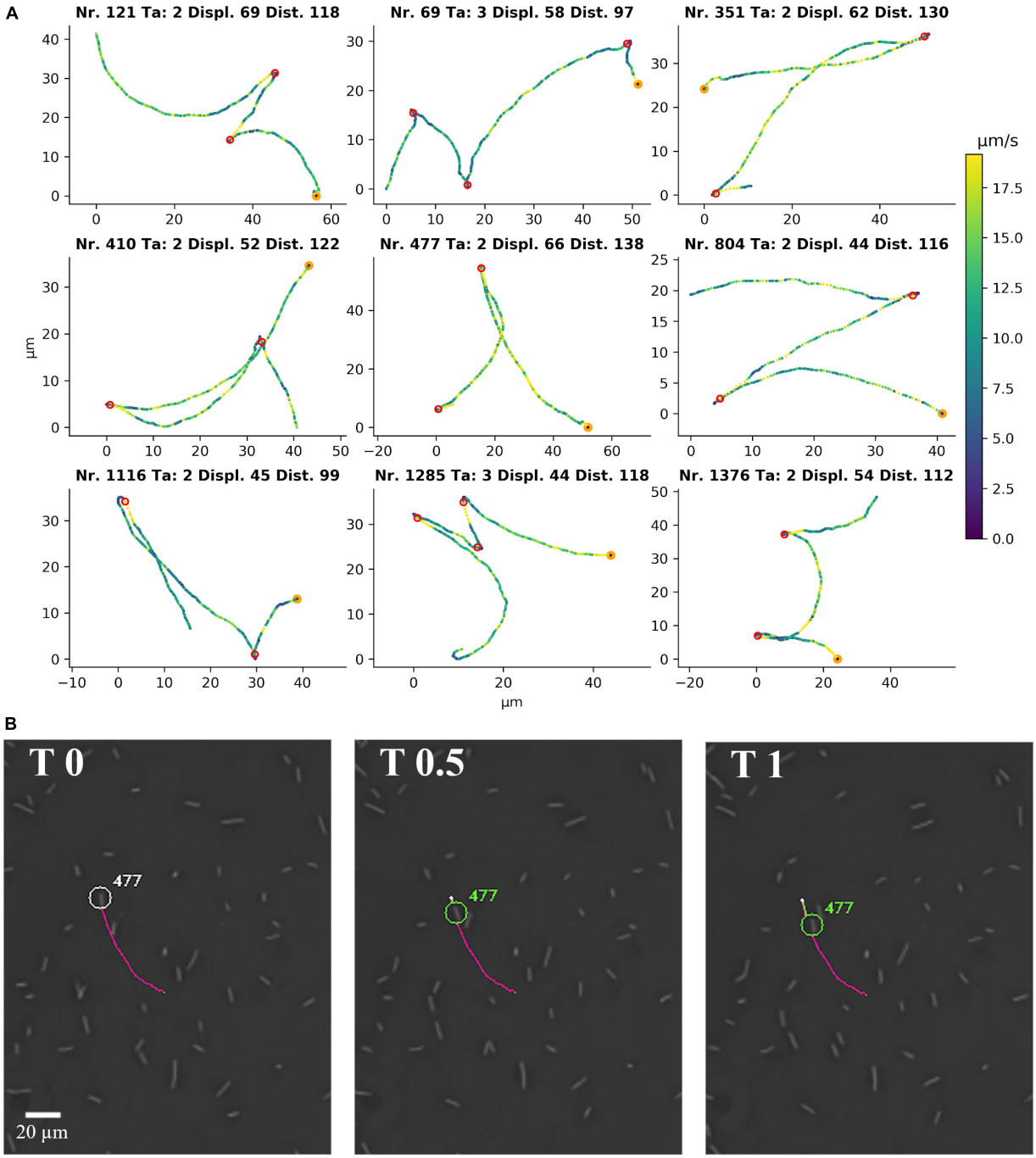

FIGURE 3 | Single cell motility of *C. difficile* 630 Δ*erm* in 1.8% PVP. **(A)** Representative single cell tracks from **Supplementary Movie 4** as detected by YSMR. Titles denote track number, number of turnarounds (Ta), displacement (Displ., µm), and total distance covered (Dist., µm). Colour of the positions indicates current speed in µm/s, with a colour bar on the right for reference. The start of the track is marked in orange. Red circles show the calculated positions of turnarounds. The bacteria associated with the displayed tracks are labelled in **Supplementary Movie 4**. The formation of tracks is shown in **Supplementary Movie 4** by the extension of a coloured line behind the respective bacterium. **(B)** A picture sequence taken from **Supplementary Movie 4** shows the first turnaround of track number 477, starting with the turnaround itself (T 0 s) and images at 0.5 and 1 s after the turnaround. The picture sequence shows the start of the backward movement without previous reorientation at the turnaround.

of flagella leads to a breakup of the flagellar bundle, followed by a random change of the cell orientation. Bacteria with a single flagellum, such as *Vibrio alginolyticus* and *Rhodobacter sphaeroides*, possess different swimming patterns. *V. alginolyticus* displays a three-step pattern, in which a forward swimming phase is followed by a reverse swimming phase and a reorientation

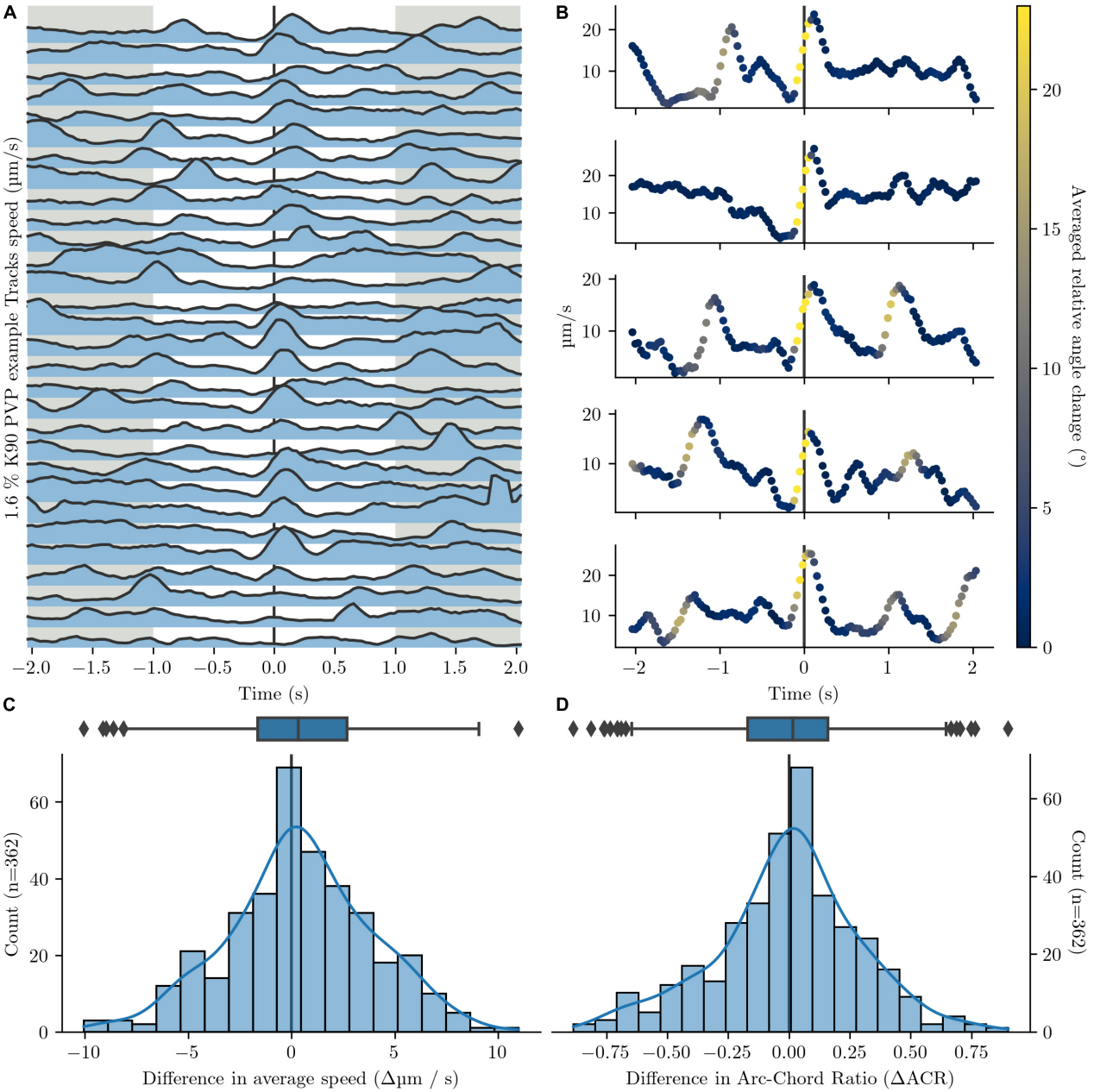

FIGURE 4 | Comparison of speed and arc-chord ratio before and after a turnaround. Events with more than one calculated turnaround within a 4 s window were excluded. Turnarounds are set to the point with local greatest change in angle. Tracks are from **Figure 1C**. **(A)** Speed profile of 30 example tracks before and after a turnaround (black line, $T = 0$). **(B)** Five additional detailed speed graphs before and after turnaround (black line, $T = 0$). The colouration indicates the relative angle change between positions. The speed maximum at or up to 0.5 s after the turnaround ranges between 16.3 and 27.2 µm/s. **(C,D)** Histograms and corresponding box plots on the speed delta **(C)** and arc-chord ratio delta **(D)** before and after turnaround. The deltas are calculated between the time intervals [-2 s, -1 s] and [1 s, 2 s] (grey regions in **A**) around the turnaround.

("flick") phase (Stocker, 2011; Xie et al., 2011). The flagellum of *R. sphaeroides* rotates in only one direction and the motility pattern follows a "stop and coil" pattern (Armitage and Macnab, 1987). Random reorientation occurs when the flagellar rotation stops. *Pseudomonas aeruginosa* performs a run-reverse-pause pattern, where reversals are marked with ∼180° angles. After pauses, the swimming direction does generally not change. Forward and backward travel directions do not differ and are achieved by clockwise or counter-clockwise turning of the single flagellum (Cai et al., 2016). Recently, a similar swimming strategy was identified in the singly flagellated proteobacterium *Caulobacter crescentus*, suggesting that the forward and backward motility pattern is more widely spread than previously expected (Grognot and Taute, 2021a). In fact, the "run and tumble"

strategy of *E. coli* has not been identified for any polar flagellated bacterium (Grognot and Taute, 2021a). *Pseudomonas putida* produces a tuft of flagella on one cell pole. It can switch between a pushing mode, a pulling mode and a wrapping mode, with reorientation taking place during switches in modes (Hintsche et al., 2017).

The PVP-induced *C. difficile* motility pattern appears to be markedly different from those previously described. In particular, an obvious reorientation phase caused by a "tumble" or a "flick" appears to be absent. Instead, *C. difficile* stops in place at the end of a run phase and performs a ∼180° turnaround by changing the movement direction from forward to backward. Turnarounds therefore lead to a direct reversal in direction, but do not play an immediate role in the random reorientation process. While at a first glance this is similar to the polar monotrichous *Pseudomonas aeruginosa*, *C. difficile* has peritrichous flagella, which leads to the question how the reversal is achieved (Lawson et al., 2016; Anjuwon-Foster and Tamayo, 2017). At the beginning of a backward run *C. difficile* travel back on a very similar path as the previous forward run. However, the curvature can change during the course of the backward run, leading to a significant net displacement of the bacterium during movement.

Generally, flagella have an energetically favourable turning direction (Antani et al., 2021). In some species a difference in torque profile based on rotational direction, likely due to stator-rotor interactions, could be shown, which leads to different motility parameter for clockwise/counter-clockwise rotation (Yuan et al., 2010; Minamino et al., 2019). The energetically favourable turning direction can translate into a preferred direction of travel. In *C. difficile*, forward and backward runs are indistinguishable, suggesting that *C. difficile* has no preferred direction of travel. *C. difficile* is able to traverse bi-directional, which appears to be a novel mode of motility for peritrichous bacteria (Grognot and Taute, 2021b). These results suggest that matrix elasticity affects the *C. difficile* flagellar motor rotation state with a strong reduction of switching frequency in an environment of high matrix elasticity. Our findings lead to the conclusion that the motility apparatus in *C. difficile* is adapted to an environment of large, high molarity molecules with the ability for bi-directional motility.

DATA AVAILABILITY STATEMENT

The original contributions presented in the study are included in the article/**Supplementary Material**, further inquiries can be directed to the corresponding author/s.

AUTHOR CONTRIBUTIONS

JS, WB, and IO: conceptualisation, methodology, and validation. JS: software, formal analysis, data curation, and visualisation. JS and IO: investigation. UG, AZ, and WB: resources, supervision, and project administration. JS and WB: writing—original draft preparation. JS, UG, AZ, and WB: writing—review and editing. UG: funding acquisition. All authors contributed to the article and approved the submitted version.

FUNDING

This work was funded by the Federal State of Lower Saxony, Niedersächsisches Vorab (VWZN2889/3215/3266).

ACKNOWLEDGMENTS

We would like to thank Dr. Joachim Schwanbeck for kindly loaning us the camera with which all images and videos were taken.

SUPPLEMENTARY MATERIAL

The Supplementary Material for this article can be found online at: https://www.frontiersin.org/articles/10.3389/fmicb.2021.715220/full#supplementary-material

Supplementary Figure 1 | Single cell motility dependency on PVP of *C. difficile* 630 Δ*erm*. The motility of *C. difficile* cells was tracked in the presence of six increasing K90 PVP concentrations (w/v) from 0.4 to 6.4% **(A–F)**. All observation durations were limited to 10 s for better comparability. The number of displayed tracks is stated in the title of each experiment. The starting position of each track is at the origin of the plot at position 0 μm/0 μm. The scale is identical for all six plots. Track colours denote the total travelled distance, with a colour bar on the right-hand side as a legend. A 5 μm scale bar is depicted in the lower left of subfigure **(A)**. The median cell lengths of *C. difficile* was determined to be between 4.81 and 5.28 μm (**Supplementary Table 1**).

Supplementary Figure 2 | Direct comparison of motility characteristics and statistical distribution within experiments for different PVP concentrations. The motility of *C. difficile* was tracked in the presence of six increasing K90 polyvinylpyrrolidone (PVP) concentrations. The PVP concentration starts at 0.4% and increase at a doubling rate up to 6.4%, with an additional step of 3.6% PVP. All observations were limited to 10 s for better comparability. Average speed **(A)** and arc-chord ratio (**B**, denoting tortuosity of path) are plotted against the displacement/bacterial length ratio (showing the maximal distance in body lengths each bacterium has covered) for each tracked bacterium. The kernel density estimate is plotted independently for each experiment and variable, denoting the distribution for each characteristic.

Supplementary Figure 3 | Single cell motility dependency on PVP of *C. difficile* 630 Δ*erm*. The motility of *C. difficile* cells was tracked in the presence of six increasing K90 PVP concentrations (w/v) from 0.4–6.4% **(A–F)**. All observation durations were limited to 10 s for better comparability. The number of displayed tracks is stated in the title of each experiment. The starting position of each track is at the origin of the plot at position 0 μm/0 μm. The scale is identical for all six plots. Track colours denote the total travelled distance, with a colour bar on the right-hand side as a legend. A 5 μm scale bar is depicted in the lower left of subfigure **(A)**. The median cell lengths of *C. difficile* was determined to be between 4.99 and 5.74 μm (**Supplementary Table 1**).

Supplementary Figure 4 | Direct comparison of motility characteristics and statistical distribution within experiments for different PVP concentrations. The motility of *C. difficile* was tracked in the presence of six increasing K90 polyvinylpyrrolidone (PVP) concentrations. The PVP concentration starts at 0.4% and increase at a doubling rate up to 6.4%, with an additional step of 3.6% PVP. All observations were limited to 10 s for better comparability. Average speed **(A)** and arc-chord ratio (**B**, denoting tortuosity of path) are plotted against the displacement/bacterial length ratio (showing the maximal distance in body lengths each bacterium has covered) for each tracked bacterium. The kernel density estimate is plotted independently for each experiment and variable, denoting the distribution for each characteristic.

Supplementary Figure 5 | Comparison of speed and arc-chord ratio before and after a turnaround. Events with more than one calculated turnaround within a 4 s window were excluded. Turnarounds are set to the point with local greatest change in angle. Tracks are from **Figure 1C**. **(A)** speed profile of 30 example tracks before and after a turnaround (black line, *T*=0). **(B)** Five additional detailed speed graphs before and after turnaround (black line, *T*=0). The colouration indicates the relative angle change between positions. The speed maximum at or up to 0.5 s after the turnaround ranges between 7.6 and 19.3 μm/s. **(C,D)** Histograms and corresponding box plots on the speed delta **(C)** and arc-chord ratio delta **(D)** before and after turnaround. The deltas are calculated between the time intervals [-2 s, -1 s] and [1 s, 2 s] (grey regions in **A**) around the turnaround.

Supplementary Figure 6 | Comparison of speed and arc-chord ratio before and after a turnaround. Events with more than one calculated turnaround within a 4 s window were excluded. Turnarounds are set to the point with local greatest change in angle. Tracks are from **Figure 1C**. **(A)** speed profile of 30 example tracks before and after a turnaround (black line, *T*=0). **(B)** Five additional detailed speed graphs before and after turnaround (black line, *T*=0). The colouration indicates the relative angle change between positions. The speed maximum at or up to 0.5 s after the turnaround ranges between 2.5 and 20.0 μm/s. **(C,D)** Histograms and corresponding box plots on the speed delta **(C)** and arc-chord ratio delta **(D)** before and after turnaround. The deltas are calculated between the time intervals [-2 s, -1 s] and [1 s, 2 s] (grey regions in **A**) around the turnaround.

Supplementary Figure 7 | Single cell motility dependency on mucin concentration of *C. difficile* 630 Δ*erm*. The motility of *C. difficile* cells was tracked in the presence of 5 increasing mucin concentrations. The mucin concentration starts at 2.5 mg/ml and increases in doubling steps up to 40 mg/ml **(A–E)**. The number of observations is stated in the title of each experiment. All observation durations were limited to 10 s for better comparability. The starting position of single *C. difficile* tracks are centred on the origin. The scale is identical for all six plots. Track colours denote the total travelled distance, with a colour bar on the right-hand side as a legend. A 5 μm scale bar is depicted in the lower left of subfigure **(A)**.

Supplementary Figure 8 | Single cell motility dependency on mucin concentration of *C. difficile* 630 Δ*erm*. The motility of *C. difficile* cells was tracked in the presence of 5 increasing mucin concentrations. The mucin concentration starts at 2.5 mg/ml and increases in doubling steps up to 40 mg/ml **(A–E)**. The number of observations is stated in the title of each experiment. All observation durations were limited to 10 s for better comparability. The starting position of single *C. difficile* tracks are centred on the origin. The scale is identical for all six plots. Track colours denote the total travelled distance, with a colour bar on the right-hand side as a legend. A 5 μm scale bar is depicted in the lower left of subfigure **(A)**.

Supplementary Figure 9 | Single cell motility dependency on mucin concentration of *C. difficile* 630 Δ*erm*. The motility of *C. difficile* cells was tracked in the presence of 5 increasing mucin concentrations. The mucin concentration starts at 2.5 mg/ml and increases in doubling steps up to 40 mg/ml **(A–E)**. The number of observations is stated in the title of each experiment. All observation durations were limited to 10 s for better comparability. The starting position of single *C. difficile* tracks are centred on the origin. The scale is identical for all six plots. Track colours denote the total travelled distance, with a colour bar on the right-hand side as a legend. A 5 μm scale bar is depicted in the lower left of subfigure **(A)**.

Supplementary Table 1 | Various statistics on individual experiments. Values are given as: average (25 % quantile, median, 75 % quantile). N: number of observations.

Supplementary Movie 1 | Motility of various *C. difficile* strains in BHIS without PVP. Video was taken with a 10x objective and converted to inverted grey-scale while filming. Shown are 630 Δ*erm* (clade 1), DSM 100002 (clade 1), R20291 (clade 2), DSM 102978 (clade 3), DSM 28670 (clade 4), and DSM 100005 (clade 4) in 100% BHIS.

Supplementary Movie 2 | Motility in 10% BHIS/PBS with 3.6% PVP. The video of *C. difficile* 630 Δ*erm* was taken with a 64x objective.

Supplementary Movie 3 | Motility in 10% BHIS/PBS with 2.5–40 mg/ml Mucin. Shown are excerpts of movies used in **Supplementary Figure 7**. The video of *C. difficile* 630 Δ*erm* was taken with a 10x objective and converted to inverted grey-scale while filming.

Supplementary Movie 4 | Motility in 10% BHIS/PBS with 1.8% PVP and annotated tracks. The video of *C. difficile* 630 Δ*erm* was taken with a 10x objective and converted to inverted grey-scale while filming. Examples of tracks are depicted in **Figure 3**.

Supplementary Movie 5 | Parts of Movies used in **Figures 1**, **2**. The videos of *C. difficile* 630 Δ*erm* were taken with a 10x objective and converted to inverted grey-scale while filming. Shown are excerpts of movies of *C. difficile* 630 Δ*erm* in increasing PVP concentrations.

Supplementary Movie 6 | Parts of Movies used in **Supplementary Figures 1**, **2**. The videos of *C. difficile* 630 Δ*erm* were taken with a 10x objective and converted to inverted grey-scale while filming. Shown are excerpts of movies of *C. difficile* 630 Δ*erm* in increasing PVP concentrations.

Supplementary Movie 7 | Parts of Movies used in **Supplementary Figures 3**, **4**. The videos of *C. difficile* 630 Δ*erm* were taken with a 10x objective and converted to inverted grey-scale while filming. Shown are excerpts of movies of *C. difficile* 630 Δ*erm* in increasing PVP concentrations.

Supplementary Movie 8 | Motility of various *C. difficile* strains in BHIS with PVP. The videos were taken with a 10x objective and converted to inverted grey-scale while filming. Shown are DSM 100002 (clade 1), R20291 (clade 2), DSM 102978 (clade 3), DSM 28670 (clade 4), and DSM 100005 (clade 4) with 2% (w/v) PVP.

Supplementary Text 1 | Settings-file used for YSMR. "**Supplementary_text 1_tracking.txt**".

Supplementary Text 2 | Mucin/PVP handling and storage.

REFERENCES

Anjuwon-Foster, B. R., and Tamayo, R. (2017). A genetic switch controls the production of flagella and toxins in *Clostridium difficile*. *PLoS Genet.* 13:e1006701. doi: 10.1371/journal.pgen.1006701

Antani, J. D., Sumali, A. X., Lele, T. P., and Lele, P. P. (2021). Asymmetric random walks reveal that the chemotaxis network modulates flagellar rotational bias in *Helicobacter pylori*. *eLife* 10:e63936. doi: 10.7554/eLife.63936

Armitage, J. P., and Macnab, R. M. (1987). Unidirectional, intermittent rotation of the flagellum of *Rhodobacter sphaeroides*. *J. Bacteriol.* 169, 514–518. doi: 10.1128/JB.169.2.514-518.1987

Baban, S. T., Kuehne, S. A., Barketi-Klai, A., Cartman, S. T., Kelly, M. L., Hardie, K. R., et al. (2013). The Role of Flagella in *Clostridium difficile* Pathogenesis: Comparison between a Non-Epidemic and an Epidemic Strain. *PLoS One* 8:e73026. doi: 10.1371/journal.pone.0073026

Bartlett, T. M., Bratton, B. P., Duvshani, A., Miguel, A., Sheng, Y., Martin, N. R., et al. (2017). A periplasmic polymer curves *Vibrio cholerae* and promotes pathogenesis. *Cell* 168, 172.e–185.e. doi: 10.1016/j.cell.2016.12.019

Batah, J., Kobeissy, H., Bui Pham, P. T., Denève-Larrazet, C., Kuehne, S., Collignon, A., et al. (2017). *Clostridium difficile* flagella induce a pro-inflammatory response in intestinal epithelium of mice in cooperation with toxins. *Sci. Rep.* 7:3256. doi: 10.1038/s41598-017-03621-z

Boin, M. A., Austin, M. J., and Hāď se, C. C. (2004). Chemotaxis in *Vibrio cholerae*. *FEMS Microbiol. Lett.* 239, 1–8. doi: 10.1016/j.femsle.2004.08.039

Bradski, G. (2000). The OpenCV Library. *Dr. Dobbs J. Softw. Tools* 120, 122–125.

Buffie, C. G., and Pamer, E. G. (2013). Microbiota-mediated colonization resistance against intestinal pathogens. *Nat. Rev. Immunol.* 13, 790–801. doi: 10.1038/nri3535

Cai, Q., Li, Z., Ouyang, Q., Luo, C., and Gordon, V. D. (2016). Singly Flagellated *Pseudomonas aeruginosa* Chemotaxes Efficiently by Unbiased Motor Regulation. *mBio* 7, e00013–e16. doi: 10.1128/mBio.00013-16

Chandrasekaran, R., and Lacy, D. B. (2017). The role of toxins in *Clostridium difficile* infection. *FEMS Microbiol. Rev.* 41, 723–750. doi: 10.1093/femsre/fux048

Courson, D. S., Pokhrel, A., Scott, C., Madrill, M., Rinehold, A. J., Tamayo, R., et al. (2019). Single cell analysis of nutrient regulation of *Clostridioides* (*Clostridium*) *difficile* motility. *Anaerobe* 59, 205–211. doi: 10.1016/j.anaerobe.2019.102080

Dannheim, H., Riedel, T., Neumann-Schaal, M., Bunk, B., Schober, I., Spröer, C., et al. (2017). Manual curation and reannotation of the genomes of *Clostridium difficile* 630Δ*erm* and *C. difficile* 630. *J. Med. Microbiol.* 66, 286–293. doi: 10.1099/jmm.0.000427

Gao, Y., Neubauer, M., Yang, A., Johnson, N., Morse, M., Li, G., et al. (2014). Altered motility of *Caulobacter crescentus* in viscous and viscoelastic media. *BMC Microbiol.* 14:322. doi: 10.1186/s12866-014-0322-3

Gómez, S., Chaves, F., and Orellana, M. A. (2017). Clinical, epidemiological and microbiological characteristics of relapse and re-infection in *Clostridium difficile* infection. *Anaerobe* 48, 147–151. doi: 10.1016/j.anaerobe.2017.08.012

Greenberg, E. P., and Canale-Parola, E. (1977). Motility of flagellated bacteria in viscous environments. *J. Bacteriol.* 132, 356–358. doi: 10.1128/JB.132.1.356-358.1977

Griffiths, D., Fawley, W., Kachrimanidou, M., Bowden, R., Crook, D. W., Fung, R., et al. (2010). Multilocus Sequence Typing of *Clostridium difficile*. *J. Clin. Microbiol.* 48, 770–778. doi: 10.1128/JCM.01796-09

Grognot, M., and Taute, K. M. (2021a). A multiscale 3D chemotaxis assay reveals bacterial navigation mechanisms. *Commun. Biol.* 4:669. doi: 10.1038/s42003-021-02190-2

Grognot, M., and Taute, K. M. (2021b). More than propellers: how flagella shape bacterial motility behaviors. *Curr. Opin. Microbiol.* 61, 73–81. doi: 10.1016/j.mib.2021.02.005

Harris, C. R., Millman, K. J., van der Walt, S. J., Gommers, R., Virtanen, P., Cournapeau, D., et al. (2020). Array programming with NumPy. *Nature* 585, 357–362. doi: 10.1038/s41586-020-2649-2

Hintsche, M., Waljor, V., Großmann, R., Kühn, M. J., Thormann, K. M., Peruani, F., et al. (2017). A polar bundle of flagella can drive bacterial swimming by pushing, pulling, or coiling around the cell body. *Sci. Rep.* 7:16771. doi: 10.1038/s41598-017-16428-9

Hunter, J. D. (2007). Matplotlib: A 2D Graphics Environment. *Comput. Sci. Eng.* 9, 90–95. doi: 10.1109/MCSE.2007.55

Johansson, M. E. V., Larsson, J. M. H., and Hansson, G. C. (2011). The two mucus layers of colon are organized by the MUC2 mucin, whereas the outer layer is a legislator of host-microbial interactions. *Proc. Natl. Acad. Sci.* 108, 4659–4665. doi: 10.1073/pnas.1006451107

Just, I., Selzer, J., Wilm, M., Eichel-Streiber, C., von, Mann, M., et al. (1995). Glucosylation of Rho proteins by *Clostridium difficile* toxin B. *Nature* 375, 500–503. doi: 10.1038/375500a0

Korolik, V. (2019). The role of chemotaxis during *Campylobacter jejuni* colonisation and pathogenesis. *Curr. Opin. Microbiol.* 47, 32–37. doi: 10.1016/j.mib.2018.11.001

Kuehne, S. A., Cartman, S. T., Heap, J. T., Kelly, M. L., Cockayne, A., and Minton, N. P. (2010). The role of toxin A and toxin B in *Clostridium difficile* infection. *Nature* 467, 711–713. doi: 10.1038/nature09397

Lai, S. K., Wang, Y.-Y., Wirtz, D., and Hanes, J. (2009). Micro- and macrorheology of mucus. *Adv. Drug Deliv. Rev.* 61, 86–100. doi: 10.1016/j.addr.2008.09.012

Lawson, P. A., Citron, D. M., Tyrrell, K. L., and Finegold, S. M. (2016). Reclassification of *Clostridium difficile* as *Clostridioides difficile* (Hall and O'Toole 1935) Prévot 1938. *Anaerobe* 40, 95–99. doi: 10.1016/j.anaerobe.2016.06.008

Leffler, D. A., and Lamont, J. T. (2015). *Clostridium difficile* Infection. *N. Engl. J. Med.* 372, 1539–1548. doi: 10.1056/NEJMra1403772

Lertsethtakarn, P., Ottemann, K. M., and Hendrixson, D. R. (2011). Motility and Chemotaxis in *Campylobacter* and *Helicobacter*. *Annu. Rev. Microbiol.* 65, 389–410. doi: 10.1146/annurev-micro-090110-102908

Lessa, F. C., Mu, Y., Bamberg, W. M., Beldavs, Z. G., Dumyati, G. K., Dunn, J. R., et al. (2015). Burden of *Clostridium difficile* Infection in the United States. *N. Engl. J. Med.* 372, 825–834. doi: 10.1056/NEJMoa1408913

Magariyama, Y., Ichiba, M., Nakata, K., Baba, K., Ohtani, T., Kudo, S., et al. (2005). Difference in Bacterial Motion between Forward and Backward Swimming Caused by the Wall Effect. *Biophys. J.* 88, 3648–3658. doi: 10.1529/biophysj.104.054049

Martinez, V. A., Schwarz-Linek, J., Reufer, M., Wilson, L. G., Morozov, A. N., and Poon, W. C. K. (2014). Flagellated bacterial motility in polymer solutions. *Proc. Natl. Acad. Sci.* 111, 17771–17776. doi: 10.1073/pnas.1415460111

Matilla, M. A., and Krell, T. (2018). The effect of bacterial chemotaxis on host infection and pathogenicity. *FEMS Microbiol. Rev.* 42:fux052. doi: 10.1093/femsre/fux052

McGuckin, M. A., Lindén, S. K., Sutton, P., and Florin, T. H. (2011). Mucin dynamics and enteric pathogens. *Nat. Rev. Microbiol.* 9, 265–278. doi: 10.1038/nrmicro2538

McKinney, W. (2010). "Data Structures for Statistical Computing in Python," in *Proceedings of the Python in Science Conference*, (Austin: Python in Science Conference), doi: 10.25080/Majora-92bf1922-00a

Minamino, T., Kinoshita, M., and Namba, K. (2019). Directional Switching Mechanism of the Bacterial Flagellar Motor. *Comput. Struct. Biotechnol. J.* 17, 1075–1081. doi: 10.1016/j.csbj.2019.07.020

Porter, S. L., Wadhams, G. H., and Armitage, J. P. (2011). Signal processing in complex chemotaxis pathways. *Nat. Rev. Microbiol.* 9, 153–165. doi: 10.1038/nrmicro2505

Purcell, E. M. (1977). Life at low Reynolds number. *Am. J. Phys.* 45, 3–11. doi: 10.1119/1.10903

Reback, J., McKinney, W., Jbrockmendel, Bossche, J. V. D., Augspurger, T., Cloud, P., et al. (2021). *pandas-dev/pandas: Pandas 1.2.1*. San Francisco: GitHub, doi: 10.5281/ZENODO.4452601

Riedel, T., Wetzel, D., Hofmann, J. D., Plorin, S. P. E. O., Dannheim, H., Berges, M., et al. (2017). High metabolic versatility of different toxigenic and non-toxigenic *Clostridioides difficile* isolates. *Int. J. Med. Microbiol.* 307, 311–320. doi: 10.1016/j.ijmm.2017.05.007

Sarkar, M. K., Paul, K., and Blair, D. (2010). Chemotaxis signaling protein CheY binds to the rotor protein FliN to control the direction of flagellar rotation in *Escherichia coli*. *Proc. Natl. Acad. Sci.* 107, 9370–9375. doi: 10.1073/pnas.1000935107

Schneider, W. R., and Doetsch, R. N. (1974). Effect of Viscosity on Bacterial Motility. *J. Bacteriol.* 117, 696–701. doi: 10.1128/JB.117.2.696-701.1974

Schwanbeck, J., Oehmig, I., Dretzke, J., Zautner, A. E., Groß, U., and Bohne, W. (2020). YSMR: a video tracking and analysis program for bacterial motility. *BMC Bioinformatics* 21:166. doi: 10.1186/s12859-020-3495-9

Semenyuk, E. G., Poroyko, V. A., Johnston, P. F., Jones, S. E., Knight, K. L., Gerding, D. N., et al. (2015). Analysis of Bacterial Communities during *Clostridium difficile* Infection in the Mouse. *Infect. Immun.* 83, 4383–4391. doi: 10.1128/IAI.00145-15

Soavelomandroso, A. P., Gaudin, F., Hoys, S., Nicolas, V., Vedantam, G., Janoir, C., et al. (2017). Biofilm Structures in a Mono-Associated Mouse Model of *Clostridium difficile* Infection. *Front. Microbiol.* 8:2086. doi: 10.3389/fmicb.2017.02086

Stecher, B., Hapfelmeier, S., Müller, C., Kremer, M., Stallmach, T., and Hardt, W.-D. (2004). Flagella and Chemotaxis Are Required for Efficient Induction of *Salmonella enterica* Serovar Typhimurium Colitis in Streptomycin-Pretreated Mice. *Infect. Immun.* 72, 4138–4150. doi: 10.1128/IAI.72.7.4138-4150.2004

Stocker, R. (2011). Reverse and flick: Hybrid locomotion in bacteria. *Proc. Natl. Acad. Sci.* 108, 2635–2636. doi: 10.1073/pnas.1019199108

Tasteyre, A., Barc, M.-C., Collignon, A., Boureau, H., and Karjalainen, T. (2001). Role of FliC and FliD Flagellar Proteins of *Clostridium difficile* in Adherence and Gut Colonization. *Infect. Immun.* 69, 7937–7940. doi: 10.1128/IAI.69.12.7937-7940.2001

Taylor, J. A., Sichel, S. R., and Salama, N. R. (2019). Bent Bacteria: A Comparison of Cell Shape Mechanisms in *Proteobacteria*. *Annu. Rev. Microbiol.* 73, 457–480. doi: 10.1146/annurev-micro-020518-115919

Theriot, C. M., and Young, V. B. (2015). Interactions Between the Gastrointestinal Microbiome and *Clostridium difficile*. *Annu. Rev. Microbiol.* 69, 445–461. doi: 10.1146/annurev-micro-091014-104115

Twine, S. M., Reid, C. W., Aubry, A., McMullin, D. R., Fulton, K. M., Austin, J., et al. (2009). Motility and Flagellar Glycosylation in *Clostridium difficile*. *J. Bacteriol.* 191, 7050–7062. doi: 10.1128/JB.00861-09

Virtanen, P., Gommers, R., Oliphant, T. E., Haberland, M., Reddy, T., et al. (2020). SciPy 1.0: fundamental algorithms for scientific computing in Python. *Nat. Methods* 17, 261–272. doi: 10.1038/s41592-019-0686-2

Waskom, M. (2021). seaborn: statistical data visualization. *J. Open Source Softw.* 6:3021. doi: 10.21105/joss.03021

Xie, L., Altindal, T., Chattopadhyay, S., and Wu, X.-L. (2011). Bacterial flagellum as a propeller and as a rudder for efficient chemotaxis. *Proc. Natl. Acad. Sci.* 108, 2246–2251. doi: 10.1073/pnas.1011953108

Yuan, J., Fahrner, K. A., Turner, L., and Berg, H. C. (2010). Asymmetry in the clockwise and counterclockwise rotation of the bacterial flagellar motor. *Proc. Natl. Acad. Sci.* 107, 12846–12849. doi: 10.1073/pnas.1007333107

Conflict of Interest: The authors declare that the research was conducted in the absence of any commercial or financial relationships that could be construed as a potential conflict of interest.

Copyright © 2021 Schwanbeck, Oehmig, Groß, Zautner and Bohne. This is an open-access article distributed under the terms of the Creative Commons Attribution License (CC BY). The use, distribution or reproduction in other forums is permitted, provided the original author(s) and the copyright owner(s) are credited and that the original publication in this journal is cited, in accordance with accepted academic practice. No use, distribution or reproduction is permitted which does not comply with these terms.

frontiers in Microbiology

ORIGINAL RESEARCH
published: 14 September 2021
doi: 10.3389/fmicb.2021.725612

The Binary Toxin of *Clostridioides difficile* Alters the Proteome and Phosphoproteome of HEp-2 Cells

Florian Stieglitz[1,2], *Ralf Gerhard*[1] *and Andreas Pich*[1,2]*

[1] Institute of Toxicology, Hannover Medical School, Hanover, Germany, [2] Core Facility Proteomics, Hannover Medical School, Hanover, Germany

Clostridioides difficile is a major cause of nosocomial infection worldwide causing antibiotic-associated diarrhea and some cases are leading to pseudomembranous colitis. The main virulence factors are toxin A and toxin B. Hypervirulent strains of *C. difficile* are linked to higher mortality rates and most of these strains produce additionally the *C. difficile* binary toxin (CDT) that possesses two subunits, CDTa and CDTb. The latter is responsible for binding and transfer of CDTa into the cytoplasm of target cells; CDTa is an ADP ribosyltransferase catalyzing the modification of actin fibers that disturbs the actin vs microtubule balance and induces microtubule-based protrusions of the cell membrane increasing the adherence of *C. difficile*. The underlying mechanisms remain elusive. Thus, we performed a screening experiment using MS-based proteomics and phosphoproteomics techniques. Epithelial Hep-2 cells were treated with CDTa and CDTb in a multiplexed study for 4 and 8 h. Phosphopeptide enrichment was performed using affinity chromatography with TiO2 and Fe-NTA; for quantification, a TMT-based approach and DDA measurements were used. More than 4,300 proteins and 5,600 phosphosites were identified and quantified at all time points. Although only moderate changes were observed on proteome level, the phosphorylation level of nearly 1,100 phosphosites responded to toxin treatment. The data suggested that CSNK2A1 might act as an effector kinase after treatment with CDT. Additionally, we confirmed ADP-ribosylation on Arg-177 of actin and the kinetic of this modification for the first time.

Keywords: binary toxin, *Clostridioides difficile*, proteome, phosphoproteome, signaling

OPEN ACCESS

Edited by:
Dieter Jahn,
Technische Universitat Braunschweig, Germany

Reviewed by:
Panagiotis Papatheodorou,
Ulm University Medical Center, Germany
William Petri,
University of Virginia, United States
Boonhiang Promdonkoy,
National Science and Technology Development Agency (NSTDA), Thailand

***Correspondence:**
Andreas Pich
pich.andreas@mh-hannover.de

Specialty section:
This article was submitted to Infectious Diseases, a section of the journal Frontiers in Microbiology

Received: *16 June 2021*
Accepted: *09 August 2021*
Published: *14 September 2021*

Citation:
Stieglitz F, Gerhard R and Pich A (2021) The Binary Toxin of Clostridioides difficile Alters the Proteome and Phosphoproteome of HEp-2 Cells. Front. Microbiol. 12:725612. doi: 10.3389/fmicb.2021.725612

INTRODUCTION

Clostridioides difficile infections are with 223,900 cases in hospitalized patients in 2017, a significant cause for nosocomial infections, and classified by the Centers for Disease Control and Prevention as an urgent threat with 12,800 deaths in 2017 in the United States (Centers for Disease Control and Prevention, 2019). The main virulence factors of *C. difficile* are the large glycosylating toxins TcdA and TcdB that target small GTPases of the Ras and Rho subfamily. Our group studied the

Abbreviations: DDA, Data-dependent acquisition; CID, Collision-induced dissociation; HCD, Higher-energy-collisional-dissociation; TMT, Tandem mass tags; PCA, Principal component analysis; IPA™, Ingenuity Pathway Analysis™; ACN, Acetonitrile; AGC, Automatic gain control.

effects of TcdA and TcdB on target cells concerning the glycosyltransferases effect via proteomic experiments. Both toxins alter the proteome of colonic cells in a time-dependent manner and effect proteins that are involved in cellular functions related to the cytopathic and cytotoxic effect of the large glucosylating toxins. Mutant TcdA with impaired glucosyltransferase activity showed no effect on the proteome of target cells; in contrast, glucosyltransferase inactive TcdB induces in epithelial cells (HEp2) a process called pyknosis that is accompanied by extensive alterations on the proteome level (Zeiser et al., 2011, 2013; Jochim et al., 2014; Erdmann et al., 2017; Junemann et al., 2017).

In recent years hypervirulent strains of *C. difficile* (e.g., NAP1/BI/027) emerged that produce additionally the binary toxin (CDT; Aktories et al., 2018). Up to 30% of clinical isolates that produce the binary toxin are linked to increased morbidity and mortality rates (Abeyawardhane et al., 2021). CDT belongs to the iota toxin family and consists of two separated subunits, the catalytically active CDTa and the pore-forming CDTb. CDT acts differently from TcdA and TcdB by ribosylating G-actin directly, subsequently prohibiting the prolongation of the F-actin, leading to depolymerization of F-actin and an imbalance of the actin microtubule homeostasis. While the actin cytoskeleton collapses, the cells form protrusions based on microtubule polymerization (Schwan et al., 2009). It has been advocated that the microtubule-based protrusions were beneficial for attachment of *C. difficile* to the epithelia. Septins play a significant role in this process since they are the primary driver of microtubule polymerization guidance (Schwan et al., 2009). Recent studies have shown that the knockout of septin prohibits microtubule-based protrusions and CDC42 involvement in septin regulation (Nölke et al., 2016). However, the underlying mechanism of microtubule stabilization and general cell response to CDT remains elusive. It has always been assumed that CDT ribosylates actin on Arg-177 like other iota-type toxins, but it has never been directly shown while general actin ribosylation by CDT has been proven (Vandekerckhove et al., 1987; Gülke et al., 2001).

This study investigated the fundamental mechanism in the cell response to CDT treatment of human epithelial cells (HEp-2) by LC-MS-based proteomics utilizing a tandem mass tags (TMT)-based phosphoproteomic approach. In a two-timepoint experiment, a detailed global phosphoproteomic analysis was carried out, and the catalytical active subunit of casein kinase 2 alpha (CSNK2A1) emerged as a potential upstream regulator of microtubule protrusions and a general regulator in the CDT response. Furthermore, we could prove for the first time CDT-mediated actin ribosylation on Arg-177.

MATERIALS AND METHODS

Cell Culture

From HeLa cells, derived cell line HEp-2 was maintained in a 75 cm^2 flask in a humidified atmosphere at 37°C and 5% CO_2. Cells were cultured in minimal essential medium supplemented with 10% fetal bovine serum, 100 U/mL penicillin, and 100 U/mL streptomycin. Depending on confluency, the cells were split to maintain vitality.

Toxin Treatment of HEp-2 Cells and Sample Preparation

Two days before toxin treatment, 7.5×10^5 cells were seeded in 10 cm dishes to achieve a 75% confluency on the day of toxin treatment. CDTa and CDTb were generated using an *Escherichia coli* expression system as previously described (Beer et al., 2018). Cells were treated with 1.5 μg/mL CDTa and 3 μg/mL CDTb. Changes in the morphology were documented by phase-contrast microscopy after 4 and 8 h, respectively. For controls, only medium was exchanged. While LPS contamination was not separately checked by an assay, classical LPS reaction pathways, e.g., ERK pathway, show no activation (**Supplementary Tables 1, 2**), and no inflammatory GO terms were enriched in GO analysis indicating that there is no major additional effect concerning LPS. After documentation, cells were washed twice with ice-cold PBS and lysed by scraping them into 600 μL lysis buffer [8 M Urea, 50 mM ammonium bicarbonate (pH 8.0), 1 mM sodium ortho-vanadate, complete EDTA-free protease inhibitor cocktail (Roche), and phosphoSTOP phosphatase inhibitor cocktail (Roche)]. Lysates were sonicated on ice two times for 5 s at 30% energy. Cell debris was removed by centrifugation for 15 min at 16,100 × *g* at 4°C. The supernatant was collected and used for further preparation.

Protein Digestion

Protein concentrations were estimated utilizing BCA assay (Thermo). Proteins were reduced with 5 mM DTT at 37°C for 1 h and afterward alkylated with 10 mM iodoacetamide at RT for 30 min. Alkylation was quenched by adding DTT to a final concentration of 5 mM. For digestion, lysates were diluted 1:5 with 50 mM ABC buffer to lower the concentration of urea below 2 M; 1 mg protein per condition was digested at 37°C for 4 h using 1:100 w/w Lys-C (Wako) followed by overnight digestion with 1/100 w/w trypsin (Promega). Digestion was stopped by adding TFA to a final concentration of 1%. Peptide solutions were then desalted with Sep Pak C18 1cc cartridges (Waters).

Phosphopeptide Enrichment and Tandem Mass Tags Labeling

Before phosphopeptide enrichment, 25 μg of peptide of each condition was set aside for the proteome measurement. Phosphopeptide enrichment was performed following Sequential Enrichment from Metal Oxide Affinity Chromatography protocol (Thermo Scientific). Phosphopeptides have to be enriched since they only resemble a small proportion of all peptides and could rarely be measured without prior enrichment. Afterward, enriched phosphopeptides were desalted by C18 spin tips. BCA assay was used before labeling to estimate the peptide concentration of each sample. Equal amounts of enriched phosphopeptides and peptides for the proteomic analysis were labeled and combined following manufactures instructions. TMT labeling is performed to quantify multiple samples in one LC-MS run and minimize technical variability

between samples. After labeling, peptides were fractionated into eight fractions by high pH fractionation (Thermo Scientific). Subsequently, peptides were vacuum dried and stored at −80°C until LC-MS measurement.

LC-MS Analysis

Samples were dissolved in 0.1% TFA/2% ACN and analyzed in an Orbitrap Fusion Lumos mass spectrometer (Thermo Fisher Scientific) equipped with a nanoelectrospray source and connected to an Ultimate 3000 RSLC nanoflow system (Thermo Fisher Scientific). Peptides were loaded on an Acclaim PepMap C18 trap (Thermo Fisher Scientific) and separated by a 50 cm μPAC^{TM} (PharmaFluidics) analytical column at 35°C column temperature. Utilizing 0.1% formic acid as solvent A and 100% ACN with 0.1% formic acid as solvent B, we used a 120-min gradient at a flow rate of 500 nl/min ramping from 3.4% B to 21% B in 65 min, to 42% B in 32 min and to 75.6% B in 2 min, kept for 3 min, then to 3.6% B in 2 min, held for 16 min. The spray voltage was set to 2 kV. A data-dependent acquisition method, in which ions are selected on the basis of their MS1 signal and isolated for further fragmentation, was used with a cycle time of 3 s and Top N setting. Dynamic exclusion was set to 60 s, AGC target at 4×10^5, maximum injection time at 50 ms, and Orbitrap resolution at 120,000 for MS1 scan. For all runs, an MS2 method was used with higher-energy-collisional-dissociation (HCD) fragmentation at 38% [for specific remeasurement for ribosylation verification collision-induced dissociation (CID) at 35% was used], first mass at 100 m/z, MS^2 maximum injection time of 110 ms, MS^2 isolation width at 0.8 m/z, and an Orbitrap resolution of 60,000. HCD and CID are fragmentation techniques that are used to fragment ions in gas phase to assess their composition and consequently to identify them. While CID is considered to use low energy for fragmentation and hence produce less fragmented ions, HCD fragmentation generates heavier fragmented ions and is very well suited to identify phosphorylated peptides including annotation of the phosphorylation site (Jedrychowski et al., 2011; Tu et al., 2016). For an in-depth review of current mass spectrometry techniques, we refer to Sinha and Mann (2020).

Data Processing

Raw data were processed with MaxQuant software (version 1.6.3.3; Cox and Mann, 2008) using the Andromeda search engine (Cox et al., 2011). Spectra were searched against the Swiss-Prot reviewed UniprotKB database (version 01/2021, 20,395 entries; The UniProt Consortium et al., 2021). Carbamidomethylation of cysteine was set as fixed modification, and as variable modifications, oxidation of methionine, N-terminal acetylation, deamidation of glutamine, and asparagine were set. To detect mono-ADP-ribosylation (541.0611 Da, $H_{21}O_{12}C_{15}N_5P_2$), this variable modification was set at cysteine, aspartate, glutamate, histidine, arginine, lysine, serine, threonine, and tyrosine residues. Similarly, phosphorylation (PO_4) was set at serine, threonine, and tyrosine residues as variable modification. False discovery rate was set to 0.01 and maximum of missed cleavage to 2. Only phosphosites and proteins were used for quantification that were measured in all three replicates. Measured phosphosites with a localization probability below 75% were excluded from further processing. Both proteome and phosphoproteome were normalized by subtracting the median intensity of each sample and the median intensity of each TMT-batch, respectively. Only phosphosites were later included in quantitative analysis that could be normalized using the corresponding protein. Data evaluation, analysis, and visualization were done using Perseus (version 1.6.2.3.; Tyanova et al., 2016). The upstream analysis was generated through ingenuity pathway analysis (IPA, QIAGEN Inc., https://www.qiagenbio-informatics.com/products/ingenuity-pathway-analysis). The IPA software predicts regulatory proteins by comparing up- and down-regulated proteins and phosphorylation events to a hand-curated database and can therefore predict regulatory proteins that could be relevant to the observed proteomic and phosphoproteomic changes. All significant regulated sites were included. R Core Team (2013) in particular, the R packages complex heat map (Gu et al., 2016) and ggplot2 (Wickham, 2016) were used for data analysis and visualization. For heat map generation, protein and phosphosite intensities were used that were tested in a Benjamini Hochberg FDR-based ANOVA. For gene ontology analysis, the STRING data base (Jensen et al., 2009) was used. The mass spectrometry proteomics data have been deposited to the ProteomeXchange Consortium via the PRIDE (Griss et al., 2016) partner repository with the dataset identifier PXD027411.

RESULTS

Alteration of Morphology After Treatment With CDT

Different concentrations of CDT for treatment of HEp-2 cells were tested, and 1.5 μg/mL was considered to be most suitable for the proteome and phosphoproteome experiments. After 4 h of treatment with CDT, most cells exhibit a rounded cell morphology but appear to be attached to the cell culture flask (**Figure 1**). After 8 h, rounding was more pronounced, and a small number of cells had detached from the ground. Detachment seemed to be a dynamic process that started only at some areas of cells, and many cells in the cell culture flasks were observed to be a little agile and seemed to stick only with a small part to the cell culture bottom while most of the cell was rounded and moved a little bit in the medium after easy panning (**Figure 1**).

Quantitative Proteome Analysis After CDT Treatment

The proteome was analyzed in a 4-plex TMT-based approach. In all three replicates, 4,348 proteins could be identified and quantified and were included in bioinformatic analysis. To assess evaluability, the data were collapsed into only two components [e.g., principal component 1 (PC1) and principal component 2 (PC2)], which explains most of their changes; the percentage sign after each component represents the percentage of the underlying data that this component describes (see **Figures 2B**, **3B**). The different time points and treatments are then compared to

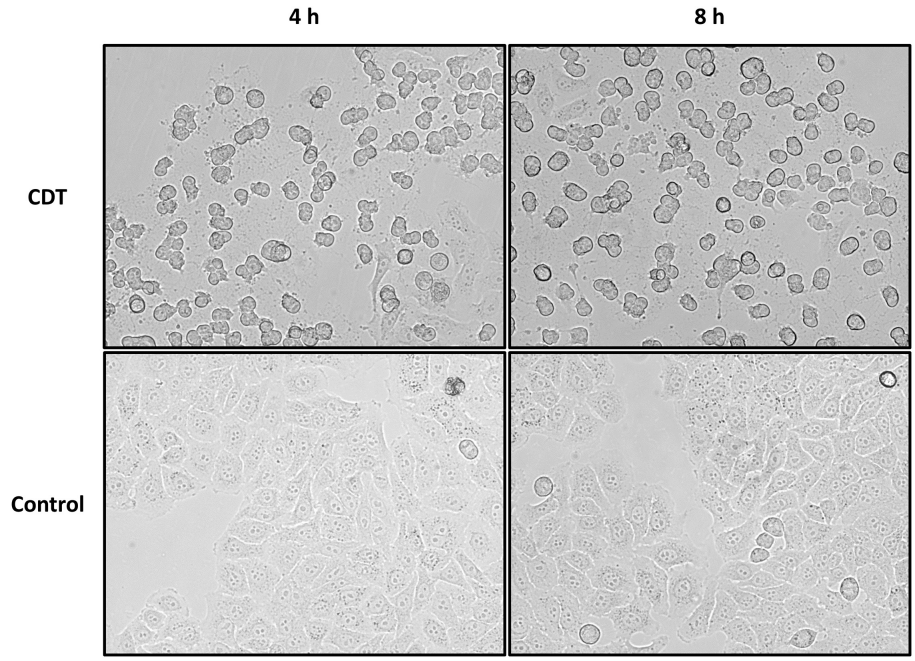

FIGURE 1 | Morphology changes of HEp-2 cells after 4 and 8 h of CDT treatment. Cells were treated with 1.5 μg/mL of CDTa and 3 μg/mL of CDTb; controls were untreated.

each other to determine whether they can be differentiated. All different time points and conditions were distinguishable via PCA and, therefore, feasible for further analysis (**Figure 2**). Only minor changes could be detected in the proteome after 4 and 8 h (**Figure 2**), respectively. Several proteins were significantly altered but 99% with a ratio of less than twofold. Notably, after 8 h, tropomyosin subunits (TPM1, TPM2, and TPM4) were significantly down-regulated by 40% compared to the untreated 8-h sample and also down-regulated compared to the 4-h timepoint (**Figure 2**).

Quantitative Phosphoproteome Analysis After CDT Treatment

In all three replicates, 5,686 phosphosites could be measured and 5,516 with a localization probability above 75%. Only phosphosites were included in a quantification that could be normalized by a corresponding protein to prohibit false hits that were only based on changed abundance of a protein; 4,619 phosphosites could be taken into analysis.

All different time points and conditions were distinguishable *via* PCA and, therefore, feasible for further analysis (**Figure 3**). 330 phosphosites were significantly regulated after 4-h treatment compared to control and, after 8 h, 61 phosphosites with a regulation above twofold change, respectively. 200 (54 with a twofold change) phosphosites significantly changed at both time points compared to the control. The top 20 significant regulated phosphosites of each condition are shown in **Supplementary Tables 3, 4**. A Fisher's exact test of the ANOVA significant phosphosites was performed to get an overview of the underlying kinase activation status. Enriched motifs were then analyzed on their phosphorylation status across the significantly changed phosphosites of both time points (**Supplementary Figure 1**). Motif phosphorylation that was regulated in the same direction at both time points was considered to play a role as a primary mechanism regulating the cell response to CDT and was therefore called "co-regulated." Down-regulated phosphorylation was primarily observed on CDK and PIM1 based motifs in both time points. Overall, up-regulated phosphorylation was detected for Casein kinase family motifs as well as BARD1 BRCT motifs (**Figure 4**).

Analysis of CSNK2A1 as a Potential Upstream Regulator

All significantly changed phosphosites of both time points were analyzed via the IPA™ software. Based on a hand-curated database, IPA™ predicts upstream regulator for phosphosites. A *Z*-score of above 2 or below −2 is considered activated or inhibited. For the 4 h time point; PIN1 and CDK6 were identified to be down-regulated. Thrombin, PASK, and HDAC1 were considered to be strongly up-regulated, and CSNK2A1 was slightly activated (**Figure 5**). For the 8 h time point, only CSNK2A1 was considered to be activated, and Thrombin was somewhat up-regulated. Since CSNK2A1 was regulated at both time points and phosphorylation of Casein kinase motifs was enhanced at both time points, potential downstream targets were further analyzed. IPA™ predicts 28 proteins to be controlled by CSNK2A1. Significantly changed phosphosites containing the casein kinase II motif are targets of CK2 according to the PhosphoSitePlus® database (Hornbeck et al., 2015), and were analyzed on their gene ontology using the STRING database

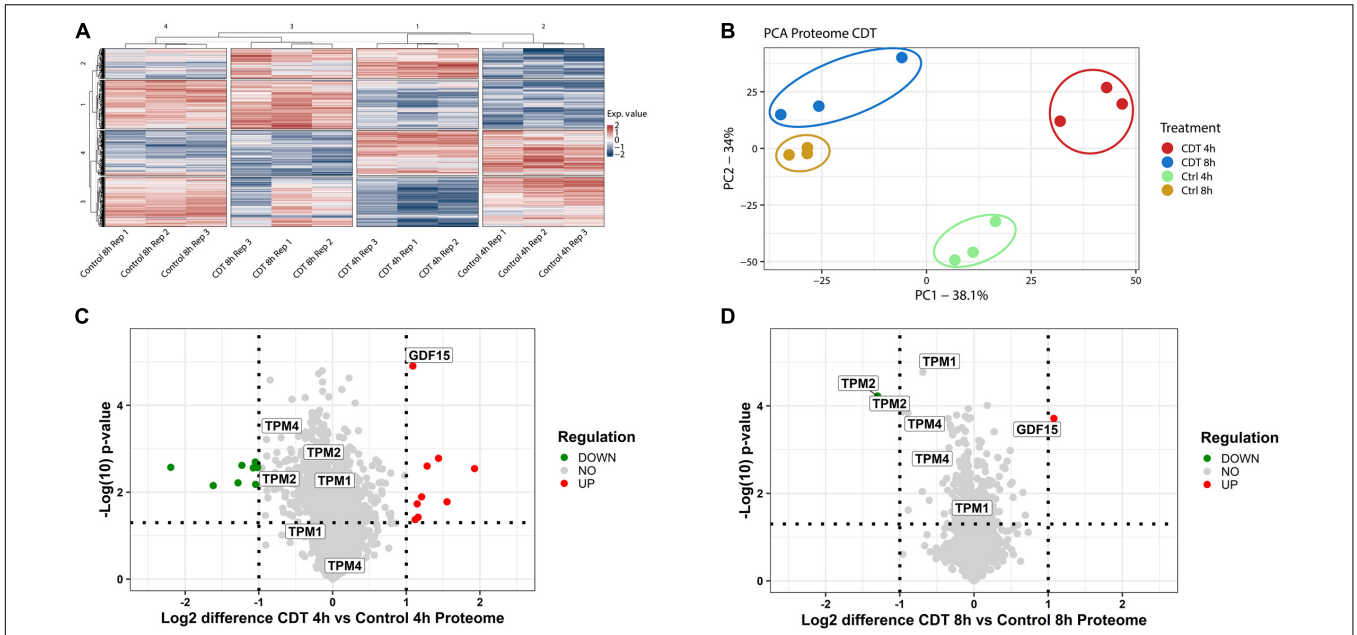

FIGURE 2 | Proteome analysis of with CDT-treated HEp-2 cells after 4 and 8 h. **(A)** Heat map of proteins that were significantly changed ($p < 0.05$) after Benjamini Hochberg FDR-based ANOVA testing. **(B)** Principal component analysis (PCA) of proteins that were significantly altered ($p < 0.05$) after FDR-based ANOVA testing. Volcano plots of proteins with CDT treated Hep-2 cells after 4 h **(C)** and 8 h **(D)**, respectively. Proteins that have been labeled with the same name resemble the isoform of that protein **(C,D)**. [**(C,D)** Horizontal dotted line indicates a *p*-value threshold of $p < 0.05$, vertical line a twofold difference, green dots: twofold significant downregulation, red dots: twofold significant upregulation; **(A)** Exp. value: expression value; numbers of row and column cluster are for coordinative reasons and have no underlying meaning; **(B)** PC1: principal component 1; PC2: principal component 2].

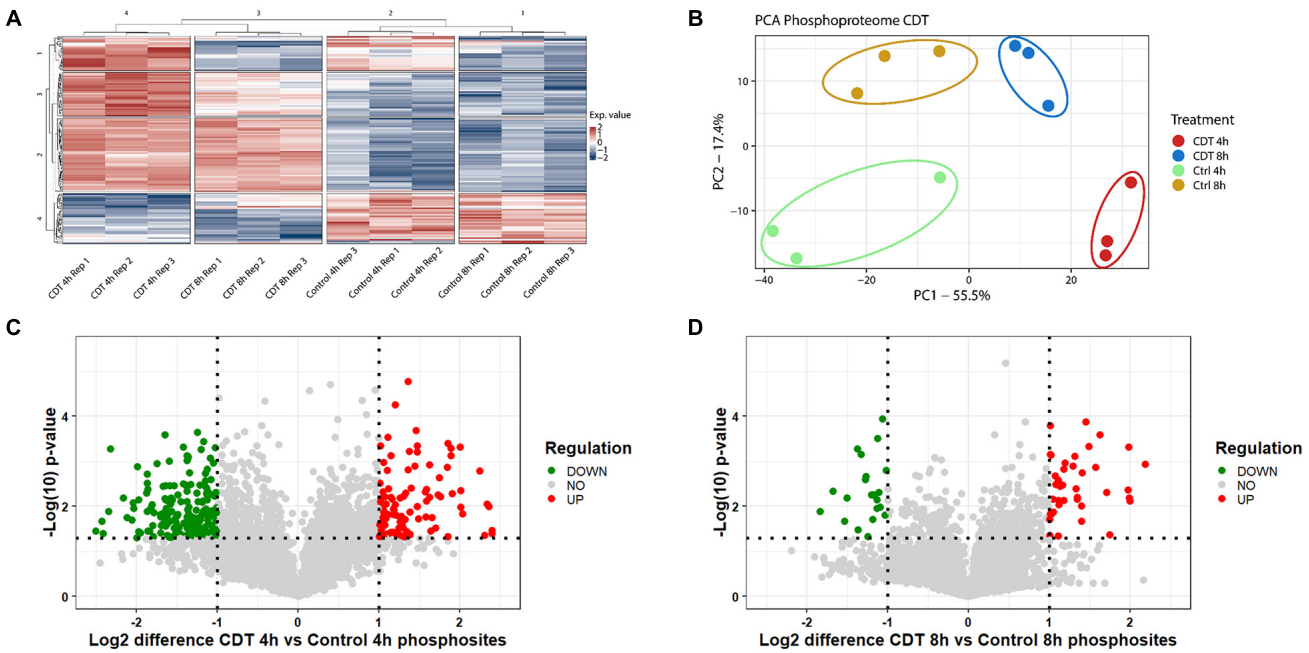

FIGURE 3 | Phosphoproteome analysis of with CDT-treated HEp-2 cells after 4 and 8 h. **(A)** Heat map of significantly changed phosphosites ($p < 0.05$) based on intensity values and Benjamini Hochberg FDR ANOVA testing; Exp. value: expression value; numbers of row and column cluster are for coordinative reasons and have no underlying meaning. **(B)** Principal component analysis (PCA) of significantly changed phosphosites ($p < 0.05$) after FDR-based ANOVA testing (PC1: principal component 1; PC2: principal component 2). Volcano plots proteins of with CDT-treated HEp-2 cells after 4 h **(C)** and 8 h **(D)**, respectively, [**(C,D)** Horizontal dotted line indicates *p*-value threshold of $p < 0.05$, vertical line twofold difference, green dots: twofold significant downregulation, red dots: twofold significant upregulation].

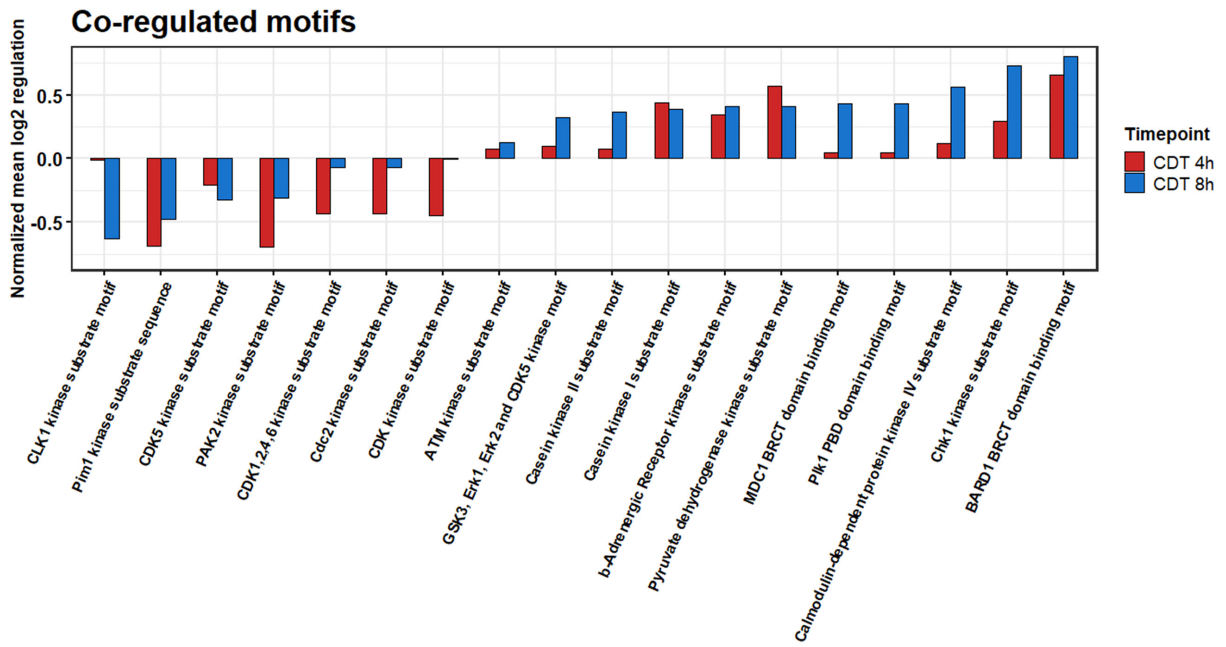

FIGURE 4 | Summed co-regulated phosphorylation of motifs of significantly changed phosphosites after 4 and 8 h of CDT treatment.

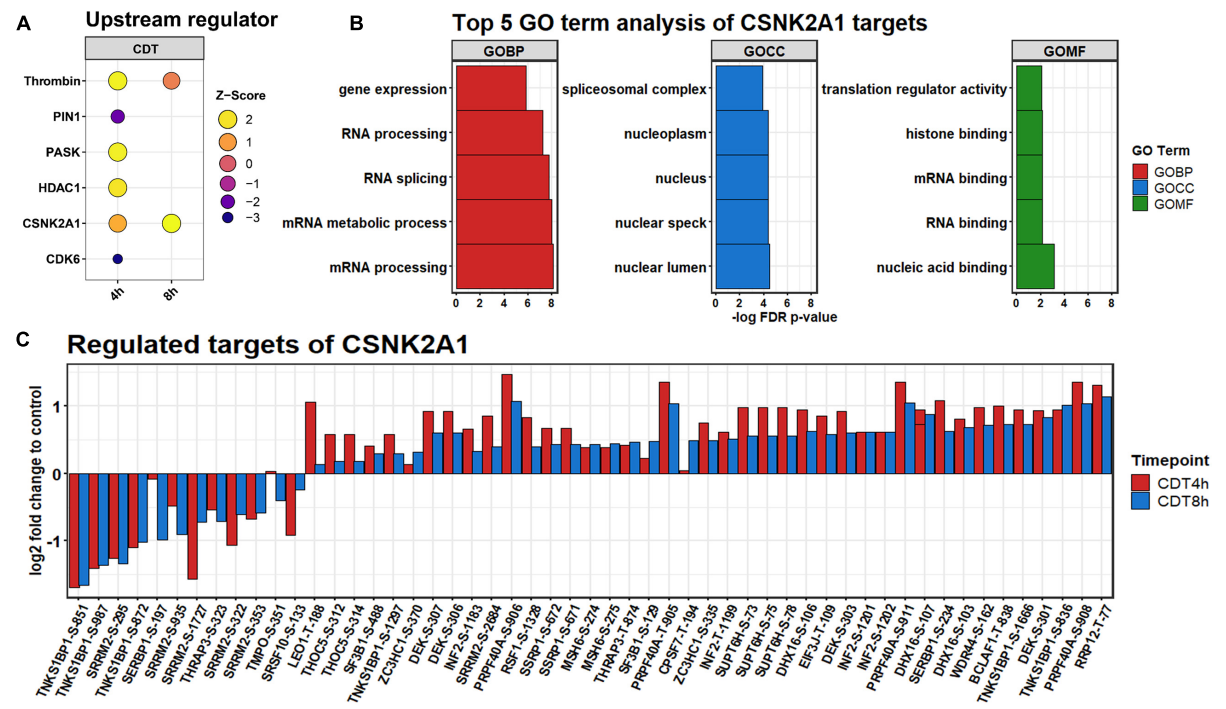

FIGURE 5 | (A) Upstream regulators predicted by IPA™. **(B)** Regulation of significantly changed predicted downstream phosphosite targets of CSNK2A1 after 4 h (red) and 8 h (blue) of CDT treatment. **(C)** GO analysis of predicted targets.

(Jensen et al., 2009). Highly enriched were GO-terms that were part of the translational process like "RNA splicing" and "translational regulator activity." The 30 most enriched GO terms for each time point are depicted in **Supplementary Figures 3, 4**.

Detection of Actin Ribosylation on Arg-177

The mono-ADP-ribosylation could be detected at Arg-177 proved by an MS2 spectrum with an Andromeda score of 214.4.

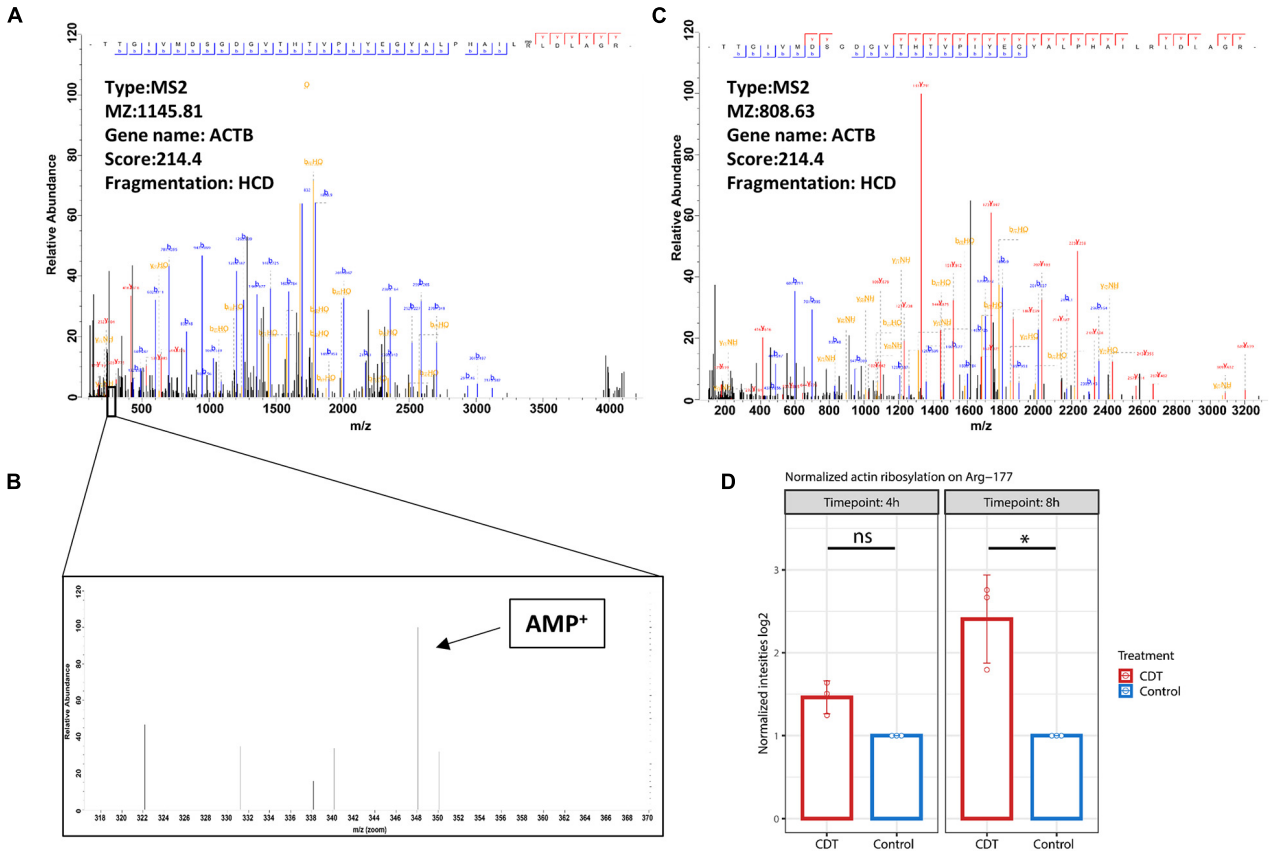

FIGURE 6 | (A) Fragment spectrum of ADP ribosylated actin on Arg-177 on the tryptic peptide TTGIVMDSGDGVTHTVPIYEGYALPHAILRLDLAGR, **(C)** the unmodified version, and **(B)** diagnostic peak of AMP at 348.2 m/z. **(D)** Normalized intensity of ADP ribosylation on Arg-177 after 4- and 8-h treatment with CDT (*$p < 0.05$, ns: non-significant).

Interestingly, no fragment ion could be seen on Arg-177 at HCD 38% despite the 348.02 peak of AMP (**Figure 6**). At CID 35%, an overlapping ion could confirm the ribosylation at Arg-177 (**Figure 6**). Furthermore, the ribosylation could be quantified with an insignificant 1.4-fold increase after 4 h of treatment and a significant 2.8-fold increase after 8 h compared to control time points (**Figure 6**).

DISCUSSION

For the first time, the effects of CDT on the proteome and phosphoproteome of target cells have been examined.

Although the proteome remains only slightly changed, distinct proteins involved in modeling the cytoskeleton were regulated in a time-dependent manner between 4 and 8 h. Tropomyosin TPM1, TPM2, TPM4, and their isoforms were significantly down-regulated during 8 h of toxin treatment and compared to the 4 h time point with a clear downward shift (**Figure 2**). Tropomyosins have been shown to be essential regulators of the actin filament function (Gunning et al., 2015). In knockout cells, it has been demonstrated that CSNK2A1 controls the abundance of tropomyosin negatively (D'Amore et al., 2019). Furthermore, the cytokine GDF-15 that promotes cell migration is significantly twofold up-regulated at both time points (**Figure 2**), and its expression is indirectly controlled by CK2 (Feng et al., 2013).

The phosphoproteome was drastically altered in contrast to the proteome. Only enriched kinase motifs were analyzed with the same phosphorylation pattern at both time points to get an overview of the underlying kinase activation status over the given period. Cyclin-dependent kinases and Pim1 motifs were less phosphorylated (**Figure 4**), and CDK6 and PIN1 also appeared as down-regulated in their activity, as evident from the IPA™ analysis (**Figure 5**). This downregulation was expected since it has been described for TcdA and TcdB that both can cause cell cycle arrest due to the collapse of the cytoskeleton that is also facilitated by CDT (Chandrasekaran and Lacy, 2017). Also, the beta-adrenergic receptor motif was stronger when phosphorylated together with the BARD1 motif. These regulations could also be foreseen considering that CDT has been described to activate the NFκB-pathway and the induction of apoptosis (Chandrasekaran and Lacy, 2017; Simpson et al., 2020).

Noticeably, changes of the phosphoproteome at the 4 h time point are more drastic than at the 8 h time point. This observation was apparently due to the collapse of the cytoskeleton between 3 and 4 h after treatment (data not shown). Accordingly,

the time point of measurement was set to 4 h to see the detailed cell reaction. At the 4 h time point, many processes were the target of imminent downregulation (e.g., cell cycle) and upregulation of damage response regulators, e.g., HDAC1 (**Figure 5A**; Miller et al., 2010). Consequently, the summed phosphorylation of different motifs compared to the control for the 4 h time point were primarily negative and do not correlate with the 8 h time point (**Supplementary Figure 1**). At the 8 h time point, those sudden changes were no longer present, and the underlying mechanism of the cell response to CDT could be viewed as more pronounced. So, only the phosphorylation of motifs regulated in the same direction was considered to describe this hidden mechanism and was further analyzed.

The phosphorylation of casein kinase motifs was up-regulated at both time points, and CSNK2A1 was strongly induced as an upstream regulator (**Figure 5**). According to a gene ontology analysis, CSNK2A1 targets that were analyzed in this dataset were mainly involved in transcriptional processes (**Figure 5**). Together with the regulated proteins, this implied an activated CSNK2A1 kinase.

A recent study suggests that SEPTINs were drivers of microtubule-based protrusions (Nölke et al., 2016). Although we did only check on general morphological changes as a marker of the CDT effect and did not look specifically for protrusions, it is noteworthy that SEPT2 is a target of CSNK2A1 with a phosphorylation site at S228. This site was found significantly altered in ANOVA-FDR-based testing and slightly up-regulated but not significant at both time points (**Supplementary Table 3**). This phosphorylation has been shown to positively influence the GTP binding of SEPTINs (Huang et al., 2006). Additionally, it has been demonstrated that in CSNK2A1 knockout cell, SEPTIN2 is significantly down-regulated (Borgo et al., 2017). This indicates a distinct regulatory mechanism, via CSNK2A1, SEPTIN, and GTPases, that could steer the microtubule polymerization and cause protrusions in the CDT setting.

While general actin ribosylation by CDT has already been shown (Gülke et al., 2001), here we could confirm for the first time that CDT ribosylates actin specifically on Arg-177. Interestingly, HCD fragmentation produces no fragment ion containing the ribosylation site on Arg-177, despite detecting the mono-ADP-ribose fragment at 348.2 m/z (**Figure 6**), described as a diagnostic ADP ribosylation marker (Schröder et al., 2018). However, the CID fragmentation method produced fragment ions containing the modification and served as an additional verification on the localization of the ADP ribosylation (**Supplementary Figure 2**).

This study offers a first glimpse of the underlying mechanisms that concern the detailed cell response to CDT. However, more experiments must be made to solidify those first suggestions that CSNK2A1 acts as an upstream regulator by, e.g., knockout experiments following experiments with primary cells instead of cell lines. In further investigations, it would also be beneficial to add more time points, especially to identify phosphorylation changes very early, e.g., 10–60 min after toxin addition. Of exceptional interest in those early time points would be the lipolysis-stimulated lipoprotein receptor (LSR) described hitherto as the only receptor for CDT (Papatheodorou et al., 2011) which could also act as an early upstream regulator. We found the phosphorylation of LSR on site S643 with a CSNK2A1 motif significantly altered after 4 h (data not shown), but since have not measured the corresponding protein, we could not include this into our analysis. Yet, it could hint that CSNK2A1 and LSR are connected and interact in a feedback loop. A different methodical setup must be applied in the following study to take receptor phosphorylation status into account since membrane proteins are challenging to analyze *via* LC-MS-based proteomics (Vit and Petrak, 2017).

Taken together, we describe the first phosphoproteome and proteome analysis after treatment of cells with CDT and offer first insights into the cellular response to this toxin. More studies have to be made to deepen these findings and elaborate on them further.

DATA AVAILABILITY STATEMENT

The dataset presented in this study has been deposited to the ProteomeXchange Consortium via the PRIDE (Griss et al., 2016) partner repository with the dataset identifier PXD027411.

AUTHOR CONTRIBUTIONS

AP designed and coached the experiments, analyzed the data, and wrote and submitted the manuscript. FS designed and performed the experiments, analyzed the data, and wrote the manuscript. RG produced the toxins and supported the experiments. All authors contributed to the article and approved the submitted version.

FUNDING

This work was partially funded by the Federal State of Lower Saxony, Niedersächsisches Vorab (VWZN2889) and a Ph.D. scholarship by Hanns-Seidel-Stiftung e.V.

SUPPLEMENTARY MATERIAL

The Supplementary Material for this article can be found online at: https://www.frontiersin.org/articles/10.3389/fmicb.2021.725612/full#supplementary-material

REFERENCES

Abeyawardhane, D. L., Godoy-Ruiz, R., Adipietro, K. A., Varney, K. M., Rustandi, R. R., Pozharski, E., et al. (2021). The importance of therapeutically targeting the binary toxin from clostridioides difficile. *Int. J. Mol. Sci.* 22:2926. doi: 10.3390/ijms22062926

Aktories, K., Papatheodorou, P., and Schwan, C. (2018). Binary *Clostridium* difficile toxin (CDT) – a virulence factor disturbing the cytoskeleton. *Anaerobe* 53, 21–29. doi: 10.1016/j.anaerobe.2018.03.001

Beer, L.-A., Tatge, H., Schneider, C., Ruschig, M., Hust, M., Barton, J., et al. (2018). The binary toxin CDT of clostridium difficile as a tool for intracellular delivery of bacterial glucosyltransferase domains. *Toxins (Basel)* 10:225.

Borgo, C., Franchin, C., Scalco, S., Bosello-Travain, V., Donella-Deana, A., Arrigoni, G., et al. (2017). Generation and quantitative proteomics analysis of CK2α/α'(-/-) cells. *Sci. Rep.* 7:42409. doi: 10.1038/srep42409

Centers for Disease Control and Prevention. (2019). *Antibiotic Resistance Threatsin The United States: 2019*. Atlanta, GA: U.S. Department of Health and Human Services.

Chandrasekaran, R., and Lacy, D. B. (2017). The role of toxins in *Clostridium* difficile infection. *FEMS Microbiol. Rev.* 41, 723–750. doi: 10.1093/femsre/fux048

Cox, J., and Mann, M. (2008). MaxQuant enables high peptide identification rates, individualized p.p.b.-range mass accuracies and proteome-wide protein quantification. *Nat. Biotechnol.* 26, 1367–1372. doi: 10.1038/nbt.1511

Cox, J., Neuhauser, N., Michalski, A., Scheltema, R. A., Olsen, J. V., and Mann, M. (2011). Andromeda: a peptide search engine integrated into the MaxQuant environment. *J. Proteome Res.* 10, 1794–1805. doi: 10.1021/pr101065j

D'Amore, C., Salizzato, V., Borgo, C., Cesaro, L., Pinna, L. A., and Salvi, M. (2019). A journey through the cytoskeleton with protein kinase CK2. *Curr. Protein Pept. Sci.* 20, 547–562. doi: 10.2174/1389203720666190119124846

Erdmann, J., Junemann, J., Schröder, A., Just, I., Gerhard, R., and Pich, A. (2017). Glucosyltransferase-dependent and -independent effects of TcdB on the proteome of HEp-2 cells. *Proteomics* 17:1600435. doi: 10.1002/pmic.201600435

Feng, H., Chen, L., Wang, Q., Shen, B., Liu, L., Zheng, P., et al. (2013). Calumenin-15 facilitates filopodia formation by promoting TGF-β superfamily cytokine GDF-15 transcription. *Cell Death Dis.* 4:e870. doi: 10.1038/cddis.2013.403

Griss, J., Perez-Riverol, Y., Lewis, S., Tabb, D. L., Dianes, J. A., Del-Toro, N., et al. (2016). Recognizing millions of consistently unidentified spectra across hundreds of shotgun proteomics datasets. *Nat. Methods* 13, 651–656. doi: 10.1038/nmeth.3902

Gu, Z., Eils, R., and Schlesner, M. (2016). Complex heatmaps reveal patterns and correlations in multidimensional genomic data. *Bioinformatics* 32, 2847–2849. doi: 10.1093/bioinformatics/btw313

Gülke, I., Pfeifer, G., Liese, J., Fritz, M., Hofmann, F., Aktories, K., et al. (2001). Characterization of the enzymatic component of the ADP-ribosyltransferase toxin CDTa from Clostridium difficile. *Infect. Immun.* 69, 6004–6011. doi: 10.1128/IAI.69.10.6004-6011.2001

Gunning, P. W., Hardeman, E. C., Lappalainen, P., and Mulvihill, D. P. (2015). Tropomyosin - master regulator of actin filament function in the cytoskeleton. *J. Cell Sci.* 128, 2965–2974. doi: 10.1242/jcs.172502

Hornbeck, P. V., Zhang, B., Murray, B., Kornhauser, J. M., Latham, V., and Skrzypek, E. (2015). PhosphoSitePlus, 2014: mutations, PTMs and recalibrations. *Nucleic Acids Res.* 43, D512–D520. doi: 10.1093/nar/gku1267

Huang, Y.-W., Surka, M. C., Reynaud, D., Pace-Asciak, C., and Trimble, W. S. (2006). GTP binding and hydrolysis kinetics of human septin 2. *FEBS J.* 273, 3248–3260. doi: 10.1111/j.1742-4658.2006.05333.x

Jedrychowski, M. P., Huttlin, E. L., Haas, W., Sowa, M. E., Rad, R., and Gygi, S. P. (2011). Evaluation of HCD- and CID-type fragmentation within their respective detection platforms for murine phosphoproteomics. *Mol. Cell. Proteomics* 10:M111.009910. doi: 10.1074/mcp.M111.009910

Jensen, L. J., Kuhn, M., Stark, M., Chaffron, S., Creevey, C., Muller, J., et al. (2009). STRING 8–a global view on proteins and their functional interactions in 630 organisms. *Nucleic Acids Res.* 37, D412–D416. doi: 10.1093/nar/gkn760

Jochim, N., Gerhard, R., Just, I., and Pich, A. (2014). Time-resolved cellular effects induced by TcdA from Clostridium difficile. *Rapid Commun. Mass Spectrom.* 28, 1089–1100. doi: 10.1002/rcm.6882

Junemann, J., Birgin, G., Erdmann, J., Schröder, A., Just, I., Gerhard, R., et al. (2017). Toxin A of the nosocomial pathogen *Clostridium* difficile induces primary effects in the proteome of HEp-2 cells. *Proteomics Clin. Appl.* 11:1600031. doi: 10.1002/prca.201600031

Miller, K. M., Tjeertes, J. V., Coates, J., Legube, G., Polo, S. E., Britton, S., et al. (2010). Human HDAC1 and HDAC2 function in the DNA-damage response to promote DNA nonhomologous end-joining. *Nat. Struct. Mol. Biol.* 17, 1144–1151. doi: 10.1038/nsmb.1899

Nölke, T., Schwan, C., Lehmann, F., Østevold, K., Pertz, O., and Aktories, K. (2016). Septins guide microtubule protrusions induced by actin-depolymerizing toxins like Clostridium difficile transferase (CDT). *Proc. Natl. Acad. Sci. U. S. A.* 113, 7870–7875. doi: 10.1073/pnas.1522717113

Papatheodorou, P., Carette, J. E., Bell, G. W., Schwan, C., Guttenberg, G., Brummelkamp, T. R., et al. (2011). Lipolysis-stimulated lipoprotein receptor (LSR) is the host receptor for the binary toxin *Clostridium difficile* transferase (CDT). *Proc. Natl. Acad. Sci. U.S.A.* 108, 16422–16427. doi: 10.1073/pnas.1109772108

R Core Team. (2013). *R: A Language and Environmentfor Statistical Computing*. Vienna: R Foundation for Statistical Computing.

Schröder, A., Benski, A., Oltmanns, A., Just, I., Rohrbeck, A., and Pich, A. (2018). MS-based quantification of RhoA/B and RhoC ADP-ribosylation. *J. Chromatogr. B Analyt. Technol. Biomed. Life Sci.* 1092, 268–271. doi: 10.1016/j.jchromb.2018.06.007

Schwan, C., Stecher, B., Tzivelekidis, T., van Ham, M., Rohde, M., Hardt, W.-D., et al. (2009). *Clostridium* difficile toxin CDT induces formation of microtubule-based protrusions and increases adherence of bacteria. *PLoS Pathog.* 5:e1000626. doi: 10.1371/journal.ppat.1000626

Simpson, M., Frisbee, A., Kumar, P., Schwan, C., Aktories, K., and Petri, W. A. (2020). Clostridioides difficile binary toxin (CDT) is recognized by the TLR2/6 heterodimer to induce an NF-κB response. *J. Infect. Dis.* 0022-1899:jiaa620. doi: 10.1093/infdis/jiaa620

Sinha, A., and Mann, M. (2020). A beginner's guide to mass spectrometry–based proteomics. *Biochemist* 42, 64–69. doi: 10.1042/BIO20200057

The UniProt Consortium, Bateman, A., Martin, M.-J., Orchard, S., Magrane, M., Agivetova, R., et al. (2021). UniProt: the universal protein knowledgebase in 2021. *Nucleic Acids Res.* 49, D480–D489. doi: 10.1093/nar/gkaa1100

Tu, C., Li, J., Shen, S., Sheng, Q., Shyr, Y., and Qu, J. (2016). Performance investigation of proteomic identification by HCD/CID fragmentations in combination with high/low-resolution detectors on a tribrid. High-field orbitrap instrument. *PLoS One* 11:e0160160. doi: 10.1371/journal.pone.0160160

Tyanova, S., Temu, T., Sinitcyn, P., Carlson, A., Hein, M. Y., Geiger, T., et al. (2016). The Perseus computational platform for comprehensive analysis of (prote)omics data. *Nat. Methods* 13, 731–740. doi: 10.1038/nmeth.3901

Vandekerckhove, J., Schering, B., Bärmann, M., and Aktories, K. (1987). Clostridium perfringens iota toxin ADP-ribosylates skeletal muscle actin in Arg-177. *FEBS Lett.* 225, 48–52. doi: 10.1016/0014-5793(87)81129-8

Vit, O., and Petrak, J. (2017). Integral membrane proteins in proteomics. How to break open the black box? *J. Proteomics* 153, 8–20. doi: 10.1016/j.jprot.2016.08.006

Wickham, H. (2016). *ggplot2: Elegant Graphics for Data Analysis*. Cham: Springer.

Zeiser, J., Gerhard, R., Just, I., and Pich, A. (2013). Substrate specificity of clostridial glucosylating toxins and their function on colonocytes analyzed by proteomics techniques. *J. Proteome Res.* 12, 1604–1618. doi: 10.1021/pr300973q

Zeiser, J. J., Klodmann, J., Braun, H.-P., Gerhard, R., Just, I., and Pich, A. (2011). Effects of *Clostridium* difficile toxin A on the proteome of colonocytes studied by differential 2D electrophoresis. *J. Proteomics* 75, 469–479. doi: 10.1016/j.jprot.2011.08.012

Conflict of Interest: The authors declare that the research was conducted in the absence of any commercial or financial relationships that could be construed as a potential conflict of interest.

Publisher's Note: All claims expressed in this article are solely those of the authors and do not necessarily represent those of their affiliated organizations, or those of the publisher, the editors and the reviewers. Any product that may be evaluated in this article, or claim that may be made by its manufacturer, is not guaranteed or endorsed by the publisher.

Copyright © 2021 Stieglitz, Gerhard and Pich. This is an open-access article distributed under the terms of the Creative Commons Attribution License (CC BY). The use, distribution or reproduction in other forums is permitted, provided the original author(s) and the copyright owner(s) are credited and that the original publication in this journal is cited, in accordance with accepted academic practice. No use, distribution or reproduction is permitted which does not comply with these terms.

frontiers in Microbiology

ORIGINAL RESEARCH
published: 05 October 2021
doi: 10.3389/fmicb.2021.735616

FliW and CsrA Govern Flagellin (FliC) Synthesis and Play Pleiotropic Roles in Virulence and Physiology of *Clostridioides difficile* R20291

*Duolong Zhu, Shaohui Wang and Xingmin Sun**

Department of Molecular Medicine, Morsani College of Medicine, University of South Florida, Tampa, FL, United States

Clostridioides difficile flagellin FliC is associated with toxin gene expression, bacterial colonization, and virulence, and is also involved in pleiotropic gene regulation during *in vivo* infection. However, how *fliC* expression is regulated in *C. difficile* remains unclear. In *Bacillus subtilis*, flagellin homeostasis and motility are coregulated by flagellar assembly factor (FliW), flagellin Hag (FliC homolog), and Carbon storage regulator A (CsrA), which is referred to as partner-switching mechanism "FliW-CsrA-Hag." In this study, we characterized FliW and CsrA functions by deleting or overexpressing *fliW*, *csrA*, and *fliW-csrA* in *C. difficile* R20291. We showed that *fliW* deletion, *csrA* overexpression in R20291, and *csrA* complementation in R20291ΔWA (*fliW-csrA* codeletion mutant) dramatically decreased FliC production, but not *fliC* gene transcription. Suppression of *fliC* translation by *csrA* overexpression can be relieved mostly when *fliW* was coexpressed, and no significant difference in FliC production was detected when only *fliW* was complemented in R20291ΔWA. Further, loss of *fliW* led to increased biofilm formation, cell adhesion, toxin production, and pathogenicity in a mouse model of *C. difficile* infection (CDI), while *fliW-csrA* codeletion decreased toxin production and mortality *in vivo*. Our data suggest that CsrA negatively modulates *fliC* expression and FliW indirectly affects *fliC* expression through inhibition of CsrA post-transcriptional regulation. In light of "FliW-CsrA-Hag" switch coregulation mechanism reported in *B. subtilis*, our data also suggest that "FliW-CsrA-*fliC*/FliC" can regulate many facets of *C. difficile* R20291 pathogenicity. These findings further aid us in understanding the virulence regulation in *C. difficile*.

Keywords: ***Clostridioides difficile*, FliW, FliC, CsrA, R20291, virulence**

OPEN ACCESS

Edited by:
Meina Neumann-Schaal, German Collection of Microorganisms and Cell Cultures GmbH (DSMZ), Germany

Reviewed by:
Susanne Sievers, University of Greifswald, Germany
Sarah Anna Kuehne, University of Birmingham, United Kingdom
Joshua Robert Fletcher, University of Minnesota Twin Cities, United States

***Correspondence:**
Xingmin Sun
sun5@usf.edu

Specialty section:
This article was submitted to Infectious Agents and Disease, a section of the journal Frontiers in Microbiology

Received: *02 July 2021*
Accepted: *13 September 2021*
Published: *05 October 2021*

Citation:
Zhu D, Wang S and Sun X (2021) FliW and CsrA Govern Flagellin (FliC) Synthesis and Play Pleiotropic Roles in Virulence and Physiology of Clostridioides difficile R20291. Front. Microbiol. 12:735616. doi: 10.3389/fmicb.2021.735616

INTRODUCTION

Clostridioides difficile (Lawson et al., 2016; Oren and Garrity, 2018) is a Gram-positive, spore-forming, toxin-producing, anaerobic bacterium that is a leading cause of nosocomial antibiotic-associated diarrhea in the developed countries (Sebaihia et al., 2006). *Clostridioides difficile* infection (CDI) can result in a spectrum of symptoms, ranging from mild diarrhea to pseudomembranous colitis and potential death (Lessa et al., 2012). *Clostridioides difficile* has many virulence factors, among which toxin A (TcdA) and toxin B (TcdB) are the major ones

(Lyras et al., 2009; Kuehne et al., 2010). These toxins can disrupt the actin cytoskeleton of intestinal cells through glucosylation of the Rho family of GTPases, and induce mucosal inflammation and symptoms associated with CDI (Peniche et al., 2013).

CsrA, the carbon storage regulator A, has been reported to control various physiological processes, such as flagella synthesis, virulence, central carbon metabolism, quorum sensing, motility, and biofilm formation in pathogens including *Pseudomonas aeruginosa*, *Pseudomonas syringae*, *Borrelia burgdorferi*, *Salmonella typhimurium*, and *Proteus mirabilis* (Sabnis et al., 1995; Pessi et al., 2001; Lawhon et al., 2003; Lucchetti-Miganeh et al., 2008; Timmermans and Van Melderen, 2010; Karna et al., 2011; Morris et al., 2013; Ferreiro et al., 2018). Recently, the role of CsrA on carbon metabolism and virulence-associated processes in *C. difficile* 630Δ*erm* was analyzed by overexpressing the *csrA* gene (Gu et al., 2018). Authors showed that the *csrA* overexpression resulted in flagella defect, poor motility, and induced carbon metabolism change. Oppositely, toxin production and cell adherence increased in the *csrA* overexpression strain. CsrA is a widely distributed RNA binding protein that post-transcriptionally modulates gene expression through regulating mRNA stability and/or translation initiation of target mRNA (Romeo et al., 1993; Liu et al., 1995; Timmermans and Van Melderen, 2010). It typically binds to multiple specific sites that are located nearby or overlapping the cognate Shine–Dalgarno (SD) sequence in the target transcripts (Sorger-Domenigg et al., 2007; Yakhnin et al., 2007). The roles of CsrA in *Bacillus subtilis* have been well-studied (Yakhnin et al., 2007; Mukherjee et al., 2011; Oshiro et al., 2019). Flagellin Hag (FliC homolog), a main structure flagellar component, has been reported to be regulated by CsrA in *B. subtilis*. Yakhnin et al. (2007) first reported that CsrA in *B. subtilis* can regulate translation initiation of Hag by preventing ribosome binding to the *hag* transcript. Mukherjee et al. (2011) elucidated that the interaction between CsrA and FliW could govern flagellin homeostasis and checkpoint on flagellar morphogenesis in *B. subtilis*. FliW, the first protein antagonist of CsrA activity, was also identified and characterized in *B. subtilis*. They elegantly demonstrated a novel regulation system "a partner-switching mechanism" (Hag-FliW-CsrA) on flagellin synthesis in *B. subtilis*. Briefly, following the flagellar assembly checkpoint of hook completion, FliW was released from a FliW-Hag complex. Afterward, FliW binds to CsrA which will relieve CsrA-mediated *hag* translation repression for flagellin synthesis concurrent with filament assembly. Thus, flagellin homeostasis restricts its own expression on the translational level. Results also suggested that CsrA has an ancestral role in flagella assembly and has evolved to coregulate multiple cellular processes with motility. Oshiro et al. (2019) further quantitated the interactions in the Hag-FliW-CsrA system. They found that Hag-FliW-$CsrA^{dimer}$ functions at nearly 1:1:1 stoichiometry in *B. subtilis*. The Hag-FliW-$CsrA^{dimer}$ system is hypersensitive to the cytoplasmic Hag concentration and is robust to perturbation.

Clostridioides difficile flagellin gene *fliC* is associated with toxin gene expression, bacterial colonization, and virulence, and is responsible for pleiotropic gene regulation during *in vivo* infection (Tasteyre et al., 2001; Aubry et al., 2012; Baban et al., 2013; Barketi-Klai et al., 2014; Stevenson et al., 2015). The delicate regulations among *fliC* gene expression, toxin production, bacterial motility, colonization, and pathogenicity in *C. difficile* are indicated. Though the important roles of CsrA in flagellin synthesis and flagellin homeostasis have been studied in other bacteria (Yakhnin et al., 2007; Mukherjee et al., 2011; Oshiro et al., 2019), the regulation of FliW, CsrA, and FliC and the function of *fliW* in *C. difficile* remain unclear.

In this communication, we aimed to study the involvement of FliW and CsrA in *fliC* expression and *C. difficile* virulence and physiology by constructing and analyzing *fliW* and *fliW-csrA* deletion mutants of *C. difficile* R20291. We evaluated these mutants in the expression of *fliC*, motility, adhesion, biofilm formation, toxin production, sporulation, germination, and pathogenicity in a mouse model of CDI.

MATERIALS AND METHODS

Bacteria, Plasmids, and Culture Conditions

Table 1 lists the strains and plasmids used in this study. *Clostridioides difficile* strains were cultured in BHIS media (brain heart infusion broth supplemented with 0.5% yeast extract and 0.1% L-cysteine, and 1.5% agar for agar plates) at 37°C in an anaerobic chamber (90% N_2, 5% H_2, and 5% CO_2). For spores preparation, *C. difficile* strains were cultured in Clospore media and purified as described earlier (Perez et al., 2011). *Escherichia coli* DH5α and *E. coli* HB101/pRK24 were grown aerobically at 37°C in LB media (1% tryptone, 0.5% yeast extract, and 1% NaCl). *Escherichia coli* DH5α was used as a cloning host, and *E. coli* HB101/pRK24 was used as a conjugation donor host. Antibiotics were added when needed for *E. coli*, 15 μg/ml chloramphenicol; for *C. difficile*, 15 μg/ml thiamphenicol, 250 μg/ml D-cycloserine, 50 μg/ml kanamycin, 8 μg/ml cefoxitin, and 500 ng/ml anhydrotetracycline.

DNA Manipulations and Chemicals

DNA manipulations were carried out according to standard techniques (Chong, 2001). Plasmids were conjugated into *C. difficile* as described earlier (Heap et al., 2010). The DNA markers, protein markers, PCR product purification kit, DNA gel extraction kit, restriction enzymes, cDNA synthesis kit, and SYBR Green RT-qPCR kit were purchased from ThermoFisher Scientific (Waltham, United States). PCRs were performed with the high-fidelity DNA polymerase NEB Q5 Master Mix, and PCR products were assembled into target plasmids with NEBuilder HIFI DNA Assembly Master Mix (New England, United Kingdom). Primers (**Supplementary Table 1**) were purchased from IDT (Coralville, United States). All chemicals were purchased from Sigma-Aldrich (St. Louis, United States) unless those stated otherwise.

TABLE 1 | Bacteria and plasmids utilized in this study.

Strains or plasmids	Genotype or phenotype	Reference
Strains		
E. coli DH5α	Cloning host	NEB
E. coli HB101/pRK24	Conjugation donor	Williams et al., 1990
C. difficile R20291	Clinical isolate; ribotype 027	Stabler et al., 2009
R20291ΔW	R20291 deleted *fliW* gene	This work
R20291ΔWA	R20291 deleted *fliW-csrA* genes	This work
R20291-E	R20291 containing blank plasmid pMTL84153	This work
R20291ΔW-E	R20291ΔW containing blank plasmid pMTL84153	This work
R20291ΔWA-E	R20291ΔWA containing blank plasmid pMTL84153	This work
R20291ΔW-W	R20291ΔW complemented with pMTL84153-*fliW*	This work
R20291ΔWA-WA	R20291ΔWA complemented with pMTL84153-*fliW-csrA*	This work
R20291ΔWA-W	R20291ΔWA complemented with pMTL84153-*fliW*	This work
R20291ΔWA-A	R20291ΔWA complemented with pMTL84153-*csrA*	This work
R20291-W	R20291 containing pMTL84153-*fliW*	This work
R20291-A	R20291 containing pMTL84153-*csrA*	This work
R20291-WA	R20291 containing pMTL84153-*fliW-csrA*	This work
Plasmids		
pDL1	AsCpfI based gene deletion plasmid	This work
pUC57-PsRNA	sRNA promoter template	This work
pDL1-*fliW*	*fliW* gene deletion plasmid	This work
pDL1-*csrA*	*csrA* gene deletion plasmid	This work
pDL1-*fliW-csrA*	*fliW-csrA* gene deletion plasmid	This work
pMTL84153	Complementation plasmid	Heap et al., 2009
pMTL84153-*fliW-csrA*	pMTL84153 containing *fliW-crsA* genes	This work
pMTL84153-*fliW*	pMTL84153 containing *fliW* gene	This work
pMTL84153-*csrA*	pMTL84153 containing *crsA* gene	This work

Gene Deletion, Complementation, and Overexpression in R20291

Gene edit plasmid pDL-1 containing Cas12a (AsCpfI) under the control of tetracycline-inducing promoter was constructed and used for *C. difficile* gene deletion according to a previous report (Hong et al., 2018). The target sgRNA was designed with an available website tool,[1] and the off-target prediction was analyzed on the Cas-OFFinder website.[2] The sgRNA, up- and down-homologous arms, were assembled into pDL-1. Two target sgRNAs for one gene deletion were selected and used for gene deletion plasmid construction in *C. difficile*, respectively. Briefly, the gene deletion plasmid was constructed in the cloning host *E. coli* DH5α and was transformed into the donor host *E. coli* HB101/pRK24, and subsequently was conjugated into R20291. Potential successful transconjugants were selected with selective antibiotic BHIS-TKC plates (15 μg/ml thiamphenicol, 50 μg/ml kanamycin, and 8 μg/ml cefoxitin). The transconjugants were cultured in BHIS-Tm broth (15 μg/ml thiamphenicol) to log phase, then the subsequent cultures were diluted with PBS serially and plated on the inducing plates (BHIS-Tm-ATc: 15 μg/ml thiamphenicol and 500 ng/ml anhydrotetracycline). The plates were incubated at 37°C in the anaerobic chamber for 24–48 h, then 20–40 colonies were used as templates for colony PCR test with check primers for correct gene deletion colony isolation. The correct gene deletion colony was sub-cultured into BHIS broth without antibiotics and was passaged several times to cure the deletion plasmid, and then the cultures were plated on BHIS plates and subsequent colonies were replica plated on BHIS-Tm plates to isolate pure gene deletion mutants. The genome of R20291Δ*fliW* (referred hereafter as R20291ΔW) and R20291Δ*fliW-csrA* (referred hereafter as R20291ΔWA) were isolated and used as templates for the PCR test with check primers, and the PCR products were sequenced to confirm the correct gene deletion.

The *fliW* (396 bp; primers 3-F/R), *csrA* (213 bp; primers 4-F/R), and *fliW-csrA* (599 bp; primers 5-F/R) genes were amplified and assembled into *Sac*I-*Bam*HI digested pMTL84153 plasmid, yielding the complementation plasmid pMTL84153-*fliW*, pMTL84153-*csrA*, and pMTL84153-*fliW-csrA*, and were subsequently conjugated into R20291ΔWA, R20291ΔW, and R20291 yielding complementation strain R20291ΔWA/pMTL84153-*fliW* (referred as R20291ΔWA-W), R20291ΔWA/pMTL84153-*csrA* (R20291ΔWA-A), R20291ΔWA/pMTL84153-*fliW-csrA* (R20291ΔWA-WA), and R20291ΔW/pMTL84153-*fliW* (R20291ΔW-W), and overexpression strain R20291/pMTL84153-*fliW* (R20291-W), R20291/pMTL84153-*csrA* (R20291-A), and R20291/pMTL84153- *fliW-csrA* (R20291-WA).

Growth Profile, Motility, and Biofilm Assay

Clostridioides difficile strains were incubated to an optical density of OD_{600} of 0.8 in BHIS media and were diluted to an OD_{600} of 0.2. Then, 1% of the culture was inoculated into fresh BHIS, followed by measuring OD_{600} for 32 h.

To examine the effect of *fliW* and *fliW-csrA* deletion on *C. difficile* motility, R20291, R20291ΔWA, and R20291ΔW were cultured to an OD_{600} of 0.8. For swimming analysis, 2 μl of *C. difficile* culture was penetrated into soft BHIS agar (0.175%) plates, meanwhile, 2 μl of culture was dropped onto 0.3% BHIS agar plates for swarming analysis. The swimming assay plates were incubated for 24 h, and the swarming plates were incubated for 48 h, respectively.

For biofilm formation analysis, wild-type and mutant strains were cultured to an OD_{600} of 0.8, and 1% of *C. difficile* cultures were inoculated into reinforced clostridial medium (RCM) with eight-well repeats in a 96-well plate and incubated in the anaerobic chamber at 37°C for 48 h. Biofilm formation was analyzed by crystal violet dye. Briefly, *C. difficile* cultures were

[1]http://big.hanyang.ac.kr/cindel/
[2]http://www.rgenome.net/cas-offinder/

removed by pipette carefully. Then, 100 µl of 2.5% glutaraldehyde was added into the well to fix the bottom biofilm, and the plate was kept at room temperature for 30 min. Next, the wells were washed with PBS three times and dyed with 0.25% (w/v) crystal violet for 10 min. The crystal violet solution was removed, and the wells were washed five times with PBS, followed by the addition of acetone into wells to dissolve the crystal violet of the cells. The dissolved solution was further diluted with ethanol 2–4 times, and biomass was determined at OD_{570}.

Adherence of *C. difficile* Vegetative Cells to HCT-8 Cells

Clostridioides difficile adhesion ability was evaluated with HCT-8 cells (ATCC CCL-244; Janvilisri et al., 2010). Briefly, HCT-8 cells were grown to 95% confluence (2×10^5/well) in a 24-well plate and then moved into the anaerobic chamber, followed by infecting with 6×10^6 of log phase of *C. difficile* vegetative cells at a multiplicity of infection (MOI) of 30:1. The plate was cultured at 37°C for 30 min. After incubation, the infected cells were washed with 300 µl of PBS three times, and then suspended in RPMI media with trypsin and plated on BHIS agar plates to enumerate the adhered *C. difficile* cells. The adhesion ability of *C. difficile* to HCT-8 cells was calculated as follows: CFU of adhered bacteria/total cell numbers.

To visualize the adherence of *C. difficile* to HCT-8 cells, *C. difficile* vegetative cells were labeled with the chemical 5(6)-CFDA (5- and −6)-Carboxyfluorescein diacetate (Fuller et al., 2000). Briefly, *C. difficile* strains were cultured to an OD_{600} of 0.8, then washed with PBS 3 times and resuspended in fresh BHIS supplemented with 50-mM 5(6)-CFDA, followed by incubation at 37°C for 30 min in the anaerobic chamber. After post-incubation, the labeled *C. difficile* cells were collected and washed with PBS three times, and then resuspended in RPMI medium. Afterward, the labeled *C. difficile* cells were used for the infection experiment as described above. After 30-min post-infection, the fluorescence of each well was scanned by the multi-mode reader (excitation, 485 nm; emission, 528 nm), the relative fluorescence unit (RFU) was recorded as F0. Following, the plates were washed with PBS three times to remove unbound *C. difficile* cells, then the plates were scanned, and the RFU was recorded as F1. The adhesion ratio was calculated as follows: F1/F0. After scanning, the infected cell plates were further detected by the fluorescence microscope.

fliC Expression Assay

For *fliC* transcription analysis, 2 ml of 24-h post-inoculated *C. difficile* cultures were centrifuged at 4°C, 12,000 × *g* for 5 min, respectively. Then, the total RNA of different strains was extracted with TRIzol reagent. The transcription of *fliC* was measured by RT-qPCR with primers Q-*fliC*-F/R. All RT-qPCRs were repeated in triplicate, independently. Data were analyzed by the comparative CT ($2^{-\Delta\Delta CT}$) method with 16 s rRNA as a control.

To analyze the FliC protein level, *C. difficile* cell lysates from overnight cultures were used for Western blot analysis. Briefly, overnight *C. difficile* cultures were collected and washed three times with PBS and then resuspended in 5 ml of distilled water. The suspensions were lysed with TissueLyser LT (Qiagen), followed centrifuged at 4°C, 25,000 × *g* for 1 h. The final pellets were resuspended in 30 µl of PBS, and the total protein concentration was measured by using a BCA protein assay (Thermo Scientific, Suwanee, GA, United States). Protein extracts were subjected to 10% SDS-PAGE. Sigma A protein (SigA) was used as a loading control protein in SDS-PAGE (Mukherjee et al., 2013). FliC and SigA proteins on the gel were detected with anti-FliC and anti-SigA primary antibody (1:1,000, a generous gift from Dr. Daniel Kearns at Indiana University) and horseradish peroxidase-conjugated secondary antibody goat anti-mouse (Cat: ab97023, IgG, 1:3,000, Abcam, Cambridge, MA, United States) by Western blot, respectively. Anti-FliC antibody used in the Western blot analysis is an anti-FliCD serum, generated in the laboratory. FliCD is a fusion protein containing *C. difficile* FliC and FliD (Wang et al., 2018). The relative intensity of blot bands was analyzed by ImageJ software, and FliC relative intensity was normalized to SigA control.

Toxin Expression Assay

To evaluate toxin expression in *C. difficile* strains, one single colony from each strain was inoculated into 25 ml of BHIS and incubated in an anaerobic chamber at 37°C, and 10 ml of *C. difficile* cultures from different strains were collected at 24- and 48-h post-incubation. The cultures were adjusted to the same OD_{600} value with fresh BHIS. Then, the collected *C. difficile* cultures were centrifuged at 4°C, 8,000 × *g* for 15 min, filtered with 0.22 µm filters, and used for ELISA. Anti-TcdA (PCG4.1, Novus Biologicals, United States) and anti-TcdB (AI, Gene Tex, United States) were used as coating antibodies for ELISA, and HRP-Chicken anti-TcdA and HRP-Chicken anti-TcdB (Gallus Immunotech, United States) were used as detection antibodies.

For toxin transcription analysis, 2 ml of 24- and 48-h post-inoculated *C. difficile* cultures were centrifuged at 4°C, 12,000 × *g* for 5 min, respectively. Next, the total RNA of different strains was extracted with TRIzol reagent. The transcription of *tcdA* and *tcdB* was measured by RT-qPCR with primers Q-*tcdA*-F/R and Q-*tcdB*-F/R, respectively. All RT-qPCRs were repeated in triplicate, independently. Data were analyzed by using the comparative CT ($2^{-\Delta\Delta CT}$) method with 16 s rRNA as a control.

Germination and Sporulation Assay

Clostridioides difficile germination and sporulation analysis were conducted as reported earlier (Zhu et al., 2019). Briefly, for *C. difficile* sporulation analysis, *C. difficile* strains were cultured in Clospore media for 4 days. Afterward, the CFU of cultures from 48 and 96 h were counted on BHIS plates with 0.1% TA to detect sporulation ratio, respectively. The sporulation ratio was calculated as CFU (65°C heated, 20 min)/CFU (no heated). For *C. difficile* germination analysis, *C. difficile* spores were collected from 2-week Clospore media-cultured bacteria and purified with sucrose gradient layer (50, 45, 35, 25, and 10%). The heated purified spores were diluted to an OD_{600} of 1.0 in the germination buffer [10 mM Tris (pH 7.5), 150 mM NaCl,

100 mM glycine, and 10 mM taurocholic acid (TA)] to detect the germination ratio. The value of OD_{600} was monitored immediately (0 min, t_0), and was detected once every 2 min (t_x) for 20 min at 37°C. The germination ratio was calculated as OD_{600} (tx)/OD_{600} (T_0). Spores in germination buffer without TA were used as the negative control.

R20291, R20291ΔWA, and R20291ΔW Virulence in the Mouse Model of *C. difficile* Infection

C57BL/6 female mice (6 weeks old) were ordered from Charles River Laboratories, Cambridge, MA. All studies were approved by the Institutional Animal Care and Use Committee of University of South Florida. The experimental design and antibiotic administration were conducted as described earlier (Sun et al., 2011). Briefly, 30 mice were divided into three groups in six cages. Group 1 mice were challenged with R20291 spores, group 2 mice with R20291ΔWA spores, and group 3 mice with R20291ΔW spores, respectively. Mice were given an orally administered antibiotic cocktail (kanamycin 0.4 mg/ml, gentamicin 0.035 mg/ml, colistin 0.042 mg/ml, metronidazole 0.215 mg/ml, and vancomycin 0.045 mg/ml) in drinking water for 4 days. After 4 days of antibiotic treatment, all mice were given autoclaved water for 2 days, followed by one dose of clindamycin (10 mg/kg, intraperitoneal route) 24 h before spores challenge (Day 0). After that mice were orally gavaged with 10^6 spores and monitored daily for a week for changes in weight, diarrhea, and mortality. If body weight loss was equal to or greater than 20%, the mouse was euthanized and counted as a dead one. Mortality also included mice that were succumbed to disease. Diarrhea was defined as soft or watery feces. All survived mice were humanely euthanized on day 7 of post-*C. difficile* challenge.

Enumeration of *C. difficile* Spores and Determination of Toxin Level in Feces

Fecal pellets from post-infection day 0 to day 7 were collected from each mouse and stored at −80°C. To enumerate *C. difficile* spores, feces were diluted with PBS at a final concentration of 0.1 g/ml, followed by adding 900 µl of absolute ethanol into 100 µl of the fecal solution, and kept at room temperature for 1 h to inactivate vegetative cells. Afterward, 200 µl of vegetative cells inactivated fecal solution from the same group and the same day was mixed. Then, fecal samples were serially diluted and plated on BHIS-CCT plates (250 µg/ml D-cycloserine, 8 µg/ml cefoxitin, and 0.1% TA). After 48-h incubation, colonies were counted and expressed as CFU/g feces. To evaluate toxin tilter in feces, 0.1 g/ml of the fecal solution was diluted two times with PBS, followed by examining TcdA and TcdB ELISA.

Statistical Analysis

The reported experiments were conducted in independent biological triplicates, and each sample was additionally taken in technical triplicates. Animal survivals were analyzed by Kaplan–Meier survival analysis and compared by the log-rank test. One-way ANOVA with *post hoc* Tukey test was used for more than two groups' comparison. Results were expressed as mean ± SEM. Differences were considered statistically significant if $p < 0.05$ (*).

TABLE 2 | Alignments of *fliW-csrA* DNA and protein sequences in *Clostridioides difficile* strains.

Strain	Sequence type (ribotype)	Genome accession	Identity (%)		
			DNA	Protein	
			fliW-csrA	FliW	CsrA
C. difficile DH	ST42 (RT106)	CP022524.1	100	100	100
C. difficile CD196	ST1 (RT027)	FN538970.1	100	100	100
C. difficile ATCC8689	ST3 (RT001)	CP011968.1	99.17	99.23	100
C. difficile TW11	ST11 (RT078)	CP035499.1	96.99	98.46	97.14
C. difficile M120	ST11 (RT078)	FN665653.1	96.99	98.46	97.14
C. difficile Z31	ST3 (RT009)	CP013196.1	88.98	83.85	92.86
C. difficile DSM27639	ST54 (RT012)	CP011847.1	88.81	83.85	92.86
C. difficile 630	ST54 (RT012)	CP010905.2	88.81	83.08	92.86
C. difficile CDT4	ST35 (RT046)	CP029152.1	88.65	83.08	92.86
C. difficile M68	ST37 (RT017)	FN668375.1	88.65	83.08	92.86

RESULTS

Highly Conserved *fliW* and *csrA* Genes in *C. difficile*

DNA and protein sequences of *fliW* and *csrA* from 10 *C. difficile* strains belonging to different ribotypes (RTs), including RT106, RT027, RT001, RT078, RT009, RT012, RT046, and RT017 were selected and aligned to those of R20291 (**Table 2**). We found that *fliW* and *csrA* genes are broadly found in *C. difficile* genomes, and both DNA and protein sequences of *fliW* and *csrA* are conserved across different *C. difficile* strains. These results motivated us to investigate the functions of *fliW* and *csrA* in *C. difficile*.

Construction of *fliW* and *fliW-csrA* Deletion Mutants and Complementation Strains

The *C. difficile* R20291 flagellar gene operon was analyzed through the *IMG/M* website,[3] and the late-stage flagellar genes (F1) are drawn as **Figure 1A** (Stevenson et al., 2015). Among them, *fliW* and *csrA* genes have a 10 bp overlap and were demonstrated as cotranscription by RT-PCR (**Supplementary Figure 1**).

To analyze the role of *fliW* and *csrA* in R20291 (NC_013316.1), CRISPR-AsCpfI-based plasmid pDL1 (pMTL82151-Ptet-AscpfI)

[3]https://img.jgi.doe.gov/

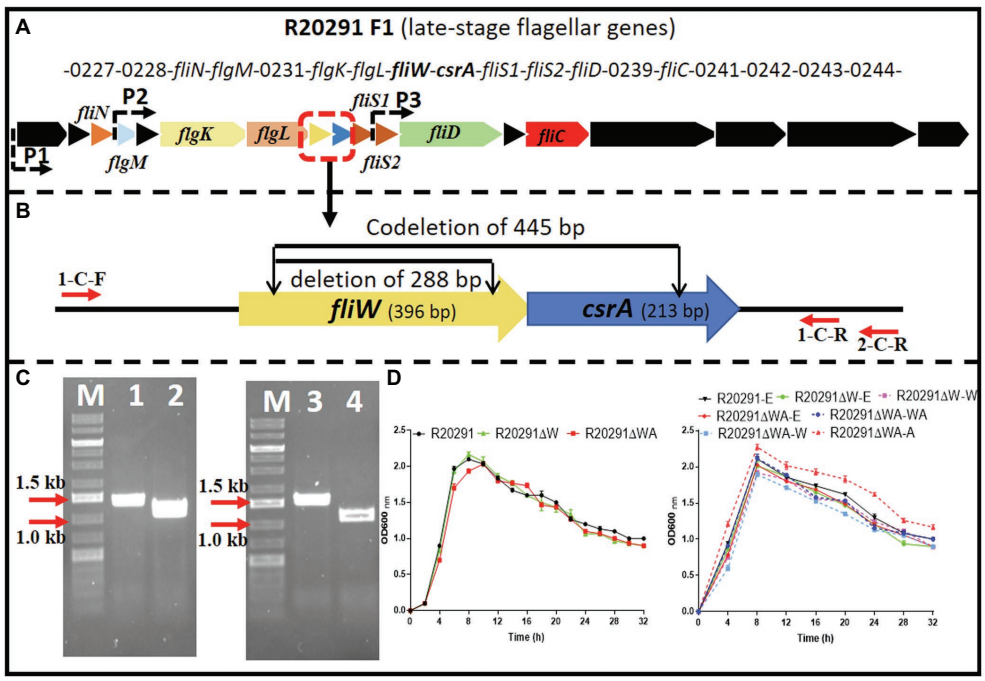

FIGURE 1 | R20291 late-stage flagellar genes (F1) and *fliW* and *fliW-csrA* deletion. **(A)** Schematic representation of late-stage flagellar genes (F1). Dotted arrows (P1, P2, and P3) indicate the potential promoters in F1. **(B)** Deletion of *fliW* and *fliW-csrA* genes. 1-C-F/R were used to verify *fliW* deletion, and 1-C-F and 2-C-R were used to test *fliW-csrA* codeletion. **(C)** Verification of *fliW* and *fliW-csrA* deletions by PCR. M, DNA ladder; 1, R20291 genome as PCR template; 2, R20291ΔW genome as PCR template; 3, R20291 genome as PCR template; and 4, R20291ΔWA genome as PCR template. **(D)** Growth profile of parent strain and gene deletion mutants. Experiments were independently repeated thrice. Bars stand for mean ± SEM. One-way ANOVA with *post hoc* Tukey test was used for statistical significance.

was constructed for gene deletion in *C. difficile* (Zhu et al., 2021). pDL1-*fliW* and pDL1-*csrA* gene deletion plasmids were constructed, and the *fliW* gene (288 bp deletion; R20291ΔW) was deleted successfully. However, after several trials, we could not get the *csrA* gene deletion mutant possibly due to its small size (213 bp) or particularly unknown roles for R20291. We also tried to use Clostron and *pyrE* gene edit system to delete *csrA* gene, but failed to get the correct mutant. Therefore, we constructed *fliW-csrA* codeletion plasmid pDL1-*fliW-csrA*. Part of *fliW-csrA* (445 bp deletion) gene was codeleted, and the plasmid curing mutant R20291ΔWA was obtained (**Figure 1B,C**). To study the role of *csrA* in R20291, the single gene complementation strain R20291ΔWA-W and R20291ΔWA-A were constructed. R20291, R20291-pMTL84153 (R20291-E), R20291ΔW-pMTL84153 (R20291ΔW-E), and R20291ΔWA-pMTL84153 (R20291ΔWA-E) were used as control strains when needed.

The effects of *fliW* and *fliW-csrA* deletion on R20291 growth were evaluated. **Figure 1D** shows that there was no significant difference in bacterial growth between parent strain and mutants in BHIS media.

Effects of *fliW* and *fliW-csrA* Deletions on *C. difficile* Motility and Biofilm Formation

To characterize the effects of *fliW* and *fliW-csrA* deletions on *C. difficile* motility, swimming, and swarming motilities of R20291, R20291ΔWA, and R20291ΔW were first analyzed at 24 and 48-h post-inoculation (**Figure 2A**; **Supplementary Figure 2**), respectively. The diameter of the swimming halo of R20291ΔWA increased by 27.2% ($p < 0.05$), while that of R20291ΔW decreased by 58.4% ($p < 0.05$) compared to that of R20291. Next, we examined the motility of the complementation strains (**Figure 2B**; **Supplementary Figure 2**), and similar results were obtained among R20291-E, R20291ΔWA-E (with the swimming halo increased by 74.8%, $p < 0.05$), and R20291ΔW-E (with the swimming halo decreased by 59.2%, $p < 0.05$; **Figure 2B**). No significant difference was detected between complementation strain R20291ΔWA-WA, R20291ΔWA-W, R20291ΔW-W, and the parent strain R20291-E except R20291ΔWA-A which decreased by 52.0% ($p < 0.05$) in swimming halo (**Figure 2B**). The swarming (48 h) and swimming (24 h) motilities analyzed on agar plates are shown in **Supplementary Figure 2**.

The effects of *fliW* and *fliW-csrA* deletions on *C. difficile* biofilm formation were also analyzed. In comparison with R20291, the biofilm formation of R20291ΔW increased by 49.5% ($p < 0.01$), and no significant difference in biofilm formation was detected in R20291ΔWA (**Figure 2C**). The biofilm formation of R20291ΔW-E increased 112.3% ($p < 0.001$) and R20291ΔWA-A increased by 79.9% ($p < 0.001$) compared to R20291-E (**Figure 2D**). Meanwhile, the biofilm formation

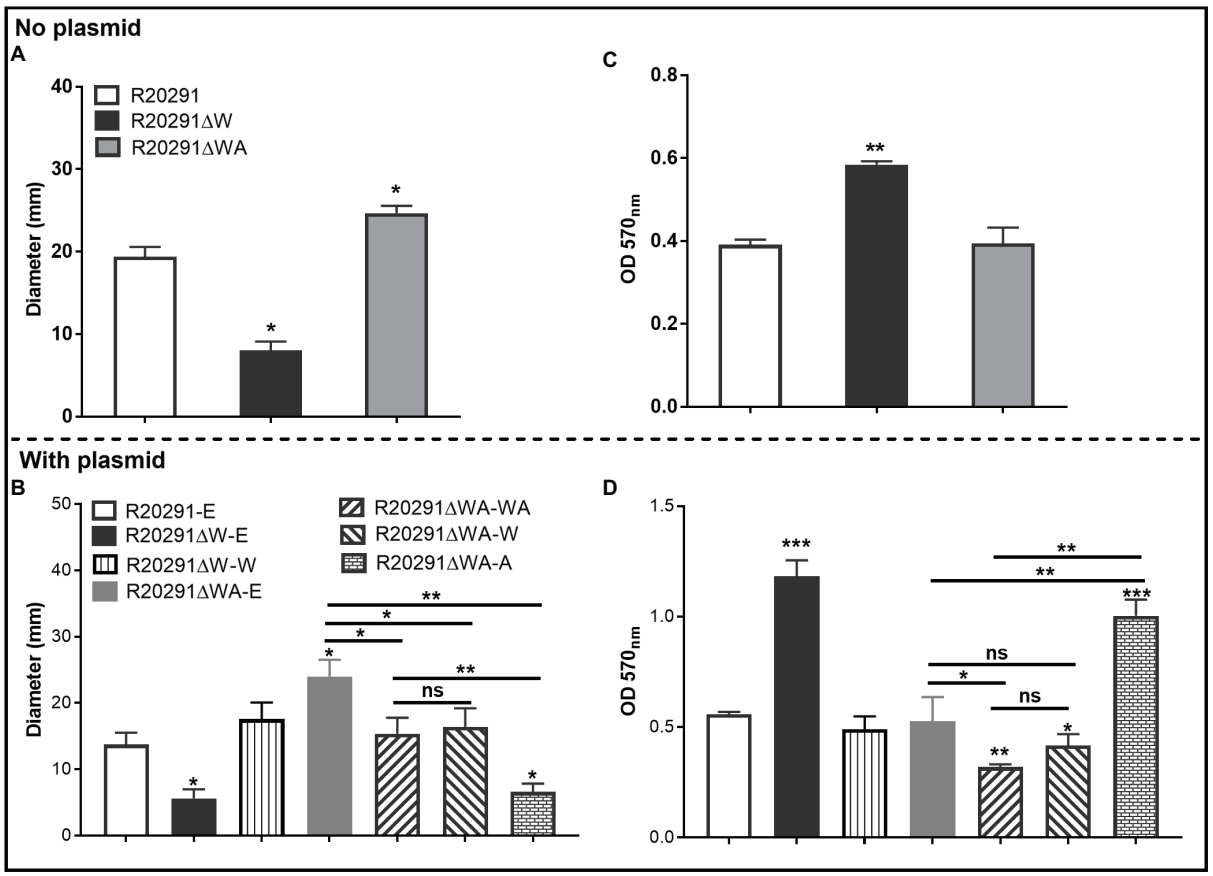

FIGURE 2 | Motility and biofilm analysis. **(A,B)**: Halo diameter of motility (swimming analysis on 0.175% agar plate). **(C,D)**: Biofilm formation analysis. Bars stand for mean ± SEM (*$p < 0.05$, **$p < 0.01$, and ***$p < 0.001$). One-way ANOVA with *post hoc* Tukey test was used for statistical significance. ***directly upon the column means the significant difference of the experimental strain compared to R20291 or R20291-E.

of R20291ΔWA-WA and R20291ΔWA-W decreased by 42.8% ($p < 0.01$) and 25.2% ($p < 0.05$), respectively.

Together, these data indicate that loss of FliW impairs *C. difficile* motility, and increases biofilm production. The decrease of motility and increase in biofilm production were also detected in R20291ΔWA-A, which was largely restored by coexpressing *fliW* with *csrA* in R20291ΔWA (**Figures 2B**,**D**), indicating that FliW could antagonize CsrA to regulate bacterial motility and biofilm production.

Effects of *fliW* and *fliW-csrA* Deletions on Bacterial Adherence *in vitro*

The ability of *C. difficile* vegetative cells to adhere to HCT-8 cells *in vitro* was analyzed. **Figure 3A** shows that the mean adhesion number of R20291 was 2.40 ± 0.70 bacteria/cell, while that of R20291ΔW was 7.17 ± 0.61, which was 3.0-fold ($p < 0.0001$) of R20291. No significant difference was detected between R20291ΔWA and R20291. In the complementation strains, we detected a similar result which showed that the mean adhesion number of R20291ΔW-E (6.17 ± 0.64) was 3.20-fold ($p < 0.0001$) of R20291-E (1.93 ± 0.25; **Figure 3B**). The adhesion ability of complementation strains nearly recovered to that of wild-type strain except for R20291ΔWA-A (7.13 ± 0.66, $p < 0.0001$) which was 3.69-fold of R20291-E in the mean adhesion number (**Figure 3B**).

To visualize the adhesion of *C. difficile* to HCT-8 cells, the *C. difficile* vegetative cells were labeled with the chemical 5(6)-CFDA. **Figures 3C**,**D** shows that the fluorescence intensity of R20291ΔW was 3.50-fold ($p < 0.0001$) of that in R20291, and the fluorescence intensity of R20291ΔW-E was 2.36-fold ($p < 0.001$), and R20291ΔWA-A was 4.08-fold ($p < 0.0001$) of that in R20291-E, respectively, which is consistent with the results shown in **Figures 3A**,**B**. Meanwhile, the adherence of *C. difficile* to HCT-8 cells was also visualized by fluorescence microscopy (**Supplementary Figure 3**).

Our data showed that FliW negatively affects bacterial adherence. CsrA complementation in R20291ΔWA increased adherence, while the phenotype change can be recovered partially when *fliW* was coexpressed with *csrA* in R20291ΔWA, suggesting that FliW could antagonize CsrA to regulate bacterial adherence. The results from bacterial adherence analysis were consistent with biofilm production analysis indicating the close relation between biofilm production and adherence in *C. difficile*.

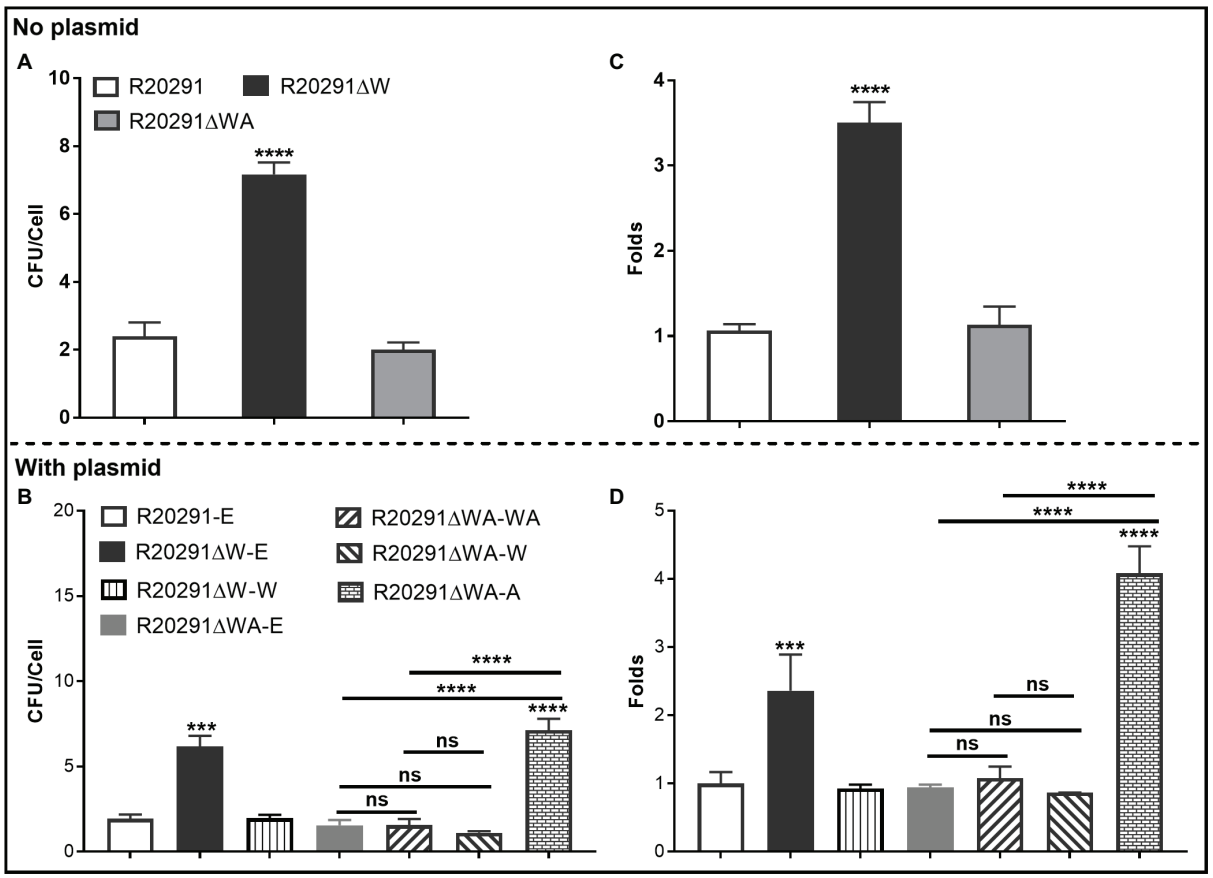

FIGURE 3 | Adhesion analysis **(A,B)**: Adherence of *C. difficile* vegetative cells to HCT-8 cells *in vitro*. **(C,D)**: Adhesion analysis with 5(6)-CFDA dye. The fluorescence intensity was scanned by the multi-mode reader (excitation, 485 nm; emission, 528 nm). The original relative fluorescence unit (RFU) was recorded as F0, after PBS wash, the RFU was recorded as F1. The adhesion ratio was calculated as follows: F1/F0. Experiments were independently repeated thrice. Bars stand for mean ± SEM (*$p < 0.05$, **$p < 0.01$, ***$p < 0.001$, and ****$p < 0.0001$). One-way ANOVA with *post hoc* Tukey test was used for statistical significance. * directly upon the column means the significant difference of the experimental strain compared to R20291 or R20291-E.

Effects of Deletion and Overexpression of *fliW* and *fliW-csrA* on *fliC* Expression

In *B. subtilis*, FliW interacts with CsrA to regulate *hag* (a homolog of *fliC*) translation. We reasoned that FliW and CsrA would also regulate *fliC* expression in *C. difficile*. As shown in **Figure 4A**, the transcription of *fliC* in R20291ΔWA increased 1.12-fold ($p < 0.05$), while the *fliW* deletion impaired the *fliC* transcription slightly while no significant difference. **Figure 4B** shows the production of FliC in R20291ΔW dramatically decreased (10.4-fold reduction, $p < 0.001$), while that of R20291ΔWA increased significantly (increased by 27.5%, $p < 0.05$). To further determine the role of the single-gene *csrA* on FliC synthesis, *csrA* and *fliW* were complemented into R20291ΔWA or overexpressed in R20291, respectively. Results showed that the significant difference of *fliC* transcription could only be detected in R20291ΔWA-E (increased by 32.3%, $p < 0.05$; **Figure 4C**) and R20291-W (increased by 69.8%) compared to R20291-E (**Figure 4E**). Interestingly, the FliC production of R20291ΔWA-A decreased 3.2-fold ($p < 0.001$) compared to that of R20291-E, while that of R20291ΔWA-WA only decreased by 14.3% ($p < 0.05$), and no significant difference of FliC production in R20291ΔWA-W was detected (**Figure 4D**). As shown in **Figures 4E,F**, the *fliC* transcription of R20291-A was not affected compared to R20291-E, but the FliC production in R20291-A decreased 5.3-fold ($p < 0.0001$). The decrease in FliC production in R20291-A can be partially recovered when *fliW* was coexpressed with *csrA* (R20291-WA decreased by 16.2%, $p < 0.05$).

Collectively, our data indicate that CsrA negatively modulates *fliC* expression post-transcriptionally and FliW antagonizes CsrA to regulate *fliC* expression possibly through inhibiting CsrA-mediated negative post-transcriptional regulation.

Effects of *fliW* and *fliW-csrA* Deletions on Toxin Expression

It has been reported that the expression of *csrA* could affect toxin expression in *C. difficile* (Gu et al., 2018). To evaluate the effects of *fliW* and *fliW-csrA* deletions on toxin production, the supernatants of *C. difficile* cultures were collected at 24- and 48-h post-inoculation, and the toxin concentration was

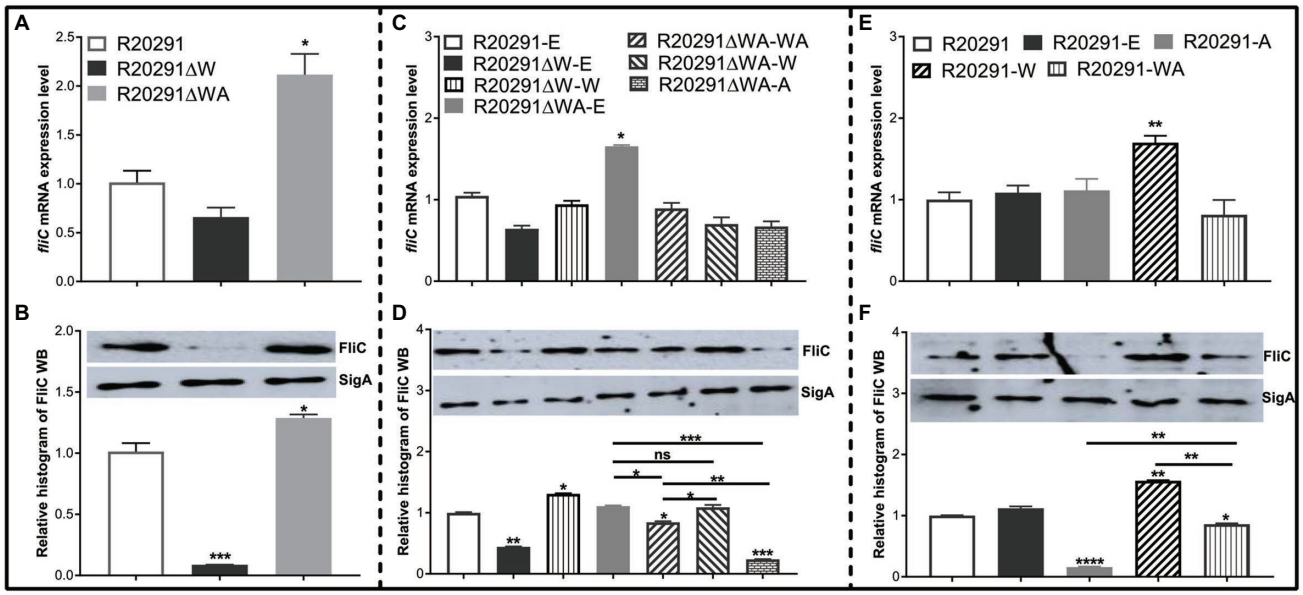

FIGURE 4 | *fliC* expression analysis. **(A,C,E)** Analysis of *fliC* expression on transcription level. **(B,D,F)** Analysis of *fliC* expression on translation level by Western blot. SigA protein was used as a loading control. Experiments were independently repeated thrice. Bars stand for mean ± SEM (*$p < 0.05$, **$p < 0.01$, ***$p < 0.001$, and ****$p < 0.0001$). One-way ANOVA with *post hoc* Tukey test was used for statistical significance. **** upon the column directly means the significant difference of experimental strain compared to R20291 or R20291-E.

determined by ELISA. **Figure 5A** shows that the TcdA concentration of R20291ΔWA decreased by 28.6% ($p < 0.05$), while R20291ΔW increased by 65.1% ($p < 0.01$) compared to R20291 at 24-h post-inoculation. However, after 48-h incubation, no significant difference was detected. In **Figure 5B**, TcdB concentration of R20291ΔWA decreased by 26.4% ($p < 0.05$) at 24-h post-inoculation, while that of R20291ΔW increased by 93.6% ($p < 0.01$) at 24 h and 33.0% ($p < 0.05$) at 48 h. Similar results were also detected in the complementation strains group (**Figures 5C**,**D**). As shown in **Figures 5C**,**D**, after 24-h post-inoculation, TcdA (**Figure 5C**) concentration of R20291ΔWA-E and R20291ΔWA-W decreased by 33.0% (*$p < 0.05$) and 47.7% ($p < 0.01$), and TcdB (**Figure 5D**) concentration of R20291ΔWA-E and R20291ΔWA-W decreased by 37.9% ($p < 0.05$) and 31.3% ($p < 0.05$), respectively, while TcdA concentration of R20291ΔW-E, R20291ΔWA-A, and R20291ΔW-W increased by 83.1% ($p < 0.01$), 64.7% ($p < 0.05$), and 56.5% ($p < 0.05$), respectively. Meanwhile, TcdB concentration of R20291ΔW-E increased by 100.2% ($p < 0.01$). At 48-h post-inoculation, though no significant difference in TcdA production was detected among different *C. difficile* strains, TcdB concentration of R20291ΔWA-A increased by 28.5% ($p < 0.05$) compared to R20291-E.

To analyze the transcription of *tcdA* and *tcdB* in the complementation strains, RT-qPCR was performed. As shown in **Figures 5E**,**F**, the transcription of *tcdA* and *tcdB* of R20291ΔWA-E and R20291ΔWA-W decreased significantly ($p < 0.05$), while that of R20291ΔW-E increased significantly ($p < 0.05$). Interestingly, the *tcdA* transcription of R20291ΔWA-A also showed a significant increase ($p < 0.05$) compared to the wild-type strain. Our data indicate that FliW negatively regulates toxin expression, while CsrA plays a positive regulation role in toxin expression.

Effects of *fliW* and *fliW-csrA* Deletions on Sporulation and Germination

To assay the sporulation ratio of *C. difficile* strains, R20291, R20291ΔWA, and R20291ΔW were cultured in Clospore media for 48 and 96 h, respectively. Results (**Supplementary Figure 4A**) showed that no significant difference in the sporulation ratio was detected between the wild-type strain and the mutants. The germination ratio of *C. difficile* spores was evaluated as well. Purified spores of R20291, R20291ΔWA, and R20291ΔW were incubated in the germination buffer supplemented with taurocholic acid (TA). As shown in **Supplementary Figure 4B**, there was no significant difference in the germination ratio between the wild-type strain and the mutants.

Evaluation of *fliW* and *fliW-csrA* Deletions on Bacterial Virulence in the Mouse Model of CDI

To evaluate the effects of *fliW* and *fliW-csrA* deletions on *C. difficile* virulence *in vivo*, the mouse model of CDI was used. Thirty mice ($n = 10$ per group) were orally challenged with R20291, R20291ΔWA, or R20291ΔW spores (1×10^6 spores/mouse) after antibiotic treatment. As shown in **Figure 6A**, the R20291ΔW infection group lost more weight at post-challenge days 1 ($p < 0.05$), and the R20291ΔWA infection group lost less weight at post-challenge days 3 ($p < 0.05$) compared to the R20291 infection group. **Figure 6B** shows that 60% of mice succumbed to severe disease within 4 days

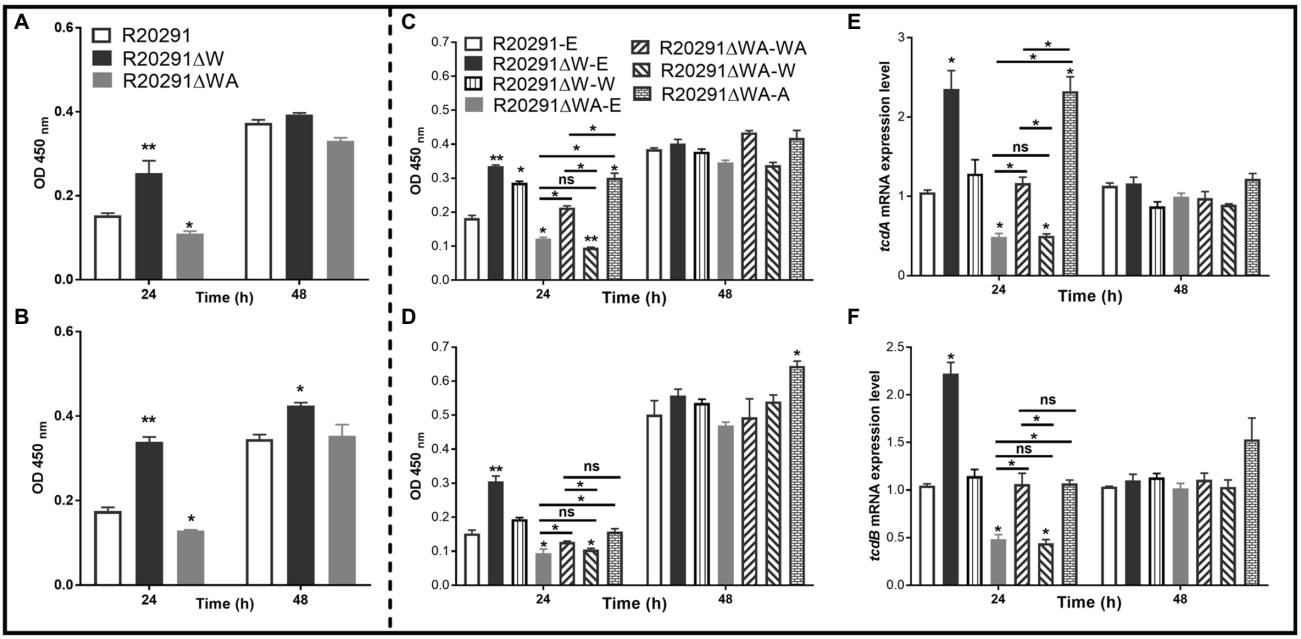

FIGURE 5 | Toxin expression analysis. **(A)** TcdA concentration in the supernatants of R20291, R20291ΔWA, and R20291ΔW. **(B)** TcdB concentration in the supernatants of R20291, R20291ΔWA, and R20291ΔW. **(C)** TcdA concentration in the supernatants of parental and gene complementation strains. **(D)** TcdB concentration in the supernatants of parental and gene complementation strains. **(E)** Transcription of *tcdA* in the supernatants of parental and gene complementation strains. **(F)** Transcription of *tcdB* in the supernatants of parental and gene complementation strains. Experiments were independently repeated thrice. Bars stand for mean ± SEM (*$p < 0.05$, **$p < 0.01$). One-way ANOVA with *post hoc* Tukey test was used for statistical significance. ** upon the column directly means the significant difference of experimental strain compared to R20291 or R20291-E.

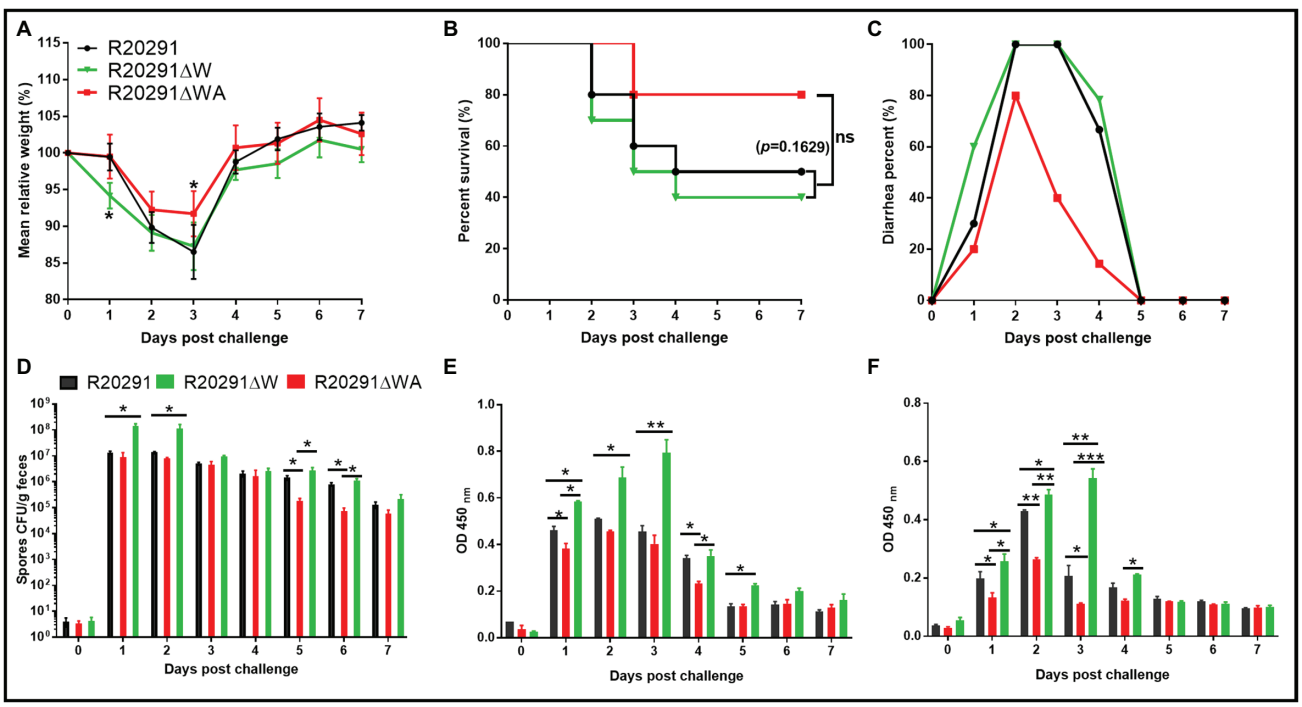

FIGURE 6 | Effects of *fliW* and *fliW-csrA* deletion on *C. difficile* virulence in mice. **(A)** Mean relative weight changes. **(B)** Survival curve. **(C)** Diarrhea percentage. **(D)** *Clostridioides difficile* in feces. **(E)** TcdA titer of fecal sample. **(F)** TcdB titer of fecal sample. Bars stand for mean ± SEM (*$p < 0.05$, **$p < 0.01$, ***$p < 0.001$). One-way ANOVA with *post hoc* Tukey test was used for statistical significance. Animal survivals were analyzed by Kaplan–Meier survival analysis with a log-rank test of significance.

in the R20291ΔW infection group and 20% in the R20291ΔWA infection group compared to 50% mortality in the R20291 infection group (no significant difference with log-rank analysis, $p = 0.1629$). Meanwhile, 100% of mice developed diarrhea in both the R20291ΔW and R20291 infection groups vs. 80% in the R20291ΔWA infection group at post-challenge days 2 (**Figure 6C**). As shown in **Figure 6D**, the spores CFU of the R20291ΔW infection group increased in the fecal shedding samples at post-challenge days 1 and 2 ($p < 0.05$), while the spores CFU of the R20291ΔWA infection group decreased at post-challenge days 1, 5, and 6 ($p < 0.05$) compared to the R20291 infection group. Interestingly, while we did not detect significant differences in bacterial growth, germination, and sporulation between the wild-type strain and mutants, the spore numbers from different infection groups were different (**Figure 6D**). This kind of difference implied that the culture media we used *in vitro* cannot simulate the complicated intestine environment well, which can lead to the different outcomes in bacterial physiology between *in vitro* and *in vivo* analysis. CsrA, as a carbon storage regulator, its regulation on carbon metabolization, and other potential roles in the complicated gut environment *in vivo* remain to be further studied.

To evaluate the toxin level in the gut, the concentrations of TcdA and TcdB in the feces were measured by ELISA. In comparison with the R20291 infection group, the TcdA of the R20291ΔW infection group increased significantly at post-challenge days 1 ($p < 0.05$), 2 ($p < 0.05$), 3 ($p < 0.01$), and 5 ($p < 0.05$; **Figure 6E**), while the TcdA of the R20291ΔWA infection group decreased significantly at post-challenge days 1 ($p < 0.05$) and 4 ($p < 0.05$; **Figure 6E**). As shown in **Figure 6F**, the TcdB concentration of the R20291ΔWA infection group decreased significantly at post-challenge days 1 ($p < 0.05$), 2 ($p < 0.05$), and 3 ($p < 0.05$), and that of the R20291ΔW increased significantly at post-challenge days 1 ($p < 0.05$), 2 ($p < 0.01$), and 3 ($p < 0.01$). Taken together, our results indicate that the FliW defect increases R20291 pathogenicity *in vivo*, while the *fliW-csrA* codeletion impairs R20291 pathogenicity.

DISCUSSION

In this study, we sought to characterize the impacts of FliW, CsrA, and FliC on *C. difficile* pathogenicity. Our data suggest that CsrA negatively modulates *fliC* expression post-transcriptionally, and FliW affects *fliC* expression possibly through inhibiting CsrA-mediated negative post-transcriptional regulation. Our data also indicate that FliW negatively affects *C. difficile* pathogenicity possibly by antagonizing CsrA *in vivo*. Based on our current pleiotropic phenotype analysis, a similar partner-switching mechanism "FliW-CsrA-*fliC*/FliC" (FliC binds FliW, FliW binds CsrA, and CsrA regulates *fliC* translation by binding to 5′ untranslated *region* of *fliC* transcripts) is predicted in *C. difficile*, though more direct experimental data are needed to uncover the molecular interactions of CsrA, FliW, and *fliC*/FliC in *C. difficile* (**Supplementary Figure 5**).

It has been reported that overexpression of the *csrA* gene could result in flagella defects, poor motility, and increased toxin production and adhesion in *C. difficile* 630Δerm (Gu et al., 2018). In our study, we found that CsrA and FliW widely exist in *C. difficile* (**Table 2**), even in the *C. difficile* strains without flagella like *C. difficile* M120 (Stabler et al., 2009), indicating a potentially important role of FliW-CsrA in *C. difficile*. Interestingly, while there are no flagella in *C. difficile* M120, six flagellar structure genes (*fliS*, *fliN*, *flgK*, *flgL*, *fliC*, and *fliD*) are still found in the genome, which inspired us to explore the potential roles of *fliW*, *csrA*, and *fliC* in *C. difficile* by deleting or overexpressing *fliW*, *csrA*, and *fliW-csrA* genes. However, after several trials with different gene edit methods in *C. difficile*, we could not get the *csrA* gene deletion mutant possibly due to its small size. This result motivated us to construct *fliW-csrA* double deletion mutant. While we did not get the single *csrA* gene deletion, we complemented the single *fliW* gene in the *fliW-csrA* double deletion mutant for simulation of the *csrA* deletion effects. The important roles of CsrA in flagellin synthesis and flagellin homeostasis have been reported (Yakhnin et al., 2007; Mukherjee et al., 2011; Gu et al., 2018; Oshiro et al., 2019). A previous study had shown that the overexpression of the *csrA* gene can cause a dramatic motility reduction and a significant Hag decrease in *B. subtilis* (Yakhnin et al., 2007). FliW (the first protein regulator of CsrA activity) deletion abolished the *B. subtilis* swarming and swimming motility and decreased the number of flagella and flagellar length (Mukherjee et al., 2011, 2016). In this study, we obtained similar results that FliW defect impaired R20291 motility significantly (**Figure 2A**) and increased biofilm formation (**Figures 2C**,**D**). Interestingly, the *csrA* gene complementation in R20291ΔWA dramatically suppressed bacterial motility and showed a similar result to R20291ΔW, indicating that CsrA can suppress *C. difficile* motility and increase biofilm production, while FliW antagonizes *csrA* to regulate bacteria motility and biofilm formation indirectly.

The partner-switching mechanism "Hag-FliW-CsrA" on flagellin synthesis was elucidated in *B. subtilis*, and the intracellular concentration of the flagellar filament protein Hag is restricted tightly by the Hag-FliW-CsrA system (Mukherjee et al., 2011). To investigate whether FliW and CrsA coregulate the *fliC* expression in *C. difficile*, we evaluated both the transcriptional and translational expression level of *fliC* gene. Our data (**Figure 4**) showed that the *fliW* deletion resulted in a 10.4-fold decrease in FliC accumulation, while the *fliW-csrA* codeletion increased FliC production, indicating that CsrA could suppress the *fliC* translation and FliW antagonizes CsrA to regulate FliC production. In *csrA*, *fliW*, and *fliW-csrA* overexpression experimental groups, we found that the *csrA* overexpression dramatically decreased FliC production (5.3-fold reduction) and the reduction in FliC production in R20291-A can be partially recovered when *fliW-csrA* was coexpressed. The FliW complementation in R20291ΔWA did not affect FliC production, but the *fliW* overexpression in R20291 increased FliC production. Taken together, our data suggest that CsrA negatively modulates *fliC* expression post-transcriptionally and FliW antagonizes CsrA to regulate *fliC* expression through inhibiting CsrA-mediated negative post-transcriptional regulation, indicating a similar partner-switching mechanism

"FliW-CsrA-FliC" in *C. difficile*. In *B. subtilis*, two CsrA binding sites (BS1: A51 to A55; BS2: C75 to G82) were identified in the *hag* leader of the mRNA (Yakhnin et al., 2007). Based on the *hag* 5'-UTR sequence and CsrA conserved binding sequence, a 91 bp 5'-UTR structure with two potential CsrA binding sites (BS1: 5'-TGACAAGGATGT-3′, BS2: 5'-CTAAGGAGGG-3′) of *fliC* gene was predicted (**Supplementary Figure 6**; Dubey et al., 2005). Recently, it was also reported that cytoplasmic Hag levels play a central role in maintaining proper intracellular architecture, and the Hag-FliW-CsrA^{dimer} system works at nearly 1:1:1 stoichiometry in *B. subtilis* (Oshiro et al., 2019). Further studies on the exquisite interactions of CsrA, FliW, and *fliC*/FliC in *C. difficile* are still needed.

Flagella play multiple roles in bacterial motility, colonization, growth, toxin production, and survival optimization (Harshey, 2003; Duan et al., 2013; Stevenson et al., 2015). Recently, several papers have reported that the flagellar genes can affect toxin expression in *C. difficile*, but results from different research groups were controversial (Aubry et al., 2012; Baban et al., 2013; Stevenson et al., 2015). Aubry et al. (2012) reported that disruption of some early-stage flagellar genes (F3), such as *fliF*, *fliG*, and *fliM*, could lead to a significant reduction in *tcdR*, *tcdE*, *tcdA*, and *tcdB* expression in *C. difficile* 630Δ*erm*, but no significant difference of *tcdC* expression was detected. Inversely, disruption of late-stage flagellar genes (F1) such as *fliC* increased toxin expression in *C. difficile* 630Δ*erm*. In 2013, Baban et al. (2013) reported that the mutation of *flgE* (one of the F3 genes) resulted in a tenfold reduction in *tcdA* expression and corroborated that the expression of *tcdA* in a *fliC* mutant increased 44.4-fold compared to the wild-type strain *C. difficile* 630Δ*erm*. Surprisingly, Aubry et al. (2012) found that a glycosylation gene (CD0240, one of F2 region genes) mutation, which can totally abolish *C. difficile* 630 motility, but did not change toxin expression. Meanwhile, cyclic diguanylate (C-di-GMP), a cellular second messenger, was also reported to be involved in bacterial motility, biofilm formation, and toxin production by repressing the expression of flagellar genes in *C. difficile* (Purcell et al., 2012; McKee et al., 2013). While we did not detect the C-di-GMP concentration in *C. difficile*, it could be perturbed by *fliW* and *csrA* deletion affecting *C. difficile* physiology. It was hypothesized that the regulation of the flagellar genes on toxin expression could be caused by the direct change or loss of flagellar genes (such as *fliC* gene deletion) rather than loss of the functional flagella (Stevenson et al., 2015). Future study about *fliC* deletion in M120 will be very interesting and will further address the *fliC* gene function in *C. difficile* as there are no flagella in RT078 strains. In our study, data indicate that CsrA negatively modulates *fliC* translation and also plays a positive regulation in toxin expression. Inversely, FliW works against CsrA to regulate *fliC* expression, which can negatively regulate toxin production. While studies of flagellar effects on motility and toxin production in *C. difficile* from different groups were controversial, the role of the flagella in *C. difficile* pathogenicity cannot be overlooked. Dingle et al. (2011) and Baban et al. (2013) both showed higher mortality of the *fliC* mutant in the animal model of CDI compared to the wild-type strains. Our study showed results similar to the published data suggesting that R20291ΔW whose FliC production was dramatically suppressed exhibited higher fatality, while R20291ΔWA showed a decreased pathogenicity compared to R20291 (**Figure 6**). In 2014, Barketi-Klai et al. (2014) examined the pleiotropic roles of the *fliC* gene in R20291 during colonization in mice. Interestingly, the transcription of *fliW* and *csrA* in the *fliC* mutant was 2.03- and 4.36-fold, respectively, of that in R20291 *in vivo* experiment (Barketi-Klai et al., 2014), which further corroborated that there is a coregulation among *fliC*, *fliW*, and *csrA*. Surprisingly, transcription of *treA*, a trehalose-6-phosphate hydrolase, increased 177.63-fold in the *fliC* mutant compared to that of R20291 during *in vivo* infection (Barketi-Klai et al., 2014). Recently, Collins et al. (2018) hypothesized that dietary trehalose can contribute to the virulence of epidemic *C. difficile*. The relationship of FliW, CsrA, FliC, and trehalose metabolization is another interesting question in *C. difficile*, and some other carbon metabolism affected by the *fliC* mutation could also facilitate *C. difficile* pathogenesis *in vivo*. Previous studies have also highlighted that the flagella of *C. difficile* play an important role in toxin production, biofilm formation, and bacterial adherence to the host (Tasteyre et al., 2001; Dingle et al., 2011; Aubry et al., 2012; Baban et al., 2013; Ethapa et al., 2013). In this study, we showed that the FliW defect led to a significant motility decrease, while the biofilm, adhesion, and toxin production increased significantly. Inversely, R20291ΔWA-W, which can imitate the *csrA* gene deletion, showed an increase in motility and a decrease in biofilm formation, toxin production, and adhesion.

In conclusion, we characterized the function of FliW and CsrA and showed the pleiotropic functions of FliW and CsrA in R20291. Our data suggest that *fliW* and *csrA* play important roles in flagellin (FliC) synthesis, which could contribute to *C. difficile* pathogenicity. Currently, *in vitro* study of the interactions of CsrA, FliW, and *fliC*/FliC in *C. difficile* is underway in our group.

DATA AVAILABILITY STATEMENT

The original contributions presented in the study are included in the article/**Supplementary Material**, further inquiries can be directed to the corresponding author.

ETHICS STATEMENT

The animal study was reviewed and approved by the Institutional Animal Care and Use Committee of University of South Florida.

AUTHOR CONTRIBUTIONS

DZ and XS designed the experiments. DZ wrote the manuscript. DZ and SW performed the experiments. DZ and XS revised the manuscript. All authors contributed to the article and approved the submitted version.

FUNDING

This work was supported in part by the National Institutes of Health grants (R01-AI132711 and R01-AI149852).

ACKNOWLEDGMENTS

The authors thank Dr. Abhraham L. Sonnenshein at Tufts University, Dr. Joseph Sorg at Texas A&M, and Dr. Daniel Kearns at Indiana University for the gifts *C. difficile* R20291, *E.coli* HB101/pRK24, and anti-SigA primary antibody, respectively. We thank Dr. Nigel Minton at the University of Nottingham for the gift plasmids pMTL84151 and pMTL83353. We also thank Jessica Bullock and Dr. Heather Danhof for their mindful revision and comments.

SUPPLEMENTARY MATERIAL

The Supplementary Material for this article can be found online at: https://www.frontiersin.org/articles/10.3389/fmicb.2021.735616/full#supplementary-material

REFERENCES

Aubry, A., Hussack, G., Chen, W., KuoLee, R., Twine, S. M., Fulton, K. M., et al. (2012). Modulation of toxin production by the flagellar regulon in *Clostridium difficile*. *Infect. Immun.* 80, 3521–3532. doi: 10.1128/IAI.00224-12

Baban, S. T., Kuehne, S. A., Barketi-Klai, A., Cartman, S. T., Kelly, M. L., Hardie, K. R., et al. (2013). The role of flagella in *Clostridium difficile* pathogenesis: comparison between a non-epidemic and an epidemic strain. *PLoS One* 8:e73026. doi: 10.1371/journal.pone.0073026

Barketi-Klai, A., Monot, M., Hoys, S., Lambert-Bordes, S., Kuehne, S. A., Minton, N., et al. (2014). The flagellin FliC of *Clostridium difficile* is responsible for pleiotropic gene regulation during in vivo infection. *PLoS One* 9:e96876. doi: 10.1371/journal.pone.0096876

Chong, L. (2001). Molecular cloning—A laboratory manual, 3rd edition. *Science* 292:446. doi: 10.1126/science.1060677

Collins, J., Robinson, C., Danhof, H., Knetsch, C. W., van Leeuwen, H. C., Lawley, T. D., et al. (2018). Dietary trehalose enhances virulence of epidemic *Clostridium difficile*. *Nature* 553, 291–294. doi: 10.1038/nature25178

Dingle, T. C., Mulvey, G. L., and Armstrong, G. D. (2011). Mutagenic analysis of the *Clostridium difficile* flagellar proteins, FliC and FliD, and their contribution to virulence in hamsters. *Infect. Immun.* 79, 4061–4067. doi: 10.1128/IAI.05305-11

Duan, Q., Zhou, M., Zhu, L., and Zhu, G. (2013). Flagella and bacterial pathogenicity. *J. Basic Microbiol.* 53, 1–8. doi: 10.1002/jobm.201100335

Dubey, A. K., Baker, C. S., Romeo, T., and Babitzke, P. (2005). RNA sequence and secondary structure participate in high-affinity CsrA-RNA interaction. *RNA* 11, 1579–1587. doi: 10.1261/rna.2990205

Ethapa, T., Leuzzi, R., Ng, Y. K., Baban, S. T., Adamo, R., Kuehne, S. A., et al. (2013). Multiple factors modulate biofilm formation by the anaerobic pathogen *Clostridium difficile*. *J. Bacteriol.* 195, 545–555. doi: 10.1128/JB.01980-12

Ferreiro, M. D., Nogales, J., Farias, G. A., Olmedilla, A., Sanjuan, J., and Gallegos, M. T. (2018). Multiple CsrA proteins control key virulence traits in pseudomonas syringae pv. Tomato DC3000. *Mol. Plant-Microbe Interact.* 31, 525–536. doi: 10.1094/MPMI-09-17-0232-R

Fuller, M. E., Streger, S. H., Rothmel, R. K., Mailloux, B. J., Hall, J. A., Onstott, T. C., et al. (2000). Development of a vital fluorescent staining method for monitoring bacterial transport in subsurface environments. *Appl. Environ. Microbiol.* 66, 4486–4496. doi: 10.1128/AEM.66.10.4486-4496.2000

Gu, H., Qi, H., Chen, S., Shi, K., Wang, H., and Wang, J. (2018). Carbon storage regulator CsrA plays important roles in multiple virulence-associated processes of *Clostridium difficile*. *Microb. Pathog.* 121, 303–309. doi: 10.1016/j.micpath.2018.05.052

Harshey, R. M. (2003). Bacterial motility on a surface: many ways to a common goal. *Annu. Rev. Microbiol.* 57, 249–273. doi: 10.1146/annurev.micro.57.030502.091014

Heap, J. T., Kuehne, S. A., Ehsaan, M., Cartman, S. T., Cooksley, C. M., Scott, J. C., et al. (2010). The ClosTron: mutagenesis in clostridium refined and streamlined. *J. Microbiol. Methods* 80, 49–55. doi: 10.1016/j.mimet.2009.10.018

Heap, J. T., Pennington, O. J., Cartman, S. T., and Minton, N. P. (2009). A modular system for clostridium shuttle plasmids. *J. Microbiol. Methods* 78, 79–85. doi: 10.1016/j.mimet.2009.05.004

Hong, W., Zhang, J., Cui, G., Wang, L., and Wang, Y. (2018). Multiplexed CRISPR-Cpf1-mediated genome editing in *Clostridium difficile* toward the understanding of pathogenesis of *C. difficile* infection. *ACS Synth. Biol.* 7, 1588–1600. doi: 10.1021/acssynbio.8b00087

Janvilisri, T., Scaria, J., and Chang, Y. F. (2010). Transcriptional profiling of *Clostridium difficile* and Caco-2 cells during infection. *J. Infect. Dis.* 202, 282–290. doi: 10.1086/653484

Karna, S. L., Sanjuan, E., Esteve-Gassent, M. D., Miller, C. L., Maruskova, M., and Seshu, J. (2011). CsrA modulates levels of lipoproteins and key regulators of gene expression critical for pathogenic mechanisms of Borrelia burgdorferi. *Infect. Immun.* 79, 732–744. doi: 10.1128/IAI.00882-10

Kuehne, S. A., Cartman, S. T., Heap, J. T., Kelly, M. L., Cockayne, A., and Minton, N. P. (2010). The role of toxin A and toxin B in *Clostridium difficile* infection. *Nature* 467, 711–713. doi: 10.1038/nature09397

Lawhon, S. D., Frye, J. G., Suyemoto, M., Porwollik, S., McClelland, M., and Altier, C. (2003). Global regulation by CsrA in salmonella typhimurium. *Mol. Microbiol.* 48, 1633–1645. doi: 10.1046/j.1365-2958.2003.03535.x

Lawson, P. A., Citron, D. M., Tyrrell, K. L., and Finegold, S. M. (2016). Reclassification of *Clostridium difficile* as Clostridioides difficile (Hall and O'Toole 1935) Prevot 1938. *Anaerobe* 40, 95–99. doi: 10.1016/j.anaerobe.2016.06.008

Lessa, F. C., Gould, C. V., and McDonald, L. C. (2012). Current status of *Clostridium difficile* infection epidemiology. *Clin. Infect. Dis.* 55, S65–S70. doi: 10.1093/cid/cis319

Liu, M. Y., Yang, H., and Romeo, T. (1995). The product of the pleiotropic *Escherichia coli* gene csrA modulates glycogen biosynthesis via effects on mRNA stability. *J. Bacteriol.* 177, 2663–2672. doi: 10.1128/jb.177.10.2663-2672.1995

Lucchetti-Miganeh, C., Burrowes, E., Baysse, C., and Ermel, G. (2008). The post-transcriptional regulator CsrA plays a central role in the adaptation of bacterial pathogens to different stages of infection in animal hosts. *Microbiology* 154, 16–29. doi: 10.1099/mic.0.2007/012286-0

Lyras, D., O'Connor, J. R., Howarth, P. M., Sambol, S. P., Carter, G. P., Phumoonna, T., et al. (2009). Toxin B is essential for virulence of *Clostridium difficile*. *Nature* 458, 1176–1179. doi: 10.1038/nature07822

McKee, R. W., Mangalea, M. R., Purcell, E. B., Borchardt, E. K., and Tamayo, R. (2013). The second messenger cyclic Di-GMP regulates *Clostridium difficile* toxin production by controlling expression of sigD. *J. Bacteriol.* 195, 5174–5185. doi: 10.1128/JB.00501-13

Morris, E. R., Hall, G., Li, C., Heeb, S., Kulkarni, R. V., Lovelock, L., et al. (2013). Structural rearrangement in an RsmA/CsrA ortholog of Pseudomonas aeruginosa creates a dimeric RNA-binding protein, RsmN. *Structure* 21, 1659–1671. doi: 10.1016/j.str.2013.07.007

Mukherjee, S., Babitzke, P., and Kearns, D. B. (2013). FliW and FliS function independently to control cytoplasmic flagellin levels in *Bacillus subtilis*. *J. Bacteriol.* 195, 297–306. doi: 10.1128/JB.01654-12

Mukherjee, S., Oshiro, R. T., Yakhnin, H., Babitzke, P., and Kearns, D. B. (2016). FliW antagonizes CsrA RNA binding by a noncompetitive allosteric mechanism. *Proc. Natl. Acad. Sci. U. S. A.* 113, 9870–9875. doi: 10.1073/pnas.1602455113

Mukherjee, S., Yakhnin, H., Kysela, D., Sokoloski, J., Babitzke, P., and Kearns, D. B. (2011). CsrA-FliW interaction governs flagellin homeostasis and a checkpoint on flagellar morphogenesis in *Bacillus subtilis*. *Mol. Microbiol.* 82, 447–461. doi: 10.1111/j.1365-2958.2011.07822.x

Oren, A., and Garrity, G. M. (2018). Notification of changes in taxonomic opinion previously published outside the IJSEM. *Int. J. Syst. Evol. Microbiol.* 68, 2137–2138. doi: 10.1099/ijsem.0.002830

Oshiro, R. T., Rajendren, S., Hundley, H. A., and Kearns, D. B. (2019). Robust stoichiometry of FliW-CsrA governs flagellin homeostasis and cytoplasmic organization in *Bacillus subtilis*. *MBio* 10, e00533–e00519. doi: 10.1128/mBio.00533-19

Peniche, A. G., Savidge, T. C., and Dann, S. M. (2013). Recent insights into *Clostridium difficile* pathogenesis. *Curr. Opin. Infect. Dis.* 26, 447–453. doi: 10.1097/01.qco.0000433318.82618.c6

Perez, J., Springthorpe, V. S., and Sattar, S. A. (2011). Clospore: a liquid medium for producing high titers of semi-purified spores of *Clostridium difficile*. *J. AOAC Int.* 94, 618–626. doi: 10.1093/jaoac/94.2.618

Pessi, G., Williams, F., Hindle, Z., Heurlier, K., Holden, M. T., Camara, M., et al. (2001). The global posttranscriptional regulator RsmA modulates production of virulence determinants and N-acylhomoserine lactones in Pseudomonas aeruginosa. *J. Bacteriol.* 183, 6676–6683. doi: 10.1128/JB.183.22.6676-6683.2001

Purcell, E. B., McKee, R. W., McBride, S. M., Waters, C. M., and Tamayo, R. (2012). Cyclic diguanylate inversely regulates motility and aggregation in *Clostridium difficile*. *J. Bacteriol.* 194, 3307–3316. doi: 10.1128/JB.00100-12

Romeo, T., Gong, M., Liu, M. Y., and Brun-Zinkernagel, A. M. (1993). Identification and molecular characterization of csrA, a pleiotropic gene from Escherichia coli that affects glycogen biosynthesis, gluconeogenesis, cell size, and surface properties. *J. Bacteriol.* 175, 4744–4755. doi: 10.1128/jb.175.15.4744-4755.1993

Sabnis, N. A., Yang, H., and Romeo, T. (1995). Pleiotropic regulation of central carbohydrate metabolism in Escherichia coli via the gene csrA. *J. Biol. Chem.* 270, 29096–29104. doi: 10.1074/jbc.270.49.29096

Sebaihia, M., Wren, B. W., Mullany, P., Fairweather, N. F., Minton, N., Stabler, R., et al. (2006). The multidrug-resistant human pathogen *Clostridium difficile* has a highly mobile, mosaic genome. *Nat. Genet.* 38, 779–786. doi: 10.1038/ng1830

Sorger-Domenigg, T., Sonnleitner, E., Kaberdin, V. R., and Blasi, U. (2007). Distinct and overlapping binding sites of *Pseudomonas aeruginosa* Hfq and RsmA proteins on the non-coding RNA RsmY. *Biochem. Biophys. Res. Commun.* 352, 769–773. doi: 10.1016/j.bbrc.2006.11.084

Stabler, R. A., He, M., Dawson, L., Martin, M., Valiente, E., Corton, C., et al. (2009). Comparative genome and phenotypic analysis of *Clostridium difficile* 027 strains provides insight into the evolution of a hypervirulent bacterium. *Genome Biol.* 10:R102. doi: 10.1186/gb-2009-10-9-r102

Stevenson, E., Minton, N. P., and Kuehne, S. A. (2015). The role of flagella in *Clostridium difficile* pathogenicity. *Trends Microbiol.* 23, 275–282. doi: 10.1016/j.tim.2015.01.004

Sun, X., Wang, H., Zhang, Y., Chen, K., Davis, B., and Feng, H. (2011). Mouse relapse model of *Clostridium difficile* infection. *Infect. Immun.* 79, 2856–2864. doi: 10.1128/IAI.01336-10

Tasteyre, A., Barc, M. C., Collignon, A., Boureau, H., and Karjalainen, T. (2001). Role of FliC and FliD flagellar proteins of *Clostridium difficile* in adherence and gut colonization. *Infect. Immun.* 69, 7937–7940. doi: 10.1128/IAI.69.12.7937-7940.2001

Timmermans, J., and Van Melderen, L. (2010). Post-transcriptional global regulation by CsrA in bacteria. *Cell. Mol. Life Sci.* 67, 2897–2908. doi: 10.1007/s00018-010-0381-z

Wang, Y., Wang, S., Bouillaut, L., Li, C., Duan, Z., Zhang, K., et al. (2018). Oral immunization with nontoxigenic *Clostridium difficile* strains expressing chimeric fragments of TcdA and TcdB elicits protective immunity against *C. difficile* infection in both mice and hamsters. *Infect. Immun.* 86, e00489–e00418. doi: 10.1128/IAI.00489-18

Williams, D. R., Young, D. I., and Young, M. (1990). Conjugative plasmid transfer from *Escherichia coli* to clostridium acetobutylicum. *J. Gen. Microbiol.* 136, 819–826. doi: 10.1099/00221287-136-5-819

Yakhnin, H., Pandit, P., Petty, T. J., Baker, C. S., Romeo, T., and Babitzke, P. (2007). CsrA of Bacillus subtilis regulates translation initiation of the gene encoding the flagellin protein (hag) by blocking ribosome binding. *Mol. Microbiol.* 64, 1605–1620. doi: 10.1111/j.1365-2958.2007.05765.x

Zhu, D., Bullock, J., He, Y., and Sun, X. (2019). Cwp22, a novel peptidoglycan cross-linking enzyme, plays pleiotropic roles in *Clostridioides difficile*. *Environ. Microbiol.* 21, 3076–3090. doi: 10.1111/1462-2920.14706

Zhu, D., Patabendige, H., Tomlinson, B.R., Wang, S., Hussain, S., Flores, D., et al. (2021). Cwl0971, a novel peptidoglycan hydrolase, plays pleiotropic roles in *Clostridioides difficile* R20291. *Environ. Microbiol.* [Epub ahead of print] doi: 10.1111/1462-2920.15529.

Conflict of Interest: The authors declare that the research was conducted in the absence of any commercial or financial relationships that could be construed as a potential conflict of interest.

Publisher's Note: All claims expressed in this article are solely those of the authors and do not necessarily represent those of their affiliated organizations, or those of the publisher, the editors and the reviewers. Any product that may be evaluated in this article, or claim that may be made by its manufacturer, is not guaranteed or endorsed by the publisher.

Copyright © 2021 Zhu, Wang and Sun. This is an open-access article distributed under the terms of the Creative Commons Attribution License (CC BY). The use, distribution or reproduction in other forums is permitted, provided the original author(s) and the copyright owner(s) are credited and that the original publication in this journal is cited, in accordance with accepted academic practice. No use, distribution or reproduction is permitted which does not comply with these terms.

frontiers in Microbiology

ORIGINAL RESEARCH
published: 29 November 2021
doi: 10.3389/fmicb.2021.784856

The Compound U18666A Inhibits the Intoxication of Cells by *Clostridioides difficile* Toxins TcdA and TcdB

Panagiotis Papatheodorou[1], Selina Kindig[1], Adriana Badilla-Lobo[2], Stephan Fischer[1], Ebru Durgun[1†], Tharani Thuraisingam[1†], Alexander Witte[3†], Shuo Song[3†], Klaus Aktories[3], Esteban Chaves-Olarte[2], César Rodríguez[2] and Holger Barth[1]*

[1] Institute of Pharmacology and Toxicology, Ulm University Medical Center, Ulm, Germany, [2] Centro de Investigación en Enfermedades Tropicales and Facultad de Microbiología, Universidad de Costa Rica, San José, Costa Rica, [3] Institute of Experimental and Clinical Pharmacology and Toxicology, Albert Ludwig University Freiburg, Freiburg, Germany

OPEN ACCESS

Edited by:
Meina Neumann-Schaal, German Collection of Microorganisms and Cell Cultures GmbH (DSMZ), Germany

Reviewed by:
Harald Genth, Hannover Medical School, Germany
Glen Carter, The University of Melbourne, Australia

***Correspondence:**
Panagiotis Papatheodorou
panagiotis.papatheodorou@uni-ulm.de

†Present address:
Ebru Durgun, Institute of Anatomy and Cell Biology, Ulm University, Ulm, Germany
Tharani Thuraisingam, Nuvisan GmbH, Neu-Ulm, Germany
Alexander Witte, Pfizer Manufacturing Deutschland GmbH, Freiburg, Germany
Shuo Song, Central Laboratory, Shenzhen Samii International Medical Center, Shenzhen, China

Specialty section:
This article was submitted to Infectious Agents and Disease, a section of the journal Frontiers in Microbiology

Received: 28 September 2021
Accepted: 01 November 2021
Published: 29 November 2021

Citation:
Papatheodorou P, Kindig S, Badilla-Lobo A, Fischer S, Durgun E, Thuraisingam T, Witte A, Song S, Aktories K, Chaves-Olarte E, Rodríguez C and Barth H (2021) The Compound U18666A Inhibits the Intoxication of Cells by Clostridioides difficile Toxins TcdA and TcdB. Front. Microbiol. 12:784856. doi: 10.3389/fmicb.2021.784856

The intestinal pathogen *Clostridioides (C.) difficile* is a major cause of diarrhea both in hospitals and outpatient in industrialized countries. This bacterium produces two large exotoxins, toxin A (TcdA) and toxin B (TcdB), which are directly responsible for the onset of clinical symptoms of *C. difficile*-associated diseases (CDADs), such as antibiotics-associated diarrhea and the severe, life-threatening pseudomembranous colitis. Both toxins are multidomain proteins and taken up into host eukaryotic cells via receptor-mediated endocytosis. Within the cell, TcdA and TcdB inactivate Rho and/or Ras protein family members by glucosylation, which eventually results in cell death. The cytotoxic mode of action of the toxins is the main reason for the disease. Thus, compounds capable of inhibiting the cellular uptake and/or mode-of-action of both toxins are of high therapeutic interest. Recently, we found that the sterol regulatory element-binding protein 2 (SREBP-2) pathway, which regulates cholesterol content in membranes, is crucial for the intoxication of cells by TcdA and TcdB. Furthermore, it has been shown that membrane cholesterol is required for TcdA- as well as TcdB-mediated pore formation in endosomal membranes, which is a key step during the translocation of the glucosyltransferase domain of both toxins from endocytic vesicles into the cytosol of host cells. In the current study, we demonstrate that intoxication by TcdA and TcdB is diminished in cultured cells preincubated with the compound U18666A, an established inhibitor of cholesterol biosynthesis and/or intracellular transport. U18666A-pretreated cells were also less sensitive against TcdA and TcdB variants from the epidemic NAP1/027 *C. difficile* strain. Our study corroborates the crucial role of membrane cholesterol for cell entry of TcdA and TcdB, thus providing a valuable basis for the development of novel antitoxin strategies in the context of CDADs.

Keywords: bacterial toxin, toxin inhibitor, cholesterol biosynthesis, cholesterol transport, cholesterol

INTRODUCTION

Clostridioides difficile is a (nosocomial) pathogen of the human gut and the major cause of antibiotics-associated diarrhea and pseudomembranous colitis. This bacterium produces two exotoxins, toxin A (TcdA) and toxin B (TcdB), that belong to the family of the clostridial glucosylating toxins (CGTs), also referred to as large clostridial cytotoxins (LCCs). The onset of clinical symptoms after *C. difficile* infections (CDIs) is strictly dependent on the toxins'

actions on target cells in the human gut (Kelly and LaMont, 2008; Aktories et al., 2017; Chandrasekaran and Lacy, 2017).

TcdA and TcdB are glucosylating toxins that specifically modify host cell target proteins by covalent attachment of a glucose moiety (Just et al., 1995). Both toxins utilize UDP-glucose for the mono-O-glucosylation of GTPases from the Rho and/or Ras family, which renders them inactive. Rho family members are master regulators of the actin cytoskeleton and numerous other cellular processes (Hall, 1994). Consequently, the intoxication of cultured mammalian cells with TcdA or TcdB leads amongst other effects to cell rounding due to the destruction of the actin cytoskeleton (Aktories and Just, 2005).

In order to reach their target proteins in the host cell cytosol, TcdA and TcdB need to enter cells via receptor-mediated, clathrin-dependent endocytosis (Papatheodorou et al., 2010). Both toxins are single-chain, multidomain toxins, which bind to host cell surface receptors via at least two independent, C-terminally located receptor-binding domains (Gerhard, 2017; Papatheodorou et al., 2018). After internalization of the toxin/receptor complexes, the pH of the endosomal lumen decreases, triggering membrane insertion and pore formation by a central region within TcdA and TcdB, denoted as translocation domain (TD) (Barth et al., 2001; Orrell et al., 2017). The glucosyltransferase domain (GTD) and the adjacent cysteine protease domain (CPD) are located at the N-terminus of both toxins (Jank and Aktories, 2008). The TD enables the translocation of the GTD and CPD across the endosomal membrane. Eventually, binding of cytosolic inositol hexakisphosphate to CPD triggers autocatalytic cleavage and release of the GTD into the cytosol (Giesemann et al., 2008; Egerer et al., 2009).

Earlier findings indicated that membrane cholesterol is crucial for the generation of translocation pores formed by TcdA and TcdB in endosomal membranes (Giesemann et al., 2006). More recently, we were able to show that an active sterol regulatory element–binding protein 2 (SREBP-2) pathway, which regulates cholesterol content in membranes, is required for efficient uptake of TcdA and TcdB into target cells (Papatheodorou et al., 2019). In addition, we demonstrated that the cholesterol-lowering drug simvastatin significantly reduces the intoxication of mouse embryonic fibroblasts (MEF cells) with TcdB *in vitro* (Papatheodorou et al., 2019).

Prompted by these observations and based on the recognized inhibitory role of the amphipathic steroid U18666A (3-β-[2-(diethylamino)ethoxy]androst-5-en-17-one) in cholesterol biosynthesis and/or intracellular transport (Cenedella, 2009), we investigated whether preincubation with the compound U18666A turns green monkey kidney epithelial cells (Vero), human cervix- (HeLa) and colon- (CaCo-2) cancer cells less prone to intoxication by TcdB. Importantly, U18666A exhibited a protective effect against TcdB in the tested cell lines. In addition, U18666A also protected cells from TcdA as well as from TcdA and TcdB from the epidemic NAP1/027 *C. difficile* strain, which is of particular clinical relevance.

Overall, the results corroborate the crucial role of membrane cholesterol for cell entry of TcdA and TcdB and should pave the way for the development of novel pharmacological antitoxin strategies for the supportive therapy after CDI.

MATERIALS AND METHODS

Cell Culture

Minimum Essential Medium (MEM; Fisher Scientific GmbH, Schwerte, Germany; #11524426) supplemented with 10% fetal calf serum (FCS), 1% sodium pyruvate, 1% non-essential amino acids, and 1% penicillin/streptomycin was used for the cultivation of HeLa and Vero cells. CaCo-2 cells (CLS Cell Line Service GmbH, Eppelheim, Germany; #300137) were cultivated in Dulbecco's Modified Eagle's Medium (DMEM; Fisher Scientific GmbH, Schwerte, Germany; #11594486) supplemented with 10% FCS, 1% sodium pyruvate, 1% non-essential amino acids, and 1% penicillin/streptomycin. Alternatively, HeLa cells were grown in DMEM (Fisher Scientific GmbH, Schwerte, Germany; #13345364) supplemented with 10% FCS and 1% penicillin/streptomycin. Cells were maintained in the incubator under humidified conditions at 37°C and 5% CO_2.

Toxins and Reagents

TcdA from *C. difficile* VPI 10463 as well as TcdA and TcdB from a NAP1/027 strain were purified from 72 h culture supernatants using dialysis culture in Brain Heart Infusion broth as previously described (Lyerly et al., 1988; Pruitt et al., 2010). Toxin cross-contaminations were excluded by MALDI-TOF analysis. TcdB from *C. difficile* VPI 10463 was purified as described before (Just et al., 2008).

U18666A was ordered from Biomol (Hamburg, Germany; Cay10009085) or from Merck/Sigma-Aldrich (Darmstadt, Germany; U3633), dissolved in dimethyl sulfoxide (DMSO) to obtain a 20 mM stock solution and aliquoted prior to storage at −20°C.

If not otherwise stated, incubation of cells with *C. difficile* toxins and/or the U18666A compound occurred at 37°C.

Microscopy

The following microscopes were used for monitoring toxin-induced cell rounding: Axiovert 40 CFL microscope (Carl Zeiss Microscopy, Jena, Germany) equipped with a ProgRes C10 plus camera (Jenoptik, Jena, Germany); Leica DMi1 equipped with a Leica MC170 HD camera (Leica, Wetzlar, Germany); Primovert (Carl Zeiss Microscopy, Jena, Germany); Lionheart FX Automated Microscope (BioTek, Vermont, United States). Toxin-induced cell rounding was manually quantified in microscopic images and, optionally, facilitated by the Neuralab online tool (https://neuralab.de).

Preparation of Whole-Cell Lysates and Immunoblotting

Whole-cell lysates from cells growing in the wells from a 24-well plate were generated directly in wells by removing the growth medium and resuspending cell monolayers in 2.5-fold pre-heated Laemmli buffer (typically 30 μl per well). Lysate

samples were heated at 95°C for 5 min, prior to SDS-PAGE and Western blotting of lysate proteins onto a nitrocellulose membrane. For the immunodetection of non-glucosylated Rac1 and GAPDH, primary mouse anti-Rac1 (clone 102; BD Biosciences, Heidelberg, Germany; #610651) and mouse anti-GAPDH (G-9; Santa Cruz Biotechnology, Dallas, United States; sc-365062) antibodies were used, respectively. Horseradish peroxidase (HRP)-coupled mouse IgG kappa binding protein (m-IgGκ BP-HRP; Santa Cruz Biotechnology, Dallas, United States; sc-516102) was used for developing antibody signals by the enhanced chemiluminescence (ECL) reaction.

Measurement of Transepithelial Electrical Resistance

The EVOMX apparatus equipped with the STX2 electrode (World Precision Instruments, Sarasota, United States) was used for measuring the transepithelial electrical resistance (TEER) of CaCo-2 cells. At day 0, 1.2×10^5 cells were seeded into 24-well hanging cell culture inserts (Brand GmbH, Wertheim, Germany; polyester membrane with pore size 0.4 μm) and incubated at 37°C until day 4. Optionally, at day 3, the U18666A compound was added basolaterally to the cells at a final concentration of 10 μM. Prior to TEER measurement at day 4, cell culture inserts were transferred into new wells containing only pre-warmed medium and further incubated at 37°C until TEER values (∼2,000 Ω) were stabilized. Then, TcdB (100 pM) was added apically to the cells and TEER measured every 30 min for up to 6 h. TEER values were normalized to time point 0 (t_0, addition of the toxin), which was set to 100%.

Statistics

Microsoft Excel (Student's) *t*-test was used for calculating the significance of differences between mean values. Resulting *p*-values were indicated by asterisks as follows: $^{*}p < 0.05$, $^{**}p < 0.01$, $^{***}p < 0.001$.

RESULTS

U18666A Inhibits the Intoxication of HeLa Cells by TcdB

We initiated our study by using TcdB (derived from the historical *C. difficile* VPI 10463 strain) as representative for both *C. difficile* large glucosylating toxins and the human HeLa cervical carcinoma cell line as established model system for *in vitro* intoxication experiments. At first, we confirmed the biological activity of the prepared TcdB and identified an operable toxin concentration by analyzing cell rounding, which is a typical, specific, and well-established hallmark of intoxication of cells with TcdB or TcdA. **Supplementary Figure 1A** shows that TcdB (10 pM) directly added to HeLa cells lead to obvious cell rounding after 90 min of incubation and after 210 min, almost all cells were round. In contrast, without toxin treatment, the cells maintained their flat morphology (**Supplementary Figure 1A**). Thus, 10 pM of TcdB were used for the further experiments with HeLa cells.

U18666A is a pharmacological inhibitor of cholesterol biosynthesis and/or its intracellular transport (Cenedella, 2009). Therefore, a long-term incubation of cells with this compound is required to achieve a recognizable decrease in membrane cholesterol levels without causing cell toxicity. In this context, HeLa cells were incubated for 24 h with increasing concentrations of U18666A and their morphology was monitored microscopically for the same time period to identify the maximal tolerable concentration of U18666A. While HeLa cells tolerated U18666A concentrations up to 20 μM after overnight treatment (**Supplementary Figure 1B**), 50 μM U18666A was moderately toxic, as indicated by rounding up of a small proportion of cells, and 100 μM U18666A lead to complete disruption of the cell layer and detachment of the cells. Therefore, overnight treatment with up to 20 μM U18666A appears to be tolerable for HeLa cells. Nevertheless, we decided to limit the U18666A concentration at 10 μM in subsequent experiments.

Next, we incubated HeLa cells with increasing concentrations of U18666A (0, 0.1, 1, and 10 μM) for 24 h, followed by the direct addition of 10 pM TcdB into the medium. Microscopic analysis of the cell morphology was performed at different time points after toxin application for up to 300 min. **Figure 1A** shows representative images at time points 0 and 180 min after TcdB addition. In direct comparison, preincubation of cells with 10 μM U18666A, but not with 0.1 μM or 1 μM U18666A, decreased the number of rounded cells in TcdB-treated cells (**Figure 1A**). Quantification of TcdB-induced cell rounding over time confirmed that HeLa cells pretreated with 10 μM U18666A were less affected by the toxin (∼25–30% reduced cell rounding after 180 min and 240 min), when compared to mock-pretreated cells and cells pretreated with 1 μM U18666A (**Figure 1B**).

Incubation Time Impacts the U18666A-Mediated Inhibition of TcdB in HeLa Cells

Since U18666A interferes with the cholesterol biosynthesis and/or intracellular transport, the incubation time with the compound correlates with the extent of decrease in membrane cholesterol levels. Thus, we aimed to analyze the consequences of various incubation periods during pretreatment of HeLa cells with the U18666A compound on the subsequent intoxication of the cells by TcdB. To this end, we pretreated HeLa cells with 10 μM U18666A for 0, 2, 4, and 24 h, and exchanged the U18666A-containing medium with fresh medium including 10 pM TcdB. We then analyzed microscopically and quantified TcdB-induced cell rounding over time up to 300 min. In comparison to the cells without U18666A pretreatment, TcdB-induced cell rounding was inhibited only moderately (∼10% reduced cell rounding at time point 180 min) in cells pretreated for 2 and 4 h, respectively, and most prominent inhibition (∼25% reduced cell rounding at time point 180 min) was observed with a 24 h U18666A pretreatment (**Figure 2A**). Thus, comparatively short incubation periods of cells with the U18666A compound correlate with less efficient protection against TcdB intoxication. Since TcdB intoxication took place after removal of the U18666A compound by medium exchange, direct inhibitory effects of U18666A on the activity of the toxin in the cell culture supernatant can be excluded.

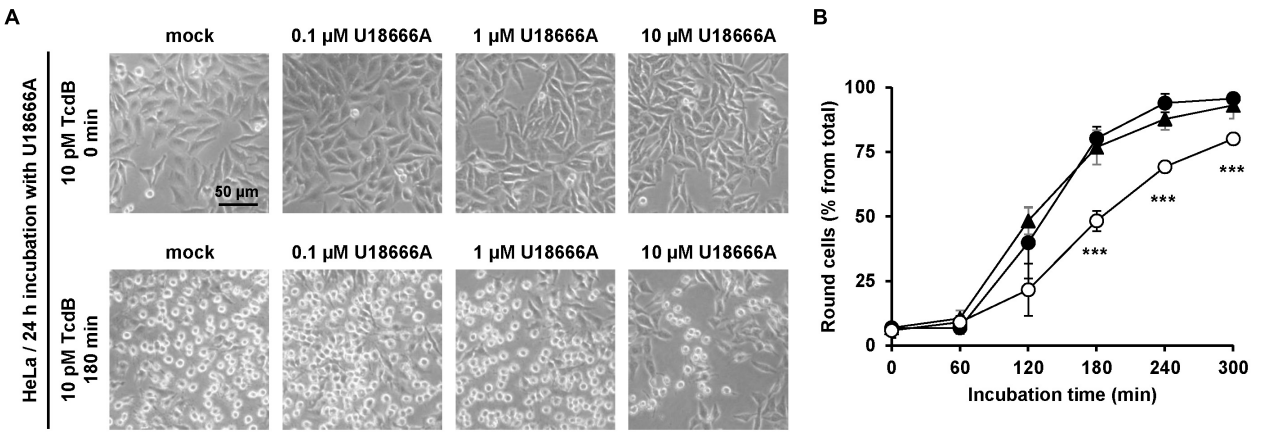

FIGURE 1 | Effect of U18666A on intoxication of HeLa cells by TcdB. **(A)** HeLa cells were pretreated for 24 h with increasing concentrations of U18666A as indicated or were left untreated (mock), prior to addition of 10 pM TcdB. Microscopic images shown were taken after time point 0 min (upper row) and 180 min (lower row). **(B)** Quantification of the TcdB-induced cell rounding over time in mock-treated (black filled circles) and 24 h U18666A-pretreated HeLa cells (1 µM, black filled triangles; 10 µM, white filled circles). Graph shows mean (percentage values of round cells) from three experiments performed in parallel in independent wells. Error bars represent ± SD. Asterisks indicate statistical significance compared to control (mock-treated HeLa cells) with $^{***}p < 0.001$.

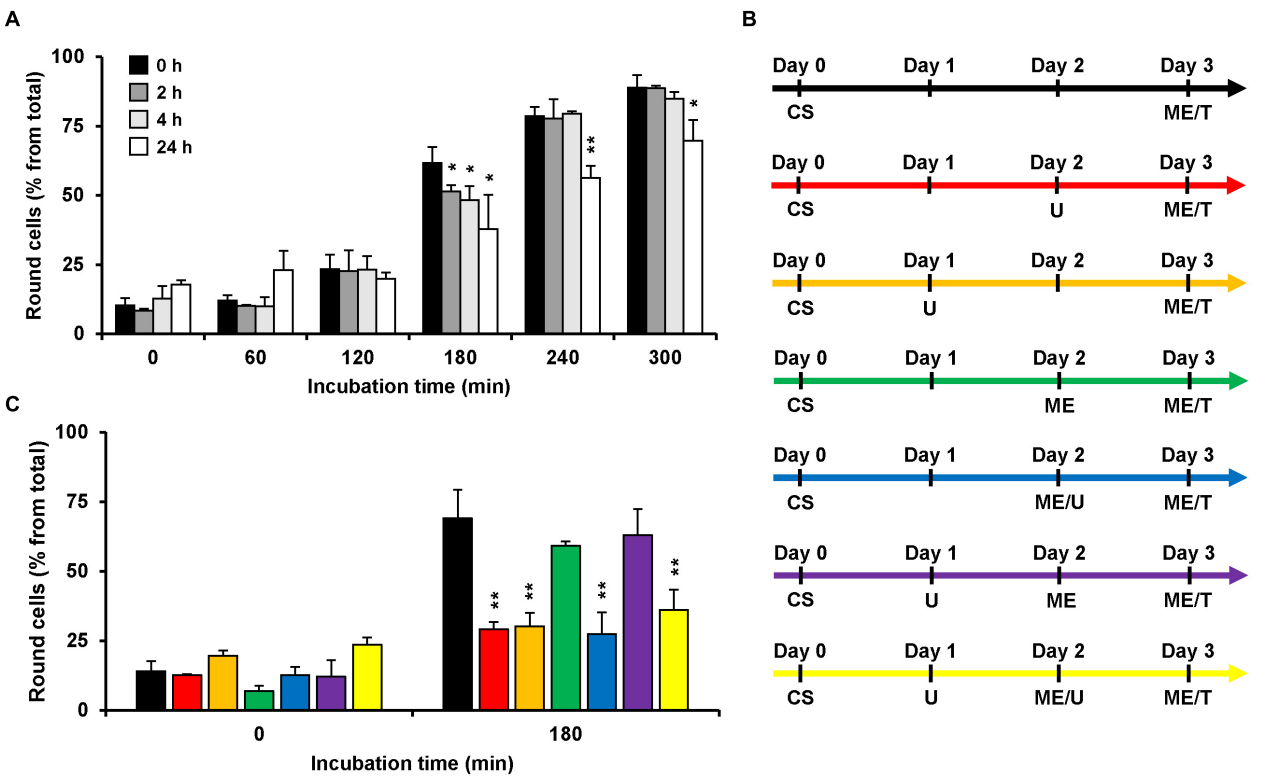

FIGURE 2 | Effect of U18666A preincubation conditions on the TcdB intoxicaton of HeLa cells. **(A)** HeLa cells were preincubated for 0 h (black bars), 2 h (dark gray bars), 4 h (light gray bars), and 24 h (white bars) with U18666A, followed by TcdB intoxication (10 pM) and microscopic analysis of TcdB-induced cell rounding over time. The bar chart shows mean percentages of round cells at the indicated incubation times after addition of the toxin. Error bars represent ± SD. Asterisks indicate statistical significance at each time point compared to control (black bar) with $^{*}p < 0.05$ and $^{**}p < 0.01$. **(B,C)** The various U18666A pretreatment- and TcdB-intoxication conditions shown in **(C)** are schematically depicted with different colors in **(B)**. Cell seeding (CS) of HeLa cells at day 0 was followed by the addition of 10 µM U18666A (U) at day 1 (orange, purple and yellow) and/or at day 2 without (red) or with medium exchange (ME; blue, yellow) and TcdB intoxication (10 pM) by medium exchange (ME/T) at day 3. The bar chart in **(C)** shows the percentages of round cells at the indicated incubation times after addition of the toxin. Error bars represent ± SD. Asterisks indicate statistical significance at each time point compared to control (black bar for red and orange bar; green bar for blue, purple and yellow bar) with $^{**}p < 0.01$. In all cases, data was obtained in three parallel experiments performed in independent wells.

Next, we wanted to identify the best condition for the pretreatment of HeLa cells with U18666A, which are summarized schematically in **Figure 2B**, regarding the inhibition of TcdB intoxication in HeLa cells. For all conditions, cells were seeded into wells at day 0 and intoxicated at day 3 for 180 min with TcdB by exchanging the medium with fresh medium including 10 pM TcdB. In the control condition (**Figure 2B**, black arrow), cells were not pretreated with the U18666A inhibitor and cell rounding occurred in ∼70% of the cells (**Figure 2C**, black bar). Direct addition of 10 μM U18666A at day 2 (**Figure 2B**, red arrow; 24 h pretreatment) or day 1 (**Figure 2B**, orange arrow; 48 h pretreatment), reduced cell rounding equally to ∼30% (**Figure 2C**, red vs. orange bar). Thus, 48 h pretreatment of HeLa cells with U18666A was not superior to the 24 h pretreatment, in terms of TcdB inhibition. We also tested the sequential addition of 10 μM U18666A to cells, first by direct addition at day 1 and then by medium exchange at day 2 (**Figure 2B**, yellow arrow). Although cells were pretreated under this condition for a total of 48 h with the U18666A compound (but with U18666A renewal at day 2), TcdB inhibition was not superior to the 48 h pretreatment with U18666A without repeated application of the compound (**Figure 2C**, orange vs. yellow bar). Addition of 10 μM U18666A to cells at day 2 by medium exchange (**Figure 2B**, blue arrow) or by direct transfer into the wells (**Figure 2B**, red arrow), inhibited TcdB-induced cell rounding to equal extents (**Figure 2C**, red vs. blue bar). Interestingly, when U18666A (10 μM) was added to the cells at day 1 and removed again by medium exchange at day 2 (**Figure 2B**, purple arrow), TcdB-induced cell rounding was not inhibited and indistinguishable from the corresponding control without U18666A pretreatment at day 1 and medium exchange at day 2 (**Figure 2C**, green vs. purple bar). This finding suggests that membrane cholesterol levels recovered when U18666A was removed 24 h before toxin addition, either by cellular uptake from the medium or by biosynthesis.

U18666A Confers Resistance Toward TcdB Intoxication in Vero Cells

Next, the protective effect of U18666A against TcdB intoxication in a second cell line was investigated. African green monkey kidney (Vero) cells were used. Due to their flat morphology, Vero cells are a well-established model cell line for studying TcdB effects. Vero cells were pretreated for 24 h with increasing U18666A concentrations (0, 1, 2, 5, 10 μM) and, subsequently, TcdB was added to the cells at a final concentration of 10 and 100 pM, respectively. TcdB-induced cell rounding was analyzed microscopically for up to 300 min (10 pM TcdB) or 240 min (100 pM TcdB). **Figures 3A,C** show representative images of

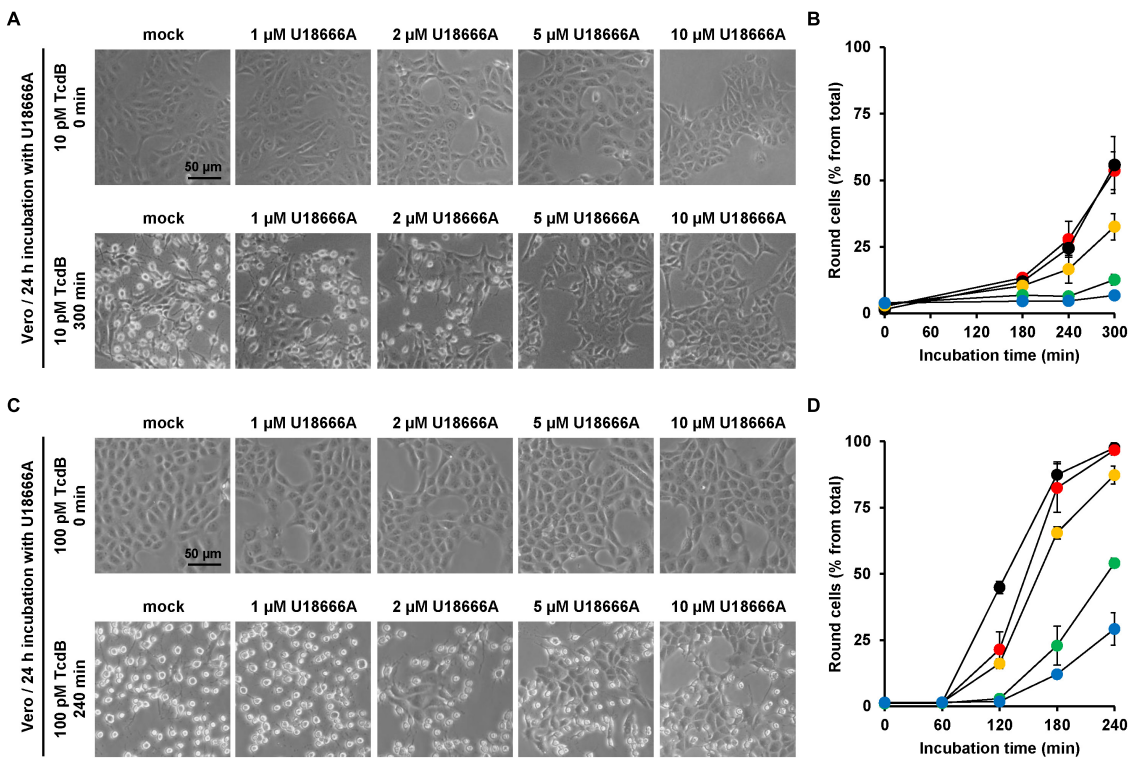

FIGURE 3 | Effect of U18666A on the TcdB-induced cell rounding of Vero cells. **(A,C)** Vero cells pretreated for 24 h with increasing concentrations of U18666A as indicated or without pretreatment (mock) were intoxicated with **(A)** 10 pM or **(C)** 100 pM TcdB. Representative images were taken microscopically after time point 0 min [upper row in **(A,C)**] and 300 min [lower row in **(A)**] or 240 min [lower row in **(C)**]. **(B,D)** Quantification of the TcdB-induced cell rounding over time in mock-treated (black filled circles) and 24 h U18666A-pretreated HeLa cells (1 μM, red filled circles; 2 μM, orange filled circles; 5 μM, green filled circles, 10 μM, blue filled circles). Graphs in **(B,D)** show mean percentage values of round cells as indicated by three parallel experiments performed in independent wells. Error bars represent ± SD.

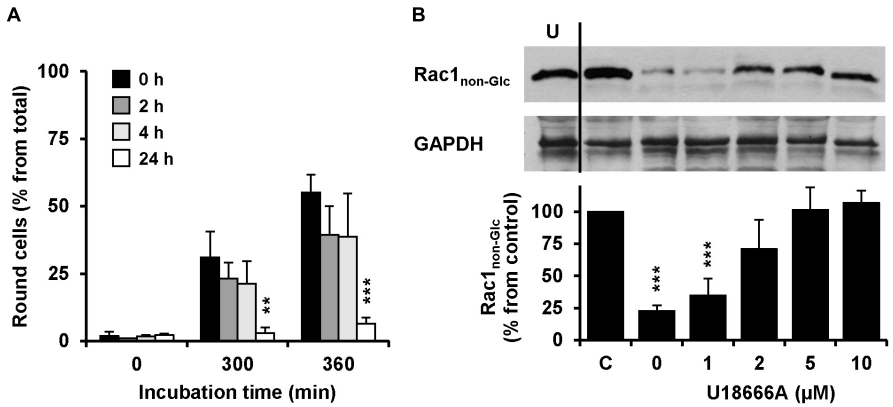

FIGURE 4 | Effect of U18666A on the TcdB-induced Rac1 glucosylation and role of U18666A pretreatment duration on TcdB-induced cell rounding in Vero cells. **(A)** Vero cells were preincubated for 0 h (black bars), 2 h (dark gray bars), 4 h (light gray bars), and 24 h (white bars) with the U18666A compound, prior to TcdB intoxication (10 pM) and microscopic analysis of TcdB-induced cell rounding over time. The mean percentage values of round cells at the indicated incubation times after addition of the toxin and from three parallel experiments performed in independent wells are plotted in the bar chart. Error bars represent ± SD. Asterisks indicate statistical significance at each time point compared to control (black bar) with $^{**}p < 0.01$ and $^{***}p < 0.001$. **(B)** Immunoblots against non-glucosylated Rac1 ($Rac1_{non-Glc}$) and GAPDH (loading control) are shown (upper panel), obtained with whole-cell lysates that were generated from Vero cells pretreated for 24 h with increasing concentrations of U18666A as indicated and after intoxication for 120 min with 100 pM TcdB. In a control sample (C) cells were left without U18666A pretreatment and toxin addition. In another control (U) cells were preincubated with 10 μM U18666A but were left without toxin treatment. The bar chart (lower panel) shows the quantification of the Rac1 signals (normalized with the signals of the GAPDH loading control) relative to the control sample (C), which was set to 100%. Error bars represent ± SEM, calculated from six experiments performed in independent wells (three experiments in parallel on two different days). Asterisks indicate statistical significance at each time point compared to control (C) with $^{***}p < 0.001$.

mock- and U18666A-pretreated Vero cells at time points zero and 300 min (10 pM TcdB) and at time points zero and 240 min (100 pM), respectively, after toxin addition. Diagrams in **Figures 3B,D** show the corresponding quantification of TcdB-induced cell rounding over time for 10 pM or 100 pM TcdB, respectively. After 300 min, cell rounding induced by 10 pM TcdB was strongly reduced to ∼10% in Vero cells pretreated with 5 and 10 μM U18666A vs. mock-pretreated cells (∼60% cell rounding) (**Figure 3B**). In cells intoxicated with 100 pM TcdB, nearly 100% cell rounding was observed after 210 min, which was decreased to ∼50% by pretreatment with 5 μM U18666A and to ∼25% by pretreatment with 10 μM U18666A. Thus, U18666A confers robust resistance in Vero cells toward 10 pM TcdB and moderate resistance toward 100 pM TcdB. Notably, the protective effect of U18666A against TcdB was more pronounced in Vero than in HeLa cells.

The influence of the pretreatment time of U18666A on the intoxication of Vero cells with TcdB was analyzed. To this end, Vero cells were pretreated with 10 μM U18666A for 0, 2, 4, and 24 h, prior to intoxication with 10 pM TcdB. Eventually, TcdB-induced cell rounding was analyzed microscopically and quantified after 0, 300, and 360 min. Importantly, 24 h pretreatment with the U18666A compound strongly inhibited TcdB-induced cell rounding (from ∼60% in mock-pretreated cells to ∼10% after 360 min of TcdB intoxication) (**Figure 4A**, black bar vs. white bar). Pretreatment with 10 μM U18666A for 2 and 4 h did not reduce TcdB-induced cell rounding significantly after 300 and 360 min of intoxication, when compared to mock-pretreated cells (**Figure 4A**, black bar vs. dark gray bar and black bar vs. light gray bar). Thus, also in Vero cells the incubation time has a major impact on the U18666A-mediated inhibition of TcdB. Similarly as observed with HeLa cells, a short incubation of Vero cells with the U18666A compound inefficiently protects these cells against TcdB intoxication.

To confirm our findings with another experimental approach, we generated whole-cell lysates from Vero cells intoxicated for 120 min with 100 pM TcdB, followed by immunoblotting against the TcdB target protein Rac1 with an antibody that detects only the non-glucosylated form of Rac1. Prior to TcdB intoxication the cells were pretreated for 24 h with increasing concentrations of U18666A (0, 1, 2, 5, and 10 μM). Whole-cell lysates obtained from untreated cells were used as control for maximal non-glucosylated Rac1 signal in the immunoblot. As expected, the Rac1 signal in whole-cell lysates obtained from TcdB-intoxicated cells without U18666A pretreatment was decreased to ∼10–20% from control (100%) (**Figure 4B**). However, the Rac1 signal was present almost to the level of the control in TcdB-intoxicated cells pretreated either with 5 or 10 μM U18666A. Lower U18666A concentrations (1 or 2 μM) protected cells less effectively toward TcdB intoxication, because the Rac1 signal was found to be reduced to ∼30% (1 μM U18666A) and ∼70% (2 μM U18666A), respectively, in these samples. Notably, pretreatment of cells with U18666A had no influence on the Rac1 expression level or on the binding by the glucosylation-sensitive anti-Rac1 antibody.

U18666A Decreases the Sensitivity of Human Intestinal Epithelial CaCo-2 Cells Against TcdB

Since *C. difficile* is a pathogen of the human intestine, it was relevant to test whether U18666A confers resistance toward TcdB intoxication in the medically and physiologically more

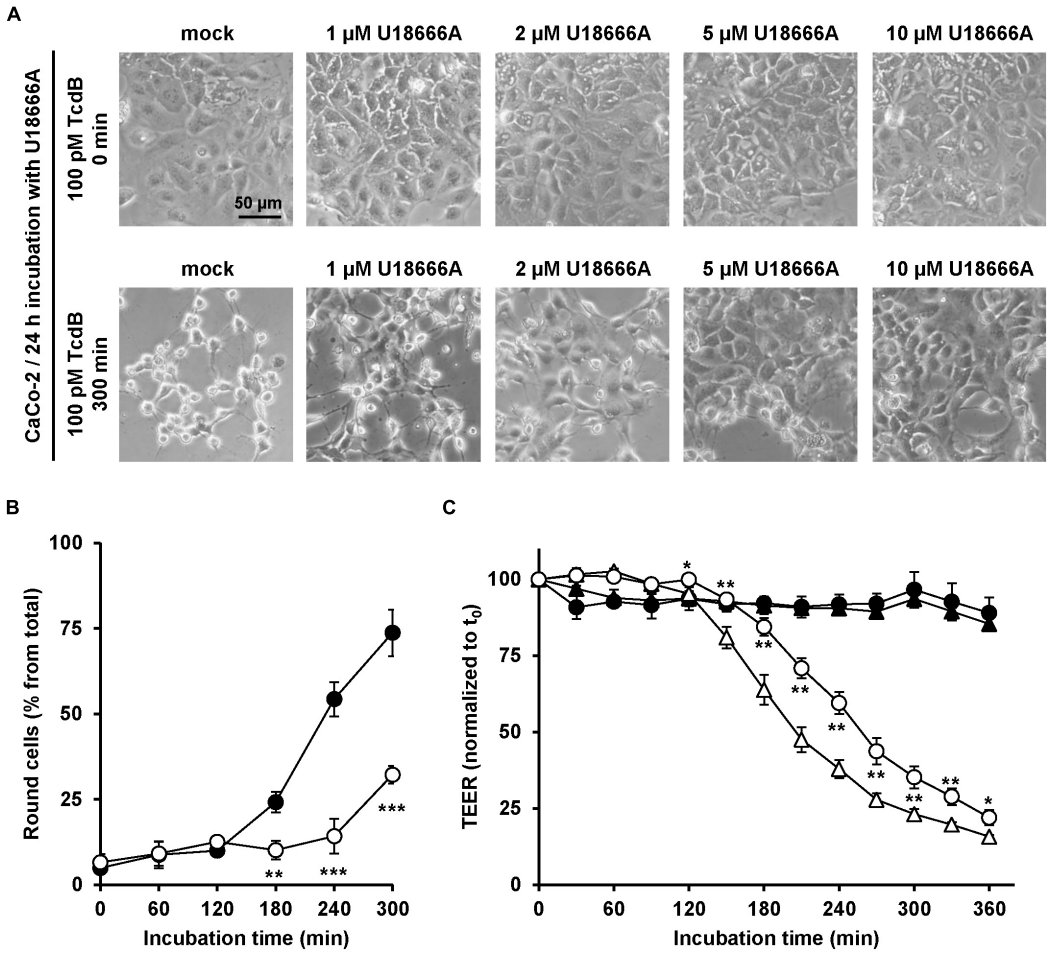

FIGURE 5 | Effect of U18666A on the intoxication of CaCo-2 cells by TcdB. **(A)** After pretreatment of CaCo-2 cells for 24 h with increasing concentrations of U18666A as indicated or without pretreatment (mock), cells were intoxicated with 100 pM TcdB for 300 min and cell morphology analyzed microscopically. Representative images after time point 0 min (upper row) and 300 min (lower row) are shown. **(B)** Quantification of the TcdB-induced cell rounding over time in mock-treated (black filled circles) and 24 h U18666A (10 μM)-pretreated CaCo-2 cells (white filled circles). Graph shows mean values (percentage of round cells) from three parallel experiments performed in independent wells. Error bars represent ± SD. Asterisks indicate statistical significance compared to control (mock-treated CaCo-2 cells) with $^{**}p < 0.01$ and $^{***}p < 0.001$. **(C)** CaCo-2 cells grown in inserts were pretreated for 24 h with 10 μM U18666A (circles) or were left without pretreatment (triangles), prior to apical addition of 100 pM TcdB (white filled circles and triangles) at time point 0 (t_0) and measurement of the transepithelial electrical resistance (TEER) at indicated incubation times. Parallel samples were not treated with TcdB (black filled circles and triangles). Diagram shows relative TEER values normalized to time point 0 (t_0). Error bars represent ± SD. Asterisks indicate statistical significance at each time point between white filled triangles (–U18666A/+TcdB) and white filled circles (+U18666A/+TcdB), with $^{*}p < 0.05$ and $^{**}p < 0.01$.

relevant human colon carcinoma cell line CaCo-2. To this end, CaCo-2 cells were preincubated for 24 h with increasing concentrations of U18666A (0, 1, 2, 5, and 20 μM), prior to addition of 100 pM TcdB and subsequent microscopic analysis of the cell morphology over time. Pretreatment of CaCo-2 cells with increasing U18666A concentrations correlated with less microscopically observable cell rounding after incubation with TcdB for 300 min, when compared to mock-pretreated cells (**Figure 5A**). The quantification of TcdB-induced cell rounding over time of mock- and 10 μM U18666A-pretreated cells confirmed the protective effect of U18666A against TcdB also in CaCo-2 cells (**Figure 5B**). Pretreatment of CaCo-2 cells with 10 μM U18666A decreased TcdB-induced cell rounding to ∼25% after 300 min of intoxication.

To investigate the protective effect of U18666A on the intoxication of CaCo-2 cells by TcdB by a further end point, the integrity of the barrier of function of CaCo-2 cells, grown as polarized monolayers in hanging cell culture inserts, was analyzed in terms of the transepithelial electrical resistance (TEER). Accordingly, CaCo-2 cell monolayers were pretreated with 10 μM U18666A for 24 h or were left untreated (mock) before apical addition of 100 pM TcdB. Then, TEER was measured every 30 min over a period of 6 h after intoxication. In direct comparison, the TcdB-induced TEER decrease over time was delayed in U18666A-pretreated CaCo-2 cells when compared to mock-pretreated cells (**Figure 5C**). Thus, U18666A pretreatment reduced the TcdB-induced disruption of the epithelial integrity of CaCo-2 cells.

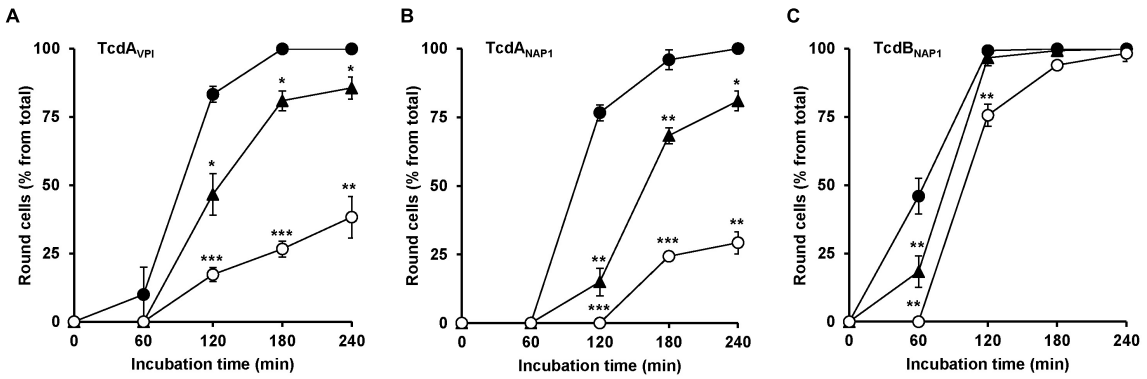

FIGURE 6 | Effect of U18666A on the intoxication of HeLa cells by TcdA$_{VPI}$, TcdA$_{NAP1}$ and TcdB$_{NAP1}$. HeLa cells preincubated with increasing concentrations of U18666A (0 μM, black filled circles; 1.25 μM, black filled triangles and 10 μM, white filled circles) were intoxicated with **(A)** 10 pM VPI-derived TcdA (TcdA$_{VPI}$), **(B)** 10 pM NAP1/027-derived TcdA (TcdA$_{NAP1}$) or **(C)** 1 pM NAP1/027-derived TcdB (TcdB$_{NAP1}$), prior to microscopic analysis of the cell morphology over time. Graphs in **(A–C)** show means (percentage values of round cells) from three experiments performed in parallel in independent wells. Error bars represent ± SD. Asterisks indicate statistical significance compared to control (mock-treated HeLa cells) with $^{*}p < 0.05$, $^{**}p < 0.01$, and $^{***}p < 0.001$.

U18666A Confers Protection Against VPI 10463-Derived TcdA and NAP1/027-Derived TcdA and TcdB

Finally, it was tested whether U18666A also protects cells against TcdA from the historical *C. difficile* strain VPI 10463 and against TcdA and TcdB from the epidemic *C. difficile* strain NAP/027. For that purpose, HeLa cells were pretreated for 24 h with increasing concentrations of U18666A (0, 1.25, and 10 μM), prior to addition of 10 pM VPI-derived TcdA (TcdA$_{VPI}$), 10 pM NAP1/027-derived TcdA (TcdA$_{NAP1}$) or 1 pM NAP1/027-derived TcdB (TcdB$_{NAP1}$). Subsequently, microscopic analysis of the cell morphology was performed. As summarized in **Figure 6**, a 24 h pretreatment of HeLa cells with 10 μM U18666A effectively diminished cell rounding induced by TcdA$_{VPI}$ (**Figure 6A**), TcdA$_{NAP1}$ (**Figure 6B**) or TcdB$_{NAP1}$ (**Figure 6C**). It is of note, however, that the reduction of TcdB$_{NAP1}$ intoxication by U18666A was less effective when compared to TcdA$_{VPI}$ and TcdA$_{NAP1}$, respectively, both of which were inhibited to an equal extent by the U18666A pretreatment.

DISCUSSION

The crucial role of membrane cholesterol for pore formation of TcdA and TcdB during their endocytic uptake into target cells was first described by the Aktories group in 2006 (Giesemann et al., 2006). Along with this finding, we found more recently that an active and functional SREBP-2 pathway, which plays a major role in cholesterol metabolism, is required in target cells for the cytotoxicity of TcdA and TcdB and showed that the hypocholesterolemic drug simvastatin, which inhibits the HMG-CoA reductase, a key enzyme in cholesterol biosynthesis, efficiently protected cultured mammalian cells from TcdB intoxication (Papatheodorou et al., 2019). Since there is no structure of membrane-embedded TcdA or TcdB, the exact interaction between membrane cholesterol and TcdA/TcdB is not known. However, a recently discovered "mirror code" controlling protein-cholesterol interactions in the outer and inner membrane leaflets (Fantini et al., 2016) seems to be present also within a region of TcdA and TcdB (amino acids 830–990) (Gerhard, 2017), which is in charge of pore formation (Genisyuerek et al., 2011). Cholesterol might be crucial for the insertion of the translocation domain of the toxins into the endosomal membrane. Otherwise, membrane cholesterol could serve as a platform for the correct positioning of transmembrane segments of the toxins within the endosomal membrane for generating a translocation-competent pore.

Prompted by the above mentioned observations that membrane cholesterol is crucial for the uptake of TcdA and TcdB in target cells, the U18666A compound came into our focus, since it has been described by several studies as potent inhibitor of cholesterol biosynthesis and/or intracellular trafficking (Cenedella, 2009). At least three membrane-bound enzymes in the cholesterol biosynthetic pathway, namely 2,3-oxidosqualene cyclase, desmosterol reductase and cholestenol delta-isomerase, are known to be inhibited by the U18666A compound (Duriatti et al., 1985; Bae and Paik, 1997; Moebius et al., 1998). The activity of HMG-CoA reductase, another key enzyme in cholesterol biosynthesis, is decreased by addition of low concentrations of U18666A, but increased at higher drug levels (Panini et al., 1984). Another feature of U18666A is the inhibition of the intracellular transport of cholesterol, namely from the lysosome to the endoplasmic reticulum (ER) and to the plasma membrane (PM), respectively, and from the PM to the ER (Liscum and Dahl, 1992; Underwood et al., 1998). Effects of U18666A on intracellular cholesterol trafficking are explained by its direct interference with the lysosomal membrane protein Niemann-Pick type C1 (NPC1), which transports cholesterol from receptor-mediated uptake of low-density lipoproteins (LDL) to post-lysosomal destinations (Carstea et al., 1997; Blanchette-Mackie, 2000; Lange et al., 2000; Lu et al., 2015).

The present study revealed that the U18666A compound confers increased protection to various mammalian cell lines

against the *C. difficile* toxin TcdB. In addition, TcdA-inhibition by U18666A-pretreatment was confirmed in HeLa cells and TcdA-inhibition by U18666A was more prominent when compared to TcdB, irrespective of the source strain of both toxins. Inhibition of TcdB is more challenging most likely due to the fact that TcdB preparations are up to 1,000-fold more toxic than TcdA preparations (Rothman et al., 1984). It is also feasible that TcdA membrane insertion and/or pore formation in endosomal membranes is more prone to changes of membrane cholesterol levels. Moreover, pretreatment with the U18666A compound was not equally protective against TcdB among the various tested cells. For instance, the inhibition of TcdB-intoxication by U18666A pretreatment was more prominent in Vero cells when compared to HeLa cells at equal inhibitor concentrations. Possible explanations for this observation could be that either the compound is more efficiently taken up into Vero cells or that the compound is more efficiently degraded or excreted from HeLa cells by drug transporters. It is also feasible that membrane cholesterol levels and/or cholesterol uptake, intracellular transport and biosynthesis capabilities are vastly differing between HeLa and Vero cells, thus influencing the inhibitory potential of the U18666A compound in each cell line.

The replication of many viruses is associated with intact cholesterol biosynthesis and intracellular transport. Thus, it has been reported that U18666A suppress the replication of several viruses, such as ebola virus, dengue virus, human hepatitis C virus, and type I feline coronavirus (Poh et al., 2012; Lu et al., 2015; Elgner et al., 2016; Takano et al., 2017). The mechanism underlying the U18666A-mediated inhibition of TcdB and TcdA is likely related to a blockage of cholesterol biosynthetic enzymes and of the intracellular transport of endocytosed cholesterol from the culture medium to the plasma membrane and/or to endocytic vesicles. Consistent with this hypothesis, cells were strongly protected from toxin intoxication, when they were pretreated for at least 24 h with U18666A, but not after shorter incubation periods with the compound. We widely excluded the possibilities of (i) an inactivating effect of U18666A by direct binding to the toxins or (ii) through alteration of endosomal membranes through U18666A incorporation, because there was no efficient protection from TcdB after short incubation periods with U18666A, but protection when the U18666A-containing medium on top of cells was removed by replacement with TcdB-containing medium during the intoxication step.

The cholesterol-dependent pore formation by TcdA or TcdB in endosomal membranes is a crucial step during cell entry of both toxins and this study corroborated that this specific step can be targeted by pharmacological tools such as U18666A. Importantly, U18666A also inhibited TcdA and TcdB variants from the epidemic NAP1/027 *C. difficile* strain. This finding indicates that cholesterol seems to be a conserved player in TcdA/TcdB intoxication. Thus, the development of cholesterol-lowering drugs, such as U18666A, as potential therapeutics against TcdA and TcdB might be of interest not only for the treatment of infections caused by non-epidemic *C. difficile* strains (such as VPI 10463), but also for the treatment of diseases associated with infections caused by the epidemic NAP1/027 *C. difficile* strain. However, the safety profile of U18666A for clinical use is not evaluated so far yet. Cataracts were described in rats that were treated daily with 10 mg/kg U18666A, but not when the rats were treated every fourth day with the U18666A compound (Cenedella and Bierkamper, 1979). Thus, the drug application form (enteral or rectal administration) and interval should be carefully considered in potential clinical studies on the efficacy and safety of U18666A and derivatives in the (supportive) treatment of severe CDI.

DATA AVAILABILITY STATEMENT

The raw data supporting the conclusions of this article will be made available by the authors, without undue reservation.

AUTHOR CONTRIBUTIONS

PP, SF, EC-O, and HB designed the research. PP, SK, AB-L, SF, ED, TT, AW, and SS performed the research. PP, SK, AB-L, SF, KA, EC-O, CR, and HB analyzed the data. PP, KA, CR, and HB wrote the manuscript. All authors contributed to the article and approved the submitted version.

FUNDING

Research funding was received in the group of HB from the Deutsche Forschungsgemeinschaft (DFG; grant number Ba 2087/8-1, project no. 450938962) and in the group of EC-O and CR from the Vice-Presidency for Research of the University of Costa Rica (project no. B9450).

ACKNOWLEDGMENTS

We would like to thank Anna Anastasia, Monika Berther and Jana Kuhn for excellent technical assistance.

SUPPLEMENTARY MATERIAL

The Supplementary Material for this article can be found online at: https://www.frontiersin.org/articles/10.3389/fmicb.2021.784856/full#supplementary-material

REFERENCES

Aktories, K., and Just, I. (2005). Clostridial Rho-inhibiting protein toxins. *Curr. Top. Microbiol. Immunol.* 291, 113–145.

Aktories, K., Schwan, C., and Jank, T. (2017). Clostridium difficile toxin biology. *Annu. Rev. Microbiol.* 71, 281–307.

Bae, S. H., and Paik, Y. K. (1997). Cholesterol biosynthesis from lanosterol: development of a novel assay method and characterization of rat liver

microsomal lanosterol Δ24-reductase. *Biochem. J.* 326, 609–616. doi: 10.1042/bj3260609

Barth, H., Pfeifer, G., Hofmann, F., Maier, E., Benz, R., and Aktories, K. (2001). Low ph-induced formation of Ion channels by Clostridium difficile toxin B in target cells. *J. Biol. Chem.* 276, 10670–10676. doi: 10.1074/jbc.M009445200

Blanchette-Mackie, E. J. (2000). Intracellular cholesterol trafficking: role of the NPC1 protein. *Biochim. Biophys. Acta Mol. Cell Biol. Lipids* 1486, 171–183.

Carstea, E. D., Morris, J. A., Coleman, K. G., Loftus, S. K., Zhang, D., Cummings, C., et al. (1997). Niemann-Pick C1 disease gene: homology to mediators of cholesterol homeostasis. *Science* 277, 228–231. doi: 10.1126/science.277.5323.228

Cenedella, R. J. (2009). Cholesterol synthesis inhibitor U18666A and the role of sterol metabolism and trafficking in numerous pathophysiological processes. *Lipids* 44, 477–487. doi: 10.1007/s11745-009-3305-7

Cenedella, R. J., and Bierkamper, G. G. (1979). Mechanism of cataract production by 3-β(2-diethylaminoethoxy) androst-5-en-17-one hydrochloride, U18666A: an inhibitor of cholesterol biosynthesis. *Exp. Eye Res.* 28, 673–688. doi: 10.1016/0014-4835(79)90068-x

Chandrasekaran, R., and Lacy, D. B. (2017). The role of toxins in clostridium difficile infection. *FEMS Microbiol. Rev.* 41, 723–750. doi: 10.1093/FEMSRE/FUX048

Duriatti, A., Bouvier-Nave, P., Benveniste, P., Schuber, F., Delprino, L., Balliano, G., et al. (1985). In vitro inhibition of animal and higher plants 2,3-oxidosqualene-sterol cyclases by 2-aza-2,3-dihydrosqualene and derivatives, and by other ammonium-containing molecules. *Biochem. Pharmacol.* 34, 2765–2777. doi: 10.1016/0006-2952(85)90578-7

Egerer, M., Giesemann, T., Herrmann, C., and Aktorles, K. (2009). Autocatalytic processing of Clostridium difficile toxin B: binding of inositol hexakisphosphate. *J. Biol. Chem.* 284, 3389–3395. doi: 10.1074/JBC.M806002200

Elgner, F., Ren, H., Medvedev, R., Ploen, D., Himmelsbach, K., Boller, K., et al. (2016). The Intracellular cholesterol transport inhibitor U18666A inhibits the exosome-dependent release of mature Hepatitis C Virus. *J. Virol.* 90, 11181–11196. doi: 10.1128/JVI.01053-16

Fantini, J., Di Scala, C., Evans, L. S., Williamson, P. T. F., and Barrantes, F. J. (2016). A mirror code for protein-cholesterol interactions in the two leaflets of biological membranes. *Sci. Rep.* 6:21907. doi: 10.1038/SREP21907

Genisyuerek, S., Papatheodorou, P., Guttenberg, G., Schubert, R., Benz, R., and Aktories, K. (2011). Structural determinants for membrane insertion, pore formation and translocation of Clostridium difficile toxin B. *Mol. Microbiol.* 79, 1643–1654. doi: 10.1111/J.1365-2958.2011.07549.X

Gerhard, R. (2017). Receptors and binding structures for clostridium difficile toxins A and B. *Curr. Top. Microbiol. Immunol.* 406, 79–96. doi: 10.1007/82_2016_17

Giesemann, T., Egerer, M., Jank, T., and Aktories, K. (2008). Processing of Clostridium difficile toxins. *J. Med. Microbiol.* 57, 690–696. doi: 10.1099/JMM.0.47742-0

Giesemann, T., Jank, T., Gerhard, R., Maier, E., Just, I., Benz, R., et al. (2006). Cholesterol-dependent pore formation of Clostridium difficile toxin A. *J. Biol. Chem.* 281, 10808–10815. doi: 10.1074/jbc.m512720200

Hall, A. (1994). Small GTP-binding proteins and the regulation of the actin cytoskeleton. *Annu. Rev. Cell Biol.* 10, 31–54. doi: 10.1146/annurev.cb.10.110194.000335

Jank, T., and Aktories, K. (2008). Structure and mode of action of clostridial glucosylating toxins: the ABCD model. *Trends Microbiol.* 16, 222–229. doi: 10.1016/J.TIM.2008.01.011

Just, I., Selzer, J., Hofmann, F., and Aktories, K. (2008). "Clostridium difficile Toxin B as a Probe for Rho GTPases," in *Bacterial Toxins - Tools in Cell Biology and Pharmacology*, ed. K. Aktories (Weinheim: Chapman & Hall), 159–168.

Just, I., Selzer, J., Wilm, M., Von Eichel-Streiber, C., Mann, M., and Aktories, K. (1995). Glucosylation of Rho proteins by Clostridium difficile toxin B. *Nature* 375, 500–503.

Kelly, C. P., and LaMont, J. T. (2008). Clostridium difficile - more difficult than ever. *N. Engl. J. Med.* 359, 1932–1940. doi: 10.1056/nejmra0707500

Lange, Y., Ye, J., Rigney, M., and Steck, T. (2000). Cholesterol movement in Niemann-Pick type C cells and in cells treated with amphiphiles. *J. Biol. Chem.* 275, 17468–17475. doi: 10.1074/jbc.M000875200

Liscum, L., and Dahl, N. K. (1992). Intracellular cholesterol transport. *J. Lipid Res.* 33, 1239–1254.

Lu, F., Liang, Q., Abi-Mosleh, L., Das, A., de Brabander, J. K., Goldstein, J. L., et al. (2015). Identification of NPC1 as the target of U18666A, an inhibitor of lysosomal cholesterol export and Ebola infection. *Elife* 4:e12177. doi: 10.7554/eLife.12177

Lyerly, D. M., Krivan, H. C., and Wilkins, T. D. (1988). Clostridium difficile: its disease and toxins. *Clin. Microbiol. Rev.* 1, 1–18. doi: 10.1128/cmr.1.1.1-18.1988

Moebius, F. F., Reiter, R. J., Bermoser, K., Glossmann, H., Cho, S. Y., and Paik, Y. K. (1998). Pharmacological analysis of sterol Δ8=Δ7 isomerase proteins with [3H]fenprodil. *Mol. Pharmacol.* 54, 591–598. doi: 10.1124/mol.54.3.591

Orrell, K. E., Zhang, Z., Sugiman-Marangos, S. N., and Melnyk, R. A. (2017). Clostridium difficile toxins A and B: receptors, pores, and translocation into cells. *Crit. Rev. Biochem. Mol. Biol.* 52, 461–473. doi: 10.1080/10409238.2017.1325831

Panini, S. R., Sexton, R. C., and Rudney, H. (1984). Regulation of 3-hydroxy-3-methylglutaryl coenzyme A reductase by oxysterol by-products of cholesterol biosynthesis. Possible mediators of low density lipoprotein action. *J. Biol. Chem.* 259, 7767–7771. doi: 10.1016/s0021-9258(17)42859-6

Papatheodorou, P., Barth, H., Minton, N., and Aktories, K. (2018). Cellular uptake and mode-of-action of Clostridium difficile toxins. *Adv. Exp. Med. Biol.* 1050, 77–96. doi: 10.1007/978-3-319-72799-8_6

Papatheodorou, P., Song, S., López-Ureña, D., Witte, A., Marques, F., Ost, G. S., et al. (2019). Cytotoxicity of Clostridium difficile toxins A and B requires an active and functional SREBP-2 pathway. *FASEB J.* 33, 4883–4892. doi: 10.1096/fj.201801440R

Papatheodorou, P., Zamboglou, C., Genisyuerek, S., Guttenberg, G., and Aktories, K. (2010). Clostridial glucosylating toxins enter cells via clathrin-mediated endocytosis. *PLoS One* 5:e10673. doi: 10.1371/journal.pone.0010673

Poh, M. K., Shui, G., Xie, X., Shi, P. Y., Wenk, M. R., and Gu, F. (2012). U18666A, an intra-cellular cholesterol transport inhibitor, inhibits dengue virus entry and replication. *Antiviral Res.* 93, 191–198. doi: 10.1016/j.antiviral.2011.11.014

Pruitt, R. N., Chambers, M. G., Ng, K. K. S., Ohi, M. D., and Lacy, D. B. (2010). Structural organization of the functional domains of Clostridium difficile toxins A and B. *Proc. Natl. Acad. Sci. U. S. A.* 107, 13467–13472. doi: 10.1073/pnas.1002199107

Rothman, S. W., Brown, J. E., Diecidue, A., and Foret, D. A. (1984). Differential cytotoxic effects of toxins A and B isolated from Clostridium difficile. *Infect. Immun.* 46, 324–331. doi: 10.1128/IAI.46.2.324-331.1984

Takano, T., Endoh, M., Fukatsu, H., Sakurada, H., Doki, T., and Hohdatsu, T. (2017). The cholesterol transport inhibitor U18666A inhibits type I feline coronavirus infection. *Antiviral Res.* 145, 96–102. doi: 10.1016/J.ANTIVIRAL.2017.07.022

Underwood, K. W., Jacobs, N. L., Howley, A., and Liscum, L. (1998). Evidence for a cholesterol transport pathway from lysosomes to endoplasmic reticulum that is independent of the plasma membrane. *J. Biol. Chem.* 273, 4266–4274. doi: 10.1074/jbc.273.7.4266

Conflict of Interest: The authors declare that the research was conducted in the absence of any commercial or financial relationships that could be construed as a potential conflict of interest.

Publisher's Note: All claims expressed in this article are solely those of the authors and do not necessarily represent those of their affiliated organizations, or those of the publisher, the editors and the reviewers. Any product that may be evaluated in this article, or claim that may be made by its manufacturer, is not guaranteed or endorsed by the publisher.

Copyright © 2021 Papatheodorou, Kindig, Badilla-Lobo, Fischer, Durgun, Thuraisingam, Witte, Song, Aktories, Chaves-Olarte, Rodríguez and Barth. This is an open-access article distributed under the terms of the Creative Commons Attribution License (CC BY). The use, distribution or reproduction in other forums is permitted, provided the original author(s) and the copyright owner(s) are credited and that the original publication in this journal is cited, in accordance with accepted academic practice. No use, distribution or reproduction is permitted which does not comply with these terms.

frontiers in Microbiology

ORIGINAL RESEARCH
published: 21 December 2021
doi: 10.3389/fmicb.2021.752549

Clostridioides difficile Toxin CDT Induces Cytotoxic Responses in Human Mucosal-Associated Invariant T (MAIT) Cells

Isabel Marquardt[1,2,3†], Josefine Jakob[1,2,3†], Jessica Scheibel[1], Julia Danielle Hofmann[4], Frank Klawonn[1], Meina Neumann-Schaal[4,5], Ralf Gerhard[6], Dunja Bruder[2,3‡] and Lothar Jänsch[1*‡]*

[1]Cellular Proteomics, Helmholtz Centre for Infection Research, Braunschweig, Germany, [2]Institute of Medical Microbiology and Hospital Hygiene, Infection Immunology, Health Campus Immunology, Infectiology and Inflammation, Otto-von-Guericke University Magdeburg, Magdeburg, Germany, [3]Immune Regulation, Helmholtz Centre for Infection Research, Braunschweig, Germany, [4]Braunschweig Integrated Centre of Systems Biology (BRICS), Department of Bioinformatics and Biochemistry, Technical University Braunschweig, Braunschweig, Germany, [5]Metabolomics, Leibniz Institute DSMZ-German Collection of Microorganisms and Cell Cultures, Braunschweig, Germany, [6]Institute of Toxicology, Hannover Medical School, Hannover, Germany

Clostridioides difficile is the major cause of antibiotic-associated colitis (CDAC) with increasing prevalence in morbidity and mortality. Severity of CDAC has been attributed to hypervirulent *C. difficile* strains, which in addition to toxin A and B (TcdA, TcdB) produce the binary toxin *C. difficile* transferase (CDT). However, the link between these toxins and host immune responses as potential drivers of immunopathology are still incompletely understood. Here, we provide first experimental evidence that *C. difficile* toxins efficiently activate human mucosal-associated invariant T (MAIT) cells. Among the tested toxins, CDT and more specifically, the substrate binding and pore-forming subunit CDTb provoked significant MAIT cell activation resulting in selective MAIT cell degranulation of the lytic granule components perforin and granzyme B. CDT-induced MAIT cell responses required accessory immune cells, and we suggest monocytes as a potential CDT target cell population. Within the peripheral blood mononuclear cell fraction, we found increased IL-18 levels following CDT stimulation and MAIT cell response was indeed partly dependent on this cytokine. Surprisingly, CDT-induced MAIT cell activation was found to be partially MR1-dependent, although bacterial-derived metabolite antigens were absent. However, the role of antigen presentation in this process was not analyzed here and needs to be validated in future studies. Thus, MR1-dependent induction of MAIT cell cytotoxicity might be instrumental for hypervirulent *C. difficile* to overcome cellular barriers and may contribute to pathophysiology of CDAC.

Keywords: MAIT cells, *C. difficile*, TcdA, TcdB, CDT, CDAC, IL-18, MR1-mediated MAIT cell activation

OPEN ACCESS

Edited by:
George Grant, University of Aberdeen, United Kingdom

Reviewed by:
Dominic Paquin Proulx, United States Military HIV Research Program, United States
Sidonia Barbara Guiomar Eckle, Peter Doherty Institute for Infection and Immunity, Australia
Lucy Garner, University of Oxford, United Kingdom

***Correspondence:**
Dunja Bruder
dunja.bruder@med.ovgu.de
Lothar Jänsch
lothar.jaensch@helmholtz-hzi.de

†These authors have contributed equally to this work and share first authorship
‡These authors have contributed equally to this work and share last authorship

Specialty section:
This article was submitted to Infectious Agents and Disease, a section of the journal Frontiers in Microbiology

Received: *03 August 2021*
Accepted: *24 November 2021*
Published: *21 December 2021*

Citation:
Marquardt I, Jakob J, Scheibel J, Hofmann JD, Klawonn F, Neumann-Schaal M, Gerhard R, Bruder D and Jänsch L (2021) Clostridioides difficile Toxin CDT Induces Cytotoxic Responses in Human Mucosal-Associated Invariant T (MAIT) Cells. Front. Microbiol. 12:752549. doi: 10.3389/fmicb.2021.752549

INTRODUCTION

Clostridioides difficile infections (CDI) are the major cause of antibiotic-associated colitis and an emerging threat for hospitalized patients. In general, clinical symptoms including pseudomembranous colitis are associated with *C. difficile* toxin A (TcdA) and toxin B (TcdB; Pothoulakis, 1996; Chumbler et al., 2016). So-called hypervirulent *C. difficile* ribotypes that in addition to TcdA and TcdB express the binary toxin *C. difficile* transferase (CDT) are responsible for outbreaks and cause severe *C. difficile*-associated colitis (CDAC) with increased recurrence, morbidity, and mortality (Kuijper et al., 2008; Bacci et al., 2011; He et al., 2013). The presence of *C. difficile* toxins in the blood (toxemia) was linked to severe courses of CDI in animals and improved techniques for the detection of toxemia in CDI patients are being established (Steele et al., 2012; Yu et al., 2015).

C. difficile toxins introduce post-translational modifications to host signaling components following their endocytosis together with different surface receptors. TcdA and TcdB are glucosyltransferases, which post-translationally modify and inactivate GTPases in target cells resulting in breakdown of tight junctions and epithelial integrity (Just et al., 1995a,b; Feltis et al., 2000). In contrast to monomeric TcdA and TcdB, CDT consists of two subunits, the substrate binding component CDTb and the enzymatic component CDTa that ADP-ribosylates actin and thereby inactivates host cell actin polymerization, ultimately leading to increase of cell surface protrusion (Gülke et al., 2001). These toxin-induced modulations of host cell organization facilitate successful *C. difficile* colonization at the intestinal epithelium (Schwan et al., 2009, 2014; Kasendra et al., 2014; Cowardin et al., 2016a; Buccigrossi et al., 2019). Toxin-dependent effects on innate immune response in CDI include the induction of pro-inflammatory cytokine production, apoptosis of epithelial cells and macrophages and subsequent attraction of pro-inflammatory neutrophils that are major drivers of CDAC-specific immunopathology (Pothoulakis et al., 1988; Mahida et al., 1996; Rocha et al., 1997; Souza et al., 1997; Saavedra et al., 2018). While there is evidence that *C. difficile* toxins affect migration and chemotaxis of conventional T cells (Wu et al., 2013), it remains largely elusive to date whether and how these toxins interfere with functionally distinct T cell subsets. In this context, we demonstrated previously that compared to less toxigenic strains, hypervirulent *C. difficile* trigger superior responses in human mucosal-associated invariant T (MAIT) cells (Bernal et al., 2018).

MAIT cells constitute up to 10% of total T cells in the lamina propria (Treiner et al., 2003). They express high levels of the C-type lectin CD161 and the T cell receptor (TCR) α-chain Vα7.2 (Tilloy et al., 1999; Martin et al., 2009). This semi-invariant TCR, together with a limited TCRβ repertoire, restricts them to the major histocompatibility complex (MHC) class I-related protein MR1, which is expressed on antigen presenting cells and epithelial cells (Treiner et al., 2003; Le Bourhis et al., 2010; Dusseaux et al., 2011). MR1 presents riboflavin (vitamin B2)-derived metabolite variants that constitute a recently described class of antigens (Kjer-Nielsen et al., 2012; Corbett et al., 2014). Upon TCR stimulation, MAIT cells are able to immediately execute effector functions (Dusseaux et al., 2011). Beside the semi-invariant TCR, MAIT cells constitutively express IL-12 and IL-18 receptors enabling their cytokine-mediated activation (Ussher et al., 2014). Activated MAIT cells can mediate cytotoxicity by release of lytic granules containing effector molecules such as perforin and a set of granzymes, e.g., granzyme B (Kurioka et al., 2015). However, MAIT cells can as well execute inflammatory Th1 immunity for instance by interferon-γ (IFNγ) secretion. Previous reports have already demonstrated that MAIT cells can be activated by superantigenic toxins produced by *Staphylococcus aureus* and *Streptococcus pyogenes*, resulting in a substantial cytokine response (Shaler et al., 2017; Emgård et al., 2019).

Here, we have studied the responsiveness of peripheral human MAIT cells to *C. difficile* toxins and identified CDT to be most competent in inducing a cytotoxic effector phenotype in MAIT cells. Interestingly, CDT-induced MAIT cell responses depend on both the interleukin-18 (IL-18) and the MR1-dependent signaling pathway. We identified monocytes to be involved in MR1-dependent activation of MAIT cells following CDT stimulation. Data obtained in frame of this study suggest that MAIT cell cytotoxicity might contribute to clearance of toxemia or to pronounced immunopathology observed in CDAC that is caused by hypervirulent *C. difficile*.

MATERIALS AND METHODS

C. difficile Cultures

C. difficile clinical isolates were provided by Leibniz Institute DSMZ – German Collection of Microorganisms and Cell Cultures (Braunschweig). DSM 102859 (RT023; depositor: Lutz von Müller) strain was cultured in riboflavin-free casamino acids containing medium (CDMM) under anaerobic conditions (Neumann-Schaal et al., 2015; Riedel et al., 2017). Cells were harvested at the mid exponential phase (OD_{max} 0.5). Bacterial numbers were determined using a Neubauer improved counting chamber (C-Chip, NanoEnTek). Bacterial cell pellets were harvested by centrifugation (13.000 *g*, 10 min, 4°C) and fixed with 2% paraformaldehyde (PFA) solution, were washed three times with PBS and stored at −80°C. Prior PBMC stimulation, the bacterial cells were resuspended in PBS to a final concentration of 3×10^8 bacteria/ml.

Expression and Purification of Recombinant *C. difficile* Toxins

Recombinant TcdA and TcdB as well as their glucosyltransferase deficient mutants were produced in the Gram positive and LPS-free *Bacillus megaterium* expression system (MoBiTec, Germany) as described before (Burger et al., 2003). Coding sequences for strain VPI10463 TcdA and TcdB were cloned into a modified pWH1520 vector (TcdA, TcdA D285/287 N) or into pHIS1522 vector (TcdB, TcdB D286/288 N) to obtain C-terminal His6-tagged proteins. The glucosyltransferase deficient mutants (TcdA D285/287 N, TcdB D286/288 N) were generated by site directed mutagenesis (QuikChange II Site-Directed Mutagenesis Kit, Stratagene) according to supplied protocol.

For expression of proteins the *B. megaterium* strain WH320 was used. In contrast to the large clostridial glucosyltransferases both components of the binary toxin CDT (CDTa and CDTb from *C. difficile* strain R20291) were expressed in *E. coli* TG1. The coding sequence for mature CDTa, lacking the export sequence, was cloned into pQE30 vector for expression as N-terminally His6-tagged protein. Mature CDTb was expressed in *E. coli* as GST fusion protein using the pGEX2T vector (GE Healthcare) as described earlier (Beer et al., 2018). GST-CDTb was purified *via* glutathione (GSH)-sepharose columns according to standard protocol. After elution from GSH-sepharose beads the GST-CDTb fusion protein was activated by limited digestion with trypsin (0.2 µg trypsin per µg GST-CDTb) for 30 min at room temperature. Thereby, the GST-tag as well as the N-terminal inhibitory part of CDTb was removed, resulting in activated CDTb. Incubation with trypsin was terminated by addition of 2 mM 4-(2-Aminoethyl)-benzensulfonylfluorid (AEBSF). All His6-tagged proteins were purified *via* Ni2 + -NTA sepharose (Protino Ni-IDA columns, Macherey-Nagel, Germany). After buffer exchange *via* ZEBA desalting columns (Pierce/Thermofischer, Germany) all toxins were stored in 20 mM Tris–HCl, pH7.2, and 50 mM NaCl at −80°C. The specific concentration and purity of toxins was estimated by SDS gel electrophoresis. We have produced CDT as authors of this study have described before in Stieglitz et al. (2021). This report provides evidence by 1,000 CDT-regulated phosphorylation sites that CDT used in this study is LPS-free and did not induce any classical LPS-dependent signaling pathway such as the ERK pathway [**Supplementary Tables 1** and **2** in Stieglitz et al. (2021)].

Blood Donations

This study was conducted in accordance with the rules of the Regional Ethics Committee of Lower Saxony, Germany and the declaration of Helsinki. Buffy coats from blood donations of healthy human volunteers, who provided informed consent, were obtained from the Institute for Clinical Transfusion Medicine, Klinikum Braunschweig, Germany. Blood donors' health was assessed prior blood donation. This procedure also includes standardized laboratory tests for infections with HIV1/2, HBV, HCV and *Treponema pallidum* (serology and/or nucleic acid testing) and hematological cell counts.

PBMC Isolation and Stimulation

Buffy Coats were produced from whole blood donations by using the Top & Bottom Extraction Bag System (Polymed Medical Devices). Peripheral blood mononuclear cells (PBMCs) were isolated from buffy coats by Ficoll® Paque PLUS density gradient centrifugation (GE Healthcare GmbH). PBMCs were rested overnight in RPMI 1640 medium (Gibco/Life Technologies) supplemented with 10% fetal bovine serum gold (PAA Laboratories), 2 mM L-glutamine, 50 units/ml penicillin and 50 µg/ml streptomycin (all Gibco/Life Technologies) at 37°C in a humid 7.5% CO_2 atmosphere. 0.5×10^6 PBMCs were either left untreated or stimulated with PFA-fixed bacteria at different multiplicities of infection (MOI) and/or with 100 ng/ml *C. difficile* toxins for 20 h at 37°C. To validate the role of MR1 or IL-18, PBMCs were incubated with 5 µg/ml anti-IL18 (MBL International, clone 126-2H), 20 µg/ml anti-MR1 (Biolegend, clone 26.5), 20 µg/ml Isotype control (Biolegend, Mouse IgG1, κ isotype) or different concentrations of Ac-6-FP (Cayman Chemical) 1 h prior stimulation with CDT at 37°C. CDT was then added with 100 ng/ml and cells were incubated for 20 h at 37°C. For intracellular staining, Brefeldin A was added for the last 4 h of stimulation.

Quantification of Cytokines

0.5×10^6 PBMCs were left either untreated or stimulated in duplicates with fixed *C. difficile* bacteria at MOI 1 or with 100 ng/ml recombinant *C. difficile* toxins for 20 h at 37°C in duplicates. Supernatants of respective samples were pooled and enzyme-linked immunosorbent assays were performed to detect human IL-12 using Human IL-12 (p70) ELISA MAX™ kit (BioLegend), human IL-15 using Human IL-15 ELISA MAX™ kit (BioLegend), and human IL-18 using Human IL-18 ELISA kit (MBL).

Fluorescence-Activated Cell Sorting (FACS) of MAIT Cells and Stimulation With *C. difficile* Toxins

PBMCs were isolated as described above. MAIT cells were sorted as $CD3^+$ $V\alpha7.2^+$ $CD161^{++}$ lymphocytes using a FACSAria II flow cytometer (BD Biosciences; Bionozzle size: 70 µm; system pressure: 70 PSI; flow rate 30,000 events/s; laser: 488 nm with 100 mWatt for FITC, PE-Cy5, and PE-Cy7, 640 nm with 60 mWatt for APC; detection with bandpass filters for FITC 525/50, PE-Cy5 670/14, PE-Cy7 780/60, and APC 670/30). Sorted cells were washed with FACS buffer and rested overnight in RPMI 1640 medium (Gibco/Life Technologies) supplemented with 10% fetal bovine serum gold (PAA Laboratories), 2 mM L-glutamine, 50 units/ml penicillin and 50 µg/ml streptomycin (all Gibco/Life Technologies) at 37°C in a humid 7.5% CO_2 atmosphere. 20,000 MAITs were either left untreated or stimulated with 100 ng/ml *C. difficile* toxins for 20 h at 37°C. For bi-cellular stimulation, monocytes were sorted as $CD14^+$ cells (BV510, Biolegend, clone M5E2) and washed as described for MAIT cells. Directly after sorting, 20,000 monocytes were combined with 20,000 MAIT cells per well and treated with *C. difficile* CDT as described before. 5-OP-RU was used as a positive control and was kindly provided by Dr. Olivier Lantz (Institut Curie, Paris). 5-OP-RU was added for 20 h to the co-culture of MAIT cells and monocytes. As in other bicellular studies, MAIT cells were stimulated by using a concentration of 50 ng/ml 5-OP-RU, which induces efficient pro-inflammatory responses while maintaining viability of MAIT cells (Hagel et al., 2020). For intracellular staining, Brefeldin A was added for the last 4 h of stimulation.

Antibodies

For cytometric assessment of MAIT cell phenotype, bulk PBMCs were stained with LIVE/DEAD™ Fixable Blue Dead Cell Stain Kit (Invitrogen) or Annexin V Apoptosis Detection Kit with 7-AAD FITC (Biolegend), with Fc receptor blocking reagent (Miltenyi Biotec) and a combination of the following antibodies

(from BioLegend except as noted): CD3 BV605 (clone OKT3), CD161 APC (clone DX12, BD Biosciences), Vα7.2 PE-Cy7 (clone 3C10), CD69 PE (clone FN50), CD107a PerCP-Cy5.5 (clone H4A3), GzmB Pacific Blue (clone GB11), perforin FITC (clone), and IFNγ APC-Cy7 (clone 4S.B3). For MR1 expression analysis on antigen presenting cells, bulk PBMCs were stained with Fc receptor blocking reagent (Miltenyi Biotec), LIVE/DEAD™ Fixable Near-IR Dead Cell Stain Kit (Invitrogen), and a combination of the following antibodies (from BioLegend): CD11c BV421 (clone 3.9), CD123 BV510 (clone 6H6), CD14 BV421 (clone 3D3), CD3 BV605 (clone OKT3), CD45 FITC (clone 2D1), CD56 BV711 (clone 5.1H11), CD16 APC (clone 3G8), HLA-DR PE-Cy7 (clone LN3), and MR1 PE (clone 26.5).

Extracellular and Intracellular Cell Staining

Stimulated PBMCs were washed with PBS and stained with Fc receptor blocking reagent (Miltenyi Biotec) and LIVE/DEAD™ Fixable Blue/Near-IR Dead Cell Stain Kit (Invitrogen). Cells were washed with FACS buffer and stained for extracellular surface marker at 4°C for 30 min. MR1 surface staining was performed together with the staining for extracellular surface marker. Cell fixation and permeabilization were performed using BD Cytofix/Cytoperm™ (BD Biosciences) followed by intracellular staining for 30 min at 4°C. Cells were washed twice with permeabilization buffer and cell pellet was resuspended in FACS buffer and subsequently analyzed on BD LSR-II SORP and BD LSR-Fortessa flow cytometer. Data was analyzed by FlowJo (TreeStar, v10.4.2) and Prism (GraphPad Software, v7.0c). To determine significant differences, Wilcoxon matched-pairs signed rank test was used. All *p*-values were corrected by strict Bonferroni Holm correction.

RESULTS

Toxins of Hypervirulent *C. difficile* Activate Human MAIT Cells

We previously demonstrated that hypervirulent *C. difficile* bacteria, which express the toxins TcdA, TcdB and CDT, exhibit superior capacities than less toxigenic TcdA/B$^+$ RT012 to activate human MAIT cells (Bernal et al., 2018). To further define the individual contribution of these major virulence factors to the observed MAIT cell activation, we generated recombinant TcdA, TcdB, their glucosyltransferase-deficient variants (GT-dTcdA and GT-TcdB), and binary *C. difficile* transferase (CDT) and studied their capacities to activate MAIT cells (purity of toxins shown in **Supplementary Figure 1**; gating strategy shown in **Supplementary Figure 2**). To this end, peripheral blood mononuclear cells (PBMCs) from healthy individuals were stimulated with increasing concentrations of CDT for 20 h from 1 to 100 ng/ml. Despite relatively pronounced donor variations, indeed all concentrations of CDT induced a significant increase in CD69 expression on MAIT cells, whereas the concentration of 100 ng/ml of CDT induced the highest MAIT cell activation (**Supplementary Figure 3A**). This concentration has also been shown (i) to induce effective innate immune response, (ii) to have no significant cytotoxic effect on the PBMC fraction, and (iii) to be within the range of concentrations present in fecal specimen of CDI patients (Lee et al., 2009; Ryder et al., 2010; Cowardin et al., 2016b; Yu et al., 2017). Therefore, we decided to investigate the role of the *C. difficile* virulence factors on MAIT cell activation using the concentration of 100 ng/ml. Interestingly, at 100 ng/ml not only CDT, but also TcdA and TcdB induced MAIT cell activation as indicated by a significantly increased CD69 expression (**Figures 1A–C**).

MAIT cell activation by TcdA and TcdB was further analyzed using glycosyltransferase-deficient TcdA (GT-dTcdA) or TcdB (GT-dTcdB). Both glycosyltransferase-deficient toxins induced a lower CD69 expression than their enzymatically active counterparts, indicating a glycosyltransferase-dependent mechanism (**Supplementary Figure 4**).

In contrast to TcdA and TcdB, CDT-mediated MAIT cell activation appeared to be less dependent on its enzymatic activity since the stimulation with the binding component CDTb was sufficient to induce full MAIT cell activation even in the absence of the enzymatic component CDTa. Adding increasing concentrations of CDTa to a fixed concentration of CDTb did not further increase MAIT cell activation (**Supplementary Figures 3B,C**). In contrast, adding increasing concentrations of CDTb to a defined concentration of CDTa indeed resulted in increased MAIT cell activation. This further emphasized the important role of the binding component CDTb in the mechanism of MAIT cell activation.

In conclusion, we found all three *C. difficile* toxins to activate human MAIT cells whereby CDT most effectively activated MAIT cells by its pore-forming unit CDTb. CDT is the hallmark of hypervirulent *C. difficile* strains and was therefore the focus in our following studies on endotoxin-mediated MAIT cell activation.

CD161^{++} Vα7.2$^+$ T Cells Are Efficiently Activated by CDT

CDT expression is a hallmark of hypervirulent and most pathogenic *C. difficile* strains that are associated with severe pathogenesis of CDAC. In general, CDT can enhance bacterial adhesion to host cells but its role in T cell-mediated immunity has not been studied so far (Schwan et al., 2009). Since CDT induced a significant MAIT cell activation, we wondered whether this observation is restricted to CD161 and Vα7.2. To evaluate this, PBMCs from healthy individuals were stimulated with CDT as described before, followed by flow cytometric analysis of CD69 on either CD161^{++}Vα7.2$^+$ (MAIT cells), CD161$^-$Vα7.2$^+$ or CD161$^{+/-}$ Vα7.2$^-$ T cells (**Figure 2**). In addition, we included stimulation of PBMCs with *C. difficile* RT023 as positive control. High donor variations were observed for stimulation with RT023 and CDT.

Although there was a moderate activation of CD161$^-$Vα7.2$^+$ and CD161$^{+/-}$ Vα7.2$^-$ T cells after stimulation with CDT, MAIT cell activation defined by high expression of CD161 and Vα7.2 was more profound. Moreover, CD161^{++} Vα7.2$^+$ MAIT cell activation after CDT stimulation was significantly increased in comparison to CD161$^-$Vα7.2$^+$ or CD161$^{+/-}$ Vα7.2$^-$ T cells. For CD161$^-$Vα7.2$^+$ T cells, the ΔMFI of CD69 after CDT

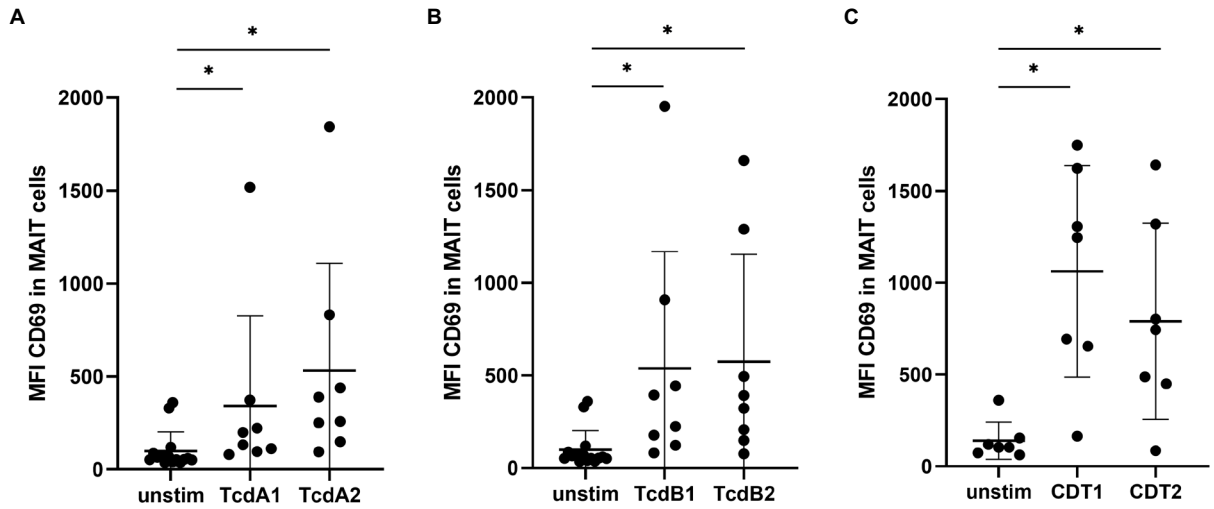

FIGURE 1 | *C. difficile* toxin-induced MAIT cell activation. PBMCs were isolated from healthy donors and stimulated with 100 ng/ml *C. difficile* toxin from two different production batches. TcdA1 or TcdA2 **(A)**, TcdB1 or TcdB2 **(B)** and CDT1 or CDT2 **(C)** stimulation for 20 h followed by flow cytometric analysis of mean fluorescence intensity (MFI) of total CD69 of MAIT cells. MAIT cells were gated on CD161^{++} Vα7.2^{+} CD3^{+} T cells. Data represent two to four independent experiments from seven to eight donors. Horizontal lines indicate mean ± SD. Asterisks indicate significant differences as determined by three Wilcoxon matched-pairs signed rank tests between all given conditions with Bonferroni Holm correction: $^{*}p < 0.05$.

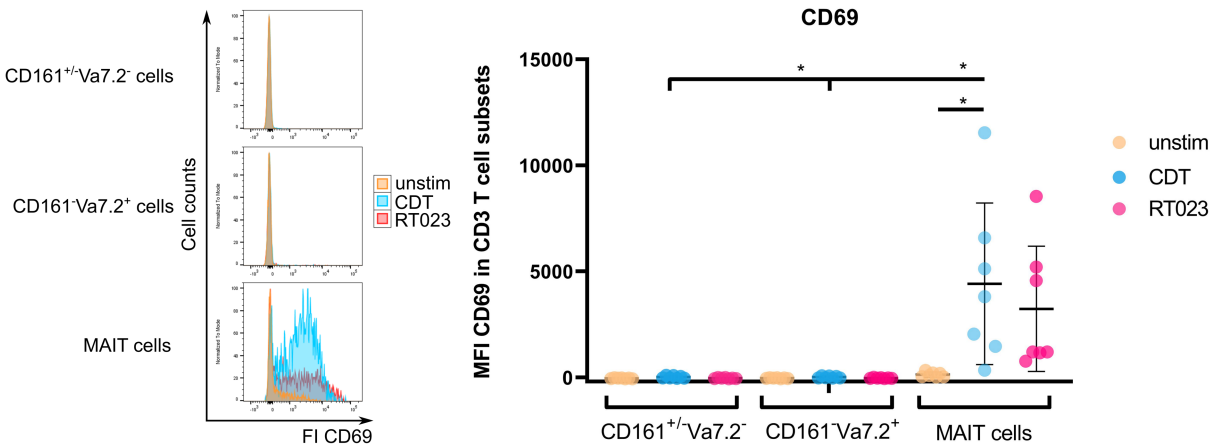

FIGURE 2 | Activation of MAIT cells, CD161$^{+/-}$ Vα7.2^{-}, and CD161^{-} Vα7.2^{+} cells following stimulation with *C. difficile* CDT. PBMCs were isolated from healthy donors and stimulated with 100 ng/ml CDT for 20 h followed by flow cytometric analyses of CD69 surface expression. Cells were gated on either CD161^{++} Vα7.2^{+}, CD161$^{+/-}$ Vα7.2^{-} or CD161^{-} Vα7.2^{+} CD3^{+} T cells and median fluorescence intensity of CD69 is displayed. Horizontal lines indicate mean ± SD. Asterisks indicate significant differences determined by eight Wilcoxon matched-pairs signed rank tests with Bonferroni Holm correction: $^{*}p < 0.05$. The following conditions were pairwise compared within all subsets: unstimulated (unstim) vs. CDT or unstim vs. RT023. Additionally, CDT of MAIT cells vs. CDT of CD161$^{+/-}$ Vα7.2^{-} or CD161^{-} Vα7.2^{+} were also compared. Data represent five independent experiments from seven donors.

stimulation was +58.4 and for CD161$^{+/-}$ Vα7.2^{-} T cells +49.9, whereas it was +4286.6 for MAIT cells.

Thus, T cell activation by CDT requires CD161^{++} Vα7.2^{+} suggesting CDT as a potent regulator of MAIT cell-related immune responses.

CDT-Activated MAIT Cells Exhibit a Cytotoxic Phenotype

Upon activation, MAIT cells mediate effector functions including cytotoxic response and secretion of cytokines. Strong or persistent activation, however, can promote MAIT cell apoptosis as well (Cosgrove et al., 2013; Zhang et al., 2019). Thus, we investigated whether stimulation with *C. difficile* toxin CDT would induce MAIT cell apoptosis, cytotoxicity and/or cytokine expression. As shown before, MAIT cells readily responded to CDT stimulation by significant upregulation of CD69. We then evaluated cell viabilities by assessing live, early and late apoptotic/dead MAIT cells by Annexin-V and 7-AAD staining. We found no evidence that under the chosen experimental conditions CDT induces MAIT cell apoptosis or cell death (**Figures 3A,B**). However,

CDT-activated MAIT cells showed significantly increased expression of lytic granule components granzyme B (GzmB) as well as perforin. Furthermore, CDT-activated MAIT cells were found to upregulate the degranulation marker CD107a at their surface (**Figures 3C–E**) indicating preceding degranulation and the release of cytotoxic lytic granules. Strikingly, CDT stimulation did not induce IFNγ expression in MAIT cells (**Figure 3F**). In conclusion, CDT-mediated activation of MAIT cells promotes their cytotoxicity, which is however uncoupled from an inflammatory IFNγ response.

CDT-Induced MAIT Cell Cytotoxicity Involves MR1 and IL-18

So far, it is unknown whether MAIT cells are direct targets of CDT. To test this, sorted MAIT cells were stimulated with CDT and CD69 surface expression was assessed. The CD69 expression was not increased, i.e., CDT stimulation of purified MAIT cells did not induce their activation, suggesting that previously observed CDT-dependent MAIT cell activation requires accessory cells (**Figure 4A**). Assuming that CDT affects cells other than MAIT cells in the PBMC fraction, we investigated whether those would release MAIT cell-activating cytokines (IL-12, IL-15, and IL-18) following stimulation with CDT. While IL-12 and IL-15 were not detectable (data not shown), CDT stimulation resulted in increased IL-18 levels in the supernatant of CDT-stimulated PBMCs (**Figure 4B**). Therefore, we next examined the role of IL-18 for the CDT-dependent MAIT cell activation.

Antibody-mediated blockade of IL-18 responses (a-IL-18) 1 h prior CDT stimulation in PBMC fractions significantly reduced the expression of the cytotoxic granule component GzmB. The expression of CD69 and CD107a was moderately but yet significantly reduced while a-IL-18 treatment did not affect the expression of perforin in MAIT cells (**Figure 4C**). We furthermore validated the role of IL-18 in the CDT-mediated activation of MAIT cells by the addition of supplementary IL-18 (r-IL18). Interestingly, IL-18 promoted CDT-induced MAIT cell cytotoxicity (significantly increased CD69, CD107a and GzmB expression). In summary, the level of IL-18 was increased in the supernatant of CDT-stimulated PBMCs and this cytokine mostly affected the CDT-induced GzmB responses while its impact on CD69 and CD107a expression was moderate with, so far, non-proven biological relevance.

Next, to activating cytokines, MAIT cell cytotoxicity can be induced by MR1 presentation of antigens to the MAIT cell invariant T cell receptor (TCR). Thus, we examined whether the MR1-TCR axis would as well contribute to the observed CDT-induced MAIT cell activation. We applied an MR1-blocking antibody and the according isotype control prior stimulation with CDT to the PBMCs and assessed MAIT cell activation and effector responses by flow cytometry (**Figure 4C** and **Supplementary Figure 5**). Surprisingly, despite the absence of bacterial antigens, antibody-mediated inhibition of MR1 attenuated MAIT cell activation and cytotoxicity (CD69, CD107a, GzmB and perforin expression). In parallel, we observed a minor downregulation of the MAIT TCR Vα7.2 upon CDT-induced activation, which is typically associated with TCR-MHC dependent activation (**Supplementary Figure 6**). However, the level of downregulation was subtle when compared to stimulation with fixed bacteria such as *E. coli* and validation of TCR-engagement needs further investigation. In contrast, MR1 blockade did not affect activation of $CD161^{+/-}$ $V\alpha7.2^{-}$ and $CD161^{-}$ $V\alpha7.2^{+}$ cells (data not shown).

Additionally, we applied the competitive inhibitor Acetyl-6-formylpterin (Ac-6-FP) to PBMCs during CDT stimulation (**Supplementary Figure 7**). Ac-6-FP is known to be loaded onto MR1 and to effectively reduce MAIT cell activation following treatment with 5-(2-oxopropylideneamino)-6-d-ribitylaminouracil (5-OP-RU; Eckle et al., 2014). Indeed, we observed an inhibitory effect of Ac-6-FP on CDT-mediated MAIT cell activation, which we found moderate though significant for CD69 and GzmB responses, whereas the effect was marginal for perforin and CD107a.

In conclusion, although the biological relevance of IL-18 was not proven in this study, the data indicate that it may promote the release of the granzyme B by MAIT cells upon CDT-stimulation. However, blockade of MR1 significantly inhibited the MAIT cell effector responses, which suggests that CDT-induced cytotoxicity involves the MR1-pathway.

MAIT Cell Activation by CDT Involves Monocytes

The fact that CDT-induced MAIT cell responses require MR1 and PBMCs indicates the relevance of antigen-presenting cells that are targeted and modulated by CDT and subsequently activate MAIT cells. To identify those cells, we first monitored MR1 surface expression in PBMCs by flow cytometry using a gating strategy to examine three major MR1-expressing immune cell subsets, i.e., monocytes, myeloid dendritic cells (mDCs) and B cells (**Supplementary Figure 8**). In the absence of CDT, highest MR1 basal expression was observed on $CD14^{+}$ monocytes (**Figure 5**, right). While CDT stimulation did not significantly alter MR1 surface expression on mDCs and B cells, a significantly increased MR1 surface expression was found on $CD14^{+}$ monocytes (**Figure 5**, left and right). These data suggest that $CD14^{+}$ monocytes are targeted by CDT.

Next, we investigated the role of $CD14^{+}$ monocytes during CDT-induced MAIT cell activation by stimulating sorted MAIT cells and sorted monocytes of the same donors in a bi-cellular model with CDT. CDT stimulation of sorted MAIT cells alone had no effect on CD69 surface expression, whereas in the presence of monocytes, CD69 expression was significantly increased (**Figure 6A**). Furthermore, CDT-activated MAIT cells showed significantly increased expression of CD107a in the bi-cellular model, indicating preceding degranulation. Expression of the lytic granule components GzmB and perforin were also increased after CDT stimulation with monocytes. However, due to relatively low donor numbers and by taking multiple testing into account by the strict Bonferroni Holm method, the *p*-values of increased GzmB and perforin expression were calculated with 0.078. Nevertheless, these data are in accordance with CDT-stimulated PBMCs (**Figure 3**) suggesting the role of monocytes for CDT-induced MAIT cell activation. We did not observe a significant increase in apoptosis of monocytes after 20 h of CDT stimulation, which largely excludes the

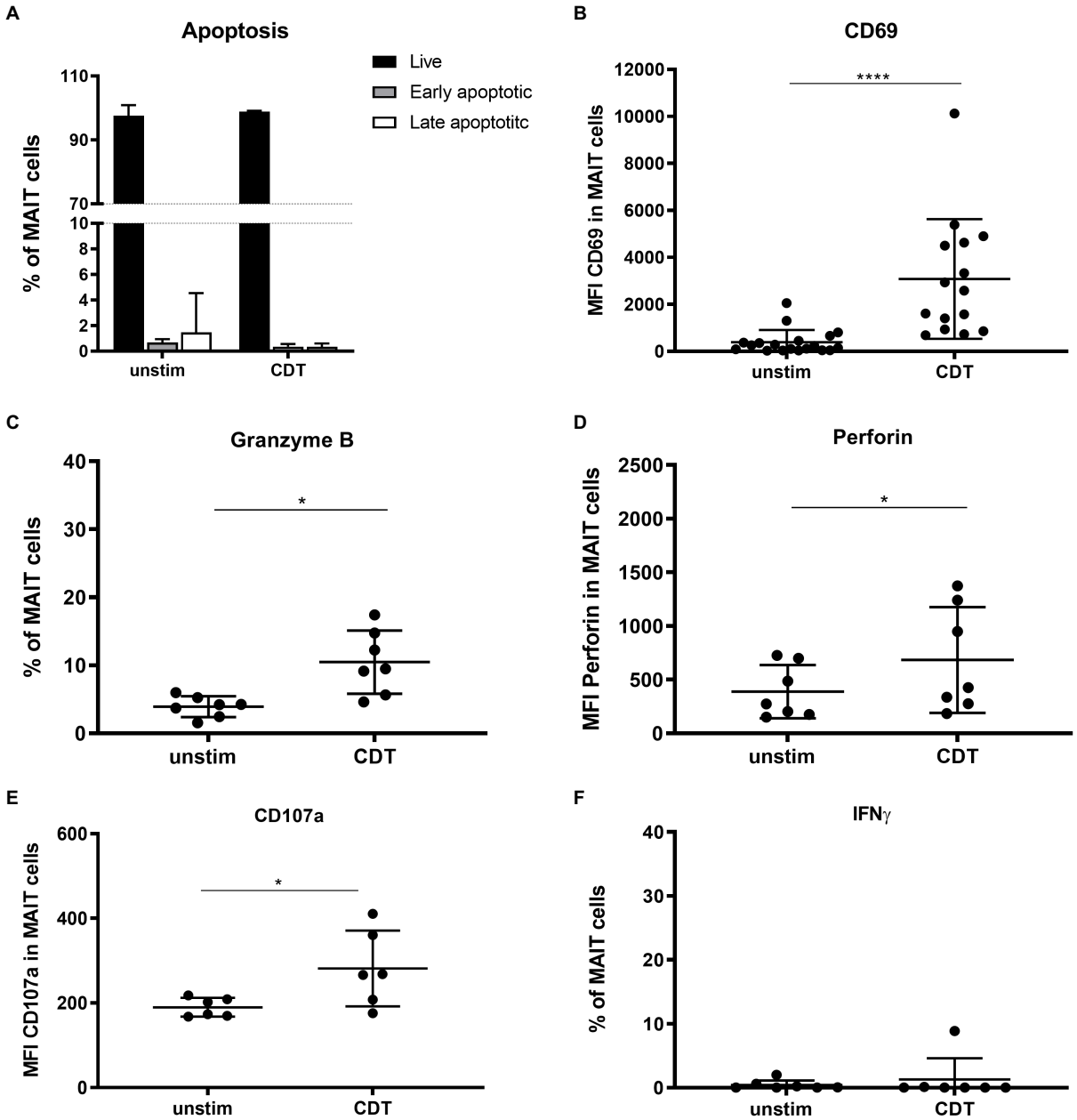

FIGURE 3 | Effector phenotype of primary human MAIT cells following stimulation with *C. difficile* CDT. PBMCs were isolated from healthy donors and stimulated with 100 ng/ml CDT for 20 h followed by flow cytometric analysis of apoptosis **(A)**, granzyme B **(B)**, CD69 **(C)**, perforin **(D)**, CD107a **(E)** and IFNγ expression **(F)**. Cells were gated on $CD161^{++}$ $V\alpha7.2^{+}$ $CD3^{+}$ T cells (MAIT cells). **(A)** Live: Annexin V^{-} and 7-AAD^{-} (black), early apoptotic Annexin V^{+} and 7-AAD^{-} (dark grey), and late apoptotic Annexin V^{+} and 7-AAD^{+} (white) MAIT cells are depicted. Horizontal lines indicate mean ± SD. Asterisks indicate significant differences determined by Wilcoxon matched-pairs signed rank test: $^{*}p < 0.05$, $^{****}p < 0.0001$. Data represent nine independent experiments from 6 to 15 donors.

possibility that MAIT cell activation and cytokine production may result from CDT-induced necrotic or apoptotic monocytes (**Figure 6F**). Responsiveness of the donors towards IFNγ response was shown by the positive control 5-OP-RU. IFNγ production was slightly increased in individual donors after CDT stimulation, but we did not observe a significant induction of IFNγ by CDT in the bi-cellular model (**Figure 6E**). Again, this finding is in agreement with our data from PBMCs (see **Figure 3F**). Likewise, MR1-dependency was validated in this bi-cellular model, since the application of anti-MR1 antibodies prior to CDT stimulation decreased MAIT cell effector responses (CD69, CD107a, GzmB, perforin).

In summary, CDT can induce MAIT cell activation and cytotoxicity, which was found to depend on MR1. Moreover, MR1-expressing monocytes were sufficient to induce significant MAIT cell activation following CDT stimulation.

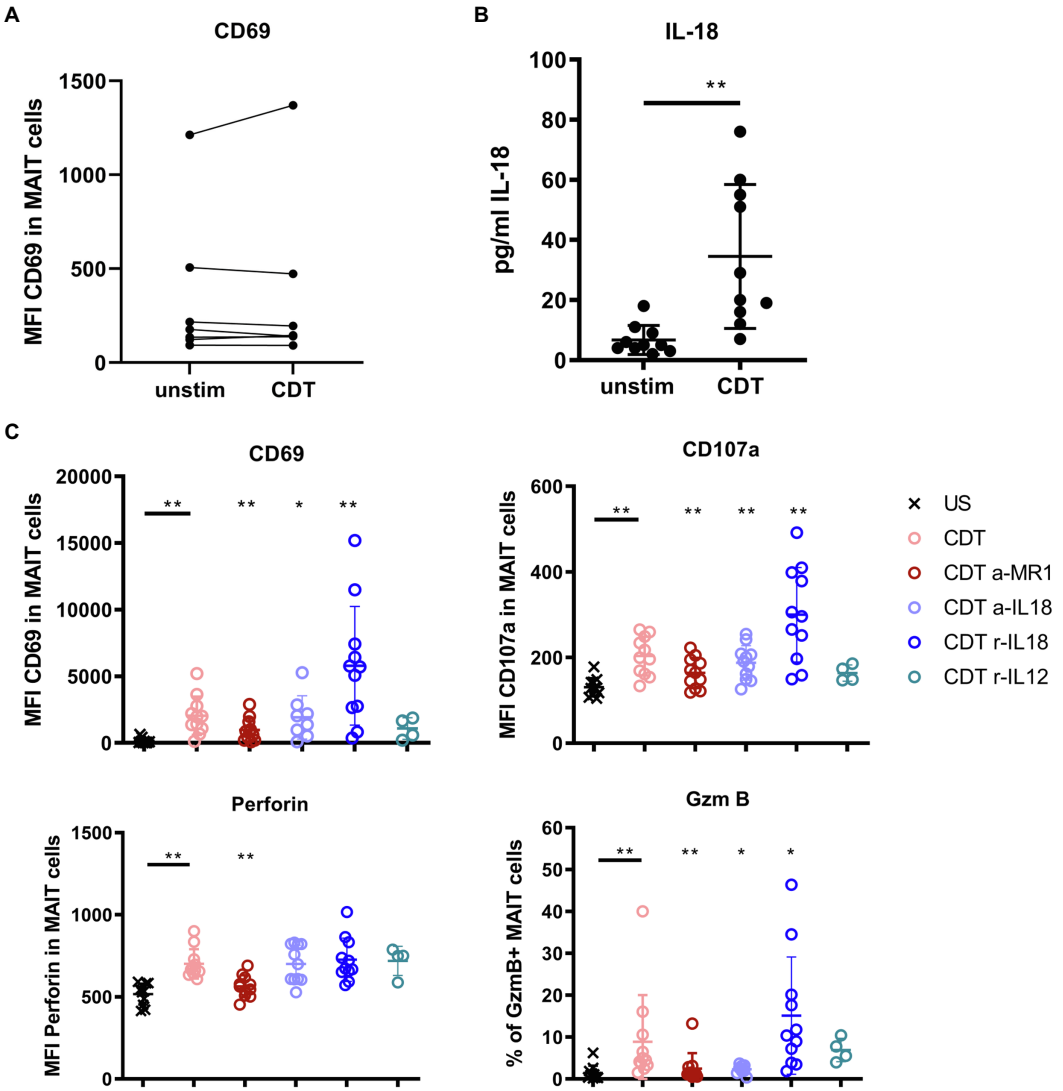

FIGURE 4 | Contribution of IL-18, IL-12, and MR1 to CDT-induced MAIT cell activation and cytotoxicity. *C. difficile* CDT (100 ng/ml) was directly applied to isolated CD161^{++} Vα7.2^{+} CD3^{+} MAIT cells from seven healthy donors for 20 h and MAIT cell activation (CD69) was examined by flow cytometric analyses **(A)**. *C. difficile* CDT (100 ng/ml) was applied to total PBMC fractions from 4 to 11 human donors for 20 h followed by quantification of IL-18 in the PBMC supernatant or flow cytometric analysis of CD69, CD107a, intracellular granzyme B (GzmB), perforin, and IFNγ in MAIT cells **(B,C)**. If indicated, PBMCs were treated with anti-IL-18 (a-IL18), recombinant IL-18 (r-IL18), recombinant IL-12 (r-IL12) or anti-MR1 (a-MR1) prior CDT stimulation. Horizontal lines indicate mean ± SD. Asterisks indicate significant differences determined by four Wilcoxon matched-pairs signed rank tests with Bonferroni Holm correction. Each condition was pairwise compared to CDT alone: $^{*}p < 0.05$, $^{**}p < 0.01$. Data represent three independent experiments from 4 to 11 donors. US: unstimulated.

CDT-Expressing Hypervirulent *C. difficile* Enhance MAIT Cell Activation

We have previously shown that hypervirulent *C. difficile* ribotypes, which under the chosen cultivation conditions did not express toxins, induce MAIT cell responses MR1-dependently (Bernal et al., 2018). Here, we demonstrate that *C. difficile* toxin CDT induces cytotoxic effector functions as well in an MR1-dependent manner. Thus, we next analyzed whether simultaneous stimulation of MAIT cells with (i) the hypervirulent *C. difficile* ribotype RT023 and (ii) CDT would have a synergistic effect in terms of MAIT cell activation and their acquisition of effector functions. To this end, PBMCs from healthy individuals were stimulated according to the previously established conditions using PFA-fixed *C. difficile* RT023 at an MOI 1 (Bernal et al., 2018), with 100 ng/ml CDT, or a combination of both. As expected, both conditions alone resulted in the activation of MAIT cells. Interestingly, co-stimulation with RT023 and CDT further increased the MAIT cell activation in individual donors as indicated by enhanced CD69 surface expression compared to stimulation with RT023 or CDT only (**Figure 7A**). However, co-stimulation with CDT did not induce further upregulation of the *C. difficile* RT023-induced expression of cytotoxic GzmB and perforin (**Figures 7B,C**). CDT-induced CD107a expression was not further increased by co-stimulation with *C. difficile* RT023 (**Figure 7D**).

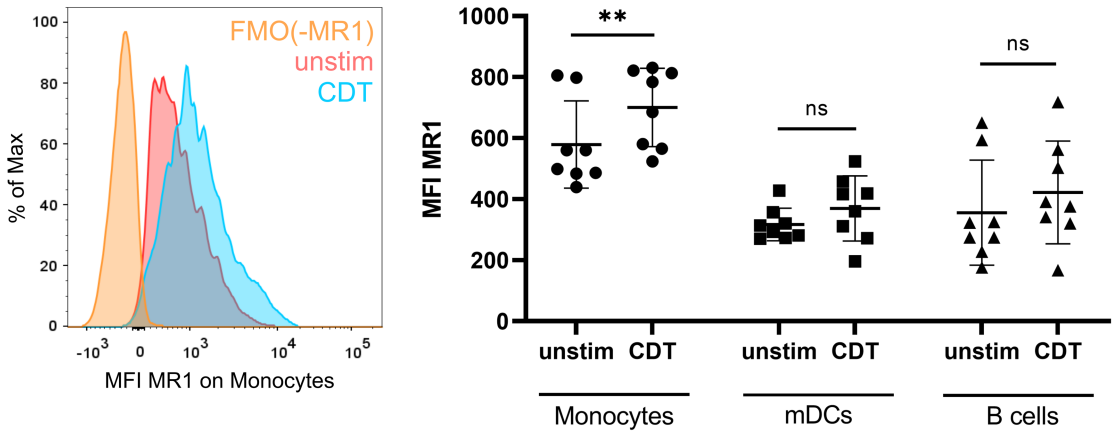

FIGURE 5 | *C. difficile* CDT-induced MR1 surface expression on monocytes. PBMCs were isolated from human donors and either left untreated or stimulated with 100 ng/ml *C. difficile* CDT for 20 h followed by flow cytometric analysis of MR1 expression. Left: Representative histogram of MR1 surface expression (MFI) on unstimulated (red) and CDT-stimulated (blue) $CD14^+$ monocytes. Fluorescence minus one (FMO) staining for MR1 is shown (orange). Right: MR1 surface expression of unstimulated or CDT-stimulated $CD14^+$ monocytes, myeloid dendritic cells (mDCs), and B cells. Horizontal lines indicate mean ± SD. Asterisks indicate significant differences determined by Wilcoxon matched-pairs signed rank tests: $^{**}p < 0.01$. Data of two independent experiments from 10 donors are shown.

Likewise and in accordance with the previously described data, CDT did not further increase the *C. difficile* RT023-induced IFNγ response (**Figure 7E**). In conclusion, co-stimulation with CDT synergizes with *C. difficile*-induced MAIT activation (CD69), while it does not further boost *C. difficile*-induced upregulation of cytotoxic perforin and GzmB as well as inflammatory IFNγ responses.

DISCUSSION

Virulent *C. difficile* is capable to produce three different exotoxins which, following receptor binding and uptake, manipulate host cell processes: TcdA, TcdB and *C. difficile* transferase CDT. The exotoxins TcdA and TcdB that contain glycosylation and ribosylation enzymatic domains inactivate Rho GTPases thereby causing *C. difficile*-associated colitis (CDAC). Hypervirulent strains additionally can produce the binary, actin ADP-ribosylating toxin CDT and these strains are associated with severe CDAC progression including pseudomembranous colitis, loss of intestinal barrier functions and life-threatening sepsis.

We show here that toxins of hypervirulent *C. difficile* are capable to activate MAIT cells in PBMC fractions of healthy individuals. In case of TcdA and TcdB, MAIT cell activation following stimulation with glycosyltransferase-deficient mutants was reduced in comparison to enzymatically active TcdA and TcdB, indicating a role of Rho GTPase signaling in this process. However, CD69 expression was analyzed from two different groups of donors in **Supplementary Figure 4**, limiting the possibility to make a final conclusion about the enzymatic dependency.

In contrast, CDT, which is only expressed by hypervirulent *C. difficile* strains, seems to activate MAIT cells in a different manner. Binary CDT consists of a substrate binding and pore-forming CDTb and an ADP-ribosyl-transferase containing CDTa domain. ADP-ribosylation of actin by CDT causes depolymerization of the host cytoskeleton and the formation of microtubule-rich protrusions, which support bacterial adhesion (Schwan et al., 2009). Interestingly, activation of MAIT cells was found to be mostly dependent on CDTb, while CDTa and its ADP-ribosyltransferase seemed to be dispensable for MAIT cell activation. Thus, CDT apparently utilizes a mechanism distinct from TcdA and TcdB to activate MAIT cell immunity. Indeed, it was previously reported that *C. difficile* CDTb is sufficient to induce necrosis in epithelial cells indicating signaling competence of the binding and pore-forming part of CDT (Landenberger et al., 2021).

In general, it was surprising that the mode-of-action of CDT in PBMCs required MR1. The prototypic MR1 antibody which is routinely used to characterize MR1-dependency almost completely blocked CDT-mediated MAIT cell responses, suggesting a CDT/MR1 non-canonical pathway being involved in the activation of MAIT cells (Huang et al., 2009). This pathway likely requires MR1 expressing non-MAIT cells since (i) MAIT cells alone turned out to be resistant against *C. difficile* toxin-induced apoptosis (**Figure 3A**) and (ii) MAIT cells were only activated CDT-dependent as part of PBMC fractions, whereas purified MAIT cells did not up-regulate CD69 following CDT treatments (**Figures 4A, 6A**). Characterizing MR1-surface expression on PBMCs indeed revealed that CDT triggers the upregulation of MR1 on monocytes and bi-cellular stimulation assays with primary MAIT cells and monocytes verified that monocytes alone are sufficient to mediate CDT-dependent MAIT cell activation. This of course did not rule out the possibility that other cell types contribute to CDT-mediated MAIT cell responses *in vivo*.

The key question by which mechanism CDT provokes MR1-dependent MAIT cell responses was not addressed and requires further studies. Lipolysis-stimulated lipoprotein receptor (LSR) is the main receptor of CDT, which is highly

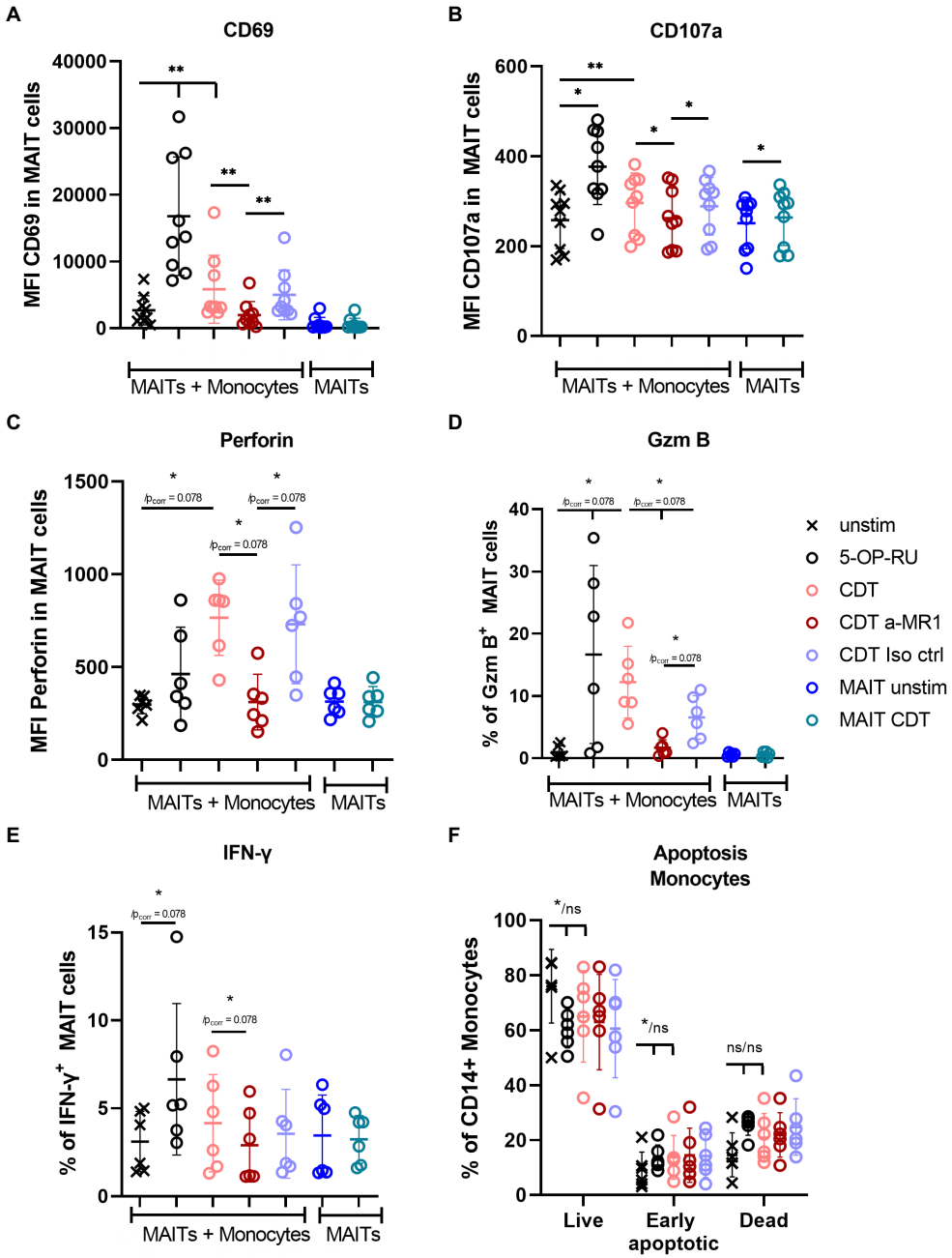

FIGURE 6 | Monocytes MR1-dependently activate MAIT cells in a bi-cellular model following CDT stimulation. *C. difficile* CDT (100 ng/ml) was directly applied to isolated CD161^{++} Vα7.2^{+} CD3^{+} MAIT cells and CD14^{+} monocytes (1:1 ratio) for 20 h. As indicated, in two conditions MAIT cells were stimulated without monocytes. MAIT cell activation was quantified by flow cytometric analysis determining CD69 **(A)**, CD107a **(B)**, intracellular perforin **(C)**, GzmB **(D)** and IFNγ **(E)** expression. Apoptosis of monocytes was determined by Annexin V Apoptosis Detection Kit with 7-AAD **(F)**. If indicated, cells were treated with anti-MR1 (a-MR1) or isotope control IgG1 (Iso ctrl) 1 h prior CDT stimulation. As positive control, cells were stimulated with 50 ng/ml 5-OP-RU for 20 h. Horizontal lines indicate mean ± SD. Asterisks indicate significant differences determined by Wilcoxon matched-pairs signed rank test with *p* values before and after Bonferroni Holm correction (*/p_{corr}); *$p < 0.05$; **$p < 0.01$. If no corrected p value is given, asterisks indicate significances after the correction. For co-incubated MAIT cells and monocytes (MAITs + Monocytes) five tests were performed **(A–E)**: unstimulated (unstim) vs. (i) 5-OP-RU, (ii) CDT and CDT vs. (iii) a-MR1, (iv) Iso ctrl, and (v) a-MR1 vs. Iso ctrl. MAIT cells alone ± CDT were tested separately. In **(F)** three tests were performed between unstim and indicated conditions. Data of two to three independent experiments from six to nine donors are shown.

expressed on colonic epithelial cells and is important for the integrity of epithelial barriers (Masuda et al., 2011). In general, immune cells have a relatively low expression of LSR compared to epithelial cells[1] with decreasing amounts

[1]https://www.proteinatlas.org/

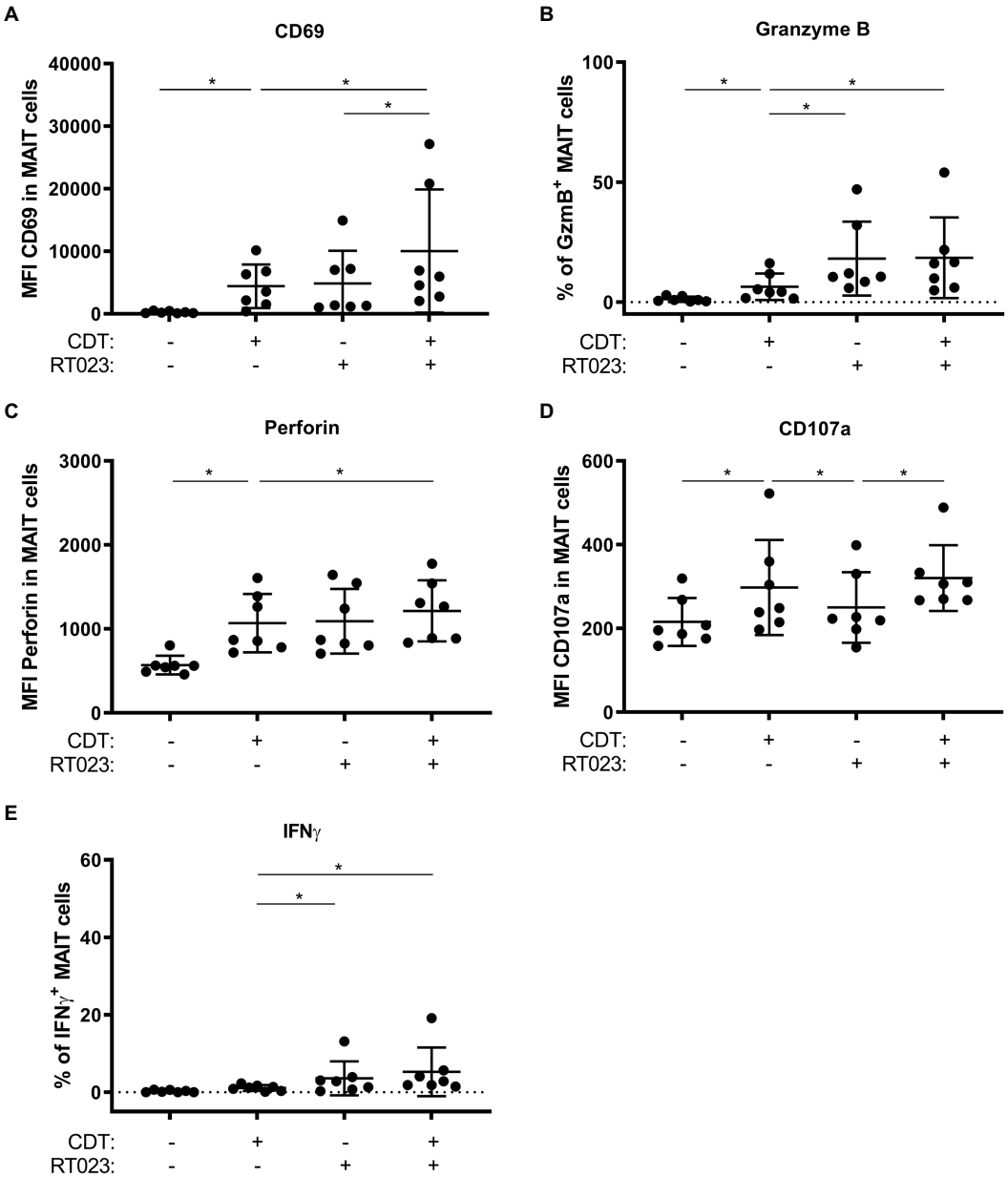

FIGURE 7 | MAIT cell effector phenotype following combined stimulation with hypervirulent *C. difficile* isolate RT023 and/or CDT. PBMCs were isolated from healthy donors and stimulated with *C. difficile* isolate with ribotype RT023 at MOI 1 and/or 100 ng/ml CDT for 20 h followed by flow cytometric analyses of CD69 **(A)** and CD107a **(D)** surface expression, internal granzyme B **(B)**, perforin **(C)**, and IFNγ **(E)** expression. Cells were gated on $CD161^{++}$ $V\alpha7.2^{+}$ $CD3^{+}$ T cells (MAIT cells). Horizontal lines indicate mean fluorescence intensity/mean percentages ± SD. Asterisks indicate significant differences determined by six Wilcoxon matched-pairs signed rank tests with Bonferroni Holm correction: $^{*}p < 0.05$. All conditions were pairwise tested against each other. Data of three independent experiments from seven donors are shown.

from T cell subsets to antigen-presenting cells. In the same line, one could also speculate about a potential role of toll-like receptor signaling since CDT is recognized by the TLR2/6 heterodimer to induce an NF-κB response and, TLR signaling in human antigen-presenting cells regulates MR1-dependent activation of MAIT cells (Ussher et al., 2016; Simpson et al., 2020). In conclusion, a mode-of-action of CDT *via* LSR is mechanistically counterintuitive due to its low surface expression on immune cells, whereas TLR signaling may co-regulate MR1 on monocytes.

Because bacterial metabolites were absent during *in vitro* CDT stimulation, we may speculate that MR1 might present endogenous metabolites (self-antigens) that are released during CDT-induced host cell modifications or necrosis. It has been described that in addition to bacterial metabolites MR1 can present non-bacterial antigens and self-antigens (Keller et al., 2017; Lepore et al., 2017).

However, this has not yet been investigated in the context of *C. difficile* toxin CDT. Such a mechanism would represent a so far undescribed non-canonical pathway enabling toxin-stimulated cells to present self-antigens MR1-dependently, thereby acting as kind of danger signals in order to induce MAIT cell cytotoxicity. Interestingly, in our experimental setting, cytotoxicity was found to depend on IL-18 (except for perforin). In direct contrast, in the canonical pathway bacteria-stimulated MAIT cells express CD107a, perforin, and GzmB independently of IL-18 (Kurioka et al., 2015). Moreover, CDT did not induce IFNγ expression in MAIT cells. Regarding IFNγ induction, one has to consider the TCR- and the cytokine-dependency of MAIT cell activation. CDT induced only IL-18, which alone is not sufficient to induce IFNγ response in MAIT cells (Ussher et al., 2014). However, in case of canonical activation pathway of bacterial antigens, TCR-dependent MAIT cell activation results in IFNγ expression, which was not observed in this study. Therefore, the absence of IFNγ production indicates a TCR-independent mechanism underlying the CDT-induced MAIT cell activation. Besides, the absence of an IFNγ response largely excludes the possibility that MAIT cells might be activated by contaminants like LPS in the recombinant produced CDT fractions and underlines that CDT specifically activates MAIT cells. Furthermore, the observed minor downregulation of the TCR on MAIT cells, which is notably low as compared to *E. coli* stimulated MAIT cells, did not indicate a significant role of the TCR in the process of CDT-induced responses (**Supplementary Figure 6**). Thus, we rather suggest a CDT mechanism widely independent from the engagement of the TCR by MR1.

Data of this study now suggest that CDT triggers a non-canonical host cell immune response that ultimately results in the degranulation of cytotoxic granules by MAIT cells. Consequently, MAIT cells might be primed to elicit targeted killing of CDT-intoxicated cells in the blood circulation, thereby contributing to clearance of toxemia. Assuming that MAIT cells exhibit cytotoxicity against CDT intoxicated epithelial cells in CDI, they might as well enhance the CDT-induced disruption of the intestinal barrier and thereby contribute to pronounced immunopathology caused by hypervirulent *C. difficile*. Other studies that investigated MAIT cell activation by Superantigens (SAgs) produced by *Staphylococcus aureus* and *Streptococcus pyogenes,* described an MR1-independent mechanism (Shaler et al., 2017; Emgård et al., 2019). However, they identified MAIT cells as the major responders of SAgs by releasing pro-inflammatory cytokines (Shaler et al., 2017). Furthermore, Emgård et al. suggest that MAIT cells may contribute to the pathological cytokine storm underlying the Streptococcal toxic shock syndrome (STSS) which is similar to our suggestion considering the pronounced immunopathology caused by hypervirulent *C. difficile.*

In general, CDT might be a promising target to manipulate the host cell immune response in CDI caused by hypervirulent *C. difficile*. Our findings suggest that CDTb is the key component of the binary CDT that induces host cell immune responses and in turn provokes MAIT cell cytotoxicity. In this context, neutralizing antibodies against CDTb have been demonstrated to reduce the adherence of *C. difficile* to human colon carcinoma cells (Schwan et al., 2009). Nevertheless, results of our study do not rule out the possibility that CDT affects also other T cell subsets, which might also contribute to pathogenicity during CDI. Thus, inhibiting MAIT cell activation by CDTb neutralizing antibodies might only partially enable to manipulate host cell immune responses during CDI. Of note, CDT-induced MAIT cell activation uncovered a remarkable donor variation concerning the individual strength of effector molecule expression. In particular, it would be important to validate these effector responses at sides of infection to clarify whether anti-CDT strategies support a required MAIT cell immunity.

In conclusion, we discovered a CDT/MR1-axis constituting a non-canonical pathway that selectively induces MAIT cell cytotoxicity. Based on our data, it is tempting to speculate that CDT expression and related cytotoxicity is instrumental for hypervirulent *C. difficile* to overcome epithelial barriers at the intestinal mucosa.

DATA AVAILABILITY STATEMENT

The raw data supporting the conclusions of this article will be made available by the authors, without undue reservation.

ETHICS STATEMENT

The studies involving human participants were reviewed and approved by Institutional Review Board of the Hanover Medical School. The patients/participants provided their written informed consent to participate in this study.

AUTHOR CONTRIBUTIONS

DB and LJ conceived and designed the research. IM, JJ, and JS designed and performed the experiments and analyzed the data. JH and MN-S provided the bacteria. RG provided the toxins. FK designed and performed the statistical analyses. IM, JJ, DB, and LJ wrote the manuscript. All authors contributed to the article and approved the submitted version.

FUNDING

This work was conducted within the context of the International Graduate School ABINEP (Analysis, Imaging, and Modelling of Neuronal and Inflammatory Processes) at Otto von Guericke University (OVGU) Magdeburg, Germany. The project was funded by the federal state Saxony-Anhalt and the European Structural and Investment Funds (ESF, 2014-2020), project number ZS/2016/08/80645. to IM and JJ, and by the Federal State of Lower Saxony, Niedersächsisches Vorab (VWZN2889/3215/3266).

SUPPLEMENTARY MATERIAL

The Supplementary Material for this article can be found online at: https://www.frontiersin.org/articles/10.3389/fmicb.2021.752549/full#supplementary-material

REFERENCES

Bacci, S., Mølbak, K., Kjeldsen, M. K., and Olsen, K. E. P. (2011). Binary Toxin and death after *Clostridium difficile* infection. *Emerg. Infect. Dis.* 17, 976–982. doi: 10.3201/eid/1706.101483

Beer, L. A., Tatge, H., Schneider, C., Ruschig, M., Hust, M., Barton, J., et al. (2018). The binary toxin CDT of *Clostridium difficile* as a tool for intracellular delivery of bacterial glucosyltransferase domains. *Toxins* 10:225. doi: 10.3390/toxins10060225

Bernal, I., Hofmann, J. D., Bulitta, B., Klawonn, F., Michel, A.-M., Jahn, D., et al. (2018). *Clostridioides difficile* activates human mucosal-associated invariant T cells. *Front. Microbiol.* 9:2532. doi: 10.3389/fmicb.2018.02532

Buccigrossi, V., Vecchio, A. L., Marano, A., and Guarino, A. (2019). Differential effects of *Clostridium difficile* toxins on ion secretion and cell integrity in human intestinal cells. *Pediatr. Res.* 85, 1048–1054. doi: 10.1038/s41390-019-0365-0

Burger, S., Tatge, H., Hofmann, F., Genth, H., Just, I., and Gerhard, R. (2003). Expression of recombinant *Clostridium difficile* toxin A using the bacillus Megaterium system. *Biochem. Biophys. Res. Commun.* 307, 584–588. doi: 10.1016/S0006-291X(03)01234-8

Chumbler, N. M., Farrow, M. A., Lapierre, L. A., Franklin, J. L., Borden, D., and Lacy., (2016). *Clostridium difficile* toxins TcdA and TcdB cause colonic tissue damage by distinct mechanisms. *Infect. Immun.* 84, 2871–2877. doi: 10.1128/IAI.00583-16

Corbett, A. J., Eckle, S. B. G., Birkinshaw, R. W., Liu, L., Patel, O., Mahony, J., et al. (2014). T-cell activation by transitory neo-antigens derived from distinct microbial pathways. *Nature* 509, 361–365. doi: 10.1038/nature13160

Cosgrove, C., Ussher, J. E., Rauch, A., Gärtner, K., Kurioka, A., Hühn, M. H., et al. (2013). Early and nonreversible decrease of CD161++/MAIT cells in HIV infection. *Blood* 121, 951–961. doi: 10.1182/blood-2012-06-436436

Cowardin, C. A., Buonomo, E. L., Saleh, M. M., Wilson, M. G., Burgess, S. L., Kuehne, S. A., et al. (2016a). The binary toxin CDT enhances *Clostridium difficile* virulence by suppressing protective colonic eosinophilia. *Nat. Microbiol.* 1:16108. doi: 10.1038/nmicrobiol.2016.108

Cowardin, C. A., Jackman, B. M., Noor, Z., Burgess, S. L., Feig, A. L., and Petri, W. A. (2016b). Glucosylation drives the innate inflammatory response to *Clostridium difficile* toxin A. *Infect. Immun.* 84, 2317–2323. doi: 10.1128/IAI.00327-16

Dusseaux, M., Martin, E., Serriari, N., Peguillet, I., Premel, V., Louis, D., et al. (2011). Human MAIT cells are xenobiotic resistant, tissue-targeted, CD161hi IL-17 secreting T cells. *Blood* 117, 1250–1260. doi: 10.1182/blood-2010-08-303339

Eckle, S. B., Birkinshaw, R. W., Kostenko, L., Corbett, A. J., McWilliam, H. E., Reantragoon, R., et al. (2014). A molecular basis underpinning the T cell receptor heterogeneity of mucosal-associated invariant T cells. *J. Exp. Med.* 211, 1585–1600. doi: 10.1084/jem.20140484

Emgård, J., Bergsten, H., McCormick, J. K., Barrantes, I., Skrede, S., Sandberg, J. K., et al. (2019). MAIT cells are major contributors to the cytokine response in group A streptococcal toxic shock syndrome. *Proc. Natl. Acad. Sci.* 116, 25923–25931. doi: 10.1073/pnas.1910883116

Feltis, B. A., Wiesner, S. M., Kim, A. S., Erlandsen, S. L., Lyerly, D. L., Wilkins, T. D., et al. (2000). *Clostridium difficile* toxins A and B can Alter epithelial permeability and promote bacterial paracellular migration through HT-29 enterocytes. *Shock* 14, 629–634. doi: 10.1097/00024382-200014060-00010

Gülke, I., Pfeifer, G., Liese, J., Fritz, M., Hofmann, F., Aktories, K., et al. (2001). Characterization of the enzymatic component of the ADP-Ribosyltransferase toxin CDTa from *Clostridium difficile*. *Infect. Immun.* 69, 6004–6011. doi: 10.1128/IAI.69.10.6004-6011.2001

Hagel, J. P., Garner, L. C., Bilton, M., Mehta, H., Leng, T., Hackstein, C. P., et al. (2020). Human MAIT cell activation in vitro. *Methods Mol. Biol.* 2098, 97–124. doi: 10.1007/978-1-0716-0207-2_7

He, M., Miyajima, F., Roberts, P., Ellison, L., Pickard, D. J., Martin, M. J., et al. (2013). Emergence and global spread of epidemic healthcare-associated *Clostridium difficile*. *Nat. Genet.* 45, 109–113. doi: 10.1038/ng.2478

Huang, S., Martin, E., Kim, S., Lawrence, Y., Soudais, C., Fremont, D. H., et al. (2009). MR1 antigen presentation to mucosal-associated invariant T cells was highly conserved in evolution. *Proc. Natl. Acad. Sci. U. S. A.* 106:8290. doi: 10.1073/pnas.0903196106

Just, I., Selzer, J., Wilm, M., von Eichel-Streiber, C., Mann, M., and Aktories, K. (1995a). Glucosylation of rho proteins by *Clostridium difficile* toxin B. *Nature* 375, 500–503. doi: 10.1038/375500a0

Just, I., Wilm, M., Selzer, J., Rex, G., von Eichel-Streiber, C., Mann, M., et al. (1995b). The enterotoxin from *Clostridium difficile* (ToxA) Monoglucosylates the rho proteins. *J. Biol. Chem.* 270, 13932–13936. doi: 10.1074/jbc.270.23.13932

Kasendra, M., Barrile, R., Leuzzi, R., and Soriani, M. (2014). *Clostridium difficile* toxins facilitate bacterial colonization by modulating the fence and gate function of colonic epithelium. *J. Infect. Dis.* 209, 1095–1104. doi: 10.1093/infdis/jit617

Keller, A. N., Eckle, S. B. G., Weijun, X., Liu, L., Hughes, V. A., Mak, J. Y. W., et al. (2017). Drugs and drug-like molecules can modulate the function of mucosal-associated invariant T cells. *Nat. Immunol.* 18, 402–411. doi: 10.1038/ni.3679

Kjer-Nielsen, L., Patel, O., Corbett, A. J., Le Nours, J., Meehan, B., Liu, L., et al. (2012). MR1 presents microbial vitamin B metabolites to MAIT cells. *Nature* 491, 717–723. doi: 10.1038/nature11605

Kuijper, E. J., Barbut, F., Brazier, J. S., Kleinkauf, N., Eckmanns, T., Lambert, M. L., et al. (2008). Update of *Clostridium difficile* infection due to PCR Ribotype 027 in Europe, 2008. *Eur. Secur.* 13:18942. doi: 10.2807/ese.13.31.18942-en

Kurioka, A., Ussher, J. E., Cosgrove, C., Clough, C., Fergusson, J. R., Smith, K., et al. (2015). MAIT cells are licensed through granzyme exchange to kill bacterially sensitized targets. *Mucosal Immunol.* 8, 429–440. doi: 10.1038/mi.2014.81

Landenberger, M., Nieland, J., Roeder, M., Nørgaard, K., Papatheodorou, P., Ernst, K., et al. (2021). The cytotoxic effect of *Clostridium difficile* pore-forming toxin CDTb. *Biochim. Biophys. Acta Biomembr.* 1863:183603. doi: 10.1016/j.bbamem.2021.183603

Le Bourhis, L., Martin, E., Péguillet, I., Guihot, A., Froux, N., Coré, M., et al. (2010). Antimicrobial activity of mucosal-associated invariant T cells. *Nat. Immunol.* 11, 701–708. doi: 10.1038/ni.1890

Lee, J. Y., Kim, H., Cha, M. Y., Park, H. G., Kim, Y.-J., Kim, I. Y., et al. (2009). *Clostridium difficile* toxin A promotes dendritic cell maturation and chemokine CXCL2 expression through P38, IKK, and the NF-KB Signaling pathway. *J. Mol. Med.* 87, 169–180. doi: 10.1007/s00109-008-0415-2

Lepore, M., Kalinichenko, A., Calogero, S., Kumar, P., Paleja, B., Schmaler, M., et al. (2017). Functionally diverse human T cells recognize non-microbial antigens presented by MR1. *elife* 6:e24476. doi: 10.7554/eLife.24476

Mahida, Y. R., Makh, S., Hyde, S., Gray, T., and Borriello, S. P. (1996). Effect of *Clostridium difficile* toxin A on human intestinal epithelial cells: induction of interleukin 8 production and apoptosis after cell detachment. *Gut* 38, 337–347. doi: 10.1136/gut.38.3.337

Martin, E., Treiner, E., Duban, L., Guerri, L., Laude, H., Toly, C., et al. (2009). Stepwise development of mait cells in mouse and human. *PLoS Biol.* 7:e54. doi: 10.1371/journal.pbio.1000054

Masuda, S., Oda, Y., Sasaki, H., Ikenouchi, J., Higashi, T., Akashi, M., et al. (2011). LSR defines cell corners for tricellular tight junction formation in epithelial cells. *J. Cell Sci.* 124, 548–555. doi: 10.1242/jcs.072058

Neumann-Schaal, M., Hofmann, J. D., Will, S. E., and Schomburg, D. (2015). Time-resolved amino acid uptake of *Clostridium difficile* 630Δerm and concomitant fermentation product and toxin formation. *BMC Microbiol.* 15:281. doi: 10.1186/s12866-015-0614-2

Pothoulakis, C. (1996). Pathogenesis of *Clostridium difficile*-associated diarrhoea. *Eur. J. Gastroenterol. Hepatol.* 8, 1041–1047. doi: 10.1097/00042737-199611000-00003

Pothoulakis, C., Sullivan, R., Melnick, D. A., Triadafilopoulos, G., Gadenne, A. S., Meshulam, T., et al. (1988). *Clostridium difficile* toxin A stimulates intracellular calcium release and chemotactic response in human granulocytes. *J. Clin. Invest.* 81, 1741–1745. doi: 10.1172/JCI113514

Riedel, T., Wetzel, D., Hofmann, J. D., Plorin, S. P. E. O., Dannheim, H., Berges, M., et al. (2017). High metabolic versatility of different toxigenic and non-toxigenic *Clostridium difficile* isolates. *Int. J. Med. Microbiol.* 307, 311–320. doi: 10.1016/j.ijmm.2017.05.007

Rocha, M. F., Maia, M. E., Bezerra, L. R., Lyerly, D. M., Guerrant, R. L., Ribeiro, R. A., et al. (1997). *Clostridium difficile* toxin A induces the release of neutrophil chemotactic factors from rat peritoneal macrophages: role of interleukin-1beta, tumor necrosis factor alpha, and Leukotrienes. *Infect. Immun.* 65, 2740–2746. doi: 10.1128/iai.65.7.2740-2746.1997

Ryder, A. B., Huang, Y., Li, H., Zheng, M., Wang, X., Stratton, C. W., et al. (2010). Assessment of *Clostridium difficile* infections by quantitative detection of TcdB toxin by use of a real-time cell analysis system. *J. Clin. Microbiol.* 48, 4129–4134. doi: 10.1128/JCM.01104-10

Saavedra, P. H. V., Huang, L., Ghazavi, F., Kourula, S., Vanden Berghe, T., Takahashi, N., et al. (2018). Apoptosis of intestinal epithelial cells restricts *Clostridium difficile* infection in a model of pseudomembranous colitis. *Nat. Commun.* 9:4846. doi: 10.1038/s41467-018-07386-5

Schwan, C., Kruppke, A. S., Nölke, T., Schumacher, L., Koch-Nolte, F., Kudryashev, M., et al. (2014). *Clostridium difficile* toxin CDT hijacks microtubule organization and reroutes vesicle traffic to increase pathogen adherence. *Proc. Natl. Acad. Sci. U. S. A.* 111, 2313–2318. doi: 10.1073/pnas.1311589111

Schwan, C., Stecher, B., Tzivelekidis, T., van Ham, M., Rohde, M., Hardt, W.-D., et al. (2009). *Clostridium difficile* toxin CDT induces formation of microtubule-based protrusions and increases adherence of bacteria. *PLoS Pathog.* 5:e1000626. doi: 10.1371/journal.ppat.1000626

Shaler, C. R., Choi, J., Rudak, P. T., Memarnejadian, A., Szabo, P. A., Tun-Abraham, M. E., et al. (2017). MAIT cells launch a rapid, robust and distinct hyperinflammatory response to bacterial superantigens and quickly acquire an anergic phenotype that impedes their cognate antimicrobial function: defining a novel mechanism of superantigen-induced immunopatho. *PLoS Biol.* 15:e2001930. doi: 10.1371/journal.pbio.2001930

Simpson, M., Frisbee, A., Kumar, P., Schwan, C., Aktories, K., and Petri, W. A. (2020). *Clostridium difficile* binary toxin (CDT) is recognized by the TLR2/6 heterodimer to induce an NF-KB response. *BioRxiv*. doi: 10.1101/2020.09.08.288209

Souza, M. H., Melo-Filho, A. A., Rocha, M. F., Lyerly, D. M., Cunha, F. Q., Lima, A. A., et al. (1997). The involvement of macrophage-derived tumour necrosis factor and lipoxygenase products on the neutrophil recruitment induced by *Clostridium difficile* toxin B. *Immunology* 91, 281–288. doi: 10.1046/j.1365-2567.1997.00243.x

Steele, J., Chen, K., Sun, X., Zhang, Y., Wang, H., Tzipori, S., et al. (2012). Systemic dissemination of *Clostridium difficile* toxins A and B is associated with severe, fatal disease in animal models. *J. Infect. Dis.* 205, 384–391. doi: 10.1093/infdis/jir748

Stieglitz, F., Gerhard, R., and Pich, A. (2021). The binary toxin of *Clostridium difficile* alters the proteome and phosphoproteome of HEp-2 cells. *Front. Microbiol.* 12:725612. doi: 10.3389/fmicb.2021.725612

Tilloy, F., Treiner, E., Park, S. H., Garcia, C., Lemonnier, F., de la Salle, H., et al. (1999). An invariant T cell receptor alpha chain defines a novel TAP-independent major histocompatibility complex class Ib-restricted alpha/Beta T cell subpopulation in mammals. *J. Exp. Med.* 189, 1907–1921. doi: 10.1084/jem.189.12.1907

Treiner, E., Duban, L., Bahram, S., Radosavljevic, M., Wanner, V., Tilloy, F., et al. (2003). Selection of evolutionarily conserved mucosal-associated invariant T cells by MR1. *Nature* 422, 164–169. doi: 10.1038/nature01433

Ussher, J. E., Bilton, M., Attwod, E., Shadwell, J., Richardson, R., de Lara, C., et al. (2014). CD161 ++ CD8 + T cells, including the MAIT cell subset, are specifically activated by IL-12+IL-18 in a TCR-independent manner. *Eur. J. Immunol.* 44, 195–203. doi: 10.1002/eji.201343509

Ussher, J. E., van Wilgenburg, B., Hannaway, R. F., Ruustal, K., Phalora, P., Kurioka, A., et al. (2016). TLR Signaling in human antigen-presenting cells regulates MR1-dependent activation of MAIT cells. *Eur. J. Immunol.* 46, 1600–1614. doi: 10.1002/eji.201545969

Wu, D., Joyee, A. G., Nandagopal, S., Lopez, M., Ma, X., Berry, J., et al. (2013). Effects of *Clostridium difficile* toxin A and B on human T lymphocyte migration. *Toxins* 5, 926–938. doi: 10.3390/toxins5050926

Yu, H., Chen, K., Jianguo, W., Yang, Z., Shi, L., Barlow, L. L., et al. (2015). Identification of Toxemia in patients with *Clostridium difficile* infection. *PLoS One* 10:e0124235. doi: 10.1371/journal.pone.0124235

Yu, H., Chen, K., Sun, Y., Carter, M., Garey, K. W., Savidge, T. C., et al. (2017). Cytokines are markers of the *Clostridium difficile*-induced inflammatory response and predict disease severity. *Clin. Vaccine Immunol.* 24, e00037–e00017. doi: 10.1128/CVI.00037-17

Zhang, M., Ming, S., Gong, S., Liang, S., Luo, Y., Liang, Z., et al. (2019). Activation-induced cell death of mucosal-associated invariant T cells is amplified by OX40 in type 2 diabetic patients. *J. Immunol.* 203, 2614–2620. doi: 10.4049/jimmunol.1900367

Conflict of Interest: The authors declare that the research was conducted in the absence of any commercial or financial relationships that could be construed as a potential conflict of interest.

Publisher's Note: All claims expressed in this article are solely those of the authors and do not necessarily represent those of their affiliated organizations, or those of the publisher, the editors and the reviewers. Any product that may be evaluated in this article, or claim that may be made by its manufacturer, is not guaranteed or endorsed by the publisher.

Copyright © 2021 Marquardt, Jakob, Scheibel, Hofmann, Klawonn, Neumann-Schaal, Gerhard, Bruder and Jänsch. This is an open-access article distributed under the terms of the Creative Commons Attribution License (CC BY). The use, distribution or reproduction in other forums is permitted, provided the original author(s) and the copyright owner(s) are credited and that the original publication in this journal is cited, in accordance with accepted academic practice. No use, distribution or reproduction is permitted which does not comply with these terms.

frontiers in Microbiology

REVIEW
published: 21 December 2021
doi: 10.3389/fmicb.2021.804949

Host Immune Responses to *Clostridioides difficile*: Toxins and Beyond

Britt Nibbering[1,2], Dale N. Gerding[3], Ed J. Kuijper[1,2], Romy D. Zwittink[1,2] and Wiep Klaas Smits[1,2]*

[1] Center for Microbiome Analyses and Therapeutics, Leiden University Medical Center, Leiden, Netherlands, [2] Department of Medical Microbiology, Leiden University Medical Center, Leiden, Netherlands, [3] Department of Veterans Affairs, Research Service, Edward Hines Jr. VA Hospital, Hines, IL, United States

Clostridioides difficile is often resistant to the actions of antibiotics to treat other bacterial infections and the resulting *C. difficile* infection (CDI) is among the leading causes of nosocomial infectious diarrhea worldwide. The primary virulence mechanism contributing to CDI is the production of toxins. Treatment failures and recurrence of CDI have urged the medical community to search for novel treatment options. Strains that do not produce toxins, so called non-toxigenic *C. difficile*, have been known to colonize the colon and protect the host against CDI. In this review, a comprehensive description and comparison of the immune responses to toxigenic *C. difficile* and non-toxigenic adherence, and colonization factors, here called non-toxin proteins, is provided. This revealed a number of similarities between the host immune responses to toxigenic *C. difficile* and non-toxin proteins, such as the influx of granulocytes and the type of T-cell response. Differences may reflect genuine variation between the responses to toxigenic or non-toxigenic *C. difficile* or gaps in the current knowledge with respect to the immune response toward non-toxigenic *C. difficile*. Toxin-based and non-toxin-based immunization studies have been evaluated to further explore the role of B cells and reveal that plasma cells are important in protection against CDI. Since the success of toxin-based interventions in humans to date is limited, it is vital that future research will focus on the immune responses to non-toxin proteins and in particular non-toxigenic strains.

Keywords: NTCD, immune response, *Clostridioides difficile*, toxins, non-toxigenic *C. difficile*, non-toxin proteins

OPEN ACCESS

Edited by:
Meina Neumann-Schaal, German Collection of Microorganisms and Cell Cultures GmbH (DSMZ), Germany

Reviewed by:
Joshua Ethan Denny, University of Pennsylvania, United States
Katie Solomon, University of Exeter, United Kingdom

****Correspondence:***
Britt Nibbering
b.nibbering@lumc.nl

Specialty section:
This article was submitted to Infectious Agents and Disease, a section of the journal Frontiers in Microbiology

Received: *29 October 2021*
Accepted: *22 November 2021*
Published: *21 December 2021*

Citation:
Nibbering B, Gerding DN, Kuijper EJ, Zwittink RD and Smits WK (2021) Host Immune Responses to Clostridioides difficile: Toxins and Beyond. Front. Microbiol. 12:804949. doi: 10.3389/fmicb.2021.804949

INTRODUCTION

Toxigenic *Clostridioides difficile* (*C. difficile*) is a multiply antibiotic resistant, anaerobic bacterium that is among the leading causes of nosocomial infectious diarrhea worldwide. An estimated 130,000 *C. difficile* infections (CDI) result in an estimated 12,400 deaths in Europe annually, imposing a significant burden on the healthcare system and economy and numbers for the United States are even higher (Lessa et al., 2012; Wiegand et al., 2012; Centers for Disease Control and Prevention [CDC], 2019). Moreover, 15–35% of CDI patients suffer from one or more recurrent infections (Singh et al., 2019).

Symptoms associated with CDI range from mild, self-limiting diarrhea to severe colitis, toxic megacolon, and bowel perforation. *C. difficile* transmission occurs via the fecal-oral route. Spores, highly resistant cells that are believed to be dormant, are ingested from the environment and survive the acidic conditions of the stomach. These cells travel down the gastrointestinal tract (GIT) and eventually germinate into vegetative cells in the duodenum (Smits et al., 2016). The germination process is influenced by many factors, such as relative and absolute levels of bile acids, the microbiota, and the host immune response (Smits et al., 2016; Zhu et al., 2018). Subsequently, vegetative cells reach the colon where toxin production is initiated and CDI can develop. Under the influence of environmental stimuli, such as nutrient deprivation, quorum sensing, and other stress signals, the vegetative cells sporulate (Higgins and Dworkin, 2012). With the expulsion of these spores in the feces, the cycle can begin anew (Smits et al., 2016).

The primary virulence mechanism of *C. difficile* is the production of one or a combination of toxin A (TcdA), toxin B (TcdB), and binary toxin (CDT) (Aktories et al., 2017). These toxins bind to their respective receptors on intestinal epithelial cells, thereby activating cellular pathways. This activation results in the breakdown of tight junctions, reduced epithelial integrity, and increased adherence of vegetative bacterial cells to the host epithelium (Papatheodorou et al., 2018). The toxin-induced damage to the intestinal barrier provokes an immune response characterized by secretion of proinflammatory cytokines and chemokines leading to the recruitment and activation of neutrophils, mast cells, monocytes, and innate lymphoid cells. This arsenal of cytokines and immune cells contributes to clinical CDI symptoms. For example, mast cell degranulation stimulates histamine release resulting in increased permeability of the intestinal barrier. Consequently, a substantial loss of fluid into the lumen causes severe diarrhea, cramps, dehydration, and toxic megacolon (Meyer et al., 2007; Leffler and Lamont, 2015; Smits et al., 2016).

Clostridioides difficile infection is challenging to manage. Presently, CDI is treated with antibiotics, such as vancomycin, fidaxomicin, and, occasionally, metronidazole (Johnson et al., 2021; van Prehn et al., 2021). However, some patients experience treatment failure, i.e., they either do not respond to treatment at all, or initially improve but experience a relapse later (Vardakas et al., 2012). To effectively address these challenges non-antibiotic treatments are essential. These treatments are limited but include bezlotoxumab infusion, fecal microbiome transplantation (FMT) and colonization with non-toxigenic *C. difficile* (NTCD) (Oksi et al., 2020). Bezlotoxumab is a monoclonal antibody against TcdB that prevents it from binding to host cells and causing damage (Navalkele and Chopra, 2018) and reduces the risk of recurrence with 10% (Wilcox et al., 2017). In an FMT, microbiome of a CDI patient is replaced with the live gut microbiome from a healthy donor and is thus considered a live biotherapeutic product. FMT is a very effective treatment for recurrent CDI (rCDI) with success rates up to 90% but it is poorly defined product (Li et al., 2016; Quraishi et al., 2017). An alternative, defined live biotherapeutic option is colonization of the GIT with an NTCD, a *C. difficile* strain that does not produce any toxins.

Non-toxigenic *C. difficile* colonization and its potential protective effects have been examined primarily in animal models. Among the prevailing hypotheses explaining the protection are nutrient and/or niche competition (Gamage et al., 2006; Merrigan et al., 2013), and the host immune response. Wilson and Sheagren (1983) were the first to show that hamsters pre-treated with cefoxitin and colonized by an NTCD were protected against a challenge with a toxigenic *C. difficile* (TCD) strain. They found that hamster survival increased from 21 to 93% (Wilson and Sheagren, 1983). Borriello and Barclay (1985) confirmed these findings yet failed to find this protective effect with heat-killed NTCD or other species of Clostridia, namely *C. perfringens, C. bifermentans,* and *C. beijerincki, failed,* and *C. sporogenes*. Furthermore, the protection was lost when the colonizing NTCD was removed using vancomycin before the challenge (Borriello and Barclay, 1985). Since then, a variety of animal models have shown that non-toxigenic strains can colonize the GIT and protect against TCD – mediated disease (Borriello and Barclay, 1985; Sambol et al., 2003; Nagaro et al., 2013; de Oliveira Júnior et al., 2016; Oliveira Júnior et al., 2019; Leslie et al., 2021). The first human clinical trial was performed in 1980s where two patients suffering from rCDI were treated with NTCD-M1 strain after vancomycin administration with a 50% clinical success rate (Seal et al., 1987). A number of phase I and II trials has been performed to determine safety, efficacy, and colonization rate using the NTCD-M3 strain (Villano et al., 2012; Gerding et al., 2015, 2018). These trials demonstrated that administration of NTCD-M3 spores was safe, i.e., no serious adverse events (SAEs) occurred, and effective in preventing subsequent CDI in patients experiencing their first CDI or first recurrent CDI episode (Villano et al., 2012; Gerding et al., 2015). Unfortunately, neither the effects on the immune system nor their role in (protection against) CDI pathogenesis have been investigated systematically in these patients.

To understand NTCD colonization as a treatment it is important to understand the immune response to these strains. Studies show that non-toxin proteins, such as flagella (Jarchum et al., 2011) and surface layer proteins (SLPs) (Ryan et al., 2011), are able to challenge the immune system. Many of these studies, however, are confounded because non-toxin factors are isolated from toxigenic strains. Nevertheless, interest in NTCDs and non-toxin proteins has slowly been increasing over the past decade. For example, non-toxin proteins have been used in studies into *C. difficile* vaccination (Ní Eidhin et al., 2008; Bruxelle et al., 2017).

Here, we review the available literature describing the host (immune) responses to toxigenic and non-toxigenic *C. difficile* and highlight the role that studying NTCD has in our understanding of the mechanism of action of NTCD-based interventions as well as *Clostridioides difficile* produces pathogenesis. We hope that the overview presented in this review will provide a framework that will aid in the analysis of immunological data from controlled animal or human infection studies in the future.

HOST IMMUNE RESPONSES TO TOXIGENIC *CLOSTRIDIOIDES DIFFICILE*

Clostridioides difficile Toxin Production

Clostridioides difficile produces various toxins that play a role in CDI, including toxin A (TcdA), toxin B (TcdB). Toxin A and Toxin B are encoded by *tcdA* and *tcdB*, respectively, which are both located within the 19.6 kb Pathogenicity loci (PaLoc) that is integrated in the chromosome of the vast majority of *C. difficile* strains (Braun et al., 1996; Monot et al., 2015). Many factors influence toxin production and a great number of regulators have been identified so far, but these have been reviewed elsewhere (Martin-Verstraete et al., 2016). Once toxin production has been initiated, toxins accumulate in the cell and are released during late stages of growth (Karlsson et al., 2003; Rupnik et al., 2009; Di Bella et al., 2016). Some strains, such as epidemic ribotype (RT) 027 and RT078, also produce a third toxin called binary toxin [or *C. difficile* transferase (CDT)]. The binary toxin is transcribed from the 6.2 kb CdtLoc and consists of an enzymatic component (CDTa) and a binding component (CDTb) (Perelle et al., 1997; Carter et al., 2007; Aktories et al., 2017). CDT^+ strains are commonly found in CDI patients and clinical studies have shown associations with increased mortality rates (Bacci et al., 2011; Stewart et al., 2013; Li et al., 2018). Rare instances have been reported where toxin genes are located on (pro-) phages (Riedel et al., 2020) and plasmids (Ramírez-Vargas and Rodríguez, 2020).

Innate Immune Responses Triggered by *Clostridioides difficile* Producing Toxin A and Toxin B

Innate immunity can be divided into three parts: physical barrier, chemical barrier, and cellular responses (summarized in **Figure 1A** and **Table 1**). The first is represented by the intestinal epithelium, including the mucosal layer. The chemical barrier is made up of antimicrobial peptides, including defensins, excreted by highly specialized epithelial cells, Paneth cells, and some commensal bacteria. Some members of the gut microbiome are known to inhibit *C. difficile* growth and germination by releasing antimicrobial peptides (AMPs) (Rea et al., 2011; Liu et al., 2014; McDonald et al., 2018). Beyond the release of AMPs, the gut microbiome can also influence *C. difficile* in other ways. Certain bacteria can deconjugate primary bile acids into secondary bile acids thereby hindering *C. difficile* germination and colonization (Staley et al., 2017). Additionally, the intestinal microbiome has been shown to affect the production of cytokines, such as IL-25 (Buonomo et al., 2016) and IL-22 (Nagao-Kitamoto et al., 2020), which can ultimately alter CDI outcomes.

TcdA and TcdB bind to their respective receptors on human colonocytes which initiates a chain reaction that leads to a loss of epithelial barrier integrity through the disruption of the skeletal structure and tight junctions, and cell death (Farrow et al., 2013; Di Bella et al., 2016; Chandrasekaran and Lacy, 2017; Orrell and Melnyk, 2021). This results in translocation of intestinal bacteria and stress in colonic epithelial cells. In response to these events, resident immune cells and intestinal epithelial cells, through activation of nuclear factor-κB (NF-κB) and activator protein 1 (AP-1) pathways, secrete pro-inflammatory cytokines and chemokines, such as interleukin 1 (IL-1), IL-8, and CXCL1. This contributes to the expression of AMPs and recruitment of circulating immune cells to the site of infection (Warny et al., 2000; Hasegawa et al., 2011; McDermott et al., 2016). Further, reactive nitrogen species (RNS) and reactive oxygen species (ROS) produced by epithelial cells limit further translocation of commensal bacteria (Abt et al., 2016). Of note, *C. difficile* appears to be less sensitive to RNS and ROS than certain other anaerobes (Ho and Ellermeier, 2011; McBride and Sonenshein, 2011; Li et al., 2021). RNS are believed to play a role in the attenuation of toxin potency (Savidge et al., 2011). Recent studies suggest that *C. difficile* metabolism, and therefore pathogenicity, is disrupted by ROS (Engevik et al., 2020). TcdB dependent glycosylation causes inactivation of RHO GTPases in colonocytes which is detected by the pyrin receptor. Consequently, this intracellular receptor binds to apoptosis-associated speck like-protein containing CARD (ASC) leading to the formation of an inflammasome, a multiprotein complex that induces one of more caspases which mediate a pro-inflammatory response for example the secretion of IL-1β (Xu et al., 2014). As an aside, it was shown that the stimulation of bone marrow derived dendritic cells (BMDCs) with TcdA and TcdB alone, in the absence of vegetative cells, induced inflammasome formation but the priming signal, such as bacterial pathogen associated molecular patterns, is required (Cowardin et al., 2015). Data from a mouse model of CDI showed that plasminogen (PLG) is recruited to the damaged epithelium where, upon binding, it remodels the surface of *C. difficile* spores and mediates gemination. This also results in increased levels of cytokines, including IL-1α, IL-10, IL-12, G-CSF, and GM-CSF (Awad et al., 2020). Using a mouse model of CDI, *in vitro* primary human colonic epithelial cells, and CDI patient material it was found that a IL-27/LL-37 axis affects CDI outcomes (Xu et al., 2021). IL-27, produced by antigen presenting cells after stimulation with toll like receptor (TLR) ligands or infectious agents (Cao et al., 2014), can stimulate human cathelicidin antimicrobial peptide (LL-37) production in human colonic epithelial cells (both *in vitro* and *in vivo*, CDI patient blood and feces IL-27 levels positively correlate with LL-37 levels). Experiments where primary human colonic epithelial cells pre-treated with different selective signaling molecule inhibitors suggest that this upregulation of LL-37 is primarily due to activation of JAK and PI3K pathways and, in part, by the P38MAPK signaling pathway. Both treatment of mice with anti-IL-27 antibodies and IL-27 receptor knock out mice (WSX–/– mice) resulted in significantly reduced levels of CRAMP (the mouse/rat variant of LL-37) in fecal and colonic tissue and reduced clearance of *C. difficile* and increased disease severity (Xu et al., 2021). Injection of CRAMP into an ileal loop of WSX–/– mice decreased their CDI associated morbidity and mortality and a significantly lower density of *C. difficile* in the caecum. Further, the categorisation of the clinical data based on disease severity showed that patients with severe CDI had lower systemic and fecal levels of IL-27 than patients suffering from non-severe CDI (Xu et al., 2021). Of note, it was shown that daily intracolonic administration of CRAMP in mice for 3 days reduces toxin A-mediated intestinal

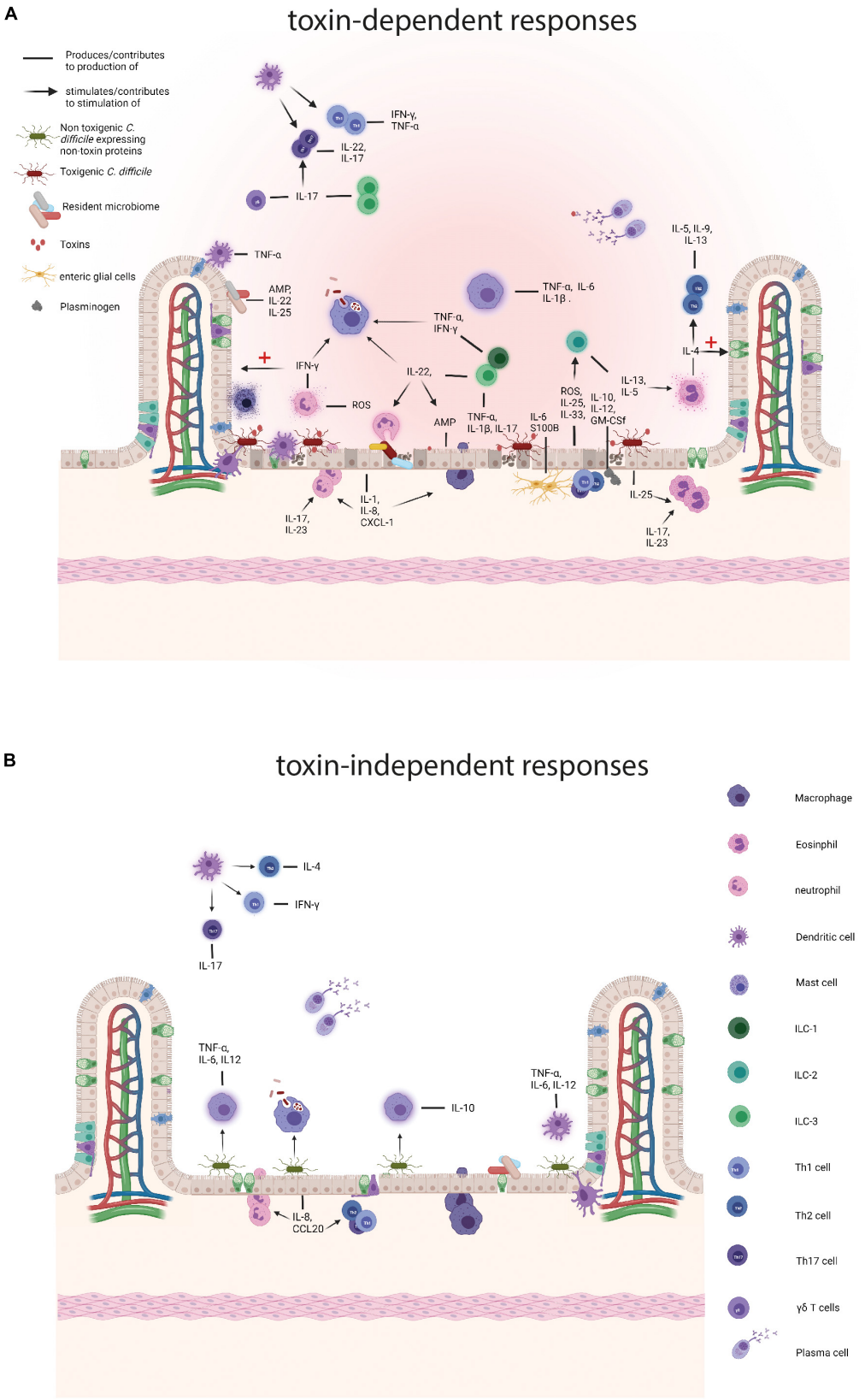

FIGURE 1 | (Continued)

FIGURE 1 | Comparison of the immune responses to toxigenic *Clostridioides difficile* (*C. difficile*) and non-toxin proteins. **(A)** Responses to toxigenic *C. difficile* and its toxins. Toxins damage colonocytes which results in the loss of epithelial barrier integrity and the production of antimicrobial peptides (AMPs), such as LL-37, interleukins (ILs), IL-25 and IL-33, and reactive oxygen species (ROS) and nitrogen oxygen species (NOS). Subepithelial enteric glial cells add to a pro-inflammatory environment by the production of S100B and IL-6 and the toxin affected epithelial cells attract plasminogen which in turn contributes to the production IL-10, IL-12, and other cytokines. The resident microbiome also contributes by producing AMPs and pro-inflammatory cytokines and as the barrier function of the colon is decreased translocation of the intestinal microbiome contributes to further enhances inflammation. Subsequently, resident colonic epithelial cells produce chemokines to attract immune cells to the site of infection, such as IL-8 and CXCL-1. Neutrophils arrive at the site of infection and provide support by tackling the vegetative cells and secreting pro-inflammatory cytokines, including interferon γ (IFN-γ) and aid in the production of other pro-inflammatory molecules, such as ROS. IFN-γ performs several actions, namely stimulation of phagocytosis by macrophages and the repair mechanisms of colonocytes. Eosinophils are drawn to the site of infection by IL-25 and produce pro-inflammatory cytokines, including IL-4, that both results in a Th2 response and a dampening of the immune response and tissue repair. During *C. difficile* infection (CDI), macrophages phagocytose vegetative cells and potentially spores and secrete pro-inflammatory cytokines, such as IL-1β and IL-6. Innate lymphoid cells are attracted by IL-33, IL-23 and IL-1β and ILC3s produce pro-inflammatory cytokines, including IL-17a, IFN- γ, and tumor necrosis factor (TNF) and in that way stimulate a Th17 response. ILCs also produce IL-22 that stimulates phagocytosis by macrophages, the killing of commensals by neutrophils, and AMP production by epithelial cells. ILC2 cells secrete IL-13 and IL-5 of which the latter attracts eosinophils. Dendritic cells (DCs) produce TNF-α in response to damaged epithelium and phagocytose these cells. Finally, plasma cells produce antibodies targeting toxins and vegetative cells. **(B)** Responses to non-toxin proteins and non-toxigenic *C. difficile*. SLPs can induce the production of IL-10 and directly stimulate phagocytosis by macrophages and SLPA has also been shown to trigger a pro-inflammatory immune response through IL-6, TNF-α, and IL-12p40 production by activated macrophages. Furthermore, SLPs activate DCs which in turn skew the adaptive immune response towards Th1 and Th17. FliC is recognized by toll like receptor 5 on colonocytes which produce IL-8 and CCL20 which attracts neutrophils, DCs, and lymphocytes. Finally, plasma cells produce antibodies against a variety of non-toxin proteins. Created with BioRender.com.

inflammation [reduced histological colonic damage and reduced tumor necrosis factor α (TNF-α) levels, among others] (Hing et al., 2013). Beneath the intestinal epithelial layer lie enteric glial cells (EGCs) that release a number of mediators, such as interleukins, NO, and S100 calcium-binding protein (S100B) and seem to be involved in the immune responses to *C. difficile* (Cirillo et al., 2011; Macchioni et al., 2017; Costa et al., 2021). In colonic biopsies from both CDI patients and CDI mice increased S100B was observed compared to control subjects and uninfected mice respectively (Costa et al., 2021). Mouse experiments with a S100B inhibitor, pentamidine, revealed that, upon inhibition of this protein, disease severity and epithelial damage are decreased while *C. difficile* shedding remained unaffected. S100B was found to regulate cytokine synthesis. Mice treated with pentamidine also showed lower colonic concentrations of pro-inflammatory cytokines, including IL-6, IL-8, IL-1β, IL-23, and GM-CS, but not IL-33 and IL-22 levels were even found to be higher compared to untreated mice (Costa et al., 2021). More specifically, the addition of TcdA and TcdB to a rat EGC cell line (EGC PK060399) showed that stimulation with *C. difficile* toxins increased both S100B release and IL-6 expression by these cells (Costa et al., 2021).

Taken together, epithelial damage caused by toxigenic *C. difficile* and/or its toxins, initiates the recruitment of circulating immune cells to the site of infection and secretion of AMPs in an attempt to clear *C. difficile* from the colon.

Next, the cellular immune response to *C. difficile* producing toxin A and toxin B will be divided according to immune cell type: neutrophils, eosinophils, macrophages, innate lymphoid cells (ILCs) and dendritic cells (DCs).

Neutrophils are crucial players in the immune response against CDI and are among the first cells to arrive at the site of infection. This is supported by a study showing antibody mediated depletion of $GR1^+$ (Ly6G) cells in a murine model of CDI leads to increased mortality (Jarchum et al., 2012). Additionally, *C. difficile* infected nucleotide binding oligomerization domain-containing protein 1 (NOD1) and ASC knock out mice, which are impaired in the formation of inflammasome, showed a decreased CXCL1 expression and neutrophil recruitment that correlated with increased morbidity and mortality (Hasegawa et al., 2011, 2012). In agreement, neutropenia is a risk factor for primary and secondary CDI in hospitalized leukemia and allogeneic hematopoietic stem cell transplant patients (Huang et al., 2014; Luo et al., 2015). Once at the site of infection, neutrophils also produce ROS and enhance phagocytosis and bacterial killing by macrophages through interactions with interferon γ (IFN-γ). Innate lymphoid cells (ILCs) also produce IFN-γ and production of this cytokine by these cells may be driven by microbiota associated acetate (Fachi et al., 2020). Contrarily, IL-22 was found to stimulate the ability of neutrophils to kill commensal bacteria through the induction of C3 deposition on pathobionts after CDI had been induced (Hasegawa et al., 2014). Additionally, antibody-mediated inhibition of neutrophil recruitment in rats (Castagliuolo et al., 1998) and rabbits (Kelly et al., 1994) was associated with a reduction in TcdA mediated enterotoxicity (Kelly et al., 1994; Castagliuolo et al., 1998; Jose and Madan, 2016). Using a severe CDI mouse model, it was demonstrated that antibody-mediated depletion of $Ly6G^+$ granulocytes, i.e., neutrophils, before initiation of infection did not affect CDI susceptibility (Chen Y. S. et al., 2020). Altogether, neutrophils seem to be a double-edged sword: these cells aid in the reduction of pathogen burden but also contribute to tissue damage.

Little is known about the role eosinophils play in the toxin-mediated innate immune responses, but some evidence suggests a protective role during CDI. A prediction model for CDI-associated mortality demonstrated that patients with peripheral eosinopenia showed higher in-hospital mortality (odds ratio: 2.26) (Kulaylat et al., 2018). Intestinal IL-25 levels are reduced in murine and human CDI, yet once IL-25 levels were restored in a mouse model the eosinophil counts went up. This was found to result in enhanced epithelial integrity and protection of the mice from CDI (Buonomo et al., 2016). A recent study demonstrated that administering IL-25 to specific pathogen free (SPF) mice led to an expansion

of IL-4 producing eosinophils which was associated with a reduction in disease severity (lower clinical score at day 3) in the recovery phase, but not mortality, compared to the control (Donlan et al., 2020). This could be explained by the known role IL-4 plays in the dampening of an inflammatory responses and tissue repair (Gieseck et al., 2018; Donlan et al., 2020).

Macrophages are also believed to shape the innate immune response to *C. difficile*. Recently, it was found that macrophage inflammatory protein-1α (MIP-1α) is associated with the defense against TcdA producing *C. difficile* in both humans and mice. By stimulating human and mouse colonic explants with TcdA and TcdB, it was shown only toxin A induced MIP-1α and decreased the expression of SLC26A3, a chloride anion exchanger. Blocking MIP-1α resulted in a recovery in SLC26A3 function in this model and prevented recurrent CDI (Wang et al., 2020). Despite that intracellular presence of *C. difficile* never has been proven in human macrophages, it is believed that phagocytosis of vegetative cells or spores by macrophages contributes to *C. difficile* clearance (Liu et al., 2018). Using mouse-derived macrophages in an *in vitro* infection setting, it was demonstrated that phagocytosis of toxigenic *C. difficile* leads to the production of pro-inflammatory cytokines, such as IL-1β, through MyD88 and toll like receptor 2 (TLR2) dependent pathways, which results inflammasome formation (Liu et al., 2018). Some studies suggest intestinal epithelial cell apoptosis as a host defense mechanism against toxigenic *C. difficile* instead of inflammasomes (Saavedra et al., 2018).

TABLE 1 | An overview of immune cells involved in the immune response to (non-)toxigenic *C. difficile* and its toxins and non-toxin proteins.

Immune cell type	Response to toxigenic *C. difficile*	References	Non-toxin proteins	References
Resident microbiome	Production of AMPs, acetate and pro-inflammatory cytokines: IL-25 and IL-22	Buonomo et al., 2016; Nagao-Kitamoto et al., 2020	–	–
Epithelial cells	Production of AMPs and pro-inflammatory cytokines and chemokines: IL-25, IL-33, IL-1 IL-8, G-CSF, GM-CSF and CXCL1. Also ROS and RNS production	Warny et al., 2000; Hasegawa et al., 2011; Xu et al., 2014; McDermott et al., 2016	Production of chemokines and pro-inflammatory cytokines: IL-23, IL-1β, CCL20, and IL-8.	Ryan et al., 2011; Batah et al., 2016; Lynch et al., 2017
Neutrophils	Bacterial killing, stimulation of phagocytosis by macrophages and production of pro-inflammatory cytokines: IFN-γ. Clearance of TcdA mediated epithelial damage.	Kelly et al., 1994; Castagliuolo et al., 1998; Hasegawa et al., 2014; Jose and Madan, 2016	–	–
Eosinophils	Production of IL-4. Enhanced epithelial integrity and stimulation of Th2 response and associated cytokine production	Cowardin et al., 2016; Donlan et al., 2020	–	–
Macrophages	Bacterial killing through phagocytosis, production of pro-inflammatory cytokines: IL-1β and IL-6	Liu et al., 2018; Saavedra et al., 2018; Wang et al., 2020	Stimulation of phagocytosis and cytokine production: IL-6, IL-12p40, and TNF-α	Lynch et al., 2017
Dendritic cells	Upregulation of *Il-23a* gene expression and production of TNF-α. Phagocytosis of damaged epithelial cells.	Cowardin et al., 2015; Huang et al., 2015	Stimulate Th1, Th2, and Th17 response	Ryan et al., 2011; Lynch et al., 2017
Innate lymphoid cells	Production of pro-inflammatory cytokines: IL-22, IL-17a, IFN-γ, TNF-α, IL-13, and IL-5. Stimulate production ROS and RNS	Buonomo et al., 2013; Geiger et al., 2014; Abt et al., 2015; Sonnenberg and Artis, 2015; Nakagawa et al., 2016; Saleh et al., 2019	–	–
Th1 cells	Production of pro-inflammatory cytokines: IFN-γ, TNF-α	Jafari et al., 2013, 2014; Yu et al., 2017; Hamo et al., 2019	Production of pro-inflammatory cytokines: IFN-γ	Ryan et al., 2011; Lynch et al., 2017
Th2 cells	Production of pro-inflammatory cytokines: IL-4, IL-5, and IL-13	Yu et al., 2017; Hamo et al., 2019	Production of pro-inflammatory cytokines: IL-4	Ryan et al., 2011
Th17 cells	Production of pro-inflammatory cytokines: IL-17 and IL-22	Buonomo et al., 2013; Jafari et al., 2013, 2014; Nakagawa et al., 2016; Yu et al., 2017; Hamo et al., 2019; Saleh et al., 2019	Production of pro-inflammatory cytokines: IL-17	Ryan et al., 2011; Lynch et al., 2017
Tfh cells	Bridge between T cell and B cell response	Rampuria et al., 2017; Amadou Amani et al., 2020	–	–
γδ T cells	Upregulation of IL-17	Chen Y. S. et al., 2020	–	–
B cells	Protective, neutralizing anti- toxin A and - toxin B IgG, IgA, and IgM antibodies	Johnson et al., 1992; Bacon and Fekety, 1994; Kyne et al., 2001; Leav et al., 2010; Gupta et al., 2016	Protective anti-SLP and anti-Flic antibodies.	Bruxelle et al., 2016, 2018; Karyal et al., 2021

However, in murine derived macrophages (RAW 264.7 cells), uptake of *C. difficile* spores was demonstrated and the spores remained dormant and retained their ability to germinate. This suggests that these spores will persist in an intestinal environment after phagocytosis (Paredes-Sabja et al., 2012). Thus, to date it seems that macrophages contribute to bacterial clearance and a proinflammatory response while forming a potential reservoir for spores as well. To unravel the complex role of macrophages in the toxin-driven immune responses and resolve some of these apparently contradictory findings further studies are required.

Innate lymphoid cells respond to the initial IL-1β, IL-12, IL-23 by producing IL-22, IL-17a, IFN-γ, and TNF-α (Abt et al., 2015; Sonnenberg and Artis, 2015). These cytokines further the attraction of neutrophils and macrophages to the site of infection, stimulate the production of RNS and ROS, and induce the expression of AMPs and repair mechanisms of colonocytes (Abt et al., 2015; Sonnenberg and Artis, 2015). It has been demonstrated that IL-17 (amongst others produced by ILC3s) contributes to pathogenesis (Nakagawa et al., 2016). IL-17A and IL-17F double knock out mice were found to be more resistant to a challenge with BI/NAP1/027 strains compared to wild type (WT) mice. Further, within 3 days post infection reduced production of IL1β, CXCL2, and IL-6 and reduced neutrophil accumulation were observed although the burden of *C. difficile* had not changed (Nakagawa et al., 2016). More recently, it was shown that blocking of IL-17RA protects against acute CDI in dextran sulfate sodium (DSS)–treated mice. Adoptive transfer of Th17 cells resulted in increased CDI severity (Saleh et al., 2019). Another study showed that IL-23 rather than IL-17A or IL-22 stimulates neutrophil recruitment and pro-inflammatory cytokines expression in the colon during CDI. Similarly, increased levels of staining for IL-23p19 in lamina propria cell infiltrates were observed in CDI patients compared to healthy controls in colon biopsy samples and *IL-23p19*$^{-/-}$ mice challenged with VPI10463 showed higher survival and improved clinical health compared to WT mice (Buonomo et al., 2013).

Mice that lack ILCs in addition to T cells and B cells (Rag1$^{-/-}$Il-2rg$^{-/-}$) show high CDI-associated mortality rates and during CDI Rag1–/– mice showed upregulated expression of ILC-1 and ILC-3 associated proteins (Abt et al., 2015). ILC-deficient mice fail to upregulate IL-22 and IFN-γ which expectedly results in induction of aberrant production of AMPs by colonocytes and decreased phagocytic mechanisms (Zheng et al., 2008; Hasegawa et al., 2014; McDermott et al., 2016). Further, *Nfil3*$^{-/-}$ mice, which are deficient for NK-cells and intestinal ILC3 cells showed similar mortality to WT mice. These mice also shed more *C. difficile* in their feces (Geiger et al., 2014). Another mechanism protecting against CDI involves IL-33 sensitive ILC2 cells (Frisbee et al., 2019). In a CDI mouse model, increased IL-33 expression led to reduced neutrophil counts and elevated eosinophil counts in the colon. This changed the Th17 to Th2-associated mucosal response and increased mouse survival mediated by ILC2 inflow that followed (Frisbee et al., 2019). IL-33 expression is also relevant in the response to *C. difficile* in humans based on analyzing IL-33 in human serum and anti-IL-33 staining of biopsies from CDI+ patients (Frisbee et al., 2019). IL-33 was shown to contribute to protection from severe CDI by increasing IL-13 and IL-5-producing ILC2s (Frisbee et al., 2019). ILC2s are considered the main producers of IL-5 (Ikutani et al., 2012) and it has recently been shown that increased IL-5 levels contribute to protection by elevating the number of eosinophils and decreasing neutrophils counts (Donlan et al., 2020). In conclusion, ILCs appear to play an important role in bridging the innate and adaptive immunity in the protection against CDI, although ILC3 can also contribute to pathogenesis of CDI and a pro-inflammatory response through IL-17 production.

Dendritic cells (DCs) form a bridge between the adaptive and innate immunity and disfunction of these cells may lead to a failure to protect the host against invasion by pathogens (Coombes and Powrie, 2008). Monocyte derived DCs, generated from peripheral blood mononuclear cells from healthy human donors, were exposed to purified toxin A and toxin B and filter sterilized culture supernatant from *C. difficile* strain R20291 (Cowardin et al., 2015). Interestingly, the stimulation with filter-sterilized supernatant from the WT R20291 strain, but not a toxin mutant resulted in upregulation of *Il-23a* gene in the DCs. Purified toxins barely induced a response, but clear induction when the R20291 toxin mutant was added in addition to purified toxins (Cowardin et al., 2015). These results may suggest an interplay between toxins and non-toxin proteins in eliciting an immune response. Co-culturing of mouse BMDCs with mouse epithelial (CT26) cells lead to an activation of the DCs. Cell surface markers, such as CD86, CD80, and CD40, were upregulated on the DC surface and they produced TNF-α as well. Furthermore, damaging of CT26 cells by exposure to TcdB even induced likely phagocytosis of the damaged CT26 cells (Huang et al., 2015). To study DC migration, mice were subcutaneously injected with the TcdB affected CT26 which led to DC recruitment to the site of infection within 24 h post injection (Huang et al., 2015). The combined information above suggests that DCs cooperate with host cells to stimulate a pro-inflammatory response, although more research is needed.

Innate Immune Responses to Binary Toxin-Producing *Clostridioides difficile*

Very few studies have been published on the host immune response to CDT, although clinical studies have shown peripheral immune cell counts in TcdA+TcdB+CDT+ strains (Bacci et al., 2011; Stewart et al., 2013; Li et al., 2018). In mice, it was found that binary toxin plays a role in the suppression of the protection against CDI by eosinophils (Cowardin et al., 2016). Using RT027 *C. difficile* strain and CdtA- and CdtB- mutants, this study showed that CDT was able to induce IL-1β production in the inflammasome which suggest that CDT acts as a priming signal for inflammasome formation. In addition, purified CDT was able to significantly activate NF-κB pathway. CDT can be recognized by TLR2 on eosinophils and upon binding the eosinophil seems to be suppressed. Furthermore, it was found that when mice that had received *TLR2*$^{-/-}$ eosinophils were significantly better

protected against CDT+ infection than WT mice (Cowardin et al., 2016). Altogether, little is yet known about CDT and its specific role in the immune response to *C. difficile* although this toxin may enhance the disruption of the host's protective mechanisms stimulated by *C. difficile* toxins.

Adaptive Immune Responses to *Clostridioides difficile* and Its Toxins

The adaptive immunity can be divided into a humoral (antibody-mediated) and a cellular response. It is characterized by its ability to mount a pathogen-specific response and to generate a memory that will preserve protection over time (Marshall et al., 2018). Immunoglobin A (IgA), IgG, and IgM are the main antibodies involved in the protection against *C. difficile*. IgA neutralizes toxins locally around the mucosal intestinal surface and IgG is responsible for general toxin neutralization. IgM is an early appearing, less specific antibody and thus characterizes the early adaptive response to *C. difficile* (Rees and Steiner, 2018). In humans, 15–30% of initial CDI patients will experience one or more relapses. Potential explanations for this include persistent disruption of the microbiome (Chang et al., 2008), persistence of spores and *C. difficile* in the colon (Gerding et al., 2015), and an inability to mount an effective host response (Keller and Kuijper, 2015).

Whereas the innate immune response is clearly relevant for acute disease, the adaptive immunity may play a role in recurrent disease. *Rag1*$^{-/-}$ mice, which lack both T cells and B cells, do not show a different recovery from acute *C. difficile* infection compared to WT mice (Hasegawa et al., 2014; Abt et al., 2015) and these mice show high CDI-associated mortality rates (Abt et al., 2015). Thus, the acute phase of CDI may be resolved by the innate immune response only, whereas rCDI is likely tackled by the adaptive immunity.

In humans, low serum antibody titers against TcdA and TcdB are associated with rCDI (De Roo and Regenbogen, 2020). It was found that TcdA- and TcdB-specific IgM was lower in CDI patients with a single CDI episode (Kyne et al., 2001). A possible explanation could be that in a more successfully matured adaptive response IgM antibodies are replaced by more specialized antibodies, such as IgA and IgG. TcdB specific IgG are more convincingly associated with CDI than antibodies against TcdA (Johnson et al., 1992; Bacon and Fekety, 1994; Leav et al., 2010). In a phase III trial where patients were treated with Actoxumab (monoclonal antibody against TcdA) and bezlotoxumab anti-TcdB monoclonal antibodies correlated better than anti-TcdA with protection against disease. In line with this, naturally occurring anti-TcdB antibodies were also correlated with protection against rCDI in the placebo arm of the study (Gupta et al., 2016; Wilcox et al., 2017). These studies could be confounded though by additional factors, such as differences in the toxin-gene content of the patient strains. Interestingly, single nucleotide polymorphisms (SNPs) in the human genome, SNP rs2516513, and the HLA alleles HLA-DRB1*07:01 and HLA-DQA1*02:01 were found to reduce bezlotoxumab treatment efficacy (Shen et al., 2020). These discoveries emphasize the need for GWAS analyses in phase 3 studies and reaffirm the importance of host factors in the immune responses in infectious CDI.

At the germinal center, Follicular helper T cells (Tfh) are the bridge between B cell and T cell responses. Tfh aid in differentiation of activated B cells into memory or plasma cells (Rampuria et al., 2017). In a mouse model, an immunization with TcdB from *C. difficile* followed by infection with the same strain led to expansion of both germinal center and non-germinal center lymph node resident T cell population in the infection model versus uninfected mice, and led to the production of toxin-specific antibodies (Amadou Amani et al., 2020). However, no good B cell response was observed, and mice were not protected from disease (Amadou Amani et al., 2020).

Clostridioides difficile can stimulate T helper 1 (Th1) and Th17 responses depending on PCR ribotype (Jafari et al., 2013, 2014). Using infected BMDC-splenocyte co-culturing, it was found that epidemic strains such as RT027 tended to increase Th1 responses (CD4+ IFN-γ producing cells) whereas non-epidemic strains, such as RT017, provoke Th17 responses (IL-17 producing cells) (Jafari et al., 2013, 2014). However, these studies used paraformaldehyde fixed bacteria which may have affected T cell epitopes. Several human studies in this area have yielded conflicting results with respect to T helper responses in CDI. One study demonstrated a higher Th1/Th2 and Th1/Th17 ratio in moderate disease compared to mild disease, whereas another established a shift from Th1 to Th17 and even Th2 in patients with severe disease (Yu et al., 2017; Hamo et al., 2019). Possibly, the timing of blood sampling is responsible for this difference.

Another type of T cell in CDI was found to be involved in the immune response to toxigenic *C. difficile*, namely the mucosal associated-invariant T (MAIT) cells (Bernal et al., 2018). These are an innate-like subset of T cells that have antibacterial properties and represent up to 10% of total T cells in the intestinal lamina propria (Treiner et al., 2003). It was found that MAIT cells are activated by *C. difficile* in an major histocompatibility complex class I-related protein (MR1)-dependent manner and in response produce IFN-γ, perforins, and granzyme B. In murine models IFN-γ is associated with protection against CDI as it presumably strengthens the immunological barrier of the gut (Abt et al., 2015; Bernal et al., 2018).

Moreover, a rapid protective role for γδ T cells was demonstrated through the increased levels of IL-17A/F in C57BL/6 mouse cecum, colon and mesenteric lymph nodes 2 days post infection with *C. difficile* spores. Using complementary loss of functions approaches, it was shown that these cells are, likely, in part responsible for neonatal resistance to CDI (Chen Y. S. et al., 2020).

As the intestinal tract is in constant contact with the outside world and many commensals dwell there, regulation of the intestinal immune response is important to maintain homeostasis. Especially in the colon, T regulatory cells (Tregs) make up an important part of the gut lamina propria (Hall et al., 2008). Interestingly, at the moment there are few studies looking at Treg involvement in the immune response mounted against *C. difficile*. SPF mouse models suggest a role in CDI for Gram-positive bacteria because vancomycin treatment was shown to

cause a reduction in the number of colonic Tregs compared to the control group. Further, the colonization of the GIT of germfree (GF) mice by a mix of commensal *Clostridium* spp. stimulated an accumulation of CTLA-4 expressing Tregs that expressed the same levels of IL-10, indicating that these Tregs are functional (Atarashi et al., 2011). It remains unclear how this comes into effect. One study, where peripheral blood was sampled from rCDI patients, showed that the percentage of CD3+ and CD4+ Tregs (FoxP3+) were slightly higher (not statistically significant) compared to healthy controls (Yacyshyn et al., 2014). These results may suggest a systemic role for Tregs in rCDI. In conclusion, at the moment there are no studies directly studying the role of Tregs play in the adaptive immune response mounted against toxigenic *C. difficile*, but their involvement cannot be ruled out.

Collectively, though it is clear that T cells play a role in CDI, more research is needed to uncover their impact on CDI progression and resolution.

Toxin-Based Immunization Strategies

To clarify the role of plasma cells in the immune response to toxigenic *C. difficile*, immunization studies will be summarized below. The following approaches will be discussed: active immunization strategies based on receptor-binding domain (RBD) and toxoid vaccines, and passive immunization strategies using anti-TcdA and anti-TcdB antibodies. Vaccination with a plasmid expressing the RBD of TcdA and TcdB has been well-studied in cells and animal models (Zhang et al., 2016; Wang et al., 2018; Luo et al., 2019). Both model systems supported the expression of the proteins and animal models (mouse and hamster) demonstrated a B cell response as a result of immunization. Using a Vero based toxin neutralisation assay (TNA), it was also shown that IgG antibodies resulting from RBD vaccination could neutralize TcdA and TcdB (Zhang et al., 2016). Other groups have studied similar RBD vaccines with similar results *in vitro* and in animal models (Gardiner et al., 2009; Baliban et al., 2014; Zhang et al., 2016; Luo et al., 2019). For example, one study confirmed that a plasmid expressing RBD from both TcdA and TcdB induced high levels of IgG1, IgG2a, and IgG2b antibodies against the antigen (Luo et al., 2019). It is remarkable that IgA was not mentioned as IgG1 antibodies generally represent a broad pro-inflammatory response while IgG4 stimulates an anti-inflammatory response and IgA is more specific for mucosal immunity, and is known to be able to enter the intestinal lumen (Castro-Dopico and Clatworthy, 2019). However, a gnotobiotic pig model was used to demonstrate the infiltration of IgG antibodies throughout the gut even through an intact barrier. Protective IgG antibodies may be transported into the gut lumen, through the neonatal Fc receptor (FcRn)-dependent and independent mechanism. Subcutaneous (s.c.) immunization of mice with the c-terminal domain (CTD) of TcdB led to the detection of anti-CTD IgG1 antibodies in feces and fecal titers correlated strongly with the serum antibody titer in the absence of epithelial damage (Amadou Amani et al., 2020). In a recent study the transport of antibodies to the gut lumen was further elucidated (Amadou Amani et al., 2021). Mice in this study were immunized with anti-CTD/PBS gel followed by intraperitoneal (i.p.) boost with anti-CTD/PBS in mice ("immunized mice" vs. untreated or "naïve" mice). Using complete FcRn knock out mice, $FcRn^{-/-}$, and partial knock out of FcRn mice, $FcRn^{+/-}$ it was found that total IgG1, IgG2b, IgG2c titers were significantly lower in $FcRn^{-/-}$ mice compared to those in the $FcRn^{+/-}$ mice. FcRn receptor-mediated transport of anti-CTD IgG1 and IgG2 was required for antibody delivery into the gut lumen. This effect was specific, as lack of FcRn expression did not affect the resident microbiota or the susceptibility to CDI in naive mice (Amadou Amani et al., 2021). Additionally, administration of immune sera from "immunized mice" through i.p. injection to FcRn-deficient mice led to reduced clinical symptoms upon challenge in the treated group compared to the group that received naïve sera. However, the lack of FcRn receptors in these mice still allowed for the transport of protective IgG into the intestinal lumen (Amadou Amani et al., 2021). Taken together, antibodies may enter the gut lumen via FcRn-dependent transport (Amadou Amani et al., 2021) and/or via the compromised intestinal barrier due to CDI infection (Spencer et al., 2014). Through both ways these antibodies may contribute to the protection against toxigenic *C. difficile* driven by systemic anti-CTD IgG.

Parental route vaccination with a next-generation Sanofi Pasteur two-component highly purified toxoid vaccine was shown to protect hamsters, that were challenged with toxigenic *C. difficile*, from death and resulted in lower clinical scores. Vaccination yielded systemic anti-toxin IgG and a IMR-90 cell-based TNA showed that this antibody response neutralized the toxins. Concluding that the results indicate that intramuscular immunization with inactivated TcdA and TcdB induce protective anti-TcdA/B IgG responses (Anosova et al., 2013, 2015). Initially, a small human study showed some success of toxoid vaccination in humans suffering from rCDI (Sougioultzis et al., 2005) and a phase II trial employing genetically and chemically inactivated toxin A and B antigen (bivalent toxoid vaccine) demonstrated that these types of vaccination are safe, well-tolerated, and immunogenic in adults aged 65–85 in a 3-dose regimen (Kitchin et al., 2020). These are encouraging results as this age group is the most affected by CDI. However, despite these seemingly successful animal and phase 2 clinical trials, no human vaccine for acute CDI has been approved for treatment of acute CDI and one 3-dose vaccine, that performed well in hamsters (Anosova et al., 2013), attempt has even failed to show a protective result in a large phase 3 clinical trial (de Bruyn et al., 2021).

Whereas the studies above induce production of anti-toxin antibodies by the host, such antibodies can also directly be administered. Another type of immunization is the direct administration of monoclonal antibodies. The best known example of this is bezlotoxumab, a monoclonal anti-TcdB antibody, which has recently been reviewed (Sehgal and Khanna, 2021). It is believed that upon intravenously administration at the end of antimicrobial therapy of CDI, the antibody is transported to the luminal compartment of the intestines through paracellular transport. As the barrier permeability increases (due to toxin-induced damage), more antibody is transported into the lumen and neutralization of toxin B would alleviate epithelial damage (Zhang et al., 2015). Though multiple clinical trials

have shown varying levels of efficacy of bezlotoxumab, results in humans are not as encouraging as in the animal models (Leav et al., 2010; Lowy et al., 2010; Wilcox et al., 2017). Nevertheless, bezlotoxumab treatment results in an absolute reduction in recurrence of 10% (27% vs. 17%) with a relative recurrence rate reduction 38% lower than standard-of-care antimicrobial treatment alone (Sehgal and Khanna, 2021).

In 2014, a humanized antibody composed of two heavy-chains-only VH (VHH) binding domains that can bind both TcdA and TcdB was developed (Yang et al., 2014). A recent study showed that oral administration of *Saccharomyces boulardii* engineered to produce this antibody protected mice from developing both primary and secondary CDI and led to a decrease in TNF-α and IL-1β was observed (Chen K. et al., 2020).

Several of these studies also applied a mix of antibodies to investigate their potential to protect against CDI. A mix of three human monoclonal anti-TcdA and TcdB antibodies protected hamsters against mortality and reduced severity of diarrhea (Anosova et al., 2015). Anti-TcdA and anti-TcdB antibodies from patients protected hamsters against CDI after a challenge with toxigenic strains (Donald et al., 2013; Anosova et al., 2015).

Collectively, these studies indicate a clear role for the adaptive immune response in rCDI during which both T and B cells are essential and underline the importance of a strong humoral toxin-mediated immune response that is associated with a reduction of disease recurrence (Kyne et al., 2001). Nevertheless, toxin or toxoid-based immunization strategies and anti-toxin therapy appear to be less successful in treatment of acute disease in humans.

HOST IMMUNE RESPONSES TO NON-TOXIN PROTEINS OF *CLOSTRIDIOIDES DIFFICILE*

Non-toxin proteins of *C. difficile* include proteins that are expressed on the outer surface of the bacterial cell, or secreted/released from the cells, and can be recognized by the immune system. Examples are cell wall protein 22 (Cwp22), Cwp84, SLPs, adherence factors, GroEL (heat shock protein), and the flagellar proteins FliD and FliC (see **Figure 2**; Drudy et al., 2004; Péchiné et al., 2005, 2018; Jarchum et al., 2011). These proteins are not necessarily unique to NTCDs and thus the immune response triggered by these proteins may be shared between non-toxigenic and toxigenic strains. Toxin-dependent immune responses are likely to mask effects of non-toxin proteins in toxigenic *C. difficile* in experimental investigations. As a result, the response to non-toxin proteins has not been studied elaborately. Below we summarize the limited information that is currently available (see **Figure 1B** and **Table 1**). The section hereafter is divided into the immune responses and immunization strategies and further organized by the type of non-toxin protein.

Innate and Adaptive Immune Responses to Non-toxin Proteins of *Clostridioides difficile*

The flagellum consists of primarily of FliC, a 39-kDa flagellar protein, and FliD, 56-kDa flagellar cap protein and plays a role in motility and adherence of the bacteria to surfaces (Tasteyre et al., 2001). Mutations in the *flic* gene in *C. difficile* have directly or indirectly been associated with increased mortality of *flic* mutant in a gnotobiotic mouse models and the mutant strains are non-motile (Barketi-Klai et al., 2014) and in other flagellated species the flagella also plays a role in adherence and regulation of other genes not directly involved in motility. *C. difficile* flagellae, as well as SLPs (that are discussed later), exhibit immune stimulating properties through binding to TLRs and pattern recognition receptors expressed on the basolateral side of intestinal epithelial cells (Ryan et al., 2011; Batah et al., 2016; Lynch et al., 2017). Purified *C. difficile* FliC specifically acts on TLR5 – through which it induces the NF-κB and P38 activation, and to a lesser degree ERK1/2 and JNK MAPKs activation, to stimulate the production and secretion of IL-8 and CCL20 (Yoshino et al., 2012; Batah et al., 2016). IL-8 attracts neutrophils to the site of infection and CCL20, in turn, engages lymphocytes and dendritic cells. Surprisingly, the role of neutrophils in the defense against non-toxigenic *C. difficile* at the site of infection has not been studied at all (Nelson et al., 2001). *C. difficile* flagellin is post-translationally modified, but there is no study on the effect of these modifications on the immune response. However, a very recent study demonstrated that modifying *Salmonella* flagellae enhances host protective immunity in an inflammasome deficient mouse model, so post translation modifications to the *C. difficile* flagellae can be expected to affect the immune responses (Tourlomousis et al., 2020). Strikingly, analysis of the innate immune cytokines produced in response to FliC clearly shows that these molecules can attract lymphocytes, indicating that adaptive immune response could play a significant role (Yoshino et al., 2012; Batah et al., 2016). Additionally, SLPs were shown to induce IL-10 production by macrophages which suggests the involvement of Tregs, which can be beneficial for survival of *C. difficile* but also the host (Grazia Roncarolo et al., 2006). Based on this limited evidence, the involvement of the adaptive immune response to non-toxin proteins is currently poorly understood.

Clostridioides difficile has a para-crystalline protein layer (S-layer) on top of the lipid bilayer containing a great of cell wall proteins, including SLPs (Fagan et al., 2011; Oatley et al., 2020). SlpA is the main S-layer precursor protein, that upon cleavage results in a high molecular weight (HMW) protein and a low molecular weight (LMW) protein (Merrigan et al., 2013; Kirk et al., 2017; see **Figure 2**). The latter is directly exposed to the environment and is therefore recognized by the immune system (Bradshaw et al., 2018).

Investigation into the innate immune responses to SlpA has demonstrated that the protein interacts with TLR4 (Ryan et al., 2011). *In vitro* experimentation using J774A.1 macrophages and BMDCs showed that activation of the NF-κB pathway and

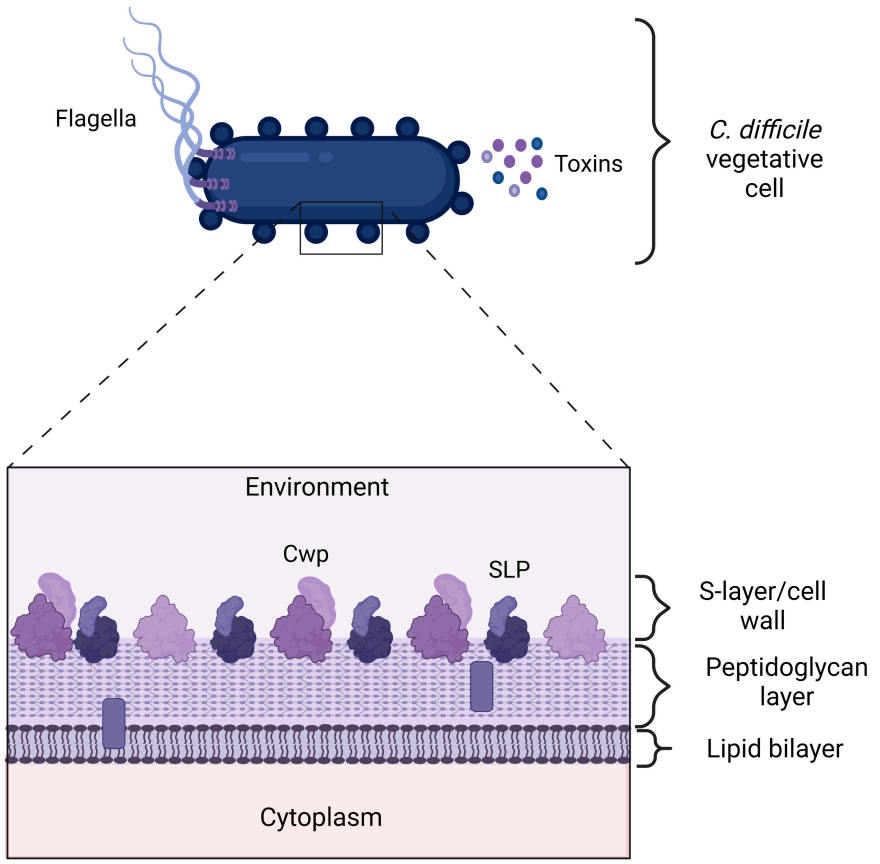

FIGURE 2 | *Clostridioides difficile* cell envelope. A vegetative *C. difficile* cell expresses many proteins on its outer surface that the immune system can recognize. Additionally, *C. difficile* toxins are highly immunogenic. The flagella consists of FliD and FliC proteins. Cell wall proteins (Cwps), such as Cwp22 and Surface layer proteins (SLPs). TcdA, TcdB, and CDT. SLPs and other Cwps consist of a high molecular weight domain (HMW) in dark purple and a low molecular weight (LMW) protein in light purple. The LMW domain is exposed to the environment and can be recognized by the immune system. The bars represent putative lipid-containing polymers (Fagan et al., 2009). Created with BioRender.com.

interferon regulator factor 3 (IRF3) leads to the production of pro-inflammatory cytokines and immune cell activation. TNF-α, IL-12p40, IL-6, and IL-10 are produced, as exemplified by the upregulation of CD40, CD80, and MHCII on DCs and macrophages. Further, the SLPs can stimulate bacterial clearance the by macrophages (Ryan et al., 2011; Collins et al., 2014; Lynch et al., 2017). SLPs have been shown to activate DCs, bridging between innate and adaptive response, which in turn skews the T cell response toward a Th1 and Th17 response (Ausiello et al., 2006). A difference in the immune responses to SLPs isolated from a variety of toxigenic *C. difficile* stains has been demonstrated (Lynch et al., 2017). SLPs isolated from epidemic strains appear to stimulate a higher secretion of IL-12p40, IL-10, and IL-6 by macrophages and a higher expression of CD40 on macrophages. Interestingly, SLPs isolated from non-epidemic strains induced a stronger phagocytosis response by the host's macrophages than SLPs from non-epidemic strains (Lynch et al., 2017). This observation may be explained by the structural variation that was found in SLPs from different strains (Fagan and Fairweather, 2014). Upon co-culturing with CD4+ T cells from mouse spleen with SLP activated DCs, it was found that the DCs stimulate a Th1, Th2, and Th17 driven T cell response, in a TLR4 dependent matter, as these T cells were found to produce IFN-γ, IL-4, and IL-17 respectively (Ryan et al., 2011). A limitation of this study is that CD8+ and γδ – T cells were excluded while, at least in the response to toxigenic *C. difficile*, research suggests some participation of these cells in the immune response (Chen Y. S. et al., 2020).

The above suggests that non-toxin proteins, such as flagellar proteins and SLPs, are highly immune potent and seem to play a role in both the clearance of *C. difficile* by the host cells and the signaling resulting from the induction of pro-inflammatory cytokines and T cell responses. Herein, structural variation of SLPs and bacterial modifications to flagella proteins may determine the severity of the immune response to these proteins. It should be noted that this research has focused so far on non-toxin proteins from toxigenic strains. The immune response to non-toxin proteins of NTCDs may contribute to the explanation of the exclusion mechanism but for lack of experimental evidence remains to be established.

Non-toxin Protein Based Immunization Strategies

Most research into the adaptive immune response to non-toxin proteins of *C. difficile* focuses on the products of B cells, antibodies, in the form of immunization studies. Non-toxin proteins are of interest because they are abundant, often surface exposed and thus easily targeted by antibodies. Additionally, they are likely involved in early stages of the colonization process, suggesting that they could be earliest point of intervention in CDI. This is particularly interesting because it was shown that immunization against toxins does not prevent colonization of the colon by *C. difficile* (Kyne et al., 2000; Ghose and Kelly, 2015).

FliC has been described as a potential vaccine candidate. I.p. immunization with FliC loaded leads to a significant increase in systemic FliC-specific IgG antibodies and protection against a challenge with toxigenic *C. difficile* (Ghose et al., 2016). Oral vaccination with FliC-loaded beads was tried as well but no antibodies were found in orally treated hamsters which suggests that a mucosal response was responsible for the protective effects (Ghose et al., 2016; Bruxelle et al., 2018). It should be noted that some studies suggest systemic IgG to be more important than intestinal IgA in improving clinical outcomes (Kyne et al., 2000, 2001).

The observation that CDI patients have detectable antibodies against SLPs has led to the study of these proteins as vaccine candidates (Bruxelle et al., 2016). A number of immunization studies has been performed in animals to design a vaccine that both protects the host against CDI and prevents *C. difficile* from colonizing the colon (Bruxelle et al., 2016, 2017, 2018; Ghose et al., 2016; Razim et al., 2019).

I.p. vaccination with a mixture of HMW and LMW *C. difficile* SLPs induced an IgG-driven humoral response without enhancing survival after challenge (Ní Eidhin et al., 2008). A recombinant SlpA vaccine has the potential to induce specific antibodies after application via two different routes, mucosal (mice) and intra-rectal (hamsters) (Bruxelle et al., 2016). The mucosal route yielded significantly more SlpA-specific IgG and IgA (local response) and a lower bacterial load in the vaccinated group compared to the control group after challenge. Additionally, a systemic response was established, because SlpA-specific IgG antibodies were significantly higher in blood of vaccinated mice. The hamster model showed that the intra-rectal route yields SlpA-specific IgA and IgG as well as a systemic response (Bruxelle et al., 2016).

Recently, oral vaccination with non-toxin protein, the lipoprotein adhesin CD0873 was reported to yield higher levels of secreted IgA (sIgA) in intestinal fluid and IgG, which were higher than those induced by the TcdB fragment after challenge with a toxigenic strain (Kovacs-Simon et al., 2014; Karyal et al., 2021). An *in vitro* assay using Caco-2 cells suggests a potential working mechanisms where sIgA covers the surface of vegetative cells, thereby blocking toxigenic *C. difficile* attachment to the intestinal cells (Karyal et al., 2021).

Oral vaccination with Cwp84 has been investigated as well. Cwp84-encapsulated beads partially protected the hamsters without an evident systemic response again pointing toward a mucosal response responsible for the observed protection (Sandolo et al., 2011). Hamsters immunized with Cwp84 were not colonized by *C. difficile* and their survival was significantly longer compared to the control group (Péchiné et al., 2011). This study did find serum anti-Cwp84 antibodies yet the titers did not always correlate with animal protection after challenge (Péchiné et al., 2011).

Finally, the heat shock protein GroEL, that plays a role in adherence and colonization (Hennequin et al., 2001), has been investigated for its immunization properties (Péchiné et al., 2013). Intranasal treatment of mice/intrarectal treatment of hamsters with recombinant GroEL protein, and in some groups an adjuvant cholera toxin, followed by a challenge with a toxigenic strain led to decreased intestinal colonization by *C. difficile* compared to control group and the anti-GroEL antibodies were detected in the hamster model (Péchiné et al., 2013).

Other Cwps may also be interesting vaccine candidates. For instance, CDI patients have antibodies against the peptidoglycan crosslinking enzyme Cwp22, and cells lacking Cwp22 are less virulent (Zhu et al., 2019). The cell wall protein Cwp22, a peptidoglycan crosslinking enzyme, was investigated as a vaccine candidate. Mutant strains of *cwp22* show reduced viability autolyse faster than WT, produce less toxins and demonstrate reduced adherence to host cells (Zhu et al., 2019).

Non-toxin proteins can also be employed as adjuvants. FliC can also be added to toxin-targeted vaccines to act as an adjuvant (Ghose et al., 2016; Bruxelle et al., 2018). Similarly, SLPs have been shown to act as an adjuvant (Brun et al., 2008; Bruxelle et al., 2017). A fragment of the 36 KDa SLP (SLP-36) can enhance humoral and cell mediated immune responses characterized by a mixed Th1/Th2 phenotype (Brun et al., 2008).

Taken together, studies of diverse routes of vaccination of animals with various non-toxin proteins has that the humoral immune response to non-toxin proteins can play a role in the protection against or resolution of CDI. Though this suggests that non-toxin proteins are could play a role as a prophylactic, studies in humans are necessary to confirm this potential.

CONCLUDING REMARKS

Clostridioides difficile is among the leading causes of nosocomial diarrhea and the rise of antimicrobial resistance is expected to worsen CDI outcomes in the future. Hence, it is important that the medical community looks into alternative methods for the prevention and/or treatment of CDI. To achieve this, a full picture of *C. difficile* colonization and pathogenesis including the host immune response to toxins (toxigenic strains) and non-toxin proteins (toxigenic and non-toxigenic strains). To date, however, our understanding of the immune response to non-toxin factors is lacking.

The host response to toxigenic *C. difficile* is highly complex but there is a clear division in the types of responses. Initial infection

seems to primarily challenge the innate immune response and re-infection or recurrence seems to involve the adaptive immune response. Despite the importance of toxins for pathogenesis, toxin-targeting interventions have so far failed to demonstrate a clear benefit in the clearance of *C. difficile* and resolution of symptoms, or the prevention of colonization.

The few studies into non-toxin proteins of *C. difficile* that have been performed provide evidence that the immune system clearly responds to bacterial proteins other than toxins as well. NTCDs or non-toxin proteins might offer a more successful route to early interventions. We note, however, that immunological evidence is so far limited to animal studies and mostly based on protein-based strategies, rather than NTCD-based interventions.

Thus, it remains unclear if and how the immune response might play a role in exclusion of TCD by NTCDs. Dedicated immunological studies in clinical trials or controlled human colonisations with NTCD should address this hiatus.

Nevertheless, the toxin- and non-toxin based immune responses share a number of similarities, such as the involvement of granulocytes and DCs (and, consequently, T cell responses). The role of neutrophils in the response to non-toxin proteins is yet to be revealed, but may be similar to that of their counterparts in the response against toxigenic *C. difficile*. Also, the role of the intestinal epithelium, that is so pronounced in the early stages of the immune responses to TCD, in the immune responses to NTCDs should be studied more elaborately as the epithelium is the first immune barrier NTCD will encounter. Anti-toxin and anti-non-toxin proteins antibodies both have been found in humans and antibody-mediated protection against CDI has been demonstrated in animal models. The roles of γδ T cells, ILCs, and epithelial cells has been shown in response to toxigenic *C. difficile* only. This may be due to the fact that their involvement in the response to non-toxin proteins has not been studied yet, or reflect inherent differences in the responses.

It is important to highlight that with the increasingly complex models, from animal to human studies, it is hard to separate the immune responses to *C. difficile* from effects mediated by the intestinal microbiome, as the latter has a great influence on both *C. difficile* colonization and pathogenesis and the intestinal immune responses (Samarkos et al., 2018). The role of the microbiome in the context of FMT has recently been reviewed elaborately (Hernández Del Pino et al., 2021; Littmann et al., 2021). Additionally, other host factors, such as immune suppressive comorbidities and antibiotic treatment, may alter the intestinal immune response even before *C. difficile* challenges the immune system (Negrut et al., 2020). Considering these aspects, as well the delicate balance between pro- and anti-inflammatory roles for the immune response (Hernández Del Pino et al., 2021), it will be a challenge to generate a complete picture of the role of the immune response in *C. difficile* colonization and pathogenesis, but we hope that the present review can provide a framework for the interpretation of immunological data from future interventions.

AUTHOR CONTRIBUTIONS

EK and DG were responsible for critically reviewing the manuscript. BN wrote the first draft of the manuscript and prepared the table and figures. RZ, WS, and BN revised the draft. All authors have made substantial contributions to this work, read and approved the manuscript.

REFERENCES

Abt, M. C., Lewis, B. B., Caballero, S., Xiong, H., Carter, R. A., Sušac, B., et al. (2015). Innate immune defenses mediated by two ILC subsets are critical for protection against acute *Clostridium difficile* infection. *Cell Host Microbe* 18, 27–37. doi: 10.1016/j.chom.2015.06.011

Abt, M. C., McKenney, P. T., and Pamer, E. G. (2016). *Clostridium difficile* colitis: pathogenesis and host defence. *Nat. Rev. Microbiol.* 14, 609–620. doi: 10.1038/nrmicro.2016.108

Aktories, K., Schwan, C., and Jank, T. (2017). *Clostridium difficile* toxin biology. *Annu. Rev. Microbiol.* 71, 281–307. doi: 10.1146/annurev-micro-090816-093458

Amadou Amani, S., Lang, G. A., Ballard, J. D., and Lang, M. L. (2021). The murine neonatal Fc receptor is required for transport of immunization-induced *C. difficile*-specific IgG to the gut and protection against disease but does not affect disease susceptibility. *Infect. Immun.* 89:e0027421. doi: 10.1128/iai.00274-21

Amadou Amani, S., Shadid, T., Ballard, J. D., and Lang, M. L. (2020). *Clostridioides difficile* infection induces an inferior IgG response to that induced by immunization and is associated with a lack of T follicular helper cell and memory B cell expansion. *Infect. Immun.* 88:e00829-19. doi: 10.1128/IAI.00829-19

Anosova, N. G., Brown, A. M., Li, L., Liu, N., Cole, L. E., Zhang, J., et al. (2013). Systemic antibody responses induced by a two-component *Clostridium difficile* toxoid vaccine protect against *C. difficile*-associated disease in hamsters. *J. Med. Microbiol.* 62(Pt 9), 1394–1404. doi: 10.1099/jmm.0.056796-0

Anosova, N. G., Cole, L. E., Li, L., Zhang, J., Brown, A. M., Mundle, S., et al. (2015). A combination of three fully human toxin A- and toxin B-specific monoclonal antibodies protects against challenge with highly virulent epidemic strains of *Clostridium difficile* in the hamster model. *Clin. Vaccine Immunol.* 22, 711–725. doi: 10.1128/CVI.00763-14

Atarashi, K., Tanoue, T., Shima, T., Imaoka, A., Kuwahara, T., Momose, Y., et al. (2011). Induction of colonic regulatory T cells by indigenous *Clostridium* species. *Science* 331, 337–341. doi: 10.1126/science.1198469

Ausiello, C. M., Cerquetti, M., Fedele, G., Spensieri, F., Palazzo, R., Nasso, M., et al. (2006). Surface layer proteins from *Clostridium difficile* induce inflammatory and regulatory cytokines in human monocytes and dendritic cells. *Microbes Infect.* 8, 2640–2646. doi: 10.1016/j.micinf.2006.07.009

Awad, M. M., Hutton, M. L., Quek, A. J., Klare, W. P., Mileto, S. J., Mackin, K., et al. (2020). Human plasminogen exacerbates *Clostridioides difficile* enteric disease and alters the spore surface. *Gastroenterology* 159, 1431–1443.e6. doi: 10.1053/j.gastro.2020.06.032

Bacci, S., Mølbak, K., Kjeldsen, M. K., and Olsen, K. E. P. (2011). Binary toxin and death after *Clostridium difficile* infection. *Emerg. Infect. Dis.* 17, 976–982. doi: 10.3201/eid/1706.101483

Bacon, A. E. III, and Fekety, R. (1994). Immunoglobulin G directed against toxins A and B of *Clostridium difficile* in the general population and patients with antibiotic-associated diarrhea. *Diagn. Microbiol. Infect. Dis.* 18, 205–209. doi: 10.1016/0732-8893(94)90021-3

Baliban, S. M., Michael, A., Shammassian, B., Mudakha, S., Khan, A. S., Cocklin, S., et al. (2014). An optimized, synthetic DNA vaccine encoding the toxin A and toxin B receptor binding domains of *Clostridium difficile* induces protective

antibody responses in vivo. *Infect. Immun.* 82, 4080–4091. doi: 10.1128/IAI.01950-14

Barketi-Klai, A., Monot, M., Hoys, S., Lambert-Bordes, S., Kuehne, S. A., Minton, N., et al. (2014). The flagellin FliC of *Clostridium difficile* is responsible for pleiotropic gene regulation during in vivo infection. *PLoS One* 9:e96876. doi: 10.1371/journal.pone.0096876

Batah, J., Denève-Larrazet, C., Jolivot, P.-A., Kuehne, S., Collignon, A., Marvaud, J.-C., et al. (2016). *Clostridium difficile* flagella predominantly activate TLR5-linked NF-κB pathway in epithelial cells. *Anaerobe* 38, 116–124. doi: 10.1016/j.anaerobe.2016.01.002

Bernal, I., Hofmann, J. D., Bulitta, B., Klawonn, F., Michel, A.-M., Jahn, D., et al. (2018). Clostridioides difficile activates human mucosal-associated invariant T cells. *Front. Microbiol.* 9:2532. doi: 10.3389/fmicb.2018.02532

Borriello, S. P., and Barclay, F. E. (1985). Protection of hamsters against *Clostridium difficile* ileocaecitis by prior colonisation with non-pathogenic strains. *J. Med. Microbiol.* 19, 339–350. doi: 10.1099/00222615-19-3-339

Bradshaw, W. J., Roberts, A. K., Shone, C. C., and Acharya, K. R. (2018). The structure of the S-layer of *Clostridium difficile*. *J. Cell Commun. Signal.* 12, 319–331. doi: 10.1007/s12079-017-0429-z

Braun, V., Hundsberger, T., Leukel, P., Sauerborn, M., and von Eichel-Streiber, C. (1996). Definition of the single integration site of the pathogenicity locus in *Clostridium difficile*. *Gene* 181, 29–38. doi: 10.1016/s0378-1119(96)00398-8

Brun, P., Scarpa, M., Grillo, A., Palù, G., Mengoli, C., Zecconi, A., et al. (2008). *Clostridium difficile* TxAC314 and SLP-36kDa enhance the immune response toward a co-administered antigen. *J. Med. Microbiol.* 57(Pt 6), 725–731. doi: 10.1099/jmm.0.47736-0

Bruxelle, J. F., Mizrahi, A., Hoys, S., Collignon, A., Janoir, C., and Péchiné, S. (2016). Immunogenic properties of the surface layer precursor of *Clostridium difficile* and vaccination assays in animal models. *Anaerobe* 37, 78–84. doi: 10.1016/j.anaerobe.2015.10.010

Bruxelle, J.-F., Mizrahi, A., Hoÿs, S., Collignon, A., Janoir, C., and Péchiné, S. (2017). *Clostridium difficile* flagellin FliC: evaluation as adjuvant and use in a mucosal vaccine against *Clostridium difficile*. *PLoS One* 12:e0187212. doi: 10.1371/journal.pone.0187212

Bruxelle, J. F., Tsapis, N., Hoys, S., Collignon, A., Janoir, C., Fattal, E., et al. (2018). Protection against *Clostridium difficile* infection in a hamster model by oral vaccination using flagellin FliC-loaded pectin beads. *Vaccine* 36, 6017–6021. doi: 10.1016/j.vaccine.2018.08.013

Buonomo, E. L., Cowardin, C. A., Wilson, M. G., Saleh, M. M., Pramoonjago, P., and Petri, W. A. Jr. (2016). Microbiota-regulated IL-25 increases eosinophil number to provide protection during *Clostridium difficile* infection. *Cell Rep.* 16, 432–443. doi: 10.1016/j.celrep.2016.06.007

Buonomo, E. L., Madan, R., Pramoonjago, P., Li, L., Okusa, M. D., and Petri, W. A. Jr. (2013). Role of interleukin 23 signaling in *Clostridium difficile* colitis. *J. Infect. Dis.* 208, 917–920. doi: 10.1093/infdis/jit277

Cao, J., Wang, D., Xu, F., Gong, Y., Wang, H., Song, Z., et al. (2014). Activation of IL-27 signalling promotes development of postinfluenza pneumococcal pneumonia. *EMBO Mol. Med.* 6, 120–140. doi: 10.1002/emmm.201302890

Carter, G. P., Lyras, D., Allen, D. L., Mackin, K. E., Howarth, P. M., O'Connor, J. R., et al. (2007). Binary toxin production in *Clostridium difficile* is regulated by CdtR, a LytTR family response regulator. *J. Bacteriol.* 189, 7290–7301. doi: 10.1128/jb.00731-07

Castagliuolo, I., Keates, A. C., Wang, C. C., Pasha, A., Valenick, L., Kelly, C. P., et al. (1998). Clostridium difficile toxin A stimulates macrophage-inflammatory protein-2 production in rat intestinal epithelial cells. *J. Immunol.* 160, 6039–6045.

Castro-Dopico, T., and Clatworthy, M. R. (2019). IgG and Fcγ receptors in intestinal immunity and inflammation. *Front. Immunol.* 10:805. doi: 10.3389/fimmu.2019.00805

Centers for Disease Control and Prevention [CDC] (2019). *Clostridioides difficile [Online]*. Available online at: https://www.cdc.gov/drugresistance/pdf/threats-report/clostridioides-difficile-508.pdf (accessed July 2020)

Chandrasekaran, R., and Lacy, D. B. (2017). The role of toxins in *Clostridium difficile* infection. *FEMS Microbiol. Rev.* 41, 723–750. doi: 10.1093/femsre/fux048

Chang, J. Y., Antonopoulos, D. A., Kalra, A., Tonelli, A., Khalife, W. T., Schmidt, T. M., et al. (2008). Decreased diversity of the fecal microbiome in recurrent *Clostridium difficile*-associated diarrhea. *J. Infect. Dis.* 197, 435–438. doi: 10.1086/525047

Chen, K., Zhu, Y., Zhang, Y., Hamza, T., Yu, H., Saint Fleur, A., et al. (2020). A probiotic yeast-based immunotherapy against *Clostridioides difficile* infection. *Sci. Transl. Med.* 12:eaax4905. doi: 10.1126/scitranslmed.aax4905

Chen, Y. S., Chen, I. B., Pham, G., Shao, T. Y., Bangar, H., Way, S. S., et al. (2020). IL-17-producing γδ T cells protect against *Clostridium difficile* infection. *J. Clin. Invest.* 130, 2377–2390. doi: 10.1172/jci127242

Cirillo, C., Sarnelli, G., Esposito, G., Turco, F., Steardo, L., and Cuomo, R. (2011). S100B protein in the gut: the evidence for enteroglial-sustained intestinal inflammation. *World J. Gastroenterol.* 17, 1261–1266. doi: 10.3748/wjg.v17.i10.1261

Collins, L., Lynch, M., Marszalowska, I., Kristek, M., Rochfort, K., O'Connell, M., et al. (2014). Surface layer proteins isolated from *Clostridium difficile* induce clearance responses in macrophages. *Microbes Infect.* 16, 391–400. doi: 10.1016/j.micinf.2014.02.001

Coombes, J. L., and Powrie, F. (2008). Dendritic cells in intestinal immune regulation. *Nat. Rev. Immunol.* 8, 435–446. doi: 10.1038/nri2335

Costa, D. V. S., Moura-Neto, V., Bolick, D. T., Guerrant, R. L., Fawad, J. A., Shin, J. H., et al. (2021). S100B inhibition attenuates intestinal damage and diarrhea severity during *Clostridioides difficile* infection by modulating inflammatory response. *Front. Cell. Infect. Microbiol.* 11:739874. doi: 10.3389/fcimb.2021.739874

Cowardin, C. A., Buonomo, E. L., Saleh, M. M., Wilson, M. G., Burgess, S. L., Kuehne, S. A., et al. (2016). The binary toxin CDT enhances *Clostridium difficile* virulence by suppressing protective colonic eosinophilia. *Nat. Microbiol.* 1:16108. doi: 10.1038/nmicrobiol.2016.108

Cowardin, C. A., Kuehne, S. A., Buonomo, E. L., Marie, C. S., Minton, N. P., and Petri, W. A. Jr. (2015). Inflammasome activation contributes to interleukin-23 production in response to *Clostridium difficile*. *mBio* 6:e02386-14. doi: 10.1128/mBio.02386-14

de Bruyn, G., Gordon, D. L., Steiner, T., Tambyah, P., Cosgrove, C., Martens, M., et al. (2021). Safety, immunogenicity, and efficacy of a *Clostridioides difficile* toxoid vaccine candidate: a phase 3 multicentre, observer-blind, randomised, controlled trial. *Lancet Infect. Dis.* 21, 252–262. doi: 10.1016/s1473-3099(20)30331-5

de Oliveira Júnior, C. A., Silva, R. O. S., Diniz, A. N., Pires, P. S., Lobato, F. C. F., and de Assis, R. A. (2016). Prevention of *Clostridium difficile* infection in hamsters using a non-toxigenic strain. *Ciência Rural* 46, 853–859.

De Roo, A. C., and Regenbogen, S. E. (2020). Clostridium difficile Infection: an epidemiology update. *Clin. Colon Rectal Surg.* 33, 49–57. doi: 10.1055/s-0040-1701229

Di Bella, S., Ascenzi, P., Siarakas, S., Petrosillo, N., and di Masi, A. (2016). *Clostridium difficile* toxins A and B: insights into pathogenic properties and extraintestinal effects. *Toxins* 8:134. doi: 10.3390/toxins8050134

Donald, R. G. K., Flint, M., Kalyan, N., Johnson, E., Witko, S. E., Kotash, C., et al. (2013). A novel approach to generate a recombinant toxoid vaccine against *Clostridium difficile*. *Microbiology (Reading)* 159(Pt 7), 1254–1266. doi: 10.1099/mic.0.066712-0

Donlan, A. N., Simpson, M. E., and Petri, W. A. Jr. (2020). Type 2 cytokines IL-4 and IL-5 reduce severe outcomes from *Clostridiodes difficile* infection. *Anaerobe* 66:102275. doi: 10.1016/j.anaerobe.2020.102275

Drudy, D., Calabi, E., Kyne, L., Sougioultzis, S., Kelly, E., Fairweather, N., et al. (2004). Human antibody response to surface layer proteins in *Clostridium difficile* infection. *FEMS Immunol. Med. Microbiol.* 41, 237–242. doi: 10.1016/j.femsim.2004.03.007

Engevik, M. A., Danhof, H. A., Shrestha, R., Chang-Graham, A. L., Hyser, J. M., Haag, A. M., et al. (2020). Reuterin disrupts *Clostridioides difficile* metabolism and pathogenicity through reactive oxygen species generation. *Gut Microbes* 12:1788898. doi: 10.1080/19490976.2020.1795388

Fachi, J. L., Sécca, C., Rodrigues, P. B., de Mato, F. C. P., Di Luccia, B., Felipe, J. d. S., et al. (2020). Acetate coordinates neutrophil and ILC3 responses against *C. difficile* through FFAR2. *J. Exp. Med.* 217:jem.20190489. doi: 10.1084/jem.20190489

Fagan, R. P., Albesa-Jové, D., Qazi, O., Svergun, D. I., Brown, K. A., and Fairweather, N. F. (2009). Structural insights into the molecular organization of the S-layer from *Clostridium difficile*. *Mol. Microbiol.* 71, 1308–1322. doi: 10.1111/j.1365-2958.2009.06603.x

Fagan, R. P., and Fairweather, N. F. (2014). Biogenesis and functions of bacterial S-layers. *Nat. Rev. Microbiol.* 12, 211–222. doi: 10.1038/nrmicro3213

Fagan, R. P., Janoir, C., Collignon, A., Mastrantonio, P., Poxton, I. R., and Fairweather, N. F. (2011). A proposed nomenclature for cell wall proteins of *Clostridium difficile*. *J. Med. Microbiol.* 60(Pt 8), 1225–1228. doi: 10.1099/jmm.0.028472-0

Farrow, M. A., Chumbler, N. M., Lapierre, L. A., Franklin, J. L., Rutherford, S. A., Goldenring, J. R., et al. (2013). *Clostridium difficile* toxin B-induced necrosis is mediated by the host epithelial cell NADPH oxidase complex. *Proc. Natl. Acad. Sci. U.S.A.* 110, 18674–18679. doi: 10.1073/pnas.1313658110

Frisbee, A. L., Saleh, M. M., Young, M. K., Leslie, J. L., Simpson, M. E., Abhyankar, M. M., et al. (2019). IL-33 drives group 2 innate lymphoid cell-mediated protection during *Clostridium difficile* infection. *Nat. Commun.* 10:2712. doi: 10.1038/s41467-019-10733-9

Gamage, S. D., Patton, A. K., Strasser, J. E., Chalk, C. L., and Weiss, A. A. (2006). Commensal bacteria influence *Escherichia coli* O157:H7 persistence and Shiga toxin production in the mouse intestine. *Infect. Immun.* 74, 1977–1983. doi: 10.1128/IAI.74.3.1977-1983.2006

Gardiner, D. F., Rosenberg, T., Zaharatos, J., Franco, D., and Ho, D. D. (2009). A DNA vaccine targeting the receptor-binding domain of *Clostridium difficile* toxin A. *Vaccine* 27, 3598–3604. doi: 10.1016/j.vaccine.2009.03.058

Geiger, T. L., Abt, M. C., Gasteiger, G., Firth, M. A., O'Connor, M. H., Geary, C. D., et al. (2014). Nfil3 is crucial for development of innate lymphoid cells and host protection against intestinal pathogens. *J. Exp. Med.* 211, 1723–1731. doi: 10.1084/jem.20140212

Gerding, D. N., Meyer, T., Lee, C., Cohen, S. H., Murthy, U. K., Poirier, A., et al. (2015). Administration of spores of nontoxigenic *Clostridium difficile* Strain M3 for prevention of recurrent *C difficile* infection: a randomized clinical trial. *JAMA* 313, 1719–1727. doi: 10.1001/jama.2015.3725

Gerding, D. N., Sambol, S. P., and Johnson, S. (2018). Non-toxigenic *Clostridioides* (formerly Clostridium) *difficile* for Prevention of *C. difficile* infection: from bench to bedside back to bench and back to bedside. *Front. Microbiol.* 9:1700. doi: 10.3389/fmicb.2018.01700

Ghose, C., Eugenis, I., Sun, X., Edwards, A. N., McBride, S. M., Pride, D. T., et al. (2016). Immunogenicity and protective efficacy of recombinant *Clostridium difficile* flagellar protein FliC. *Emerg. Microbes Infect.* 5:e8. doi: 10.1038/emi.2016.8

Ghose, C., and Kelly, C. P. (2015). The prospect for vaccines to prevent *Clostridium difficile* infection. *Infect. Dis. Clin. North Am.* 29, 145–162. doi: 10.1016/j.idc.2014.11.013

Gieseck, R. L. III, Wilson, M. S., and Wynn, T. A. (2018). Type 2 immunity in tissue repair and fibrosis. *Nat. Rev. Immunol.* 18, 62–76. doi: 10.1038/nri.2017.90

Grazia Roncarolo, M., Gregori, S., Battaglia, M., Bacchetta, R., Fleischhauer, K., and Levings, M. K. (2006). Interleukin-10-secreting type 1 regulatory T cells in rodents and humans. *Immunol. Rev.* 212, 28–50. doi: 10.1111/j.0105-2896.2006.00420.x

Gupta, S. B., Mehta, V., Dubberke, E. R., Zhao, X., Dorr, M. B., Guris, D., et al. (2016). Antibodies to toxin B are protective against *Clostridium difficile* infection recurrence. *Clin. Infect. Dis.* 63, 730–734. doi: 10.1093/cid/ciw364

Hall, J. A., Bouladoux, N., Sun, C. M., Wohlfert, E. A., Blank, R. B., Zhu, Q., et al. (2008). Commensal DNA limits regulatory T cell conversion and is a natural adjuvant of intestinal immune responses. *Immunity* 29, 637–649. doi: 10.1016/j.immuni.2008.08.009

Hamo, Z., Azrad, M., Nitzan, O., and Peretz, A. (2019). Characterization of the immune response during infection caused by *Clostridioides difficile*. *Microorganisms* 7:435. doi: 10.3390/microorganisms7100435

Hasegawa, M., Kamada, N., Jiao, Y., Liu, M. Z., Núñez, G., and Inohara, N. (2012). Protective role of commensals against *Clostridium difficile* infection via an IL-1β-mediated positive-feedback loop. *J. Immunol.* 189, 3085–3091. doi: 10.4049/jimmunol.1200821

Hasegawa, M., Yada, S., Liu, M. Z., Kamada, N., Muñoz-Planillo, R., Do, N., et al. (2014). Interleukin-22 regulates the complement system to promote resistance against pathobionts after pathogen-induced intestinal damage. *Immunity* 41, 620–632. doi: 10.1016/j.immuni.2014.09.010

Hasegawa, M., Yamazaki, T., Kamada, N., Tawaratsumida, K., Kim, Y. G., Núñez, G., et al. (2011). Nucleotide-binding oligomerization domain 1 mediates recognition of *Clostridium difficile* and induces neutrophil recruitment and protection against the pathogen. *J. Immunol.* 186, 4872–4880. doi: 10.4049/jimmunol.1003761

Hennequin, C., Porcheray, F., Waligora-Dupriet, A.-J., Collignon, A., Barc, M.-C., Bourlioux, P., et al. (2001). GroEL (Hsp60) of *Clostridium difficile* is involved in cell adherence. *Microbiology* 47, 87–96. doi: 10.1099/00221287-147-1-87

Hernández Del Pino, R. E., Barbero, A. M., Español, L. Á, Morro, L. S., and Pasquinelli, V. (2021). The adaptive immune response to *Clostridioides difficile*: a tricky balance between immunoprotection and immunopathogenesis. *J. Leukoc. Biol.* 109, 195–210. doi: 10.1002/JLB.4VMR0720-201R

Higgins, D., and Dworkin, J. (2012). Recent progress in *Bacillus subtilis* sporulation. *FEMS Microbiol. Rev.* 36, 131–148. doi: 10.1111/j.1574-6976.2011.00310.x

Hing, T. C., Ho, S., Shih, D. Q., Ichikawa, R., Cheng, M., Chen, J., et al. (2013). The antimicrobial peptide cathelicidin modulates *Clostridium difficile*-associated colitis and toxin A-mediated enteritis in mice. *Gut* 62, 1295–1305. doi: 10.1136/gutjnl-2012-302180

Ho, T. D., and Ellermeier, C. D. (2011). PrsW is required for colonization, resistance to antimicrobial peptides, and expression of extracytoplasmic function σ factors in *Clostridium difficile*. *Infect. Immun.* 79, 3229–3238. doi: 10.1128/IAI.00019-11

Huang, A., Marini, B., Frame, D., Aronoff, D., and Nagel, J. (2014). Risk factors for recurrent *Clostridium difficile* infection in hematopoietic stem cell transplant recipients. *Transpl. Infect. Dis.* 16, 744–750. doi: 10.1111/tid.12267

Huang, T., Perez Cordon, G., Shi, L., Li, G., Sun, X., Wang, X., et al. (2015). *Clostridium difficile* toxin B intoxicated mouse colonic epithelial CT26 cells stimulate the activation of dendritic cells. *Pathog. Dis.* 73:ftv008. doi: 10.1093/femspd/ftv008

Ikutani, M., Yanagibashi, T., Ogasawara, M., Tsuneyama, K., Yamamoto, S., Hattori, Y., et al. (2012). Identification of innate IL-5-producing cells and their role in lung eosinophil regulation and antitumor immunity. *J. Immunol.* 188, 703–713. doi: 10.4049/jimmunol.1101270

Jafari, N. V., Kuehne, S. A., Bryant, C. E., Elawad, M., Wren, B. W., Minton, N. P., et al. (2013). *Clostridium difficile* modulates host innate immunity via toxin-independent and dependent mechanism(s). *PLoS One* 8:e69846. doi: 10.1371/journal.pone.0069846

Jafari, N. V., Songane, M., Stabler, R. A., Elawad, M., Wren, B. W., Allan, E., et al. (2014). Host immunity to *Clostridium difficile* PCR ribotype 017 strains. *Infect. Immun.* 82, 4989–4996. doi: 10.1128/IAI.02605-14

Jarchum, I., Liu, M., Lipuma, L., and Pamer, E. G. (2011). Toll-like receptor 5 stimulation protects mice from acute *Clostridium difficile* colitis. *Infect. Immun.* 79, 1498–1503. doi: 10.1128/IAI.01196-10

Jarchum, I., Liu, M., Shi, C., Equinda, M., and Pamer, E. G. (2012). Critical role for MyD88-mediated neutrophil recruitment during *Clostridium difficile* colitis. *Infect. Immun.* 80, 2989–2996. doi: 10.1128/IAI.00448-12

Johnson, S., Gerding, D. N., and Janoff, E. N. (1992). Systemic and mucosal antibody responses to toxin A in patients infected with *Clostridium difficile*. *J. Infect. Dis.* 166, 1287–1294. doi: 10.1093/infdis/166.6.1287

Johnson, S., Lavergne, V., Skinner, A. M., Gonzales-Luna, A. J., Garey, K. W., Kelly, C. P., et al. (2021). Clinical practice guideline by the infectious diseases society of America (IDSA) and society for healthcare epidemiology of America (SHEA): 2021 focused update guidelines on management of *Clostridioides difficile* infection in adults. *Clin. Infect. Dis.* 73, e1029–e1044. doi: 10.1093/cid/ciab549

Jose, S., and Madan, R. (2016). Neutrophil-mediated inflammation in the pathogenesis of *Clostridium difficile* infections. *Anaerobe* 41, 85–90. doi: 10.1016/j.anaerobe.2016.04.001

Karlsson, S., Dupuy, B., Mukherjee, K., Norin, E., Burman, L. G., and Akerlund, T. (2003). Expression of *Clostridium difficile* toxins A and B and their sigma factor TcdD is controlled by temperature. *Infect. Immun.* 71, 1784–1793. doi: 10.1128/iai.71.4.1784-1793.2003

Karyal, C., Hughes, J., Kelly, M. L., Luckett, J. C., Kaye, P. V., Cockayne, A., et al. (2021). Colonisation factor CD0873, an attractive oral vaccine candidate against *Clostridioides difficile*. *Microorganisms* 9:306. doi: 10.3390/microorganisms9020306

Keller, J. J., and Kuijper, E. J. (2015). Treatment of recurrent and severe *Clostridium difficile* infection. *Annu. Rev. Med.* 66, 373–386. doi: 10.1146/annurev-med-070813-114317

Kelly, C. P., Becker, S., Linevsky, J. K., Joshi, M. A., O'Keane, J. C., Dickey, B. F., et al. (1994). Neutrophil recruitment in *Clostridium difficile* toxin A enteritis in the rabbit. *J. Clin. Invest.* 93, 1257–1265. doi: 10.1172/JCI117080

Kirk, J. A., Banerji, O., and Fagan, R. P. (2017). Characteristics of the *Clostridium difficile* cell envelope and its importance in therapeutics. *Microb. Biotechnol.* 10, 76–90. doi: 10.1111/1751-7915.12372

Kitchin, N., Remich, S. A., Peterson, J., Peng, Y., Gruber, W. C., Jansen, K. U., et al. (2020). A phase 2 study evaluating the safety, tolerability, and immunogenicity of two 3-dose regimens of a *Clostridium difficile* vaccine in healthy US adults aged 65 to 85 years. *Clin. Infect. Dis.* 70, 1–10. doi: 10.1093/cid/ciz153

Kovacs-Simon, A., Leuzzi, R., Kasendra, M., Minton, N., Titball, R. W., and Michell, S. L. (2014). Lipoprotein CD0873 is a novel adhesin of *Clostridium difficile*. *J. Infect. Dis.* 210, 274–284. doi: 10.1093/infdis/jiu070

Kulaylat, A. S., Buonomo, E. L., Scully, K. W., Hollenbeak, C. S., Cook, H., Petri, W. A. Jr., et al. (2018). Development and validation of a prediction model for mortality and adverse outcomes among patients with peripheral eosinopenia on admission for *Clostridium difficile* infection. *JAMA Surg.* 153, 1127–1133. doi: 10.1001/jamasurg.2018.3174

Kyne, L., Warny, M., Qamar, A., and Kelly, C. P. (2000). Asymptomatic carriage of *Clostridium difficile* and serum levels of IgG antibody against toxin A. *N. Engl. J. Med.* 342, 390–397. doi: 10.1056/nejm200002103420604

Kyne, L., Warny, M., Qamar, A., and Kelly, C. P. (2001). Association between antibody response to toxin A and protection against recurrent *Clostridium difficile* diarrhoea. *Lancet* 357, 189–193. doi: 10.1016/S0140-6736(00)03592-3

Leav, B. A., Blair, B., Leney, M., Knauber, M., Reilly, C., Lowy, I., et al. (2010). Serum anti-toxin B antibody correlates with protection from recurrent *Clostridium difficile* infection (CDI). *Vaccine* 28, 965–969. doi: 10.1016/j.vaccine.2009.10.144

Leffler, D. A., and Lamont, J. T. (2015). *Clostridium difficile* infection. *N. Engl. J. Med.* 372, 1539–1548. doi: 10.1056/NEJMra1403772

Leslie, J. L., Jenior, M. L., Vendrov, K. C., Standke, A. K., Barron, M. R., O'Brien, T. J., et al. (2021). Protection from lethal *Clostridioides difficile* infection via intraspecies competition for cogerminant. *mBio* 12:e00522-21. doi: 10.1128/mBio.00522-21

Lessa, F. C., Gould, C. V., and McDonald, L. C. (2012). Current status of *Clostridium difficile* infection epidemiology. *Clin. Infect. Dis.* 55(Suppl. 2), S65–S70. doi: 10.1093/cid/cis319

Li, C., Harmanus, C., Zhu, D., Meng, X., Wang, S., Duan, J., et al. (2018). Characterization of the virulence of a non-RT027, non-RT078 and binary toxin-positive *Clostridium difficile* strain associated with severe diarrhea. *Emerg. Microbes Infect.* 7, 211–211. doi: 10.1038/s41426-018-0211-1

Li, H., Zhou, X., Huang, Y., Liao, B., Cheng, L., and Ren, B. (2021). Reactive oxygen species in pathogen clearance: the killing mechanisms, the adaption response, and the side effects. *Front. Microbiol.* 11:622534. doi: 10.3389/fmicb.2020.622534

Li, Y. T., Cai, H. F., Wang, Z. H., Xu, J., and Fang, J. Y. (2016). Systematic review with meta-analysis: long-term outcomes of faecal microbiota transplantation for *Clostridium difficile* infection. *Aliment Pharmacol. Ther.* 43, 445–457. doi: 10.1111/apt.13492

Littmann, E. R., Lee, J.-J., Denny, J. E., Alam, Z., Maslanka, J. R., Zarin, I., et al. (2021). Host immunity modulates the efficacy of microbiota transplantation for treatment of *Clostridioides difficile* infection. *Nat. Commun.* 12:755. doi: 10.1038/s41467-020-20793-x

Liu, R., Suárez, J. M., Weisblum, B., Gellman, S. H., and McBride, S. M. (2014). Synthetic polymers active against *Clostridium difficile* vegetative cell growth and spore outgrowth. *J. Am. Chem. Soc.* 136, 14498–14504. doi: 10.1021/ja506798e

Liu, Y.-H., Chang, Y.-C., Chen, L.-K., Su, P.-A., Ko, W.-C., Tsai, Y.-S., et al. (2018). The ATP-P2X7 signaling axis is an essential sentinel for intracellular *Clostridium difficile* pathogen-induced inflammasome activation. *Front. Cell. Infect. Microbiol.* 8:84. doi: 10.3389/fcimb.2018.00084

Lowy, I., Molrine, D. C., Leav, B. A., Blair, B. M., Baxter, R., Gerding, D. N., et al. (2010). Treatment with monoclonal antibodies against *Clostridium difficile* toxins. *N. Engl. J. Med.* 362, 197–205. doi: 10.1056/NEJMoa0907635

Luo, D., Liu, X., Xing, L., Sun, Y., Huang, J., Zhang, L., et al. (2019). Immunogenicity and protection from receptor-binding domains of toxins as potential vaccine candidates for *Clostridium difficile*. *Vaccines* 7:180. doi: 10.3390/vaccines7040180

Luo, R., Greenberg, A., and Stone, C. D. (2015). Outcomes of *Clostridium difficile* infection in hospitalized leukemia patients: a nationwide analysis. *Infect. Control Hosp. Epidemiol.* 36, 794–801. doi: 10.1017/ice.2015.54

Lynch, M., Walsh, T. A., Marszalowska, I., Webb, A. E., Mac Aogain, M., Rogers, T. R., et al. (2017). Surface layer proteins from virulent *Clostridium difficile* ribotypes exhibit signatures of positive selection with consequences for innate immune response. *BMC Evol. Biol.* 17:90. doi: 10.1186/s12862-017-0937-8

Macchioni, L., Davidescu, M., Fettucciari, K., Petricciuolo, M., Gatticchi, L., Gioè, D., et al. (2017). Enteric glial cells counteract *Clostridium difficile* toxin B through a NADPH oxidase/ROS/JNK/caspase-3 axis, without involving mitochondrial pathways. *Sci. Rep.* 7:45569. doi: 10.1038/srep45569

Marshall, J. S., Warrington, R., Watson, W., and Kim, H. L. (2018). An introduction to immunology and immunopathology. *Allergy Asthma Clin. Immunol.* 14:49. doi: 10.1186/s13223-018-0278-1

Martin-Verstraete, I., Peltier, J., and Dupuy, B. (2016). The regulatory networks that control *Clostridium difficile* toxin synthesis. *Toxins (Basel)* 8:153. doi: 10.3390/toxins8050153

McBride, S. M., and Sonenshein, A. L. (2011). The dlt operon confers resistance to cationic antimicrobial peptides in *Clostridium difficile*. *Microbiology (Reading)* 157(Pt 5), 1457–1465. doi: 10.1099/mic.0.045997-0

McDermott, A. J., Falkowski, N. R., McDonald, R. A., Pandit, C. R., Young, V. B., and Huffnagle, G. B. (2016). Interleukin-23 (IL-23), independent of IL-17 and IL-22, drives neutrophil recruitment and innate inflammation during *Clostridium difficile* colitis in mice. *Immunology* 147, 114–124. doi: 10.1111/imm.12545

McDonald, J. A. K., Mullish, B. H., Pechlivanis, A., Liu, Z., Brignardello, J., Kao, D., et al. (2018). Inhibiting growth of *Clostridioides difficile* by restoring valerate, produced by the intestinal microbiota. *Gastroenterology* 155, 1495–1507.e15. doi: 10.1053/j.gastro.2018.07.014

Merrigan, M. M., Venugopal, A., Roxas, J. L., Anwar, F., Mallozzi, M. J., Roxas, B. A. P., et al. (2013). Surface-layer protein A (SlpA) is a major contributor to host-cell adherence of *Clostridium difficile*. *PLoS One* 8:e78404. doi: 10.1371/journal.pone.0078404

Meyer, G. K. A., Neetz, A., Brandes, G., Tsikas, D., Butterfield, J. H., Just, I., et al. (2007). *Clostridium difficile* toxins A and B directly stimulate human mast cells. *Infect. Immun.* 75, 3868–3876. doi: 10.1128/IAI.00195-07

Monot, M., Eckert, C., Lemire, A., Hamiot, A., Dubois, T., Tessier, C., et al. (2015). *Clostridium difficile*: new insights into the evolution of the pathogenicity locus. *Sci. Rep.* 5:15023. doi: 10.1038/srep15023

Nagao-Kitamoto, H., Leslie, J. L., Kitamoto, S., Jin, C., Thomsson, K. A., Gillilland, M. G. III, et al. (2020). Interleukin-22-mediated host glycosylation prevents *Clostridioides difficile* infection by modulating the metabolic activity of the gut microbiota. *Nat. Med.* 26, 608–617. doi: 10.1038/s41591-020-0764-0

Nagaro, K. J., Phillips, S. T., Cheknis, A. K., Sambol, S. P., Zukowski, W. E., Johnson, S., et al. (2013). Nontoxigenic *Clostridium difficile* protects hamsters against challenge with historic and epidemic strains of toxigenic BI/NAP1/027 C. difficile. *Antimicrob. Agents Chemother.* 57:5266. doi: 10.1128/AAC.00580-13

Nakagawa, T., Mori, N., Kajiwara, C., Kimura, S., Akasaka, Y., Ishii, Y., et al. (2016). Endogenous IL-17 as a factor determining the severity of *Clostridium difficile* infection in mice. *J. Med. Microbiol.* 65, 821–827. doi: 10.1099/jmm.0.000273

Navalkele, B. D., and Chopra, T. (2018). Bezlotoxumab: an emerging monoclonal antibody therapy for prevention of recurrent *Clostridium difficile* infection. *Biologics* 12, 11–21. doi: 10.2147/BTT.S127099

Negrut, N., Bungau, S., Behl, T., Khan, S. A., Vesa, C. M., Bustea, C., et al. (2020). Risk factors associated with recurrent *Clostridioides difficile* infection. *Healthcare (Basel)* 8:352. doi: 10.3390/healthcare8030352

Nelson, R. T., Boyd, J., Gladue, R. P., Paradis, T., Thomas, R., Cunningham, A. C., et al. (2001). Genomic organization of the CC chemokine mip-3alpha/CCL20/larc/exodus/SCYA20, showing gene structure, splice variants, and chromosome localization. *Genomics* 73, 28–37. doi: 10.1006/geno.2001.6482

Ní Eidhin, D. B., O'Brien, J. B., McCabe, M. S., Athié-Morales, V., and Kelleher, D. P. (2008). Active immunization of hamsters against *Clostridium difficile*

infection using surface-layer protein. *FEMS Immunol. Med. Microbiol.* 52, 207–218. doi: 10.1111/j.1574-695X.2007.00363.x

Oatley, P., Kirk, J. A., Ma, S., Jones, S., and Fagan, R. P. (2020). Spatial organization of *Clostridium difficile* S-layer biogenesis. *Sci. Rep.* 10:14089. doi: 10.1038/s41598-020-71059-x

Oksi, J., Anttila, V. J., and Mattila, E. (2020). Treatment of *Clostridioides (Clostridium) difficile* infection. *Ann. Med.* 52, 12–20. doi: 10.1080/07853890.2019.1701703

Oliveira Júnior, C. A., Silva, R. O. S., Lage, A. P., Coura, F. M., Ramos, C. P., Alfieri, A. A., et al. (2019). Non-toxigenic strain of *Clostridioides difficile* Z31 reduces the occurrence of *C. difficile* infection (CDI) in one-day-old piglets on a commercial pig farm. *Vet. Microbiol.* 231, 1–6. doi: 10.1016/j.vetmic.2019.02.026

Orrell, K. E., and Melnyk, R. A. (2021). Large clostridial toxins: mechanisms and roles in disease. *Microbiol. Mol. Biol. Rev.* 85:e0006421. doi: 10.1128/mmbr.00064-21

Papatheodorou, P., Barth, H., Minton, N., and Aktories, K. (2018). Cellular uptake and mode-of-action of *Clostridium difficile* toxins. *Adv. Exp. Med. Biol.* 1050, 77–96. doi: 10.1007/978-3-319-72799-8_6

Paredes-Sabja, D., Cofre-Araneda, G., Brito-Silva, C., Pizarro-Guajardo, M., and Sarker, M. R. (2012). *Clostridium difficile* spore-macrophage interactions: spore survival. *PLoS One* 7:e43635. doi: 10.1371/journal.pone.0043635

Péchiné, S., Bruxelle, J. F., Janoir, C., and Collignon, A. (2018). Targeting *Clostridium difficile* surface components to develop immunotherapeutic strategies against *Clostridium difficile* infection. *Front. Microbiol.* 9:1009. doi: 10.3389/fmicb.2018.01009

Péchiné, S., Denève, C., Le Monnier, A., Hoys, S., Janoir, C., and Collignon, A. (2011). Immunization of hamsters against *Clostridium difficile* infection using the Cwp84 protease as an antigen. *FEMS Immunol. Med. Microbiol.* 63, 73–81. doi: 10.1111/j.1574-695X.2011.00832.x

Péchiné, S., Hennequin, C., Boursier, C., Hoys, S., and Collignon, A. (2013). Immunization using GroEL decreases *Clostridium difficile* intestinal colonization. *PLoS One* 8:e81112. doi: 10.1371/journal.pone.0081112

Péchiné, S., Janoir, C., and Collignon, A. (2005). Variability of *Clostridium difficile* surface proteins and specific serum antibody response in patients with *Clostridium difficile*-associated disease. *J. Clin. Microbiol.* 43, 5018–5025. doi: 10.1128/JCM.43.10.5018-5025.2005

Perelle, S., Gibert, M., Bourlioux, P., Corthier, G., and Popoff, M. R. (1997). Production of a complete binary toxin (actin-specific ADP-ribosyltransferase) by *Clostridium difficile* CD196. *Infect. Immun.* 65, 1402–1407. doi: 10.1128/iai.65.4.1402-1407.1997

Quraishi, M. N., Widlak, M., Bhala, N., Moore, D., Price, M., Sharma, N., et al. (2017). Systematic review with meta-analysis: the efficacy of faecal microbiota transplantation for the treatment of recurrent and refractory *Clostridium difficile* infection. *Aliment. Pharmacol. Ther.* 46, 479–493. doi: 10.1111/apt.14201

Ramírez-Vargas, G., and Rodríguez, C. (2020). Putative conjugative plasmids with tcdB and cdtAB genes in *Clostridioides difficile*. *Emerg. Infect. Dis.* 26, 2287–2290. doi: 10.3201/eid2609.191447

Rampuria, P., Lang, G. A., Devera, T. S., Gilmore, C., Ballard, J. D., and Lang, M. L. (2017). Coordination between T helper cells, iNKT cells, and their follicular helper subsets in the humoral immune response against *Clostridium difficile* toxin B. *J. Leukoc. Biol.* 101, 567–576. doi: 10.1189/jlb.4A0616-271R

Razim, A., Pacyga, K., Martirosian, G., Szuba, A., Gamian, A., Myc, A., et al. (2019). Mapping epitopes of a novel peptidoglycan cross-linking enzyme Cwp22 recognized by human sera obtained from patients with *Clostridioides difficile* infection and cord blood. *Microorganisms* 7:565. doi: 10.3390/microorganisms7110565

Rea, M. C., Dobson, A., O'Sullivan, O., Crispie, F., Fouhy, F., Cotter, P. D., et al. (2011). Effect of broad- and narrow-spectrum antimicrobials on Clostridium difficile and microbial diversity in a model of the distal colon. *Proc. Natl. Acad. Sci. U.S.A.* 108(Suppl. 1), 4639–4644. doi: 10.1073/pnas.1001224107

Rees, W. D., and Steiner, T. S. (2018). Adaptive immune response to *Clostridium difficile* infection: a perspective for prevention and therapy. *Eur. J. Immunol.* 48, 398–406. doi: 10.1002/eji.201747295

Riedel, T., Neumann-Schaal, M., Wittmann, J., Schober, I., Hofmann, J. D., Lu, C.-W., et al. (2020). Characterization of *Clostridioides difficile* DSM 101085 with A–B–CDT+ phenotype from a late recurrent colonization. *Genome Biol. Evol.* 12, 566–577. doi: 10.1093/gbe/evaa072

Rupnik, M., Wilcox, M. H., and Gerding, D. N. (2009). *Clostridium difficile* infection: new developments in epidemiology and pathogenesis. *Nat. Rev. Microbiol.* 7, 526–536. doi: 10.1038/nrmicro2164

Ryan, A., Lynch, M., Smith, S. M., Amu, S., Nel, H. J., McCoy, C. E., et al. (2011). A role for TLR4 in *Clostridium difficile* infection and the recognition of surface layer proteins. *PLoS Pathog.* 7:e1002076. doi: 10.1371/journal.ppat.1002076

Saavedra, P. H. V., Huang, L., Ghazavi, F., Kourula, S., Vanden Berghe, T., Takahashi, N., et al. (2018). Apoptosis of intestinal epithelial cells restricts *Clostridium difficile* infection in a model of pseudomembranous colitis. *Nat. Commun.* 9:4846. doi: 10.1038/s41467-018-07386-5

Saleh, M. M., Frisbee, A. L., Leslie, J. L., Buonomo, E. L., Cowardin, C. A., Ma, J. Z., et al. (2019). Colitis-induced Th17 cells increase the risk for severe subsequent *Clostridium difficile* infection. *Cell Host Microbe* 25, 756–765.e5. doi: 10.1016/j.chom.2019.03.003

Samarkos, M., Mastrogianni, E., and Kampouropoulou, O. (2018). The role of gut microbiota in *Clostridium difficile* infection. *Eur. J. Intern. Med.* 50, 28–32. doi: 10.1016/j.ejim.2018.02.006

Sambol, S., Merrigan, M., Tang, J., Johnson, S., and Gerding, D. (2003). Colonization for the prevention of *Clostridium difficile* disease in hamsters. *J. Infect. Dis.* 186, 1781–1789. doi: 10.1086/345676

Sandolo, C., Péchiné, S., Le Monnier, A., Hoys, S., Janoir, C., Coviello, T., et al. (2011). Encapsulation of Cwp84 into pectin beads for oral vaccination against *Clostridium difficile*. *Eur. J. Pharm. Biopharm.* 79, 566–573. doi: 10.1016/j.ejpb.2011.05.011

Savidge, T. C., Urvil, P., Oezguen, N., Ali, K., Choudhury, A., Acharya, V., et al. (2011). Host S-nitrosylation inhibits clostridial small molecule-activated glucosylating toxins. *Nat. Med.* 17, 1136–1141. doi: 10.1038/nm.2405

Seal, D., Borriello, S. P., Barclay, F., Welch, A., Piper, M., and Bonnycastle, M. (1987). Treatment of relapsing *Clostridium difficile* diarrhoea by administration of a non-toxigenic strain. *Eur. J. Clin. Microbiol.* 6, 51–53. doi: 10.1007/BF02097191

Sehgal, K., and Khanna, S. (2021). Immune response against *Clostridioides difficile* and translation to therapy. *Therap. Adv. Gastroenterol.* 14:17562848211014817. doi: 10.1177/17562848211014817

Shen, J., Mehrotra, D. V., Dorr, M. B., Zeng, Z., Li, J., Xu, X., et al. (2020). Genetic association reveals protection against recurrence of *Clostridium difficile* infection with bezlotoxumab treatment. *mSphere* 5, 1–13. doi: 10.1128/mSphere.00232-20

Singh, T., Bedi, P., Bumrah, K., Singh, J., Rai, M., and Seelam, S. (2019). Updates in treatment of recurrent *Clostridium difficile* infection. *J. Clin. Med. Res.* 11, 465–471. doi: 10.14740/jocmr3854

Smits, W. K., Lyras, D., Lacy, D. B., Wilcox, M. H., and Kuijper, E. J. (2016). *Clostridium difficile* infection. *Nat. Rev. Dis. Primers* 2:16020. doi: 10.1038/nrdp.2016.20

Sonnenberg, G. F., and Artis, D. (2015). Innate lymphoid cells in the initiation, regulation and resolution of inflammation. *Nat. Med.* 21, 698–708. doi: 10.1038/nm.3892

Sougioultzis, S., Kyne, L., Drudy, D., Keates, S., Maroo, S., Pothoulakis, C., et al. (2005). *Clostridium difficile* toxoid vaccine in recurrent *C. difficile*-associated diarrhea. *Gastroenterology* 128, 764–770. doi: 10.1053/j.gastro.2004.11.004

Spencer, J., Leuzzi, R., Buckley, A., Irvine, J., Candlish, D., Scarselli, M., et al. (2014). Vaccination against *Clostridium difficile* using toxin fragments: observations and analysis in animal models. *Gut Microbes* 5, 225–232. doi: 10.4161/gmic.27712

Staley, C., Weingarden, A. R., Khoruts, A., and Sadowsky, M. J. (2017). Interaction of gut microbiota with bile acid metabolism and its influence on disease states. *Appl. Microbiol. Biotechnol.* 101, 47–64. doi: 10.1007/s00253-016-8006-6

Stewart, D. B., Berg, A., and Hegarty, J. (2013). Predicting recurrence of *C. difficile* colitis using bacterial virulence factors: binary toxin is the key. *J. Gastrointest. Surg.* 17, 118–125. doi: 10.1007/s11605-012-2056-6

Tasteyre, A., Barc, M. C., Collignon, A., Boureau, H., and Karjalainen, T. (2001). Role of FliC and FliD flagellar proteins of *Clostridium difficile* in adherence and

gut colonization. *Infect. Immun.* 69, 7937–7940. doi: 10.1128/IAI.69.12.7937-7940.2001

Tourlomousis, P., Wright, J. A., Bittante, A. S., Hopkins, L. J., Webster, S. J., Bryant, O. J., et al. (2020). Modifying bacterial flagellin to evade Nod-like receptor CARD 4 recognition enhances protective immunity against *Salmonella*. *Nat. Microbiol.* 5, 1588–1597. doi: 10.1038/s41564-020-00801-y

Treiner, E., Duban, L., Bahram, S., Radosavljevic, M., Wanner, V., Tilloy, F., et al. (2003). Selection of evolutionarily conserved mucosal-associated invariant T cells by MR1. *Nature* 422, 164–169. doi: 10.1038/nature01433

van Prehn, J., Reigadas, E., Vogelzang, E. H., Bouza, E., Hristea, A., Guery, B., et al. (2021). European society of clinical microbiology and infectious diseases: 2021 update on the treatment guidance document for *Clostridioides difficile* infection in adults. *Clin. Microbiol. Infect.* doi: 10.1016/j.cmi.2021.09.038 [Epub ahead of print].

Vardakas, K. Z., Polyzos, K. A., Patouni, K., Rafailidis, P. I., Samonis, G., and Falagas, M. E. (2012). Treatment failure and recurrence of *Clostridium difficile* infection following treatment with vancomycin or metronidazole: a systematic review of the evidence. *Int. J. Antimicrob. Agents* 40, 1–8. doi: 10.1016/j.ijantimicag.2012.01.004

Villano, S. A., Seiberling, M., Tatarowicz, W., Monnot-Chase, E., and Gerding, D. N. (2012). Evaluation of an oral suspension of VP20621, spores of nontoxigenic *Clostridium difficile* strain M3, in healthy subjects. *Antimicrob. Agents Chemother.* 56, 5224–5229. doi: 10.1128/AAC.00913-12

Wang, J., Ortiz, C., Fontenot, L., Mukhopadhyay, R., Xie, Y., Chen, X., et al. (2020). Therapeutic mechanism of macrophage inflammatory protein 1 α neutralizing antibody (CCL3) in *Clostridium difficile* infection in mice. *J. Infect. Dis.* 221, 1623–1635. doi: 10.1093/infdis/jiz640

Wang, S., Wang, Y., Cai, Y., Kelly, C. P., and Sun, X. (2018). Novel chimeric protein vaccines against *Clostridium difficile* infection. *Front. Immunol.* 9:2440. doi: 10.3389/fimmu.2018.02440

Warny, M., Keates, A. C., Keates, S., Castagliuolo, I., Zacks, J. K., Aboudola, S., et al. (2000). p38 MAP kinase activation by *Clostridium difficile* toxin A mediates monocyte necrosis, IL-8 production, and enteritis. *J. Clin. Invest.* 105, 1147–1156. doi: 10.1172/jci7545

Wiegand, P. N., Nathwani, D., Wilcox, M. H., Stephens, J., Shelbaya, A., and Haider, S. (2012). Clinical and economic burden of *Clostridium difficile* infection in Europe: a systematic review of healthcare-facility-acquired infection. *J. Hosp. Infect.* 81, 1–14. doi: 10.1016/j.jhin.2012.02.004

Wilcox, M. H., Gerding, D. N., Poxton, I. R., Kelly, C., Nathan, R., Birch, T., et al. (2017). Bezlotoxumab for prevention of recurrent *Clostridium difficile* infection. *N. Engl. J. Med.* 376, 305–317. doi: 10.1056/NEJMoa1602615

Wilson, K. H., and Sheagren, J. N. (1983). Antagonism of toxigenic *Clostridium difficile* by nontoxigenic *C. difficile*. *J. Infect. Dis.* 147, 733–736. doi: 10.1093/infdis/147.4.733

Xu, B., Wu, X., Gong, Y., and Cao, J. (2021). IL-27 induces LL-37/CRAMP expression from intestinal epithelial cells: implications for immunotherapy of *Clostridioides difficile* infection. *Gut Microbes* 13:1968258. doi: 10.1080/19490976.2021.1968258

Xu, H., Yang, J., Gao, W., Li, L., Li, P., Zhang, L., et al. (2014). Innate immune sensing of bacterial modifications of Rho GTPases by the Pyrin inflammasome. *Nature* 513, 237–241. doi: 10.1038/nature13449

Yacyshyn, M. B., Reddy, T. N., Plageman, L. R., Wu, J., Hollar, A. R., and Yacyshyn, B. R. (2014). *Clostridium difficile* recurrence is characterized by pro-inflammatory peripheral blood mononuclear cell (PBMC) phenotype. *J. Med. Microbiol.* 63(Pt 10), 1260–1273. doi: 10.1099/jmm.0.075382-0

Yang, Z., Schmidt, D., Liu, W., Li, S., Shi, L., Sheng, J., et al. (2014). A novel multivalent, single-domain antibody targeting TcdA and TcdB prevents fulminant *Clostridium difficile* infection in mice. *J. Infect. Dis.* 210, 964–972. doi: 10.1093/infdis/jiu196

Yoshino, Y., Kitazawa, T., Ikeda, M., Tatsuno, K., Yanagimoto, S., Okugawa, S., et al. (2012). *Clostridium difficile* flagellin stimulates toll-like receptor 5, and toxin B promotes flagellin-induced chemokine production via TLR5. *Life Sci.* 92, 211–217. doi: 10.1016/j.lfs.2012.11.017

Yu, H., Chen, K., Sun, Y., Carter, M., Garey, K. W., Savidge, T. C., et al. (2017). Cytokines are markers of the *Clostridium difficile*-induced inflammatory response and predict disease severity. *Clin. Vaccine Immunol.* 24:e00037-17. doi: 10.1128/cvi.00037-17

Zhang, B.-Z., Cai, J., Yu, B., Hua, Y., Lau, C. C., Kao, R. Y.-T. T., et al. (2016). A DNA vaccine targeting TcdA and TcdB induces protective immunity against *Clostridium difficile*. *BMC Infect. Dis.* 16:596. doi: 10.1186/s12879-016-1924-1

Zhang, Z., Chen, X., Hernandez, L. D., Lipari, P., Flattery, A., Chen, S. C., et al. (2015). Toxin-mediated paracellular transport of antitoxin antibodies facilitates protection against *Clostridium difficile* infection. *Infect. Immun.* 83, 405–416. doi: 10.1128/IAI.02550-14

Zheng, Y., Valdez, P. A., Danilenko, D. M., Hu, Y., Sa, S. M., Gong, Q., et al. (2008). Interleukin-22 mediates early host defense against attaching and effacing bacterial pathogens. *Nat. Med.* 14, 282–289. doi: 10.1038/nm1720

Zhu, D., Bullock, J., He, Y., and Sun, X. (2019). Cwp22, a novel peptidoglycan cross-linking enzyme, plays pleiotropic roles in *Clostridioides difficile*. *Environ. Microbiol.* 21, 3076–3090. doi: 10.1111/1462-2920.14706

Zhu, D., Sorg, J. A., and Sun, X. (2018). *Clostridioides difficile* biology: sporulation, germination, and corresponding therapies for *C. difficile* infection. *Front. Cell. Infect. Microbiol.* 8:29. doi: 10.3389/fcimb.2018.00029

Conflict of Interest: DG holds technology for the use of non-toxigenic *C. difficile* for the prevention and treatment of CDI licensed to Destiny Pharma plc, Brighton, United Kingdom. EK has received an unrestricted research grant from Vedanta Bioscience, Boston, United States.

The remaining authors declare that the research was conducted in the absence of any commercial or financial relationships that could be construed as a potential conflict of interest.

Publisher's Note: All claims expressed in this article are solely those of the authors and do not necessarily represent those of their affiliated organizations, or those of the publisher, the editors and the reviewers. Any product that may be evaluated in this article, or claim that may be made by its manufacturer, is not guaranteed or endorsed by the publisher.

Copyright © 2021 Nibbering, Gerding, Kuijper, Zwittink and Smits. This is an open-access article distributed under the terms of the Creative Commons Attribution License (CC BY). The use, distribution or reproduction in other forums is permitted, provided the original author(s) and the copyright owner(s) are credited and that the original publication in this journal is cited, in accordance with accepted academic practice. No use, distribution or reproduction is permitted which does not comply with these terms.

frontiers in Microbiology

REVIEW
published: 20 January 2022
doi: 10.3389/fmicb.2021.651081

Gut Dysbiosis and *Clostridioides difficile* Infection in Neonates and Adults

Iulia-Magdalena Vasilescu[1,2†], Mariana-Carmen Chifiriuc[1,3,4,5†], Gratiela Gradisteanu Pircalabioru[3†], Roxana Filip[6,7†], Alexandra Bolocan[8†], Veronica Lazăr[1†], Lia-Mara Diţu[1†] and Coralia Bleotu[1,3,9†]*

[1] Department of Microbiology, Faculty of Biology, University of Bucharest, Bucharest, Romania, [2] INBI "Prof. Dr. Matei Balş" – National Institute for Infectious Diseases, Bucharest, Romania, [3] Research Institute of the University of Bucharest, Bucharest, Romania, [4] Academy of Romanian Scientists, Bucharest, Romania, [5] The Romanian Academy, Bucharest, Romania, [6] Faculty of Medicine and Biological Sciences, Stefan cel Mare University of Suceava, Suceava, Romania, [7] Regional County Emergency Hospital, Suceava, Romania, [8] Department of General Surgery, University Emergency Hospital, Carol Davila University of Medicine and Pharmacy, Bucharest, Romania, [9] Ştefan S. Nicolau Institute of Virology, Romanian Academy, Bucharest, Romania

OPEN ACCESS

Edited by:
Axel Cloeckaert, Institut National de Recherche pour l'Agriculture, l'Alimentation et l'Environnement (INRAE), France

Reviewed by:
Felix Broecker, Idorsia Pharmaceuticals Ltd., Switzerland
Frédéric Barbut, AP-HP, France

***Correspondence:**
Mariana-Carmen Chifiriuc
carmen.chifiriuc@gmail.com

† These authors have contributed equally to this work

Specialty section:
This article was submitted to Infectious Agents and Disease, a section of the journal Frontiers in Microbiology

Received: *09 April 2021*
Accepted: *15 December 2021*
Published: *20 January 2022*

Citation:
Vasilescu I-M, Chifiriuc M-C, Pircalabioru GG, Filip R, Bolocan A, Lazăr V, Diţu L-M and Bleotu C (2022) Gut Dysbiosis and Clostridioides difficile Infection in Neonates and Adults. Front. Microbiol. 12:651081. doi: 10.3389/fmicb.2021.651081

In this review, we focus on gut microbiota profiles in infants and adults colonized (CDC) or infected (CDI) with *Clostridioides difficile*. After a short update on CDI epidemiology and pathology, we present the gut dysbiosis profiles associated with CDI in adults and infants, as well as the role of dysbiosis in *C. difficile* spores germination and multiplication. Both molecular and culturomic studies agree on a significant decrease of gut microbiota diversity and resilience in CDI, depletion of *Firmicutes, Bacteroidetes,* and *Actinobacteria* phyla and a high abundance of *Proteobacteria*, associated with low butyrogenic and high lactic acid-bacteria levels. In symptomatic cases, microbiota deviations are associated with high levels of inflammatory markers, such as calprotectin. In infants, colonization with *Bifidobacteria* that trigger a local anti-inflammatory response and abundance of *Ruminococcus*, together with lack of receptors for clostridial toxins and immunological factors (e.g., *C. difficile* toxins neutralizing antibodies) might explain the lack of clinical symptoms. Gut dysbiosis amelioration through administration of "biotics" or non-toxigenic *C. difficile* preparations and fecal microbiota transplantation proved to be very useful for the management of CDI.

Keywords: *Clostridium difficile* infection, gut microbiota, dysbiosis, biotics, fecal microbiota transplantation

INTRODUCTION

Clostridioides (formerly *Clostridium*) *difficile* is a Gram-positive, obligate anaerobe, spore-forming bacteria, harboring a plethora of surface and secreted proteins responsible for the colonic colonization and subsequent inflammation characteristic for *C. difficile* infection (CDI), among which the most important are the clostridial toxins: toxin A (TcdA) and toxin B (TcdB), and in some bacterial strains, the binary toxin CDT (Smits et al., 2016). Clinical symptoms range from mild diarrhea to fulminant colitis, known as pseudomembranous colitis, with its complications – toxic megacolon and large bowel perforation (McDonald et al., 2018; Dieterle et al., 2019). *C. difficile* is the number one causative agent of nosocomial post-antibiotic colitis, associated with high

morbidity and mortality (Ghose, 2013). In the last decade, both frequency and severity of CDI have increased, largely due to the emergence of a hypervirulent strain called NAP1 (North American pulsed-field gel electrophoresis type 1 strain) (Depestel and Aronoff, 2013). Moreover, in the last two decades, there has been a significant increase in the incidence of CDI in previously considered low-risk population categories, including community-associated-*Clostridioides difficile* infections (CA-CDI), with more than 30% of cases not showing typical CDI risk factors, such as antibiotic treatment or recent hospitalization (Wilcox et al., 2008; Hensgens et al., 2011). Although CDI is the preserve of the elderly population, it can also affect other age segments. In a retrospective survey performed by U.S. National Hospital Discharge Surveys from 2001 to 2010 revealed that CDI incidence was highest among elderly adults (11.6 CDI discharges/1,000 total discharges), followed by adults (3.5 CDI discharges/1,000 total discharges) and pediatrics (<12 years) (1.2 CDI discharges/1,000 total discharges). The mortality rates attributable to CDI in the elderly were significantly higher (8.8%) compared to adults (3.1%) and pediatrics (1.4%) (Pechal et al., 2016). Although there is not much information available about the epidemiology of infection in infants, however, the carriage rate of non-toxigenic *C. difficile* is very high in newborns, suggesting the commensal status of this bacterium in this population segment (Sammons et al., 2013; Borali and De Giacomo, 2016). For this reason, *C. difficile* is not considered an enteric pathogen in infants and children affected by bloody diarrhea and younger than 12 months (Cama et al., 2019). However, asymptomatic infants could be also infected by toxigenic adult infectious strains both after hospitalization and even in the community, thus, constituting a reservoir for toxigenic strains (Rousseau et al., 2011; Ferraris et al., 2020).

This review aims to present some particular aspects of gut microbiota in CDI infants and adults, taking into account that the pathophysiology of this disease suggests that the clinical manifestations occur in cases of an imbalance of the intestinal microbiota, known as dysbiosis. In this purpose, studies performing culture-dependent (*C. difficile* cultivation) and independent (16S rRNA and metagenomics) have been analyzed.

Some of the underlying causes of intestinal dysbiosis are antibiotic treatments (Kukla et al., 2020), advanced age (over 65 years), hospitalization (particularly in patients sharing the hospital room with an infected patient, in intensive care units, during prolonged hospitalization), nursing home stay, severe associated diseases, immunological suppression, gastric acidity suppression by proton pump inhibitors or histamine$_2$-receptor antagonists and prolonged use of elemental diet in the context of enteral nutrition, inflammatory bowel diseases, gastrointestinal surgery (in particular colectomy, small-bowel resection, and gastric resection were associated with the highest risk while patients undergoing cholecystectomy and appendectomy had the lowest risk), all of these circumstances being associated with characteristic changes in the configuration of the gut microbiota and with an increased CDI risk (O'Keefe, 2010; Fashner et al., 2011; Nitzan et al., 2013; Rodriguez et al., 2016; Sartelli et al., 2019; Avni et al., 2020). A strong argument regarding the impact of dysbiosis on CDI risk is offered by animal studies proving that correcting dysbiosis by administration of different substances such as phytophenolic compounds or carvacrol has been shown to decrease susceptibility to CDI. The gut dysbiosis of 6-week-old C57BL/6 mice was induced by the oral administration of an antibiotic cocktail in water simultaneously with the intra-peritoneal injection of clindamycin. The mice were infected with 10^5 CFU/ml of hypervirulent *C. difficile* ATCC 1870 spores. Carvacrol supplementation significantly reduced the incidence of diarrhea and improved mice's clinical and diarrhea scores. Microbiome analysis revealed that carvacrol increased the abundance of *Bacteroidetes* and *Firmicutes*. An increased abundance of *Lactobacillaceae* and *Lachnospiraceae* was noticed among the beneficial taxa in carvacrol treated mice. Also, carvacrol decreased the proportion of pro-inflammatory microbiota, such as *Proteobacteria* (i.e., *Enterobacteriaceae*) and *Verrucomicrobia*, without significantly affecting the gut microbiome diversity compared to the control (Mooyottu et al., 2017).

Five clinical features (potential risk factors) predict dysbiosis in CDI patients: antibiotic use within the previous 3 weeks, immunosuppression, multimorbidity, recent/multiple hospitalization, and prior CDI (Battaglioli et al., 2018). In individuals whose normal intestinal microbiota has been disrupted, ingested *C. difficile* spores germinate in the presence of bile salts in the small intestine and colonize the colon epithelial cells, releasing the inflammatory enterotoxins, which are primarily and largely responsible for the colonic inflammation in *C. difficile* diseases, inducing cytoskeletal changes, disruption of tight junctions, and induction of inflammatory cytokine production (Shen, 2012; Winston and Theriot, 2016). The *C. difficile* spores are released by the patient facilitating CDI transmission to susceptible hosts (Czepiel et al., 2019).

Clostridioides difficile INFECTION AND DYSBIOSIS IN ADULTS

The intestinal environment represents a complex network of bacterial cells and metabolic products and/or other unknown substances derived from their own structures or metabolisms, which are in close and continuous interaction, both with each other, as well as with the human intestinal cells and the host's immune system (Lazar et al., 2018, 2019).

The characterization of the baseline healthy microbiota and differences that are associated with various diseases has been possible with the contribution of large-scale projects, such as Meta-HIT and the Human Microbiome Project (HMP), using different omics technologies (Qin et al., 2010; Human Microbiome Project, 2012).

During early development, the gut microbiota undergoes subsequent changes until a stable adult state is reached. The adult microbiota has three basic characteristics: diversity (a high microbiota diversity defined by high species richness and high functional diversity being generally associated with the health condition), resilience (the property of the gut microbiota to resist to an impact and to recover and to baseline after the disturbance cessation; the capacity of a microbial community to reach a stable

TABLE 1 | Gut microbiota dysbiosis associated with *Clostridium difficile* infection in adults and infants (proposed microbiota-derived biomarkers for CDI dysbiosis are presented in bold).

Effect	Taxonomic level	Representatives	Mechanism	References
Adults				
Depletion	Gut microbiota	Cultivable/non-cultivable microbiota	Disrupted microbiota; decreased richness and diversity	Amrane et al., 2019
	Phylum	*Firmicutes*	Butyrate and short chain fatty acid production; role in gut homeostasis and inhibition of *C. difficile* germination	Antharam et al., 2013; den Besten et al., 2013; Abt et al., 2016
		Bacteroidetes	Carbohydrate digestion, producing substrates for colonocytes	den Besten et al., 2013; Zhang et al., 2015
		Actinobacteria		Amrane et al., 2019
	Families	*Bacteroidaceae*		Lozupone et al., 2012
		Bifidobacteriaceae		Lozupone et al., 2012
		Lachnospiraceae	Colonization resistance	Reeves et al., 2011, 2012; Antharam et al., 2013; Perez-Cobas et al., 2015
		Clostridiales	*C. difficile* spores germination inhibition and colonization	
		Ruminococcaceae		Franzosa et al., 2019; Lo Presti et al., 2019; Wilson et al., 2019; Berkell et al., 2021
	Genera and species	*Faecalibacterium, Roseburia, Blautia, Dorea*, *Prevotella, Megamonas*, *Subdoligranulum, Anaerostipes, Pseudobutyrivibrio, Streptococcus, Ezakiella, Odoribacter, Bacteroides sp.*, ***Alistipes***, ***B. ovatus***, *B. vulgatus*, ***Bifidobacterium adolescentis*****, *B. longum***, *Oscillibacter massiliensis, Clostridium scindens*	Decrease of luminal pH by butyrogenic and acetogenic bacteria, stimulation of mucin and antimicrobial peptides production, maintaining decreased permeability Primary bile acids conversion Production of lantibiotics (nisin O)	Guilloteau et al., 2010; Lozupone et al., 2012; Antharam et al., 2013; Hamilton et al., 2013; Solomon, 2013; Gupta et al., 2016; Milani et al., 2016; Theriot et al., 2016; Winston and Theriot, 2016; Hatziioanou et al., 2017; Vakili et al., 2020
Increase	Phylum	*Proteobacteria*		Rodriguez et al., 2020
	Families	***Enterobacteriaceae***	Increased intestinal permeability	Collins and Auchtung, 2017
	Genera/ species	*Finegoldia, Enterococcus, Lactobacillus, Fusobacterium, Mycobacterium, Enterobacter, Bacteroides*, *Parabacteroides, Escherichia coli*, ***Akkermansia muciniphila***	Lactic acid bacteria	Reeves et al., 2011, 2012; Na and Kelly, 2011; Rea et al., 2012; Rajilic-Stojanovic et al., 2013; Gevers et al., 2014; Milani et al., 2016; Ross et al., 2016
Infants				
Increase	Genera/ species	*Staphylococcus aureus, Enterococcus*, *Escherichia coli, Shigella spp., Citrobacter spp., Klebsiella spp.*	Triggering a pro-inflammatory response	Heida et al., 2016
Decrease	Phylum	*Bacteroidetes, Firmicutes*		Dobbler et al., 2017
		Bifidobacteria	Upregulation of IL-10 production	Huurre et al., 2008
	Genera/ species	*Ruminococcus*		Morelli, 2008

state in response to chemical, physical or biological perturbations of different intensities is achieved through genetically diverse resident clonal populations and population-level dynamics) and long-term stability of high taxonomic level components (Levine and d'Antonio, 1999; Lozupone et al., 2012; McBurney et al., 2019; Priya and Blekhman, 2019; Dogra et al., 2020).

Regarding the diversity, human microbiota displays a remarkable heterogeneity within and between individuals, the results of the culture-independent studies leading to the generally accepted idea that we rather share a functional core microbiome, than a core microbiota (Lozupone et al., 2012). The >1,000 estimated species-level phylotypes are belonging to few microbial phyla, which are *Firmicutes, Bacteroidetes, Actinobacteria, Proteobacteria, Fusobacteria,* and *Verrucomicrobia*; among these, the two *Firmicutes* and *Bacteroidetes* phyla are representing 90% of gut microbiota (Magne et al., 2020). *Firmicutes* comprises more than 200 different genera, such as *Lactobacillus, Bacillus, Clostridium, Enterococcus,* and *Ruminococcus* (Kachrimanidou and Tsintarakis, 2020). *Clostridium* genera represent 95% of the *Firmicutes*, while *Bacteroidetes* include as predominant genera *Bacteroidetes* and *Prevotella* (Rinninella et al., 2019). *Actinobacteria* are proportionally less abundant and mainly

represented by *Bifidobacterium* species (Rinninella et al., 2019). From the mentioned components, *Ruminococcus* and *Bifidobacterium* have been reported to exhibit protective roles against CDI (Seekatz and Young, 2014; Kho and Lal, 2018).

The gut microbiota community shows resilience to different perturbations, such as those induced by different diets, antibiotic administration, invasion by new species (called colonization resistance) (Folke et al., 2004). Under the impact of a certain disturbances, such as antibiotic administration, microbiota enters an unstable state that progresses to a new stable state. When the latter is highly similar to the pre-disturbance state, this indicates a complete recovery. However, sometimes the post-disturbance stable state is distinct and this unfortunately can be both abnormal and resilient, as a response to the perturbation persistence (e.g., poor diet, antibiotic treatments etc) (Dupont, 2011). An example of gut microbiota resilience is the success of bacteriotherapy or microbiota transplantation in treating recurrent CDI. In this case, the gut microbiota switches from an initial dysbiosis state, favoring the CDI (e.g., increased abundance of *Veillonella* and *Streptococcus*) to a baseline state, in which the taxa from the healthy donor (e.g., *Bacteroidetes*) persisted 1 month after transplantation (Gough et al., 2011). A high diversity (high species richness, α-diversity) and host immune effectors, e.g., nucleotide-binding oligomerization domain (Nod2), an intracellular innate immune sensor involved in the anti-infectious host defense, were linked to gut microbiota resilience (Tap et al., 2015; Raymond et al., 2016; Goethel et al., 2019). A low microbiota diversity was correlated with recurrent CDI, but with unknown effects on microbiota resilience (Chang et al., 2008; Khoruts et al., 2010). However, a comparable phylum-level diversity was observed in individuals with initial CDI and healthy controls, while in case of recurrent CDI the phylum-level diversity switched to different highly divergent profiles very different from the healthy state other (Chang et al., 2008).

The stability of gut microbiota is affected by different factors, including genetic factors, early-life events, travel, dietary changes, weight loss or gain, diarrheal disease, antibiotics, immunosuppressants, premeditated interventions to influence the microbiota by administration of prebiotics, probiotics, postbiotics and symbiotics, as well as fecal transplantation (Faith et al., 2013; Britton and Young, 2014).

Dysbiosis Profiles in *Clostridioides difficile* Infection Patients

In this section, we will present some of the culture-dependent and independent studies that have been performed to identify the dysbiosis profiles (**Table 1**) and specific microbial derived biomarkers in patients prone to CDI. A metagenomic and culturomic analysis of gut microbiota dysbiosis during CDI has shown a significant depletion of *Bacteroidetes* in *C. difficile* patients compared with the control group (Amrane et al., 2019). Diversity was significantly higher in the control group. *Proteobacteria* were more common in the CDI group. *Firmicutes* and *Actinobacteria* were less common in the CDI group (Lozupone et al., 2012). *Firmicutes* are involved in butyrate, and other short chain fatty acids (SCFA) production, these molecules playing a role in gut homeostasis and inhibition of *C. difficile* germination (Kachrimanidou and Tsintarakis, 2020) and *Bacteroidetes* are involved in carbohydrates digestion, producing substrates for colonocytes (den Besten et al., 2013). Depletion of these two major phyla of gut microbiota was detected in the *C. difficile* group. The bacterial families conferring resistance to CDI are *Bacteroidaceae, Bifidobacteriaceae,* and *Lachnospiraceae* (Antharam et al., 2013). Studies in animals with CDI, revealed a high abundance of *Proteobacteria* (especially *Enterobacteriaceae*) and a numerical decrease of *Lachnospiraceae* (*Firmicutes*) in diseased animals (Reeves et al., 2011). *Lachnospiraceae* strains have been shown to be able to partially restore colonization resistance, the mice inoculated with such strains showing decreased *C. difficile* colonization, lower levels of cytotoxins and lower clinical signs of severe infection (Reeves et al., 2012). An increased relative abundance of *Enterococcus, Lactobacillus, Escherichia coli*, *Enterobacter, Bacteroides*, *Parabacteroides, Akkermansia muciniphila,* and decreased *Faecalibacterium, Roseburia, Blautia, Prevotella, Megamonas*, *Streptococcus,* and *Bacteroides* levels were evidenced in the gut microbiota of CDI patients (Rea et al., 2012). The bacteria found only in the control group, which may have a role against *C. difficile,* were *Bacteroides ovatus, Bacteroides vulgatus* and *Oscillibacter massiliensis* (Lozupone et al., 2012). Only three bacteria with a potential role against *C. difficile* were detected both by culturomics and metagenomics, namely *Bifidobacterium adolescentis*, *Bifidobacterium longum* and *Bacteroides ovatus* (Lozupone et al., 2012). Overrepresentation of *Akkermansia* may be a predictive marker for the development of nosocomial diarrhea, with a worsened CDI prognosis (Hernandez et al., 2018; Vakili et al., 2020).

Dysbiosis-Associated Biochemical Features in *Clostridioides difficile* Infection Patients

The gut dysbiosis also results in biochemical and immunological disruptions like decreased short chain fatty acids (SCFAs) levels, the abundance of primary bile acids, high availability of carbohydrates, suppression of immunological mechanisms and absence of competitors, all resulting in increased colonization capacity, favoring germination and growth of *C. difficile* (Ridlon et al., 2014; Carding et al., 2015; Goh and Klaenhammer, 2015; Valdes et al., 2018; Hills et al., 2019; Toor et al., 2019). Nosocomial diarrheal syndromes, including CDI, were associated not only with decreased bacterial diversity, *Firmicutes* paucity, low numbers of *Ruminococcaceae, Lachnospiraceae* but also with low levels of butyrogenic (e.g., *Roseburia, Faecalibacterium, Subdoligranulum, Anaerostipes,* and *Pseudobutyrivibrio*) and acetogenic (e.g., *Blautia* and *Dorea*) genera and with high levels of lactic acid bacteria (e.g., *Enterococcus* sp.) (Antharam et al., 2013). A decrease in butyrate-producing bacteria and an increase in lactic acid-producing bacteria were associated with increased CDI risk (Vakili et al., 2020). The role of SCFAs depletion in facilitating *C. difficile* infection is not yet elucidated, yet however, SCFAs could act by reducing the luminal pH (unfavorable for *C. difficile*) and stimulating the defensive barrier

by production of mucin and antimicrobial peptides (defensins and cathelicidins, secreted by specialized cells, Paneth cells and leukocytes in the intestinal crypts) (Guilloteau et al., 2010; Solomon, 2013; Gupta et al., 2016). Among SCFAs, butyrate seems to have no effect on *C. difficile* colonization and toxin production, but it can protect the intestinal epithelium from the damage caused by *C. difficile* toxins by stabilizing hypoxia-inducible factor-1 (HIF-1) and increasing tight junctions, and thus decreasing intestinal epithelial permeability, inhibiting intestinal inflammation and bacterial translocation. The addition of butyrate to the drinking water of mice, administration of a pro-drug of butyrate, tributyrin, or of an inulin-rich diet (inulin can be fermented by gut commensal bacteria, which generate short-chain fatty acids, mainly acetate, propionate, and butyrate) resulted in the protection of mice against CDI (Fachi et al., 2019; Song et al., 2020).

C. difficile spore germination is regulated by the detection of bile salt and amino acid cogerminants by pseudoproteases CspC and CspA, respectively (Weingarden et al., 2014; Lawler et al., 2020). Although some cholate derivatives and the amino acid glycine could act as co-germinant factors, deoxycholate prevents vegetative growth (Sorg and Sonenshein, 2008), while chenodeoxycholate inhibits taurocholate-mediated germination (Sorg and Sonenshein, 2010). Commensal members of *Clostridiales* present in the gut contribute to the creation of an inappropriate environment for *C. difficile* germination and colonization by modulating the production of cogerminants (Perez-Cobas et al., 2015). For example, *Clostridium scindens*, a bile acid 7α-dehydroxylating intestinal strain, is associated with resistance to *C. difficile* infection, and, upon administration, it enhances resistance to infection in association with a secondary bile acid (Buffie et al., 2015). Depleting specific gut microbes responsible for converting primary bile acids into secondary antimicrobial bile acids could be associated with increased risk of CDI (Theriot et al., 2016; Winston and Theriot, 2016).

Clostridium species are among the best-described users of free amino acids as energy sources. Amino acids regulate *in vitro* toxin production and support colonization of *C. difficile* in antibiotic-treated mice. Dysbiotic microbial communities showed significantly decreased expression of multiple genes related to amino acid uptake and metabolism, resulting in increased concentrations of 12 amino acids, with proline showing significant differences when compared to healthy mice microbiota. The ability to utilize proline provides a competitive advantage to *C. difficile* in germ-free mice transplanted with healthy-like and dysbiotic human stool consortia. Fecal microbiota transplant reduced free proline and decreased CDI susceptibility in dysbiotic mice (Mooyottu et al., 2017).

Recent studies have found increased indole levels (tryptophan metabolite involved in microbial growth, virulence induction, acid resistance, biofilm development) in the intestinal lumen of CDI patients, suggesting that *C. difficile*, which cannot produce this metabolite itself, would stimulate the production of indole by other bacteria to stop the growth and the development of indole-sensitive strains, including protective gut microbiota representatives, thus ensuring an intestinal environment conducive to its survival (Darkoh et al., 2019).

A recent study evaluated the relationship between the composition of the intestinal microbiota and level of fecal calprotectin in *C. difficile* asymptomatic and symptomatic patients. The asymptomatic patients have shown a modified microbiota, comparatively with the non-colonized patients, harboring significantly lower levels of *Ruminococcaceae, Bilophila*, *Blautia, Faecalibacterium, Ruminococcus,* and *Sutterella,* and higher levels of *Enterobacteriaceae*. In symptomatic patients the main devations of gut microbiota were represented by higher levels of *Bacteroides* and lower levels of *Blautia*, *Phascolarctobacterium, Prevotella,* and *Succinivibrio*. These gut microbiota changes in symptomatic patients were accompanied by significantly higher levels of fecal calprotectin, comparatively with asymptomatic patients and controls. These data suggest that association of microbiota and inflammatory markers could be used to differentiate *C. difficile* colonization (CDC) from CDI (Han et al., 2020).

Knowledge regarding the gut microbiota in *C. difficile* colonized patients may elucidate the mechanisms that allow for colonization whilst protecting against infection (Crobach et al., 2020). To this end, a recent study by Crobach et al. (2020) analyzed the bacterial signatures associated with resistance and susceptibility to CDC and CDI. Both CDC and CDI were associated with decreased gut microbial diversity and differences in the relative abundance of taxa such as *Lachnospiraceae, Ruminococcaceae, Fusicatenibacter, Bacteroides, Veillonella*, and *Eubacterium hallii* (Crobach et al., 2020).

INFANT GUT MICROBIOTA CHARACTERISTICS AND POSSIBLE EXPLANATIONS FOR THE LOW PATHOGENICITY OF *C. difficile* IN NEONATES

During childhood, the intestinal microbiota is subject to many factors that shape the microbiota on short- and long-term. Apart from the maternal-fetal transmission of certain bacterial components, the microbiota is influenced by the type and the time of birth, the place of birth (hospitals or home births), the type of feeding (breastfeeding or artificial feeding), administration of probiotic and prebiotic supplements, dietary factors, antibiotics and other drugs, sex, and other genetic differences and environmental factors, such as exposure to pets, number of family members, rural or urban environment, hygiene, geographical factors (Combellick et al., 2018; Mohammadkhah et al., 2018; Akagawa et al., 2019).

Taking into account the numerous factors that could influence the intestinal microbiota of the newborns, the healthy profile of this age group is considered to be represented by the types of gut bacteria and the abundances found in vaginally delivered, exclusively breastfed and not exposed to antibiotics neonates (Arboleya et al., 2015; Combellick et al., 2018; Mohammadkhah et al., 2018; Akagawa et al., 2019). It has been hypothesized that bacterial colonization of the digestive tract begins *in utero,* the healthy placenta bearing

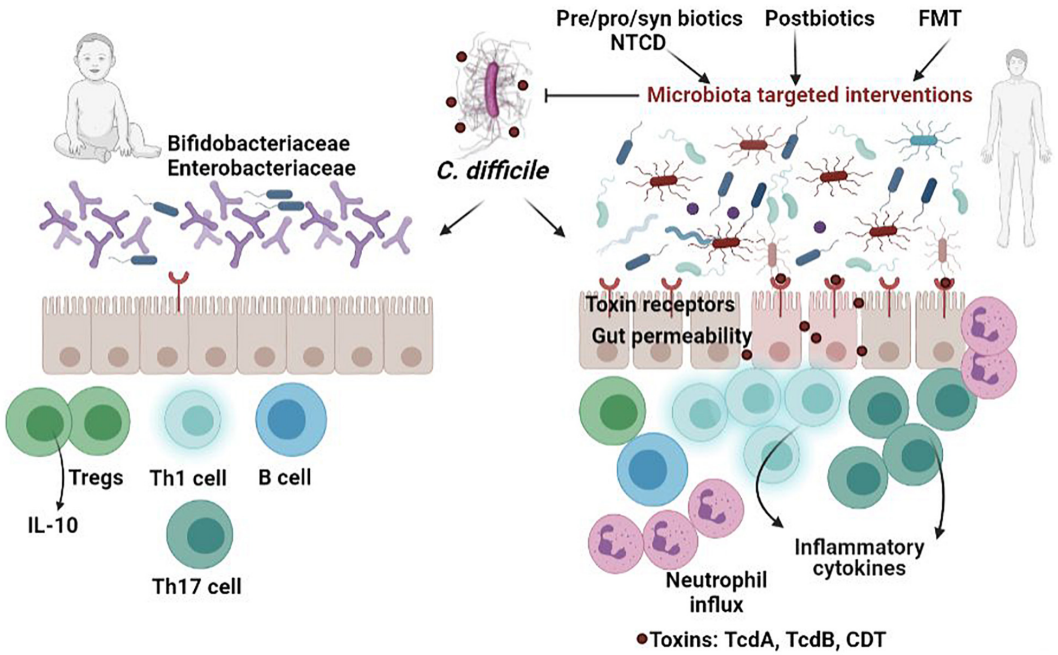

FIGURE 1 | Comparison of *C. difficile* infection in neonates versus adults. The presence of postnatal microbial species (*Bifidobacteria* and *Enterobacteriaceae*) and immaturity of the immune system as well as the lack of receptors for clostridial toxins helps to protect babies from the deleterious effects of *C. difficile* toxins, which occur in dysbiotic adults. In individuals with disrupted microbiota, ingested *C. difficile* spores germinate in the presence of bile salts in the small intestine and target the colon epithelial cells, releasing the inflammatory toxins, which subsequently induce disruption of tight junctions, and production of inflammatory cytokines. Targeting the microbiota using various strategies-probiotics, prebiotics, synbiotics, postbiotics, non-toxigenic *C. difficile* (NTCD), fecal transplant (FMT)-has proven to be effective in alleviating CDI.

a low biomass microbiome, composed of non-pathogenic species belonging to the *Tenericutes, Firmicutes, Bacteroidetes, Proteobacteria,* and *Fusobacteria* phyla, while in the amniotic fluid predominate *Proteobacteria*. However, the results reported by different studies are contradictory and depend on the sampling method and the culture-based or molecular-based approaches. Recent metagenomic studies conclude that the placenta does not harbor a specific, consistent and functional microbiota (Gschwind et al., 2020). The meconium harbors a cultivable microbiota, initially dominated by *Bacteroides-Prevotella*. The digestive contamination of the fetus occurs most probably by swallowing the amniotic fluid, starting with the 10th week after conception (Chong et al., 2018). The transfer of *Enterococcus faecium* from pregnant female mice into meconium was also demonstrated experimentally (Jimenez et al., 2008). All these lead to the conclusion that changes in the maternal internal environment may affect both fetal and newborn development (Zhuang et al., 2019).

C. difficile Colonization in Infants

Neonates are uniquely susceptible to *C. difficile* colonization because of the neonatal intestine's immaturity and intestinal microbiota instability (Lees et al., 2016). The main source of colonization seems to be the environmental exposure to *C. difficile* spores within the nursery or healthcare environment rather than the mother, the rates of *C. difficile* detection increasing with the length of stay in these units.

In infants <1 month of age, *C. difficile* has an average colonization rate of 37%, ranging between 0 and 61%. Between 1 and 6 months of age, the colonization rate is still high at 30% and drops to about 10% by the end of the first year of life (Kuiper et al., 2017). However, the colonization rates reported by different studies vary from 14 to 71% in children <12 months of age. This age group is most commonly colonized with non-toxigenic strains and they are asymptomatic (Khalaf et al., 2012). The asymptomatic carriage rate continues to drop until about 3 years of age, when it stabilizes to carriage rates of 0–3%, similar to those found in adults, together with a progressive raise in serum IgG antibody concentrations against toxins A and B between birth and 24 months of age (Antonara and Leber, 2016). Around 3 years of age, the intestinal microbiota of the child is stabilized, acquiring the characteristics of the adult microbiota, which might explain the increase of symptomatic CDI starting with this age.

Moreover, other studies are assuming that asymptomatic carriage of *C. difficile* is common in the young individuals of many other species, including dogs, pigs, and cattle (Deng and Swanson, 2015). In puppies, the association between lower bacterial community diversity and *C. difficile* colonization was statistically significant, and certain bacterial taxa were preferentially associated with *C. difficile* colonization (Berry et al., 2019). Similar associations have also been found in human studies. Unweaned puppies that were not colonized with *C. difficile* had higher relative abundance of taxa from the

clostridia genera than unweaned puppies that were colonized with *C. difficile* (Berry et al., 2019).

Many studies have found higher colonization rates with *C. difficile* in formula-fed infants than in breastfed infants (Cooperstock et al., 1983; Jangi and Lamont, 2010). Also, the breastfed infants colonized by *C. difficile* had significantly lower colony counts than formula-fed infants, probably because the human colostrum contains neutralizing antibodies to toxins A and B (Rolfe and Song, 1995; Jangi and Lamont, 2010).

There are no studies comparing *C. difficile* carriage rate regarding the delivery mode, but it might have persistent effects on microbiota beyond infancy. The lack of "bacterial baptism" of vaginal birth or other confounding factors associated with cesarean delivery, as well as maternal obesity, antibiotic administration, gestational age and breastfeeding pattern, could influence the *C. difficile* carriage rate (Kyne et al., 2000; Liu et al., 2019). However, there were found a significantly higher number of Clostridia in the stool of children vaginally delivered (VD) than in those delivered by C-section (CS) (Reyman et al., 2019). No association was found with prematurity as a risk factor for *C. difficile* infection (Lees et al., 2016).

The question arises whether the newborns and adults, which are asymptomatic carriers of *C. difficile,* might have a particular gut microbiota composition that allows colonization to occur without any clinical manifestations. Lack of disease has also been related to immature or diminished receptor sites for toxin A along the intestinal epithelium (Keel and Songer, 2007). In exchange, CDI may be more likely to manifest in certain populations of infants harboring pathological intestinal conditions, such as those with Hirschsprung's disease, all these demonstrating the link between *C. difficile* colonization and intestinal homeostasis (Sammons et al., 2013).

In conclusion, the high carriage rate of *C. difficile* colonization in neonates can be explained by the immaturity of the neonatal intestine and the presence of a less complex intestinal microbiota, as compared to adults. However, postnatal microbial species, together with the lack of receptors for clostridial toxins protect help babies from the deleterious effects of *C. difficile* toxins.

Neonate Gut Microbiota Signatures Associated With *C. difficile* Colonization

Considering that *C. difficile* only occasionally produces clinical manifestations in infants, one can state that a specific microbiota composition probably consolidating a specific environment in newborns helps protect babies from the deleterious effects of *C. difficile* toxins, which occur in dysbiotic adults.

The newborn microbiota is dominated by Gram-positive cocci, *Enterobacteriaceae* or *Bifidobacteriaceae*, with a sequential transition to a microbiota dominated by *Bifidobacteriaceae*. It is well known that *Bifidobacteria* upregulate IL-10 production by intestinal dendritic cells explaining the lack of clinical symptoms in infants colonized with *C. difficile* (Huurre et al., 2008). In CS neonates, decreased levels of T cells and CD4+ helper T cells were noticed, probably due to the failure of the immature infant immune system to activate an inflammatory response (Jangi and Lamont, 2010; Collins and Auchtung, 2017; Francino, 2018).

Prematurity might not be a risk factor for *C. difficile* infection (Lees et al., 2016), probably due to the fact that in general, the intestinal microbiota of the premature child is dominated by *Proteobacteria*, even if breastfed, and the species of *Clostridium* and *Veillonella* appear later. However, the microbiota of the premature infant is strongly influenced by pre- and postnatal antibiotic therapy (Staude et al., 2018). Hospitalization and antibiotic exposure induce indigenous microbiota imbalance (McFarland et al., 2016). Antibiotic treatment in neonate's intensive care units (NICU) was associated with a lower *C. difficile* colonization rate, but colonization with *C. difficile* occurred rapidly after cessation of antibiotics. In children in the NICU, born prematurely, the colonization with *Bifidobacteriaceae* is delayed.

Breast milk protects against infections in infants due to the presence of immunological factors such as immunoglobulin A (IgA), including neutralizing antibodies to *C. difficile* toxins A and B (Jangi and Lamont, 2010). *Ruminococcus* (which is more commonly found in the gut of breastfed infants) is thought to inhibit the growth of *Clostridia*, thereby preventing colonization by *C. difficile* (Morelli, 2008).

Increased levels of immunoglobulin-producing cells in peripheral blood have been observed in CS infants, probably due to excessive exposure to antigens at the level of the vulnerable intestinal barrier. In addition, breastfeeding contributes to the maturation of the infant's immune system and modulates microbiota development. The microbiota of breastfed children is less diverse but contains more *Bifidobacterium spp*., also explaining the protection against deleterious pro-inflammatory responses triggered by CDI (Derrien et al., 2019). However, *Bifidobacteria* significantly decrease in abundance upon cessation of breastfeeding.

In the clinical cases of neonate necrotizing enterocolitis (NEC), a decrease of bacterial diversity and of *Bacteroidetes* and *Firmicutes* phyla, as well as of *Bifidobacteria,* were observed, with the more frequent presence of potentially pathogenic organisms, such as *Staphylococcus aureus, Enterococcus*, *Escherichia coli, Shigella spp., Citrobacter spp., Klebsiella spp.* (Dobbler et al., 2017). Among the strictly anaerobic bacteria that have been associated with NEC, the majority belong to the *Clostridium* genus (e.g., *C. butyricum, C. neonatale, C. perfringens, C. paraputrificum, and C. difficile* have been associated with NEC in preterm neonates) (Zhou et al., 2015; Rozé et al., 2017; Schönherr-Hellec et al., 2018; Schönherr-Hellec and Aires, 2019). Moreover, a NEC-associated microbiota, such as *C. perfringens* has been identified in meconium samples (Heida et al., 2016).

MANIPULATION OF GUT MICROBIOTA AS ADJUNCTIVE THERAPY OF *C. difficile* INFECTION

The first step in *C. difficile* treatment is the de-escalation of antibiotic treatment. Depending on the degree of *C. difficile* risk induction, the antibiotics were divided into three groups: high (fluoroquinolones, 2nd and 3rd generation cephalosporins, clindamycin, ampicillin, broad-spectrum

TABLE 2 | Microbiota-centered therapeutic approaches with proven beneficial effects in CDI.

Type of microbiota-targeted intervention	Administration methods	Effects	References
Probiotics/prebiotics/synbiotics			
Lactobacillus plantarum Inducia	Use of xylitol as symbiotic to enhance the probiotic engraftment and effects	Total inhibition of *C. difficile* spores germination *in vitro*; reduction of mouse mortality	Ratsep et al., 2017
Bifidobacterium longum Bifidobacterium breve	Use oligo-fructosaccharides as a carbon source (symbiotic effect)	Reduction in toxicity	Valdes-Varela et al., 2016
Bacillus clausii O/C	Administered alone	Neutralization of *C. difficile* toxin inhibition of *C. difficile* toxins by bacterial secreted compounds (serine protease, M-protease)	Ripert et al., 2016; Aktories et al., 2017
Bacillus thuringiensis	Administered alone	Production of bacteriocin direct inhibition	Mills et al., 2018
Enterococcus durans	Administered alone and with bacteriocins (reuterin, nisin)	Production of durancin	Hanchi et al., 2017
Lactobacillus reuteri	Administered alone	Direct inhibition production of antibacterial substances such as reuterin obtained through fermentation of glycerol	Spinler et al., 2017
Multi-strain capsule (*Lactobacillus acidophilus NCFM, ATCC 700396; Lactobacillus paracasei Lpc-37, ATCC SD5275; Bifidobacterium lactis Bi-07, ATCC SC5220; B. lactis Bl-04, ATCC SD5219*)	Administered as multi-strain capsule	Probiotic adjunct therapy was associated with a significant improvement in diarrhea outcomes	Barker et al., 2017
Spores of *Firmicutes* phylum (e.g., SER-109; SER-262)	Administration of purified spores	Repopulation the gut microbiota	Khanna et al., 2016; Gnocchi et al., 2020
Postbiotics			
Filtered fecal supernatant	Administration of microbe-free fecal filtrates	Rapid shifts in gut microbial composition	Kelly et al., 2016; Hota et al., 2017; Ott et al., 2017
Competition for resources			
Non-toxigenic *C. difficile* (NTCD)			Gerding et al., 2015
Fecal microbiota transplantation			
Consortia of fecal bacteria quality-controlled and semi-standardized (e.g., RBX2660)	Use of fecal derivatives for the treatment of CDI	Repopulation of the gut microbiota	Orenstein et al., 2016

penicillins with inhibitors, except for ticarcillin with clavulanate, and piperacillin with tazobactam), moderate (macrolides, trimethoprim/sulfamethoxazole, other penicillins, and sulfonamides) and low risk (aminoglycosides, bacitracin, carbapenems, chloramphenicol, daptomycin, metronidazole, rifampicin, teicoplanin, tigecycline, tetracycline, and vancomycin) (Kukla et al., 2020). Current standard treatment for CDI involves treatment with antibiotics such as metronidazole, vancomycin, or fidaxomicin (Mills et al., 2018; Gnocchi et al., 2020). Vancomycin is the first-line antibiotic therapy for both first episode of infection and fulminant infections in adults (Esposito et al., 2015; Wang et al., 2020). Unfortunately, vancomycin is a strong disruptor of gut microbiota, while the rate of CDI recurrence after treatment cessation occurs in 20–30% of patients (Lessa et al., 2015; Winston and Theriot, 2016). On the other hand, metronidazole is used especially in the first episodes of mild acute CDI and less for severe disease because the concentrations in the colon become readily undetectable due to the fact that it is absorbed very quickly (Gnocchi et al., 2020). The rapid absorption from the gut is also reflected in a negligible effect on normal microbiota (Lessa et al., 2015; Chilton et al., 2018). Fidaxomicin can be used in *C. difficile* non-severe and also severe infections treatment due to the fact that it is poorly absorbed at the intestinal level, ensuring the persistence of killing concentration in the gut and has a narrow antimicrobial spectrum (e.g., Gram-positive and Gram-negative anaerobes and facultative aerobes) unaffecting the equilibrium of the normal intestinal microbiota (Tannock et al., 2010; Louie et al., 2011, 2012; Gnocchi et al., 2020). Moreover, in another study, vancomycin and metronidazole treatment, but not fidaxomicin were associated with the potentially pathogenic fungal operational taxonomic units' emergence as well as with bacterial functions enriched for xenobiotic metabolism that could contribute to dysbiosis that could favor the occurrence, persistence and recurrence of CDI (Lamendella et al., 2018).

Adjunctive therapies are frequently used due to the important role of gut microbiota disturbances in *C. difficile* pathogenesis (**Table 1** and **Figure 1**). Thus, specific manipulation of the microbiota to ameliorate dysbiotic changes and restore intestinal microbiota homeostasis could represent an essential part of the therapy (**Table 2**).

One way to modulate microbiota is using "biotics" with beneficial impact on resident microbiota that confer health benefits for the host, such as probiotics (e.g., *Saccharomyces boulardii, Lactobacillus*, *Bifidobacterium,* and probiotic mixtures), prebiotics, symbiotics or postbiotics

(Surawicz et al., 2000; Na and Kelly, 2011; Maziade et al., 2015; Collins and Auchtung, 2017). According to International Scientific Association for Probiotics and Prebiotics (ISAPP)[1], prebiotics are substrates different from fibers, that are selectively metabolized by host microorganisms. Synbiotics are complementary/synergistic mixtures comprising live microorganisms (probiotics) and prebiotics. In case of synergistics synbiotics the two components taken individually do not have to meet criteria for prebiotic or probiotic. Postbiotics are cellular fractions or structures prepared from inactivated microbes. The postbiotic preparations exclude filtrates or live cultures individual components, while inactivated probiotics are not considered automatically postbiotics, unless a health benefit is demonstrated.

Most data regarding the protective role of commensal bacteria against *C. difficile* infection were obtained by studying the effects of different probiotics. For example, *Bifidobacterium breve* (YH68), widely used in the field of food fermentation and biomedicine, has shown antibacterial activity against *C. difficile*, by inhibiting the growth, spore production, toxigenesis and virulence gene expression (Valdes-Varela et al., 2016; Yang and Yang, 2019), potentiating the effect of anti-*C. difficile* antibiotics *in vitro* (Yang and Yang, 2018) or preventing the occurrence of clinical manifestations *in vivo* (Yun et al., 2017). Probiotic use has been shown to decrease CDI incidence in high-risk populations by as much as 50%, especially when they are combined with prebiotics (Shen et al., 2017).

It was demonstrated that the administration of non-living bacteria or microbial components (e.g., proteins, lipids, or nucleic acids) has an immunostimulatory effect proving that the beneficial impact on the host health is due to the physical interaction of specific microbial components, but in order to be effective for a long period, these need continuous administration.

Many bacterial strains such as *Bacillus clausii* and *Lactobacillus reuteri* have been shown to secrete soluble compounds that directly inhibit *C. difficile* (Khalaf et al., 2012; Deng and Swanson, 2015; Antonara and Leber, 2016). Organisms that produce secondary bile acids, such as *Clostridium scindens*, enhance *C. difficile* colonization resistance (Winston and Theriot, 2016).

Fecal microbiota transplantation (FMT) is considered the most effective microbiota-targeted intervention for the treatment of antibiotic-refractory CDI (Arbel et al., 2017), but however, the long-term effects, including the risk of other diseases, are not known (Schaffler and Breitruck, 2018).

[1] https://isappscience.org/a-roundup-of-the-isapp-consensus-definitions-probiotics-prebiotics-synbiotics-postbiotics-and-fermented-foods/

Another therapeutic approach is the administration of non-toxigenic *C. difficile* strains or a mixture of spore-forming commensals, which act by providing nutritional niche competition. Despite their efficiency in decreasing CDI recurrence, there is the risk of switching to the toxigenic phenotype (Brouwer et al., 2013; Khanna et al., 2016).

CONCLUSION

The available studies suggest that *C. difficile* colonization and infection are influenced by the presence, absence or abundance of certain bacteria in the human gut, which could generate favorable conditions for germination, proliferation and production of clostridial toxins which, on their turn, will alter the integrity of the intestinal mucosa. Therefore, the clinical manifestations and severity of CDI are linked to gut dysbiosis, that could have multiple causes, among which the administration of high-risk antibiotics. The presence of protective microbial species, together with the particularities of the immune system and lack of receptors for clostridial toxins could explain the fact that in children, despite the high carriage rate, the symptomatic and severe cases are rare. However, if there is a gut microbiota composition predisposing to *C. difficile* asymptomatic carriage or clinical infection still needs clarification. Also, the mechanisms involved in *C. difficile* crosstalk with the commensal microbiota and/or particular soluble compounds remain only partially explained. Adjunctive microbiota-targeting therapies based on probiotics, prebiotics, postbiotics, synbiotics, non-toxigenic bacteria or fecal microbiota transplantation proved to be very useful for the therapeutic management of CDI.

AUTHOR CONTRIBUTIONS

All authors contributed equally to this manuscript with the conception and design of the study, literature review and analysis, drafting and critical revision and editing, and final approval of the final version.

FUNDING

This research was funded by the Research Projects PN-III-P4-ID-PCCF-2016-0114, C1.2.PFE-CDI.2021-587, and CNFIS-FDI-2021-0405 awarded to M-CC.

REFERENCES

Abt, M. C., McKenney, P. T., and Pamer, E. G. (2016). *Clostridium difficile* colitis: pathogenesis and host defence. *Nat. Rev. Microbiol.* 14, 609–620. doi: 10.1038/nrmicro.2016.108

Akagawa, S., Tsuji, S., Onuma, C., Akagawa, Y., Yamaguchi, T., Yamagishi, M., et al. (2019). Effect of delivery mode and nutrition on gut microbiota in neonates. *Ann. Nutr. Metab.* 74, 132–139. doi: 10.1159/000496427

Aktories, K., Schwan, C., and Jank, T. (2017). *Clostridium difficile* toxin biology. *Annu. Rev. Microbiol.* 71, 281–307.

Amrane, S., Hocquart, M., Afouda, P., Kuete, E., Pham, T. P., Dione, N., et al. (2019). Metagenomic and culturomic analysis of gut microbiota dysbiosis during *Clostridium difficile* infection. *Sci. Rep.* 9:12807. doi: 10.1038/s41598-019-49189-8

Antharam, V. C., Li, E. C., Ishmael, A., Sharma, A., Mai, V., Rand, K. H., et al. (2013). Intestinal dysbiosis and depletion of butyrogenic bacteria in *Clostridium*

difficile infection and nosocomial diarrhea. *J. Clin. Microbiol.* 51, 2884–2892. doi: 10.1128/JCM.00845-13

Antonara, S., and Leber, A. L. (2016). Diagnosis of *Clostridium difficile* infections in children. *J. Clin. Microbiol.* 54, 1425–1433.

Arbel, L. T., Hsu, E., and McNally, K. (2017). Cost-effectiveness of fecal microbiota transplantation in the treatment of recurrent *Clostridium difficile* infection: a literature review. *Cureus* 9:e1599.

Arboleya, S., Sanchez, B., Milani, C., Duranti, S., Solis, G., Fernandez, N., et al. (2015). Intestinal microbiota development in preterm neonates and effect of perinatal antibiotics. *J. Pediatr.* 166, 538–544. doi: 10.1016/j.jpeds.2014.09.041

Avni, T., Babitch, T., Ben-Zvi, H., Hijazi, R., Ayada, G., Atamna, A., et al. (2020). Clostridioides difficile infection in immunocompromised hospitalized patients is associated with a high recurrence rate. *Int. J. infect. Dis.* 90, 237–242. doi: 10.1016/j.ijid.2019.10.028

Barker, A. K., Duster, M., Valentine, S., Hess, T., Archbald-Pannone, L., Guerrant, R., et al. (2017). A randomized controlled trial of probiotics for *Clostridium difficile* infection in adults (PICO). *J. Antimicrob. Chemother.* 72, 3177–3180. doi: 10.1093/jac/dkx254

Battaglioli, E. J., Hale, V. L., Chen, J., Jeraldo, P., Ruiz-Mojica, C., Schmidt, B. A., et al. (2018). Clostridioides difficile uses amino acids associated with gut microbial dysbiosis in a subset of patients with diarrhea. *Sci. Transl. Med.* 10:eaam7019. doi: 10.1126/scitranslmed.aam7019

Berkell, M., Mysara, M., Xavier, B. B., van Werkhoven, C. H., Monsieurs, P., Lammens, C., et al. (2021). Microbiota-based markers predictive of development of Clostridioides difficile infection. *Nat. Commun.* 12:2241. doi: 10.1038/s41467-021-22302-0

Berry, A. S. F., Kelly, B. J., Barnhart, D., Kelly, D. J., Beiting, D. P., Baldassano, R. N., et al. (2019). Gut microbiota features associated with Clostridioides difficile colonization in puppies. *PLoS One* 14:e0215497. doi: 10.1371/journal.pone.0215497

Borali, E., and De Giacomo, C. (2016). *Clostridium Difficile* infection in children: a review. *J. Pediatr. Gastroenterol. Nutr.* 63, e130–e140.

Britton, R. A., and Young, V. B. (2014). Role of the intestinal microbiota in resistance to colonization by *Clostridium difficile*. *Gastroenterology* 146, 1547–1553.

Brouwer, M. S., Roberts, A. P., Hussain, H., Williams, R. J., Allan, E., and Mullany, P. (2013). Horizontal gene transfer converts non-toxigenic *Clostridium difficile* strains into toxin producers. *Nat. Commun.* 4:2601. doi: 10.1038/ncomms3601

Buffie, C. G., Bucci, V., Stein, R. R., McKenney, P. T., Ling, L., Gobourne, A., et al. (2015). Precision microbiome reconstitution restores bile acid mediated resistance to *Clostridium difficile*. *Nature* 517, 205–208. doi: 10.1038/nature13828

Cama, V., Pieragostini, L., Fontanelli, G., Velletri, M. R., and Mariarosa, C. (2019). *Clostridium difficile* severe infection in a newborn. *Arch. Dis. Child.* 104, A311.

Carding, S., Verbeke, K., Vipond, D. T., Corfe, B. M., and Owen, L. J. (2015). Dysbiosis of the gut microbiota in disease. *Microb. Ecol. Health Dis.* 26:26191.

Chang, J. Y., Antonopoulos, D. A., Kalra, A., Tonelli, A., Khalife, W. T., Schmidt, T. M., et al. (2008). Decreased diversity of the fecal microbiome in recurrent *Clostridium difficile*-associated diarrhea. *J. Infect. Dis.* 197, 435–438. doi: 10.1086/525047

Chilton, C. H., Pickering, D. S., and Freeman, J. (2018). Microbiologic factors affecting *Clostridium difficile* recurrence. *Clin. Microbiol. Infect.* 24, 476–482. doi: 10.1016/j.cmi.2017.11.017

Chong, C. Y. L., Bloomfield, F. H., and O'Sullivan, J. M. (2018). Factors affecting gastrointestinal microbiome development in neonates. *Nutrients* 10:274. doi: 10.3390/nu10030274

Collins, J., and Auchtung, J. M. (2017). Control of *Clostridium difficile* infection by defined microbial communities. *Microbiol. Spectr.* 5, 1–25.

Combellick, J. L., Shin, H., Shin, D., Cai, Y., Hagan, H., Lacher, C., et al. (2018). Differences in the fecal microbiota of neonates born at home or in the hospital. *Sci. Rep.* 8:15660.

Cooperstock, M., Riegle, L., Woodruff, C. W., and Onderdonk, A. (1983). Influence of age, sex, and diet on asymptomatic colonization of infants with *Clostridium difficile*. *J. Clin. Microbiol.* 17, 830–833. doi: 10.1128/jcm.17.5.830-833.1983

Crobach, M. J. T., Ducarmon, Q. R., Terveer, E. M., Harmanus, C., Sanders, I. M. J. G., Verduin, K. M., et al. (2020). The bacterial gut microbiota of adult patients infected, colonized or noncolonized by *Clostridioides difficile*. *Microorganisms* 8:677. doi: 10.3390/microorganisms8050677

Czepiel, J., Drozdz, M., Pituch, H., Kuijper, E. J., Perucki, W., Mielimonka, A., et al. (2019). *Clostridium difficile* infection: review. *Eur. J. Clin. Microbiol. Infect. Dis.* 38, 1211–1221.

Darkoh, C., Plants-Paris, K., Bishoff, D., and DuPont, H. L. (2019). *Clostridium difficile* modulates the gut microbiota by inducing the production of indole, an interkingdom signaling and antimicrobial molecule. *mSystems* 4, e00346–e00318. doi: 10.1128/mSystems.00346-18

den Besten, G., van Eunen, K., Groen, A. K., Venema, K., Reijngoud, D. J., and Bakker, B. M. (2013). The role of short-chain fatty acids in the interplay between diet, gut microbiota, and host energy metabolism. *J. Lipid Res.* 54, 2325–2340. doi: 10.1194/jlr.R036012

Deng, P., and Swanson, K. S. (2015). Gut microbiota of humans, dogs and cats: current knowledge and future opportunities and challenges. *Br. J. Nutr.* 113(Suppl.), S6–S17. doi: 10.1017/S0007114514002943

Depestel, D. D., and Aronoff, D. M. (2013). Epidemiology of *Clostridium difficile* infection. *J. Pharm. Pract.* 26, 464–475.

Derrien, M., Alvarez, A. S., and de Vos, W. M. (2019). The gut microbiota in the first decade of life. *Trends Microbiol.* 27, 997–1010. doi: 10.1016/j.tim.2019.08.001

Dieterle, M. G., Rao, K., and Young, V. B. (2019). Novel therapies and preventative strategies for primary and recurrent *Clostridium difficile* infections. *Ann. N.Y. Acad. Sci.* 1435, 110–138. doi: 10.1111/nyas.13958

Dobbler, P. T., Procianoy, R. S., Mai, V., Silveira, R. C., Corso, A. L., Rojas, B. S., et al. (2017). Low microbial diversity and abnormal microbial succession is associated with necrotizing enterocolitis in preterm infants. *Front. Microbiol.* 8:2243. doi: 10.3389/fmicb.2017.02243

Dogra, S. K., Dore, J., and Damak, S. (2020). Gut microbiota resilience: definition, link to health and strategies for intervention. *Front. Microbiol.* 11:572921. doi: 10.3389/fmicb.2020.572921

Dupont, H. L. (2011). Gastrointestinal infections and the development of irritable bowel syndrome. *Curr. Opin. Infect. Dis.* 24, 503–508. doi: 10.1097/QCO.0b013e32834a962d

Esposito, S., Umbrello, G., Castellazzi, L., and Principi, N. (2015). Treatment of *Clostridium difficile* infection in pediatric patients. *Exp. Rev. Gastroenterol. Hepatol.* 9, 747–755. doi: 10.1586/17474124.2015.1039988

Fachi, J. L., Felipe, J. S., Pral, L. P., da Silva, B. K., Correa, R. O., de Andrade, M. C. P., et al. (2019). Butyrate protects mice from *Clostridium difficile*-induced colitis through an HIF-1-dependent mechanism. *Cell Rep.* 27, 750–761.e7. doi: 10.1016/j.celrep.2019.03.054

Faith, J. J., Guruge, J. L., Charbonneau, M., Subramanian, S., Seedorf, H., Goodman, A. L., et al. (2013). The long-term stability of the human gut microbiota. *Science* 341:1237439.

Fashner, J., Garcia, M., Ribble, L., and Crowell, K. (2011). Clinical inquiry: what risk factors contribute to C difficile diarrhea? *J. Family Pract.* 60, 545–547.

Ferraris, L., Couturier, J., Eckert, C., Delannoy, J., Barbut, F., Butel, M. J., et al. (2020). Carriage and colonization of C. difficile in preterm neonates: a longitudinal prospective study. *PLoS One* 14:e0212568. doi: 10.1371/journal.pone.0212568

Folke, C., Carpenter, S., Walker, B., Scheffer, M., Elmqvist, T., Gunderson, L., et al. (2004). Regime shifts, resilience, and biodiversity in ecosystem management. *Annu. Rev. Ecol. Evol. Syst.* 35, 557–581.

Francino, M. P. (2018). Birth mode-related differences in gut microbiota colonization and immune system development. *Ann. Nutr. Metab.* 73(Suppl. 3), 12–16. doi: 10.1159/000490842

Franzosa, E. A., Sirota-Madi, A., Avila-Pacheco, J., Fornelos, N., Haiser, H. J., Reinker, S., et al. (2019). Gut microbiome structure and metabolic activity in inflammatory bowel disease. *Nat. Microbiol.* 4, 293–305.

Gerding, D. N., Meyer, T., Lee, C., Cohen, S. H., Murthy, U. K., Poirier, A., et al. (2015). Administration of spores of nontoxigenic *Clostridium difficile* strain M3 for prevention of recurrent C. difficile infection: a randomized clinical trial. *JAMA* 313, 1719–1727. doi: 10.1001/jama.2015.3725

Gevers, D., Kugathasan, S., Denson, L. A., Vazquez-Baeza, Y., Van Treuren, W., Ren, B., et al. (2014). The treatment-naive microbiome in new-onset Crohn's disease. *Cell Host Microbe* 15, 382–392.

Ghose, C. (2013). *Clostridium difficile* infection in the twenty-first century. *Emerg. Microbes Infect.* 2:e62. doi: 10.1038/emi.2013.62

Gnocchi, M., Gagliardi, M., Gismondi, P., Gaiani, F., De' Angelis, G. L., and Esposito, S. (2020). Updated management guidelines for Clostridioides difficile in paediatrics. *Pathogens* 9:291. doi: 10.3390/pathogens9040291

Goethel, A., Turpin, W., Rouquier, S., Zanello, G., Robertson, S. J., Streutker, C. J., et al. (2019). Nod2 influences microbial resilience and susceptibility to colitis following antibiotic exposure. *Mucosal Immunol.* 12, 720–732. doi: 10.1038/s41385-018-0128-y

Goh, Y. J., and Klaenhammer, T. R. (2015). Genetic mechanisms of prebiotic oligosaccharide metabolism in probiotic microbes. *Annu. Rev. Food Sci. Technol.* 6, 137–156. doi: 10.1146/annurev-food-022814-015706

Gough, E., Shaikh, H., and Manges, A. R. (2011). Systematic review of intestinal microbiota transplantation (Fecal Bacteriotherapy) for recurrent *Clostridium difficile* infection. *Clin. Infect. Dis.* 53, 994–1002. doi: 10.1093/cid/cir632

Gschwind, R., Fournier, T., Kennedy, S., Tsatsaris, V., Cordier, A. G., Barbut, F., et al. (2020). Evidence for contamination as the origin for bacteria found in human placenta rather than a microbiota. *PLoS One* 15:e0237232. doi: 10.1371/journal.pone.0237232

Guilloteau, P., Martin, L., Eeckhaut, V., Ducatelle, R., Zabielski, R., and Van Immerseel, F. (2010). From the gut to the peripheral tissues: the multiple effects of butyrate. *Nutr. Res. Rev.* 23, 366–384. doi: 10.1017/S0954422410000247

Gupta, P., Yakubov, S., Tin, K., Zea, D., Garankina, O., Ghitan, M., et al. (2016). Does alkaline colonic pH predispose to *Clostridium difficile* infection? *Southern Med. J.* 109, 91–96. doi: 10.14423/SMJ.0000000000000414

Hamilton, M. J., Weingarden, A. R., Unno, T., Khoruts, A., and Sadowsky, M. J. (2013). High-throughput DNA sequence analysis reveals stable engraftment of gut microbiota following transplantation of previously frozen fecal bacteria. *Gut Microbes* 4, 125–135.

Han, S. H., Yi, J., Kim, J. H., and Moon, A. H. (2020). Investigation of intestinal microbiota and fecal calprotectin in non-toxigenic and toxigenic *Clostridioides difficile* colonization and infection. *Microorganisms* 8:882. doi: 10.3390/microorganisms8060882

Hanchi, H., Hammami, R., Gingras, H., Kourda, R., Bergeron, M. G., Ben Hamida, J., et al. (2017). Inhibition of MRSA and of *Clostridium difficile* by durancin 61A: synergy with bacteriocins and antibiotics. *Future Microbiol.* 12, 205–212. doi: 10.2217/fmb-2016-0113

Hatziioanou, D., Gherghisan-Filip, C., Saalbach, G., Horn, N., Wegmann, U., Duncan, S. H., et al. (2017). Discovery of a novel lantibiotic nisin O from Blautia obeum A2-162, isolated from the human gastrointestinal tract. *Microbiology* 163, 1292–1305. doi: 10.1099/mic.0.000515

Heida, F. H., van Zoonen, A. G. J. F., Hulscher, J. B. F., Te Kiefte, B. J. C., Wessels, R., Kooi, E. M. W., et al. (2016). A necrotizing enterocolitis-associated gut microbiota is present in the meconium: results of a prospective study. *Clin. Infect. Dis.* 62, 863–870. doi: 10.1093/cid/ciw016

Hensgens, M. P., Goorhuis, A., van Kinschot, C. M., Crobach, M. J., Harmanus, C., and Kuijper, E. J. (2011). *Clostridium difficile* infection in an endemic setting in the Netherlands. *Eur. J. Clin. Microbiol. Infect. Dis.* 30, 587–593. doi: 10.1007/s10096-010-1127-4

Hernandez, M., de Frutos, M., Rodriguez-Lazaro, D., Lopez-Urrutia, L., Quijada, N. M., and Eiros, J. M. (2018). Fecal microbiota of toxigenic Clostridioides difficile-associated Diarrhea. *Front. Microbiol.* 9:3331. doi: 10.3389/fmicb.2018.03331

Hills, R. D. Jr., Pontefract, B. A., Mishcon, H. R., Black, C. A., Sutton, S. C., and Theberge, C. R. (2019). Gut microbiome: profound implications for diet and disease. *Nutrients* 11:1613. doi: 10.3390/nu11071613

Hota, S. S., Sales, V., Tomlinson, G., Salpeter, M. J., McGeer, A., Coburn, B., et al. (2017). Oral vancomycin followed by fecal transplantation versus tapering oral vancomycin treatment for recurrent *Clostridium difficile* infection: an open-label, randomized controlled trial. *Clin. Infect. Dis.* 64, 265–271. doi: 10.1093/cid/ciw731

Human Microbiome Project, C. (2012). Structure, function and diversity of the healthy human microbiome. *Nature* 486, 207–214. doi: 10.1038/nature11234

Huurre, A., Kalliomaki, M., Rautava, S., Rinne, M., Salminen, S., and Isolauri, E. (2008). Mode of delivery - effects on gut microbiota and humoral immunity. *Neonatology* 93, 236–240. doi: 10.1159/000111102

Jangi, S., and Lamont, J. T. (2010). Asymptomatic colonization by *Clostridium difficile* in infants: implications for disease in later life. *J. Pediatr. Gastroenterol. Nutr.* 51:2. doi: 10.1097/MPG.0b013e3181d29767

Jimenez, E., Marin, M. L., Martin, R., Odriozola, J. M., Olivares, M., Xaus, J., et al. (2008). Is meconium from healthy newborns actually sterile? *Res. Microbiol.* 159, 187–193. doi: 10.1016/j.resmic.2007.12.007

Kachrimanidou, M., and Tsintarakis, E. (2020). Insights into the role of human gut microbiota in clostridioides difficile infection. *Microorganisms* 8:200. doi: 10.3390/microorganisms8020200

Keel, M. K., and Songer, J. G. (2007). The distribution and density of *Clostridium difficile* toxin receptors on the intestinal mucosa of neonatal pigs. *Vet. Pathol.* 44, 814–822. doi: 10.1354/vp.44-6-814

Kelly, C. R., Khoruts, A., Staley, C., Sadowsky, M. J., Abd, M., Alani, M., et al. (2016). Effect of fecal microbiota transplantation on recurrence in multiply recurrent *Clostridium difficile* infection: a randomized trial. *Ann. Intern. Med.* 165, 609–616. doi: 10.7326/M16-0271

Khalaf, N., Crews, J. D., DuPont, H. L., and Koo, H. L. (2012). *Clostridium difficile*: an emerging pathogen in children. *Discov. Med.* 14, 105–113.

Khanna, S., Pardi, D. S., Kelly, C. R., Kraft, C. S., Dhere, T., Henn, M. R., et al. (2016). A novel microbiome therapeutic increases gut microbial diversity and prevents recurrent *Clostridium difficile* infection. *J. Infect. Dis.* 214, 173–181. doi: 10.1093/infdis/jiv766

Kho, Z. Y., and Lal, S. K. (2018). The Human gut microbiome - a potential controller of wellness and disease. *Front. Microbiol.* 9:1835. doi: 10.3389/fmicb.2018.01835

Khoruts, A., Dicksved, J., Jansson, J. K., and Sadowsky, M. J. (2010). Changes in the composition of the human fecal microbiome after bacteriotherapy for recurrent *Clostridium difficile*-associated diarrhea. *J. Clin. Gastroenterol.* 44, 354–360. doi: 10.1097/MCG.0b013e3181c87e02

Kuiper, G. A., van Prehn, J., Ang, W., Kneepkens, F., van der Schoor, S., and de Meij, T. (2017). *Clostridium difficile* infections in young infants: case presentations and literature review. *IDCases* 10, 7–11. doi: 10.1016/j.idcr.2017.07.005

Kukla, M., Adrych, K., Dobrowolska, A., Mach, T., Regula, J., and Rydzewska, G. (2020). Guidelines for *Clostridium difficile* infection in adults. *Prz. Gastroenterol.* 15, 1–21. doi: 10.5114/pg.2020.93629

Kyne, L., Warny, M., Qamar, A., and Kelly, C. P. (2000). Asymptomatic carriage of *Clostridium difficile* and serum levels of IgG antibody against toxin A. *N. Engl. J. Med.* 342, 390–397. doi: 10.1056/NEJM200002103420604

Lamendella, R., Wright, J. R., Hackman, J., McLimans, C., Toole, D. R., Bernard Rubio, W., et al. (2018). Antibiotic treatments for *Clostridium difficile* infection are associated with distinct bacterial and fungal community structures. *mSphere* 3, e00572-17 . doi: 10.1128/mSphere.00572-17

Lawler, A. J., Lambert, P. A., and Worthington, T. (2020). A revised understanding of Clostridioides difficile spore germination. *Trends Microbiol.* 28, 744–752. doi: 10.1016/j.tim.2020.03.004

Lazar, V., Ditu, L. M., Pircalabioru, G. G., Gheorghe, I., Curutiu, C., Holban, A. M., et al. (2018). Aspects of gut microbiota and immune system interactions in infectious diseases, immunopathology, and cancer. *Front. Immunol.* 9:1830. doi: 10.3389/fimmu.2018.01830

Lazar, V., Ditu, L. M., Pircalabioru, G. G., Picu, A., Petcu, L., Cucu, N., et al. (2019). Gut microbiota, host organism, and diet trialogue in diabetes and obesity. *Front. Nutr.* 6:21. doi: 10.3389/fnut.2019.00021

Lees, E. A., Miyajima, F., Pirmohamed, M., and Carrol, E. D. (2016). The role of *Clostridium difficile* in the paediatric and neonatal gut - a narrative review. *Eur. J. Clin. Microbiol. Infect. Dis.* 35, 1047–1057. doi: 10.1007/s10096-016-2639-3

Lessa, F. C., Mu, Y., Bamberg, W. M., Beldavs, Z. G., Dumyati, G. K., Dunn, J. R., et al. (2015). Burden of *Clostridium difficile* infection in the United States. *N. Engl. J. Med.* 372, 825–834.

Levine, J. M., and d'Antonio, C. M. (1999). Elton revisited: a review of evidence linking diversity and invasibility. *Oikos* 87, 15–26.

Liu, Y., Qin, S., Song, Y., Feng, Y., Lv, N., Xue, Y., et al. (2019). The perturbation of infant gut microbiota caused by cesarean delivery is partially restored by exclusive breastfeeding. *Front. Microbiol.* 10:598. doi: 10.3389/fmicb.2019.00598

Lo Presti, A., Zorzi, F., Del Chierico, F., Altomare, A., Cocca, S., Avola, A., et al. (2019). Fecal and mucosal microbiota profiling in irritable bowel syndrome and inflammatory bowel disease. *Front. Microbiol.* 10:1655. doi: 10.3389/fmicb.2019.01655

Louie, T. J., Cannon, K., Byrne, B., Emery, J., Ward, L., Eyben, M., et al. (2012). Fidaxomicin preserves the intestinal microbiome during and after treatment of

Clostridium difficile infection (CDI) and reduces both toxin reexpression and recurrence of CDI. *Clin. Infect. Dis.* 55(Suppl. 2), S132–S142. doi: 10.1093/cid/cis338

Louie, T. J., Miller, M. A., Mullane, K. M., Weiss, K., Lentnek, A., Golan, Y., et al. (2011). Fidaxomicin versus vancomycin for *Clostridium difficile* infection. *N. Engl. J. Med.* 364, 422–431.

Lozupone, C. A., Stombaugh, J. I., Gordon, J. I., Jansson, J. K., and Knight, R. (2012). Diversity, stability and resilience of the human gut microbiota. *Nature* 489, 220–230. doi: 10.1038/nature11550

Magne, F., Gotteland, M., Gauthier, L., Zazueta, A., Pesoa, S., Navarrete, P., et al. (2020). The firmicutes/bacteroidetes ratio: a relevant marker of gut dysbiosis in obese patients? *Nutrients* 12:1474. doi: 10.3390/nu12051474

Maziade, P. J., Pereira, P., and Goldstein, E. J. (2015). A decade of experience in primary prevention of *Clostridium difficile* infection at a community hospital using the probiotic combination *Lactobacillus acidophilus* CL1285, *Lactobacillus casei* LBC80R, and *Lactobacillus rhamnosus* CLR2 (Bio-K+). *Clin. Infect. Dis.* 60(Suppl. 2), S144–S147. doi: 10.1093/cid/civ178

McBurney, M. I., Davis, C., Fraser, C. M., Schneeman, B. O., Huttenhower, C., Verbeke, K., et al. (2019). Establishing what constitutes a healthy human gut microbiome: state of the science, regulatory considerations, and future directions. *J. Nutr.* 149, 1882–1895. doi: 10.1093/jn/nxz154

McDonald, L. C., Gerding, D. N., Johnson, S., Bakken, J. S., Carroll, K. C., Coffin, S. E., et al. (2018). Clinical practice guidelines for *Clostridium difficile* infection in adults and children: 2017 update by the Infectious Diseases Society of America (IDSA) and Society for Healthcare Epidemiology of America (SHEA). *Clin. Infect. Dis.* 66, e1–e48.

McFarland, L. V., Ozen, M., Dinleyici, E. C., and Goh, S. (2016). Comparison of pediatric and adult antibiotic-associated diarrhea and *Clostridium difficile* infections. *World J. Gastroenterol.* 22, 3078–3104. doi: 10.3748/wjg.v22.i11.3078

Milani, C., Ticinesi, A., Gerritsen, J., Nouvenne, A., Lugli, G. A., Mancabelli, L., et al. (2016). Gut microbiota composition and *Clostridium difficile* infection in hospitalized elderly individuals: a metagenomic study. *Sci. Rep.* 6:25945. doi: 10.1038/srep25945

Mills, J. P., Rao, K., and Young, V. B. (2018). Probiotics for prevention of *Clostridium difficile* infection. *Curr. Opin. Gastroenterol.* 34, 3–10. doi: 10.1097/mog.0000000000000410

Mohammadkhah, A. I., Simpson, E. B., Patterson, S. G., and Ferguson, J. F. (2018). Development of the gut microbiome in children, and lifetime implications for obesity and cardiometabolic disease. *Children* 5:160. doi: 10.3390/children5120160

Mooyottu, S., Flock, G., Upadhyay, A., Upadhyaya, I., Maas, K., and Venkitanarayanan, K. (2017). Protective effect of carvacrol against gut dysbiosis and *Clostridium difficile* associated disease in a mouse model. *Front. Microbiol.* 8:625. doi: 10.3389/fmicb.2017.00625

Morelli, L. (2008). Postnatal development of intestinal microflora as influenced by infant nutrition. *J. Nutr.* 138, 1791S–1795S. doi: 10.1093/jn/138.9.1791S

Na, X., and Kelly, C. (2011). Probiotics in *Clostridium difficile* Infection. *J. Clin. Gastroenterol.* 45(Suppl.), S154–S158.

Nitzan, O., Elias, M., Chazan, B., Raz, R., and Saliba, W. (2013). *Clostridium difficile* and inflammatory bowel disease: role in pathogenesis and implications in treatment. *World J. Gastroenterol.* 19, 7577–7585. doi: 10.3748/wjg.v19.i43.7577

O'Keefe, S. J. (2010). Tube feeding, the microbiota, and *Clostridium difficile* infection. *World J. Gastroenterol.* 16, 139–142.

Orenstein, R., Dubberke, E., Hardi, R., Ray, A., Mullane, K., Pardi, D. S., et al. (2016). Safety and durability of RBX2660 (Microbiota Suspension) for recurrent *Clostridium difficile* infection: results of the PUNCH CD Study. *Clin. Infect. Dis.* 62, 596–602. doi: 10.1093/cid/civ938

Ott, S. J., Waetzig, G. H., Rehman, A., Moltzau-Anderson, J., Bharti, R., Grasis, J. A., et al. (2017). Efficacy of sterile fecal filtrate transfer for treating patients with *Clostridium difficile* infection. *Gastroenterology* 152, 799–811.e7. doi: 10.1053/j.gastro.2016.11.010

Pechal, A., Lin, K., Allen, S., and Reveles, K. (2016). National age group trends in *Clostridium difficile* infection incidence and health outcomes in United States community hospitals. *BMC Infect. Dis.* 16:682. doi: 10.1186/s12879-016-2027-8

Perez-Cobas, A. E., Moya, A., Gosalbes, M. J., and Latorre, A. (2015). Colonization resistance of the gut microbiota against *Clostridium difficile*. *Antibiotics* 4, 337–357.

Priya, S., and Blekhman, R. (2019). Population dynamics of the human gut microbiome: change is the only constant. *Genome Biol.* 20:150. doi: 10.1186/s13059-019-1775-3

Qin, J., Li, R., Raes, J., Arumugam, M., Burgdorf, K. S., Manichanh, C., et al. (2010). A human gut microbial gene catalogue established by metagenomic sequencing. *Nature* 464, 59–65. doi: 10.1038/nature08821

Rajilic-Stojanovic, M., Shanahan, F., Guarner, F., and de Vos, W. M. (2013). Phylogenetic analysis of dysbiosis in ulcerative colitis during remission. *Inflamm. Bowel Dis.* 19, 481–488. doi: 10.1097/MIB.0b013e31827fec6d

Ratsep, M., Koljalg, S., Sepp, E., Smidt, I., Truusalu, K., Songisepp, E., et al. (2017). A combination of the probiotic and prebiotic product can prevent the germination of *Clostridium difficile* spores and infection. *Anaerobe* 47, 94–103. doi: 10.1016/j.anaerobe.2017.03.019

Raymond, F., Ouameur, A. A., Déraspe, M., Iqbal, N., Gingras, H., Dridi, B., et al. (2016). The initial state of the human gut microbiome determines its reshaping by antibiotics. *ISME J.* 10, 707–720. doi: 10.1038/ismej.2015.148

Rea, M. C., O'Sullivan, O., Shanahan, F., O'Toole, P. W., Stanton, C., Ross, R. P., et al. (2012). *Clostridium difficile* carriage in elderly subjects and associated changes in the intestinal microbiota. *J. Clin. Microbiol.* 50, 867–875. doi: 10.1128/JCM.05176-11

Reeves, A. E., Koenigsknecht, M. J., Bergin, I. L., and Young, V. B. (2012). Suppression of *Clostridium difficile* in the gastrointestinal tracts of germfree mice inoculated with a murine isolate from the family Lachnospiraceae. *Infect. Immun.* 80, 3786–3794. doi: 10.1128/IAI.00647-12

Reeves, A. E., Theriot, C. M., Bergin, I. L., Huffnagle, G. B., Schloss, P. D., and Young, V. B. (2011). The interplay between microbiome dynamics and pathogen dynamics in a murine model of *Clostridium difficile* Infection. *Gut Microbes* 2, 145–158. doi: 10.4161/gmic.2.3.16333

Reyman, M., van Houten, M. A., van Baarle, D., Bosch, A., Man, W. H., Chu, M., et al. (2019). Impact of delivery mode-associated gut microbiota dynamics on health in the first year of life. *Nat. Commun.* 10:4997.

Ridlon, J. M., Kang, D. J., Hylemon, P. B., and Bajaj, J. S. (2014). Bile acids and the gut microbiome. *Curr. Opin. Gastroenterol.* 30, 332–338.

Rinninella, E., Raoul, P., Cintoni, M., Franceschi, F., Miggiano, G. A. D., Gasbarrini, A., et al. (2019). What is the healthy gut microbiota composition? A changing ecosystem across age, environment, diet, and diseases. *Microorganisms* 7:14. doi: 10.3390/microorganisms7010014

Ripert, G., Racedo, S. M., Elie, A. M., Jacquot, C., Bressollier, P., and Urdaci, M. C. (2016). Secreted compounds of the probiotic *Bacillus clausii* strain O/C inhibit the cytotoxic effects induced by *Clostridium difficile* and *Bacillus cereus* toxins. *Antimicrob. Agents Chemother.* 60, 3445–3454. doi: 10.1128/AAC.02815-15

Rodriguez, C., Romero, E., Garrido-Sanchez, L., Alcain-Martinez, G., Andrade, R. J., Taminiau, B., et al. (2020). Microbiota insights in *Clostridium difficile* infection and inflammatory bowel disease. *Gut Microbes* 12:1725220.

Rodriguez, C., Taminiau, B., Korsak, N., Avesani, V., Van Broeck, J., Brach, P., et al. (2016). Longitudinal survey of *Clostridium difficile* presence and gut microbiota composition in a Belgian nursing home. *BMC Microbiol.* 16:229. doi: 10.1186/s12866-016-0848-7

Rolfe, R. D., and Song, W. (1995). Immunoglobulin and non-immunoglobulin components of human milk inhibit *Clostridium difficile* toxin A-receptor binding. *J. Med. Microbiol.* 42, 10–19. doi: 10.1099/00222615-42-1-10

Ross, C. L., Spinler, J. K., and Savidge, T. C. (2016). Structural and functional changes within the gut microbiota and susceptibility to *Clostridium difficile* infection. *Anaerobe* 41, 37–43. doi: 10.1016/j.anaerobe.2016.05.006

Rousseau, C., Lemée, L., Le Monnier, A., Poilane, I., Pons, J. L., and Collignon, A. (2011). Prevalence and diversity of *Clostridium difficile* strains in infants. *J. Med. Microbiol.* 60(Pt. 8), 1112–1118. doi: 10.1099/jmm.0.029736-0

Rozé, J. C., Ancel, P. Y., Lepage, P., Martin-Marchand, L., Al Nabhani, Z., Delannoy, J., et al. (2017). Nutrition EPIPAGE 2 study group; EPIFLORE study group. nutritional strategies and gut microbiota composition as risk factors for necrotizing enterocolitis in very-preterm infants. *Am. J. Clin. Nutr.* 106, 821–830. doi: 10.3945/ajcn.117.152967

Sammons, J. S., Toltzis, P., and Zaoutis, T. E. (2013). *Clostridium difficile* Infection in children. *JAMA Pediatr.* 167, 567–573.

Sartelli, M., Di Bella, S., McFarland, L. V., Khanna, S., Furuya-Kanamori, L., Abuzeid, N., et al. (2019). 2019 update of the WSES guidelines for management of Clostridioides (Clostridium) difficile infection in surgical patients. *World J. Emerg. Surg.*14:8. doi: 10.1186/s13017-019-0228-3

Schaffler, H., and Breitruck, A. (2018). *Clostridium difficile* - from colonization to infection. *Front. Microbiol.* 9:646. doi: 10.3389/fmicb.2018.00646

Schönherr-Hellec, S., and Aires, J. (2019). Clostridia and necrotizing enterocolitis in preterm neonates. *Anaerobe* 58, 6–12. doi: 10.1016/j.anaerobe.2019.04.005

Schönherr-Hellec, S., Klein, G. L., Delannoy, J., Ferraris, L., Rozé, J. C., Butel, M. J., et al. (2018). Clostridial strain-specific characteristics associated with necrotizing enterocolitis. *Appl. Environ. Microbiol.* 84, e02428-17. doi: 10.1128/AEM.02428-17

Seekatz, A. M., and Young, V. B. (2014). *Clostridium difficile* and the microbiota. *J. Clin. Investig.* 124, 4182–4189.

Shen, A. (2012). *Clostridium difficile* toxins: mediators of inflammation. *J. Innate Immun.* 4, 149–158. doi: 10.1159/000332946

Shen, N. T., Maw, A., Tmanova, L. L., Pino, A., Ancy, K., Crawford, C. V., et al. (2017). Timely use of probiotics in hospitalized adults prevents *Clostridium difficile* infection: a systematic review with meta-regression analysis. *Gastroenterology* 152, 1889–1900.e9. doi: 10.1053/j.gastro.2017.02.003

Smits, W. K., Lyras, D., Lacy, D. B., Wilcox, M. H., and Kuijper, E. J. (2016). *Clostridium difficile* infection. *Nat. Rev. Dis. Primers* 2:16020.

Solomon, K. (2013). The host immune response to *Clostridium difficile* infection. *Ther. Adv. Infect. Dis.* 1, 19–35. doi: 10.1177/2049936112472173

Song, J., Li, Q., Everaert, N., Liu, R., Zheng, M., Zhao, G., et al. (2020). Dietary inulin supplementation modulates short-chain fatty acid levels and cecum microbiota composition and function in chickens infected With *Salmonella*. *Front. Microbiol.* 11:584380. doi: 10.3389/fmicb.2020.584380

Sorg, J. A., and Sonenshein, A. L. (2008). Bile salts and glycine as cogerminants for *Clostridium difficile* spores. *J. Bacteriol.* 190, 2505–2512. doi: 10.1128/JB.01765-07

Sorg, J. A., and Sonenshein, A. L. (2010). Inhibiting the initiation of *Clostridium difficile* spore germination using analogs of chenodeoxycholic acid, a bile acid. *J. Bacteriol.* 192, 4983–4990. doi: 10.1128/JB.00610-10

Spinler, J. K., Auchtung, J., Brown, A., Boonma, P., Oezguen, N., Ross, C. L., et al. (2017). Next-generation probiotics targeting *Clostridium difficile* through precursor-directed antimicrobial biosynthesis. *Infect. Immun.* 85:e00303-17. doi: 10.1128/IAI.00303-17

Staude, B., Oehmke, F., Lauer, T., Behnke, J., Gopel, W., Schloter, M., et al. (2018). The microbiome and preterm birth: a change in paradigm with profound implications for pathophysiologic concepts and novel therapeutic strategies. *BioMed. Res. Int.* 2018, 7218187. doi: 10.1155/2018/7218187

Surawicz, C. M., McFarland, L. V., Greenberg, R. N., Rubin, M., Fekety, R., Mulligan, M. E., et al. (2000). The search for a better treatment for recurrent *Clostridium difficile* disease: use of high-dose vancomycin combined with Saccharomyces boulardii. *Clin. Infect. Dis.* 31, 1012–1017. doi: 10.1086/318130

Tannock, G. W., Munro, K., Taylor, C., Lawley, B., Young, W., Byrne, B., et al. (2010). A new macrocyclic antibiotic, fidaxomicin (OPT-80), causes less alteration to the bowel microbiota of *Clostridium difficile*-infected patients than does vancomycin. *Microbiology* 156(Pt. 11), 3354–3359. doi: 10.1099/mic.0.042010-0

Tap, J., Furet, J. P., Bensaada, M., Philippe, C., Roth, H., Rabot, S., et al. (2015). Gut microbiota richness promotes its stability upon increased dietary fibre intake in healthy adults. *Environ. Microbiol.* 17, 4954–4964. doi: 10.1111/1462-2920.13006

Theriot, C. M., Bowman, A. A., and Young, V. B. (2016). Antibiotic-induced alterations of the gut microbiota alter secondary bile acid production and allow for *Clostridium difficile* spore germination and outgrowth in the large intestine. *mSphere* 1:e00045-15. doi: 10.1128/mSphere.00045-15

Toor, D., Wsson, M. K., Kumar, P., Karthikeyan, G., Kaushik, N. K., Goel, C., et al. (2019). Dysbiosis disrupts gut immune homeostasis and promotes gastric diseases. *Int. J. Mol. Sci.* 20:2432. doi: 10.3390/ijms20102432

Vakili, B., Fateh, A., Asadzadeh Aghdaei, H., Sotoodehnejadnematalahi, F., and Siadat, S. D. (2020). Characterization of gut microbiota in hospitalized patients with Clostridioides difficile infection. *Curr. Microbiol.* 77, 1673–1680. doi: 10.1007/s00284-020-01980-x

Valdes, A. M., Walter, J., Segal, E., and Spector, T. D. (2018). Role of the gut microbiota in nutrition and health. *BMJ* 361:k2179.

Valdes-Varela, L., Hernandez-Barranco, A. M., Ruas-Madiedo, P., and Gueimonde, M. (2016). Effect of bifidobacterium upon *Clostridium difficile* growth and toxicity when co-cultured in different prebiotic substrates. *Front. Microbiol.* 7:738. doi: 10.3389/fmicb.2016.00738

Wang, Y., Schluger, A., Li, J., Gomez-Simmonds, A., Salmasian, H., and Freedberg, D. E. (2020). Does addition of intravenous metronidazole to oral vancomycin improve outcomes in Clostridioides difficile infection? *Clin. Infect. Dis.* 71, 2414–2420. doi: 10.1093/cid/ciz1115

Weingarden, A. R., Chen, C., Bobr, A., Yao, D., Lu, Y., Nelson, V. M., et al. (2014). Microbiota transplantation restores normal fecal bile acid composition in recurrent *Clostridium difficile* infection. *Am. J. Physiol. Gastrointest. Liver Physiol.* 306, G310–G319. doi: 10.1152/ajpgi.00282.2013

Wilcox, M. H., Mooney, L., Bendall, R., Settle, C. D., and Fawley, W. N. (2008). A case-control study of community-associated *Clostridium difficile* infection. *J. Antimicrob. Chemother.* 62, 388–396.

Wilson, B. C., Vatanen, T., Cutfield, W. S., and O'Sullivan, J. M. (2019). The super-donor phenomenon in fecal microbiota transplantation. *Front. Cell. Infect. Microbiol.* 9:2. doi: 10.3389/fcimb.2019.00002

Winston, J. A., and Theriot, C. M. (2016). Impact of microbial derived secondary bile acids on colonization resistance against *Clostridium difficile* in the gastrointestinal tract. *Anaerobe* 41, 44–50. doi: 10.1016/j.anaerobe.2016.05.003

Yang, J., and Yang, H. (2018). Effect of bifidobacterium breve in combination with different antibiotics on *Clostridium difficile*. *Front. Microbiol.* 9:2953. doi: 10.3389/fmicb.2018.02953

Yang, J., and Yang, H. (2019). Antibacterial activity of bifidobacterium breve against Clostridioides difficile. *Front. Cell. Infect. Microbiol.* 9:288. doi: 10.3389/fcimb.2019.00288

Yun, B., Song, M., Park, D. J., and Oh, S. (2017). Beneficial effect of *Bifidobacterium longum* ATCC 15707 on survival rate of *Clostridium difficile* infection in mice. *Korean J. Food Sci. Anim. Resourc.* 37, 368–375. doi: 10.5851/kosfa.2017.37.3.368

Zhang, L., Dong, D., Jiang, C., Li, Z., Wang, X., and Peng, Y. (2015). Insight into alteration of gut microbiota in *Clostridium difficile* infection and asymptomatic C. difficile colonization. *Anaerobe* 34, 1–7. doi: 10.1016/j.anaerobe.2015.03.008

Zhou, Y., Shan, G., Sodergren, E., Weinstock, G., Walker, W. A., and Gregory, K. E. (2015). Longitudinal analysis of the premature infant intestinal microbiome prior to necrotizing enterocolitis: a case-control study. *PLoS One* 10:e0118632. doi: 10.1371/journal.pone.0118632

Zhuang, L., Chen, H., Zhang, S., Zhuang, J., Li, Q., and Feng, Z. (2019). Intestinal microbiota in early life and its implications on childhood health. *Genomics Proteom. Bioinform.* 17, 13–25. doi: 10.1016/j.gpb.2018.10.002

Conflict of Interest: The authors declare that the research was conducted in the absence of any commercial or financial relationships that could be construed as a potential conflict of interest.

Publisher's Note: All claims expressed in this article are solely those of the authors and do not necessarily represent those of their affiliated organizations, or those of the publisher, the editors and the reviewers. Any product that may be evaluated in this article, or claim that may be made by its manufacturer, is not guaranteed or endorsed by the publisher.

Copyright © 2022 Vasilescu, Chifiriuc, Pircalabioru, Filip, Bolocan, Lazăr, Dițu and Bleotu. This is an open-access article distributed under the terms of the Creative Commons Attribution License (CC BY). The use, distribution or reproduction in other forums is permitted, provided the original author(s) and the copyright owner(s) are credited and that the original publication in this journal is cited, in accordance with accepted academic practice. No use, distribution or reproduction is permitted which does not comply with these terms.

frontiers in Microbiology

ORIGINAL RESEARCH
published: 07 March 2022
doi: 10.3389/fmicb.2022.846215

The Essential Role of Rac1 Glucosylation in *Clostridioides difficile* Toxin B-Induced Arrest of G1-S Transition

Lara Petersen[1], Svenja Stroh[2], Dennis Schöttelndreier[1], Guntram A. Grassl[3], Klemens Rottner[4,5], Cord Brakebusch[6], Jörg Fahrer[2,7†] and Harald Genth[1]*

[1]*Institute for Toxicology, Hannover Medical School, Hannover, Germany,* [2]*Department of Toxicology, University Medical Center Mainz, Mainz, Germany,* [3]*Institute of Medical Microbiology and Hospital Epidemiology and DZIF partner site Hannover, Hannover Medical School, Hannover, Germany,* [4]*Division of Molecular Cell Biology, Zoological Institute, Technische Universität Braunschweig, Braunschweig, Germany,* [5]*Department of Cell Biology, Helmholtz Centre for Infection Research, Braunschweig, Germany,* [6]*Biotech Research and Innovation Centre (BRIC), University of Copenhagen, Copenhagen, Denmark,* [7]*Rudolf-Buchheim-Institute of Pharmacology, Justus-Liebig-University Giessen, Giessen, Germany*

OPEN ACCESS

Edited by:
Meina Neumann-Schaal, German Collection of Microorganisms and Cell Cultures GmbH (DSMZ), Germany

Reviewed by:
Xingmin Sun, University of South Florida, United States
Panagiotis Papatheodorou, Ulm University Medical Center, Germany

***Correspondence:**
Harald Genth
genth.harald@mh-hannover.de

†Present address:
Jörg Fahrer, Division of Food Chemistry and Toxicology, Department of Chemistry, University of Kaiserslautern, Kaiserslautern, Germany

Specialty section:
This article was submitted to Infectious Agents and Disease, a section of the journal Frontiers in Microbiology

Received: *30 December 2021*
Accepted: *14 February 2022*
Published: *07 March 2022*

Citation:
Petersen L, Stroh S, Schöttelndreier D, Grassl GA, Rottner K, Brakebusch C, Fahrer J and Genth H (2022) The Essential Role of Rac1 Glucosylation in Clostridioides difficile Toxin B-Induced Arrest of G1-S Transition. Front. Microbiol. 13:846215. doi: 10.3389/fmicb.2022.846215

Clostridioides difficile infection (CDI) in humans causes pseudomembranous colitis (PMC), which is a severe pathology characterized by a loss of epithelial barrier function and massive colonic inflammation. PMC has been attributed to the action of two large protein toxins, Toxin A (TcdA) and Toxin B (TcdB). TcdA and TcdB mono-O-glucosylate and thereby inactivate a broad spectrum of Rho GTPases and (in the case of TcdA) also some Ras GTPases. Rho/Ras GTPases promote G1-S transition through the activation of components of the ERK, AKT, and WNT signaling pathways. With regard to CDI pathology, TcdB is regarded of being capable of inhibiting colonic stem cell proliferation and colonic regeneration, which is likely causative for PMC. In particular, it is still unclear, the glucosylation of which substrate Rho-GTPase is critical for TcdB-induced arrest of G1-S transition. Exploiting SV40-immortalized mouse embryonic fibroblasts (MEFs) with deleted Rho subtype GTPases, evidence is provided that Rac1 (not Cdc42) positively regulates Cyclin D1, an essential factor of G1-S transition. TcdB-catalyzed Rac1 glucosylation results in Cyclin D1 suppression and arrested G1-S transition in MEFs and in human colonic epithelial cells (HCEC), Remarkably, Rac1$^{-/-}$ MEFs are insensitive to TcdB-induced arrest of G1-S transition, suggesting that TcdB arrests G1-S transition in a Rac1 glucosylation-dependent manner. Human intestinal organoids (HIOs) specifically expressed Cyclin D1 (neither Cyclin D2 nor Cyclin D3), which expression was suppressed upon TcdB treatment. In sum, Cyclin D1 expression in colonic cells seems to be regulated by Rho GTPases (most likely Rac1) and in turn seems to be susceptible to TcdB-induced suppression. With regard to PMC, toxin-catalyzed Rac1 glucosylation and subsequent G1-S arrest of colonic stem cells seems to be causative for decreased repair capacity of the colonic epithelium and delayed epithelial renewal.

Keywords: cyclin D, cell cycle, p21-activated kinase, human intestinal organoids, large clostridial glucosylating toxins, colonic epithelial renewal, human colonic epithelial cells

INTRODUCTION

The *Clostridioides difficile* Toxin B (TcdB, 270 kDa) [together with Toxin A (TcdA, 307 kDa)] is causative for the pathology of *C. difficile* infection (CDI), ranging from mild diarrhea to pseudomembranous colitis (PMC; Smits et al., 2016). PMC is characterized by a loss of epithelial barrier function and massive colonic inflammation. TcdA and TcdB are large single-chain protein toxins with a multi-domain organization, allowing self-mediated entry of the N-terminal glucosyltransferase domain into mammalian target cells by receptor-mediated endocytosis (Aktories et al., 2017; Kordus et al., 2021; Orrell and Melnyk, 2021). Upon internalization into the cytosol, the glucosyltransferase domain catalyzes divalent metal ion-dependent mono-O-glucosylation and thereby inactivation of small GTPases of Rho and Ras families (Genth et al., 2014, 2016, 2018). While TcdB specifically glucosylates GTPases of the Rho, Rac, and Cdc42 subfamilies, the related TcdA exhibits a broader substrate profile, as it glucosylates Ras subtype GTPases in addition to Rho/Rac/Cdc42 subtype GTPases (Genth et al., 2018). Ras and Rho GTPases are the key regulators of cytoskeletal dynamics, of gene expression, of cell cycle progression, and of cell death/survival. Upon treatment of cultured cells with TcdB, glucosylation of Rho GTPases results in actin depolymerization (Mitchell et al., 1987; May et al., 2013) and cell death including upregulation of the cell death-regulating GTPase RhoB (Huelsenbeck et al., 2007; Matarrese et al., 2007; Farrow et al., 2013; Wohlan et al., 2014).

In the gastrointestinal tract, a single layer of epithelial cells and the mucus layer separate the body from adverse factors in the gut environment. The gastrointestinal tract, however, is vulnerable to damage induced by adverse factors including bacterial toxins (such as TcdA and TcdB), metabolites (such as cytotoxic bile acids), dietary antigens and carcinogens, and oxidative stress. Likely because of this vulnerability, the intestinal epithelium undergoes rapid self-renewal with a renewal cycle of 4–5 days. This renewal depends on stem cells that feed the compartment of rapidly cycling transit-amplifying (TA) cells, which divide 4–5 times prior to their differentiation upon crossing the crypt villus junction. The proliferative activity and the acquisition of particular cell fates are coordinated by a small number of conserved signaling pathways, including the Wnt/beta-catenin and the Notch signaling pathways (de Lau et al., 2014; Reynolds et al., 2014).

Cell cycle progression requires sequential expression of cyclins, which complexes specific cyclin-dependent kinases (Cdks). Cyclin D1 is one of the essential cyclins that (upon binding to Cdk4/6) regulate G1-S transition during normal cell-cycle progression. p21-activated kinase (PAK) promotes G1-S transition through activation of components of the ERK, AKT and Wnt signaling pathways, all of which regulate expression of Cyclin D isoforms (Radu et al., 2014). PAK1 and PAK2 are activated by Rho subfamily GTPases Rac1 and Cdc42 (Bokoch, 2003; Parri and Chiarugi, 2010).

TcdA and TcdB induce a G1-S arrest in a glucosylation-dependent manner, with concomitant glucosylation of RhoA, Rac1, and Cdc42 being regarded to be required for arrested G1-S transition (Lica et al., 2011; D'Auria et al., 2012; Wohlan et al., 2014; Fettucciari et al., 2017; He et al., 2017). This study sets out to identify those Rho GTPases regulating Cyclin D1 expression and G1-S transition. Exploiting Rac1 and Cdc42 knock-out fibroblasts, glucosylation of specifically Rac1 (not Cdc42) is shown to be required for TcdB-induced Cyclin D1 suppression and arrested G1-S transition. Furthermore, evidence on the inhibition of Rac/Cdc42-PAK signaling and subsequent Cyclin D1 suppression is provided in TcdB-treated human colonic epithelial cells (HCEC) and in human intestinal organoids (HIO).

MATERIALS AND METHODS

Materials

Commercially obtained reagents: TO-PRO-3 (Life Technologies, Darmstadt, Germany); [^{32}P]NAD; Staurosporine. Antibodies: RhoA (26C4; Santa Cruz); Rac1 (clone 102, Transduction Laboratories); Rac1 (clone 23A8, Millipore); beta-actin (AC-40, Sigma); Hsp90 (Sigma); pS144/141-PAK1/2 (EP656Y, Abcam); PAK2 (Cell Signaling); Cyclin D1 (Cell Signaling); Cdc42 (Transduction Laboratories); horseradish peroxidase conjugated secondary antibody, mouse (Rockland); horseradish peroxidase conjugated secondary antibody, rabbit (Rockland). Recombinant TcdB and TcdB-NxN were expressed in *Bacillus megaterium* and purified by Ni^{2+} affinity chromatography using Ni^{2+}-IDA columns (Macherey-Nagel, Germany; Burger et al., 2003; Wohlan et al., 2014).

Cell Culture

Human intestinal organoids were grown from surgically removed intestinal tissue as recently described (Schöttelndreier et al., 2018). Non-transformed human colonic epithelial cells (HCEC) were kindly provided by Dr. Jerry Shay (Department of Cell Biology, UT Southwestern Medical Center, Dallas, United States) in 2015. HCEC exhibit a cuboidal to spindle-shaped morphology and intact p53 signaling (Mimmler et al., 2016). HCEC were maintained as previously described and grown in a nitrogen incubator with reduced oxygen levels (Roig et al., 2010). SV40 LT-antigen-immortalized $Rac1^{-/-}$ (clone 3) and $Rac1^{fl/fl}$ (Steffen et al., 2013) and LT-antigen-immortalized $Cdc42^{-/-}$ (clone 3-9-9) and $Cdc42^{fl/-}$ (clone 3–9; Czuchra et al., 2005) mouse embryonic fibroblasts were cultivated under standard conditions in Dulbecco's modified essential medium supplemented with 10% fetal calf serum, 100 µM penicillin, 100 µM streptomycin, 1% non-essential amino acids (*NEAA*), and 1 mM sodium pyruvate at 37°C and 5% CO_2. Cells were passaged upon 80% confluence. Doubling times of either cell line were estimated by dividing the natural logarithm of two by the exponent of growth.

EdU Labeling of Replicating Cells and Confocal Microscopy

HCEC grown on coverslips were incubated with TcdB for 24 h or left untreated. As positive control, cells were starved in

serum-free medium. Cells were then labeled with EdU for 1 h. After fixation and blocking, the samples were incubated with the Click-iT® EdU Imaging Kit (Life Technologies, Darmstadt, Germany) for 1 h in the dark. After a washing step, nuclei were counterstained with TO-PRO-3 (Life Technologies, Darmstadt, Germany) and samples mounted using Vectashield® (Vector Labs, Burlingame, CA, United States). Confocal microscopy was performed using a Zeiss Axio Observer. Z1 microscope equipped with a LSM710 laser-scanning unit (Zeiss, Oberkochen, Germany). Images were acquired in optical sections of 1 µm and processed with ImageJ (NIH, USA). The number of EdU-positive cells was quantified with ImageJ (50–100 cells/treatment) and data were evaluated by using the GraphPad Prism software.

BrdU Labeling of Replicating Cells

The BrdU Cell Proliferation Assay (Merck Millipore, Darmstadt, Germany) was exploited for the analysis of G1-S transition. The assay was performed according to the manufacturers' instructions. In brief, proliferating cells were pre-loaded with BrdU, followed by TcdB treatment for 24 h. Thereby, BrdU was incorporated into the DNA of proliferating cells. Cells were fixed, permeabilized, and the labeled DNA was denatured to enable binding of the anti-BrdU monoclonal antibody. A secondary, horseradish peroxidase-labeled antibody catalyzes the conversion of the chromogenic substrate tetramethylbenzidine (TMB) from a colorless solution to a blue solution (or yellow after the addition of stopping reagent). The level of the colored reaction product was quantified by photometry using a scanning multiwell spectrophotometer.

Western Blot Analysis

Cells were seeded into 3.5-cm-diameter dishes, treated with TcdB or mock for 24 h and washed with phosphate buffered saline (PBS; 4°C). For western blot analysis, cells were lysed with a buffer containing HEPES (50 mM), NaCl (150 mM), $MgCl_2$ (5 mM), Laemmli sample buffer, PMSF (1 mM) and sodium vanadate pH 7.4. The suspension was sonified with 50% cycle for 5 s. Subsequently, the samples were incubated at 95°C for 10 min, centrifuged, and separated by SDS-PAGE (15% gels, 25 mA/gel). For Western Blotting, proteins were transferred onto nitrocellulose membranes, which were blocked with 5% (w/v) non-fat dried milk for 60 min and incubated with respective primary antibody overnight at 4°C. Following treatment of the membrane with the second antibody for 60 min, proteins were detected using ECL Femto (Pierce).

Sequential [^{32}P]ADP Ribosylation

For sequential [^{32}P]ADP ribosylation, cells were lysed in a buffer containing 150 mM NaCl, 50 nM Tris (pH 7.2), 5 mM $MgCl_2$, 1 mM PMSF and NP40 (1%). After sonification, the soluble fraction was prepared by centrifugation. The lysates were incubated with *C. botulinum* exoenzyme C3 in the presence of 0.3 µM [^{32}P]NAD and 3 µM NAD for 30 min at 37°C. The reaction was stopped by addition of Laemmli sample buffer. The samples were incubated at 95°C for 10 min, separated by SDS-PAGE and analysed using a PhosphoImager.

RESULTS

Cyclin D1 Suppression in TcdB-Treated Human Intestinal Organoids and Human Colonic Epithelial Cells

Human intestinal organoids (HIOs) were exploited as experimental model for studying the effect of TcdB on the expression of the G1-phase Cyclins Cyclin D1, Cyclin D2, and Cyclin D3. HIOs specifically expressed Cyclin D1 but neither Cyclin D2 nor Cyclin D3 (**Supplementary Figure S1**). In contrast, SV40-immortalized Rac1$^{fl/fl}$ mouse embryonic fibroblasts (MEFs) that expressed Cyclin D1, Cyclin D2, and Cyclin D3 served as a positive control (**Supplementary Figure S1**). Treatment of HIOs with TcdB caused a time-dependent suppression of Cyclin D1 (**Figures 1A,B**). TcdB-catalyzed glucosylation of Rac/Cdc42 was evaluated by immunoblot analysis using Rac1 antibody (mAb102) that detects Rac/Cdc42 (Genth et al., 2006; Brandes et al., 2012). Once Rac/Cdc42 is glucosylated by TcdB, this Rac1 antibody (mAb102) does not detect its epitope, resulting in signal loss (Genth et al., 2006; Brandes et al., 2012). Decreased detection of Rac/Cdc42 by this antibody thus reflects TcdB-catalyzed glucosylation of Rac/Cdc42. TcdB time-dependently glucosylated Rac/Cdc42 (**Figures 1A,B**), as evaluated in terms of the loss of the detection of Rac/Cdc42 by immunoblot analysis using Rac1 antibody (mAb102). The total cellular level of Rac1 was not changed upon TcdB treatment as assessed using the Rac1 antibody (mAb23A8; **Figure 1A**), confirming that decreasing detection of Rac/Cdc42 by the Rac1 antibody (mAb102) was due to glucosylation and not due to degradation. Rac/Cdc42 from HIOs are thus susceptible to TcdB-catalyzed glucosylation, consistent with a former report (Zhu et al., 2019). PAK1/2, the upstream regulator of Cyclin D, is activated by Rac/Cdc42 (Balasenthil et al., 2004; Thullberg et al., 2007). In turn, TcdB-induced Rac/Cdc42 glucosylation resulted in a time-dependent decrease of phospho-Ser-144-PAK1 and phospho-Ser-141-PAK2 (pS144/141-PAK1/2; **Figure 1A**), with PAK1/2 dephosphorylation being indicative of PAK1/2 deactivation, consistent with previous observations (May et al., 2014). The total levels of PAK2 also decreased (**Figure 1A**), showing that TcdB-induced pS144/141-PAK1/2 deactivation was based on both PAK dephosphorylation and PAK degradation. In TcdB-treated HIOs, inhibition of Rac/Cdc42-PAK signaling by TcdB, thus coincided with suppression of Cyclin D1, with the kinetics of Cyclin D1 suppression being almost comparable to that of Rac/Cdc42 glucosylation (**Figures 1A,B**). The observation that TcdB-induced inhibition of Rac/Cdc42-PAK signaling results in suppression of Cyclin D1 reinforces the paradigm that expression of Cyclin D1 is regulated by a Rac/Cdc42-PAK-dependent signaling pathway (Joyce et al., 1999; Klein et al., 2007).

Next, the TcdB effects on G1-S transition were analyzed in human colonic epithelial cells (HCEC) isogenetically

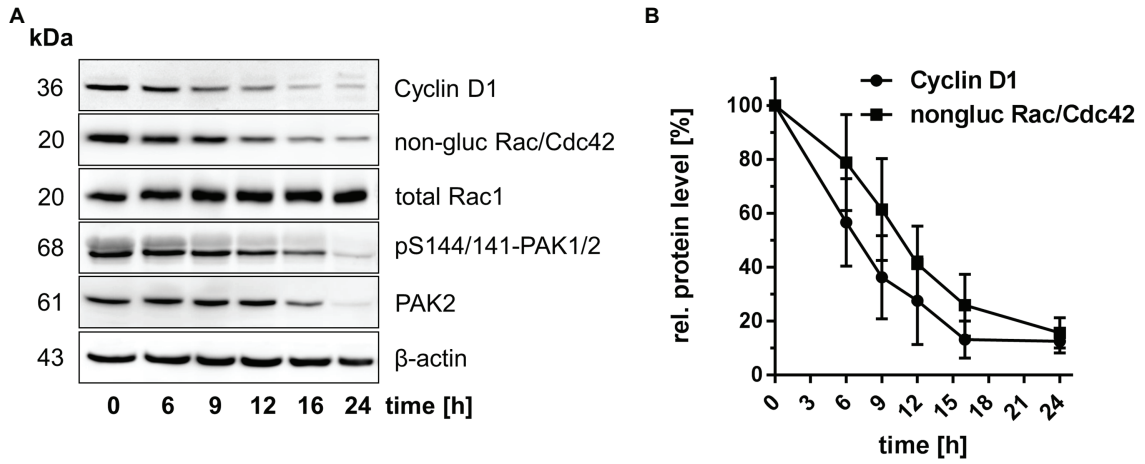

FIGURE 1 | Suppression of Cyclin D1 in TcdB-treated human intestinal organoids (HIOs). **(A)** HIOs were treated with TcdB (30 ng/ml) for the indicated times. The relative cellular concentrations of the indicated proteins were determined using Western blot analysis. Representative Western blots are presented. **(B)** Quantifications of signals were performed using Kodak software. Signal intensities obtained from immunoblots blots (n = 3) were quantified and normalized to the signal of beta-actin. The concentration of the indicated proteins in non-treated cells was set 100. Values are given as mean ± SD of three independent experiments.

transformed with Cdk4 and human telomerase. HCEC are a frequently exploited model to recapitulate colorectal cancer initiation and progression (Roig et al., 2010; Zhang et al., 2015; Mimmler et al., 2016). Treatment of HCEC with TcdB resulted in cell rounding with the formation of bipolar retraction fibers (**Supplementary Figure S2**), showing that HCEC are sensitive to TcdB. S-phase entry of HCEC was analyzed in terms of EdU incorporation. About 40% of a serum-maintained non-synchronously proliferating population of HCEC was EdU-positive (**Figures 2A,B**), reflecting those cells passing G1-S transition and S-phase within 24 h. Serum depletion resulted in an almost complete loss of EdU-positive cells, showing that in the absence of growth factors HCEC were arrested at the G1-S boundary (**Figure 2A**). TcdB concentration-dependently reduced the number of EdU-positive cells, indicating blocked G1-S transition (**Figures 2A,B**). HCEC expressed the G1-phase Cyclins Cyclin D1, Cyclin D2, and Cyclin D3 (**Figure 2C**). Interestingly, specifically the expression of Cyclin D1 (neither of Cyclin D2 nor Cyclin D3) was suppressed in TcdB-treated HCEC (**Figures 2C,D**). At the chosen relatively high TcdB concentration of 25 ng/ml, TcdB completely glucosylated Rac/Cdc42 within 1 h of TcdB treatment (**Figure 2C**), as evaluated in terms of the loss of the detection of Rac/Cdc42 Western by immunoblot analysis using Rac1 antibody (mAb102). The cellular level of Rac1 was not changed upon TcdB treatment as assessed using the Rac1 antibody (mAb23A8; **Figure 2C**), confirming that decreasing detection of Rac/Cdc42 by the Rac1 antibody (mAb102) was due to glucosylation and not due to degradation. Furthermore, prolonged treatment of HCEC with TcdB for 24 h did not result in Cyclin D2 and Cyclin D3 suppression (**Supplementary Figure S3**). In proliferating HCEC, Rac/Cdc42 glucosylation appeared earlier as compared to Cyclin D1 degradation (**Figures 2C,D**). The latter observation is consistent with the current paradigm stating that a Rac1-dependent pathways leads to transcriptional activation of cyclin D1 (Joyce et al., 1999; Klein et al., 2007). In turn, Rac1 glucosylation most likely blocks transcriptional cyclin D1 activation, resulting in degradation of pre-formed Cyclin D1. TcdB-induced Rac/Cdc42 glucosylation thus coincided with suppression of specifically Cyclin D1 and arrested G1-S transition in HCEC.

Suppression of Cyclin D1 and Cyclin D2 Correlates With Increased Doubling Time of Rac1$^{-/-}$ MEFs

To check if the inhibition of either Rac1 or Cdc42 is sufficient for suppression of Cyclin D1, SV40-immortalized mouse embryonic fibroblasts (MEFs) with a genetic deletion of either Rac1 or Cdc42 were exploited (Czuchra et al., 2005; Steffen et al., 2013). SV40-immortalized Rac1$^{fl/fl}$ MEFs were rapidly proliferating cells with a doubling time of about 13 h (**Supplementary Figure S4A**), as estimated by dividing the natural logarithm of two by the exponent of growth. In contrast, Rac1$^{-/-}$ MEFs exhibited a doubling time of about 24 h (**Supplementary Figure S4A**), indicating delayed cell cycle progression. Delayed cell cycle progression of Rac1$^{-/-}$ MEFs coincided with suppressed expression of the G1 Cyclins Cyclin D1 and Cyclin D2 in non-treated Rac1$^{-/-}$ MEFs (**Figure 3A**; **Supplementary Figure S5A**). In contrast to Cyclin D1 and Cyclin D2, Cyclin D3 was expressed in non-treated Rac1$^{-/-}$ MEFs to a level comparable to that in Rac1$^{fl/fl}$ (**Figure 3A**; **Supplementary Figure S5A**). The presence of Cyclin D3 might ensure G1-S transition and (delayed) proliferation of non-treated Rac1$^{-/-}$ MEFs, based on the idea that Cyclin D3 compensates for inactivation or loss of Cyclin D1 (Radulovich et al., 2010; Zhang et al.,

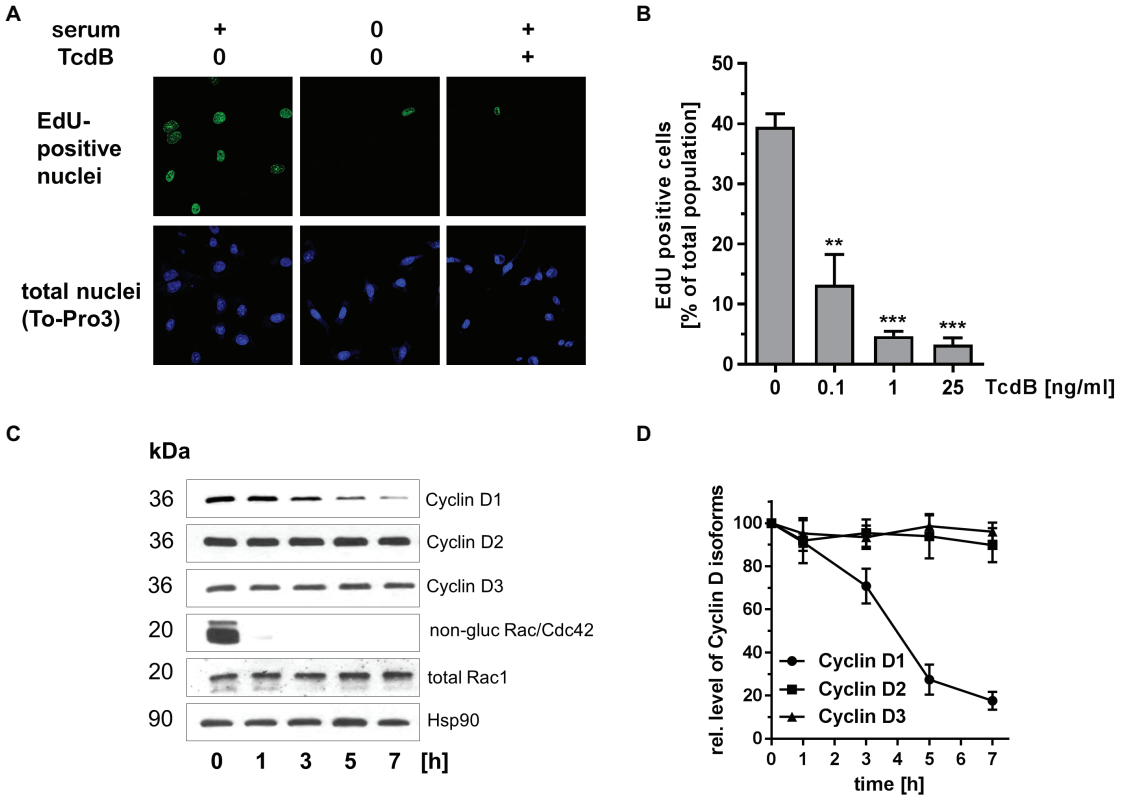

FIGURE 2 | Effects of TcdB in human colonic epithelial cells (HCEC). **(A)** HCEC were treated with TcdB (25 ng/ml) or maintained in serum-starved medium as positive control for 24 h. Actively replicating S-phase cells were labeled with EdU and visualized by confocal microscopy. Upon fixation of cells, nuclei were counterstained with TO-PRO-3. **(B)** HCEC were treated with the indicated concentrations of TcdB for 24 h. Actively replicating S-phase cells were labeled with EdU and visualized by confocal microscopy. The number of EdU-positive per TO-PRO-3-positive nuclei was determined. Signals from EdU-positive cells were quantitatively evaluated using ImageJ software ($n = 3$). $^{***}p < 0.001$, $^{**}p < 0.01$. **(C)** HCEC were treated with TcdB (25 ng/ml) for the indicated time. The relative cellular concentrations of the indicated proteins were determined using Western blot analysis. Representative Western blots are presented. **(D)** Signal intensities obtained from the Western blots ($n = 3$) were quantified and normalized to the signal of Hsp90. The concentration of the indicated proteins in non-treated cells was set 100. Values are given as mean ± SD of three independent experiments.

2011). In contrast to $Rac1^{fl/fl}$ and $Rac1^{-/-}$ MEFs, SV40-immortalized $Cdc42^{fl/-}$ and $Cdc42^{-/-}$ MEFs proliferated with almost comparable doubling times of about 14 h and 16 h, respectively (**Supplementary Figure S4B**). The level of Cyclin D1 appeared to be increased in non-treated $Cdc42^{-/-}$ MEFs as compared to non-treated $Cdc42^{fl/-}$ MEFs (**Supplementary Figure S6**) for reasons that remain to be unclear. Notwithstanding this, our observations argued for a major function of Rac1 (not Cdc42) in positively regulating Cyclin D1 expression and G1-S transition of SV40-immortalized fibroblasts.

Lacking Susceptibility of $Rac1^{-/-}$ MEFs to TcdB-Induced Arrest of G1-S Transition

The observation that Cyclin D1 and Cyclin D2 are suppressed in $Rac1^{-/-}$ MEFs (**Figure 3**) led to the hypothesis that TcdB-catalyzed Rac1 glucosylation (i.e., Rac1 inactivation) is causative for Cyclin D1 and Cyclin D2 suppression. Upon TcdB treatment for 24 h, the levels of Cyclin D1 and Cyclin D2 TcdB concentration-dependently decreased in $Rac1^{fl/fl}$ MEFs, with a TcdB concentration of 1 ng/ml being sufficient for almost complete Cyclin D1 and Cyclin D2 suppression (**Figure 3B**; **Supplementary Figure S5A**). In contrast, Cyclin D3 expression was reduced to some extent in TcdB-treated $Rac1^{fl/fl}$ MEFs but not completely suppressed even at high TcdB concentrations (**Figure 3B**; **Supplementary Figure S5A**).

To check if TcdB-induced suppression of Cyclin D1 and Cyclin D2 coincides with arrested G1-S transition, BrdU incorporation (indicative of S-phase entry) into non-synchronously proliferating cells was investigated. TcdB concentration-dependently reduced BrdU incorporation into non-synchronously proliferating $Rac1^{fl/fl}$ MEFs (**Figure 4A**). Remarkably, BrdU incorporation into non-synchronously proliferating $Rac1^{-/-}$ MEFs was not responsive to TcdB treatment (**Figure 4B**). These observations strongly suggest that TcdB inhibits G1-S transition in a Rac1 glucosylation-dependent manner. TcdB concentration-dependently reduced BrdU incorporation into both $Cdc42^{fl/-}$ and $Cdc42^{-/-}$ MEFs

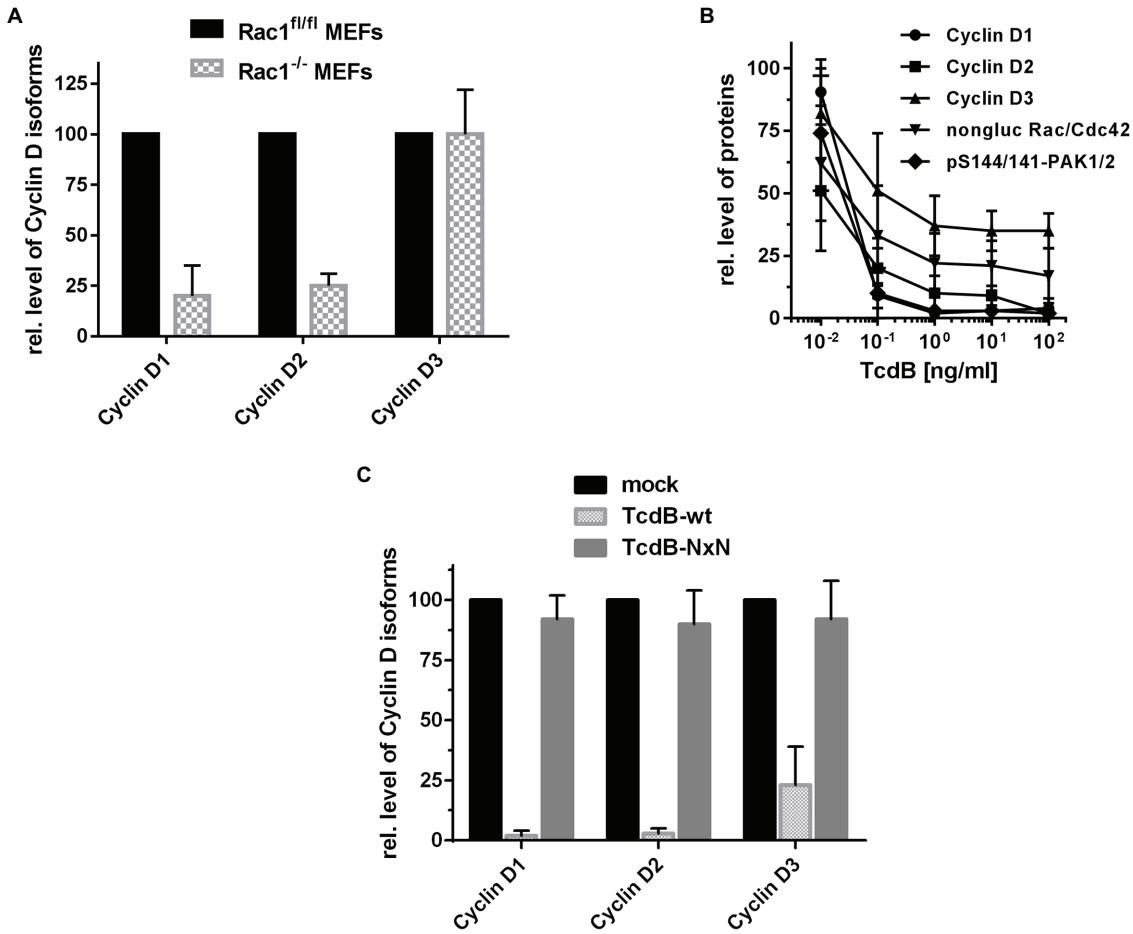

FIGURE 3 | Expression of Cyclin D isoforms upon Rac1 deletion and TcdB treatment. **(A)** Lysates from proliferating Rac1$^{fl/fl}$ and Rac1$^{-/-}$ MEFs were analyzed for the cellular concentrations of the Cyclin D isoforms using Western blot analysis. **(B)** Proliferating Rac1$^{fl/fl}$ MEFs were treated with the indicated concentrations of TcdB for 24 h. **(C)** Proliferating Rac1$^{fl/fl}$ MEFs were treated with TcdB-wt and TcdB-NxN (1 ng/ml each) or mock for 24 h. The relative cellular concentrations of the indicated proteins were determined using Western blot analysis. Signal intensities obtained from Western blots ($n = 3$) were quantified and normalized to the signal of beta-actin. The concentration of the indicated proteins in non-treated cells was set 100. Values are given as mean ± SD of three independent experiments.

(**Figures 4C,D**). In contrast to Rac1$^{-/-}$ MEFs, Cdc42$^{-/-}$ MEFs did not lack responsiveness to TcdB, most likely excluding a role of Cdc42 glucosylation in TcdB-induced G1-S arrest. TcdB-induced inhibition of G1-S transition depended on Rac1 glucosylation and coincided with suppression of Cyclin D1 and Cyclin D2.

TcdB exhibited comparable potency in Rac1$^{fl/fl}$ and Rac1$^{-/-}$ MEFs, as TcdB concentration-dependent RhoA glucosylation was comparable in Rac1$^{fl/fl}$ MEFs and Rac1$^{-/-}$ MEFs, with a TcdB concentration of 1 ng/ml being sufficient for almost complete RhoA glucosylation (**Supplementary Figures S5A,B**). RhoA/B/C glucosylation was thereby tracked in terms of sequential [^{32}P] ADP-ribosylation exploiting *C. botulinum* exoenzyme C3. Once RhoA/B/C is glucosylated by TcdB at Thr-37, sequential ADP-ribosylation of RhoA/B/C is blocked, resulting in a loss of [^{32}P]ADP-ribosylation (Just et al., 1994). Decreasing [^{32}P] ADP-ribosylation of RhoA/B/C thus reflects TcdB-catalyzed glucosylation of RhoA/B/C (**Supplementary Figures S5A,B**). Moreover, Cdc42 degradation, PAK de-activation, and RhoA/B/C glucosylation exhibited comparable kinetics in TcdB-treated Rac1$^{fl/fl}$ and Rac1$^{-/-}$ MEFs (**Supplementary Figures S5A,B**). These observations provide evidence on comparable TcdB potency in Rac1$^{fl/fl}$ and Rac1$^{-/-}$ MEFs. TcdB also exhibited comparable potency in Cdc42$^{fl/-}$ and Cdc42$^{-/-}$ MEFs, as RhoA glucosylation, RhoA degradation, PAK de-activation, and PAK degradation exhibited comparable kinetics in Cdc42$^{fl/-}$ and Cdc42$^{-/-}$ MEFs (**Supplementary Figure S6**).

In Rac1$^{-/-}$ MEFs, low levels of Cyclin D1 were still expressed, with this residual Cyclin D1 expression being sensitive to TcdB treatment (**Supplementary Figure S5A**; Cyclin D1*). The residual Cyclin D1 expression in Rac1$^{-/-}$ MEFs seems to be regulated by a TcdB substrate GTPase distinct from Rac1. Appropriate candidates are RhoA and the Cdc42 subfamily GTPase TC10, both of which are glucosylated by TcdB and are shown to regulate Cyclin D1 expression (Murphy et al., 2001; Croft and Olson, 2006; Genth et al., 2014).

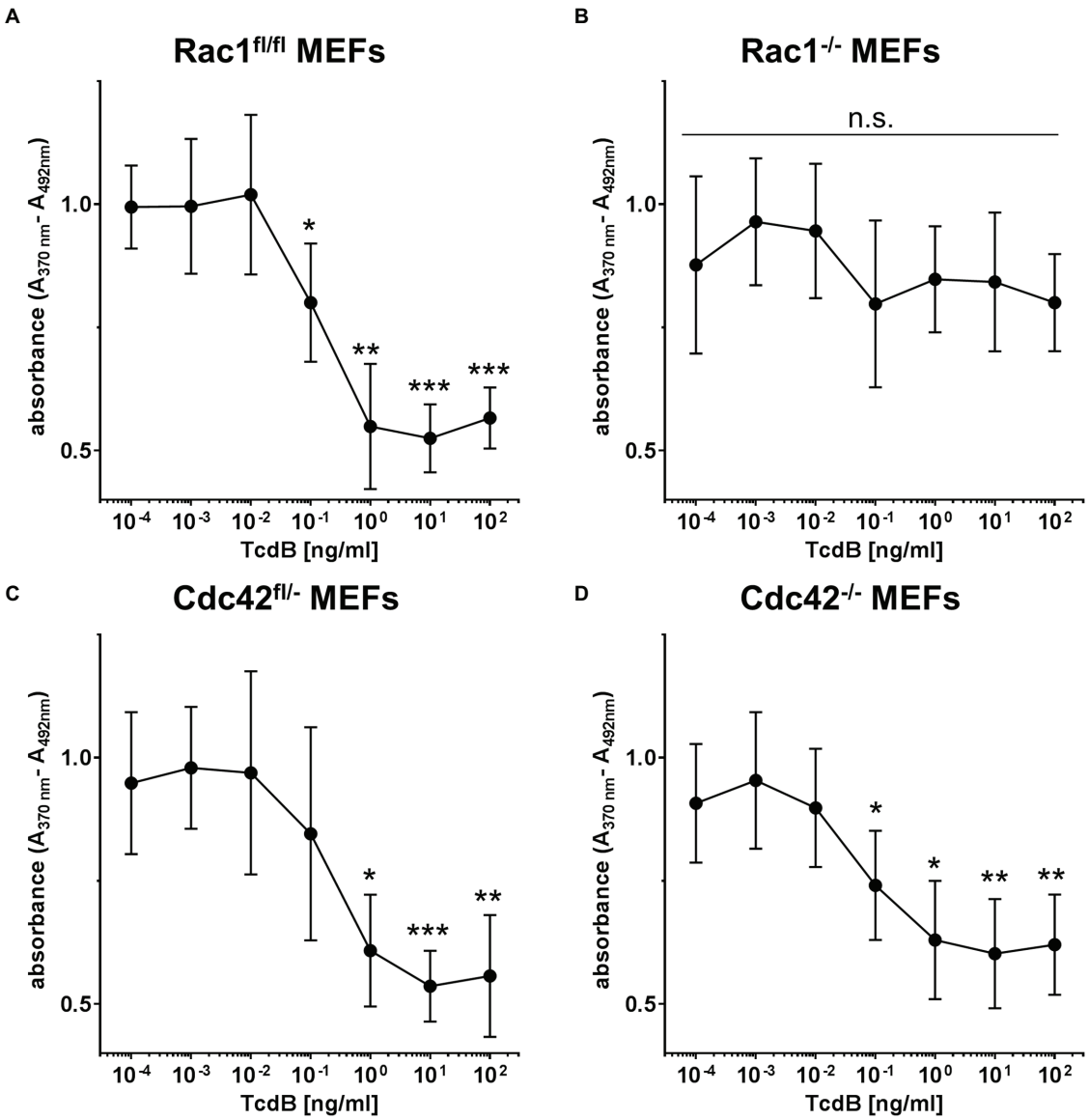

FIGURE 4 | TcdB effects on G1-S transition. Proliferating Rac1$^{fl/fl}$ MEFs **(A)**, Rac1$^{-/-}$ MEFs **(B)**, Cdc42$^{fl/-}$ MEFs **(C)**, and Cdc42$^{-/-}$ MEFs **(D)** were labeled with BrdU (10 μM) and treated with the indicated concentrations of TcdB for 24 h. DNA *de novo* synthesis is determined using a peroxidase-conjugated anti-BrdU antibody. Values are given as mean ± SD of three independent experiments. ***$p < 0.001$, **$p < 0.01$, *$p < 0.05$.

The low expression of Cyclin D1 and Cyclin D2 does not seem to regulate G1-S progression in Rac1$^{-/-}$ MEFs, as Rac1$^{-/-}$ MEFs progressed through the G1-S transition at those TcdB concentrations being sufficient for complete Cyclin D1 suppression (**Supplementary Figure S5A**; **Figure 4B**). Instead, G1-S transition in Rac1$^{-/-}$ MEFs might be promoted by Cyclin D3, the expression of which is only reduced to some extent upon TcdB treatment (**Figure 3B**; **Supplementary Figure S5A**).

TcdB harbors two adjacent aspartates at acid position 286 and 288, which mediate divalent metal ion-dependent coordination of the glucose donor UDP-glucose. Upon exchange of D286 and D286 into asparagins (TcdB-NxN), the glucosyltransferase activity is deleted (Wohlan et al., 2014). To confirm that TcdB-induced suppression of the Cyclin D isoforms depends on the glucosyltransferase activity of TcdB, Rac1$^{fl/fl}$ MEFs were treated TcdB with as a positive control. TcdB caused rounding of Rac1$^{fl/fl}$ MEFs (**Supplementary Figure S7A**), suppression of the Cyclin D isoforms (**Figure 3C**; **Supplementary Figure S7B**), Rac/Cdc42 glucosylation (**Supplementary Figure S7B**), and PAK deactivation (**Supplementary Figure S7B**). In contrast, TcdB-NxN-treated Rac1$^{fl/fl}$ MEFs exhibited expression of the Cyclin D isoforms and active Rac/Cdc42-PAK signaling, as neither Rac/Cdc42 glucosylation nor Cdc42 degradation nor PAK deactivation were observed (**Figure 3C**; **Supplementary Figure S7B**).

These findings confirmed that TcdB-induced suppression of Cyclin D isoforms depended on the glucosyltransferase activity of TcdB.

Susceptibility of Rac1$^{fl/fl}$ and Rac1$^{-/-}$ MEFs to Staurosporine-Induced Arrest of G1-S Transition

To show that G1-S transition in Rac1$^{-/-}$ MEFs is in principle susceptible to inhibition, staurosporine (STS), a broad-spectrum inhibitor of protein kinases, was applied. STS concentration-dependently reduced BrdU incorporation into both non-synchronously proliferating Rac1$^{fl/fl}$ MEFs and Rac1$^{-/-}$ MEFs (**Supplementary Figure S8A**). STS concentration-dependently induced decreasing levels of pT202/Y204-p44-MAPK(ERK1) and pT183/Y185-p42-MAPK(ERK2) in both Rac1$^{fl/fl}$ and Rac1$^{-/-}$ MEFs (**Supplementary Figure S8B**), confirming that STS acts as a kinase inhibitor. The total levels of ERK1/2 concentration-dependently decreased (**Supplementary Figure S8B**), showing that STS-induced ERK1/2 de-activation is based on both de-phosphorylation and degradation. ERK1/2 is an up-stream regulator of Cyclin D1 expression and G1-S transition (Baker et al., 2014; Radu et al., 2014). Furthermore, STS concentration-dependently induced Cyclin D1 suppression in Rac1$^{fl/fl}$ MEFs (**Supplementary Figure S8B**). In STS-treated Rac1$^{fl/fl}$ MEFs, Cyclin D1 suppression thus coincided with arrested G1-S transition. The responsiveness of G1-S transition in Rac1$^{-/-}$ MEFs to STS proved that Rac1$^{-/-}$ MEFs were in principle susceptible to a G1-S arrest.

DISCUSSION

The Rac1/Cdc42-PAK pathway promotes G1-S transition through the activation of components of the ERK, AKT, and Wnt signaling pathways, all of which regulate expression of Cyclin D isoforms (Radu et al., 2014). In this study, MEFs with genetic deletion of either Rac1 or Cdc42 were exploited to provide evidence that the genetic deletion of Rac1 (not Cdc42) results in suppression of Cyclin D1 and Cyclin D2 (**Figure 3**). Consistently, suppression of Cyclin D1 and D2 coincides with an increased doubling time of Rac1$^{-/-}$ MEFs (**Supplementary Figure S4**). As delayed G2-M transition hardly contributes to the increased doubling time of Rac1$^{-/-}$ MEFs, delayed cell cycle progression of Rac1$^{-/-}$ MEFs can be associated with delayed G1-S transition (May et al., 2014). Rac1 (not Cdc42) seems thus to be the upstream regulator of Cyclin D1 and Cyclin D2 and of G1-S transition in murine fibroblasts. Consistently, inactivation of Rac1 by TcdB-catalyzed glucosylation results in suppression of Cyclin D1 and Cyclin D2 and (to some extent) Cyclin D3 in MEFs (**Figure 3B**; **Supplementary Figure S5A**). These observations are consistent with former findings providing evidence on reduced expression of the cyclin d1 gene upon TcdB treatment (D'Auria et al., 2012). Furthermore, the related TcdA has been shown to suppress Cyclin D1 expression (Bezerra Lima et al., 2014). Interestingly, TcdA-induced inhibition of the Wnt/β-Catenin Pathway is shown to be preserved upon expression of non-glucosylatable Rac1-Q61L (Martins et al., 2020). In sum, Rac1 seems to be the critical upstream regulator of G1 phase Cyclins on the level of Rho GTPases, which glucosylation by either TcdA or TcdB results in Cyclin D1 suppression.

TcdB-induced suppression of Cyclin D1 and Cyclin D2 coincides with a G1-S arrest in MEFs (**Figure 4**), as evidenced in terms of reduced BrdU incorporation. These observations nicely complement former observations on TcdB-induced G1-S arrest, as analyzed in terms of a loss of the S-phase population and an increased 2 N population on FACS analysis of propidium iodide-stained cells (Nottrott et al., 2007; Lica et al., 2011; D'Auria et al., 2012; Wohlan et al., 2014). The observations that Rac1$^{-/-}$ MEFs (not Cdc42$^{-/-}$ MEFs) are insensitive to TcdB-induced arrest of G1-S transition (**Figure 4**) suggest that TcdB arrested G1-S transition in a Rac1 glucosylation-dependent manner. In Rac1$^{-/-}$ MEFs, other Rho subfamily GTPases - dependently or independently of the "invisible hand" of Rho GDI-1-might compensate for the loss of Rac1. In TcdB-treated Rac1$^{-/-}$ MEFs, such compensation can most likely be excluded, as TcdB completely inactivates the Rho, Rac, and Cdc42 subfamily GTPases (Boulter et al., 2010; Genth et al., 2018).

In human colonic epithelial cells (HCEC), expression of specifically Cyclin D1 (not Cyclin D2 or Cyclin D3) seems to depend on Rho subtype GTPases (most likely Rac1), as Cyclin D1 expression (not expression of Cyclin D2 and Cyclin D3) is sensitive to TcdB treatment (**Figure 2**). Comparable to MEFs, Cyclin D1 suppression coincides with arrested G1-S transition (**Figure 2**). In HCEC, TcdB-induced suppression of Cyclin D1 (not Cyclin D2 or D3) seems to be causative for the G1-S arrest.

Together with former studies on the cell cycle effect of TcdB, TcdB blocks cell proliferation by inhibition of several Rac1-/RhoA-dependent pathways regulating cell cycle progression: (1) TcdB-catalyzed Rac1 glucosylation results in delayed G2-M transition (Ando et al., 2007; May et al., 2014); (2) TcdB-catalysed RhoA glucosylation prevents contractile ring formation in cytokinesis, resulting in inhibited cell division (Huelsenbeck et al., 2009; Lica et al., 2011); (3) TcdB-induced G1-S arrest depends on Rac1 glucosylation (this study; **Figure 5**).

Several lines of evidence have highlighted Rac1 as a driver of colonic stem cell proliferation and colonic regeneration (Myant et al., 2013; McKernan and Egan, 2015). Most recently, TcdB (rather than TcdA) has been identified as the driver of colonic stem cell damage in CDI (Mileto et al., 2020). The observations of this study nicely complement the current model: Cyclin D1 seems to be the only G1 phase cyclin expressed in the colon, as deduced from our observations from HIOs (**Supplementary Figure S1**). TcdB-induced Rac1 glucosylation and PAK deactivation and subsequent suppression of Cyclin D1 and arrested G1-S transition seem to be causative for colonic damage, including a diminished LGR5+ stem cell compartment, and a damaged stem cell population. In consequence, the repair capacity of the colonic epithelium must be regarded to be decreased

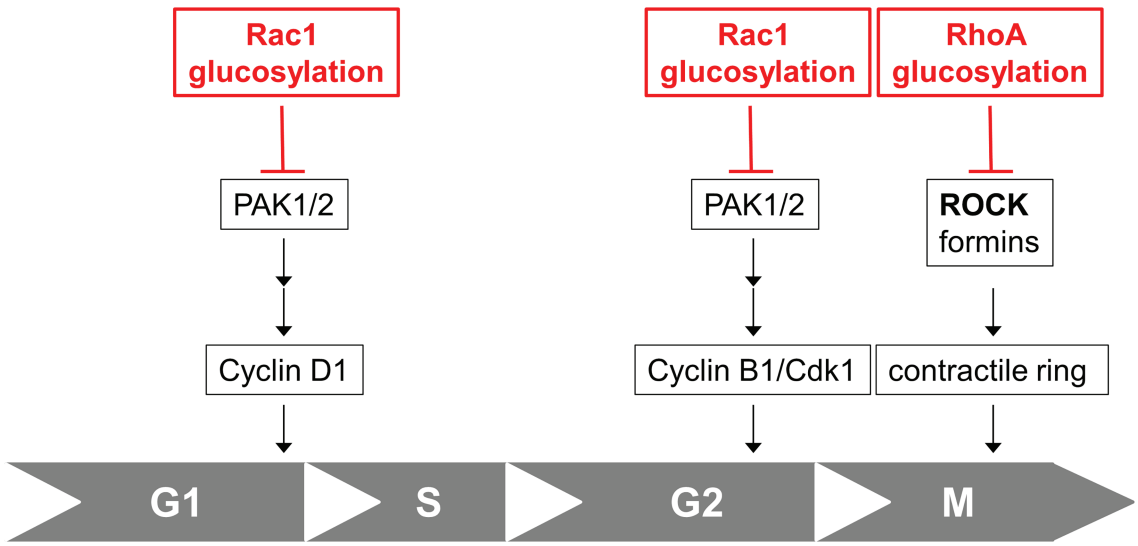

FIGURE 5 | Cell cycle effects of TcdB. Rac1 glucosylation by TcdB results in inhibition of Rac1/PAK-dependent pathways regulating expression of Cyclin D1 and subsequent arrested G1-S transition. Rac1 glucosylation by TcdB also results in inhibition of Rac1/PAK-dependent pathways leading to Cyclin B/Cdk1 complex and subsequent delayed G2-M transition. RhoA glucosylation by TcdB blocks formation of the contractile actin-myosin ring (CAR) in cytokinesis, resulting in arrested cell division in M-phase.

and the epithelial renewal to be delayed (Barker, 2014; Mileto et al., 2020).

DATA AVAILABILITY STATEMENT

The original contributions presented in the study are included in the article/**Supplementary Material**, and further inquiries can be directed to the corresponding author.

AUTHOR CONTRIBUTIONS

HG, JF, and GG conceived the study. LP, SS, and DS performed the experiments. KR and CB supplied reagents. LP, HG, JF, GG, and DS analyzed the data and wrote the manuscript. All authors contributed to the article and approved the submitted version.

FUNDING

This work was funded by the Federal State of Lower Saxony, Niedersächsisches Vorab (VWZN3215/ZN3266).

SUPPLEMENTARY MATERIAL

The Supplementary Material for this article can be found online at: https://www.frontiersin.org/articles/10.3389/fmicb.2022.846215/full#supplementary-material

REFERENCES

Aktories, K., Schwan, C., and Jank, T. (2017). Clostridium difficile Toxin Biology. *Annu. Rev. Microbiol.* 71, 281–307. doi: 10.1146/annurev-micro-090816-093458

Ando, Y., Yasuda, S., Oceguera-Yanez, F., and Narumiya, S. (2007). Inactivation of rho GTPases with Clostridium difficile toxin B impairs centrosomal activation of Aurora-A in G2/M transition of HeLa cells. *Mol. Biol. Cell* 18, 3752–3763. doi: 10.1091/mbc.e07-03-0281

Baker, N. M., Yee Chow, H., Chernoff, J., and Der, C. J. (2014). Molecular pathways: targeting RAC-p21-activated serine-threonine kinase signaling in RAS-driven cancers. *Clin. Cancer Res.* 20, 4740–4746. doi: 10.1158/1078-0432.CCR-13-1727

Balasenthil, S., Sahin, A. A., Barnes, C. J., Wang, R. A., Pestell, R. G., Vadlamudi, R. K., et al. (2004). p21-activated kinase-1 signaling mediates cyclin D1 expression in mammary epithelial and cancer cells. *J. Biol. Chem.* 279, 1422–1428. doi: 10.1074/jbc.M309937200

Barker, N. (2014). Adult intestinal stem cells: critical drivers of epithelial homeostasis and regeneration. *Nat. Rev. Mol. Cell Biol.* 15, 19–33. doi: 10.1038/nrm3721

Bezerra Lima, B., Faria Fonseca, B., Da Graca Amado, N., Moreira Lima, D., Albuquerque Ribeiro, R., Garcia Abreu, J., et al. (2014). *Clostridium difficile* toxin A attenuates Wnt/beta-catenin signaling in intestinal epithelial cells. *Infect. Immun.* 82, 2680–2687. doi: 10.1128/IAI.00567-13

Bokoch, G. M. (2003). Biology of the p21-activated kinases. *Annu. Rev. Biochem.* 72, 743–781. doi: 10.1146/annurev.biochem.72.121801.161742

Boulter, E., Garcia-Mata, R., Guilluy, C., Dubash, A., Rossi, G., Brennwald, P. J., et al. (2010). Regulation of Rho GTPase crosstalk, degradation and activity by RhoGDI1. *Nat. Cell Biol.* 12, 477–483. doi: 10.1038/ncb2049

Brandes, V., Schelle, I., Brinkmann, S., Schulz, F., Schwarz, J., Gerhard, R., et al. (2012). Protection from *Clostridium difficile* toxin B-catalysed Rac1/Cdc42 glucosylation by tauroursodeoxycholic acid-induced Rac1/Cdc42 phosphorylation. *Biol. Chem.* 393, 77–84. doi: 10.1515/BC-2011-198

Burger, S., Tatge, H., Hofmann, F., Genth, H., Just, I., and Gerhard, R. (2003). Expression of recombinant *Clostridium difficile* toxin A using the Bacillus megaterium system. *Biochem. Biophys. Res. Commun.* 307, 584–588. doi: 10.1016/S0006-291X(03)01234-8

Croft, D. R., and Olson, M. F. (2006). The Rho GTPase effector ROCK regulates cyclin A, cyclin D1, and p27Kip1 levels by distinct mechanisms. *Mol. Cell. Biol.* 26, 4612–4627. doi: 10.1128/MCB.02061-05

Czuchra, A., Wu, X., Meyer, H., Van Hengel, J., Schroeder, T., Geffers, R., et al. (2005). Cdc42 is not essential for filopodium formation, directed migration, cell polarization, and mitosis in fibroblastoid cells. *Mol. Biol. Cell* 16, 4473–4484. doi: 10.1091/mbc.e05-01-0061

D'auria, K. M., Donato, G. M., Gray, M. C., Kolling, G. L., Warren, C. A., Cave, L. M., et al. (2012). Systems analysis of the transcriptional response of human ileocecal epithelial cells to *Clostridium difficile* toxins and effects on cell cycle control. *BMC Syst. Biol.* 6:2. doi: 10.1186/1752-0509-6-2

De Lau, W., Peng, W. C., Gros, P., and Clevers, H. (2014). The R-spondin/Lgr5/Rnf43 module: regulator of Wnt signal strength. *Genes Dev.* 28, 305–316. doi: 10.1101/gad.235473.113

Farrow, M. A., Chumbler, N. M., Lapierre, L. A., Franklin, J. L., Rutherford, S. A., Goldenring, J. R., et al. (2013). *Clostridium difficile* toxin B-induced necrosis is mediated by the host epithelial cell NADPH oxidase complex. *Proc. Natl. Acad. Sci. U. S. A.* 110, 18674–18679. doi: 10.1073/pnas.1313658110

Fettucciari, K., Ponsini, P., Gioe, D., Macchioni, L., Palumbo, C., Antonelli, E., et al. (2017). Enteric glial cells are susceptible to *Clostridium difficile* toxin B. *Cell. Mol. Life Sci.* 74, 1527–1551. doi: 10.1007/s00018-016-2426-4

Genth, H., Huelsenbeck, J., Hartmann, B., Hofmann, F., Just, I., and Gerhard, R. (2006). Cellular stability of rho-GTPases glucosylated by *Clostridium difficile* toxin B. *FEBS Lett.* 580, 3565–3569. doi: 10.1016/j.febslet.2006.04.100

Genth, H., Junemann, J., Lammerhirt, C. M., Lucke, A. C., Schelle, I., Just, I., et al. (2018). Difference in mono-O-glucosylation of Ras subtype GTPases between toxin A and toxin B from *Clostridioides difficile* strain 10463 and lethal toxin from *Clostridium sordellii* strain 6018. *Front. Microbiol.* 9:3078. doi: 10.3389/fmicb.2018.03078

Genth, H., Pauillac, S., Schelle, I., Bouvet, P., Bouchier, C., Varela-Chavez, C., et al. (2014). Haemorrhagic toxin and lethal toxin from *Clostridium sordellii* strain vpi9048: molecular characterization and comparative analysis of substrate specificity of the large clostridial glucosylating toxins. *Cell. Microbiol.* 16, 1706–1721. doi: 10.1111/cmi.12321

Genth, H., Schelle, I., and Just, I. (2016). Metal ion activation of Clostridium sordellii lethal toxin and *Clostridium difficile* toxin B. *Toxins* 8:109. doi: 10.3390/toxins8040109

He, R., Peng, J., Yuan, P., Yang, J., Wu, X., Wang, Y., et al. (2017). Glucosyltransferase activity of *Clostridium difficile* toxin B triggers autophagy-mediated cell growth arrest. *Sci. Rep.* 7:10532. doi: 10.1038/s41598-017-11336-4

Huelsenbeck, J., Dreger, S. C., Gerhard, R., Fritz, G., Just, I., and Genth, H. (2007). Upregulation of the immediate early gene product RhoB by exoenzyme C3 from *Clostridium limosum* and toxin B from *Clostridium difficile*. *Biochemistry* 46, 4923–4931. doi: 10.1021/bi602465z

Huelsenbeck, S. C., May, M., Schmidt, G., and Genth, H. (2009). Inhibition of cytokinesis by *Clostridium difficile* toxin B and cytotoxic necrotizing factors—reinforcing the critical role of RhoA in cytokinesis. *Cell Motil. Cytoskeleton* 66, 967–975. doi: 10.1002/cm.20390

Joyce, D., Bouzahzah, B., Fu, M., Albanese, C., D'amico, M., Steer, J., et al. (1999). Integration of Rac-dependent regulation of cyclin D1 transcription through a nuclear factor-kappaB-dependent pathway. *J. Biol. Chem.* 274, 25245–25249. doi: 10.1074/jbc.274.36.25245

Just, I., Fritz, G., Aktories, K., Giry, M., Popoff, M. R., Boquet, P., et al. (1994). *Clostridium difficile* toxin B acts on the GTP-binding protein rho. *J. Biol. Chem.* 269, 10706–10712. doi: 10.1016/S0021-9258(17)34116-9

Klein, E. A., Yang, C., Kazanietz, M. G., and Assoian, R. K. (2007). NFkappaB-independent signaling to the cyclin D1 gene by Rac. *Cell Cycle* 6, 1115–1121. doi: 10.4161/cc.6.9.4147

Kordus, S. L., Thomas, A. K., and Lacy, D. B. (2021). *Clostridioides difficile* toxins: mechanisms of action and antitoxin therapeutics. *Nat. Rev. Microbiol.* doi: 10.1038/s41579-021-00660-2 [Epub ahead of print].

Lica, M., Schulz, F., Schelle, I., May, M., Just, I., and Genth, H. (2011). Difference in the biological effects of *Clostridium difficile* toxin B in proliferating and non-proliferating cells. *Naunyn Schmiedeberg's Arch. Pharmacol.* 383, 275–283. doi: 10.1007/s00210-010-0595-5

Martins, C. S., Costa, D. V. S., Lima, B. B., Leitao, R. F. C., Freire, G. E., Silva, G. F. M., et al. (2020). Clostridioides difficile toxin A-induced Wnt/beta-catenin pathway inhibition is mediated by Rac1 Glucosylation. *Front. Microbiol.* 11:1998. doi: 10.3389/fmicb.2020.01998

Matarrese, P., Falzano, L., Fabbri, A., Gambardella, L., Frank, C., Geny, B., et al. (2007). Clostridium difficile toxin B causes apoptosis in epithelial cells by thrilling mitochondria. Involvement of ATP-sensitive mitochondrial potassium channels. *J. Biol. Chem.* 282, 9029–9041. doi: 10.1074/jbc.M607614200

May, M., Schelle, I., Brakebusch, C., Rottner, K., and Genth, H. (2014). Rac1-dependent recruitment of PAK2 to G2 phase centrosomes and their roles in the regulation of mitotic entry. *Cell Cycle* 13, 2211–2221. doi: 10.4161/cc.29279

May, M., Wang, T., Muller, M., and Genth, H. (2013). Difference in F-actin depolymerization induced by toxin B from the Clostridium difficile strain VPI 10463 and toxin B from the variant Clostridium difficile serotype F strain 1470. *Toxins* 5, 106–119. doi: 10.3390/toxins5010106

Mckernan, D. P., and Egan, L. J. (2015). The intestinal epithelial cell cycle: uncovering its 'cryptic' nature. *Curr. Opin. Gastroenterol.* 31, 124–129. doi: 10.1097/MOG.0000000000000154

Mileto, S. J., Jarde, T., Childress, K. O., Jensen, J. L., Rogers, A. P., Kerr, G., et al. (2020). Clostridioides difficile infection damages colonic stem cells via TcdB, impairing epithelial repair and recovery from disease. *Proc. Natl. Acad. Sci. U. S. A.* 117, 8064–8073. doi: 10.1073/pnas.1915255117

Mimmler, M., Peter, S., Kraus, A., Stroh, S., Nikolova, T., Seiwert, N., et al. (2016). DNA damage response curtails detrimental replication stress and chromosomal instability induced by the dietary carcinogen PhIP. *Nucleic Acids Res.* 44, 10259–10276. doi: 10.1093/nar/gkw791

Mitchell, M. J., Laughon, B. E., and Lin, S. (1987). Biochemical studies on the effect of Clostridium difficile toxin B on actin in vivo and in vitro. *Infect. Immun.* 55, 1610–1615. doi: 10.1128/iai.55.7.1610-1615.1987

Murphy, G. A., Jillian, S. A., Michaelson, D., Philips, M. R., D'eustachio, P., and Rush, M. G. (2001). Signaling mediated by the closely related mammalian rho family GTPases TC10 and Cdc42 suggests distinct functional pathways. *Cell Growth Differ.* 12, 157–167.

Myant, K. B., Cammareri, P., Mcghee, E. J., Ridgway, R. A., Huels, D. J., Cordero, J. B., et al. (2013). ROS production and NF-kappaB activation triggered by RAC1 facilitate WNT-driven intestinal stem cell proliferation and colorectal cancer initiation. *Cell Stem Cell* 12, 761–773. doi: 10.1016/j.stem.2013.04.006

Nottrott, S., Schoentaube, J., Genth, H., Just, I., and Gerhard, R. (2007). *Clostridium difficile* toxin A-induced apoptosis is p53-independent but depends on glucosylation of rho GTPases. *Apoptosis* 12, 1443–1453. doi: 10.1007/s10495-007-0074-8

Orrell, K. E., and Melnyk, R. A. (2021). Large Clostridial toxins: mechanisms and roles in disease. *Microbiol. Mol. Biol. Rev.* 85:e0006421. doi: 10.1128/MMBR.00064-21

Parri, M., and Chiarugi, P. (2010). Rac and Rho GTPases in cancer cell motility control. *Cell Commun. Signal.* 8:23. doi: 10.1186/1478-811X-8-23

Radu, M., Semenova, G., Kosoff, R., and Chernoff, J. (2014). PAK signalling during the development and progression of cancer. *Nat. Rev. Cancer* 14, 13–25. doi: 10.1038/nrc3645

Radulovich, N., Pham, N. A., Strumpf, D., Leung, L., Xie, W., Jurisica, I., et al. (2010). Differential roles of cyclin D1 and D3 in pancreatic ductal adenocarcinoma. *Mol. Cancer* 9:24. doi: 10.1186/1476-4598-9-24

Reynolds, A., Wharton, N., Parris, A., Mitchell, E., Sobolewski, A., Kam, C., et al. (2014). Canonical Wnt signals combined with suppressed TGFbeta/BMP pathways promote renewal of the native human colonic epithelium. *Gut* 63, 610–621. doi: 10.1136/gutjnl-2012-304067

Roig, A. I., Eskiocak, U., Hight, S. K., Kim, S. B., Delgado, O., Souza, R. F., et al. (2010). Immortalized epithelial cells derived from human colon biopsies express stem cell markers and differentiate *in vitro*. *Gastroenterology* 138, e1011–e1015. doi: 10.1053/j.gastro.2009.11.052

Schöttelndreier, D., Seeger, K., Grassl, G. A., Winny, M. R., Lindner, R., and Genth, H. (2018). Expression and (lacking) internalization of the cell surface receptors of *Clostridioides difficile* toxin B. *Front. Microbiol.* 9:1483. doi: 10.3389/fmicb.2018.01483

Smits, W. K., Lyras, D., Lacy, D. B., Wilcox, M. H., and Kuijper, E. J. (2016). *Clostridium difficile* infection. *Nat. Rev. Dis. Primers.* 2:16020. doi: 10.1038/nrdp.2016.20

Steffen, A., Ladwein, M., Dimchev, G. A., Hein, A., Schwenkmezger, L., Arens, S., et al. (2013). Rac function is crucial for cell migration but is not required for spreading and focal adhesion formation. *J. Cell Sci.* 126, 4572–4588. doi: 10.1242/jcs.118232

Thullberg, M., Gad, A., Beeser, A., Chernoff, J., and Stromblad, S. (2007). The kinase-inhibitory domain of p21-activated kinase 1 (PAK1) inhibits cell cycle progression independent of PAK1 kinase activity. *Oncogene* 26, 1820–1828. doi: 10.1038/sj.onc.1209983

Wohlan, K., Goy, S., Olling, A., Srivaratharajan, S., Tatge, H., Genth, H., et al. (2014). Pyknotic cell death induced by *Clostridium difficile* TcdB: chromatin condensation and nuclear blister are induced independently of the glucosyltransferase activity. *Cell. Microbiol.* 16, 1678–1692. doi: 10.1111/cmi.12317

Zhang, L. Z., Li, Y. S., and Liu, H. Z. (2015). Meta-analysis of the relationship between XRCC3 T241M polymorphism and colorectal cancer susceptibility. *Genet. Mol. Res.* 14, 14831–14839. doi: 10.4238/2015.November.18.48

Zhang, Q., Sakamoto, K., Liu, C., Triplett, A. A., Lin, W. C., Rui, H., et al. (2011). Cyclin D3 compensates for the loss of cyclin D1 during ErbB2-induced mammary tumor initiation and progression. *Cancer Res.* 71, 7513–7524. doi: 10.1158/0008-5472.CAN-11-1783

Zhu, Z., Schnell, L., Muller, B., Muller, M., Papatheodorou, P., and Barth, H. (2019). The antibiotic bacitracin protects human intestinal epithelial cells and stem cell-derived intestinal Organoids from *Clostridium difficile* toxin TcdB. *Stem Cells Int.* 2019:4149762. doi: 10.1155/2019/4149762

Conflict of Interest: The authors declare that the research was conducted in the absence of any commercial or financial relationships that could be construed as a potential conflict of interest.

Publisher's Note: All claims expressed in this article are solely those of the authors and do not necessarily represent those of their affiliated organizations, or those of the publisher, the editors and the reviewers. Any product that may be evaluated in this article, or claim that may be made by its manufacturer, is not guaranteed or endorsed by the publisher.

Copyright © 2022 Petersen, Stroh, Schöttelndreier, Grassl, Rottner, Brakebusch, Fahrer and Genth. This is an open-access article distributed under the terms of the Creative Commons Attribution License (CC BY). The use, distribution or reproduction in other forums is permitted, provided the original author(s) and the copyright owner(s) are credited and that the original publication in this journal is cited, in accordance with accepted academic practice. No use, distribution or reproduction is permitted which does not comply with these terms.

frontiers in Microbiology

ORIGINAL RESEARCH
published: 10 March 2022
doi: 10.3389/fmicb.2021.787451

Molecular Epidemiology and Antimicrobial Resistance of *Clostridioides difficile* in Hospitalized Patients From Mexico

Emmanuel Aguilar-Zamora[1,2], Bart C. Weimer[3], Roberto C. Torres[1], Alejandro Gómez-Delgado[1], Nayeli Ortiz-Olvera[4], Gerardo Aparicio-Ozores[5], Varenka J. Barbero-Becerra[6], Javier Torres[1] and Margarita Camorlinga-Ponce[1]**

[1] Unidad de Investigación Medica en Enfermedades Infecciosas y Parasitarias, UMAE Pediatría, CMN Siglo XXI, IMSS, México City, Mexico, [2] Escuela Nacional de Ciencias Biológicas, Instituto Politécnico Nacional, México City, Mexico, [3] Department of Population Health and Reproduction, School of Veterinary Medicine, 100K Pathogen Genome Project, University of California, Davis, Davis, CA, United States, [4] Departamento de Gastroenterología, UMAE Hospital de Especialidades, Instituto Mexicano del Seguro Social, México City, Mexico, [5] Departamento de Microbiología, Escuela Nacional de Ciencias Biológicas, Instituto Politécnico Nacional, México City, Mexico, [6] Translational Research Unit, Medica Sur Clinic and Foundation, México City, Mexico

OPEN ACCESS

Edited by:
Uwe Groß, University Medical Center Göttingen, Germany

Reviewed by:
Martinique Frentrup, German Collection of Microorganisms and Cell Cultures GmbH (DSMZ), Germany
Maja Rupnik, National Laboratory of Health, Environment and Food, Slovenia

***Correspondence:**
Javier Torres
uimeip@gmail.com
Margarita Camorlinga-Ponce
margaritacamorlinga@yahoo.com

Specialty section:
This article was submitted to Infectious Agents and Disease, a section of the journal Frontiers in Microbiology

Received: *30 September 2021*
Accepted: *29 December 2021*
Published: *10 March 2022*

Citation:
Aguilar-Zamora E, Weimer BC, Torres RC, Gómez-Delgado A, Ortiz-Olvera N, Aparicio-Ozores G, Barbero-Becerra VJ, Torres J and Camorlinga-Ponce M (2022) Molecular Epidemiology and Antimicrobial Resistance of Clostridioides difficile in Hospitalized Patients From Mexico. Front. Microbiol. 12:787451. doi: 10.3389/fmicb.2021.787451

Clostridioides difficile is a global public health problem, which is a primary cause of antibiotic-associated diarrhea in humans. The emergence of hypervirulent and antibiotic-resistant strains is associated with the increased incidence and severity of the disease. There are limited studies on genomic characterization of *C. difficile* in Latin America. We aimed to learn about the molecular epidemiology and antimicrobial resistance in *C. difficile* strains from adults and children in hospitals of México. We studied 94 *C. difficile* isolates from seven hospitals in Mexico City from 2014 to 2018. Whole-genome sequencing (WGS) was used to determine the genotype and examine the toxigenic profiles. Susceptibility to antibiotics was determined by *E*-test. Multilocus sequence typing (MLST) was used to determine allelic profiles. Results identified 20 different sequence types (ST) in the 94 isolates, mostly clade 2 and clade 1. ST1 was predominant in isolates from adult and children. Toxigenic strains comprised 87.2% of the isolates that were combinations of *tcdAB* and *cdtAB* (*tcdA+/tcdB+/cdtA+/cdtB+*, followed by *tcdA+/tcdB+/cdtA−/cdtB−*, *tcdA−/tcdB+/cdtA−/ cdtB−,* and *tcdA−/tcdB−/cdtA+/cdtB+*). Toxin profiles were more diverse in isolates from children. All 94 isolates were susceptible to metronidazole and vancomycin, whereas a considerable number of isolates were resistant to clindamycin, fluroquinolones, rifampicin, meropenem, and linezolid. Multidrug-resistant isolates (≥3 antibiotics) comprised 65% of the isolates. The correlation between resistant genotypes and phenotypes was evaluated by the kappa test. Mutations in *rpoB* and *rpoC* showed moderate concordance with resistance to rifampicin and mutations in *fusA* substantial concordance with fusidic acid resistance. *cfrE*, a gene recently described in one Mexican isolate, was present in 65% of strains linezolid resistant, all ST1 organisms. WGS is a powerful tool to genotype and characterize virulence and antibiotic susceptibility patterns.

Keywords: *Clostridioides difficile*, antibiotic resistance, whole-genome sequencing, mutation, multilocus sequence typing, adults and children

INTRODUCTION

Clostridioides (*Clostridium*) *difficile* is a spore-forming, gram-positive, and anaerobic bacillus found in the environment and in the intestinal tract of animals and humans. In humans, the infection is the leading cause of antibiotic-associated diarrhea and of a wide range of gastrointestinal syndromes (Knight et al., 2015; Turner and Anderson, 2020). The molecular epidemiology of *C. difficile* infection (CDI) has shown that the bacterial genome and the disease have become very variable in the last decades. The incidence of CDI markedly increased worldwide at the end of the twentieth century (Czepiel et al., 2019), which was associated with the rapid spread of the hypervirulent strain NAP1/B1/027/ST01 [North American Pulse field type 1/restriction endonuclease analysis type BI/ribotype 027/multilocus sequence typing (MLST)] (Krutova et al., 2018; Lv et al., 2019; Guerrero-Araya et al., 2020). In addition, CDI cases attributed to other ribotypes such as RT078, RT001, RT018, and RT126 are emerging in Europe (Couturier et al., 2018), and, currently, CDI is the most frequently identified health care–associated infection in the United States (Guh and Kutty, 2018).

A number of major factors contribute to the virulence of *C. difficile* including the production of toxin A (TcdA) and toxin B (TcdB), which are monoglycosyltransferases that disrupt the gut epithelium (Monot et al., 2015), as well as other factors that participate in colonization like adhesins, pili, and flagella (Janoir, 2016). The toxins are encoded by *tcdA* and *tcdB* genes that are situated in the pathogenicity locus (PaLoc) and are implicated in progression and severity of CDI (Monot et al., 2015). In addition, some *C. difficile* strains express an ADP-ribosylating toxin named *C. difficile* transferase (CDT) that modifies actin and is encoded by the genes *cdtA* and *cdtB* located in the CdTLoc locus (Gerding et al., 2014).

The use of antibiotics induces transmission of *C. difficile*. Many antibiotics are associated with CDI; ampicillin, amoxicillin, cephalosporins, clindamycin, and fluoroquinolones continue to be associated with the highest risk for CDI (Spigaglia, 2016; Banawas, 2018). Understanding the mechanisms of resistance of *C. difficile* is a key issue in the strategy to control spread of CDI (Peng et al., 2017). Resistance to tetracycline, chloramphenicol, and linezolid is less frequently associated with CDI with differences between countries (Sholeh et al., 2020).

C. difficile has a versatile genome content, with a wide range of mobile elements, many of them encoding for antibiotic resistance (Spigaglia, 2016). Transposons that confer resistance to lincomycin and streptogramin B (Tn5398 and Tn6194) (Mullany et al., 2015), to chloramphenicol (Tn4453a and Tn4453b) (Mullany et al., 2015; Peng et al., 2017), to erythromycin (Tn5398), or to tetracycline (Tn916-like and Tn5397) exist in various isolates (Spigaglia et al., 2018). Recently, a *cfr*-like gene named *cfrE* was described in a Mexican *C. difficile* isolate and appears to be associated with resistance to phenicols, lincosamides, oxazolidinones, pleuromutilins, and streptogramin A (Stojković et al., 2020). Mutations in *gyrA* and *gyrB* are associated with resistance to fluoroquinolones, whereas missense mutations in the *rpoB* gene confer resistance to rifaximin and rifampicin (Peng et al., 2017). Currently, standard CDI therapies include metronidazole and vancomycin as the first choice for primary mild and severe CDI, respectively (Spigaglia et al., 2010); however, some studies have recently reported resistance or reduced susceptibility to metronidazole and vancomycin (Chahine, 2018). At present, rifaximin and fidaxomicin are recommended as the antibiotic of choice for relapsing or recurrent CDI (Spigaglia, 2016).

Whole-genome sequencing (WGS) is a tool that allows studies on the diversity, plasticity, and population structure of the *C. difficile* genomes and helps understand the complexity of CDI management including antibiotic resistance (Knight et al., 2015; Saldanha et al., 2020) and toxin variants (Li et al., 2020). It also facilitates understanding the *C. difficile* epidemiology, providing information on the spread, emergence, and detection of strains with increased virulence using genome differences (Knetsch et al., 2013). MLST analyses of housekeeping genes are accepted as a reliable tool for routine typing of CDI; it provides highly reproducible and easy to interpret results as compared to other typing methods (Kamboj et al., 2021), although it is not the best choice for epidemiological studies, where genome-based analyses are currently applied, including core genome MLST (cgMLST) (Bletz et al., 2018; Janezic and Rupnik, 2019).

Although CDI is an important cause of hospital-acquired diarrhea and colitis in Latin America (Muñoz et al., 2018; Guerrero-Araya et al., 2020), little is known about antibiotic resistance and molecular epidemiology of *C. difficile* in this region. In recent years, studies in Mexico have focused mainly on molecular typing of *C. difficile* strains, particularly on the identification of the hypervirulent strain RT027 using PCR ribotyping (Camacho-Ortiz et al., 2015; Martínez-Meléndez et al., 2018). The aim of this study was to examine the molecular epidemiology of *C. difficile* strains isolated from patients at hospitals in Mexico. WGS was used to genotype, determining the genotype of antibiotic resistance, and the profile of toxins in *C. difficile* strains isolated from adults and children.

MATERIALS AND METHODS

Patients and Isolation of *Clostridioides difficile*

A total of 94 *C. difficile* strains were isolated from stool samples of patients with hospital acquired diarrhea; of these, 31 were isolated from children and 63 from adults. Patients were recruited from seven hospitals (one pediatric and six general hospitals) in Mexico City between 2014 and 2018. Hospitals requested *C. difficile* culture from clinically suspected cases, and, from a collection of 160 isolated strains, we selected 63 strains from adults and 31 from children for WGS; selected isolates were those that were sequentially recovered from our frozen collection, and the total number was limited by the available funds for sequencing.

To isolate C. *difficile*, stool samples were treated with 96% ethanol at room temperature for 50 min followed by centrifugation at 4,000 rpm for 10 min. The cell pellets were inoculated onto taurocholate–cefoxitin–cycloserine fructose agar plates and incubated at 37°C for 5 days in an anaerobic jar with

an atmosphere containing 85% N_2, 5% H_2, and 10% CO_2 that was generated using the Anoxomat system (MART Microbiology B.V., The Netherlands). *C. difficile* isolates were identified by their characteristic colony morphology, gram stain, colony fluorescence, and odor. Identification was confirmed using the Vitek MS combined with detection of the *tpi* gene by PCR using primers and conditions previously reported (Lemee et al., 2004). All isolates were frozen at −70°C in Brucella broth medium supplemented with 10% glycerol for subsequent analysis.

Ethical Considerations

The study protocol was approved by the ethical committee of Instituto Mexicano del Seguro Social, and all adult participants or guardians of children were informed about the study and asked to sign a consent letter.

Antimicrobial Susceptibility Assay

The antimicrobial susceptibility of *C. difficile* to clindamycin, ciprofloxacin, levofloxacin, moxifloxacin, linezolid, metronidazole, and vancomycin was determined by the Epsilometric method (*E*-test) on pre-reduced Brucella agar (BBL BD, United States) containing 5% of defibrinated sheep blood, vitamin K (1 μg/ml), and hemin (5 μg/ml). *E*-test strips (Liofilchem, Italy) were placed on the plate and incubated at 37°C for 48 h, in anaerobic conditions (85%N_2, 5%H_2, and 10% CO_2). The minimal inhibitory concentration (MIC) was defined by the point of intersection of the inhibitory zone with the strip, whereas susceptibility to tetracycline, rifampicin, fusidic acid, and meropenem was determined by the agar dilution method. Brucella Agar (BBL BD, United States) was also used but mixed with the antimicrobial agent solution, following the guidelines by the Clinical and Laboratory Standards Institute (CLSI) (Clinical and Laboratory Standards Institute, 2018) and the guidelines by the European Committee on Antimicrobial Susceptibility Testing (EUCAST) (v.2.0).[1] Cutoff values were adopted from the CLSI and EUCAST guidelines for anaerobic bacteria; the breakpoints used to define resistance were as follows: >16 μg/ml for rifampicin, meropenem, and tetracycline; >4 μg/ml for linezolid; 0.5 μg/ml for fusidic acid; >32 μg/ml for metronidazole; >4 for vancomycin; and >8 μg/ml for moxifloxacin, levofloxacin, clindamycin, and ciprofloxacin.

DNA Extraction and Amplification of *Clostridioides difficile* Housekeeping and Toxins Genes

Genomic DNA was prepared from Brucella broth culture of *C. difficile* strains grown under anaerobic conditions at 37°C for 48 h. The culture was harvested by centrifugation (14,000 rpm for 2 min); washed in sterile phosphate buffered solution (PBS); resuspended in 180 μl of lysis buffer comprising 20 mM Tris-HCl, pH 8.0, 2 mM EDTA, and lysozyme (20 mg/ml); and incubated for 30 min at 37°C. DNA was extracted using a DNeasy® Kit (Qiagen, Hilden Germany) according to the manufacturer's instructions (Aguayo et al., 2015). The housekeeping genes *tpi* and *tcdA* (toxin A), *tcdB* (toxin B), and cdtA/*cdtB* (binary toxin) were amplified by PCR as previously described (Lemee et al., 2004; Persson et al., 2008). Positive controls consisted of DNA template from *C. difficile* ATCC 630 and *C. difficile* ATCC 9689.

Whole-Genome Sequencing and Phylogenomic Analysis

Isolates were sequenced at the University of California, Davis (United States) within the 100K Pathogen Genome Project (Weimer, 2017). WGS of the 94 Mexican *C. difficile* strains was done using PE150 on a HiSeq 2500 platform (Illumina Inc., San Diego, CA, United States) (Miller et al., 2019). Genomes were assembled *de novo* with the Shovill pipeline[2] (Trinetta et al., 2020) using default settings, and the quality of assemblies was assessed using QUAST v.5.0.0[3]; genomes with contamination or low coverage (<33×) were discarded. The contigs were annotated using rapid annotation pipeline Prokka v.1.13[4] (Seemann, 2014). All genome sequences were deposited in the NCBI as part of the 100K Pathogen Genome Project BioProject under the accession number PRJNA203445; **Supplementary Table 1** describes the accession number for each genome sequence.

Genomes were screened for the *tcdA*, *tcdB*, and *cdtA*/*cdtB* and other virulence genes using the Virulence Factors Database from Resfinder[5] (Hu et al., 2020) as well as the annotation provided by Prokka (see text footnote 4) (Seemann, 2014).

Raw sequence data files of the isolates were uploaded to EnteroBase web–based platform[6] for core genome analysis. Analysis includes pre-processing, trimming, assembly, post-correction, and filtering, and the output is a FASTA file used for analysis including MLST on different levels (Zhou et al., 2020). EnteroBase includes up to now 23,632 C. *difficile* genomes. We choose the cgMLST scheme, which contains a subset of 2,556 loci, to analyze our 94 strains. Each genome has been assigned to hierarchical sets of single-linkage clusters by cgMLST distances. This hierarchical clustering is used to identify and name populations of *C. difficile* for epidemiological studies (Frentrup et al., 2020). The phylogenetic cluster analysis was plotted by neighbor joining tree that was visualized using the R packages ggplot2 (v3.0.0) (Wickham, 2016) and ggtree (v2.4.1) (Yu et al., 2017).

Multi-Locus Sequence Typing Analysis

Multi-Locus Sequence Typing (MLST) of all isolates was performed using seven housekeeping genes as previously described (Griffiths et al., 2010). The assignation of *C. difficile* sequence type (ST) and clades was done according to PubMLST database using MLST v.2.10.[7] To show the genetic diversity of the MLST results, a maximum-likelihood tree was generated with MUSCLE-aligned concatenated allele sequences using PhyML

[1] http://www.eucast.org

[2] https://github.com/tseemann/shovill

[3] http://bioinf.spbau.ru/quast

[4] https://github.com/tseemann/prokka

[5] https://cge.cbs.dtu.dk/services/ResFinder/

[6] https://enterobase.warwick.ac.uk

[7] http://github.com/tseemann/mlst

v3.0 with a Hasegawa–Kishino–Yano evolutionary model and 1,000 random bootstrap replicates (Edgar, 2004; Guindon et al., 2009).

Bioinformatic Analysis of Antibiotic Resistance

We identified antimicrobial resistance (ARG) genes by screening contigs with ResFinder (Bortolaia et al., 2020) and CARD[8] using ABRicate version 1.0.1[9] (Seemann, 2020). The HMMER program v.2.1.1 was used to build Hidden Markov Model to search for *cfrE* gene. Analysis of previously reported substitutions related to antibiotic resistance in *gyrA*, *gyrB*, *rpoB*, *rpoC*, *fusA*, *pbp2*, and *pbp3* (Isidro et al., 2018) was retrieved using Snippy v.4.6.0,[10] mapping the assembled *C. difficile* Mexican genomes against *C. difficile* 630 reference genome (sequence accession number AM180355.1). Analysis of single nucleotide polymorphisms (SNPs) within antibiotic resistance genes was also done using Snippy (v.4.6.0) BWA. MEM 1.2.0 (Li and Durbin, 2010; see text footnote 10).

To determine the relation between *C. difficile* clades and antimicrobial resistance, a phylogenetic tree was constructed with whole-genome sequences using virtual genome fingerprint with VAMPhyRE software[11] with a probe set of 13 mers, allowing one mismatch and using a threshold of 17 nucleotides.

Statistical Analysis

The frequency of resistance to one or more antibiotics among the study populations was analyzed, and their 95% confidence intervals were estimated. *Z*-test for comparison for two proportions was used to evaluate the frequency of differences in antibiotic resistance, toxin profile, and MLST clades between both children and adult isolates. All statistical analyses were performed in OMS-Epidata version 4.2 (2016).[12] The agreement between antibiotic resistance phenotype and genotype was tested using a Cohen's kappa statistics. A kappa coefficient value of <0.4, 0.4–0.6, 0.61–0.8, and 0.81–1.0 indicated low, moderate, substantial, and perfect agreement, respectively (Liou et al., 2011). In addition, a p-value <0.05 was considered as statistically significant in the above tests.

RESULTS

Clostridioides difficile Isolates

A total of 94 *C. difficile* strains were obtained from patients from seven hospitals in Mexico City. Thirty-one isolates were from children (mean age, 7.4 ± 5.8; 12 females and 19 males), whereas 63 were isolated from adults (mean age, 58.9 ± 17.3 years; 38 females and 24 males).

[8]https://card.mcmaster.ca

[9]https://github.com/tsee-mann/abricate

[10]https://github.com/tseemann/snippy

[11]http://biomedbiotec.encb.ipn.mx/VAMPhyRE

[12]http://www.sergas.es/Saude-publica/EPIDAT

Toxin Profile

The presence of *tcdA, tcdB, cdtA*, and *cdtB* genes was examined using PCR initially and confirmed with the WGS in all strains. **Figure 1A** depicts the toxins profiles. A toxigenic profile (those containing at least one toxin gene) was found in 82 (87.2%) of the isolates, whereas 12 (12.7%) isolates contained no toxin genes and were considered to be non-toxigenic. Among the 82 toxigenic strains (24 from children and 58 from adults), the most frequent toxin profile was *tcdA+/tcdB+/cdtA+/cdtB+*. This profile was significantly different between children (41.9%) and adults (81%) (p = 0.02). Conversely, the toxin profile *tcdA+/tcdB+/cdtB−/cdtB−* was more frequent in children (25.8%) than adults (12%) (p = 0.067). The *tcdA−/tcdB+/cdtA−/cdtB− was* present in five *C. difficile* isolates (four from adults and one from children). One *C. difficile* isolate from children contained only the *cdtB+* gene, and another isolate from a child contained the unusual *tcdA−/tcdB+/cdtA+/cdtB+* combination of toxin genes.

Multi-Locus Sequence Typing

The MLST relationships of the 94 *C. difficile* isolates formed four clades and 20 different ST groups (**Figure 1B**). Clade 2 was the most frequent, although its frequency was higher in adults (74.6%) than in children (48.3%) (p = 0.012). In contrast, clade 1 was more frequent in children (41.9%) than in adults (19%) (p = 0.018) (**Figure 1C**). Four isolates from adults and two from children were in clade 4 and only one isolate from a child belonged to clade 5. ST1 (NAP1/027) was the most common type, accounting for 63% of all the isolates, corresponding to 45/63 (71.4%) and 13/31 (41.9%) of the strains isolated from adult and children, respectively (**Figure 1D**). The remaining STs were represented by one or two isolates, except ST26 (RT039/140, clade 1) identified in four isolates from children. Of note, the following STs were identified only in isolates from children, ST8 (RT002, clade 1), ST11 (RT078, clade 5), ST36 (RT011, clade 1), ST41 (RT244, clade 2), ST310 (clade 4), and ST708. Whereas ST2 (RT014/020/076/220, clade 1), ST16 (RT050, clade 1), ST48 (clade 1), ST58 (clade 1), ST95 (clade 2), and ST109 (clade 4) were identified only in adult isolates.

Antibiotic Resistance

Antimicrobial susceptibility testing of the 94 isolates was done using 11 antimicrobial agents (**Table 1**). The pattern of resistance was similar in both *C. difficile* isolates from children and adults except for levofloxacin, rifampicin, and linezolid where resistance was significantly lower in pediatric isolates (**Table 1**). Isolates from children were resistant to fluoroquinolones at 100% for both ciprofloxacin and moxifloxacin and 77.4% for levofloxacin. Similarly, isolates from adult were largely resistant to fluoroquinolones with moxifloxacin (90.5%), ciprofloxacin (98.4%), and levofloxacin (95.2%). Resistance to tetracycline and fusidic acid was common among isolates from children and adults.

Multiple resistance pattern to clindamycin, ciprofloxacin, and meropenem was frequent in *C. difficile* isolates from both children (64.5%) and adults (65%). Resistance to five

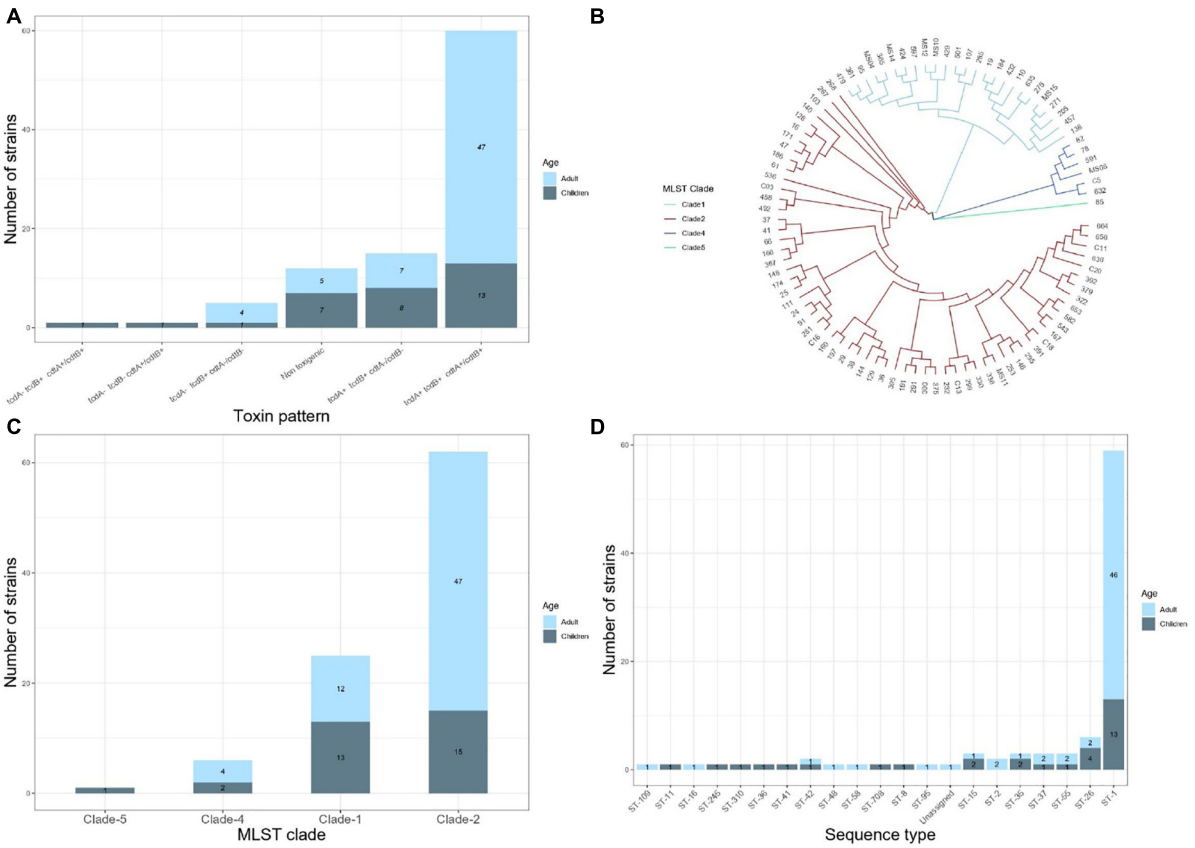

FIGURE 1 | Results of analysis of the whole genome sequences of 94 *Clostridiodes difficile* isolates from 63 adults and 31 children. **(A)** Distribution of toxins profile of the isolates. **(B)** Vamphyre phylogenetic circular tree based on MLST analysis to illustrate the genetic relationships between 20 STs that involve four clades of *C. difficile.* Each color corresponds to clades (Clade 1 blue, Clade 2 red, Clade 4 dark blue, Clade 5 green). **(C)** Number of *C. difficile* strains per MLST clade. **(D)** Number of STs identified by MLST in the studied isolates.

TABLE 1 | Distribution of resistance pattern among Mexican *C. difficile* strains.

Resistance pattern	**Number of strains**				
	Adults ***n*** **= 63**		**Children** ***n*** **= 31**		
Antibiotic	**No.**	**%(95CI)**	**No.**	**%(95CI)**	***p*-value**
Clindamycin (CLIN)	56	88.8 (78.4–95.4)	27	87.1 (70.1–96.4)	0.799
Levofloxacin (LEV)	60	95.2 (86.7–99.0)	24	77.4 (58.9–90.4)	0.008
Ciprofloxacin (CIPRO)	62	98.4 (91.4–99.9)	31	100 (–)	0.958
Moxifloxacin (MOX)	57	90.4 (80.4–96.4)	31	100 (–)	0.749
Rifampicin (RIF)	54	85.7 (74.6–93.2)	20	64.5 (45.3–80.7)	0.018
Linezolid (LIN)	43	68.2 (55.3–79.4)	14	45.1 (27.3–63.9)	0.031
Meropenem (MER)	42	66.6 (53.6–78.0)	23	74.1 (55.3–88.1)	0.458
Fusidic Acid (FUS)	6	9.5 (3.5–19.5)	5	16.1 (5.4–33.7)	0.349
Tetracycline (TET)	6	9.5 (3.5–19.5)	1	3.2 (0.08–16.7)	0.274
Vancomycin (VAN)		0		0	
Metronidazole (MET)		0		0	
Multiple resistance					
CLIN, CIPRO, MERO	41	65.0 (52.0–76.6)	20	64.5 (45.3–80.7)	0.957
CLIN,LEV,CIPRO,RIF, LIN	28	44.4 (31.9–57.5)	12	38.7 (21.8–57.8)	0.597
CLIN,LEV,CIPRO,RIF, MER	38	60.3 (47.2–72.4)	14	45.1 (27.3–63.9)	0.165
CLIN,LEV,CIPRO,RIF, MER, TET	4	6.3 (1.7–15.4)		0	

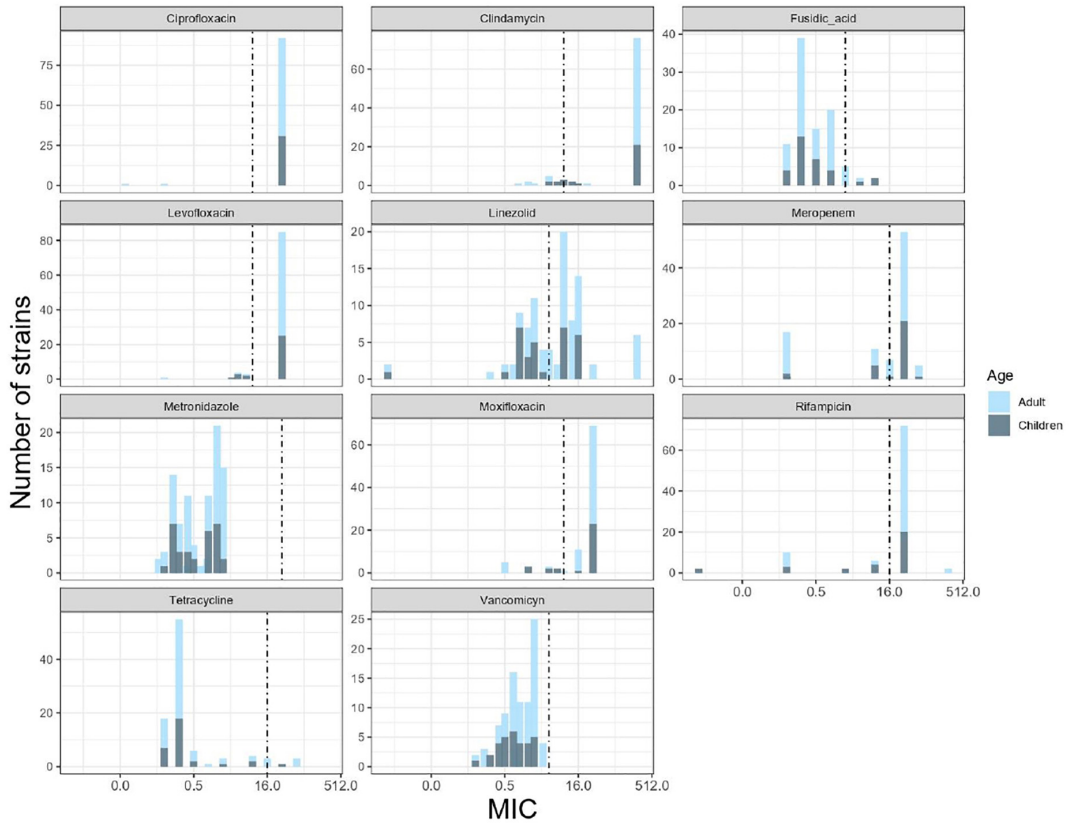

FIGURE 2 | Minimum inhibitory concentration (MIC) distributions for 11 antibiotics against 94 *C. difficile* isolates of children and adults. The graphs show the number of isolates across a range of MIC values. Black dashed lines indicate the clinical breakpoints according to the European Committee for Antimicrobial Susceptibility Testing (EUCAST).

antibiotics was common among isolates from adults (44%) and children (40%). Four isolates from adults contained resistance to six antibiotics (6.3%). The distribution of MIC values for each antibiotic is shown in **Figure 2**. High MIC values were observed for ciprofloxacin, levofloxacin, moxifloxacin clindamycin, meropenem, and rifampicin, with MIC values of 1.5–32 μg/ml for fluoroquinolones and 1.5–256 μg/ml for clindamycin. Among the other antibiotics tested, fusidic acid and tetracycline demonstrated a wide distribution of MIC values ranging from 0.125 to 8 μg/ml and from 0.125 to 64 μg/ml, respectively. All 94 *C. difficile* isolates tested were found susceptible to vancomycin and metronidazole (MICs 0.125–3 μg/ml and 0.094–2 μg/ml, respectively). Regarding the ST, over 95% of the ST1 isolates were resistant to ciprofloxacin, clindamycin, levofloxacin, moxifloxacin, and rifampin, whereas 74% were resistant to linezolid and meropenem, 41.3% to fusidic acid, and 6.8% to tetracycline.

Molecular Analysis of Mechanisms of Resistance

No correlation was observed between the presence of mutations in antimicrobial resistant genes and phenotypic resistance in the *C. difficile* strains (**Table 2**), except in three cases. Three mutations in *rpoB* and one in *rpoC* presented a moderate agreement with resistance to rifampicin, whereas the mutation Glu117Lys in *fusA* showed a substantial agreement with resistance to fusidic acid. High levels of rifampicin resistance (MIC above 16.0 μg/ml) could be due, in part, to multiple substitutions in RNA polymerase sub-unit B *rpoB* (Arg505Lys, Ile548Met, Ile750Met/Val, Asp1160Glu, and Asp1232Glu) that were detected in 70 *C. difficile* isolates from children and adults (**Figure 3**). Furthermore, substitution of Ile833Leu in *rpoC* was also frequent and probably also affecting susceptibility to rifampicin (kappa coefficient of 0.479).

The substitutions Thr82Ile, Leu406Ile, Asp468Asn, Met299Val, and Met324Ile in *gyrA* were detected in 68 *C. difficile* strains (**Figure 3**); however, there was disagreement with phenotypic resistance for these substitutions. In addition, the substitutions Ser366Ala, Gln160His, Ser416Ala, Val130Ile, Arg488Met, and Ile139Arg in *gyrB* were found in 14 C. *difficile* isolates. These substitutions were not associated with resistance in the measured phenotype.

Seven ST1 isolates contained a SNP in *fusA* (Glu117Lys) with very high linkage with phenotypic resistance as determined using a kappa coefficient of 0.7176. Finally, 59 strains contained the A555T substitution in penicillin-binding protein 2 (*pbp2*) but only one had a Y721S substitution in *pbp3*. This substitution

TABLE 2 | Concordance between genotypic and phenotypic drug resistance.

Gene	Antibiotic	Mutation	Kappa Coefficiency (95%CI)
		Thr82Ile	0.2937 [0.0933 – 0.4940]
		Leu406Ile	0.3491 [0.1654 – 0.5328]
gyrA	Moxifloxacin	Asp468Asn	0.3215 [0.1444 – 0.4985]
		Met299Val	0.0034 [−0.0035 – 0.0104]
		Met324Ile	−0.0215 [−0.0637 – 0.0208]
		Thr82Ile	0.0257 [−0.0721 – 0.1236]
		Leu406Ile	0.0773 [−0.0252 – 0.1798]
gyrA	Ciprofloxacin	Asp468Asn	0.0707 [−0.0236 – 0.1650]
		Met299Val	0.0005 [−0.0007 – 0.0016]
		Met324Ile	0.0215 [−0.0639 – 0.0209]
		Ser366Ala	−0.0305 [−0.0919 – 0.0309]
		Gln160His	0.0034 [−0.0035 – 0.0104]
gyrB	Moxifloxacin	Ser416Ala	0.0034 [−0.0035 – 0.0104]
		Val130Ile	−0.0370 [−0.0978 – 0.0237]
		Arg488Met	0.0034 [−0.0035 – 0.0104]
		Ile139Arg	−0.0182 [−0.0608 – 0.0244]
		Ser366Ala	−0.0202 [−0.0626 – 0.0221]
		Gln160His	0.0005 [−0.0007 – 0.0016]
gyrB	Ciprofloxacin	Ser416Ala	0.0005 [−0.0007 – 0.0016]
		Val130Ile	−0.0208 [−0.0631 – 0.0216]
		Arg488Met	0.0005 [−0.0007 – 0.0016]
		Ile139Arg	0.0009 [−0.0009 – 0.0028]
		Arg505Lys	0.4764 [0.2961 – 0.6567]
		Ile548Met	0.4764 [0.2961 – 0.6567]
rpoB	Rifampicin	Asp1232Glu	0.4592 [0.2908 – 0.6670]
		Ile750Met	0.0544 [−0.1297 – 0.0209]
		Asp1160Glu	−0.01 [−0.0549 – 0.0348]
		Ile750Val	−0.0377 [−0.0986 – 0.0232]
		Ile833Leu	0.4789 [0.2908 – 0.6670]
rpoC	Rifampicin	Asn564Lys	0.0058 [−0.0058 – 0.0174]
		Thr543Ile	−0.0214 [−0.0636 – 0.0207]
fusA	Fusidic Acid	Glu117Lys	0.7176 [0.5245 – 0.9107]
pbp2	Meropenem	Ala555Thr	0.1039 [−0.0991 – 0.3068]
pbo3	Meropenem	Tyr721Cys	−0.0214 [−0.0634 – 0.0206]

has been linked with an increase in meropenem resistance; however, the kappa coefficient showed a very low correlation with phenotype resistance in both cases (see **Table 2**).

The genomic analysis showed than all 94 *C. difficile* isolates contained the multidrug and toxic compound extrusion (MATE) multidrug efflux transporter *cdeA* (**Figure 4**), whereas 66 isolates (70.2%) were positive for the methyltransferase *ermB* and only one for *ermQ*. In addition, two linezolid resistant strains (2.1%) also carried the rRNA methyltransferase *cfrB*; whereas the recently described *cfrE* gene was identified in 37 of 57 (64.9%) linezolid resistant strains, showing a perfect agreement with phenotype (kappa coefficient of 0.85). Moreover, a diverse collection of tetracycline resistance genes was identified with a varied distribution in MLST clades, and *tetM, tetO, tetB*, and *tetA* were found in 18.1, 4.3, 1.1, and 1.1% of the isolates, respectively. Components of an aminoglycoside-streptothricin resistance cassette (*ant6-sat4-alph-III*) were identified in 11.7% of the isolates. Three genes encoding putative aminoglycoside-modifying enzymes, termed *aadE* (aminoglycoside 6-adenylytrasnfesare), *aadA27* (aminoglycoside (3″) (9) adenylyltransferase), and *aac(6′)-Ie-aph(2″)-Ia* [bifunctional aminoglycoside N-acetyltransferase AAC(6′)-Ie/aminoglycoside O-phosphotransferase APH(2″)-Ia] were found in 11.7, 2.1, and 8.5% of the isolates, respectively. The chloramphenicol resistance gene *catP* was present in one only (1.1%) strain. Finally, β-lactamase *blaCCD1* and *blaCDD2* were found in 19.1% (n = 18) and 79.8% (n = 75) of the 94 genomes, respectively (**Figure 3**).

Whole-Genome Analyses and Correlation With Resistance, Toxins Profile, and Epidemiologic Variables

A phylogenetic analysis was done with the whole genomes using VAMPhyRE (**Figure 4**) that showed clade 2 with a reduced diversity in ST and resistant genes as compared with the other clades. The genome analysis clearly separated clusters within clades 1 and 4 and even within clade 2 where the analysis clearly separated three isolates (103, 267, and 268) from the other strains. Most strains in clade 2 were closely related and presented the *blaCDD2*, *cdeA*, and *emB* resistance-associated genes, as well as *cfrE*, a gene that has not been reported in other *C. difficile* populations. The other resistance-associated genes were variable present within clusters of clades 1, 4, and 5. Mutations associated to antibiotic resistance were more common among clade 2 isolates (**Figure 3**), and some mutations (Ser366Ala) were found only in clade 4 isolates.

Genomes were submitted to EnteroBase for a cgMLST analysis (**Figure 5**). The study grouped strains following the pattern of the clades, although the extended core analysis resulted in a more detailed clustering within clades, similar to the virtual hybridization assay. Genomic diversity was higher within strains of clades 1, 3, and 4, as compared to clade 2 where genomes seem to be more related. Still, within clade 2, there were clusters grouping isolates by age, hospital, and year of isolation (adult strains 38, 167, 166, and 232 during 2014–2015; and children strains 392 and 379 during 2017). All strains from clade 2 were *tcdA+/tcdB+/cdtA+/cdtB+*, except for two that clearly separated from most other isolates 267 (*tcdA+/tcdB+/cdtB−/cdtB−*) and 268 (*tcdA−/tcdB−/cdtA+/cdtB+*). Distances between genomes of clade 1 were relatively large, with few clusters like adult strains MS10 and MS12 isolated in 2018 or adult strains 19 and 432 together with children strain 184 recovered during 2014, 2015, and 2016. Toxins profiles in clade 1 were mostly *tcdA+/tcdB+/cdtB−/cdtB−* or *tcdA−/tcdB−/cdtA−/cdtB−*. The few strains from clade 4 were also very distant, except for adult strains 82 and 78 recovered in 2014; strains from this clade were non-toxigenic (*tcdA−/tcdB−/cdtA−/cdtB−*) or producing only one toxin (*tcdA−/tcdB+/cdtA−/cdtB−*). The single strain recovered from clade 5, children isolate 85, was very distant from all other isolates and presented the unusual pattern *tcdA−/tcdB+/cdtA+/cdtB+*. Thus, toxigenic

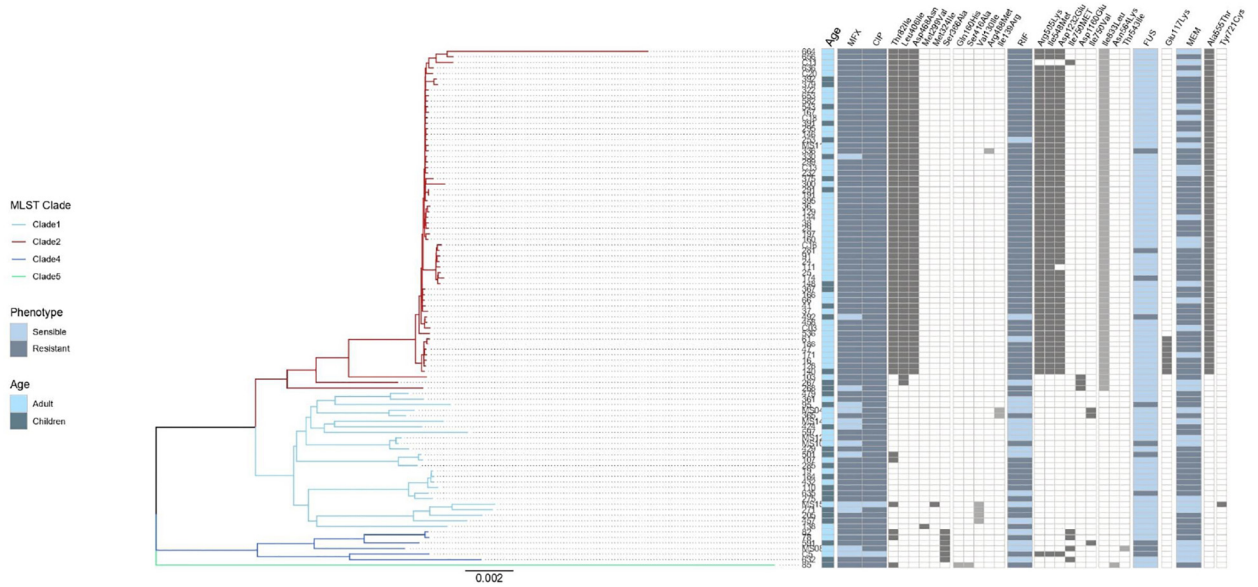

FIGURE 3 | Result of genomic analysis of 94 *C. difficile* strains from Mexican patients and presence of resistance associated mutations. A phylogenetic tree based on whole genome sequences was constructed using virtual hybridization analysis (VAMPhyRE) and correlated with clades, patient's age and with the presence of antibiotic resistance mutations. Presence of mutations is indicated by gray rectangles and absence by white rectangles. The sensitive and resistant phenotype are denoted by gray or blue rectangles, respectively, MFX (Moxifloxacin), CIP (Ciprofloxacin), RIF (Rifampicin) FUS (Fusidic acid), MEM (Meropenem). The presence and absence of mutations are denoted by black and white rectangles, respectively.

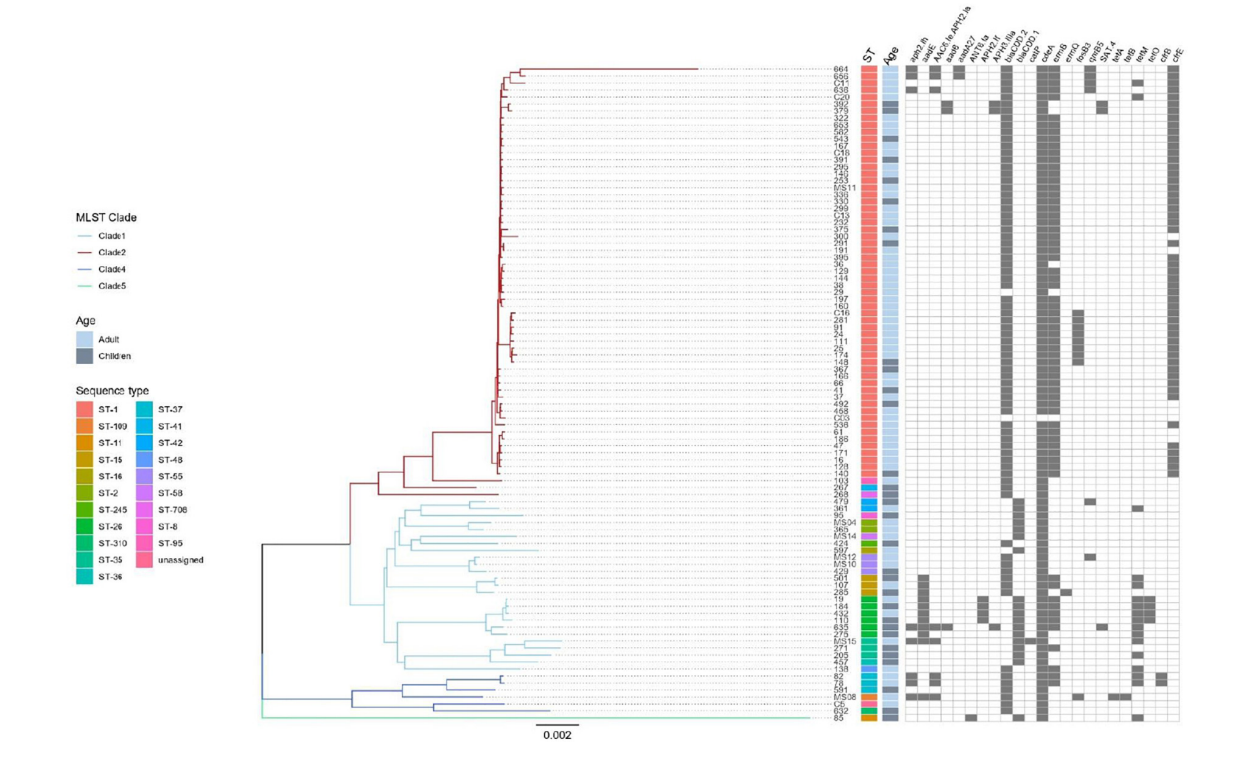

FIGURE 4 | Result of genomic analysis of 94 *C. difficile* strains from Mexican patients and presence of resistance associated genes. Phylogenetic tree based on whole genome sequences was constructed using virtual hybridization analysis (VAMPhyRE) and correlated with clades, STs, patient's age and with the presence of antibiotic resistance genes. Presence is indicated by gray rectangles and absence by white rectangles.

strains *tcdA+/tcdB+/cdtA+/cdtB+* from clade 2 have remained as the most prevalent strains in different adult and pediatric hospitals in Mexico City during the period 2014–2019, whereas strains from clades 1 and 3 varied genomically between hospitals and year of isolation.

DISCUSSION

Antimicrobial therapy is one of the most common risk factors for the development of CDI (Pépin et al., 2004). Consequently, drug resistance is a well-recognized problem among clinical isolates of *C. difficile* that has continued to increase in recent years (Mutai et al., 2021). In 2019, the Center for Disease Control and Prevention classified *C. difficile* as one of five urgent health threats and called for aggressive actions to counteract the significant risks associated with antimicrobial overuse (Mutai et al., 2021). Molecular epidemiology studies of CDI will provide better understand of virulence mechanisms in combination with resistance profiles to commonly used antibiotics so as to define links between distribution, prevalence, and associations with outbreaks that can be targeted for controlling and limiting health consequences. In this study, we used WGS with 94 *C. difficile* isolates to determine the phylogeny, cgMLST allelic profiles, toxin gene profile, and phenotypic and genotypic resistance to antibiotics in strains from pediatric and adult patients in Mexico. Consistent with other studies, the majority of toxigenic strains were *tcdA+/tcdB+/cdtA+/cdtB+* (RT027/ST1) (Aguayo et al., 2015), a toxin profile associated with many ribotypes including the globally distributed RT078 and RT 027.

In contrast to previous studies, we included in the analysis a group of pediatric patients to discover that the frequency of the *tcdA+/tcdB+/cdtA+/cdtB+* was significantly higher in adults compared to children (81% vs. 41.9%; $p = 0.02$). This observation highlights the need to understand the difference between the patient populations to understand how different toxin profiles impact the distribution and prevalence of CDI isolates linked to outbreaks. This agrees with the relatively few studies that reported infection in children with this toxins profile (Lukkarinen et al., 2009; Lees et al., 2020). Five isolates contained the combination of toxins *tcdA−/tcdB+/cdtA−/cdtB−* (four from adults and one from a child), which has been rarely reported in North America, although cases with this toxin combination genotype are increasing in Europe (Freeman et al., 2020) and Asia (Azimirad et al., 2018). Interestingly, this toxin grouping is commonly reported in pediatric cases in the Netherlands (12%) (Van Dorp et al., 2017). It should be noted that the toxin profiles were confirmed by genome sequence and thus not influenced by gene variants that could be missed by PCR. The use of orthogonal methods to find (PCR) and confirm (WGS) these results suggests that these observations are accurate and reflect the clinical situation in Mexico.

In pediatric patients, a significantly higher number of non-toxigenic isolates were found compared to those from adults (22.5% vs. 7.9%; $p = 0.045$), and this agrees with previous studies reporting that children are often colonized by non-toxigenic *C. difficile* isolates (Camorlinga-Ponce et al., 1987; Spigaglia and Barbanti, 2020). Of interest, isolates lacking one or more toxin genes were also more frequently isolated from children. This observation brings into question the role of these organisms in diarrheal episodes in pediatric cases.

MLST typing was determined from WGS of the 94 strains of *C. difficile* to reveal that 20 STs are circulating in hospitals within Mexico City. Differences in the diversity of STs in different geographical regions have been reported, for example, in one Asian region, 68 different STs were reported, whereas, in Colombia, 11 were found (Luo et al., 2019; Muñoz et al., 2019). According to the seven MLST housekeeping genes, a total of five distinct phylogenetic clades (clades 1, 2, 3, 4, and 5) have been described (Janezic and Rupnik, 2019). Four of these clades were identified in the isolates from this study (clade 1, 2, 4, and 5). *C. difficile* clade 2 (ST1) was the dominant MLST type in isolates from Mexico in children and adults. This MLST type (NAP1/ST1) is recognized to be hypervirulent and is responsible for outbreaks worldwide (Badilla-Lobo and Rodríguez, 2021). A previous report in Mexico identified *C. difficile* NAP1/027 hypervirulent in adults with nosocomial diarrhea (Camacho-Ortiz et al., 2015). In children, there has been a notable increase in CDI cases since 2002. In addition, reports suggest that they occur with disease increased severity (Noor and Krilov, 2018). However, there are few studies on infection with hypervirulent *C. difficile* NAP1/RT-027 in pediatric patients (Alvarez and Rathore, 2019). In this study, it was found that children in Mexico were frequently (48.3%) colonized with *C. difficile* clade 2 (ST1) strains. A previous report suggests that CDI is higher in children with cancer (Alvarez and Rathore, 2019) and, in our study, six of the 31 children were oncology patients. However, this study found that children with hospital-acquired diarrhea are often colonized with non-toxigenic strains (22.5%) or isolates that lack *cdt* toxin gene (*tcdA+/tcdB+/cdtA−/cdtB−*) (25.8%), a genotype profile that contrast with that observed in adults.

The epidemiology of CDI is highly dynamic with new strains continually emerging worldwide (Diniz et al., 2019). In contrast, studies in Mexico during the last 5 years suggest that the epidemiology of CDI has remained stable, with ST1 as the dominant MLST type (Camacho-Ortiz et al., 2015; Martínez-Meléndez et al., 2018). Clade 1 was the second most frequent MLST observed (28.2%) with 12 different STs and with different toxin profiles, most of them non-toxigenic (34%) or partially toxigenic (62%) and a very low fraction toxigenic (3.8%). It is well documented that a clade can be associated with more than one RT (Knight et al., 2015), and clade 1 is the most heterogeneous not only in terms of STs but also in its toxigenic profiles (Janezic and Rupnik, 2015), which agrees with our findings. Of note, 42% of the *C. difficile* isolates from children were of clade 1, whereas only 19% of those from adults belonged to this clade ($p = 0.012$), which suggest marked differences in the molecular epidemiology between adult and pediatric *C. difficile* strains.

Five strains were grouped in clade 4, and three of these strains were ST37, which is related to RT017 /ST37 present in Europe, North America, and Argentina (Goorhuis et al., 2009; Imwattana et al., 2019). The presence of this clade is relevant because this ST has been associated with high levels of antibiotic

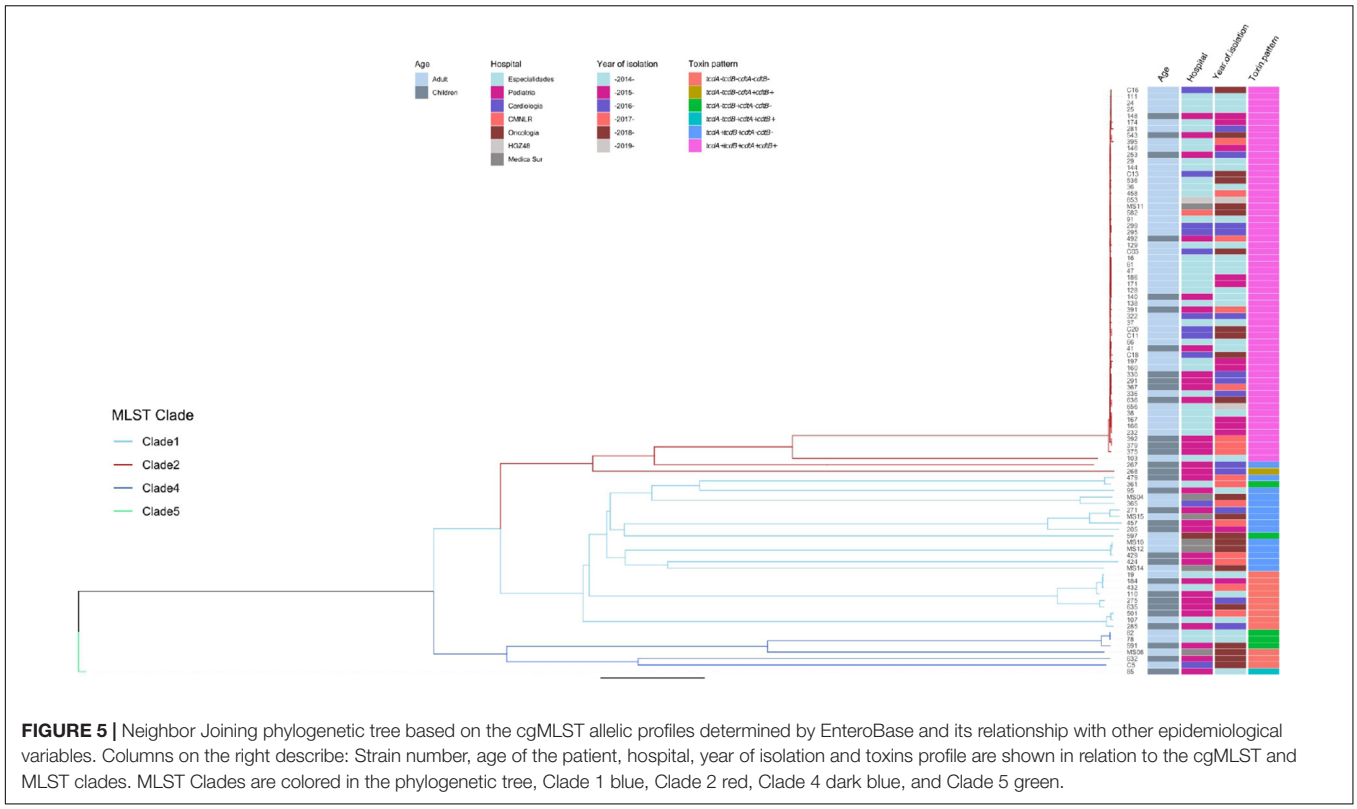

FIGURE 5 | Neighbor Joining phylogenetic tree based on the cgMLST allelic profiles determined by EnteroBase and its relationship with other epidemiological variables. Columns on the right describe: Strain number, age of the patient, hospital, year of isolation and toxins profile are shown in relation to the cgMLST and MLST clades. MLST Clades are colored in the phylogenetic tree, Clade 1 blue, Clade 2 red, Clade 4 dark blue, and Clade 5 green.

resistance, which complicates CDI treatment and increases recurrence risk and the emergence of outbreaks.

One pediatric strain isolated in 2014 belonged to clade 5 (ST11), related to RT078, an emerging and hypervirulent strain reported in China, Japan, Australia, and Europe (Freeman et al., 2015; Li et al., 2019). This genotype was usually associated with infections in animals (Janezic and Rupnik, 2019), but it has now become a significant public health problem in humans. Finally, non-toxigenic strains in clade 1 (STs 15 and 26) have been reported only in Oxfordshire, United Kingdom (Dingle et al., 2011), but, now, we documented its presence in Mexico.

We found that all the isolates were susceptible to metronidazole and vancomycin, which is consistent with the use of these antibiotics as the first-line for treatment of CDI (Spigaglia, 2016; Peng et al., 2017; Mutai et al., 2021). A low prevalence of resistance to metronidazole and vancomycin has been reported in some countries (Goudarzi et al., 2013; Muñoz et al., 2019), although reports of treatment failure with metronidazole are increasing (Chahine, 2018). Resistance to vancomycin has been documented in strains from Iran, Israel, Italy, and Spain (Peng et al., 2017), and resistance as high as 58% was found in strains from Brazil (Fraga et al., 2016).

We found a high proportion of resistance to fluoroquinolone in both children and adult isolates, except for levofloxacin that was significantly lower in isolates from children (see **Table 1**). A lower resistance to moxifloxacin in children than in adult strains has also been reported (Kociolek et al., 2016). The high resistance of *C. difficile* to fluoroquinolones is possibly related to the high proportion of NAP1/RT-027 strains found in our isolates, because high resistance to fluoroquinolones has been reported worldwide in this genotype (Miller et al., 2010; Kociolek et al., 2016). In agreement with the high prevalence of resistance to fluoroquinolones, we found substitutions in the *gyrA* or *gyrB* genes in most of the isolates (69%), although with a higher frequency in adults than in pediatric isolates. Among the 88 strains resistant to moxifloxacin 65 (73.8%) contained a SNP in *gyrA* or *gyrB* presenting the SNPs Thr82Ile, Leu406Ile, and Asp468Asn that are the same observed in most resistant *C. difficile* strains worldwide (Spigaglia et al., 2010; Mac Aogáin et al., 2015). Interestingly, these three SNPs had a low concordance with the phenotype, whereas all other SNPs in both *gyrA* and *gyrB* showed no agreement.

Resistance to erythromycin and clindamycin is the most common phenotype among *C. difficile* strains isolated in Europe (Wasels et al., 2015) and the *erm(B)* gene, the most common determinant of resistance to the macrolide–lincosamide–streptogramin (MLS_B) family. In this study, we identified *erm(B)* in 60 of 83 (72.2%) *C. difficile* isolates that were resistant to clindamycin. In contrast, Ackermann et al. (2003) found that 51% of MLS_B-resistant C. *difficile* strains were negative for *ermB* and suggested that resistance could be the result of mutations in the target sequences in the 23S rRNA gene.

Analysis of the sensitivity of *C. difficile* to rifamycin showed a higher number of resistant strains in adults (85%) than in children (64.5%) (p = 0.018). Reports in other regions have found lower resistance rates; a study in the United States reported resistant to rifampicin in 1.6% of pediatric and 6.7% of adult isolates (Kociolek et al., 2016), whereas a European

study found 13.4% of resistance for this antibiotic (Freeman et al., 2015). Resistance has been associated with point mutations in the *rpoB* gene (O'Connor et al., 2008), and we detected mutations in the *rpoB* (Arg505Lys, Ile548Met, and Asp1232Glu) and *rpoC* (Ile833Leu) genes that showed a moderate agreement with the phenotype.

Resistance to linezolid has been occasionally described in clinical isolates of *C. difficile* (Marín et al., 2015), and it has been associated with *cfr* genes (Stojković et al., 2020). A previous report identified the *cfr* gene as possible mechanism of resistance to linezolid in seven of nine resistant strains (Marín et al., 2015), and, recently, *cfr*E was identified in a Mexican strain resistant to linezolid (Stojković et al., 2020). In this study, we described the presence of *cfrE* gene in linezolid resistant ST1 strains from children and adults and confirmed its dissemination among strains in Mexico (Stojković et al., 2020).

Sequencing of *C. difficile* genome offers an opportunity to identify genes and mutations associates with resistance to antibiotics and allows prediction of the antibiotic resistance phenotype, but validation of the phenotype–genotype correlation in each region is needed. We found no or low phenotype–genotype correlation for most of the studied mutations related to quinolones and meropenem resistance. However, a moderate agreement was found for rifampicin and an excellent agreement for fusidic acid (**Table 2**), suggesting the utility of these markers in our community. The *tet*M gene was a poor predictor for tetracycline susceptibility phenotype, similar to results reported by Xu et al. (2021).

We analyzed the genomes of our isolates with virtual hybridization and cgMLST using the EnteroBase platform for better reference with other studies. Genome analyses allowed a better discrimination of strains and showed that closely related strains belonging to clade 2, toxigenic, and with high antibiotic resistance have been predominant in children and adult isolates from different hospital during the last 5 years. The analysis also showed the high genome diversity within strains from clades 1 and 4 with no clustering across years of isolation or hospitals as observed with clade 2 isolates. Thus, strains with variable toxins profile or antibiotic resistance and high genome diversity are continuously emerging and should be regularly monitored.

In summary, in the current study, we reported the molecular epidemiology of *C. difficile* strains based on a WGS analysis of genotypes, virulence genes, and antimicrobial resistance in hospitals of Mexico. An important strength of this study is the inclusion of *C. difficile* isolates from pediatric and adult patients. Our data show a high prevalence of NAP1/ST1 infection and significant diversity in ST and in toxins profiles, with differences between adult and pediatric isolates. Whereas all *C. difficile* strains were sensitive to metronidazole and vancomycin, a high prevalence of multi-resistance to fluoroquinolones, clindamycin, rifampicin, linezolid, and meropenem was found. The genotype and phenotype agreement were low for most antimicrobials, except for quinolones and fusidic acid. Effective antimicrobial administration and infection control programs are needed to prevent and contain the spread of multidrug resistant and potentially epidemic strains of *C. difficile*.

DATA AVAILABILITY STATEMENT

The datasets presented in this study can be found in online repositories. The names of the repository/repositories and accession number(s) can be found in the article/ **Supplementary Material**.

ETHICS STATEMENT

The studies involving human participants were reviewed and approved by the Ethics Committee Comite Nacional de Investigación Cientifica Numero R-2015-785-089. Written informed consent to participate in this study was provided by the participants' legal guardian/next of kin.

AUTHOR CONTRIBUTIONS

MC-P and JT designed and coordinated the study and wrote the manuscript. EA-Z performed the isolation, antimicrobial susceptibility, analysis of results, and wrote the manuscript. NO-O selected patients. AG-D participated in statistical analysis. GA-O and VB-B contributed to revising the article and isolation of *C. difficile* strains. RT participated in the bioinformatic analysis. BW performed the sequencing of the genome. All authors contributed to the article and approved the submitted version.

FUNDING

This work was supported by the "Coordinación Nacional de Investigación en Salud, Instituto Mexicano del Seguro Social, México, Grand: FIS/IMSS/PROT/PRIO/16/059." The genomes were sequenced using the 100K Pathogen Genome Project resources.

SUPPLEMENTARY MATERIAL

The Supplementary Material for this article can be found online at: https://www.frontiersin.org/articles/10.3389/fmicb.2021.787451/full#supplementary-material

REFERENCES

Ackermann, G., Degner, A., Cohen, S. H., Silva, J., and Rodloff, A. C. (2003). Prevalence and association of macrolide-lincosamide-streptogramin B (MLSB) resistance with resistance to moxifloxacin in *Clostridium difficile*. *J. Antimicrob. Chemother.* 51, 599–603. doi: 10.1093/jac/dkg112

Aguayo, C., Flores, R., Levesque, S., Araya, P., Ulloa, S., Lagos, J., et al. (2015). Rapid spread of *Clostridium difficile* NAP1/027/ST1 in Chile confirms the emergence of the epidemic strain in Latin America. *Epidemiol. Infect.* 143, 3069–3073. doi: 10.1017/S0950268815000023

Alvarez, A. M., and Rathore, M. H. (2019). *Clostridium difficile* infection in children. *Adv. Pediatr.* 66, 263–280. doi: 10.1016/j.yapd.2019.03.010

Azimirad, M., Noukabadi, F., Lahmi, F., and Yadegar, A. (2018). Prevalence of binari-toxin gens (cdtA and cdtB) among clinical strains of *Clostridium difficile* isolated from diarrheal patients in Iran. *Gastroenterol. Hepathol. Bed Bench* 11(Suppl), 59–65.

Badilla-Lobo, A., and Rodríguez, C. (2021). Microbiological features, epidemiology, and clinical presentation of *Clostridioides difficile* strains from MLST Clade 2: a narrative review. *Anaerobe* 69:102355. doi: 10.1016/j.anaerobe.2021.102355

Banawas, S. S. (2018). *Clostridium difficile* infections: a global overview of drug sensitivity and resistance mechanisms. *Bio Med. Res. Intern.* 2018:8414257. doi: 10.1155/2018/8414257

Bletz, S., Janesic, S., Harmsen, D., Rupnik, M., and Mellmann, A. (2018). Defining and evaluating a core genome multilocus sequence typing scheme for genome -wide typing of *Clostridium difficile*. *J. Clin. Microbiol.* 56:e01987-17. doi: 10.1128/JCM.01987-17

Bortolaia, V., Kaas, R. S., Ruppe, E., Roberts, M. C., Schwarz, S., Cattoir, V., et al. (2020). ResFinder 4.0 for predictions of phenotypes from genotypes. *J. Antimicrob. Chemother.* 75, 3491–3500. doi: 10.1093/JAC/DKAA345

Camacho-Ortiz, A., López-Barrera, D., Hernández-García, R., Galván-De los Santos, A. M., Flores-Treviño, S. M., Llaca-Díaz, J. M., et al. (2015). First report of *Clostridium difficile* NAP1/027 in a Mexican Hospital. *PLoS One* 10:e0122627. doi: 10.1371/journal.pone.0122627

Camorlinga-Ponce, M., Gamboa, M., Barragan, J. J., Munoz, O., Fekety, F. R., and Torres, J. F. (1987). Epidemiological aspects of *Clostridium difficile* in a pediatric hospital and its role in diarrheal disease. *Eur. J. Clin. Microbiol.* 6, 542–546. doi: 10.1007/BF02014243

Chahine, E. B. (2018). The rise and fall of metronidazole for *Clostridium difficile* infection. *Ann. Pharmacother.* 52, 600–602. doi: 10.1177/1060028018757446

Clinical and Laboratory Standards Institute (2018). *Performance Standards for Antimicrobial Susceptibility Testing. Twenty Eighth Informational Supplement*, 28th Edn. Wayne, PA: Clinical and Laboratory Standard Institute.Couturier.

Couturier, J., Davies, K., Gateau, C., and Barbut, F. (2018). Ribotypes and new virulent strains across Europe. *Adv. Exp. Med. Biol.* 1050, 45–58. doi: 10.1007/978-3-319-72799-8_4

Czepiel, J., Drozdz, M., Pituch, H., Kuijper, E. J., Perucki, W., Mielimonka, A., et al. (2019). *Clostridium difficile* infection: review. *Eur. J. Clin. Microbiol. Infect. Dis.* 38, 1211–1221. doi: 10.1007/s10096-019-03539-6

Dingle, K. E., Griffits, D., Evans, J., Vaughan, A., Kachrimanidou, M., and Stoesser, N. (2011). Clinical *Clostridium difficile* clonality and pathogenicity locus diversity. *PLoS One* 6:e19993. doi: 10.1371/journal.pone.0019993

Diniz, A., de Olivera, J., Vilela, E., Figueredo, H., Rupnik, M., Wilcox, M., et al. (2019). Molecular epidemiology of *Clostridiodes*(previously *Clostridium difficile* isolates from a university hospital in Minas Gerais. *Brazil.Anaerobe.* 56, 34–39. doi: 10.1016/j.anaerobe.2019.01.010

Edgar, R. C. (2004). MUSCLE: multiple sequence alignment with high accuracy and high throughput. *Nucleic Acids Res.* 32, 1792–1797. doi: 10.1093/nar/gkh340

Fraga, E. G., Nicodemo, A. C., and Sampaio, J. L. M. (2016). Antimicrobial susceptibility of Brazilian *Clostridium difficile* strains determined by agar dilution and disk diffusion. *Braz. J. Infect. Dis.* 20, 476–481. doi: 10.1016/j.bjid.2016.07.004

Freeman, J., Vernon, J., Morris, K., Nicholson, S., Todhunter, S., Longshaw, C., et al. (2015). Pan-European longitudinal surveillance of antibiotic resistance among prevalent *Clostridium difficile* ribotypes. *Clin. Microbiol. Infect.* 21, 248.e9–248.e16. doi: 10.1016/j.cmi.2014.09.017

Freeman, J., Vernon, J., Pilling, S., Morris, K., Nicholson, S., Shearmn, S., et al. (2020). Five year pan European, longitudinal surveillance of *Clostridium difficile* ribotype prevalence and antimicrobial resistance: the extended CloSER study. *Eur. J. Microbiol. Infect. Dis.* 39, 169–177. doi: 10.1007/s10096-019-03708-7

Frentrup, M., Zhou, Z., Steglich, M., Meier-Kolthoff, J. P., Goker, M., and Riedel, T. (2020). A publicly accessible database for *Clostridium difficile* genome sequences supports tracing of transmission chains and epidemics. *Microbial. Genomics* 6:mgen000410. doi: 10.1099/mgen.0.000410

Gerding, D. N., Johnson, S., Rupnik, M., and Aktories, K. (2014). *Clostridium difficile* binary toxin CDT: mechanism, epidemiology, and potential clinical importance. *Gut Microbes* 5, 15–27. doi: 10.4161/gmic.26854

Goorhuis, A., Legaria, M. C., van den Berg, R. J., Harmanus, C., Klaassen, C. H. W., Brazier, J. S., et al. (2009). Application of multiple-locus variable-number tandem-repeat analysis to determine clonal spread of toxin A-negative *Clostridium difficile* in a general hospital in Buenos Aires, Argentina. *Clin. Microbiol. Infect.* 15, 1080–1086. doi: 10.1111/j.1469-0691.2009.02759.x

Goudarzi, M., Goudarzi, H., Alebouyeh, M., Azimi Rad, M., Shayegan Mehr, F. S., Zali, M. R., et al. (2013). Antimicrobial susceptibility of *Clostridium difficile* clinical isolates in Iran. *Iran. Red. Crescent. Med. J.* 15, 704–711. doi: 10.5812/ircmj.5189

Griffiths, D., Fawley, W., Kachrimanidou, M., Bowden, R., Crook, D. W., Fung, R., et al. (2010). Multilocus sequence typing of *Clostridium difficile*. *J. Clin. Microbiol.* 48, 770–778. doi: 10.1128/JCM.01796-09

Guerrero-Araya, E., Meneses, C., Castro-Nallar, E., Guzmán, D. A. M., Álvarez-Lobos, M., Quesada-Gómez, C., et al. (2020). Origin, genomic diversity and microevolution of the *Clostridium difficile* b1/nap1/rt027/st01 strain in costa rica, Chile, Honduras and Mexico. *Microb. Genomics* 6:e000355. doi: 10.1099/mgen.0.000355

Guh, A. Y., and Kutty, P. K. (2018). Clostridioides difficile infection. *Ann. Intern. Med.* 169, 1–16. doi: 10.7326/AITC201810020

Guindon, S., Delsuc, F., Dufayard, J. F., and Gascuel, O. (2009). Estimating maximum likelihood phylogenies with PhyML. *Methods Mol. Biol.* 537, 113–137. doi: 10.1007/978-1-59745-251-9_6

Hu, Q., Liu, C., Zhang, D., Wang, R., Qin, L., Xu, Q., et al. (2020). Effects of low-dose antibiotics on gut immunity and antibiotic resistomes in weaned piglets. *Front. Immunol.* 11:903. doi: 10.3389/fimmu.2020.00903

Imwattana, K., Knight, D. R., Kullin, B., Collins, D. A., Putsathit, P., Kiratisin, P., et al. (2019). *Clostridium difficile* ribotype 017–characterization, evolution and epidemiology of the dominant strain in Asia. *Emerg. Microbes Infect.* 8, 796–807. doi: 10.1080/22221751.2019.1621670

Isidro, J., Menezes, J., Serrano, M., Borges, V., Paixão, P., Mimoso, M., et al. (2018). Genomic study of a *Clostridium difficile* multidrug resistant outbreak-related clone reveals novel determinants of resistance. *Front. Microbiol.* 9:2994. doi: 10.3389/fmicb.2018.02994

Janezic, S., and Rupnik, M. (2015). Genomic diversity of *Clostridium* strains. *Res. Microbiol.* 166, 353–360. doi: 10.1016/j.resmic.2015.02.002

Janezic, S., and Rupnik, M. (2019). Develoment and implementation of whole genome sequencing- based typing schemes for *Clostridiodes difficile*. *Front. Public Health.* 24:309. doi: 10.3389/fpubh.2019.00309

Janoir, C. (2016). Virulence factors of *Clostridium difficile* and their role during infection. *Anaerobe* 37, 13–24. doi: 10.1016/j.anaerobe.2015.10.009

Kamboj, M., McMillen, T., Syed, M., Yan Chow, H., Jani, K., Aslam, A., et al. (2021). Evaluation of a combined multilocus sequence typing and whole genome sequencing two-step algorithm for routine typing of *Clostridiodes difficile*. *J. Clin Microbiol.* 59:e01955-20. doi: 10.1128/JCM.01955-20

Knetsch, C. W., Lawley, T. D., Hensgens, M. P., Corver, J., Wilcox, M. W., and Kuijper, E. J. (2013). Current application and future perspectives of molecular typing methods to study *Clostridium difficile* infections. *Euro Surveillance* 18:20381. doi: 10.2807/ese.18.04.20381-en

Knight, D. R., Elliott, B., Chang, B. J., Perkins, T. T., and Riley, T. V. (2015). Diversity and evolution in the genome of *Clostridium difficile*. *Clin. Microbiol. Rev.* 28, 721–741. doi: 10.1128/CMR.00127-14

Kociolek, L. K., Gerding, D. N., Osmolski, J. R., Patel, S. J., Snydman, D. R., McDermott, L. A., et al. (2016). Differences in the molecular epidemiology and antibiotic susceptibility of *Clostridium difficile* isolates in pediatric and adult patients. *Antimicrob. Agents Chemother.* 60, 4896–4900. doi: 10.1128/AAC.00714-16

Krutova, M., Kinross, P., Barbut, F., Hajdu, A., Wilcox, M. H., and Kuijper, E. J. (2018). How to: surveillance of *Clostridium difficile* infections. *Clin. Microbiol. Infect.* 24, 469–475. doi: 10.1016/j.cmi.2017.12.008

Lees, E. A., Carrol, E. D., Ellaby, N. A. F., Roberts, P., Corless, C. E., Lenzi, L., et al. (2020). Characterization of circulating *Clostridium difficile* strains, host response and intestinal microbiome in hospitalized children with Diarrhea. *Pediatr. Infect. Dis. J.* 39, 221–228. doi: 10.1097/INF.0000000000002559

Lemee, L., Dhalluin, A., Testelin, S., Mattrat, M.-A., Maillard, K., Lemeland, J.-F., et al. (2004). Multiplex PCR Targeting tpi (Triose Phosphate Isomerase), tcdA (Toxin A), and tcdB (Toxin B) Genes for Toxigenic Culture of *Clostridium difficile*. *J. Clin. Microbiol.* 42, 5710–5714. doi: 10.1128/JCM.42.12.5710-5714.2004

Li, H., and Durbin, R. (2010). Fast and accurate long-read alignment with Burrows-Wheeler transform. *Bioinformatics.* 26, 589–595. doi: 10.1093/bioinformatics/btp698

Li, H., Wg, L., Zhang, W., Sb, Y., Zj, L., Zhang, X., et al. (2019). Antibiotic resistance of clinical isolates of *Clostridium difficile* in China and its association with geographical regions and patient age. *Anaerobe* 60:102094. doi: 10.1016/j.anaerobe.2019.102094

Li, Z., Lee, K., Rajyaguru, U., HalJones, C., Janezic, S., Rupnik, M., et al. (2020). Ribotype classification of *Clostridium difficile* isolates is not predictive of amino acid sequence diversity of the toxin virulence factors TcdA and TcdB. *Front. Microbiol.* 11:1310. doi: 10.3389/fmicb.2020.01310

Liou, J.-M., Chang, C.-Y., Sheng, W.-H., Wang, Y.-C., Chen, M.-J., Lee, Y.-C., et al. (2011). Genotypic resistance in *Helicobacter pylori* strains correlates with susceptibility test and treatment outcomes after levofloxacin- and clarithromycin-based therapies. *Antimicrob. Agents Chemother.* 55:1123. doi: 10.1128/AAC.01131-10

Lukkarinen, H., Eerola, E., Ruohola, A., Vainionpää, R., Jalava, J., Kotila, S., et al. (2009). *Clostridium difficile* ribotype 027-associated disease in children with norovirus infection. *Pediatr. Infect. Dis. J.* 28, 847–848. doi: 10.1097/INF.0b013e31819d1cd9

Luo, Y., Cheong, E., Bian, Q., Collins, D. A., Ye, J., Shin, J. H., et al. (2019). Different molecular characteristics and antimicrobial resistance profiles of *Clostridium difficile* in the Asia- Pacific region. *Emerg Microbs Infect.* 8, 1553–1562.

Lv, T., Chen, Y., Guo, L., Xu, Q., Gu, S., Shen, P., et al. (2019). Whole genome analysis reveals new insights into the molecular characteristics of *Clostridium difficile* NAP1/B1/O27/ST1 clinical isolates in the people's Republic of China. *Infect. Drug. Resistant.* 12, 1783–1794. doi: 10.2147/IDR.S203238

Mac Aogáin, M., Kilkenny, S., Walsh, C., Lindsay, S., Moloney, G., Morris, T., et al. (2015). Identification of a novel mutation at the primary dimer interface of GyrA conferring fluoroquinolone resistance in *Clostridium difficile*. *J. Glob. Antimicrob. Resist.* 3, 295–299. doi: 10.1016/j.jgar.2015.09.007

Marín, M., Martín, A., Alcalá, L., Cercenado, E., Iglesias, C., Reigadas, E., et al. (2015). *Clostridium difficile* isolates with high linezolid MICs harbor the multiresistance gene cfr. *Antimicrob. Agents Chemother.* 59, 586–589. doi: 10.1128/AAC.04082-14

Martínez-Meléndez, A., Tijerina-Rodríguez, L., Morfin-Otero, R., Camacho-Ortíz, A., Villarreal-Treviño, L., Sánchez-Alanís, H., et al. (2018). Circulation of highly drug-resistant *Clostridium difficile* Ribotypes 027 and 001 in Two Tertiary-Care Hospitals in Mexico. *Microb. Drug Resist.* 24, 386–392. doi: 10.1089/mdr.2017.0323

Miller, B., Kets, V. V., Rooyen, B. V., Whitehorn, H., Jones, P., and Ranik, M. (2019). *A novel, Single Tube Enzymatic Fragmentation and Library Construction Method Enables Fast Turnaround Times and Improved Data Quality for Microbial Whole-Genome Sequencing. Technical Note APP109001*. Wilmington, MA: Kapa Biosystem, doi: 10.21769/bioprotoc.1010550

Miller, M., Gravel, D., Mulvey, M., Taylor, G., Boyd, D., Simor, A., et al. (2010). Health care-associated *Clostridium difficile* infection in Canada: patient age and infecting strain type are highly predictive of severe outcome and mortality. *Clin. Infect. Dis.* 50, 194–201. doi: 10.1086/649213

Monot, M., Eckert, C., Lemire, A., Hamiot, A., Dubois, T., Tessier, C., et al. (2015). *Clostridium difficile*: new insights into the evolution of the pathogenicity locus. *Sci. Rep.* 5:15023. doi: 10.1038/srep15023

Mullany, P., Allan, E., and Roberts, A. P. (2015). Mobile genetic elements in *Clostridium difficile* and their role in genome function. *Res. Microbiol.* 166, 361–367. doi: 10.1016/j.resmic.2014.12.005

Muñoz, M., Restrepo-Montoya, D., Kumar, N., Iraola, G., Camargo, M., Díaz-Arévalo, D., et al. (2019). Integrated genomic epidemiology and phenotypic profiling of *Clostridium difficile* across intra-hospital and community populations in Colombia. *Sci. Rep.* 9:11293. doi: 10.1038/s41598-019-47688-2

Muñoz, M., Ríos-Chaparro, D. I., Herrera, G., Soto-De Leon, S. C., Birchenall, C., Pinilla, D., et al. (2018). New insights into *Clostridium difficile* (CD) infection in Latin America: novel description of toxigenic profiles of diarrhea-associated to CD in Bogotá, Colombia. *Front. Microbiol.* 9:74. doi: 10.3389/fmicb.2018.00074

Mutai, W. C., Mureithi, M. W., Anzala, O., Revathi, G., Kullin, B., Burugu, M., et al. (2021). High prevalence of multidrug-resistant *Clostridioides difficile* following extensive use of antimicrobials in hospitalized patients in Kenya. *Front. Cell. Infect. Microbiol.* 10:604986. doi: 10.3389/fcimb.2020.604986

Noor, A., and Krilov, L. R. (2018). *Clostridium difficile* infection in children. *Pediatr. Ann.* 47, e359–e365. doi: 10.3928/19382359-20180803-01

O'Connor, J. R., Galang, M. A., Sambol, S. P., Hecht, D. W., Vedantam, G., Gerding, D. N., et al. (2008). Rifampin and rifaximin resistance in clinical isolates of *Clostridium difficile*. *Antimicrob. Agents Chemother.* 52, 2813–2817. doi: 10.1128/AAC.00342-08

Peng, Z., Jin, D., Kim, H. B., Stratton, C. W., Wu, B., Tang, Y.-W., et al. (2017). An update on antimicrobial resistance in *Clostridium difficile*?: resistance mechanisms and antimicrobial susceptibility testing. *J. Clin. Microbiol.* 55, 1998–2008. doi: 10.1128/JCM.02250-16

Pépin, J., Valiquette, L., Alary, M. E., Villemure, P., Pelletier, A., Forget, K., et al. (2004). *Clostridium difficile*-associated diarrhea in a region of Quebec from 1991 to 2003: a changing pattern of disease severity. *CMAJ* 171, 466–472. doi: 10.1503/cmaj.1041104

Persson, S., Torpdahl, M., and Olsen, K. (2008). New multiplex PCR method for the detection of *Clostridium difficile* toxin A(tcdA) and toxin B(tcdB) and the binary toxin(cdtA/cdtB) genes applied to a Danish strain collection. *Clin. Microbiol. Infect.* 14, 1057–1064. doi: 10.1111/j.1469-0691.2008.02092.x

Saldanha, G. Z., Pires, R. N., Rauber, A. P., de Lima-Morales, D., Falci, D. R., Caierão, J., et al. (2020). Genetic relatedness, Virulence factors and Antimicrobial Resistance of *C. difficile* strains from hospitalized patients in a multicentric study in Brazil. *J. Glob. Antimicrob. Resist.* 22, 117–121. doi: 10.1016/j.jgar.2020.01.007

Seemann, T. (2014). prrokka: repid prokaryotic genome annotation. *Bioinformatics* 30, 2068–2069. doi: 10.1093/bioinformatics/btu153

Seemann, T. (2020). *Abricate*. San Francisco, CA: Github.

Sholeh, M., Krutova, M., Forouzesh, M., Mironov, S., Sadeghifard, S., Molaeipour, L., et al. (2020). Antimicrobial resistance in *Clostridiodes* (*Clostridium difficile*) derived from humans: a systematic review and meta analysis. *Antimicrob. Resist Infect. Control.* 9, 158–164. doi: 10.1186/s13756-020-00815-5

Spigaglia, P. (2016). Recent advances in the understanding of antibiotic resistance in *Clostridium difficile* infection. *Ther. Adv. Infect. Dis.* 3, 23–42. doi: 10.1177/2049936115622891

Spigaglia, P., Barbanti, F., Dionisi, A. M., and Mastrantonio, P. (2010). *Clostridium difficile* isolates resistant to fluoroquinolones in Italy: emergence of PCR ribotype 018. *J. Clin. Microbiol.* 48, 2892–2896. doi: 10.1128/JCM.02482-09

Spigaglia, P., and Barbanti, F. (2020). Microbiological characteristics of human and animal isolates of *Clostridiodes difficile* in Italy: results of the Istituto Superiore di Sanita in the years 2006-2016. *Anaerobe.* 61:102136. doi: 10.1016/j.anaerobe.2019.102136

Spigaglia, P., Mastrantonio, P., and Barbanti, F. (2018). Antibiotic resistances of *Clostridium difficile*. *Adv Exp Med Biol.* 1050, 137–159. doi: 10.1007/978-3-319-72799-8_9

Stojković, V., Ulate, M. F., Hidalgo-Villeda, F., Aguilar, E., Monge-Cascante, C., Pizarro-Guajardo, M., et al. (2020). Cfr(B), cfr(C), and a New cfr-Like Gene, cfr(E), in *Clostridium difficile* Strains Recovered across Latin America. *Antimicrob. Agents Chemother.* 64:e01074-19. doi: 10.1128/AAC.01074-19

Trinetta, V., Magossi, G., Allard, M. W., Tallent, S. M., Brown, E. W., and Lomonaco, S. (2020). Characterization of *Salmonella enterica* isolates from selected U.S. Swine feed mills by whole-genome sequencing. *Foodborne Pathog. Dis.* 17, 126–136. doi: 10.1089/fpd.2019.2701

Turner, N. A., and Anderson, D. J. (2020). Hospital Infection Control: *Clostridiodes difficile* Clin. *Colon. Rectal. Surg.* 33, 98–108. doi: 10.1055/s-0040-1701234

Van Dorp, S. M., Smajlovic, E., Knetsch, C. W., Notermans, D. W., De Greeff, S. C., and Kuijper, E. J. (2017). Clinical and Microbiological Characteristics of *Clostridium difficile* Infection Among Hospitalized Children in the Netherlands. *Clin. Infect. Dis.* 64, 192–198. doi: 10.1093/cid/ciw699

Wasels, F., Kuehne, S. A., Cartman, S. T., Spigaglia, P., Barbanti, F., Minton, N. P., et al. (2015). Fluoroquinolone resistance does not impose a cost on the fitness of *Clostridium difficile in vitro*. *Antimicrob. Agent Chemother.* 59, 1794–1796. doi: 10.1128/AAC.04503-14

Weimer, B. C. (2017). 100K Pathogen Genome Project. *Genome Announc.* 5, 3–4. doi: 10.1128/genomea.00594-17

Wickham, H. (2016). *Programming with ggplot2. ggplot2. Use R!*. Cham: Springer, doi: 10.1007/978-3-319-24277-4

Xu, X., Luo, Y., Chen, H., Song, X., Bian, Q., Wang, X., et al. (2021). Genomic evolution and virulence association of Clostridioides difficile sequence type 37

(ribotype 017) in China. *Emerg. Microbes Infect.* 10, 1331–1345. doi: 10.1080/22221751.2021.1943538

Yu, G., Smith, D. K., Zhu, H., Guan, Y., and Lam, T. T. Y. (2017). ggtree: an r package for visualization and annotation of phylogenetic trees with their covariates and other associated data. *Methods Ecol. Evol.* 8, 28–36. doi: 10.1111/2041-210X.12628

Zhou, Z., Alikhan, N. F., Mohamed, K., Fan, Y., and Achtman, M. (2020). The EnteroBase user's guide, with case studies on *Salmonella* transmissions, *Yersinia pestis*, phylogeny, and *Escherichia* core genomic diversity. *Genome Res.* 30, 138–152. doi: 10.1101/gr.251678.119

Conflict of Interest: The authors declare that the research was conducted in the absence of any commercial or financial relationships that could be construed as a potential conflict of interest.

Publisher's Note: All claims expressed in this article are solely those of the authors and do not necessarily represent those of their affiliated organizations, or those of the publisher, the editors and the reviewers. Any product that may be evaluated in this article, or claim that may be made by its manufacturer, is not guaranteed or endorsed by the publisher.

Copyright © 2022 Aguilar-Zamora, Weimer, Torres, Gómez-Delgado, Ortiz-Olvera, Aparicio-Ozores, Barbero-Becerra, Torres and Camorlinga-Ponce. This is an open-access article distributed under the terms of the Creative Commons Attribution License (CC BY). The use, distribution or reproduction in other forums is permitted, provided the original author(s) and the copyright owner(s) are credited and that the original publication in this journal is cited, in accordance with accepted academic practice. No use, distribution or reproduction is permitted which does not comply with these terms.

frontiers in Microbiology

ORIGINAL RESEARCH
published: 24 March 2022
doi: 10.3389/fmicb.2022.814692

Destination and Specific Impact of Different Bile Acids in the Intestinal Pathogen *Clostridioides difficile*

*Nicole G. Metzendorf[1], Lena Melanie Lange[2], Nina Lainer[2], Rabea Schlüter[3], Silvia Dittmann[2], Lena-Sophie Paul[2], Daniel Troitzsch[2] and Susanne Sievers[2]**

[1] Department of Pharmacy, Uppsala University, Uppsala, Sweden, [2] Department of Microbial Physiology and Molecular Biology, Institute of Microbiology, Center for Functional Genomics of Microbes, University of Greifswald, Greifswald, Germany, [3] Imaging Center of the Department of Biology, University of Greifswald, Greifswald, Germany

The anaerobic bacterium *Clostridioides difficile* represents one of the most problematic pathogens, especially in hospitals. Dysbiosis has been proven to largely reduce colonization resistance against this intestinal pathogen. The beneficial effect of the microbiota is closely associated with the metabolic activity of intestinal microbes such as the ability to transform primary bile acids into secondary ones. However, the basis and the molecular action of bile acids (BAs) on the pathogen are not well understood. We stressed the pathogen with the four most abundant human bile acids: cholic acid (CA), chenodeoxycholic acid (CDCA), deoxycholic acid (DCA) and lithocholic acid (LCA). Thin layer chromatography (TLC), confocal laser scanning microscopy (CLSM), and electron microscopy (EM) were employed to track the enrichment and destination of bile acids in the bacterial cell. TLC not only revealed a strong accumulation of LCA in *C. difficile*, but also indicated changes in the composition of membrane lipids in BA-treated cells. Furthermore, morphological changes induced by BAs were determined, most pronounced in the virtually complete loss of flagella in LCA-stressed cells and a flagella reduction after DCA and CDCA challenge. Quantification of both, protein and RNA of the main flagella component FliC proved the decrease in flagella to originate from a change in gene expression on transcriptional level. Notably, the loss of flagella provoked by LCA did not reduce adhesion ability of *C. difficile* to Caco-2 cells. Most remarkably, extracellular toxin A levels in the presence of BAs showed a similar pattern as flagella expression. That is, CA did not affect toxin expression, whereas lower secretion of toxin A was determined in cells stressed with LCA, DCA or CDCA. In summary, the various BAs were shown to differentially modify virulence determinants, such as flagella expression, host cell adhesion and toxin synthesis. Our results indicate differences of BAs in cellular localization and impact on membrane composition, which could be a reason of their diverse effects. This study is a starting point in the elucidation of the molecular mechanisms underlying the differences in BA action, which in turn can be vital regarding the outcome of a *C. difficile* infection.

Keywords: *Clostridioides difficile*, bile acids, toxin A, flagella, adhesion

OPEN ACCESS

Edited by:
Uwe Groß, University Medical Center Göttingen, Germany

Reviewed by:
Guillermo Tellez-Isaias, University of Arkansas, United States
Rishi Drolia, Purdue University, United States

****Correspondence:***
Susanne Sievers
susanne.sievers@uni-greifswald.de

Specialty section:
This article was submitted to Infectious Agents and Disease, a section of the journal Frontiers in Microbiology

Received: *14 November 2021*
Accepted: *09 February 2022*
Published: *24 March 2022*

Citation:
Metzendorf NG, Lange LM, Lainer N, Schlüter R, Dittmann S, Paul L-S, Troitzsch D and Sievers S (2022) Destination and Specific Impact of Different Bile Acids in the Intestinal Pathogen Clostridioides difficile. Front. Microbiol. 13:814692. doi: 10.3389/fmicb.2022.814692

INTRODUCTION

The intestinal pathogen *Clostridioides difficile* is a strictly anaerobic bacterium and causes one of the most frequent hospital-acquired infections in developed countries called CDI for *Clostridioides difficile* infection. *C. difficile* produces two major toxins (toxins A and B) that provoke diarrhea in the first instance (Thomas et al., 2003), and in more advanced and serious cases pseudomembranous colitis, toxic megacolon and possibly even an intestinal perforation leading to sepsis (Rupnik et al., 2009). The bacterium is capable of forming extremely resistant spores that persist antibiotic treatment resulting in very high relapse rates. It is commonly appreciated that an intact intestinal microbiota can prevent bacterial infections, a phenomenon which was called colonization resistance (Buffie and Pamer, 2013). A disturbed intestinal microbiota (dysbiosis), as it can be found after antibiotic treatment, constitutes a welcome opportunity for bacterial pathogens to proliferate in the intestinal tract. In fact, systemic antibiotic treatment and subsequent dysbiosis represent the major risk factor to develop a CDI (Reeves et al., 2011). However, the mechanisms behind the microbiota-mediated colonization resistance are only poorly understood. It is assumed that the structural rearrangements in the microbiota after antibiotic treatment come along with functional and thus metabolic changes creating a basis for germination, growth and toxin production of *C. difficile* (Theriot and Young, 2014, 2015). In 2014, Theriot et al. (2014) could substantiate such metabolic alterations in mice and showed that antibiotic treatment led to an increase of primary bile acids (PBAs), which are produced by the human liver. Concurrently, a decrease in the levels of secondary bile acids (SBAs), which are formed from PBAs by the microbiota was detected. BAs are also thought to be one of the main reasons for the success of fecal microbiota transplantations (FMTs) applied in very heavy cases of CDI (Cammarota et al., 2014). It could be demonstrated that *via* FMT a dysregulated BA composition of CDI patients could be corrected to a composition that suppresses germination of *C. difficile* spores and inhibits growth of the pathogen (Weingarden et al., 2016).

Bile acids are amphiphilic compounds with a steroid structure produced from cholesterol in the liver and secreted into the intestine. They facilitate the absorption and digestion of dietary lipids, but also represent natural antimicrobials due to their soap-like character (Begley et al., 2005). The PBAs cholic acid (CA) and chenodeoxycholic acid (CDCA) are mostly conjugated to taurine or glycine. After deconjugation by specific species of the microbiota in a first step, they can be further converted to the SBAs deoxycholic acid (DCA) and lithocholic acid (LCA), respectively, by dehydroxylation at C7. Along the intestinal tract, the composition of BAs changes due to the conversion of PBAs to SBAs by species of the microbiota, and the total concentration of BAs constantly decreases with passage through the intestines, since up to 95% of BAs are re-absorbed by intestinal epithelial cells (Hofmann, 2009). Only during the last years the key players in the complex human microbiota, that are capable of modifications of BAs, could be pinpointed (Theriot and Young, 2014). Specifically, the ability of *C. scindens* of a 7-alpha-dehydroxylation on the steroid body to form SBAs enhances resistance to CDI (Buffie et al., 2015). However, SBAs are a double-edged sword, since they do not only protect from CDI but are also associated with some diseases such as gallstone formation and colon cancer (Ridlon et al., 2016). In light of this fact, it is of utmost importance to understand the action of BAs on a molecular level, before they or analogs of them could be considered as drugs for treating and preventing CDI.

Membrane-damaging is the most reported effect of BAs on bacteria which could be attributed to their amphiphilic nature. However, at lower concentrations the effect of BAs can be more subtle as minor changes in the membrane do not result in loss of cell integrity but rather in changes in membrane fluidity, transmembrane fluxes or activity of membrane-bound enzymes (Begley et al., 2005). *Vice versa*, stress-mediated alterations in membrane architecture and composition, e.g., by temperature, significantly influence BA resistance (Fernández Murga et al., 1999). All known sublethal stresses that provide cross-protection to BAs are known to induce membrane changes (Begley et al., 2005). In addition to the membrane-disturbing effect, BAs were also reported to structurally alter other macromolecules as RNA, DNA and proteins (Begley et al., 2005). LCA was even reported to cause single strand breaks in DNA in mouse lymphoblasts (Kulkarni et al., 1980).

Bile acid stress experiments in bacteria were mostly carried out using a complex BA mixture isolated from ox or pig (Begley et al., 2002). Thus, very few specific BAs effects are reported and almost nothing is known on the signal transduction of the BA stimulus, e.g., if it is sensed by a two-component system, by a specific receptor or merely indirectly by disruption of membrane integrity or BA-induced alterations in the structure of macromolecules. However, reports on contrary responses to BAs by different species hint at specific receptors and signal transduction pathways. For instance, BAs have been shown to upregulate the flagellar promoter in *Campylobacter jejuni* (Allen and Griffiths, 2001) and motility in *Vibrio cholerae* (Krukonis and DiRita, 2003), but in *Salmonella*, flagellar synthesis and motility was reduced in the presence of BAs (Prouty et al., 2004).

Regarding the action of BAs on *C. difficile*, some specific effects have been described. Already decades ago, Wilson reported a stimulation of spore germination by specific bile preparations (Wilson, 1983). In 2008 CA was elucidated to be the active bile component that instigates spore germination (Sorg and Sonenshein, 2008) and eventually, the protease CspC on the spore surface was demonstrated to be the receptor (Francis et al., 2013) for taurocholate which initiates germination. CspC is the only direct BA receptor in *C. difficile* so far contrasting the human host, where far-reaching effects of BAs due their specific binding to diverse BA receptors (Fiorucci and Distrutti, 2015) have been recognized. BAs do not only act on *C. difficile* spores. An inhibitory effect of SBAs on growth and virulence of *C. difficile* has been frequently described (Lewis et al., 2016; Winston and Theriot, 2016; Thanissery et al., 2017). Interestingly, also a restraining action of BAs on the toxins has been found pointing at a possible direct interaction of BAs and *C. difficile* toxins (Brandes et al., 2012; Darkoh et al., 2013). Lewis et al. (2016) found that *C. difficile* strains that exhibit a high tolerance

to LCA *in vitro* are more virulent in animals and very recently, DCA was confirmed to promote biofilm formation in *C. difficile* (Dubois et al., 2019). Furthermore, Kang et al. (2019) reported an increased inhibitory effect of tryptophan-derived antibiotics on *C. difficile* in the presence of DCA and LCA but not CA. The dissimilar impact of various BAs in *C. difficile* is reflected by the difference of proteomic stress signatures as described recently (Sievers et al., 2019).

In order to understand and to anticipate the susceptibility of patients to develop a CDI as well as to consider BA analogs for treatment or prevention of this infectious disease, more precise knowledge on the targets and mode of action of BAs in *C. difficile* has to be attained. In this study, the effect of four infection-relevant BAs on important virulent traits of *C. difficile* has been characterized. We could show a reduction of flagella in the presence of selected BAs and could ascribe the origin of reduced flagella to transcriptional level. The similar effect could be demonstrated for the abundance of secreted toxin A. However, adhesion to Caco-2 cells did not follow the same pattern and seems not to be exclusively dependent on flagella. Tracking the destination of the four BAs revealed a high accumulation of LCA in *C. difficile* and a distinct distribution of the other BAs in the *C. difficile* cell. In summary, the results do not only disclose specific and infection-relevant novel phenotypes of *C. difficile* in response to various BAs, but also point at the different target location of BAs in the cell to be one of the reasons for the specific phenotypes.

MATERIALS AND METHODS

Strains and Growth Conditions

Strains R20291 and 630 of *C. difficile* obtained from the "German Collection of Microorganisms and Cell Cultures GmbH" (DSM27147 and DSM27543, respectively) were used in this study. For long-term (LT)-stress experiments, *C. difficile* was inoculated to an A_{600} of 0.01 in brain heart infusion medium (BHI, Oxoid Limited, Hampshire, United Kingdom) and grown anaerobically at 37°C (Don Whitley Scientific Limited, Herzlake, Germany) in the presence of growth-inhibiting concentrations of the sodium salts of the four main bile acids (BAs), which are cholic acid (CA) at 15 mM, chenodeoxycholic acid (CDCA) at 0.8 mM, deoxycholic acid (DCA) at 0.8 mM and lithocholic acid (LCA) at 0.08 mM. All BAs were obtained from Sigma Aldrich (Taufkirchen, Germany) except for LCA which was from Steraloids Inc. BA treated cells and untreated cells were harvested anaerobically at exponential growth phase (A_{600} = 0.4–0.6) and at stationary phase (A_{600} = 1.0–1.2 for stressed cells, >2.0 for untreated cells and cells stressed with LCA).

RNA Preparation and Northern Blot Analysis

Bacterial suspension was harvested under anaerobic conditions and collected in ice-cold falcon tubes. The samples were quickly cooled down by placing them carefully in liquid nitrogen. Pelleting of cells was done by centrifugation at 10,200 × *g* at 4°C for 3 min. The supernatant was discarded, the pellet dissolved in sterile suspension buffer (3 mM EDTA, 200 mM NaCl, pH 8.0) and after mechanical disruption proceeded with an acid-phenol extraction of RNA (Nicolas et al., 2012). Quality of the RNA was analyzed on a 1.5% agarose gel and concentration was determined with NanoDrop DeNovix DS-11 Spectrophotometer (DeNovix, Wilmington, United States). RNA was extracted in quadruplicates from independent cultures.

Northern blot analysis was carried out as previously described (Troitzsch et al., 2021). The digoxigenin-labeled RNA probes were synthesized by *in vitro* transcription with T7 RNA polymerase using gene-specific primers (fliC-NB forw 5′-ATGAGAGTTAATACAAATGTAAGTGC-3′ and fliC-NB rev 5′-CTAATACGACTCACTATAGGGAGACTATCCTAATAATTGT AAAACTCC-3′) on chromosomal DNA as template. 10 μg of total RNA were separated on a 1.5% agarose gel per sample. Chemiluminescent signals were detected with a Lumi-Imager (Intas Science Imaging Instruments GmbH). Intensity signals of Northern Blot bands were quantified with Fiji (Schindelin et al., 2012).

Purification of Cell Surface Proteins and Western Blot Analysis

Cell envelope proteins were purified as described earlier by Delmée et al. (1990) and Twine et al. (2009) with a few adaptations (Delmée et al., 1990; Twine et al., 2009). In brief, 100 μL of a *C. difficile* 630 overnight culture were plated on BHI agar plates containing the four BAs at concentrations used for LT-stress and the plates were incubated at anaerobic conditions at 37°C for 48 h. The bacterial lawn was harvested by adding 2 mL water and carefully scraped off with a plastic inoculation loop. The suspensions were intensely shaken on a vortex mixer at maximum power for 3 min followed by centrifugation at 13,500 × *g* at 4°C for 5 min. The supernatants were lyophilized, resuspended in 300 μL water and desalted by using Micron®centrifugal filter devices (Amicon) at 14,000 × g at 4°C for 20 min. Protein concentration was determined using Roti®Nanoquant (Carl Roth, Karlsruhe, Germany). 10 μg of each protein sample was separated on a 10% SDS-PAGE (Amplichem) at constant voltage of 80 V. Gels were stained with Coomassie Brilliant Blue R (Sigma Aldrich, Taufkirchen, Germany) or for Western Blot analysis blotted onto a PVDF membrane (Merck) for 90 min at 100 V. The membrane was incubated for 1 h in Tris-buffered saline (TBS; 10 mM Tris, 150 mM NaCl, 20 mM NaN_3; pH 8.0) buffer containing 0.1% (v/v) Tween-20 (Serva, TBST) and 5% (w/v) skimmed milk powder (Carl Roth, Karlsruhe, Germany). After three washing steps in TBST, the first antibody (chicken anti-FliC *C. difficile* IgY kindly provided by Glen Armstrong) 1:20,000 (v/v) and rabbit anti-FliD *C. difficile* (kindly provided by Severine Pechine) 1:1,000 (v/v) was added in TBST with 5% (w/v) skimmed milk powder and incubated overnight at 4°C. The membrane was washed three times in TBST, before incubation with the secondary antibody (anti-chicken alkaline phosphatase (AP)-conjugated (Sigma Aldrich, Taufkirchen, Germany) 1:10,000 (v/v), anti-rabbit AP-conjugated (Sigma Aldrich, Taufkirchen, Germany) 1:10,000 (v/v) diluted in TBST, 5% (w/v) skimmed milk powder for 45 min at room

temperature (RT). The membrane was washed 3 times in TBST followed by another wash step with ice-cold alkaline phosphatase AP-buffer (0.1 M Tris–Hcl, 0.1 M NaCl, pH9.5). The signal was detected by adding NBT (5% p-nitroblue tetrazolium chloride in 70% (w/v) dimethylformamide) and BCIP [5% 5-bromo-4-chloro-3-indolyl phosphate in 100% dimethylformamide (w/v)] in a ratio of 2:1 (v/v) in AP-buffer. The reaction was stopped with H_2O. Intensity of Western Blot signals was quantified using Fiji (Schindelin et al., 2012).

Eukaryotic Cell Culture

Co-cultivation of *C. difficile* with the human colon carcinoma cell line Caco-2 (ATCC No. HTB-37) was based on a previously described protocol (Natoli et al., 2012). Cells were routinely grown in Dublecco's Modified Eagle's Medium (DMEM, Gibco, Thermo Fisher Scientific) supplemented with 10% inactivated fetal calf serum (FCS) (Sigma Aldrich, Taufkirchen, Germany) and 1% MEM non-essential amino acids (Gibco) in a 5% CO_2 atmosphere at 37°C. Confluency occurred after 5–6 days of incubation. For the adhesion assay, propagated cells were seeded at 5×10^4 per well onto pre-cleaned and poly-L-lysine-coated (PLL; Sigma, 1:10 (v/v) in deionized water) 10 or 18-mm-diameter high precision coverslips (Paul Marienfeld GmbH, Lauda-Königshof, Germany) in a 12-well tissue culture plate (TPP Techno Plastic Products AG, Trasadingen, Switzerland). The culture medium was changed every other day. Cells were used 7 days (almost confluent monolayers) after seeding. The state of polarization and morphological differentiation was monitored by scanning electron microscopy (SEM).

Adhesion Assay

C. difficile adhesion on Caco-2 cells was assayed according to an adapted protocol from Cerquetti et al. (2002). Caco-2 cells were carefully washed with PBS and kept in DMEM without phenol red (Gibco) supplemented with 10% FCS in a 5% CO_2 atmosphere at 37°C until co-cultivation. Bacterial cells were harvested by centrifugation at 630 x *g* for 10 min at RT in air-tight falcons (TPP Techno Plastic Products AG, Trasadingen, Switzerland), washed once with phosphate buffered saline (PBS; 137 mM NaCl, 2.7 mM KCl, 1.4 mM KH_2PO_4, 10 mM $Na_2HPO_4 \times 2\ H_2O$; pH 7.4) and diluted 1:10 (v/v; 1×10^8 bacteria mL^{-1}) in DMEM without phenol red supplemented with 10% FCS. 1 mL of these bacterial suspensions was added to each tissue-culture plate well and incubated for 2 h anaerobically. The bacterial cell suspension was carefully removed and cells were washed 3 times with sterile anaerobic PBS and finally incubated with 1% (v/v) Triton X-100 (Serva) for 5 min at 37°C within the anaerobic chamber. The suspension was removed and dilutions were plated on pre-equilibrated BHI agar plates (Oxoid Limited, Hampshire, United Kingdom). After 24 h the counts of adherent bacteria released from Caco-2 cells were determined. The results were expressed as number of adherent bacteria per cell. For this purpose, Caco-2 cells from a number of non-infected monolayers were collected by trypsinization and counted in parallel. Each experiment was carried out in technical triplicates of three independent experiments. For scanning electron microscopy (SEM), infected monolayers were grown on 10-mm-diameter high precision coverslips (Paul Marienfeld GmbH, Lauda-Königshof, Germany), which were fixed in the medium with 2% (v/v) glutaraldehyde (GA, Sigma Aldrich, Taufkirchen, Germany) and 5% (v/v) paraformaldehyde (PFA, Science Services GmbH, Munich, Germany) for 30 min at RT followed by an incubation at 4°C overnight. The coverslips were then transferred in a 12-well dish containing fixative No. 2 (100 mM HEPES, 50 mM NaN_3, 2% (v/v) GA, 5% (v/v) PFA) and stored at 4°C until further processing.

Confocal Laser Scanning Microscopy

Infected monolayers of Caco-2 cells were fixed with 4% (v/v) PFA in PBS for 12 min in the anaerobic chamber. *C. difficile* in suspension were either pelleted at 160 × g for 5 min and 4% (v/v) PFA was added to the pellet for 12 min at RT or added to PLL-treated 18-mm-diameter coverslips (Paul Marienfeld GmbH, Lauda-Königshof, Germany) and incubated to attach for approx. 30 min proceeded by fixation with 4% (v/v) PFA under anaerobic conditions. All cells were washed for 5 min with PBS thrice and optionally permeabilized with 0.25% (v/v) Triton-X-100 (Serva) for 5 min at RT and carefully rinsed with PBS. Blocking was done with 0.5% (w/v) BSA (Sigma Aldrich, Taufkirchen, Germany) for 1 h at RT. *C. difficile* were labeled using rabbit anti-*C. difficile* No. 501 diluted 1:1,000 (v/v), (provided by Rob Fagan), followed by incubation with the secondary goat anti-rabbit IgG (H + L) Alexa Fluor 488 antibody [1:1,000 (v/v), Thermo Fisher Scientific].

For preparation of sections, cells were fixed as described for transmission electron microscopy (see below). The following day, samples were centrifuged at 1,500 × *g* for 5 min, the pellet was washed with washing buffer (100 mM cacodylate buffer; pH 7.4) thrice for 5 min each and after a final centrifugation step at 9,600 × *g*, the pellet was embedded in low gelling agarose. The material was washed with washing buffer three times for 10 min at RT, dehydrated in graded series of ethanol (30, 50, 70, 90, and 100% for 30 min each step on ice) and subsequently infused with the acryl resin LR White (Plano GmbH, Wetzlar, Germany). Embedding and the following steps were carried as described by Petersen et al. (2020) for sample preparation for serial sectioning and immunofluorescence labeling.

Bile acids were each detected with a 1:100 (v/v) dilution of mouse anti-CA (Dianova), mouse anti-CDCA (Dianova), rabbit anti-DCA (Cloudclone Corp., Hölzel Diagnostika, Köln, Germany) and rabbit anti-LCA (Hölzel Diagnostika, Köln, Germany) followed by incubation with a goat anti-mouse IgG (H + L) Alexa Fluor 546 (Invitrogen) or goat anti-rabbit IgG (H + L) Alexa Fluor 488 (Thermo Fisher Scientific) secondary antibody, respectively, both diluted 1:1,000 (v/v). Caco-2 cells were visualized with 1:1,000 (v/v) Rhodamine-phalloidine stain Alexa Fluor 568 (Thermo Fisher Scientific). DNA was labeled with 1:1,000 (v/v) of 4′,6-diamidino-2-phenylindole (DAPI, Thermo Fisher Scientific) and the membrane visualized with a dilution of 1:1,000 (v/v) Nile red (Thermo Fisher Scientific). All antibody dilutions were prepared in 0.5% (w/v) BSA in PBS and cells were incubated for 2 h with the first antibody and 45 min with the secondary. After antibody incubation, cells were always washed 3 times for 5 min with PBS and once with water before mounting in Mowiol (Carl Roth, Karlsruhe,

Germany). Fluorescence images were acquired using an inverted laser scanning confocal microscope (Zeiss LSM 510 Meta, Carl Zeiss Microscopy GmbH) equipped with a 100 × oil objective (NA 1.4) and the ZEN 2009 software (Carl Zeiss Microscopy GmbH). An argon/krypton laser (488/568 nm) as well as a HeNe-laser (633 nm) were used at 25% intensity. A diode laser (405 nm) was used at 15% intensity. The excitation and emission wavelengths employed were 488 and 510 nm for Alexa Fluor 488, 532, and 570 nm for Alexa Fluor 546 and 568 and 590 nm for Alexa Fluor 568, respectively. Images were captured using a 512 × 512-pixel frame. Gain settings were between 600 and 800. Scan speed was set to 7 and the mean of 4 lines was used. The zoom function and airy unit was set to one. Z-series were used to capture out of focus filaments.

Scanning Electron Microscopy

C. difficile bacterial suspensions were fixed in the medium with 2% (v/v) GA (Sigma Aldrich, Taufkirchen, Germany) and 5% (v/v) PFA (Science Services GmbH, Munich, Germany) for 30 min at RT followed by an incubation at 4°C overnight. Cells were subsequently added on PLL-treated coverslips and left to attach in a humid chamber for approx. 60 min at RT. The remaining liquid was carefully removed, the coverslips were transferred into a 12-well dish containing fixative No. 2 (see above) and stored at 4°C. All coverslips (with single cells or with infected monolayers) were washed with washing buffer (100 mM cacodylate buffer, 1 mM $CaCl_2$; pH 7) three times for 5 min each. Then, the samples were dehydrated in a graded series of aqueous ethanol solutions (10, 30, 50, 70, 90, and 100%) on ice for 15 min each step. Before the final change of 100% ethanol, the samples were allowed to reach room temperature and then critical point-dried with liquid CO_2. Finally, samples were mounted on aluminum stubs, sputtered with gold/palladium and examined with a scanning electron microscope EVO LS10 (Carl Zeiss Microscopy Deutschland GmbH, Oberkochen, Germany). All micrographs were edited by using Adobe Photoshop CS6. Scanning electron micrographs were analyzed with Fiji (Schindelin et al., 2012) to determine the length of the cells (stationary phase: CA $n = 37$, DCA $n = 61$, CDCA $n = 58$, LCA $n = 55$, untreated $n = 65$). All data were further analyzed using Prism (version 9.2.0). The average was calculated and the standard deviation is indicated. Statistical significance was assessed by an unpaired Student's *t*-Test ($^{***}p < 0.001$).

Transmission Electron Microscopy

The used Transmission Electron Microscopy (TEM) procedure is adapted to a protocol kindly provided by Aimee Shen.

C. difficile cells were pelleted in air-tight and pre-equilibrated Falcon tubes (TPP Techno Plastic Products AG, Trasadingen, Switzerland) by centrifugation at 4,000 x *g* for 10 min at 4°C. Cells were washed once with sterile-filtered (0.2 μm) PBS and transferred to 1.5 mL SafeSeal Microcentrifuge Tubes (Sorenson^{TM} BioScience Inc., Allentown, PA, United States) to repeat the centrifugation step. The supernatant was discarded and the pellet was resuspended in PBS and fixative (100 mM cacodylate buffer, 2% (v/v) PFA, 2% (v/v) GA, 5 mM $CaCl_2$, 10 mM $MgCl_2$, 50 mM NaN_3; pH 7.4) in a ratio of 1:5 (v/v). The samples were incubated for 10 min at 20°C and then shifted to 4°C slightly nutating overnight. The following day, samples were centrifuged at 1,500 × *g* for 5 min and the pellet was washed with washing buffer (100 mM cacodylate buffer; pH 7.4) three times for 5 min each. After a final centrifugation step at 9,600 × *g* the pellet was embedded in low gelling agarose. Cells were postfixed in 1% osmium tetroxide in washing buffer for 1 h at 4°C, and then stained with 0.5% uranyl acetate in 0.9% (w/v) sodium chloride at 4°C overnight with washing steps in between. After dehydration in graded series of ethanol (35 – 100% ethanol), the material was transferred stepwise into propylene oxide and finally embedded in AGAR-LV resin (Plano, Wetzlar, Germany). Sections were cut on an ultramicrotome (Reichert Ultracut, Leica UK Ltd., Wetzlar, Germany), stained with 4% aqueous uranyl acetate for 5 min followed by lead citrate for 1 min and analyzed with a transmission electron microscope LEO 906 (Carl Zeiss Microscopy Deutschland GmbH, Oberkochen, Germany). All micrographs were edited by using Adobe Photoshop CS6.

Preparation of Extracellular Proteins for Toxin A Western Blot Analysis

C. difficile R20291 and 630 were anaerobically cultivated in tryptone medium (3% (w/v) tryptone, 2% (w/v) yeast extract, and 0.12% thioglycolic acid) at 37°C in three biological replicates. Cultures were inoculated to an A_{600} of 0.05, treated with growth-inhibiting concentrations of the sodium salts of CA, CDCA, DCA, and LCA as previously described (Sievers et al., 2019) and cultivated for 72 h. Subsequently, 20 mL of each culture was centrifuged at 10,200 × *g* for 20 min at 4°C. The supernatant was transferred into a new centrifuge tube and precipitated with 10% (v/v) trichloroacetic acid overnight at 4°C. Thereafter, precipitated extracellular proteins were pelleted *via* centrifugation for 1 h at 10,200 × *g* at 4°C. Pellets were washed in 1 mL 70% (v/v) ethanol, transferred to a new reaction tube and centrifuged at 11,000 × *g* for 5 min at 4°C. The washing step was repeated twice with 100% ethanol. Pellets were dried and subsequently dissolved in 100 μL urea buffer (8 M urea, 10 mM EDTA, 200 mM EDTA, 1% (w/v) CHAPS). Protein concentration was determined using Pierce^{TM} BCA Protein Assay Kit (Thermo Fisher Scientific) following the manual for the "enhanced protocol."

In total, 150 μg of each protein sample was separated *via* SDS-PAGE. The gel was run at 70 V until samples migrated into the 8% separating gel und was then run at 100 V until samples passed the complete gel. Subsequently, proteins were blotted onto polyvinylidene fluoride (PVDF) membranes (Merck Millipore, Darmstadt, Germany) for 2 h at 100 V. Blotted membranes were treated and detected as described above, but using a primary antibody against TcdA (1:10,000 (v/v), tgcBiomics, Bingen, Germany) and an anti-mouse antibody as secondary antibody (1:25,000 (v/v), Sigma Aldrich, Taufkirchen, Germany) Blots were scanned and signals were quantified using ImageJ (Schneider et al., 2012).

Thin Layer Chromatography

Lipids were extracted according to an adapted protocol by Nakayasu et al. (2016). Briefly, bacterial cells were pelleted by

centrifugation at 10,200 x *g* for 10 min at 4°C. The supernatant was discarded and the pellets were resuspended in freshly prepared 150 mM ammonium bicarbonate and subjected to vortex mixing for 30 sec. A volume of four-fold excess of pre-warmed 38°C chloroform-methanol 2:1 (v/v) was added to the samples, mixed thoroughly and left to incubate for 5 min on ice. Samples were vortexed again and subsequently centrifuged at 14,000 × *g* for 10 min at 4°C. Three phases appeared and for lipid analysis the bottom organic phase was collected and transferred into a new reaction tube. Samples were air-dried in a Speedvac and pellets were reconstituted in 12 μL chloroform-methanol 2:1 (v/v). Samples were applied onto a thin layer chromatography silica gel 60G coated glass plate (Merck) and separated by using chloroform/methanol p.a./H_2O (75%: 25%: 2.5%) as the solvent system. Lipids were visualized with 10% (w/v) phosphomolybdic acid in ethanol.

RESULTS

Expression and Abundance of Flagella

It was previously shown that distinct BAs have an impact on the presence of flagella on the cell surface of *C. difficile* influencing motility of the bacterial cell (Sievers et al., 2019). In the present work these data could be verified and extended. In Confocal Laser Scanning Microscopy (CLSM) and SEM analyses it was demonstrated that *C. difficile* cells challenged with CA feature just as many flagella as non-stressed bacteria. DCA and CDCA stress result in a reduced number of flagella while LCA challenge leads to an almost complete loss of flagella (**Figures 1A,B**). This is in perfect accordance with the data in our previous work, where flagella abundance was exactly quantified (Sievers et al., 2019). It should be noted that the different BA concentrations used in this study were adapted to provide a comparable extent of growth inhibition of *C. difficile*. The question remained, if the reduced number of flagella is caused by the sole loss of the filaments from the cell surface during sample preparation for microscopic analyses or if the cellular synthesis of flagellar components is influenced by BA. To give an answer, antibodies against FliC and FliD, both representing flagellar proteins, were used to determine the abundance of these two proteins on the cell surface of *C. difficile*. Extracts of *C. difficile* surface proteins were prepared, the proteins separated *via* SDS-PAGE and FliC and FliD quantified by Western Blot analysis. Western Blot signals reflect a lower abundance of flagella proteins in the presence of DCA and CDCA, and even more pronounced in the presence of LCA (**Figure 2A**), once more indicating a reduced flagella synthesis during BA stress with the exception of CA. In a next step, it should be clarified if differences in flagella abundance have their origin already on transcriptional level. For this reason, *fliC* mRNA abundance after challenge with different BAs was assayed in Northern Blot analysis (**Figure 2B**). The mRNA abundance resembles protein levels meaning that the lower expression of flagellar proteins, specifically FliC, during LCA, DCA, and CDCA challenge, is already implemented on transcriptional level.

Adhesion to Epithelial Cells

In a previous study it was shown that BAs can cause a reduced motility of *C. difficile* with LCA-stressed cells being essentially immotile (Sievers et al., 2019). In this work, the ability of BA-challenged *C. difficile* cells to adhere to intestinal epithelial cells (Caco-2 cells) was tested, since adherence is not only a key feature for the infection process but also known to be mediated by flagella (Tasteyre et al., 2001). As expected, and in accordance with flagella abundance data, adhesion of CA-stressed *C. difficile* cells is comparable to unstressed cells (**Figure 3**). Also anticipated

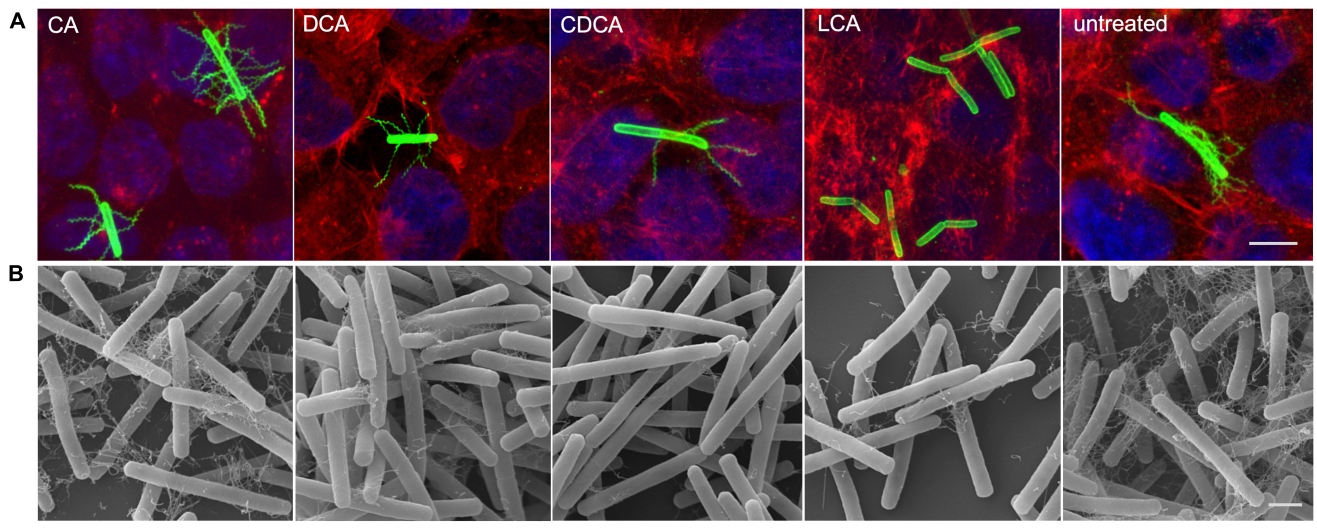

FIGURE 1 | Flagella abundance. **(A)** Immunofluorescence (IF) of *C. difficile* challenged with the four different bile acids (CA, cholic acid; DCA, deoxycholic acid; CDCA, chenodeoxycholic acid; LCA, lithocholic acid) and untreated cells co-cultivated on Caco-2 cells. IF staining: green – anti-*C. difficile* antibody, red – Rhodamine-phalloidine and blue – DAPI, scale bar = 5 μm. **(B)** Scanning electron micrographs of exponential phase *C. difficile* cells challenged with BAs prior to co-cultivation with Caco-2 cells, scale bar = 1 μm.

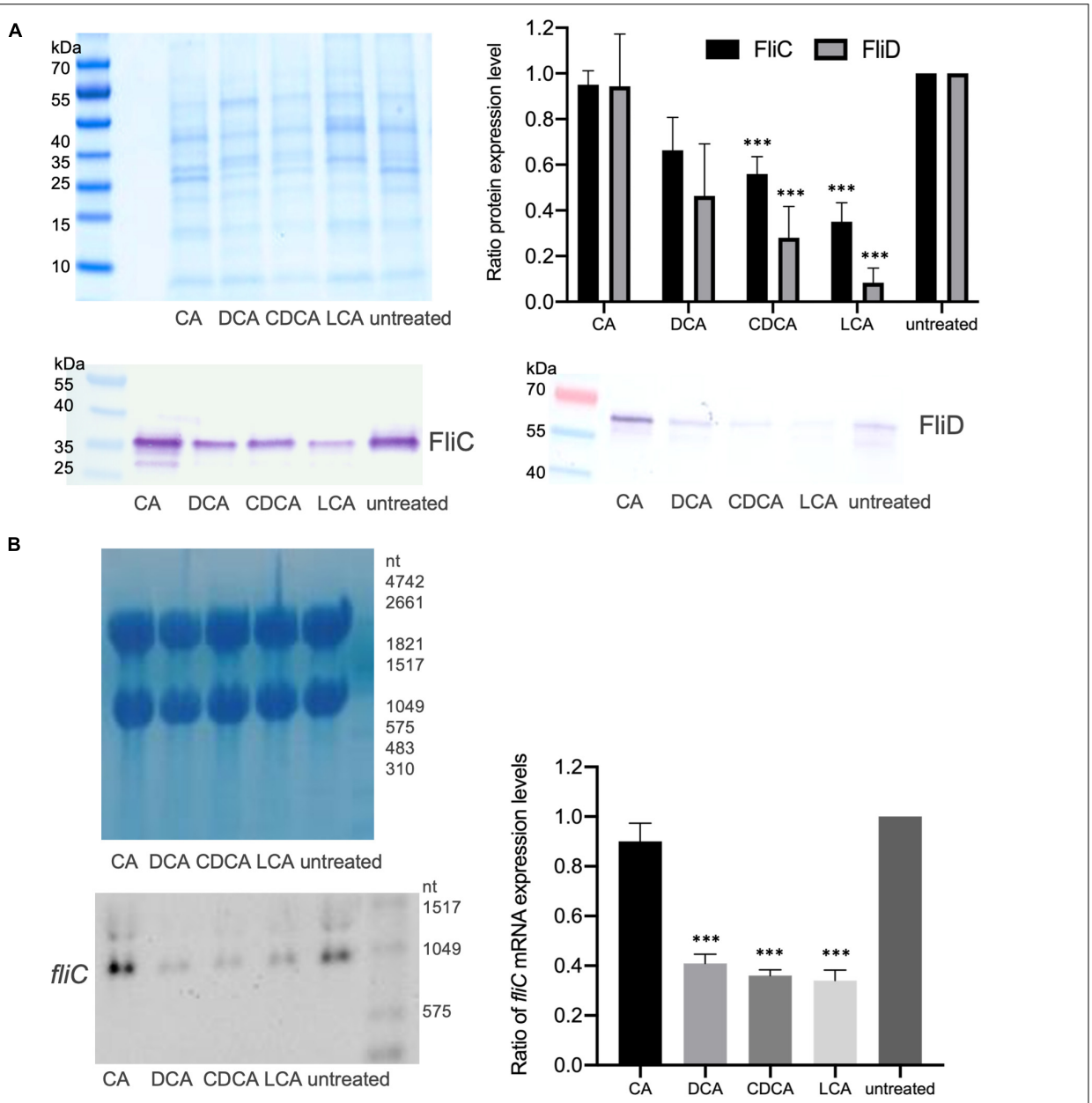

FIGURE 2 | Flagella protein expression. **(A)** Western Blot analysis of FliC and FliD expression in untreated cells and in cells stressed with the four different BAs with a Coomassie-stained gel in the upper left corner that was run as a loading control in parallel. Right (top): Average quantification of signal intensities of FliC as well as FliD bands of three replicates normalized to untreated condition. **(B)** Transcriptional profiling of *fliC* expression by Northern Blotting. Left (top): Methylene blue staining of RNA gel serving as a loading control. Left (bottom): Exemplary *fliC*-specific Northern Blot. Right: Three biological replicates were analyzed and normalized to the control condition. Standard deviation is indicated and values significantly different by a Student's *t*-test compared to untreated cells are marked (***p-value <0.001).

was the decrease in adherence of *C. difficile* stressed with DCA and CDCA, but unexpected was the persistent adherence of *C. difficile* which was stressed with LCA. These cells are almost devoid of flagella and must mediate their adherence to Caco-2 cells by some kind of flagella-independent way. This data was confirmed by repeating the adhesion assay with stationary *C. difficile* stressed with the four bile acids (**Figures 4C,D**). In stationary phase LCA-treated *C. difficile* have regained flagella growth (**Figure 4A**) but the number of bacteria that adhere to the Caco-2 cells remains very similar to cells grown to exponential phase only (**Figures 4D**, **3B**).

Toxin Expression

It has been shown that flagella expression correlates with toxin expression in *C. difficile* (Aubry et al., 2012). Thus, we investigated if the presence of BAs has also an impact on the amount of toxins produced by *C. difficile*. The toxins are mostly synthesized in the late stationary phase with some strains

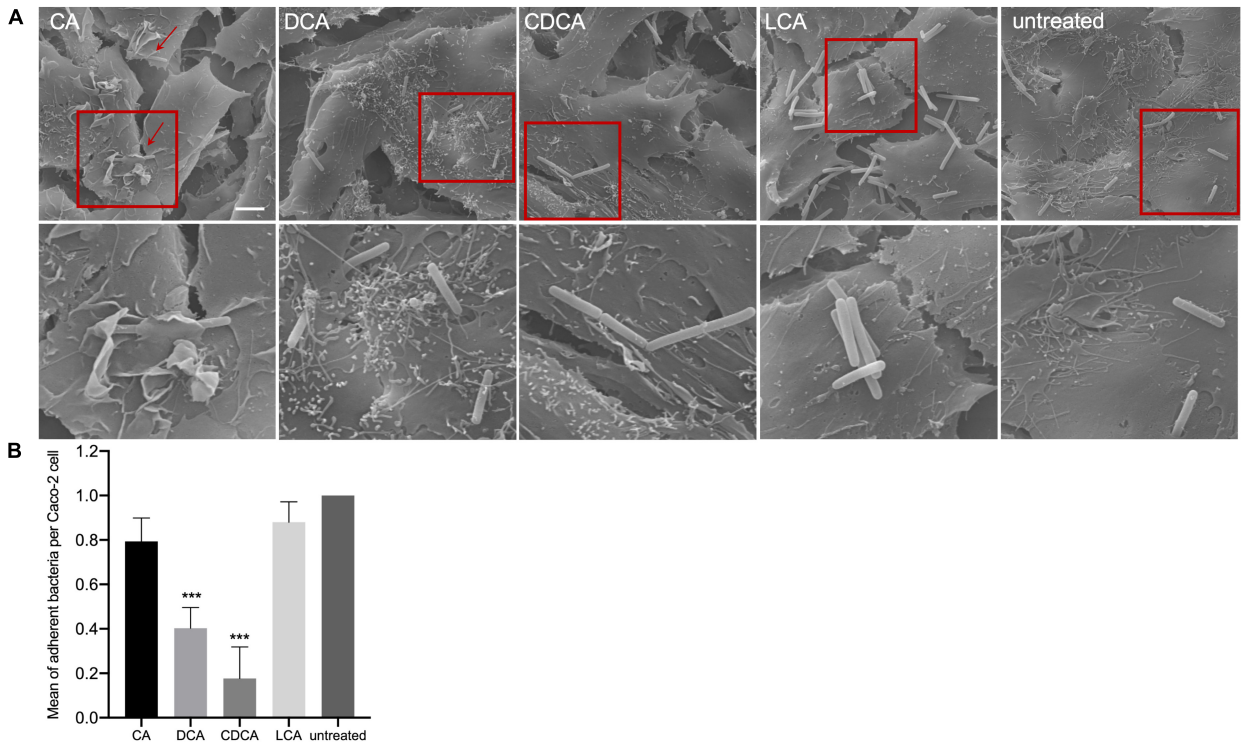

FIGURE 3 | Co-cultivation of bile acid stressed *C. difficile* with Caco-2 cells. **(A)** Scanning electron micrographs of co-cultivation of Caco-2 cells with untreated *C. difficile* and *C. difficile* challenged with four different bile acids (CA, cholic acid; DCA, deoxycholic acid; CDCA, chenodeoxycholic acid; LCA, lithocholic acid), scale bar = 5 μm. Red squares indicate zoomed in area shown below. **(B)** Adhesion assay after co-cultivation of Caco-2 cells with bile acid stressed *C. difficile*. Colony forming units of three independent experiments with three technical replicates each were determined and the number of adherent bacteria per Caco-2 cell was visualized. Standard deviation is indicated and values significantly different by a Student's *t*-test compared to untreated cells are marked (***p-value <0.001).

producing more toxin than others (e.g., strain R20291). Growth media lacking specific nutrients, such as glucose and cysteine, even facilitate toxin expression (Bouillaut et al., 2015). In this study, *C. difficile* strains 630 and R20291 were grown for 72 h in tryptone medium containing different BAs. To measure toxin expression, the abundance of toxin A in the extracellular protein fraction was determined by Western Blot analysis (**Figure 5** and **Supplementary Figure 1**). The amount of toxin A secreted by *C. difficile* into the medium correlates very well with flagella expression in exponentially growing cells stressed with different BAs. Both strains produce higher amounts of toxin in the absence of BAs. CA does not hamper toxin synthesis, but the other three BAs provoke a clear reduction of secreted toxin A.

Cellular Location of Bile Acids

Different BAs have different impact on *C. difficile*, not only on the expression of flagella, host cell adherence and toxin secretion as shown in this study, but also on germination, growth, biofilm formation and toxin action (Sorg and Sonenshein, 2008; Darkoh et al., 2013; Thanissery et al., 2017; Dubois et al., 2019). However, the molecular understanding for most of such differences is still missing. To elucidate the mode and place of action of BAs in the *C. difficile* cell, information on the cellular location of the single BAs is mandatory. There is no information yet on how efficiently external BAs from growth media or the gut lumen enter a *C. difficile* cell. In this study, we aimed for a first and semi-quantitative view in this regard. *C. difficile* cells stressed with growth-inhibiting concentrations of different BAs were obtained and their lipid fractions were extracted for a separation *via* TLC. Aside, pure BAs were applied on TLC plates and served as reference to pinpoint the single BAs on the plates. Although LCA was used in a much lower concentration compared to the other BAs, one can easily realize an extreme accumulation of LCA in *C. difficile* cells (**Figure 6**). This vast amount of LCA can already be detected in exponentially growing cells grown for 5 h in medium containing the BAs. In contrast, *C. difficile* cells challenged with DCA and CDCA show an enrichment in BAs first in stationary but barely in exponential growth phase. A clear accumulation of CA could be detected in stationary phase cells as well. The CA spot of the exponential growth phase sample overlays with signals of other lipids. Besides the enormous accumulation of LCA in *C. difficile*, differences can be noticed in lipid patterns comparing the different BA conditions. Especially in stationary phase, lipid composition of BA stressed cells appears to be different from untreated cells possibly caused by an adjustment of the cell membrane composition in response to BA stress.

In addition to TLC experiments, microscopic methods were consulted to gain evidence on the cellular location of BAs. TEM revealed interesting differences on the impact of BAs in *C. difficile*

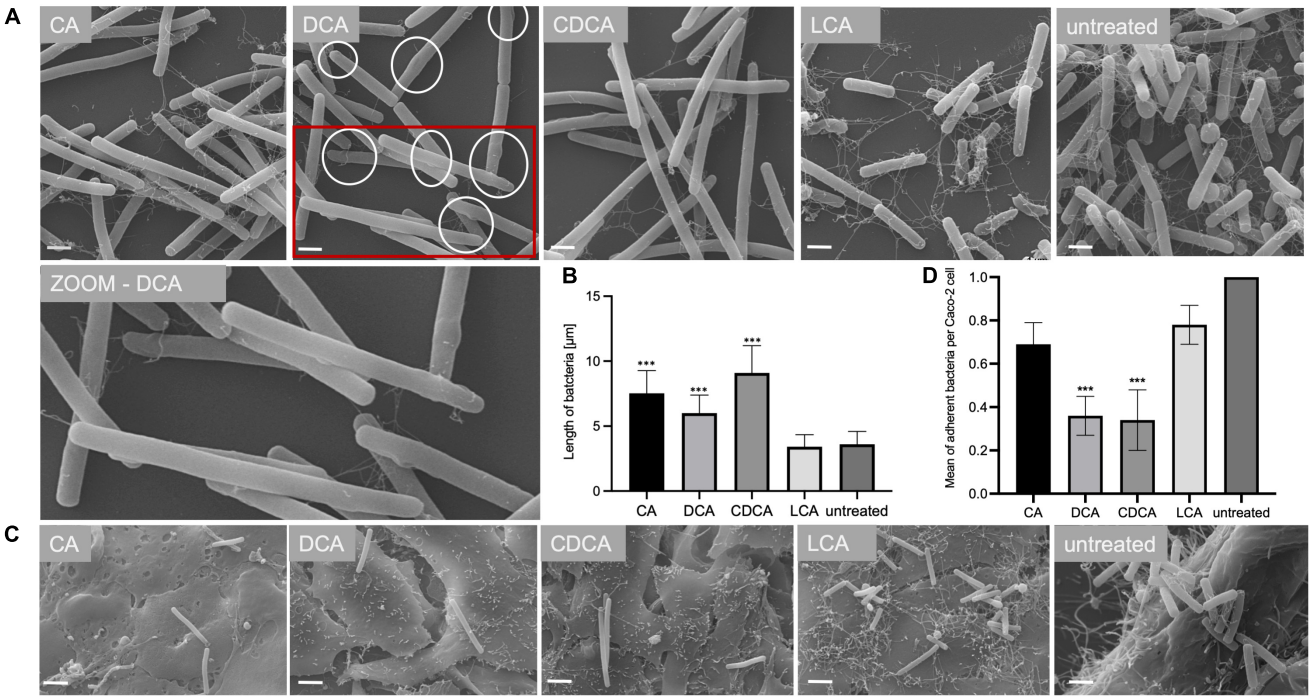

FIGURE 4 | Morphology of bile acid stressed *C. difficile* in stationary phase. **(A)** Scanning electron micrographs of untreated *C. difficile* (untreated) and *C. difficile* challenged with four different bile acids (CA, cholic acid, DCA, deoxycholic acid; CDCA, chenodeoxycholic acid; LCA, lithocholic acid). Scale bar = 1 µm. Circles in DCA micrograph indicate "swellings." **(B)** Average length of bacterial cells is given in µm. **(C)** Scanning electron micrographs of co-cultivated untreated *C. difficile* and *C. difficile* challenged with four different bile acids (CA, DCA, CDCA, and LCA) with Caco-2 cells, scale bar = 2 µm. **(D)** Adhesion assay after co-cultivation of Caco-2 cells with bile acid stressed *C. difficile* from stationary phase. Colony forming units of 3 independent experiments with three technical replicates each were determined and the number of adherent bacteria per Caco-2 cell was visualized. Standard deviation is indicated and values significantly different by a Student's *t*-test compared to untreated cells are marked (***p-value <0.001).

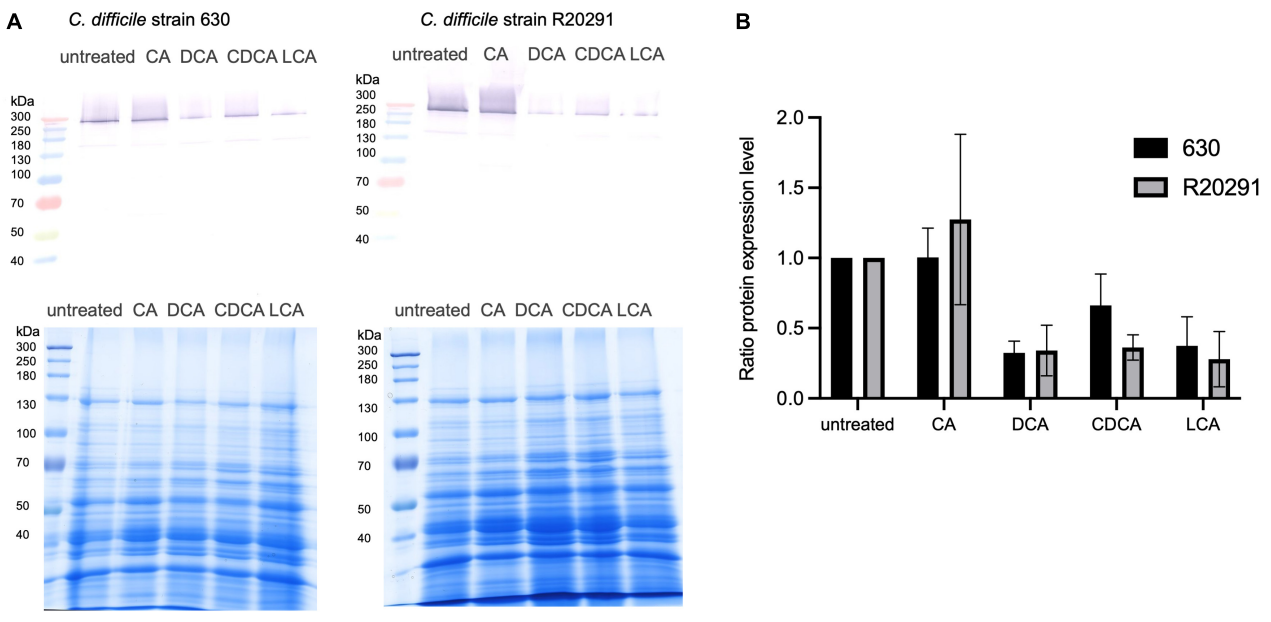

FIGURE 5 | Western Blot analysis of secreted toxin A. **(A)** *C. difficile* strain 630 (left) and strain R20291 (right) were cultivated for 72 h in the presence of four different bile acids (CA, cholic acid; DCA, deoxycholic acid; CDCA, chenodeoxycholic acid; LCA, lithocholic acid) and without any stress conditions (untreated). Secreted proteins were extracted from cultivation supernatant and an amount of 150 µg was separated *via* SDS-PAGE (loading control in the bottom) to subsequently detect toxin A by Western Blot analysis (top). **(B)** Three biological replicates were analyzed and related to the untreated condition. Standard deviations are indicated.

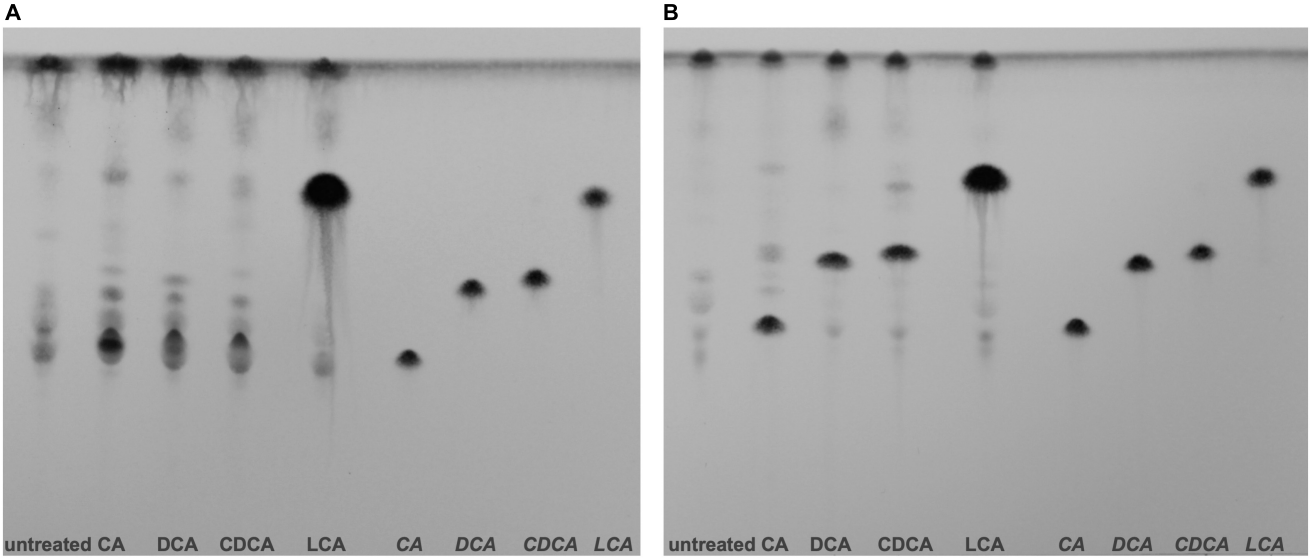

FIGURE 6 | Thin layer chromatography (TLC) of *C. difficile* lipid extracts. **(A)** Lipids of exponentially growing cells and **(B)** stationary phase cells under control conditions (untreated) and challenged with different bile acids (CA, cholic acid; DCA, deoxycholic acid; CDCA, chenodeoxycholic acid; LCA, lithocholic acid) were extracted and separated *via* TLC. Hydrophobic species were stained with phosphomolybdic acid. References of the four bile acids were separated on the right side of each TLC plate. Two additional biological replicates for exponentially growing cells and stationary phase cells are provided **Supplementary Figure 3**.

(**Figure 7**). Especially, in DCA-challenged cells a formation of bleb-like structures ("swelling") on the inner surface layer of the cell is most striking. Not as prevalent but also observable those swellings occur in CA-stressed cells. In untreated and LCA-stressed *C. difficile* none of such structures could be seen. Interestingly, in cells challenged with CDCA no swellings, but a distinct additional layer on the inner surface of the bacterial membrane was observed. In SEM of exponentially growing *C. difficile* cells stressed with different BAs these morphological changes were not visible, but differences in the expression of flagella became once more obvious (**Figure 7**). However, in SEM of stationary phase cells being challenged with BAs for a longer time, the swellings of DCA-stressed cells could be visualized (**Figure 4**). Furthermore, big differences in the length of bacteria were determined as was previously shown for exponentially growing cells (Sievers et al., 2019). Especially CDCA causes elongation with cells being twice as long as untreated stationary phase cells (**Figure 4**). However, most striking was the recurrence of flagella in LCA-stressed stationary phase cells, whereas *C. difficile* grown to stationary phase in the presence of DCA or CDCA still features a reduced number of flagella (**Figure 4**).

Besides electron microscopy we also employed CLSM to test for the fate of different BAs in *C. difficile* (**Figure 7**). This was possible since specific antibodies against each of the four tested BAs are commercially available. A proof of specificity and absence of cross-reactivity is provided in **Supplementary Figure 2**. Although resolution of the applied CLSM method is the limiting factor for an unequivocal determination of the exact cellular location of the single BAs, the results essentially resemble the TEM data. The immunofluorescence (IF) signal of the DCA antibody appears in separate spots apparently at the bacterial membrane. Such fluorescence spots could resemble the swellings seen in electron micrographs. Also in CA-challenged *C. difficile*, the IF signal originating from the BA antibody appears clustered but not distributed all over the cell. This becomes especially obvious when CA is detected *via* IF in an ultramicrotome section as it was prepared for TEM (**Figure 7**). In contrast, in cells challenged with CDCA the IF signal is not as focused but rather evolving from the entire cell envelope which corresponds very well with the phenomenon of an extra layer at the inner side of the cytoplasmic membrane as it was observed *via* TEM. Although, no abnormality was detected in electron micrographs of LCA-stressed cells, IF revealed an accumulation of LCA in several clusters over the cell comparable to what was observed for DCA.

DISCUSSION

Previously, comprehensive proteome signatures characterizing the stress response of the human intestinal pathogen *C. difficile* to the four most abundant BA lead structures have been published. They showed different and specific changes in *C. difficile's* proteome depending on the nature of the BA (Sievers et al., 2018). Data of this study demonstrate that the expression of several virulence traits of *C. difficile* is diversely affected in the presence of various BAs as well. Our data revealed the close to complete loss of flagella in LCA challenged *C. difficile* cells and reduced number of flagella in cells cultivated in the presence of DCA and CDCA. The latter observation correlates very well with the observation made by Dubois et al. who determined an increased biofilm formation for DCA and CDCA stressed cells (Dubois et al., 2019),

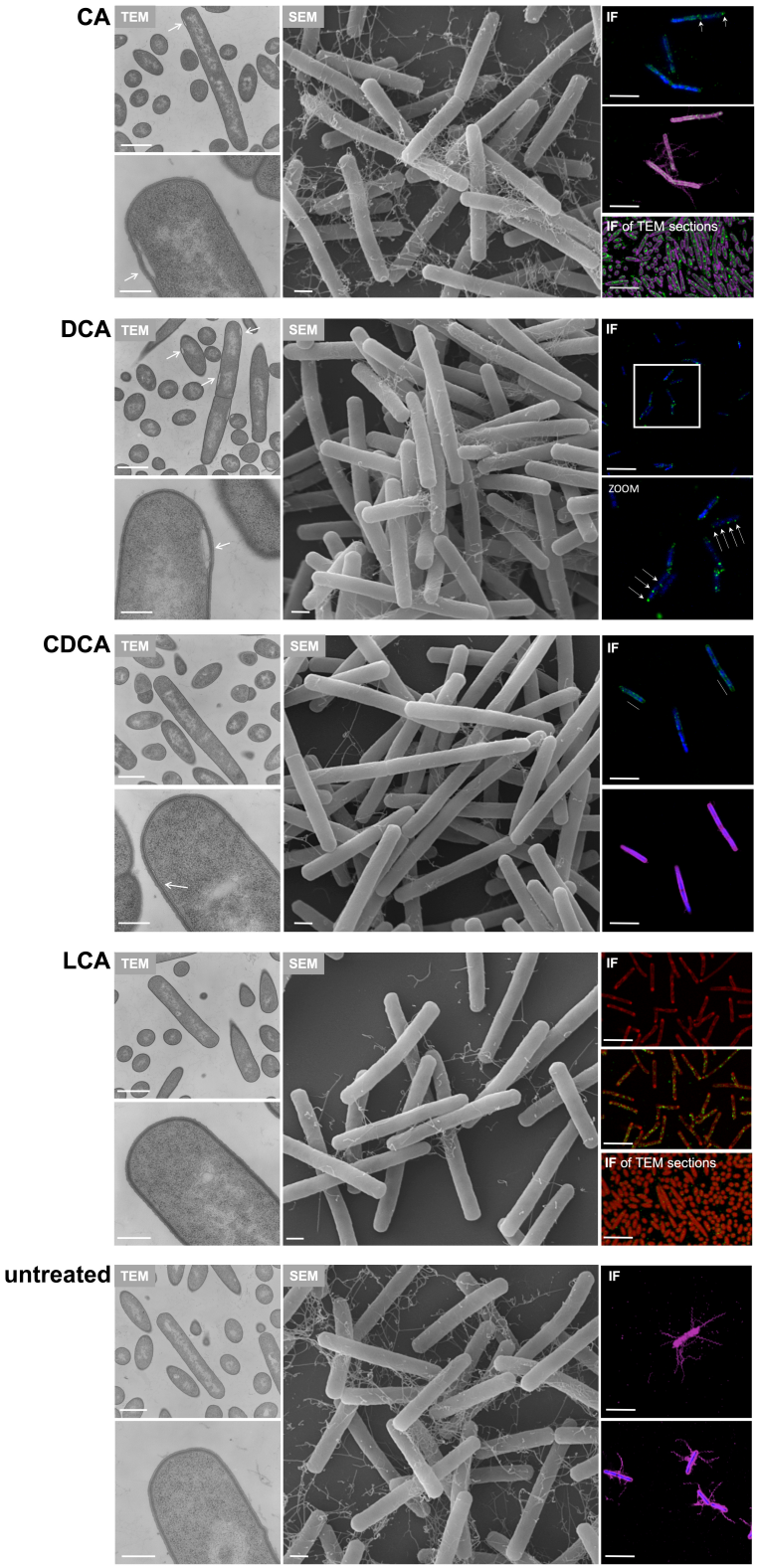

FIGURE 7 | Putative localization of various BAs in the *C. difficile* cell. Left: Transmission electron micrographs of *C. difficile* challenged with the four different bile acids (CA, cholic acid, DCA, deoxycholic acid, CDCA, chenodeoxycholic acid, LCA, lithocholic acid) and of untreated cells, all in exponential growth phase. Morphological

(*Continued*)

FIGURE 7 | changes are highlighted as white arrows. Scale bars, top 1 μm and bottom 200 nm. Middle: Scanning electron micrographs of *C. difficile* challenged with four different bile acids (CA, DCA, CDCA, and LCA) and of untreated cells, scale bar = 1 μm. Right top and center: Immunofluorescence (IF) of *C. difficile* challenged with BAs and stained with mouse anti-CA antibody (green), mouse anti-CDCA antibody (green), rabbit anti-DCA antibody (green), rabbit anti-LCA antibody (green) as well as DAPI (blue) and rabbit anti-*C. difficile* antibody (purple). Due to the same antibody host (rabbit), LCA samples were not counterstained with anti-*C. difficile* but with Nile red (red) and DCA challenged cells were only co-stained with DAPI. Scale bars = 5 μm. Right bottom: IF of TEM sections of *C. difficile* challenged with BAs and stained with anti-CA (green) and counterstained with anti-*C. difficile* (purple) and anti-LCA (green) counterstained with Nile red (red). An IF staining of TEM sections of DCA, CDCA and untreated samples was not possible. Scale bars = 5 μm.

which could be reasoned by less motile cells with fewer flagella. Flagella play an important role for the pathogenicity of *C. difficile*. They do not only allow for motility of the bacterium but also mediate adhesion to biotic and abiotic surfaces (Stevenson et al., 2015). The here presented results on the reduced adherence of *C. difficile* challenged with DCA and CDCA to Caco-2 cells, a cell line of human colorectal adenocarcinoma cells, was thus expected. However, astonishing was the consistent adherence capability of LCA-challenged *C. difficile* cells, although earlier studies demonstrated the importance of flagella in *C. difficile* colonization (Tasteyre et al., 2001). Cells of *C. difficile* 630 tested in the present study, that lost flagella after LCA treatment, were obviously able to adhere to Caco-2 cells by a flagella-independent mechanism. This finding corresponds very well to recent observations in which strain 630Δ*erm* mutated in the structural flagella components *fliC* and *fliD* featured an even stronger adherence to Caco-2 cells than the wildtype (Dingle et al., 2011; Baban et al., 2013), but is contradictory to results obtained in strain R20291, in which the loss of flagella resulted in a decreased adherence to Caco-2 cells (Baban et al., 2013). The origin of such differences in adherence between strains and the mechanistic background of a flagella-independent cell adhesion still needs to be elucidated.

Flagella are not just important virulence determinants in terms of motility and cell host adherence of a pathogen. It is known that they are highly immunogenic with the ability to modulate the host immune response by triggering proinflammatory cytokines which is mediated by the Toll-like receptor 5 (Hayashi et al., 2001), also shown for *C. difficile* (Yoshino et al., 2013). Hence, *C. difficile* strains devoid of flagella can possibly hide away from clearance by the immune system and infect the host even more successfully than strains expressing flagella (Dingle et al., 2011). The here determined differential impact of various BAs on flagella expression could thus make a big difference on how *C. difficile* is recognized by the host immune system along the intestinal tract. Higher concentrations of DCA, CDCA and LCA, that are generally thought to counteract a *C. difficile* infection, reduce flagella on the bacterial surface and thus might prevent a fast clearance of the pathogen by the immune system.

In this work, we could show that the non-existence of flagella is not just caused by mechanical loss from the cell surface due to presence of specific BAs, but a result of changes in gene expression, specifically gene transcription. Hence, BAs either enter the cells and directly hamper transcription of flagellar genes or they have their locus of action somewhere else in the cell, but the signal is transduced to affect *fliC* gene transcription. Whatever mechanism holds true, it is interesting that the tested BAs act differently in this respect. The regulation of flagella expression in *C. difficile* is not fully understood. However, the genes encoding for numerous components to build the flagellar apparatus are located in three adjacent genetic regions and are divided into early- and late-stage flagellar genes, allowing for their hierarchical expression. Expression of the late-stage flagellar genes, such as the main structural flagellar component *fliC* and the flagellar cap *fliD*, is facilitated by sigma factor FliA (SigD), which itself is encoded in the region for early-stage flagellar genes (Aubry et al., 2012). These early-stage genes have recently been shown to be under control of a genetic switch upstream of their coding sequences deciding on their "ON" or "OFF" state and consequently, *via* SigD, also on late-stage flagellar gene expression (Anjuwon-Foster and Tamayo, 2017). Interestingly, the locus of early-stage flagellar genes is additionally regulated by a riboswitch located in the untranslated 5′ region of the corresponding mRNA. Binding of c-di-GMP to the riboswitch leads to premature termination of transcription (Soutourina et al., 2013). In our work, we detected a reduced amount of the late-stage flagellar proteins FliC and FliD and also of the *fliC* mRNA in the presence of the secondary BAs DCA and LCA and also of the primary BA CDCA. Several groups have already demonstrated a co-regulation of flagella and genes of the pathogenicity locus (PaLoc) including the two main toxins, toxin A and toxin B. Aubry et al. (2012) have shown an increased toxin production of *C. difficile* when the *fliC* or *fliD* gene is deleted accompanied by an increased virulence of such mutants in a hamster model. Our observation is the opposite with reduced levels of secreted toxin A comparable to the influence of the single BAs on *fliC* and *fliD* expression. A reduction of toxin synthesis was previously observed when genes of the early-stage flagellar locus are deleted (Aubry et al., 2012) leading us to the conclusion that the reduction of the late-stage flagellar components FliC and FliD and of toxin A, as determined in this work, is an indirect effect that results from repression of the early-stage flagellar operon. Specifically, the reduced amount of SigD, which is required for transcription initiation of both, the late-stage flagellar genes and the PaLoc (El Meouche et al., 2013) is assumed to be the cause of lower *fliC*, *fliD* and toxin A expression. We thus conclude that the BAs DCA, CDCA and especially LCA hamper expression of the early-stage flagellar gene region. Hitherto, BAs were known to affect spore germination and vegetative growth of *C. difficile*. Our observation endows them with another vital feature, i.e., the influence on the expression of important virulence traits such as flagella formation and toxin synthesis. Thus LCA, DCA and CDCA might counteract a *C. difficile* infection by suppressing transcription of early-stage flagellar genes and subsequently transcription of toxins, which once more underscores how the BA-composition in the host's intestines

can decide on the outcome of a CDI. A plethora of regulatory cellular processes to control the expression of the PaLoc in *C. difficile* has been described involving various sigma factors, other global transcriptional regulators and small metabolites (Martin-Verstraete et al., 2016). We propose the regulation of toxin synthesis by specific BAs to be indirect and mediated by SigD. However, it cannot be excluded that other regulatory mechanisms play a role that directly affect toxin expression after BA challenge or act indirectly *via* the expression of flagellar genes. Hence, the question on the exact molecular mechanisms of how BAs specifically modify transcription of flagellar and toxin genes remains to be answered and will be a challenging task for future studies.

An important issue that has been neglected in research so far is the question of the place and mode of action of BAs in bacteria. Of course, it is assumed that due to their amphiphilic and soap-like character, BAs primarily challenge cell envelope integrity. Stressing bacteria with high concentrations of BAs in *in vitro* studies will at a certain point simply lead to abrupt cell lysis. However, in addition to the membrane-disturbing effect, BAs were also reported to structurally alter other macromolecules as RNA, DNA and proteins (Begley et al., 2005). LCA was even reported to cause single strand breaks in mouse lymphoblasts (Kulkarni et al., 1980). In contrast to SDS or other chemical detergents represent BAs naturally occurring compounds. Especially with respect to intestinal bacteria they occur in concentrations that will not kill the bacterium, but will challenge it and will result in adaptation processes and stress responses, or will have certain signaling function to implement specific virulence mechanisms. The BA taurocholate as trigger for spore germination of *C. difficile* is a good example of such a signaling function with an essential meaning for the virulence of the pathogen (Sorg and Sonenshein, 2008). However, it is neither known to date, how much of externally applied BAs actually enter the bacterial cell to be effective there, nor what the exact mode of action on the bacterial surface, specifically in the cytoplasmic membrane, is. Since it is widely appreciated by now, that specific BAs can be beneficial to avoid a CDI while others are rather detrimental, one aim of this study was to get an idea on how efficiently different BAs enter the cell. The concentration of every BA used in this study was adjusted in such a way that the effect on *C. difficile* growth was comparable, as described before (Sievers et al., 2018). This should prevent any indirect and growth-dependent effects on flagella formation, adhesion and toxin synthesis that were also analyzed in this study. But it meant that the concentrations of CDCA, DCA and especially CA that were used to stress *C. difficile* were much higher than the one of LCA. It can be assumed that the effect amphiphilic substances can exert on bacteria highly depends on their capability of entering the cells. With respect to BAs, the fewer hydroxy-groups a BA has, the more hydrophobic it is and the more efficiently it embeds into or even crosses membranes (Schubert et al., 1983; Cabral et al., 1987; Kamp et al., 1993). This was shown on model membranes that consisted of only one or a few different lipids. Later it was found that the membrane-crossing ability of BAs does not only depend on the hydrophobicity of the BA but also on the lipid composition of the membrane (Hofmann et al., 2001). Proteins embedded in the membrane, as it is the case in real biological membranes, would add another factor of impact on membrane intercalation of BAs. To exactly answer the question of how well an amphiphilic substance interacts with or crosses the cellular membrane of a bacterium, the substance needs to be tested on the specific bacterium itself. There is only very little known on the membrane composition of *C. difficile*. A first phospholipid profiling of membranes of 11 different *C. difficile* strains was carried out by Drucker et al. (1996). Later, plasmalogens, which are ether lipids restricted to strictly anaerobic organisms and animals, and cardiolipin, a rigid lipid composed of a phosphatidylglycerol dimer, were identified in *C. difficile* membranes (Guan et al., 2014). However, information on *C. difficile*'s lipidome is still scarce and to our knowledge no lipidomics analysis tracking the changes in membrane lipid composition with changing conditions has been performed. For a start we aimed to determine the relative amount of the different BAs that were taken up or adsorbed by *C. difficile* using thin layer chromatography (TLC). Although this approach is only semi-quantitative, a clear difference could be observed between the single BAs. LCA, which was provided in only very small quantities to the medium compared to the other BAs, was taken up in huge amounts already in exponential growth phase. In fact, there is no further increase in LCA noticeable in stationary phase, i.e., LCA can obviously enter *C. difficile* very fast and efficiently. On the contrary, there is no clear signal of the other three BAs in exponential growth phase, although for CA this cannot be unambiguously stated, since there is an accumulation and overlay of several lipids on the TLC plate at the height of CA. In general, the lipid pattern of CA, DCA, and CDCA stressed cells is slightly different from control cells in exponential phase, indicating that *C. difficile* already adapted its membrane lipid composition. This difference comes even clearer in stationary phase cells. Now, a clear accumulation of CA, DCA and CDCA in *C. difficile* can be observed, although not as dominant as for LCA challenged cells. Furthermore, the signals of lipids apart from the BAs show distinct patterns for CA, DCA, and CDCA stressed cells. *C. difficile* cells challenged with LCA show the most similar pattern to the control sample despite the strong accumulation of LCA. Altogether, TLC results indicate that there is not just a proteomic stress response of *C. difficile* specific for every tested BA (Sievers et al., 2018), but that there are also BA specific rearrangements in the lipid composition of the pathogen.

As anticipated, the most hydrophobic BA LCA readily entered the *C. difficile* cell, but the other three BAs featuring more hydroxy groups were first detectable after a long incubation time. However, DCA and CDCA, which have the same empirical molecular formular, have a different impact in the cell as determined by proteomics profiling (Sievers et al., 2018) and by the TLC results presented in this study. It will be most interesting to characterize particular and BA-specific lipid changes in qualitative and quantitative detail making use of modern lipidomics techniques. The question remains, if there exist specific receptor molecules in the *C. difficile* cell and in bacteria in general. Most BA stress experiments

on bacteria were carried out using a complex BA mixture isolated from ox or pig. Thus, very few examples of the impact of specific BAs are published so far. However, contrary reports on how bacteria respond to BAs point at the presence of specific receptors and signal transduction pathways. For instance, BAs have been shown to upregulate the flagellar promoter in *Campylobacter jejuni* (Allen and Griffiths, 2001) and motility in *Vibrio cholerae* (Krukonis and DiRita, 2003) but in *Salmonella enterica*, flagellar synthesis and motility was reduced in the presence of BAs (Prouty et al., 2004) comparable with what we observed in *C. difficile*. In 2013, Francis et al. (2013) determined the spore surface protease CspC to be the specific receptor of taurocholate to induce spore germination of *C. difficile*. CspC is the first and only receptor identified so far. However, in consideration of the numerous specific BA receptors that have already been described in human (Fiorucci and Distrutti, 2015), additional receptors aside from CspC are conceivable.

While TLC was used in this study to determine if and to what extent BAs accumulate in *C. difficile*, we tried to determine the exact location of BAs by different microscopic approaches. Especially for DCA a clear concentration of this BA into a few bleb-like clusters in the cell could be observed by electron microscopy as well as by CLSM. Although DCA and CDCA differ only in the position of one single hydroxy group on the steroid scaffold, such an accumulation could not be seen for the latter one. CDCA in *C. difficile* seems to uniformly disseminate at the entire inner layer of the cell envelope. It can be speculated that the clustered accumulation of BAs in the cell might be an adaptation strategy of *C. difficile* to the stress, since such an accumulation of BAs in form of micelles would lead to an inhomogeneous distribution in the cell and thus to a reduction of the local BA concentration in the cell allowing metabolic processes still to take place. However, there remains the question why some BAs accumulate in blebs in *C. difficile* while others do not. It is tempting to reason that based on their hydrophobic character BAs have different abilities to interact with the specific structure of the membrane. It is long known that the membrane of eukaryotic cells is not a homogeneous compartment, but rather structured in domains that consist of high amounts of specific lipids such as cholesterol and proteins for signal transduction pathways (lipid rafts) (Lingwood and Simons, 2010). Recently, lipid raft equivalents were also discovered in bacteria. They were named functional membrane microdomains (FMM) and comprise highly active membrane segments including processes of signal transduction and transport (López and Kolter, 2010). These FMM are characterized by a higher concentration of rigid lipids and a special protein called flotillin or flotillin-like protein (Langhorst et al., 2005). Whereas in eukaryotes cholesterol represents the rigid lipid of lipid rafts, bacteria are not able to produce cholesterol and enrich other lipids in their FMM, e.g., cardiolipin which was already identified from *C. difficile* membranes (Guan et al., 2014).

Bile acids featuring a steroid structure are reminiscent of rigid lipids. It is thus conceivable, that the interaction of specific BAs with FMMs is different than with other parts of the bacterial membrane and also dependent on the nature of the BA. In a human carcinoma cell line, a change in membrane domains was detected after BA stress, and by using radio-labeled BAs a differential interaction of these BAs with membrane domains was determined (Jean-Louis et al., 2006). Also in baby hamster kidney cells, BAs reorganize membrane structure and stabilize membrane domains resulting in a non-receptor-mediated signaling in these cells (Zhou et al., 2013). These results turn BAs into potential regulators of cell signaling and they call for an elucidation of the exact signal cascades that are initiated in bacteria of the digestive tract including intestinal pathogens as *C. difficile*. The knowledge could help to shed light on observations that were recently made. Kang et al. (2019) reported an increased inhibitory effect of tryptophan-derived antibiotics on *C. difficile* in the presence of DCA and LCA but not CA. Although the authors could not explain this additive effect of selected BAs and antibiotics yet, it is possible, that it is caused by an impact some BAs have on membrane structure formation but others do not. Especially with regard to pathogenic bacteria, the perturbation of FMM possibly leads to a loss of essential virulence traits as it was impressively pictured for methicillin-resistant *Staphylococcus aureus* that could be re-sensitized for penicillin after FMM disruption (García-Fernández et al., 2017).

In the meantime, it is widely appreciated that intestinal BA composition can decide on the outcome of an infection with *C. difficile*. To smartly employ the intestinal microbiota and its ability to convert BAs in CDI prevention and therapy, detailed knowledge on the molecular action of BAs on pathogenic intestinal bacteria such as *C. difficile* is mandatory.

DATA AVAILABILITY STATEMENT

The original contributions presented in the study are included in the article/**Supplementary Material**, further inquiries can be directed to the corresponding author.

AUTHOR CONTRIBUTIONS

NM and SS designed all experiments of this study, analysed and interpreted the data and wrote the manuscript. LL and NM performed the TLC experiments. NL and NM prepared flagella extracts and performed Western Blot analysis to check for FliC and FliD protein abundance. DT and NM analyzed fliC mRNA expression by Northern Blot analysis. NM prepared the extracts for visualization by CLSM, TEM, and SEM and carried out the CLSMimage analysis. RS performed the electron microscopy studies. SD and NM performed cell culture experiments. SD, L-SP, and DT performed the preparation of extracellular proteins and Toxin A detection by Western Blot analysis. All authors contributed to the article and approved the submitted version.

FUNDING

This work was funded by a grant of the German Research Foundation (231396381/GRK1947) to SS, the "Ministerium für Bildung, Wissenschaft und Kultur Mecklenburg-Vorpommern" (UG16001) and by a Käthe–Kluth-Scholarship of the University of Greifswald granted to SS.

ACKNOWLEDGMENTS

We are very grateful to Glen Armstrong (University of Calgary), Séverine Péchiné (University Paris-Sud) and Robert Fagan (University of Sheffield) for generously providing us with anti-FliC, anti-FliD and anti-*C. difficile* antibodies, respectively. Furthermore, we very much appreciate the sharing of a protocol for transmission electron microscopy of *C. difficile* by Aimee Shen (Tufts University, Boston, MA, United States). We also thank Annette Meuche and Stefan Bock for excellent technical assistance regarding electron microscopy.

SUPPLEMENTARY MATERIAL

The Supplementary Material for this article can be found online at: https://www.frontiersin.org/articles/10.3389/fmicb.2022.814692/full#supplementary-material

Supplementary Material 1 | Western Blot analyses of toxin A from supernatants of *C. difficile* (strains 630 and R20291) stressed with different bile acids and of unstressed cells.

Supplementary Material 2 | Verification of specificity and exclusion of cross reactivity of four bile acid-specific antibodies.

Supplementary Material 3 | Thin layer chromatography (TLC) of lipid extracts of *C. difficile* stressed with bile acids and of unstressed cells.

REFERENCES

Allen, K. J., and Griffiths, M. W. (2001). Effect of environmental and chemotactic stimuli on the activity of the *Campylobacter jejuni* flaA sigma(28) promoter. *FEMS Microbiol. Lett.* 205, 43–48. doi: 10.1111/j.1574-6968.2001.tb10923.x

Anjuwon-Foster, B. R., and Tamayo, R. (2017). A genetic switch controls the production of flagella and toxins in *Clostridium difficile*. *PLoS Genet.* 13:e1006701. doi: 10.1371/journal.pgen.1006701

Aubry, A., Hussack, G., Chen, W., KuoLee, R., Twine, S. M., Fulton, K. M., et al. (2012). Modulation of toxin production by the flagellar regulon in *Clostridium difficile*. *Infect. Immun.* 80, 3521–3532. doi: 10.1128/IAI.00224-12

Baban, S. T., Kuehne, S. A., Barketi-Klai, A., Cartman, S. T., Kelly, M. L., Hardie, K. R., et al. (2013). The role of flagella in *Clostridium difficile* pathogenesis: comparison between a non-epidemic and an epidemic strain. *PLoS One* 8:e73026. doi: 10.1371/journal.pone.0073026

Begley, M., Gahan, C. G. M., and Hill, C. (2002). Bile stress response in *Listeria monocytogenes* LO28: adaptation, cross-protection, and identification of genetic loci involved in bile resistance. *Appl. Environ. Microbiol.* 68, 6005–6012. doi: 10.1128/AEM.68.12.6005-6012.2002

Begley, M., Gahan, C. G. M., and Hill, C. (2005). The interaction between bacteria and bile. *FEMS Microbiol. Rev.* 29, 625–651. doi: 10.1016/j.femsre.2004.09.003

Bouillaut, L., Dubois, T., Sonenshein, A. L., and Dupuy, B. (2015). Integration of metabolism and virulence in *Clostridium difficile*. *Res. Microbiol.* 166, 375–383. doi: 10.1016/j.resmic.2014.10.002

Brandes, V., Schelle, I., Brinkmann, S., Schulz, F., Schwarz, J., Gerhard, R., et al. (2012). Protection from *Clostridium difficile* toxin B-catalysed Rac1/Cdc42 glucosylation by tauroursodeoxycholic acid-induced Rac1/Cdc42 phosphorylation. *Biol. Chem.* 393, 77–84. doi: 10.1515/BC-2011-198

Buffie, C. G., Bucci, V., Stein, R. R., McKenney, P. T., Ling, L., Gobourne, A., et al. (2015). Precision microbiome reconstitution restores bile acid mediated resistance to *Clostridium difficile*. *Nature* 517, 205–208. doi: 10.1038/nature13828

Buffie, C. G., and Pamer, E. G. (2013). Microbiota-mediated colonization resistance against intestinal pathogens. *Nat. Rev. Immunol.* 13, 790–801. doi: 10.1038/nri3535

Cabral, D. J., Small, D. M., Lilly, H. S., and Hamilton, J. A. (1987). Transbilayer movement of bile acids in model membranes. *Biochemistry* 26, 1801–1804. doi: 10.1021/bi00381a002

Cammarota, G., Ianiro, G., and Gasbarrini, A. (2014). Fecal microbiota transplantation for the treatment of *Clostridium difficile* infection: a systematic review. *J. Clin. Gastroenterol.* 48, 693–702. doi: 10.1097/MCG.0000000000000046

Cerquetti, M., Serafino, A., Sebastianelli, A., and Mastrantonio, P. (2002). Binding of *Clostridium difficile* to Caco-2 epithelial cell line and to extracellular matrix proteins. *FEMS Immunol. Med. Microbiol.* 32, 211–218. doi: 10.1111/j.1574-695X.2002.tb00556.x

Darkoh, C., Brown, E. L., Kaplan, H. B., and DuPont, H. L. (2013). Bile salt inhibition of host cell damage by *Clostridium difficile* toxins. *PLoS One* 8:e79631. doi: 10.1371/journal.pone.0079631

Delmée, M., Avesani, V., Delferriere, N., and Burtonboy, G. (1990). Characterization of flagella of *Clostridium difficile* and their role in serogrouping reactions. *J. Clin. Microbiol.* 28, 2210–2214. doi: 10.1128/JCM.28.10.2210-2214.1990

Dingle, T. C., Mulvey, G. L., and Armstrong, G. D. (2011). Mutagenic analysis of the *Clostridium difficile* flagellar proteins, FliC and FliD, and their contribution to virulence in hamsters. *Infect. Immun.* 79, 4061–4067. doi: 10.1128/IAI.05305-11

Drucker, D. B., Wardle, H. M., and Boote, V. (1996). Phospholipid profiles of *Clostridium difficile*. *J. Bacteriol.* 178, 5844–5846. doi: 10.1128/jb.178.19.5844-5846.1996

Dubois, T., Tremblay, Y. D. N., Hamiot, A., Martin-Verstraete, I., Deschamps, J., Monot, M., et al. (2019). A microbiota-generated bile salt induces biofilm formation in *Clostridium difficile*. *NPJ Biofilms Microbiomes* 5:14. doi: 10.1038/s41522-019-0087-4

El Meouche, I., Peltier, J., Monot, M., Soutourina, O., Pestel-Caron, M., Dupuy, B., et al. (2013). Characterization of the SigD regulon of *C. difficile* and its positive control of toxin production through the regulation of tcdR. *PLoS One* 8:e83748. doi: 10.1371/journal.pone.0083748

Fernández Murga, M. L., Bernik, D., Font de Valdez, G., and Disalvo, A. E. (1999). Permeability and stability properties of membranes formed by lipids extracted from *Lactobacillus acidophilus* grown at different temperatures. *Arch. Biochem. Biophys.* 364, 115–121. doi: 10.1006/abbi.1998.1093

Fiorucci, S., and Distrutti, E. (2015). Bile acid-activated receptors, intestinal microbiota, and the treatment of metabolic disorders. *Trends Mol. Med.* 21, 702–714. doi: 10.1016/j.molmed.2015.09.001

Francis, M. B., Allen, C. A., Shrestha, R., and Sorg, J. A. (2013). Bile acid recognition by the *Clostridium difficile* germinant receptor, CspC, is important for establishing infection. *PLoS Pathog.* 9:e1003356. doi: 10.1371/journal.ppat.1003356

García-Fernández, E., Koch, G., Wagner, R. M., Fekete, A., Stengel, S. T., Schneider, J., et al. (2017). Membrane microdomain disassembly inhibits MRSA antibiotic resistance. *Cell* 171, 1354–1367.e20. doi: 10.1016/j.cell.2017.10.012

Guan, Z., Katzianer, D., Zhu, J., and Goldfine, H. (2014). *Clostridium difficile* contains plasmalogen species of phospholipids and glycolipids. *Biochim. Biophys. Acta* 1842, 1353–1359. doi: 10.1016/j.bbalip.2014.06.011

Hayashi, F., Smith, K. D., Ozinsky, A., Hawn, T. R., Yi, E. C., Goodlett, D. R., et al. (2001). The innate immune response to bacterial flagellin is mediated by Toll-like receptor 5. *Nature* 410, 1099–1103. doi: 10.1038/35074106

Hofmann, A. F. (2009). The enterohepatic circulation of bile acids in mammals: form and functions. *Front. Biosci.* 14, 2584–2598. doi: 10.2741/3399

Hofmann, M., Schumann, C., Zimmer, G., Henzel, K., Locher, U., and Leuschner, U. (2001). LUV's lipid composition modulates diffusion of bile acids. *Chem. Phys. Lipids* 110, 165–171. doi: 10.1016/s0009-3084(01)00131-1

Jean-Louis, S., Akare, S., Ali, M. A., Mash, E. A., Meuillet, E., and Martinez, J. D. (2006). Deoxycholic acid induces intracellular signaling through membrane perturbations. *J. Biol. Chem.* 281, 14948–14960. doi: 10.1074/jbc.M506710200

Kamp, F., Hamilton, J. A., and Westerhoff, H. V. (1993). Movement of fatty acids, fatty acid analogues, and bile acids across phospholipid bilayers. *Biochemistry* 32, 11074–11086. doi: 10.1021/bi00092a017

Kang, J. D., Myers, C. J., Harris, S. C., Kakiyama, G., Lee, I.-K., Yun, B.-S., et al. (2019). Bile Acid 7α-Dehydroxylating gut bacteria secrete antibiotics that inhibit *Clostridium difficile*: role of secondary bile acids. *Cell Chem. Biol.* 26, 27–34.e4. doi: 10.1016/j.chembiol.2018.10.003

Krukonis, E. S., and DiRita, V. J. (2003). From motility to virulence: sensing and responding to environmental signals in *Vibrio cholerae*. *Curr. Opin. Microbiol.* 6, 186–190. doi: 10.1016/s1369-5274(03)00032-8

Kulkarni, M. S., Heidepriem, P. M., and Yielding, K. L. (1980). Production by Lithocholic Acid of DNA strand breaks in Li 210 Cells. *Cancer Res.* 2666–2669.

Langhorst, M. F., Reuter, A., and Stuermer, C. A. O. (2005). Scaffolding microdomains and beyond: the function of reggie/flotillin proteins. *Cell. Mol. Life Sci.* 62, 2228–2240. doi: 10.1007/s00018-005-5166-4

Lewis, B. B., Carter, R. A., and Pamer, E. G. (2016). Bile acid sensitivity and in vivo virulence of clinical *Clostridium difficile* isolates. *Anaerobe* 41, 32–36. doi: 10.1016/j.anaerobe.2016.05.010

Lingwood, D., and Simons, K. (2010). Lipid rafts as a membrane-organizing principle. *Science* 327, 46–50. doi: 10.1126/science.1174621

López, D., and Kolter, R. (2010). Functional microdomains in bacterial membranes. *Genes Dev.* 24, 1893–1902. doi: 10.1101/gad.1945010

Martin-Verstraete, I., Peltier, J., and Dupuy, B. (2016). The regulatory networks that control *Clostridium difficile* toxin synthesis. *Toxins* 8:153. doi: 10.3390/toxins8050153

Nakayasu, E. S., Nicora, C. D., Sims, A. C., Burnum-Johnson, K. E., Kim, Y.-M., Kyle, J. E., et al. (2016). MPLEx: a robust and universal protocol for single-sample integrative proteomic, metabolomic, and lipidomic analyses. *mSystems* 1:e00043-16. doi: 10.1128/mSystems.00043-16

Natoli, M., Leoni, B. D., D'Agnano, I., Zucco, F., and Felsani, A. (2012). Good Caco-2 cell culture practices. *Toxicol. In Vitro* 26, 1243–1246. doi: 10.1016/j.tiv.2012.03.009

Nicolas, P., Mäder, U., Dervyn, E., Rochat, T., Leduc, A., Pigeonneau, N., et al. (2012). Condition-dependent transcriptome reveals high-level regulatory architecture in *Bacillus subtilis*. *Science* 335, 1103–1106. doi: 10.1126/science.1206848

Petersen, I., Schlüter, R., Hoff, K. J., Liebscher, V., Bange, G., Riedel, K., et al. (2020). Non-invasive and label-free 3D-visualization shows *in vivo* oligomerization of the staphylococcal alkaline shock protein 23 (Asp23). *Sci. Rep.* 10:125. doi: 10.1038/s41598-019-56907-9

Prouty, A. M., Brodsky, I. E., Manos, J., Belas, R., Falkow, S., and Gunn, J. S. (2004). Transcriptional regulation of *Salmonella enterica* serovar Typhimurium genes by bile. *FEMS Immunol. Med. Microbiol.* 41, 177–185. doi: 10.1016/j.femsim.2004.03.002

Reeves, A. E., Theriot, C. M., Bergin, I. L., Huffnagle, G. B., Schloss, P. D., and Young, V. B. (2011). The interplay between microbiome dynamics and pathogen dynamics in a murine model of *Clostridium difficile* Infection. *Gut Microbes* 2, 145–158. doi: 10.4161/gmic.2.3.16333

Ridlon, J. M., Wolf, P. G., and Gaskins, H. R. (2016). Taurocholic acid metabolism by gut microbes and colon cancer. *Gut Microbes* 7, 201–215. doi: 10.1080/19490976.2016.1150414

Rupnik, M., Wilcox, M. H., and Gerding, D. N. (2009). *Clostridium difficile* infection: new developments in epidemiology and pathogenesis. *Nat. Rev. Microbiol.* 7, 526–536. doi: 10.1038/nrmicro2164

Schindelin, J., Arganda-Carreras, I., Frise, E., Kaynig, V., Longair, M., Pietzsch, T., et al. (2012). Fiji: an open-source platform for biological-image analysis. *Nat. Methods* 9, 676–682. doi: 10.1038/nmeth.2019

Schneider, C. A., Rasband, W. S., and Eliceiri, K. W. (2012). NIH Image to ImageJ: 25 years of image analysis. *Nat. Methods* 9, 671–675. doi: 10.1038/nmeth.2089

Schubert, R., Jaroni, H., Schoelmerich, J., and Schmidt, K. H. (1983). Studies on the mechanism of bile salt-induced liposomal membrane damage. *Digestion* 28, 181–190. doi: 10.1159/000198984

Sievers, S., Dittmann, S., Jordt, T., Otto, A., Hochgräfe, F., and Riedel, K. (2018). Comprehensive Redox Profiling of the Thiol Proteome of *Clostridium difficile*. *Mol. Cell Proteomics* 17, 1035–1046. doi: 10.1074/mcp.TIR118.000671

Sievers, S., Metzendorf, N. G., Dittmann, S., Troitzsch, D., Gast, V., Tröger, S. M., et al. (2019). Differential view on the bile acid stress response of *Clostridioides difficile*. *Front. Microbiol.* 10:258. doi: 10.3389/fmicb.2019.00258

Sorg, J. A., and Sonenshein, A. L. (2008). Bile salts and glycine as cogerminants for *Clostridium difficile* spores. *J. Bacteriol.* 190, 2505–2512. doi: 10.1128/JB.01765-07

Soutourina, O. A., Monot, M., Boudry, P., Saujet, L., Pichon, C., Sismeiro, O., et al. (2013). Genome-wide identification of regulatory RNAs in the human pathogen *Clostridium difficile*. *PLoS Genet.* 9:e1003493. doi: 10.1371/journal.pgen.1003493

Stevenson, E., Minton, N. P., and Kuehne, S. A. (2015). The role of flagella in *Clostridium difficile* pathogenicity. *Trends Microbiol.* 23, 275–282. doi: 10.1016/j.tim.2015.01.004

Tasteyre, A., Barc, M. C., Collignon, A., Boureau, H., and Karjalainen, T. (2001). Role of FliC and FliD flagellar proteins of *Clostridium difficile* in adherence and gut colonization. *Infect. Immun.* 69, 7937–7940. doi: 10.1128/IAI.69.12.7937-7940.2001

Thanissery, R., Winston, J. A., and Theriot, C. M. (2017). Inhibition of spore germination, growth, and toxin activity of clinically relevant *C. difficile* strains by gut microbiota derived secondary bile acids. *Anaerobe* 45, 86–100. doi: 10.1016/j.anaerobe.2017.03.004

Theriot, C. M., Koenigsknecht, M. J., Carlson, P. E., Hatton, G. E., Nelson, A. M., Li, B., et al. (2014). Antibiotic-induced shifts in the mouse gut microbiome and metabolome increase susceptibility to *Clostridium difficile* infection. *Nat. Commun.* 5:3114. doi: 10.1038/ncomms4114

Theriot, C. M., and Young, V. B. (2014). Microbial and metabolic interactions between the gastrointestinal tract and *Clostridium difficile* infection. *Gut Microbes* 5, 86–95. doi: 10.4161/gmic.27131

Theriot, C. M., and Young, V. B. (2015). Interactions between the gastrointestinal microbiome and *Clostridium difficile*. *Annu. Rev. Microbiol.* 69, 445–461. doi: 10.1146/annurev-micro-091014-104115

Thomas, C., Stevenson, M., and Riley, T. V. (2003). Antibiotics and hospital-acquired *Clostridium difficile*-associated diarrhoea: a systematic review. *J. Antimicrob. Chemother.* 51, 1339–1350. doi: 10.1093/jac/dkg254

Troitzsch, D., Zhang, H., Dittmann, S., Düsterhöft, D., Möller, T. A., Michel, A.-M., et al. (2021). A point mutation in the transcriptional repressor PerR results in a constitutive oxidative stress response in *Clostridioides difficile* 630Δerm. *mSphere* 6:e00091-21. doi: 10.1128/mSphere.00091-21

Twine, S. M., Reid, C. W., Aubry, A., McMullin, D. R., Fulton, K. M., Austin, J., et al. (2009). Motility and flagellar glycosylation in *Clostridium difficile*. *J. Bacteriol.* 191, 7050–7062. doi: 10.1128/jb.00861-09

Weingarden, A. R., Dosa, P. I., DeWinter, E., Steer, C. J., Shaughnessy, M. K., Johnson, J. R., et al. (2016). Changes in colonic bile acid composition following fecal microbiota transplantation are sufficient to control *Clostridium difficile* Germination and Growth. *PLoS One* 11:e0147210. doi: 10.1371/journal.pone.0147210

Wilson, K. H. (1983). Efficiency of various bile salt preparations for stimulation of *Clostridium difficile* spore germination. *J. Clin. Microbiol.* 18, 1017–1019. doi: 10.1128/jcm.18.4.1017-1019.1983

Winston, J. A., and Theriot, C. M. (2016). Impact of microbial derived secondary bile acids on colonization resistance against *Clostridium difficile* in the gastrointestinal tract. *Anaerobe* 41, 44–50. doi: 10.1016/j.anaerobe.2016.05.003

Yoshino, Y., Kitazawa, T., Ikeda, M., Tatsuno, K., Yanagimoto, S., Okugawa, S., et al. (2013). *Clostridium difficile* flagellin stimulates toll-like receptor 5, and toxin B promotes flagellin-induced chemokine production via TLR5. *Life Sci.* 92, 211–217. doi: 10.1016/j.lfs.2012.11.017

Zhou, Y., Maxwell, K. N., Sezgin, E., Lu, M., Liang, H., Hancock, J. F., et al. (2013). Bile acids modulate signaling by functional perturbation of plasma membrane domains. *J. Biol. Chem.* 288, 35660–35670. doi: 10.1074/jbc.M113.519116

Conflict of Interest: The authors declare that the research was conducted in the absence of any commercial or financial relationships that could be construed as a potential conflict of interest.

Publisher's Note: All claims expressed in this article are solely those of the authors and do not necessarily represent those of their affiliated organizations, or those of the publisher, the editors and the reviewers. Any product that may be evaluated in this article, or claim that may be made by its manufacturer, is not guaranteed or endorsed by the publisher.

Copyright © 2022 Metzendorf, Lange, Lainer, Schlüter, Dittmann, Paul, Troitzsch and Sievers. This is an open-access article distributed under the terms of the Creative Commons Attribution License (CC BY). The use, distribution or reproduction in other forums is permitted, provided the original author(s) and the copyright owner(s) are credited and that the original publication in this journal is cited, in accordance with accepted academic practice. No use, distribution or reproduction is permitted which does not comply with these terms.

Advantages of publishing in Frontiers

OPEN ACCESS
Articles are free to read for greatest visibility and readership

FAST PUBLICATION
Around 90 days from submission to decision

HIGH QUALITY PEER-REVIEW
Rigorous, collaborative, and constructive peer-review

TRANSPARENT PEER-REVIEW
Editors and reviewers acknowledged by name on published articles

Frontiers
Avenue du Tribunal-Fédéral 34
1005 Lausanne | Switzerland

Visit us: www.frontiersin.org
Contact us: frontiersin.org/about/contact

REPRODUCIBILITY OF RESEARCH
Support open data and methods to enhance research reproducibility

DIGITAL PUBLISHING
Articles designed for optimal readership across devices

FOLLOW US
@frontiersin

IMPACT METRICS
Advanced article metrics track visibility across digital media

EXTENSIVE PROMOTION
Marketing and promotion of impactful research

LOOP RESEARCH NETWORK
Our network increases your article's readership